

**INVESTIGATIONS ON THE EFFECTS OF  
ELECTROMAGNETIC RADIATION  
ON INDIAN FLORA**

**THESIS SUBMITTED BY**

**ARDHENDU KUNDU**

**DOCTOR OF PHILOSOPHY (ENGINEERING)**

**DEPARTMENT OF ELECTRONICS AND  
TELECOMMUNICATION ENGINEERING**

**FACULTY COUNCIL OF ENGINEERING AND TECHNOLOGY**

**JADAVPUR UNIVERSITY**

**KOLKATA, INDIA**

**2022**



**INVESTIGATIONS ON THE EFFECTS OF  
ELECTROMAGNETIC RADIATION  
ON INDIAN FLORA**

**THESIS SUBMITTED IN PARTIAL FULFILMENT  
OF THE REQUIREMENT FOR THE DEGREE OF  
DOCTOR OF PHILOSOPHY (PH.D.)**

**IN  
ENGINEERING**

**BY  
ARDHENDU KUNDU**

**DEPARTMENT OF ELECTRONICS AND  
TELECOMMUNICATION ENGINEERING  
FACULTY COUNCIL OF ENGINEERING AND TECHNOLOGY  
JADAVPUR UNIVERSITY  
KOLKATA, INDIA**

**2022**





**JADAVPUR UNIVERSITY**

**KOKATA – 700032, INDIA**

**INDEX NO. 180/15/E**

**1. Name of the Thesis:**

INVESTIGATIONS ON THE EFFECTS OF ELECTROMAGNETIC RADIATION  
ON INDIAN FLORA

**2. Name, Designation & Institution of the Supervisors:**

DR. BHASKAR GUPTA

Professor, Dept. of Electronics and Telecommunication Engineering,  
Jadavpur University, Kolkata – 700032, West Bengal, India

DR. AMIRUL ISLAM MALLICK

Associate Professor, Dept. of Biological Sciences, Indian Institute of  
Science Education and Research Kolkata, Mohanpur, Nadia – 741246, West  
Bengal, India

**3. List of Publications:** Kindly refer to **Appendix I**

**4. List of Patents:** NIL

**5. List of Presentations in National/International Conferences/Workshops:**

Kindly refer to **Appendix II**



## STATEMENT OF ORIGINALITY

I, **Ardhendu Kundu**, registered on **18/12/2015** do hereby declare that this thesis entitled “**Investigations on the Effects of Electromagnetic Radiation on Indian Flora**” contains literature survey and original research work done by the undersigned candidate as part of Doctoral studies.


All information in this thesis have been obtained and presented in accordance with existing academic rules and ethical conduct. I declare that, as required by these rules and conduct, I have fully cited and referred all materials and results that are not original to this work.


I also declare that I have checked this thesis as per the “Policy on Anti Plagiarism, Jadavpur University, 2019”, and the level of similarity as checked by iThenticate software is 1 %.

*Ardhendu Kundu*  
Signature of Candidate

Date: *12-12-2022*

Certified by Supervisor(s):

*B Gupta 12/12/22*  
  
Dr. Bhaskar Gupta  
Professor, Dept. of ETCE  
Jadavpur University, Kolkata, India – 700032  
Prof. Bhaskar Gupta  
Professor  
Dept. of E. & T.C. Engg.  
Jadavpur University  
Kolkata

*A Amirul*  
*12/12/2022*  
  
Dr. Amirul Islam Mallick  
Associate Professor, Dept. of Biological Sciences  
IISER Kolkata, India – 741246  
DR. AMIRUL ISLAM MALLICK  
M.V.Sc, Ph.D  
Associate Professor  
Dept. Of Biological Science  
Indian Institute of Science Education & Research Kolkata  
Mohanpur, Nadia, West Bengal, Pin - 741246





## CERTIFICATE FROM THE SUPERVISORS

This is to certify that the thesis entitled “**Investigations on the Effects of Electromagnetic Radiation on Indian Flora**” submitted by **Shri Ardhendu Kundu**, who got his name registered on **18/12/2015** for the award of Ph.D. (Engg.) degree of Jadavpur University is absolutely based upon his own work under the supervision of **Prof. Bhaskar Gupta**, Dept. of Electronics and Telecommunication Engineering, Jadavpur University, Kolkata – 700032, West Bengal, India, and **Dr. Amirul Islam Mallick**, Associate Professor, Dept. of Biological Sciences, Indian Institute of Science Education and Research Kolkata, Mohanpur, Nadia – 741246, West Bengal, India, and that neither his thesis nor any part of the thesis has been submitted for any degree/diploma or any other academic award anywhere before.

*hupt 12/12/22*  
**Dr. Bhaskar Gupta**  
Professor, Dept. of ETCE  
Jadavpur University, Kolkata, India – 700032



*Prof. Bhaskar Gupta*  
Professor  
Dept. of E. & T.C. Engg.  
Jadavpur University  
Kolkata

*AM Mallick*  
*12/12/2022*

**Dr. Amirul Islam Mallick**  
Associate Professor, Dept. of Biological Sciences  
IISER Kolkata, India – 741246



**DR. AMIRUL ISLAM MALLICK**  
M.V.Sc, Ph.D  
Associate Professor  
Dept. Of Biological Science  
Indian Institute of Science Education & Research Kolkata  
Mohanpur, Nadia, West Bengal, Pin - 741246



*Dedicated to the Memory of My Grandfather*  
*Late Dhirendra Lal Kundu*





# Acknowledgements

---

The journey to pursue doctoral research work is stretched over a number of years – thus, at times it seems difficult for the doctoral scholar to continue research work in the right direction without proper motivation, guidance and support. While preparing the doctoral dissertation just prior to submission, the scholar stops for a moment to recapitulate the entire journey over the past years. At that very moment, he realizes that there are indirect and direct contributions from a number of well wishers behind successful completion of his doctoral research work. The scholar further realizes that he will not get a second chance to write this particular acknowledgement section in his entire life – thus, he writes this section with utmost care, honest feelings and personal touch. The words expressed in this acknowledgement section are indeed honest and open. A research scholar feels satisfied while writing this section and the feeling stays with him for the rest of his life.

It is indeed difficult to find an appropriate way to express gratitude to everyone who motivated, guided and supported throughout my research journey and during the preparation of this doctoral dissertation. However to start with, I would like to express sincere gratitude to my research supervisors, **Dr. Bhaskar Gupta** (Professor), Department of Electronics and Telecommunication Engineering, Jadavpur University and **Dr. Amirul Islam Mallick** (Associate Professor), Department of Biological Sciences, Indian Institute of Science Education and Research Kolkata, who always managed time (out of their busy schedules) to discuss research ideas, analyze the roots of failure and also celebrate success. Their continuous motivation and guidance enriched my knowledge and understanding in the fields of science, engineering, technology and interdisciplinary research – thus, helped me to sail the boat forward to achieve doctoral research goals. In addition, I am indeed thankful to **Dr. Somnath Bhattacharyya** (Professor), Department of Genetics and Plant Breeding, Bidhan Chandra Krishi Viswavidyalaya for his generous guidance, advice and support in planning and conducting practical investigations.

I am also indebted to present Head of the Department of Electronics and Telecommunication Engineering, Jadavpur University namely **Dr. Manotosh Biswas** (Professor) for his generous

## Acknowledgements

support and assistance in making my thesis submission formalities easier, comfortable and an experience to cherish forever. During my research tenure at this department, I had the privilege to receive advices, suggestions and assistance from previous Heads of this Department and other faculty members whenever I came across any crisis. Therefore, I would like to express my gratitude from the core of my heart to each of them. In addition, I am also thankful to all the departmental staff members, administrative staff members and officers of the University at the Department of Electronics and Telecommunication Engineering, Faculty of Engineering and Technology office, Research Section, Technical Education Quality Improvement Programme (TEQIP) Section, or in any other department – whose cordial assistance made my research journey comfortable and a pleasant experience to cherish forever.

It is indeed true that research supervisors motivate and guide the scholar to explore new avenues for achieving his doctoral research goals. However, the motivation, support and assistance received from senior researchers, fellow laboratory co-researchers and friends must also be acknowledged. Hence, I would like to take the opportunity to acknowledge my senior researchers and fellow co-researchers – **Dr. S. Sankaralingam, Dr. Rajendra Prasad Ghosh, Dr. Arindam Deb, Dr. Sayantan Dhar, Dr. Sudipta Maity, Dr. Amrita Chakraborty, Dr. Buddhadev Pradhan, Dr. Kaushik Patra, Dr. Sourav Banik, Dr. Rinki Ghosal, Dr. Suman Pradhan, Dr. Amartya Banerjee, Mr. Sharanbasappa B. Belangi, Mr. Sumit Kumar Mitra, Mr. Joydeep Pal, Mr. Mishor Biswas and Mr. Sayan Sarkar** for their active cooperation. I will always remember those moments when we discussed technical problems, explored techniques to handle new instruments and standardized measurement protocols even during extended lab hours – I would like to have more such fruitful moments of interaction in future. In addition, I would also like to thank **Dr. Ayona Chakraborty, Dr. Balaka Biswas and Dr. Arka Bhattacharyya** for their cooperation, support and encouragement. Apart from this, I must acknowledge the technical support received from **Dr. Sathish Vangaru** (PhD from BCKV, WB) while carrying out collaborative research work. I also acknowledge the motivation and guidance received from my friend **Dr. Sanjay Ghosh** (PhD from IISc, Bangalore) who is currently conducting postdoctoral research at University of California, San Francisco. Furthermore, I would like to thank the M.E. & B.E. students at Department of Electronics and Telecommunication Engineering, Jadavpur University whose keen questions triggered me to dig

deeper into technical topics and enriched my knowledge. I had the opportunity to interact with a number of professors, scientists, research scholars and industry experts from India and abroad – therefore, I must acknowledge their contributions in sharpening my technical knowledge and skills. I also take this opportunity to thank all the faculty members of MCKV Institute of Engineering where I pursued my B. Tech in Electronics and Communication Engineering – the learning over those four years has helped me a lot to shape my research career.

Without a strong support from the family, it would have never been possible to complete this dissertation. Therefore, I would like to thank my parents **Mr. Ritendu Kundu** and **Mrs. Kakali Kundu**, for whom words are falling short to express what they have sacrificed and bore with for fulfilling my dream of higher education and research. I also appreciate my sister **Mrs. Moumita Kundu** for the continuous inspiration. Before concluding, from the bottom of my heart, I acknowledge the sacrifice, motivation and moral support received from my spouse **Mrs. Susmita Biswas** through these years of PhD tenure.



**ARDHENDU KUNDU**

Date: *12-12-2022*

Place: Kolkata, India

# Abstract

---

With the widespread deployment of wireless communication infrastructure, electromagnetic radiation is steadily increasing in the open environment over multiple frequency bands – in fact, electromagnetic radiation is omnipresent all around the globe. Presence of enormous water and ion substances in the majority of living tissues contributes to reasonably high permittivity ( $\epsilon_r'$ ) and electrical conductivity ( $\sigma$ ). Therefore, biological objects are quite capable of absorbing electromagnetic energy over wide frequency spectrum. Till date, scientists and researchers have majorly investigated electromagnetic energy absorption rates in several human models along with associated biological effects – however, similar investigations on prototyped fruit and plant models are rarely available. Furthermore, all existing global and national electromagnetic exposure regulatory standards have been prescribed entirely based on immediate thermal effects of electromagnetic radiation on humans. As a consequence, prescribed reference power density and Specific Absorption Rate (SAR) limits have been set only for humans. However, arguments can be put to investigate SAR values for fruit, flower and plant structures as those get exposed to uninterrupted electromagnetic radiation at multiple frequencies from the radiating antennas. Besides, higher surface-to-volume ratio of plant structures makes increased interaction with incident electromagnetic field possible. Therefore, in addition to investigating SAR data and spatial distributions, periodic (long duration) as well as one-time (hours long) electromagnetic irradiation induced plant responses should also be investigated at physiological and molecular levels. This thesis entitled “**Investigations on the Effects of Electromagnetic Radiation on Indian Flora**” aims at such investigations of complex dielectric properties ( $\epsilon_r$ ) of fruit and plant tissues, SAR distributions in prototyped fruit and plant models, tissue equivalent phantom liquids for SAR measurement, and periodic (long duration) as well as one-time (hours long) electromagnetic irradiation induced physiological and molecular responses in plants. In this thesis, a chapter is dedicated to the fundamental concepts of material dielectric properties ( $\epsilon_r$ ) and broadband dielectric properties ( $\epsilon_r$ ) characterization of fruit and plant tissue specimens. Furthermore, a novel technique to determine multi-tissue layers equivalent homogeneous phantom liquid formulation (for practical SAR measurement) has also been discussed in the same chapter. SAR data and associated spatial distributions in several tropical fruit models have

been demonstrated in the next chapter. The dependence of SAR data and spatial distributions in fruit and plant models on electromagnetic exposure regulatory guidelines, frequency of operation, angle of incidence and wave polarization has also been demonstrated. Reported findings indicate towards the necessity of harmonizing global and national electromagnetic exposure regulatory standards worldwide. The following chapter covers fruit and plant tissue equivalent homogeneous phantom liquid preparation for performing practical SAR measurement in future. Custom-made phantom liquid recipes have been prepared for twenty fruit and plant tissue layers at 947.50 MHz, 1842.50 MHz and 2450.00 MHz. In this thesis, the subsequent chapters by and large report induced plant responses under electromagnetic irradiation. The immediate next chapter covers investigations on electromagnetic propagation loss due to presence of plants inside an anechoic chamber and initial plant responses under long duration cell phone radiation. Being motivated by the initial plant responses, further investigations have been carried out to investigate periodic (long duration) as well as one-time (hours long), controlled and deterministic electromagnetic irradiation induced physiological and molecular plant responses in two subsequent chapters. Periodic electromagnetic irradiation (1837.50 MHz, 2.75 mW/m<sup>2</sup>) induced physiological and molecular responses have been investigated in two rice variants (*Oryza sativa*) at different growth stages – inside a simple electromagnetic reverberation chamber. Reduced rice seed germination rate, photosynthetic pigment concentration levels and upregulated stress-sensitive gene expressions were noted under the periodic electromagnetic irradiation. Furthermore, investigations have been conducted to examine molecular responses in rice plants following one-time electromagnetic irradiation for 2 h 30 min. Transcript accumulations of selected stress-sensitive genes have been noted even following this one-time electromagnetic irradiation. Thus, reported findings indicate that plants in general perceive electromagnetic irradiation as an abiotic stress. Reported outcome in this thesis can lead to potential planning for minimizing electromagnetic energy absorption in fruits and plants along with associated biological effects without compromising sustainable telecommunication development.

# Contents

---

Acknowledgements	i
Abstract	iv
Contents	vi
List of Figures	xv
List of Tables	xxv
List of Acronyms	xxix
<b>CHAPTER 1: INTRODUCTION</b>	<b>1</b>
1.1 Motivation	2
1.2 Organization of the Thesis	5
<b>CHAPTER 2: LITERATURE REVIEW</b>	<b>13</b>
2.1 Motivation	13
2.2 Dielectric Properties of Different Plant Tissue Specimens	14
2.3 Specific Absorption Rate Assessment Technique	16
2.4 Disagreement among Different Electromagnetic Guidelines	19
2.5 Multilayer Tissues Equivalent Homogeneous Phantom Liquid	21
2.6 Phantom Liquid Recipes for SAR Measurement	22
2.7 Electromagnetic Irradiation Induced Responses in Plants	24
2.8 Conclusions	28
<b>CHAPTER 3: DIELECTRIC PROPERTIES CHARACTERIZATION AND MULTILAYER TISSUE MODELING</b>	<b>42</b>
<b>Part I: Dielectric Properties Characterization</b>	<b>42</b>
3.1 Concept of Dielectric Properties	42

3.1.1 Dipole Moment and Electronic Polarization	43
3.1.2 Polarization Vector	44
3.1.3 Electric Susceptibility and Relative Permittivity	45
3.1.4 Local Electric Field and Clausius-Mossotti Equation	45
3.1.5 Electronic Polarization – Covalent Bond	47
3.1.6 Ionic Polarization Mechanism	48
3.1.7 Orientational (Dipolar) Polarization Mechanism	49
3.1.8 Interfacial Polarization Mechanism	51
3.1.9 Total Polarization	52
3.1.10 Frequency Dependence: Dielectric Constant and Loss Factor	52
3.1.11 Dielectric Properties and Polarizations in Plant Tissues	56
3.2 Dielectric Characterization Techniques – Special Emphasis on Plant Specimen Measurements	57
3.2.1 Open Ended Coaxial Probe Technique – A Non-Destructive Dielectric Characterization System	59
3.3 Dielectric Properties Characterization of Different Plant Tissues	65
3.3.1 Dielectric Properties of Coconut Tissues	65
3.3.2 Dielectric Properties of Mango Tissues	67
3.3.3 Dielectric Properties of Orange Tissues	69
3.3.4 Dielectric Properties of Water Apple Tissue	70
3.3.5 Dielectric Properties of Sapodilla Tissues	72
3.3.6 Dielectric Properties of Grape Tissue	73
3.3.7 Dielectric Properties of Apple Tissue	75
3.3.8 Dielectric Properties of Tomato Tissue	77
3.3.9 Dielectric Properties of Brinjal Tissue	79
3.3.10 Dielectric Properties of Guava Tissue	81
3.4 Conclusions	83
<b>Part II: Multilayer Tissue Modeling</b>	<b>85</b>
3.5 Introduction to Multilayer Tissue Modeling	85
3.6 A Brief Outline of the Problem	87
3.7 Multilayer Equivalent Phantom Liquid Formulation Technique	87

3.8 Multilayer Equivalent Homogeneous Phantom Liquid for Plane Wave Exposure in Far Field Scenario	92
3.8.1 Plane Wave Exposure – A Typical Four Equal Layer Model	92
3.8.1.1 A Brief Description of the Electromagnetic Simulation Setup	94
3.8.1.2 Results and Discussion (Plane Wave – Four Equal Layers)	95
3.8.2 Plane Wave Exposure – A Typical Four Unequal Layer Model	99
3.8.2.1 Results and Discussion (Plane Wave – Four Unequal Layers)	100
3.9 Multilayer Equivalent Homogeneous Phantom Liquid Close to Radiating Antenna in Near Field Scenario	104
3.9.1 Antenna Proximity Radiation Exposure – A Typical Four Equal Layer Model	104
3.9.1.1 Results and Discussion (In Close Proximity of Antenna – Four Equal Layers)	105
3.9.2 Antenna Proximity Radiation Exposure – A Typical Four Unequal Layer Model	109
3.9.2.1 Results and Discussion (In Close Proximity of Antenna – Four Unequal Layers)	110
3.10 Discussions	112
3.11 Conclusions	114
<b>CHAPTER 4: SPECIFIC ABSORPTION RATE EVALUATION FOR PROTOTYPED FRUIT AND PLANT MODELS</b>	<b>123</b>
4.1 Introduction	123
4.2 SAR Analyses in Different Tropical Fruit Models	125
4.2.1 SAR Analysis in a Typical Multilayer Coconut Model	126
4.2.1.1 Existing Electromagnetic Exposure Standards in India	126
4.2.1.2 Material Density and Dielectric Properties of Coconut	128
4.2.1.3 A Typical Multilayer Coconut Modeling in CST MWS 2010	129
4.2.1.4 SAR Computational Technique	130
4.2.1.5 SAR Results in Twig Connected Coconut Structure	132
4.2.1.6 SAR Distribution on Surface of the Coconut Model	135
4.2.1.7 Conclusions	135
4.2.2 SAR Analysis in Single Apple, Guava and Grape Models	137
4.2.2.1 Density and Dielectric Properties of Apple, Guava and Grape	138
4.2.2.2 Modeling of Apple, Guava and Grape in CST MWS 2010	139



4.2.2.3 SAR Computational Technique	140
4.2.2.4 Indian Electromagnetic Exposure Standards	141
4.2.2.5 SAR Computational Results	142
4.2.2.6 SAR Data Analyses	145
4.2.2.7 Conclusions	146
4.2.3 SAR Analysis in a Typical Bunch of Grapes Model	147
4.2.3.1 Indian Electromagnetic Regulatory Guidelines	147
4.2.3.2 Material Density and Dielectric Properties of Grapes	148
4.2.3.3 A Typical Bunch of Grapes Modeling in CST MWS 2010	150
4.2.3.4 SAR Computational Scheme	150
4.2.3.5 SAR Results and Discussion	151
4.2.3.6 Conclusions	154
4.3 Contrast in SAR Data for Fruit and Plant Specimens – due to Discrepancy among Electromagnetic Regulatory Guidelines	155
4.3.1 Contrast in SAR Data for a Bunch of Sapodilla Fruits Model	156
4.3.1.1 Introduction	156
4.3.1.2 Disparity among Different Electromagnetic Standards	157
4.3.1.3 Material Density and Dielectric Properties Characterization	158
4.3.1.4 A Bunch of Sapodilla Fruits Modeling in CST MWS 2014	159
4.3.1.5 SAR Simulation Setup	161
4.3.1.6 Comparative SAR Data and Analysis	163
4.3.1.7 Conclusions	169
4.3.2 Contrast in SAR Data for a Typical Plant Model	170
4.3.2.1 Introduction	170
4.3.2.2 Disparity among Different Electromagnetic Standards	173
4.3.2.3 Material Density and Dielectric Properties Characterization	173
4.3.2.4 <i>Catharanthus roseus</i> Plant Modeling in CST MWS 2014	175
4.3.2.5 Computational Scheme for SAR Estimation	176
4.3.2.6 Computed SAR Data and Analysis	177
4.3.2.7 Conclusions	183

## Contents

4.4 Dependence of SAR Data and Spatial Distribution in Fruit Specimens on Angle of Incidence and Wave Polarization	185
4.4.1 Dependence of SAR in Homogeneous Fruits Model	186
4.4.1.1 Introduction	186
4.4.1.2 Indian Electromagnetic Exposure Guidelines	186
4.4.1.3 Dielectric Properties and Material Density of Water Apple	187
4.4.1.4 Bunch of Water Apples Model and SAR Simulation Setup	189
4.4.1.5 SAR Results and Discussion	191
4.4.1.6 Conclusions	197
4.4.2 Dependence of SAR in Multilayer Fruits Model	197
4.4.2.1 Introduction	197
4.4.2.2 Dielectric Properties and Material Density of Mango Tissues	198
4.4.2.3 Bunch of Mango Fruits and SAR Simulation Setup	199
4.4.2.4 Contrast among Different Electromagnetic Standards	201
4.4.2.5 SAR Data and Analysis	202
4.4.2.6 Conclusions	211
<b>CHAPTER 5: PHANTOM LIQUID PREPARATION FOR DIFFERENT FRUIT AND PLANT SAMPLES TO PERFORM PRACTICAL SPECIFIC ABSORPTION RATE MEASUREMENT</b>	<b>221</b>
5.1 Introduction	221
5.2 Phantom Liquid Preparation for Fruit and Plant Specimens	222
5.3 Target Dielectric Properties of Fruit and Plant Specimens	223
5.4 Phantom Liquid Preparation for Fruit and Plant Specimens	225
5.4.1 Phantom Liquids Preparation for Coconut Specimens	225
5.4.1.1 Phantom Liquids for Coconut Green Skin	226
5.4.1.2 Phantom Liquids for Coconut Pulp	229
5.4.1.3 Phantom Liquids for Coconut Water	233
5.4.2 Phantom Liquids Preparation for Apple Specimen	237
5.4.3 Phantom Liquids Preparation for Guava Specimen	241

5.4.4 Phantom Liquids Preparation for Grape Specimen	245
5.4.5 Phantom Liquids Preparation for Tomato Specimen	249
5.4.6 Phantom Liquids Preparation for Brinjal Specimen	253
5.4.7 Phantom Liquids Preparation for Sapodilla Specimens	257
5.4.7.1 Phantom Liquids Preparation for Sapodilla Fruit Specimen	257
5.4.7.2 Phantom Liquids Preparation for Sapodilla Leaf Specimen	261
5.4.8 Phantom Liquids Preparation for <i>Catharanthus roseus</i> Specimens	265
5.4.8.1 Phantom Liquids Preparation for <i>Catharanthus roseus</i> Leaf Specimen	265
5.4.8.2 Phantom Liquids Preparation for <i>Catharanthus roseus</i> Flower Specimen	269
5.4.8.3 Phantom Liquids Preparation for <i>Catharanthus roseus</i> Stem Specimen	273
5.4.9 Phantom Liquids Preparation for Green Mango Specimens	277
5.4.9.1 Phantom Liquids Preparation for Green Mango Pulp Specimen	277
5.4.9.2 Phantom Liquids Preparation for Green Mango Seed Specimen	281
5.4.9.3 Phantom Liquids Preparation for Green Mango Leaf Specimen	285
5.4.10 Phantom Liquids Preparation for Water Apple Specimen	289
5.4.11 Phantom Liquids Preparation for Orange Specimens	293
5.4.11.1 Phantom Liquids Preparation for Orange Pulp Specimen	293
5.4.11.2 Phantom Liquids Preparation for Orange Peel Specimen	297
5.4.12 Phantom Liquids Preparation for Black Grape Specimen	301
5.5 Discussions	305
5.6 Conclusions	305

## **CHAPTER 6: ELECTROMAGNETIC PROPAGATION LOSS DUE TO PLANTS AND INITIAL RESPONSES UNDER LONG DURATION CELL PHONE IRRADIATION 308**

<b>Part I: Electromagnetic Propagation Loss due to Plants – A Preliminary Investigation</b>	<b>308</b>
6.1 Introduction	308
6.2 Research Statement	309
6.3 Materials and Equipment	309
6.4 Investigation Technique	311
6.5 Results and Analyses	312

## Contents

6.6 Discussions	314
6.7 Conclusions	314
<b>Part II: Initial Plant Responses under Long Duration Cell Phone Irradiation</b>	<b>315</b>
6.8 Introduction	315
6.9 Materials, Equipment and Experimental Method	317
6.9.1 Materials and Equipment	317
6.9.2 Experimental Method	317
6.10 Antenna Received Power Measurement	318
6.11 Radiation Effects on Seed Germination and Sapling Growth	321
6.11.1 Reduced Seed Germination	322
6.11.2 Increased Sapling Height and Leaf Length	325
6.11.3 Wrinkled Top Leaves	325
6.12 Discussions and Conclusions	326
<b>CHAPTER 7: PERIODIC AND CONTROLLED ELECTROMAGNETIC IRRADIATION EVOKED PHYSIOLOGICAL AND MOLECULAR RESPONSES IN PLANTS</b>	<b>331</b>
7.1 Introduction	331
7.2 Electromagnetic Reverberation Chamber	334
7.2.1 A Brief Theoretical Description	334
7.2.2 A Simple Custom-Made Reverberation Chamber	337
7.3 Periodic EM Irradiation Evoked Responses in <i>Satabdi</i> Rice Plant	340
7.3.1 Plant culture and growth conditions	340
7.3.2 Intermediate Protocols to Inspect Plant Responses	342
7.3.2.1 Seed Germination Rate Inspection	342
7.3.2.2 Photosynthetic Pigment Concentrations Estimation	342
7.3.2.3 Spectrophotometric Analysis of Photosynthetic Pigments	343
7.3.2.4 Periodic EM Irradiation Induced Gene Expressions	343
7.3.3 Physiological Responses in <i>Satabdi</i> Rice Plant	345
7.3.3.1 Effect on Seed Germination Rate	345
7.3.3.2 Effect on Photosynthetic Pigment Profile	346

7.3.4 Molecular Responses in <i>Satabdi</i> Rice Plant	346
7.3.5 Discussions	348
7.4 Periodic EM Irradiation Evoked Responses in <i>Swarnaprabha</i> Rice Plant	350
7.4.1 Plant culture and growth conditions	352
7.4.2 Intermediate Protocols to Inspect Plant Responses	352
7.4.3 Physiological Responses in <i>Swarnaprabha</i> Rice Plant	352
7.4.3.1 Effect on Seed Germination Rate	352
7.4.3.2 Effect on Photosynthetic Pigment Profile	352
7.4.4 Molecular Responses in <i>Swarnaprabha</i> Rice Plant	353
7.4.5 Discussions	355
7.5 Conclusions	356
<b>CHAPTER 8: ONE-TIME CONTROLLED ELECTROMAGNETIC IRRADIATION EVOKED MOLECULAR RESPONSES IN PLANTS</b>	<b>368</b>
8.1 Introduction	368
8.2 Electromagnetic Reverberation Chamber	370
8.3 One-Time Controlled Electromagnetic Irradiation Evoked Molecular Responses in <i>Satabdi</i> Rice Plant	371
8.3.1 Plant culture and growth conditions	372
8.3.2 Electromagnetic Irradiation on <i>Satabdi</i> Rice Plant	373
8.3.3 Plant RNA Extraction and cDNA Synthesis ( <i>Satabdi</i> )	373
8.3.4 Quantitative Real-Time PCR (qRT-PCR)	373
8.3.5 Statistical Analysis	374
8.3.6 Molecular Responses in <i>Satabdi</i> Rice Plant	376
8.3.7 Discussions	376
8.4 One-Time Controlled Electromagnetic Irradiation Evoked Molecular Responses in <i>Swarnaprava</i> Rice Plant	377
8.4.1 Plant culture and growth conditions	377
8.4.2 Electromagnetic Irradiation on <i>Swarnaprabha</i> Rice Plant	379
8.4.3 Plant RNA Extraction and cDNA Synthesis ( <i>Swarnaprabha</i> )	379

## Contents

8.4.4 Quantitative Real-Time PCR (qRT-PCR)	379
8.4.5 Statistical Analysis	379
8.4.6 Molecular Responses in <i>Swarnaprabha</i> Rice Plant	379
8.4.7 Discussions	380
8.5 Conclusions	381
<b>CHAPTER 9: CONCLUSIONS AND FUTURE SCOPE</b>	<b>386</b>
9.1 Introduction	386
9.2 A Qualitative Summary of Research Achievements	386
9.3 Future Scope for this Dissertation	387
<b>APPENDIX I</b>	<b>I</b>
<b>APPENDIX II</b>	<b>IV</b>

# List of Figures

---

Fig. 3.1: High frequency lumped equivalent circuit for open ended coaxial probe [14-23]	59
Fig. 3.2: Open ended coaxial probe for broadband dielectric properties measurement [41]	62
Fig. 3.3: Open ended coaxial probe setup for broadband dielectric properties ( $\epsilon_r$ ) measurements of (a) mango pulp tissue and (b) de-ionized water at 25 °C	63
Fig. 3.4: Open ended coaxial probe setup for broadband dielectric properties measurement of coconut tissue specimens (a) green skin, (b) yellowish pulp	65
Fig. 3.5: Broadband dielectric properties of coconut green skin, yellowish pulp and fresh coconut water specimens up to 8.5 GHz (a) permittivity and (b) loss tangent	66
Fig. 3.6: Open ended coaxial probe setup for broadband dielectric properties measurement of mango pulp specimen (a) total measurement setup, (b) close-up view	67
Fig. 3.7: Broadband dielectric properties of green mango pulp, seed and leaf specimens up to 8.5 GHz (a) permittivity and (b) loss tangent	68
Fig. 3.8: Open ended coaxial probe setup for broadband dielectric properties measurement of orange tissue specimens (a) orange pulp – measurement setup, (b) orange pulp – enlarged view, (c) orange peel – measurement setup and (d) orange peel – enlarged view	69
Fig. 3.9: Broadband dielectric properties of orange pulp and peel specimens up to 8.5 GHz (a) permittivity and (b) loss tangent	70
Fig. 3.10: Open ended coaxial probe setup for broadband dielectric properties measurement of water apple tissue specimen (a) total measurement setup, (b) a close-up view	71
Fig. 3.11: Broadband dielectric properties of water apple specimens up to 8.5 GHz (a) permittivity and (b) loss tangent	71
Fig. 3.12: Open ended coaxial probe setup for broadband dielectric properties measurement of sapodilla pulp specimen (a) total measurement setup, (b) close-up view	72
Fig. 3.13: Broadband dielectric properties of sapodilla pulp and leaf specimens up to 8.5 GHz (a) permittivity and (b) loss tangent	73
Fig. 3.14: Open ended coaxial probe setup for broadband dielectric properties measurement of ripe grape fruit specimen (a) total measurement setup, (b) close-up view	74
Fig. 3.15: Frequency dependent variation in broadband dielectric properties of ripe grape tissue specimen up to 8.5 GHz (a) permittivity and (b) loss tangent	74
Fig. 3.16: Open ended coaxial probe setup for broadband dielectric properties measurement of apple tissue specimen (a) total measurement setup, (b) a close-up view	76
Fig. 3.17: Temperature dependent variations in broadband dielectric properties of apple tissue specimens up to 8.5 GHz (a) permittivity and (b) loss tangent	77

## List of Figures

- Fig. 3.18: Open ended coaxial probe setup for broadband dielectric properties measurement of ripe tomato specimen (a) total measurement setup, (b) a close-up view 78
- Fig. 3.19: Temperature dependent variations in broadband dielectric properties of ripe tomato tissue specimens up to 8.5 GHz (a) permittivity and (b) loss tangent 79
- Fig. 3.20: Open ended coaxial probe setup for broadband dielectric properties measurement of mature brinjal specimen (a) total measurement setup, (b) a close-up view 80
- Fig. 3.21: Temperature dependent variations in broadband dielectric properties of mature brinjal tissue specimens up to 8.5 GHz (a) permittivity and (b) loss tangent 81
- Fig. 3.22: Open ended coaxial probe setup for broadband dielectric properties measurement of mature guava specimen (a) total measurement setup, (b) a close-up view 82
- Fig. 3.23: Temperature dependent variations in broadband dielectric properties of mature guava tissue specimens up to 8.5 GHz (a) permittivity and (b) loss tangent 83
- Fig. 3.24: Electromagnetic wave incidence on multilayer tissue model and an equivalent homogeneous phantom formulation (a) a linearly polarized plane wave impinges on the first layer and propagates through all the subsequent layers of n-layer tissue model, (b) an equivalent homogeneous problem with single phantom dielectric layer of thickness  $z_t$  88
- Fig. 3.25: A plane wave with linear polarization at 2.45 GHz impinges on the four equal tissue layers model ( $L_1$  to  $L_4$  respectively) – each tissue layer possesses different dielectric properties but equal thickness (1 cm) 94
- Fig. 3.26: Four equal tissue layers model – plane wave exposure in far field scenario (a)  $Max(f_{i(jk)})$  plot for varied permittivity and loss tangent of equivalent model, (b) comparison of electric field distributions between four equal layers model and equivalent dielectric properties (50, 0.20) that lead to smallest  $Max(f_{i(jk)})$ , (c) difference in peak  $E$  field distribution for equivalent dielectric properties (50, 0.20), (d)  $Max(f'_{i(jk)})$  plot for varied permittivity and loss tangent of equivalent model, (e) comparison of electric field distributions between four equal layers model and equivalent dielectric properties (40, 0.35) that result in smallest  $Max(f'_{i(jk)})$ , (f) difference in peak  $E$  field distribution for equivalent dielectric properties (40, 0.35) 96
- Fig. 3.27: Four equal tissue layers model – plane wave exposure in far field scenario (a)  $Max(g_{i(jk)})$  plot for varied permittivity and loss tangent of equivalent model, (b) comparison of point SAR distributions between four equal layer model and equivalent dielectric properties (25, 0.30) that lead to smallest  $Max(g_{i(jk)})$ , (c) difference in point SAR distribution for equivalent dielectric properties (25, 0.30), (d)  $Max(g'_{i(jk)})$  plot for varied permittivity and loss tangent of equivalent model, (e) comparison of point SAR distributions between four equal layer model and equivalent dielectric properties (40, 0.35) that result in smallest  $Max(g'_{i(jk)})$ , (f) difference in point SAR distribution for equivalent dielectric properties (40, 0.35) 98
- Fig. 3.28: Four unequal tissue layers model – plane wave exposure in far field scenario (a)  $Max(f_{i(jk)})$  plot for varied permittivity and loss tangent of equivalent model, (b) comparison of electric field distributions between four unequal layers model and equivalent dielectric properties (55, 0.20) that lead to smallest  $Max(f_{i(jk)})$ , (c) difference in peak  $E$  field distribution for equivalent dielectric properties (55, 0.20), (d)  $Max(f'_{i(jk)})$  plot for varied permittivity



and loss tangent of equivalent model, (e) comparison of electric field distributions between four unequal layers model and equivalent dielectric properties (60, 0.20) that result in smallest  $Max(f'_{i(jk)})$ , (f) difference in peak  $E$  field distribution for equivalent dielectric properties (60, 0.20) 101

Fig. 3.29: Four unequal tissue layers model – plane wave exposure in far field scenario (a)  $Max(g_{i(jk)})$  plot for varied permittivity and loss tangent of equivalent model, (b) comparison of point SAR distributions between four unequal layer model and equivalent dielectric properties (60, 0.30) that lead to smallest  $Max(g_{i(jk)})$ , (c) difference in point SAR distribution for equivalent dielectric properties (60, 0.30), (d)  $Max(g'_{i(jk)})$  plot for varied permittivity and loss tangent of equivalent model, (e) comparison of point SAR distributions between four unequal layer model and equivalent dielectric properties (60, 0.25) that result in smallest  $Max(g'_{i(jk)})$ , (f) difference in point SAR distribution for equivalent dielectric properties (60, 0.25) 103

Fig. 3.30: A rectangular microstrip antenna radiates at 2.45 GHz in proximity to the four equal tissue layers model ( $L_1$  to  $L_4$  respectively) – each tissue layer possesses different dielectric properties but equal thickness (1 cm) 105

Fig. 3.31: Four equal tissue layers model – close to the radiating antenna in near field scenario (a)  $Max(f_{i(jk)})$  plot for varied permittivity and loss tangent of equivalent model, (b) comparison of electric field distributions between four equal layers model and equivalent dielectric properties (30, 0.35) that lead to smallest  $Max(f_{i(jk)})$ , (c) difference in peak  $E$  field distribution for equivalent dielectric properties (30, 0.35), (d)  $Max(f'_{i(jk)})$  plot for varied permittivity and loss tangent of equivalent model, (e) comparison of electric field distributions between four equal layers model and equivalent dielectric properties (55, 0.25) that result in smallest  $Max(f'_{i(jk)})$ , (f) difference in peak  $E$  field distribution for equivalent dielectric properties (55, 0.25) 106

Fig. 3.32: Four equal tissue layers model – close to the radiating antenna in near field scenario (a)  $Max(g_{i(jk)})$  plot for varied permittivity and loss tangent of equivalent model, (b) comparison of point SAR distributions between four equal layers model and equivalent dielectric properties (30, 0.30) that lead to smallest  $Max(g_{i(jk)})$ , (c) difference in point SAR distribution for equivalent dielectric properties (30, 0.30), (d)  $Max(g'_{i(jk)})$  plot for varied permittivity and loss tangent of equivalent model, (e) comparison of point SAR distributions between four equal layers model and equivalent dielectric properties (50, 0.35) that result in smallest  $Max(g'_{i(jk)})$ , (f) difference in point SAR distribution for equivalent dielectric properties (50, 0.35) 108

Fig. 3.33: Four unequal tissue layers model – close to the radiating antenna in near field scenario (a)  $Max(f_{i(jk)})$  plot for varied permittivity and loss tangent of equivalent model, (b) comparison of electric field distributions between four unequal layers model and equivalent dielectric properties (45, 0.20) that lead to smallest  $Max(f_{i(jk)})$ , (c) difference in peak  $E$  field distribution for equivalent dielectric properties (45, 0.20), (d)  $Max(f'_{i(jk)})$  plot for varied permittivity and loss tangent of equivalent model, (e) comparison of electric field distributions between four unequal layers model and equivalent dielectric properties (55, 0.35) that result in smallest  $Max(f'_{i(jk)})$ , (f) difference in peak  $E$  field distribution for equivalent dielectric properties (55, 0.35) 111

Fig. 3.34: Four unequal tissue layers model – close to the radiating antenna in near field scenario (a)  $Max(g_{i(jk)})$  plot for varied permittivity and loss tangent of equivalent model, (b) comparison of point SAR distributions between

## List of Figures

four unequal layers model and equivalent dielectric properties (45, 0.35) that lead to smallest $Max(g_{i(jk)})$ , (c) difference in point SAR distribution for equivalent dielectric properties (45, 0.35), (d) $Max(g'_{i(jk)})$ plot for varied permittivity and loss tangent of equivalent model, (e) comparison of point SAR distributions between four unequal layers model and equivalent dielectric properties (60, 0.35) that result in smallest $Max(g'_{i(jk)})$ , (f) difference in point SAR distribution for equivalent dielectric properties (60, 0.35)	113
Fig. 4.1: Electromagnetic exposure zones around a base station antenna	127
Fig. 4.2: Dielectric properties measurement for coconut layers (a) green skin, (b) yellowish pulp	129
Fig. 4.3: Twig connected multilayer coconut structure modeled in CST MWS 2010 [49]	131
Fig. 4.4: Comparative SAR analysis for the twig connected coconut structure at 947.5 MHz, 1842.5 MHz and 2450 MHz as per the existing electromagnetic standards in India [11]	134
Fig. 4.5: (a) A linearly polarized plane wave at 2450 MHz (with peak electric field 27.46 V/m) impinges on the twig connected multilayer coconut structure, (b) 1g averaged SAR distribution on three dimensional surface of the twig connected multilayer coconut structure at 2450 MHz in Indian scenario	136
Fig. 4.6: (a) Top view of the twig connected multilayer coconut structure illustrating 1g averaged SAR distribution at 2450 MHz as per the existing Indian electromagnetic exposure scenario, (b) Side view of the twig connected multilayer coconut structure illustrating 1g averaged SAR distribution at 2450 MHz as per the existing Indian electromagnetic exposure scenario	136
Fig. 4.7: Dielectric properties ( $\epsilon_r$ ) measurement setup for an apple specimen	139
Fig. 4.8: Simplified models of (a) apple, (b) guava and (c) grape fruits	140
Fig. 4.9: MLP and 1g averaged SAR data analyses for apple model as per public electromagnetic exposure guidelines in India	143
Fig. 4.10: MLP and 1g averaged SAR data analyses for guava model as per public electromagnetic exposure guidelines in India	143
Fig. 4.11: MLP and 1g averaged SAR data analyses for grape model as per public electromagnetic exposure guidelines in India	145
Fig. 4.12: Broadband dielectric measurement setup for grape samples at 25 °C using open ended coaxial probe technique	149
Fig. 4.13: Measured dielectric parameters for two typical grape samples at 25 °C using open ended coaxial probe technique (a) permittivity vs. frequency, (b) loss tangent vs. frequency	149
Fig. 4.14: (a) A typical bunch of grapes modeled in CST MWS 2010, (b) The bunch of grapes is exposed to GSM 1842.5 MHz linearly polarized plane wave radiation	151
Fig. 4.15: (a) Three dimensional 1g averaged SAR distribution at 1842.5 MHz, (b) Two dimensional 1g averaged SAR distribution on $x$ - $z$ plane of the prototyped bunch of grapes model at 1842.5 MHz and (c) Two dimensional 1g averaged SAR distribution on $y$ - $z$ plane of the prototyped bunch of grapes model at 1842.5 MHz	154
Fig. 4.16: Broadband permittivity and loss tangent measurement setup using Agilent 85070E dielectric measurement kit and E5071B ENA series Vector Network Analyzer (VNA) (a) sapodilla fruit, (b) enlarged view of open ended coaxial probe on flat cut surface of sapodilla fruit and (c) sapodilla leaves	160

Fig. 4.17: Three dimensional CAD model of the bunch of sapodilla fruits with linearly polarized plane wave at 1842.50 MHz in accordance with FCC public exposure scenario	161
Fig. 4.18: (a) Simulated point SAR profile on surface of sapodilla bunch at 1842.50 MHz in accordance with FCC public exposure scenario and (b) Simulated 1g averaged SAR profile on surface of sapodilla bunch at 1842.50 MHz in accordance with FCC public exposure scenario	163
Fig. 4.19: Disparity among SAR data for the bunch of sapodilla model due to variation among different electromagnetic regulatory guidelines (a) 947.5 MHz, (b) 1842.5 MHz, (c) 2150 MHz, (d) 2350 MHz, (e) 2450 MHz and (f) cumulative SAR data over all five frequencies	167
Fig. 4.20: (a) Entire dielectric properties measurement setup for <i>Catharanthus roseus</i> leaf samples, (b) An enlarged view of the coaxial probe with leaf samples	174
Fig. 4.21: Simplified three dimensional model of <i>Catharanthus roseus</i> plant designed in CST MWS 2014 [49]	176
Fig. 4.22: (a) A linearly polarized plane wave passes through <i>Catharanthus roseus</i> plant model at 2150 MHz with field strength set as per FCC guidelines for public zone, (b) Evaluated 1g averaged SAR profile on surface of <i>Catharanthus roseus</i> model at 2150 MHz	178
Fig. 4.23: Contrast in 1g averaged SAR data for <i>Catharanthus roseus</i> plant model due to variation among different global and national public electromagnetic standards	184
Fig. 4.24: Contrast in cumulative SAR data for <i>Catharanthus roseus</i> plant model due to variation among electromagnetic standards prescribed by different global and national organizations	184
Fig. 4.25: (a) Open ended coaxial probe setup for broadband dielectric properties characterization of water apples, (b) Measured permittivity data for different water apple samples and (c) Measured loss tangent data for different water apple samples	189
Fig. 4.26: (a) A linearly polarized plane wave incidence on the bunch of water apples [Direction of Propagation (DoP): $z = -1$ , $E$ field: $x$ axis], (b) MLP SAR distribution at 1842.50 MHz [Direction of Propagation (DoP): $z = -1$ , $E$ field: $x$ axis], (c) 1g SAR distribution at 1842.50 MHz [Direction of Propagation (DoP): $z = -1$ , $E$ field: $x$ axis] and (d) 10g SAR distribution at 1842.50 MHz [Direction of Propagation (DoP): $z = -1$ , $E$ field: $x$ axis]	190
Fig 4.27: (a) to (e) Variations in magnitude and position of MLP SAR for six different combinations of direction of propagation and wave polarization at 947.50 MHz, 1842.50 MHz, 2150 MHz, 2350 MHz and 2450 MHz	195
Fig 4.28: (a) to (e) Variation in magnitude and position of 1g averaged SAR for six different combinations of direction of propagation and wave polarization at 947.50 MHz, 1842.50 MHz, 2150 MHz, 2350 MHz and 2450 MHz	195
Fig 4.29: (a) to (e) Variation in magnitude and position of 10g averaged SAR for six different combinations of direction of propagation and wave polarization at 947.50 MHz, 1842.50 MHz, 2150 MHz, 2350 MHz and 2450 MHz	196
Fig. 4.30: Variation in magnitude of WBA SAR at 947.50 MHz, 1842.50 MHz, 2150 MHz, 2350 MHz and 2450 MHz	196

## List of Figures

- Fig. 4.31: (a) Dielectric properties measurement setup for mango pulp, (b) Close-up view of dielectric properties measurement setup for mango pulp, (c) Measured permittivity for different mango tissues over broad frequency range and (d) Measured loss tangent for different mango tissues over broad frequency range 199
- Fig. 4.32: (a) Three dimensional perspective of the designed bunch of mango fruits model with marked coordinates, (b) The bunch of mango fruits model is exposed to a linearly polarized plane wave propagating along  $x$ -axis and electric field along  $z$ -axis, (c) 1 g SAR distribution on three dimensional surfaces of the bunch of mango fruits model at 2.45 GHz as per the existing Indian public scenario, (d) 1 g SAR distribution on a two dimensional cut plane of the bunch of mango fruits model at 2.45 GHz as per the existing Indian public scenario 202
- Fig. 4.33: SAR data as per the FCC public electromagnetic standards (a) to (c) MLP SAR, 1 g averaged and 10 g averaged SAR distribution at 947.5 MHz due to variations in direction of arrival and polarization; (d) to (f) MLP SAR, 1 g averaged and 10 g averaged SAR distribution at 1842.5 MHz due to variations in direction of arrival and polarization; (g) to (i) MLP SAR, 1 g averaged and 10 g averaged SAR distribution at 2150 MHz due to variations in direction of arrival and polarization; (j) to (l) MLP SAR, 1 g averaged and 10 g averaged SAR distribution at 2350 MHz due to variations in direction of arrival and polarization; (m) to (o) MLP SAR, 1 g averaged and 10 g averaged SAR distribution at 2450 MHz due to variations in direction of arrival and polarization; (p) WBA SAR data over all five frequencies due to variations in direction of arrival and polarization 208
- Fig. 4.34: SAR data as per the existing Indian public electromagnetic standards (a) to (c) MLP SAR, 1 g averaged and 10 g averaged SAR distribution at 947.5 MHz due to variations in direction of arrival and polarization; (d) to (f) MLP SAR, 1 g averaged and 10 g averaged SAR distribution at 1842.5 MHz due to variations in direction of arrival and polarization; (g) to (i) MLP SAR, 1 g averaged and 10 g averaged SAR distribution at 2150 MHz due to variations in direction of arrival and polarization; (j) to (l) MLP SAR, 1 g averaged and 10 g averaged SAR distribution at 2350 MHz due to variations in direction of arrival and polarization; (m) to (o) MLP SAR, 1 g averaged and 10 g averaged SAR distribution at 2450 MHz due to variations in direction of arrival and polarization; (p) WBA SAR data over all five frequencies due to variations in direction of arrival and polarization 210
- Fig. 5.1: Open-ended coaxial probe and dielectric properties ( $\epsilon_r$ ) measurement setup (a) 85070E high temperature open-ended coaxial dielectric measurement probe, (b) broadband dielectric properties ( $\epsilon_r$ ) measurement setup for characterizing phantom liquids 223
- Fig. 5.2: Coconut green skin tissue equivalent phantom liquid at 947.50 MHz (a) permittivity and (b) loss tangent 225
- Fig. 5.3: Coconut green skin tissue equivalent phantom liquid at 1842.50 MHz (a) permittivity and (b) loss tangent 226
- Fig. 5.4: Coconut green skin tissue equivalent phantom liquid at 2450.00 MHz (a) permittivity and (b) loss tangent 227
- Fig. 5.5: Coconut pulp tissue equivalent phantom liquid at 947.50 MHz (a) permittivity and (b) loss tangent 229
- Fig. 5.6: Coconut pulp tissue equivalent phantom liquid at 1842.50 MHz (a) permittivity and (b) loss tangent 230
- Fig. 5.7: Coconut pulp tissue equivalent phantom liquid at 2450.00 MHz (a) permittivity and (b) loss tangent 231
- Fig. 5.8: Coconut water equivalent phantom liquid at 947.50 MHz (a) permittivity and (b) loss tangent 233

Fig. 5.9: Coconut water equivalent phantom liquid at 1842.50 MHz (a) permittivity and (b) loss tangent	234
Fig. 5.10: Coconut water equivalent phantom liquid at 2450.00 MHz (a) permittivity and (b) loss tangent	235
Fig. 5.11: Apple tissue equivalent phantom liquid at 947.50 MHz (a) permittivity and (b) loss tangent	237
Fig. 5.12: Apple tissue equivalent phantom liquid at 1842.50 MHz (a) permittivity and (b) loss tangent	238
Fig. 5.13: Apple tissue equivalent phantom liquid at 2450.00 MHz (a) permittivity and (b) loss tangent	239
Fig. 5.14: Guava tissue equivalent phantom liquid at 947.50 MHz (a) permittivity and (b) loss tangent	241
Fig. 5.15: Guava tissue equivalent phantom liquid at 1842.50 MHz (a) permittivity and (b) loss tangent	242
Fig. 5.16: Guava tissue equivalent phantom liquid at 2450.00 MHz (a) permittivity and (b) loss tangent	243
Fig. 5.17: Grape tissue equivalent phantom liquid at 947.50 MHz (a) permittivity and (b) loss tangent	245
Fig. 5.18: Grape tissue equivalent phantom liquid at 1842.50 MHz (a) permittivity and (b) loss tangent	246
Fig. 5.19: Grape tissue equivalent phantom liquid at 2450.00 MHz (a) permittivity and (b) loss tangent	247
Fig. 5.20: Tomato tissue equivalent phantom liquid at 947.50 MHz (a) permittivity and (b) loss tangent	249
Fig. 5.21: Tomato tissue equivalent phantom liquid at 1842.50 MHz (a) permittivity and (b) loss tangent	250
Fig. 5.22: Tomato tissue equivalent phantom liquid at 2450.00 MHz (a) permittivity and (b) loss tangent	251
Fig. 5.23: Brinjal tissue equivalent phantom liquid at 947.50 MHz (a) permittivity and (b) loss tangent	253
Fig. 5.24: Brinjal tissue equivalent phantom liquid at 1842.50 MHz (a) permittivity and (b) loss tangent	254
Fig. 5.25: Brinjal tissue equivalent phantom liquid at 2450.00 MHz (a) permittivity and (b) loss tangent	255
Fig. 5.26: Sapodilla fruit tissue equivalent phantom liquid at 947.50 MHz (a) permittivity and (b) loss tangent	257
Fig. 5.27: Sapodilla fruit tissue equivalent phantom liquid at 1842.50 MHz (a) permittivity and (b) loss tangent	258
Fig. 5.28: Sapodilla fruit tissue equivalent phantom liquid at 2450.00 MHz (a) permittivity and (b) loss tangent	259
Fig. 5.29: Sapodilla leaf tissue equivalent phantom liquid at 947.50 MHz (a) permittivity and (b) loss tangent	261
Fig. 5.30: Sapodilla leaf tissue equivalent phantom liquid at 1842.50 MHz (a) permittivity and (b) loss tangent	262
Fig. 5.31: Sapodilla leaf tissue equivalent phantom liquid at 2450.00 MHz (a) permittivity and (b) loss tangent	263
Fig. 5.32: <i>Catharanthus roseus</i> leaf tissue equivalent phantom liquid at 947.50 MHz (a) permittivity and (b) loss tangent	265
Fig. 5.33: <i>Catharanthus roseus</i> leaf tissue equivalent phantom liquid at 1842.50 MHz (a) permittivity and (b) loss tangent	266
Fig. 5.34: <i>Catharanthus roseus</i> leaf tissue equivalent phantom liquid at 2450.00 MHz (a) permittivity and (b) loss tangent	267
Fig. 5.35: <i>Catharanthus roseus</i> flower tissue equivalent phantom liquid at 947.50 MHz (a) permittivity and (b) loss tangent	269
Fig. 5.36: <i>Catharanthus roseus</i> flower tissue equivalent phantom liquid at 1842.50 MHz (a) permittivity and (b) loss tangent	270
Fig. 5.37: <i>Catharanthus roseus</i> flower tissue equivalent phantom liquid at 2450.00 MHz (a) permittivity and (b) loss tangent	271
Fig. 5.38: <i>Catharanthus roseus</i> stem tissue equivalent phantom liquid at 947.50 MHz (a) permittivity and (b) loss tangent	273

## List of Figures

Fig. 5.39: <i>Catharanthus roseus</i> stem tissue equivalent phantom liquid at 1842.50 MHz (a) permittivity and (b) loss tangent	274
Fig. 5.40: <i>Catharanthus roseus</i> stem tissue equivalent phantom liquid at 2450.00 MHz (a) permittivity and (b) loss tangent	275
Fig. 5.41: Green mango pulp tissue equivalent phantom liquid at 947.50 MHz (a) permittivity and (b) loss tangent	277
Fig. 5.42: Green mango pulp tissue equivalent phantom liquid at 1842.50 MHz (a) permittivity and (b) loss tangent	278
Fig. 5.43: Green mango pulp tissue equivalent phantom liquid at 2450.00 MHz (a) permittivity and (b) loss tangent	279
Fig. 5.44: Green mango seed tissue equivalent phantom liquid at 947.50 MHz (a) permittivity and (b) loss tangent	281
Fig. 5.45: Green mango seed tissue equivalent phantom liquid at 1842.50 MHz (a) permittivity and (b) loss tangent	282
Fig. 5.46: Green mango seed tissue equivalent phantom liquid at 2450.00 MHz (a) permittivity and (b) loss tangent	283
Fig. 5.47: Green mango leaf tissue equivalent phantom liquid at 947.50 MHz (a) permittivity and (b) loss tangent	285
Fig. 5.48: Green mango leaf tissue equivalent phantom liquid at 1842.50 MHz (a) permittivity and (b) loss tangent	286
Fig. 5.49: Green mango leaf tissue equivalent phantom liquid at 2450.00 MHz (a) permittivity and (b) loss tangent	287
Fig. 5.50: Water apple tissue equivalent phantom liquid at 947.50 MHz (a) permittivity and (b) loss tangent	289
Fig. 5.51: Water apple tissue equivalent phantom liquid at 1842.50 MHz (a) permittivity and (b) loss tangent	290
Fig. 5.52: Water apple tissue equivalent phantom liquid at 2450.00 MHz (a) permittivity and (b) loss tangent	291
Fig. 5.53: Orange pulp tissue equivalent phantom liquid at 947.50 MHz (a) permittivity and (b) loss tangent	293
Fig. 5.54: Orange pulp tissue equivalent phantom liquid at 1842.50 MHz (a) permittivity and (b) loss tangent	294
Fig. 5.55: Orange pulp tissue equivalent phantom liquid at 2450.00 MHz (a) permittivity and (b) loss tangent	295
Fig. 5.56: Orange peel tissue equivalent phantom liquid at 947.50 MHz (a) permittivity and (b) loss tangent	297
Fig. 5.57: Orange peel tissue equivalent phantom liquid at 1842.50 MHz (a) permittivity and (b) loss tangent	298
Fig. 5.58: Orange peel tissue equivalent phantom liquid at 2450.00 MHz (a) permittivity and (b) loss tangent	299
Fig. 5.59: Black grape tissue equivalent phantom liquid at 947.50 MHz (a) permittivity and (b) loss tangent	301
Fig. 5.60: Black grape tissue equivalent phantom liquid at 1842.50 MHz (a) permittivity and (b) loss tangent	302
Fig. 5.61: Black grape tissue equivalent phantom liquid at 2450.00 MHz (a) permittivity and (b) loss tangent	303
Fig. 6.1: A typical Chinese <i>Tabernaemontana divaricata</i> plant ( $L_1, L_2, S$ and $T$ represent height of foliage, width of foliage, height of stem and height of earthen pot respectively)	310
Fig. 6.2: Reflection coefficients ( $S_{11}$ ) for transmitting and receiving half-wave dipole antennas	310

- Fig. 6.3: (a) Experimental setup inside semi-anechoic chamber for measuring propagation loss due to presence of the plants, (b) Microwave signal generator with the transmitting half-wave dipole antenna at 1.75 GHz and (c) HSA connected with the receiving half-wave dipole antenna 311
- Fig. 6.4: Decline in half-wave dipole antenna received power due to propagation loss / attenuation in Chinese *Tabernaemontana divaricata* plants present in between the transmitting and receiving antennas (a) at 1.73 GHz, (b) at 1.75 GHz and (c) at 1.77 GHz 313
- Fig. 6.5: (a) Fifty *Capsicum annuum* seeds have been spread in the 1<sup>st</sup> earthen pot (kept in natural environment) and (b) Fifty *Capsicum annuum* seeds have been spread in the 2<sup>nd</sup> earthen pot (exposed to GSM cell phone radiation) 316
- Fig. 6.6: (a) Half-wave dipole antenna at 1750 MHz with SMA to coaxial N-type adapter and (b) Measured reflection coefficient ( $S_{11}$ ) characteristics of the fabricated half-wave dipole antenna 319
- Fig. 6.7: (a) Handheld power meter along with fabricated half-wave dipole antenna at 1750 MHz and (b) Half-wave dipole antenna received power measurement in close vicinity of the 2<sup>nd</sup> earthen pot placed next to GSM cell phone 319
- Fig. 6.8: Observation on 15<sup>th</sup> day (a) thirty six saplings in the 1<sup>st</sup> earthen pot kept in natural environment and (b) twenty two saplings in the 2<sup>nd</sup> earthen pot next to GSM mobile phone 323
- Fig. 6.9: Observation on 22<sup>nd</sup> day (a) forty five saplings in the 1<sup>st</sup> earthen pot kept in natural environment and (b) twenty seven saplings in the 2<sup>nd</sup> earthen pot next to GSM mobile phone 324
- Fig. 6.10: Observation on 50<sup>th</sup> day (a) thirty eight saplings in the 1<sup>st</sup> earthen pot kept in natural environment and (b) twenty five saplings in the 2<sup>nd</sup> earthen pot next to GSM mobile phone 324
- Fig. 6.11: Observation on 50<sup>th</sup> day (a) healthy glowing leaves in the 1<sup>st</sup> earthen pot kept in natural environment and (b) wrinkled leaves in the 2<sup>nd</sup> earthen pot next to GSM mobile phone 326
- Fig. 7.1: Simple electromagnetic reverberation chamber and transmitting system (a) schematic representation of the simple reverberation chamber, (b) transmitting system inside the simple reverberation chamber 339
- Fig. 7.2: Graphical schemes of seed germination, photosynthetic pigment profiling and gene expression profiling experiments in *Satabdi* rice under periodic electromagnetic irradiation (a) seed germination experiment, (b) gene expression profiling experiment in 12 days old *Satabdi* rice seedlings and (c) photosynthetic pigment profiling and gene expression profiling experiment in 32 days old *Satabdi* rice plants 341
- Fig. 7.3: Effect of periodic electromagnetic irradiation on seed germination rate and photosynthetic pigment concentrations (data represent mean value  $\pm$  SEM from at least three independent experiments) (a) significant reduction in *Satabdi* seed germination rate due to 1837.50 MHz periodic electromagnetic irradiation, (b) marginal reduction in photosynthetic pigment concentration levels among 32 days old *Satabdi* rice plants due to periodic electromagnetic exposure at 1837.50 MHz 346
- Fig. 7.4: Effect of periodic electromagnetic irradiation on relative gene expression levels (data represent mean value  $\pm$  SEM from three independent experiments) (a) comparison of relative gene expression levels among 12 days old *Satabdi* rice variant due to periodic electromagnetic exposure at 1837.50 MHz, (b) comparison of relative gene expression levels among 32 days old *Satabdi* rice variant due to periodic electromagnetic exposure at 1837.50 MHz

- 347
- Fig. 7.5: Graphical schemes of seed germination, photosynthetic pigment profiling and gene expression profiling experiments in *Swarnaprabha* rice under periodic electromagnetic irradiation (a) seed germination experiment, (b) gene expression profiling experiment in 12 days old *Swarnaprabha* rice seedlings and (c) photosynthetic pigment profiling and gene expression profiling experiment in 32 days old *Swarnaprabha* rice plants 351
- Fig. 7.6: Effect of periodic electromagnetic irradiation on seed germination rate and photosynthetic pigment concentrations (data represent mean value  $\pm$  SEM from at least three independent experiments) (a) no such alteration in *Swarnaprabha* seed germination rate due to 1837.50 MHz periodic electromagnetic irradiation, (b) significant reduction in photosynthetic pigment concentration levels among 32 days old *Swarnaprabha* rice plants due to periodic electromagnetic exposure at 1837.50 MHz 353
- Fig. 7.7: Effect of periodic electromagnetic irradiation on relative gene expression levels (data represent mean value  $\pm$  SEM from three independent experiments) (a) comparison of relative gene expression levels among 12 days old *Swarnaprabha* rice variant due to periodic electromagnetic exposure at 1837.50 MHz, (b) comparison of relative gene expression levels among 32 days old *Swarnaprabha* rice variant due to periodic electromagnetic exposure at 1837.50 MHz 354
- Fig. 8.1: Fabricated transmitting antenna and its reflection coefficient ( $S_{11}$ ) measurement (a) microstrip patch antenna designed at 1837.50 MHz, (b) reflection coefficient ( $S_{11}$ ) measurement 371
- Fig. 8.2: Graphical scheme of gene expression profiling experiment in 12 days old *Satabdi* rice seedlings following one-time electromagnetic irradiation 372
- Fig. 8.3: Comparison of relative gene expression levels in 12 days old *Satabdi* rice seedlings following one-time electromagnetic irradiation at 1837.50 MHz, 2.75 mW/m<sup>2</sup> for 2 h 30 min (data represent mean value  $\pm$  SEM from three independent experiments) 375
- Fig. 8.4: Graphical scheme of gene expression profiling experiment in 40 days old *Swarnaprabha* rice plants following one-time electromagnetic irradiation 378
- Fig. 8.5: Comparison of relative gene expression levels in 40 days old *Swarnaprabha* rice plants following one-time electromagnetic irradiation at 1837.50 MHz, 2.75 mW/m<sup>2</sup> for 2 h 30 min (data represent mean value  $\pm$  SEM from three independent experiments) 380



# List of Tables

---

Table 2.1: Lack of harmonization among different international and national electromagnetic exposure regulatory standards [37-42, 76]	20
Table 3.1: Thickness and dielectric properties ( $\epsilon_r$ ) of four equal tissue layers model	93
Table 3.2: Thickness and dielectric properties ( $\epsilon_r$ ) of four unequal tissue layers model	100
Table 4.1: Existing revised Indian public electromagnetic exposure guidelines [11]	127
Table 4.2: Measured material densities ( $\rho$ ) of different coconut layers	129
Table 4.3: Measured dielectric properties ( $\epsilon_r$ ) of different coconut layers	129
Table 4.4: Modeling specifications of the twig connected multilayer coconut model	131
Table 4.5: SAR results for twig connected coconut with electric field set as per revised Indian electromagnetic exposure standards [11]	134
Table 4.6: Measured material densities ( $\rho$ ) of apple, guava and grape	139
Table 4.7: Measured dielectric properties ( $\epsilon_r$ ) of apple, guava and grape	139
Table 4.8: Modeling specifications of apple, guava and grape	140
Table 4.9: Revised Indian electromagnetic exposure guidelines for public scenario [11]	141
Table 4.10: SAR data for apple model as per public electromagnetic exposure guidelines in India	142
Table 4.11: SAR data for guava model as per public electromagnetic exposure guidelines in India	144
Table 4.12: SAR data for grape model as per public electromagnetic exposure guidelines in India	144
Table 4.13: Measured dielectric properties of grape samples	149
Table 4.14: Modeling specifications for the bunch of grapes model	150
Table 4.15: Revised Indian electromagnetic regulatory guidelines for public exposure zone	152
Table 4.16: SAR data for a typical bunch of grapes model as per the existing Indian electromagnetic regulatory guidelines	152
Table 4.17: Disparity among different global and national electromagnetic exposure regulatory guidelines [9-12]	158
Table 4.18: Measured material density ( $\rho$ ) of sapodilla fruit, leaf and twig samples	158
Table 4.19: Measured permittivity and loss tangent of sapodilla fruit, leaf and twig samples	160
Table 4.20: Modeling specifications of the bunch of sapodilla fruits model	162
Table 4.21: Disparity among SAR data for bunch of sapodilla model at 947.5 MHz as per different global and national electromagnetic standards	164
Table 4.22: Disparity among SAR data for bunch of sapodilla model at 1842.5 MHz as per different global and national electromagnetic standards	164
Table 4.23: Disparity among SAR data for bunch of sapodilla model at 2150 MHz as per different global and national electromagnetic standards	165

## List of Tables

Table 4.24: Disparity among SAR data for bunch of sapodilla model at 2350 MHz as per different global and national electromagnetic standards	165
Table 4.25: Disparity among SAR data for bunch of sapodilla model at 2450 MHz as per different global and national electromagnetic standards	166
Table 4.26: Measured density ( $\rho$ ) of <i>Catharanthus roseus</i> leaf, flower and stem samples	173
Table 4.27: Measured dielectric properties of <i>Catharanthus roseus</i> leaf, flower and stem	174
Table 4.28: Modeling specifications of <i>Catharanthus roseus</i> leaf, flower and stem	175
Table 4.29: Comparative SAR data for <i>Catharanthus roseus</i> plant model at 947.5 MHz as per different global and national electromagnetic regulatory guidelines	181
Table 4.30: Comparative SAR data for <i>Catharanthus roseus</i> plant model at 1842.5 MHz as per different global and national electromagnetic regulatory guidelines	181
Table 4.31: Comparative SAR data for <i>Catharanthus roseus</i> plant model at 2150 MHz as per different global and national electromagnetic regulatory guidelines	182
Table 4.32: Comparative SAR data for <i>Catharanthus roseus</i> plant model at 2350 MHz as per different global and national electromagnetic regulatory guidelines	182
Table 4.33: Comparative SAR data for <i>Catharanthus roseus</i> plant model at 2450 MHz as per different global and national electromagnetic regulatory guidelines	183
Table 4.34: Reference power density and equivalent electric field strength in India [11]	187
Table 4.35: Measured parameters of water apple tissue	189
Table 4.36: SAR data for different directions of propagation and wave polarizations at 947.50 MHz	192
Table 4.37: SAR data for different directions of propagation and wave polarizations at 1842.50 MHz	192
Table 4.38: SAR data for different directions of propagation and wave polarizations at 2150 MHz	193
Table 4.39: SAR data for different directions of propagation and wave polarizations at 2350 MHz	193
Table 4.40: SAR data for different directions of propagation and wave polarizations at 2450 MHz	194
Table 4.41: Measured parameters of different mango tissues	200
Table 4.42: Comparative SAR data at 947.5 MHz for different directions of arrival and polarizations of incident wave	203
Table 4.43: Comparative SAR data at 1842.5 MHz for different directions of arrival and polarizations of incident wave	203
Table 4.44: Comparative SAR data at 2150 MHz for different directions of arrival and polarizations of incident wave	204
Table 4.45: Comparative SAR data at 2350 MHz for different directions of arrival and polarizations of incident wave	204
Table 4.46: Comparative SAR data at 2450 MHz for different directions of arrival and polarizations of incident wave	205
Table 4.47: Typical Max-to-Min SAR ratio for different combinations of direction of arrival and polarization of incident wave	211

Table 5.1: Measured dielectric properties ( $\epsilon_r$ ) of the targeted fruit and plant specimens	224
Table 5.2: Final compositions of coconut green skin tissue equivalent phantom liquids	228
Table 5.3: Difference between the measured dielectric properties ( $\epsilon_r$ ) of coconut green skin tissue specimen and equivalent phantom liquids	228
Table 5.4: Final compositions of coconut pulp tissue equivalent phantom liquids	232
Table 5.5: Difference between the measured dielectric properties ( $\epsilon_r$ ) of coconut pulp tissue specimen and equivalent phantom liquids	232
Table 5.6: Final compositions of coconut water equivalent phantom liquids	236
Table 5.7: Difference between the measured dielectric properties ( $\epsilon_r$ ) of coconut water specimen and equivalent phantom liquids	236
Table 5.8: Final compositions of apple tissue equivalent phantom liquids	240
Table 5.9: Difference between the measured dielectric properties ( $\epsilon_r$ ) of apple tissue specimen and equivalent phantom liquids	240
Table 5.10: Final compositions of guava tissue equivalent phantom liquids	244
Table 5.11: Difference between the measured dielectric properties ( $\epsilon_r$ ) of guava tissue specimen and equivalent phantom liquids	244
Table 5.12: Final compositions of grape tissue equivalent phantom liquids	248
Table 5.13: Difference between the measured dielectric properties ( $\epsilon_r$ ) of grape tissue specimen and equivalent phantom liquids	248
Table 5.14: Final compositions of tomato tissue equivalent phantom liquids	252
Table 5.15: Difference between the measured dielectric properties ( $\epsilon_r$ ) of tomato tissue specimen and equivalent phantom liquids	252
Table 5.16: Final compositions of brinjal tissue equivalent phantom liquids	256
Table 5.17: Difference between the measured dielectric properties ( $\epsilon_r$ ) of brinjal tissue specimen and equivalent phantom liquids	256
Table 5.18: Final compositions of sapodilla fruit tissue equivalent phantom liquids	260
Table 5.19: Difference between the measured dielectric properties ( $\epsilon_r$ ) of sapodilla fruit tissue specimen and equivalent phantom liquids	260
Table 5.20: Final compositions of sapodilla leaf tissue equivalent phantom liquids	264
Table 5.21: Difference between the measured dielectric properties ( $\epsilon_r$ ) of sapodilla leaf tissue specimen and equivalent phantom liquids	264
Table 5.22: Final compositions of <i>Catharanthus roseus</i> leaf tissue equivalent phantom liquids	268
Table 5.23: Difference between the measured dielectric properties ( $\epsilon_r$ ) of <i>Catharanthus roseus</i> leaf tissue specimen and equivalent phantom liquids	268
Table 5.24: Final compositions of <i>Catharanthus roseus</i> flower tissue equivalent phantom liquids	272
Table 5.25: Difference between the measured dielectric properties ( $\epsilon_r$ ) of <i>Catharanthus roseus</i> flower tissue specimen and equivalent phantom liquids	272

## List of Tables

Table 5.26: Final compositions of <i>Catharanthus roseus</i> stem tissue equivalent phantom liquids	276
Table 5.27: Difference between the measured dielectric properties ( $\epsilon_r$ ) of <i>Catharanthus roseus</i> stem tissue specimen and equivalent phantom liquids	276
Table 5.28: Final compositions of green mango pulp tissue equivalent phantom liquids	280
Table 5.29: Difference between the measured dielectric properties ( $\epsilon_r$ ) of green mango pulp tissue specimen and equivalent phantom liquids	280
Table 5.30: Final compositions of green mango seed tissue equivalent phantom liquids	284
Table 5.31: Difference between the measured dielectric properties ( $\epsilon_r$ ) of green mango seed tissue specimen and equivalent phantom liquids	284
Table 5.32: Final compositions of green mango leaf tissue equivalent phantom liquids	288
Table 5.33: Difference between the measured dielectric properties ( $\epsilon_r$ ) of green mango leaf tissue specimen and equivalent phantom liquids	288
Table 5.34: Final compositions of water apple tissue equivalent phantom liquids	292
Table 5.35: Difference between the measured dielectric properties ( $\epsilon_r$ ) of water apple tissue specimen and equivalent phantom liquids	292
Table 5.36: Final compositions of orange pulp tissue equivalent phantom liquids	296
Table 5.37: Difference between the measured dielectric properties ( $\epsilon_r$ ) of orange pulp tissue specimen and equivalent phantom liquids	296
Table 5.38: Final compositions of orange peel tissue equivalent phantom liquids	300
Table 5.39: Difference between the measured dielectric properties ( $\epsilon_r$ ) of orange peel tissue specimen and equivalent phantom liquids	300
Table 5.40: Final compositions of black grape tissue equivalent phantom liquids	304
Table 5.41: Difference between the measured dielectric properties ( $\epsilon_r$ ) of black grape tissue specimen and equivalent phantom liquids	304
Table 6.1: Dimensions of three <i>Tabernaemontana divaricata</i> plants (refer to Fig. 6.1)	310
Table 6.2: Comparison of half-wave dipole antenna received power data next to 1 <sup>st</sup> earthen pot (natural low electromagnetic environment) and the 2 <sup>nd</sup> earthen pot (beside GSM mobile phone)	320
Table 6.3: Radiation exposure duration of <i>Capsicum annuum</i> seeds and subsequent saplings in the 2 <sup>nd</sup> earthen pot over 50 days duration	320
Table 6.4: Germinated sapling count and mean sapling height over 50 days	323
Table 6.5: Comparison of largest sapling height and largest leaf length between the 1 <sup>st</sup> and 2 <sup>nd</sup> earthen pots	325
Table 7.1: Primer information for rice ( <i>Oryza sativa</i> ) housekeeping and target genes	345
Table 8.1: Primer information for rice ( <i>Oryza sativa</i> ) housekeeping and target genes	375

# List of Acronyms

---

AEC	Adenylate Energy Charge
ATP	Adenosine Triphosphate
BAN	Body-Area-Network
bZIP	Basic Leucine Zipper
CDPK	Calcium-Dependent Protein Kinase
CMBP	Chloroplast mRNA-Binding Protein
CST MWS	CST Microwave Studio
CT	Cycle Threshold
DoP	Direction of Propagation
DoT	Department of Telecommunications
DI	De-Ionized
FCC	Federal Communications Commission
FDTD	Finite Difference Time Domain
FIT	Finite Integration Technique
GSM	Global System for Mobile Communication
HSA	Handheld Spectrum Analyzer
ICNIRP	International Commission on Non-Ionizing Radiation Protection
IEC	International Electrotechnical Commission
LOS	Line-of-Sight
MLP SAR	Maximum Local Point SAR
MSRC	Mode Stirred Reverberation Chamber
MUT	Material under Test
NCBI	National Center for Biotechnology Information
OATS	Open Area Test Site
PAR	Photosynthetically Active Radiation

## List of Acronyms

PEC	Perfect Electric Conductor
PIFs	Phytochrome Interacting Factors
PIN	Proteinase Inhibitor
PMLs	Perfectly Matched Layers
Q Factor	Quality Factor
qRT-PCR	Quantitative Real Time Polymerase Chain Reaction
RAP-DB	Rice Annotation Project Database
RF	Radio Frequency
SAEFL	Swiss Agency for the Environment, Forests and Landscape
SAR	Specific Absorption Rate
SEM	Standard Error of the Mean
TB1	Teosinte Branched 1
TD	Time Domain
TE	Transverse Electric
TFs	Transcription Factors
TM	Transverse Magnetic
VNA	Vector Network Analyzer
WBA SAR	Whole Body Averaged SAR
1g SAR	SAR Averaged over 1 g of Contiguous Tissue Mass
10g SAR	SAR Averaged over 10 g of Contiguous Tissue Mass

# Chapter 1

## Introduction

---

In the present era of seamless wireless connectivity, electromagnetic radiation from different antennas over multiple frequency bands is omnipresent all over the world. Electromagnetic energy emission is gradually increasing with the widespread deployment of modern wireless telecommunication infrastructure – as a consequence, presence of electromagnetic fields at multiple frequencies is increasing all over the environment. Significant presence of water and ion content in human, animal and plant tissues contribute to high permittivity ( $\epsilon_r'$ ) and electrical conductivity ( $\sigma$ ) [1-11]. As a consequence, biological objects in general are quite capable of perceiving and absorbing incident electromagnetic energy that impinges on them. Though electromagnetic energy absorption rates have majorly been investigated for a number of human models along with associated biological effects [12-24], similar investigations on prototyped fruit and plant models is rarely available in literature. In addition, existing electromagnetic exposure regulatory norms have been set entirely based on immediate thermal effects of electromagnetic radiation on humans – thus, maximum reference power density and Specific Absorption Rate (SAR) limits have been prescribed only for human exposure [25-30]. In this context, arguments can be put to investigate SAR values for different fruit, flower and plant models – as, those get uninterrupted electromagnetic exposure at multiple frequencies from a number of radiating antennas. Over and above, higher surface-to-volume ratio of plants makes increased interaction with the incident electromagnetic energy possible [31]. Therefore, long duration as well as short duration deterministic electromagnetic irradiation evoked plant responses should also be investigated at physiological and molecular levels. This thesis entitled **“Investigations on the Effects of Electromagnetic Radiation on Indian Flora”** aims at such investigations of complex dielectric properties ( $\epsilon_r$ ) of fruit and plant tissues, SAR distributions in prototyped fruit and plant models, tissue equivalent dielectric liquids for SAR measurement, and long duration as well as short duration electromagnetic irradiation induced physiological and molecular responses in plants. The outcomes of these investigations also suggest solutions to minimize electromagnetic energy absorption in fruits and plants along with associated biological

effects – while maintaining a sustainable telecommunication growth for seamless wireless connectivity.

## 1.1 Motivation

At initial stage, to start exploring the wide interdisciplinary research spectrum of electromagnetic energy absorption in biological objects, associated interaction mechanisms and consequent biological responses – it seems to be a standard approach to begin the investigations with broadband complex dielectric properties ( $\epsilon_r$ ) characterization of different fruit, flower and plant tissue specimens. It is so because there are some articles available in the literature on dielectric properties ( $\epsilon_r$ ) measurements of similar fruit and plant specimens – therefore, the adopted measurement technique, measured permittivity ( $\epsilon'_r$ ) and loss tangent ( $\tan \delta$ ) data can be verified along with a firm grasp on the underlying physics behind the adopted measurement system [4-11, 32-41]. Among different dielectric properties measurement techniques, open ended coaxial measurement technique has been adopted mostly for characterizing dielectric properties ( $\epsilon_r$ ) of soft semi-solid or liquid biological tissue specimens [35-41]. In spite of the fact that decades ago, researchers and scientists initiated exploring electromagnetic energy absorption in human models along with associated biological consequences [12-24] – electromagnetic energy absorption rates in different fruit and plant models have never been investigated before primarily due to mobile tower antenna emission at multiple frequency bands. Thus, with the ever-increasing utilization of electromagnetic energy in wireless telecommunication systems, investigating spatial SAR distributions in different fruit and plant models along with associated biological responses seems absolutely necessary.

Investigations on permittivity ( $\epsilon'_r$ ) and loss tangent ( $\tan \delta$ ) measurement of different fruit / plant tissues, spatial SAR distributions in prototyped fruit / plant models, plant tissue equivalent phantom liquids, along with long duration and short duration electromagnetic irradiation evoked plant responses are gaining importance with the extensive utilization of electromagnetic energy over a wide frequency spectrum. Not only from the research perspective – it should be noted that, outcome of the above mentioned investigations can also facilitate different electromagnetic exposure regulatory committees and policy makers to re-evaluate existing regulatory norms and prepare revised electromagnetic regulatory guidelines in future.



In this dissertation, a chapter is dedicated to the fundamental concepts of material dielectric properties ( $\epsilon_r$ ) [42], underlying physics behind different polarization mechanisms [42-43], polarization phenomena and dielectric properties ( $\epsilon_r$ ) in plant tissues, appropriate dielectric properties ( $\epsilon_r$ ) measurement techniques with special emphasis on open ended coaxial probe technique [35-41], broadband dielectric properties ( $\epsilon_r$ ) characterization of several fruit and plant tissue specimens, and subsequently a novel technique to determine multi-tissue layers equivalent homogeneous phantom liquid formulation for practical SAR measurement. As mentioned before, this chapter has primarily been divided into two parts – the first part deals with dielectric properties ( $\epsilon_r$ ) characterization, whereas, the other part focuses on multilayer tissue modeling for practical SAR measurement. This particular chapter has been arranged after the initial two chapters i.e. Introduction and Literature Review presented in this thesis. Thus, this chapter provides a recapitulation of the fundamental concepts of material dielectric properties ( $\epsilon_r$ ) and polarization mechanisms, reports dielectric properties ( $\epsilon_r$ ) of several fruit and plant tissue samples, and formulates a novel protocol to define multilayer equivalent homogeneous phantom liquid for SAR measurement.

The next chapter includes SAR data evaluation for several prototyped fruit and plant models with appropriate frequency dependent dielectric properties ( $\epsilon_r$ ), as reported in the preceding chapter. At initial phase, SAR data and associated spatial distributions have been evaluated in a number of tropical fruit models due to plane wave incidence with linear polarization at multiple frequency bands. Subsequently, disparities in SAR data for different fruit and plant models have been reported due to wide contrast among different international and national electromagnetic exposure regulatory standards [25-30]. At last, variations of SAR data and associated spatial distributions in different fruit models have been evaluated for different combinations of incidence angle and wave polarization. Reported findings in this chapter indicate towards the necessity of harmonizing different international and national electromagnetic exposure regulatory standards worldwide [25-30, 44].

The chapter on SAR evaluation in different fruit and plant models is followed by practical work on homogeneous phantom liquids preparation for different fruit and plant tissue specimens – in order to perform practical SAR measurement in future. In the past, human head and body equivalent homogeneous phantom liquids were prepared and standardized for SAR measurements and validations [45-50]. Hence, following similar methodology, custom-made

homogeneous phantom liquids have been prepared for twenty fruit and plant tissue layers chosen out of twelve fruit and plant specimens (some fruits are multilayer). Reference permittivity ( $\epsilon_r'$ ) and loss tangent ( $\tan \delta$ ) values for all fruit or plant specimens have been attained either using sucrose (sugar), sodium chloride (NaCl), De-Ionized (DI) water based solution or employing diethylene glycol monobutyl ether (glycol), sodium chloride (NaCl) and DI water based solution. Fruit and plant tissue equivalent homogeneous phantom liquids have been prepared at 947.50 MHz, 1842.50 MHz and 2450.00 MHz – in total, sixty phantom liquid recipes have been formulated for SAR measurement in future.

Following the earlier chapters related to electromagnetic energy deposition in fruit and plant models, subsequent chapters focus on electromagnetic irradiation induced responses in model plants. The immediate next chapter consists of two topics – first part describes a basic investigation on electromagnetic propagation loss due to presence of single or multiple plants inside test environment, whereas a time study on initial plant responses under long duration cell phone exposure has been reported in the following part. In the first investigation, higher propagation loss has been noted as number of plants increases in the channel between transmitting and receiving antennas near 1800 MHz – the observations have been explained using plant absorption and scattering phenomena. In 50 days time study, reduced seed germination rate, enhanced sapling growth and wrinkled leaf specimens have been observed among *Capsicum annuum* (commonly known as Chilli) saplings under long-duration cell phone irradiation. These initial observations motivated further to investigate long-duration as well as short-duration controlled and deterministic electromagnetic irradiation induced physiological and molecular plant responses in subsequent chapters.

The next chapter reports periodic and controlled electromagnetic irradiation induced responses in rice plants (*Oryza sativa*) at physiological and molecular levels. It should be noted, Roux et al. and Vian et al. first introduced using Mode Stirred Reverberation Chamber (MSRC) for investigating controlled electromagnetic exposure evoked molecular responses in tomato plants – stress-responsive gene expression alterations were reported following the electromagnetic irradiation [31, 51-53]. Reported investigations, in 7<sup>th</sup> chapter of this dissertation, have been carried out after gaining inspiration from the past work on short duration electromagnetic irradiation induced gene expression alterations in tomato plants [31, 51-54]. Physiological and

molecular effects under long-duration, periodic and controlled electromagnetic irradiation (1837.50 MHz, 2.75 mW/m<sup>2</sup>) have been investigated in *Satabdi* and *Swarnaprabha* rice variants at different growth stages – inside a simple electromagnetic reverberation chamber. Irrespective of variant and growth stage, the periodic electromagnetic irradiation causes significant physiological or molecular response alterations in rice plants. In general, rice seed germination rate and photosynthetic pigment concentration levels were reduced – whereas, stress-sensitive gene expressions were upregulated under periodic electromagnetic irradiation at 1837.50 MHz, 2.75 mW/m<sup>2</sup>.

In continuation of the work reported in the last chapter, further investigation has been carried out to determine molecular responses in rice plants following one-time controlled electromagnetic irradiation at 1837.50 MHz, 2.75 mW/m<sup>2</sup>. Inside the custom-made reverberation chamber, stress-sensitive gene expressions have been investigated in both 12 days old *Satabdi* rice seedlings and 40 days old *Swarnaprabha* rice plants following one-time electromagnetic irradiation (2 h 30 min). Relative expressions for stress-responsive genes have been assayed using real-time quantitative Polymerase Chain Reaction (PCR) technique – transcript accumulation of selected stress related rice genes has been noted following the one-time electromagnetic irradiation. It should further be noted, 2 h 30 min electromagnetic irradiation induced transcript accumulation in rice plants is in line with the earlier molecular responses under periodic electromagnetic exposure at 1837.50 MHz, 2.75 mW/m<sup>2</sup>. The reported stress-responsive gene expressions upregulation confirms that plants perceive electromagnetic irradiation as an abiotic stress – similar findings, though limited, are available in literature [31, 51-54].

## 1.2 Organization of the Thesis

Based on the chronological progress of work, the organization of this dissertation is described in this section.

**Chapter 2** summarizes an initial literature review report on the past research articles which were studied in detail to prepare the preliminary foundation for this research work. To be a bit specific, this chapter contains an extensive and multi-dimensional review of articles from cross-disciplinary research domains. Research articles have been read to comprehend electromagnetic properties of plant tissues, SAR assessment techniques, electromagnetic exposure regulatory

standards, homogeneous phantom liquid formulation for SAR measurement and electromagnetic irradiation induced plant responses [5-20, 25-30, 45-55].

**Chapter 3** starts with the fundamental concepts of material dielectric properties ( $\epsilon_r$ ) and associated polarization mechanisms – thereafter, dielectric properties ( $\epsilon_r$ ) and polarization mechanisms in plant tissues have been discussed. Different dielectric properties ( $\epsilon_r$ ) measurement techniques have also been recapitulated in this chapter with special emphasis on open ended coaxial probe technique [32-41]. Furthermore, broadband permittivity ( $\epsilon_r'$ ) and loss tangent ( $\tan \delta$ ) data have been reported for several fruit and plant tissue specimens – these measured data have been utilized in subsequent research work. The second part, in this chapter, focuses on multilayer equivalent homogeneous dielectric modeling for SAR measurement.

**Chapter 4** reports SAR data simulations in a number of fruit and plant models due to plane wave irradiation with linear polarization. Measured dielectric properties ( $\epsilon_r$ ) have been fed into the realistic fruit and plant models at the frequencies of interest – thereafter, spatial SAR distributions have been evaluated. For any particular fruit or plant model, variations in SAR data have been investigated due to lack of harmonization among different electromagnetic exposure standards [25-30]. Furthermore, variations in peak SAR value and spatial distribution have also been investigated in fruit models for various angles of incidence and wave polarizations.

In **Chapter 5**, different fruit and plant tissue equivalent homogeneous phantom liquids have been formulated for practical SAR measurement in future. At three frequencies (i.e. 947.50 MHz, 1842.50 MHz and 2450.00 MHz), homogeneous dielectric liquid recipes have been prepared for twenty fruit or plant tissue specimens. Thus, altogether, sixty phantom liquid recipes have been reported in this chapter.

**Chapter 6**, in its first part, reports electromagnetic path loss due to presence of plants in a test propagation channel. Propagation loss has been explained with absorption and scattering phenomena due to presence of plants in the wireless channel. Furthermore, a preliminary investigation on visible plant responses under continuous cell phone irradiation has been reported in the subsequent part. Reduced seed germination, enhanced sapling growth and wrinkled leaves have been observed among *Capsicum annuum* plants following the cell phone irradiation.

In **Chapter 7**, physiological and molecular responses have been investigated in rice plants (*Oryza sativa*) following periodic, controlled and deterministic electromagnetic exposure at

1837.50 MHz. Rice seeds and subsequent plants have been exposed to controlled electromagnetic radiation inside a simple metallic reverberation chamber. Periodic electromagnetic irradiation induced effects on seed germination rate, chlorophyll concentrations and stress-responsive gene expressions have been investigated in two rice variants at different growth stages. Seed germination rate and chlorophyll contents reduced – whereas, stress-responsive gene expressions were upregulated under the periodic electromagnetic irradiation.

**Chapter 8** continues the work and reports further investigations on transcript accumulation of stress-responsive genes in rice plants following one-time, controlled and deterministic electromagnetic irradiation at 1837.50 MHz. These investigations have also been carried out inside the above mentioned custom-made reverberation chamber using the same exposure setup. Based on real-time quantitative PCR assay, upregulated stress-sensitive gene expressions have been noted in two rice variants following the 2 h 30 min electromagnetic irradiation.

**Chapter 9** summarizes the concluding remarks and scope for future research.

## References

- [1] C. Gabriel, S. Gabriel, and Y. E. Corthout, ‘The Dielectric Properties of Biological Tissues: I. Literature Survey’, *Physics in Medicine & Biology*, Vol. 41, No. 11, pp. 2231-2249, 1996.
- [2] S. Gabriel, R. W. Lau, and C. Gabriel, ‘The Dielectric Properties of Biological Tissues: II. Measurements in the Frequency Range 10 Hz to 20 GHz’, *Physics in Medicine & Biology*, Vol. 41, No. 11, pp. 2251-2269, 1996.
- [3] S. Gabriel, R. W. Lau, and C. Gabriel, ‘The Dielectric Properties of Biological Tissues: III. Parametric Models for the Dielectric Spectrum of Tissues’, *Physics in Medicine & Biology*, Vol. 41, No. 11, pp. 2271-2293, 1996.
- [4] M. A. Stuchly, T. W. Athey, G. M. Samaras, and G. E. Taylor, ‘Measurement of Radio Frequency Permittivity of Biological Tissues with an Open-Ended Coaxial Line: Part II - Experimental Results’, *IEEE Transactions on Microwave Theory and Techniques*, Vol. 30, No. 1, pp. 87-92, 1982.
- [5] G. P. De Loor, and F. W. Meijboom, ‘The Dielectric Constant of Foods and other Materials with High Water Contents at Microwave Frequencies’, *International Journal of Food Science & Technology*, Vol. 1, No. 4, pp. 313-322, 1966.

- [6] S. O. Nelson, 'Microwave Dielectric Properties of Grain and Seed', *Transactions of the ASAE*, Vol. 16, No. 5, pp. 902-905, 1973.
- [7] S. O. Nelson, 'Dielectric Properties of Some Fresh Fruits and Vegetables at Frequencies of 2.45 to 22 GHz', *Transactions of the ASAE*, Vol. 26, No. 2, pp. 613-616, 1983.
- [8] S. O. Nelson, 'Dielectric Properties of Agricultural Products – Measurements and Applications', *IEEE transactions on Electrical Insulation*, Vol. 26, No. 5, pp.845-869, 1991.
- [9] W. Kuang, and S. O. Nelson, 'Dielectric Relaxation Characteristics of Fresh Fruits and Vegetables from 3 to 20 GHz', *Journal of Microwave Power and Electromagnetic Energy*, Vol. 32, No. 2, pp. 114-122, 1997.
- [10] W. C. Guo, S. O. Nelson, S. Trabelsi, and S. J. Kays, '10–1800-MHz Dielectric Properties of Fresh Apples during Storage', *Journal of Food Engineering*, Vol. 83, No. 4, pp. 562-569, 2007.
- [11] S. O. Nelson, and S. Trabelsi, 'Dielectric Spectroscopy Measurements on Fruit, Meat, and Grain', *Transactions of the ASABE*, Vol. 51, No. 5, pp. 1829-1834, 2008.
- [12] S. S. Stuchly, M. A. Stuchly, A. Kraszewski, and G. Hartsgrove, 'Energy Deposition in a Model of Man: Frequency Effects', *IEEE Transactions on Biomedical Engineering*, Vol. 33, No. 7, 1986.
- [13] K. Meier, V. Hombach, R. Kästle, R. Y. Tay, and N. Kuster, 'The Dependence of Electromagnetic Energy Absorption upon Human-Head Modelling at 1800 MHz', *IEEE Transactions on Microwave Theory and Techniques*, Vol. 45, No. 11, 1997.
- [14] T. Yelkenci, 'Effects of Metallic Objects on Specific Absorption Rate in the Human Head for 915 and 1900 MHz Mobile Phones', *Frequenz*, Vol. 60, No. 3-4, pp. 46-50, 2006.
- [15] O. P. Gandhi, 'Yes the Children are More Exposed to Radiofrequency Energy from Mobile Telephones than Adults', *IEEE Access*, Vol. 3, pp. 985-988, 2015.
- [16] J. Cooper, B. Marx, J. Buhl, and V. Hombach, 'Determination of Safety Distance Limits for a Human near a Cellular Base Station Antenna, Adopting the IEEE Standard or ICNIRP Guidelines', *Bioelectromagnetics*, Vol. 23, No. 6, pp. 429-443, 2002.
- [17] A. Christ, A. Klingenböck, T. Samaras, C. Goiceanu, and N. Kuster, 'The Dependence of Electromagnetic Far-Field Absorption on Body Tissue Composition in the Frequency Range from 300 MHz to 6 GHz', *IEEE Transactions on Microwave Theory and Techniques*, Vol. 54, No. 5, 2006.

- [18] M. A. A. Karunarathna, and I. J. Dayawansa, 'Energy Absorption by the Human Body from RF and Microwave Emissions in Sri Lanka', *Sri Lankan Journal of Physics*, Vol. 7, pp. 35-47, 2006.
- [19] A. Hirata, N. Ito, O. Fujiwara, T. Nagaoka, and S. Watanabe, 'Conservative Estimation of Whole-Body-Averaged SARs in Infants with a Homogeneous and Simple-Shaped Phantom in the GHz Region', *Physics in Medicine and Biology*, Vol. 53, No. 24, pp. 7215-7223, 2008.
- [20] T. Wessapan, S. Srisawatdhisukul, and P. Rattanadecho, 'Specific Absorption Rate and Temperature Distributions in Human Head Subjected to Mobile Phone Radiation at Different Frequencies', *International Journal of Heat and Mass Transfer*, Vol. 55, No. 1-3, pp. 347-359, 2012.
- [21] R. J. Aitken, L. E. Bennetts, D. Sawyer, A. M. Wiklendt, and B. V. King, 'Impact of Radio Frequency Electromagnetic Radiation on DNA Integrity in the Male Germline', *International Journal of Andrology*, Vol. 28, No. 3, pp. 171-179, 2005.
- [22] BioInitiative Working Group, '*BioInitiative 2012: A Rationale for a Biologically-Based Exposure Standards for Low-Intensity Electromagnetic Radiation*', In C. Sage, and D. O. Carpenter (eds): *The BioInitiative Report 2012*, 2012. [www.bioinitiative.org](http://www.bioinitiative.org) [Last accessed 03 April 2022].
- [23] Y. H. Hao, L. Zhao, and R. Y. Peng, 'Effects of Microwave Radiation on Brain Energy Metabolism and Related Mechanisms', *Military Medical Research*, Vol. 2, No. 1, pp. 1-8, 2015.
- [24] Y. F. Lai, H. Y. Wang, and R. Y. Peng, 'Establishment of Injury Models in Studies of Biological Effects Induced by Microwave Radiation', *Military Medical Research*, Vol. 8, Article No. 12, pp. 1-18, 2021.
- [25] R. F. Cleveland, Jr., D. M. Sylvar, and J. L. Ulcek, '*Evaluating Compliance with FCC Guidelines for Human Exposure to Radiofrequency Electromagnetic Fields*', FCC OET Bulletin, Vol. 65, Edition 97-01, Washington D.C., 1997.
- [26] International Commission on Non-Ionizing Radiation Protection (ICNIRP), 'Guidelines for Limiting Exposure to Electromagnetic Fields (100 kHz to 300 GHz)', *Health Physics*, Vol. 118, No. 5, pp. 483-524, 2020.
- [27] Department of Telecommunications (DoT), '*A Journey for EMF*', 2012, [www.dot.gov.in/journey-emf](http://www.dot.gov.in/journey-emf) [Last accessed 03 April 2022].

- [28] Swiss Agency for the Environment, Forests and Landscape (SAEFL), ‘*Electrosmog in the Environment*’, pp. 1-56, Switzerland, 2005.
- [29] Ministry of Health of the Russian Federation, ‘*SanPiN 2.1.8/2.2.4.1190-03: Arrangement and Operation of Land Mobile Radiocommunication Facilities – Hygienic Requirements*’, pp. 1-17, Russia, 2003.
- [30] The President of the Council of Ministers (Italy), ‘*Establishment of Exposure Limits, Attention Values, and Quality Goals to Protect the Population against Electric, Magnetic, and Electromagnetic Field Generated at Frequencies between 100 kHz and 300 GHz*’, unofficial translation by P. Vecchia, pp. 1-6, Italy, 2003.
- [31] A. Vian, C. Faure, S. Girard, E. Davies, F. Hallé, P. Bonnet, G. Ledoigt, and F. Paladian, ‘Plants Respond to GSM-Like Radiations’, *Plant Signaling & Behaviour*, Vol. 2, No. 6, pp. 522-524, 2007.
- [32] M. S. Venkatesh, and G. S. V. Raghavan, ‘An Overview of Dielectric Properties Measuring Techniques’, *Canadian Biosystems Engineering*, Vol. 47, No. 7, pp. 15-30, 2005.
- [33] S. N. Jha, K. Narsaiah, A. L. Basediya, R. Sharma, P. Jaiswal, R. Kumar, and R. Bhardwaj, ‘Measurement Techniques and Application of Electrical Properties for Nondestructive Quality Evaluation of Foods – A Review’, *Journal of Food Science and Technology*, Vol. 48, No. 4, pp. 387-411, 2011.
- [34] A. P. Gregory, and R. N. Clarke, ‘A Review of RF and Microwave Techniques for Dielectric Measurements on Polar Liquids’, *IEEE Transactions on Dielectrics and Electrical Insulation*, Vol. 13, No. 4, pp. 727-743, 2006.
- [35] G. Deschamps, ‘Impedance of an Antenna in a Conducting Medium’, *IRE Transactions on Antennas and Propagation*, Vol. 10, No. 5, pp. 648-650, 1962.
- [36] L. Liu, D. Xu, and Z. Jiang, ‘Improvement in Dielectric Measurement Technique of Open-Ended Coaxial Line Resonator Method’, *Electronics Letters*, Vol. 22, No. 7, pp. 373-375, 1986.
- [37] D. Xu, L. Liu, and Z. Jiang, ‘Measurement of the Dielectric Properties of Biological Substances using an Improved Open-Ended Coaxial Line Resonator Method’, *IEEE Transactions on Microwave Theory and Techniques*, Vol. 35, No. 12, pp. 1424-1428, 1987.
- [38] M. A. Stuchly, and S. S. Stuchly, ‘Coaxial Line Reflection Method for Measuring Dielectric Properties of Biological Substances at Radio and Microwave Frequencies – A Review’, *IEEE Transactions on Instrumentation and Measurement*, Vol. 29, No. 3, pp 176-183, 1980.



- [39] T. W. Athey, M. A. Stuchly, and S. S. Stuchly, 'Measurement of Radio Frequency Permittivity of Biological Tissues with an Open-Ended Coaxial Line: Part I', *IEEE Transactions on Microwave Theory and Techniques*, Vol. 30, No. 1, pp 82-86, 1982.
- [40] R. Zajíček, L. Oppl, and J. Vrba, 'Broadband Measurement of Complex Permittivity using Reflection Method and Coaxial Probes', *Radioengineering*, Vol.17, No. 1, pp. 14-19, 2008.
- [41] J. S. Bobowski, and T. Johnson, 'Permittivity Measurements of Biological Samples by an Open-Ended Coaxial Line', *Progress in Electromagnetics Research B*, Vol. 40, pp. 159-183, 2012.
- [42] S. O. Kasap, '*Principles of Electronic Materials and Devices*', McGraw-Hill, New York, Third Ed., 2006.
- [43] D. Kumar, N. Ahmad, V. Kumar, V. K. Jha, S. Kulshrestha, R. Saini, and M. S. Shekhawat, 'Various Polarization Mechanisms Involved in Ionic Crystals', *AIP Conference Proceedings*, Vol. 2220, No. 1, Article ID. 040036, pp. 1-6, May, 2020.
- [44] K. R. Foster, 'Exposure Limits for Radiofrequency Energy: Three Models', *Proceedings of the Eastern European Regional EMF Meeting and Workshop (Criteria for EMF Standards Harmonization)*, pp. 1-6, Varna, Bulgaria, 2001.
- [45] V. Hombach, K. Meier, M. Burkhardt, E. Kuhn, and N. Kuster, 'The Dependence of EM Energy Absorption upon Human Head Modeling at 900 MHz', *IEEE Transactions on Microwave Theory and Techniques*, Vol. 44, No. 10, pp. 1865-1873, 1996.
- [46] K. Meier, M. Burkhardt, T. Schmid, and N. Kuster, 'Broadband Calibration of E-field Probes in Lossy Media [Mobile Telephone Safety Application]', *IEEE Transactions on Microwave Theory and Techniques*, Vol. 44, No. 10, pp. 1954-1962, 1996.
- [47] K. Ito, K. Furuya, Y. Okano, and L. Hamada, 'Development and Characteristics of a Biological Tissue-equivalent Phantom for Microwaves', *Electronics and Communications in Japan (Part I: Communications)*, Vol. 84, No. 4, pp. 67-77, 2001.
- [48] T. Onishi, R. Ishido, T. Takimoto, K. Saito, S. Uebayashi, M. Takahashi, and K. Ito, 'Biological Tissue-Equivalent Agar-Based Solid Phantoms and SAR Estimation using the Thermographic Method in the Range of 3-6 GHz', *IEICE Transactions on Communications*, Vol. 88, No. 9, pp. 3733-3741, 2005.

- [49] K. Quelever, T. Coradin, C. Bonhomme, O. Meyer, B. Derat, ‘Composition Simulating the Dielectric Properties of the Human Body and Use Thereof for SAR Measurement’, *U.S. Patent PCT WO2013079621 (A1)*, 2013.
- [50] A. P. Gregory, K. Quéléver, D. Allal, and O. Jawad, ‘Validation of a Broadband Tissue-Equivalent Liquid for SAR Measurement and Monitoring of its Dielectric Properties for Use in a Sealed Phantom’, *Sensors*, Vol. 20, No. 10, Article No. 2956, pp. 1-13, 2020.
- [51] D. Roux, A. Vian, S. Girard, P. Bonnet, F. Paladian, E. Davies, and G. Ledoigt, ‘Electromagnetic Fields (900 MHz) Evoke Consistent Molecular Responses in Tomato Plants’, *Physiologia Plantarum*, Vol. 128, No. 2, pp. 283-288, 2006.
- [52] A. Vian, D. Roux, S. Girard, P. Bonnet, F. Paladian, E. Davies, and G. Ledoigt, ‘Microwave Irradiation Affects Gene Expression in Plants’, *Plant Signaling & Behavior*, Vol. 1, No. 2, pp. 67-69, 2006.
- [53] D. Roux, A. Vian, S. Girard, P. Bonnet, F. Paladian, E. Davies, and G. Ledoigt, ‘High Frequency (900MHz) Low Amplitude ( $5V\ m^{-1}$ ) Electromagnetic Field: A Genuine Environmental Stimulus that Affects Transcription, Translation, Calcium and Energy Charge in Tomato’, *Planta*, Vol. 227, No. 4, pp. 883-891, 2008.
- [54] A. Vian, E. Davies, M. Gendraud, and P. Bonnet, ‘Plant Responses to High Frequency Electromagnetic Fields’, *BioMed Research International*, Article ID: 1830262, 2016.
- [55] E. Beaubois, S. Girard, S. Lallechere, E. Davies, F. Paladian, P. Bonnet, G. Ledoigt, and A. Vian, ‘Intercellular Communication in Plants: Evidence for Two Rapidly Transmitted Systemic Signals Generated in Response to Electromagnetic Field Stimulation in Tomato’, *Plant, Cell and Environment*, Vol. 30, No. 7, pp. 834-844, 2007.

# Chapter 2

## Literature Review

---

### 2.1 Motivation

Modern wireless communication has evolved through multiple development cycles since the pioneering theoretical and practical research work by Maxwell, Hertz, Marconi and Bose. With the worldwide deployment of advanced wireless communication infrastructure – the utilization of electromagnetic energy over multiple frequency bands has increased by a large extent. Biological bodies irrespective of humans, animals or plants possess fairly high permittivity ( $\epsilon'_r$ ) and electrical conductivity ( $\sigma$ ), in principle, due to the respective presence of water and ion contents [1-17] – thus, biological tissues possess great capabilities to perceive electromagnetic energy present in open environment. Since last few decades, electromagnetic energy absorption rates in human models along with associated biological consequences are being investigated [18-36]. Furthermore, based on immediate thermal effects on humans, a number of international and national electromagnetic exposure regulatory guidelines have been prescribed across the globe [37-42]. It is unfortunate that these guidelines are not harmonized in terms of the prescribed power density or equivalent electromagnetic field strength – rather, those are prescribed wide apart from each other.

In contrast, electromagnetic energy absorption rates in different fruits, plants and crops haven't been explored yet – though, those are exposed to microwave radiation from a number of wireless antennas (such as, mobile tower antennas) throughout their lifespan. Moreover, larger surface-to-volume ratio of plant structures facilitates higher interaction with the incident electromagnetic wave [43] – in spite of this fact, electromagnetic irradiation induced physiological and molecular responses in plants haven't been investigated to sufficient extent [43-47].

Therefore, this chapter aims at rapid recapitulation of the significant developments in above mentioned research areas – as also, how these concepts directed the motivation of this thesis towards investigating dielectric properties ( $\epsilon_r$ ) of fruit / plant tissues, electromagnetic energy absorption rate analyses in prototyped fruit / plant models and electromagnetic irradiation evoked biological responses in selected plants with an aim for a sustainable development.

## 2.2 Dielectric Properties of Different Plant Tissue Specimens

Major research work on characterizing dielectric properties ( $\epsilon_r$ ) of different plant, fruit and crop specimens have been initiated at around 1970 – at subsequent phase, prompt research progresses have been noticed in this particular field [7-17]. At initial instance, core motivation behind this work was several agricultural applications, food processing using dielectric tissue heating and pest control using microwave during crop storage. In 1973, S. O. Nelson reported dielectric properties ( $\epsilon_r$ ) of several crop and seed specimens such as wheat, sorghum, oats, alfalfa and soybean using three different microwave characterization techniques [7]. Later in 1980, dielectric properties ( $\epsilon_r$ ) of few fresh fruit and vegetable specimens were reported by Nelson at 2.45 GHz using short circuited coaxial line measurement technique – permittivity ( $\epsilon_r'$ ) and loss factor have been measured for some peach cultivars, two sweet potato cultivars and individual cultivars of potato, apple, cantaloupe and carrot [8]. Next, complex dielectric properties ( $\epsilon_r$ ) of potato, sweet potato, peach, watermelon, cantaloupe and cucumber specimens have been reported by Nelson at three different frequencies i.e. 2.45 GHz, 11.7 GHz and 22.0 GHz. In addition, correlations have been investigated between the complex dielectric properties ( $\epsilon_r$ ) of the tissue specimens and their respective moisture content levels [9]. In 1991, Nelson discussed the dependence of dielectric properties ( $\epsilon_r$ ) on frequency, temperature, moisture content and density of agricultural product [10]. In the same paper, different dielectric measurement techniques have also been reviewed – moreover, practical applications such as dielectric heating for seed treatment, improving grain qualities for long-duration storage, insect control during grain storage, crop quality assessment and determining moisture content etc. have also been discussed [10]. In 1997, the Debye equation has been utilized for analyzing measured dielectric properties ( $\epsilon_r$ ) of a number of fruit and vegetable samples over 3 GHz to 20 GHz; Kuang and Nelson have scrutinized Cole-Cole plots for the selected fruit and vegetable tissues to determine how close the measured data fit to Debye relaxation model [11]. Dielectric properties ( $\epsilon_r$ ) of apple cultivars have been reported by Ikediala et al. in the year of 2000. In the present twenty first century, Nelson and his research colleagues (such as W. C. Guo, S. Trabelsi etc.) have made significant advancement in this research domain – this group reported numerous experimental dielectric data analyses for a number of plant and fruit tissue specimens [12-17].

In connection with dielectric properties ( $\epsilon_r$ ) measurement of plant tissues, suitable dielectric characterization techniques should also be discussed in this section. Appropriate measurement technique is chosen based on material type (solid, granular, semi-solid, gel or liquid), electrical characteristics, material density, particle size distribution, sample shape, surface smoothness, frequency range, temperature, accuracy and precision levels [8, 10-11, 13-17, 48-50]. Suitable sample holder design and lumped equivalent circuit modeling at microwave spectrum are the main challenges for dielectric constant ( $\epsilon_r$ ) characterization [48-51]. Complex dielectric constant ( $\epsilon_r$ ) of test material can be characterized after solving the lumped equivalent system equations over desired microwave spectrum [5, 50, 52-60]. Closed resonant structures or open resonant structures are employed as two-port devices to characterize transmission coefficient – whereas, reflection coefficient is measured in one-port devices for deriving complex dielectric constant ( $\epsilon_r$ ) of the test material [48, 61]. Solid, semi-solid or liquid dielectric specimens can be characterized using several techniques such as cavity perturbation technique, waveguide or coaxial transmission line, free space transmission technique, microstrip transmission line, time domain reflectometry and open ended coaxial probe [48-50]. Complex dielectric properties ( $\epsilon_r$ ) of grains, fruits and vegetables can be measured using several techniques – as reported in literature [4, 6, 62-65]. At lower frequencies, grain and seed dielectric properties ( $\epsilon_r$ ) was measured with coaxial line sample holder and Q meter – based on resonant circuit model [10, 48, 66]. Moreover, coaxial line or rectangular waveguide sample holder (along with different microwave components) based dielectric characterization techniques have been used for seed, grain, fruit and vegetable specimens over 1 GHz to 22 GHz [7-10, 48, 67]. Some of the widely adopted dielectric characterization techniques above 1 GHz are transmission line method, resonant cavity structure and free space transmission method [48, 61, 68-69]. However, open ended coaxial probe setup (one-port system with reflection coefficient measurement) is the most preferred non-destructive dielectric properties ( $\epsilon_r$ ) characterization system for biological tissues – plant and fruit specimens are no exception [5, 51-60]. In this technique, amplitude and phase information of reflected signal at the coaxial probe open end is utilized to characterize the dielectric properties ( $\epsilon_r$ ) of tissue specimen. The lumped equivalent circuit and detailed mathematical analyses are well established and available in literature [5, 52-60]. Agilent Technologies (currently known as Keysight Technologies) have produced a commercial version of this dielectric properties characterization setup – the same is known as 85070E open ended

coaxial probe kit and can measure permittivity ( $\epsilon_r'$ ) and loss tangent ( $\tan \delta$ ) over a broad frequency spectrum while connected with a vector network analyzer [70].

It's true that, in past, dielectric properties ( $\epsilon_r$ ) characterizations of fruit, crop and plant tissues have been performed primarily aiming at different agricultural and food processing applications [10, 17]. However, it can be argued that these past developments related to the dielectric properties of different crop, fruit and plant tissue specimens i.e. measurement setup calibration, theoretical calculations, experimental measurements and detailed data analyses have helped a lot to shape the direction of this thesis work – in particular for characterizing broadband permittivity ( $\epsilon_r'$ ) and loss tangent ( $\tan \delta$ ) of different plant tissues, estimating electromagnetic energy absorption rates for prototyped plant / fruit models and formulating different plant / fruit tissue equivalent phantom liquids.

### **2.3 Specific Absorption Rate Assessment Technique**

In this era of extensive virtual communication, electromagnetic energy is being utilized over various frequency bands to sustain high speed wireless data services along with support for uninterrupted voice calls. Now, as an unavoidable consequence, living biological objects including humans, animals and plants are getting uninterrupted exposure to simultaneous electromagnetic radiation at numerous frequency bands from multiple transmitting antennas. Researchers have reported that deterministic exposure to electromagnetic radiation can lead to reversible or irreversible biological alterations or responses in humans and plants [31-36, 43-47, 71-74]. Thus, scientists and researchers have started investigating electromagnetic energy absorption rates in different human phantom models at distinct exposure scenarios – in this connection, they have also coined a term ‘Specific Absorption Rate (SAR)’ to quantify electromagnetic energy absorption rate in living biological object while an incident electromagnetic wave impinges on it [18-30]. SAR data and its spatial distribution have been investigated using theoretical calculations, numerical simulations and practical measurements for different human body and head equivalent phantom models [18-30].

In 1986, Stuchly et al. investigated electromagnetic energy deposition in a human model at three different frequencies i.e. at 160 MHz, 350 MHz and 915 MHz respectively. A computer controlled field scanning setup and non-perturbing field probes were employed to investigate spatial electric field distributions in a full length homogeneous human model at the above

mentioned frequencies both in far and near field of the resonant dipole antennas. Frequency dependent spatial SAR distributions and average values were analyzed. It was reported that, in far-field exposure scenario, SAR value reduces exponentially with the direction of propagation in torso at all frequencies of interest [18]. Later in 1997, Meier et al. reported dependence of electromagnetic energy absorption rate on human head phantom modeling in particular at 1800 MHz. This investigation was of immense importance since few peripheral tissue layer thicknesses are of the order of  $\lambda/4$  to  $\lambda/2$  thickness in between 1.5 GHz and 2.5 GHz (bands utilized then for mobile communications) [19]. In 2006, SAR values inside a human head equivalent phantom model have been simulated using Finite Difference Time Domain (FDTD) method (mesh sizes of 2 mm) due to cellular phone exposure at 915 MHz and 1900 MHz – the effects on SAR values due to presence of a metallic spectacle frame and metallic tooth caps have also been investigated in the multi-tissue layer head and hand phantom models. In this article, Yelkenci reported that presence of the metallic spectacle frame can increase SAR values – however, metallic tooth caps had insignificant contribution on reported SAR values [20]. In 2015, Gandhi confirmed that mobile phone exposure induced electromagnetic energy absorption rate among children is higher while compared to adults [21]. Takei et al. reported variation in SAR values due to various positions of a smart phone near the torso at 900 MHz and 2 GHz. The numerical simulations have been performed using realistic Japanese male and female adult models. Irrespective of smart phone position and placement, the 10g averaged SAR value (10g SAR) was reported to be higher at 2 GHz compared to 900 MHz. Over and above, 10g SAR had a trend to increase while the smart phone was positioned in vertical orientation with respect to torso. Observations indicate 10g SAR value primarily depends on tilt angle but not on placement height [22]. In 2002, Cooper et al. reported an investigation to determine safe distance for human body in near field of a cellular base station antenna – this work has been carried out in accordance with the IEEE standard and ICNIRP guidelines [23]. Christ et al. investigated and reported the dependence of electromagnetic energy absorption on body tissue composition particularly in far-field exposure scenarios over 300 MHz to 6 GHz. The article, published in 2006, further indicated that for some specific separation in between the half-wave dipole antenna and body (around  $\lambda/3$ ), strong standing wave phenomena dominate in the coupling mechanism and thus lead to increased SAR value in layered tissue mediums [24]. In 2006, Karunarathna and Dayawansa investigated and reported electromagnetic energy absorption in human body due to

microwave emissions in Sri Lanka. In this article, SAR values have been investigated over 100 MHz to 2500 MHz for human organs like eye, testis, brain and kidney – results indicate that in general the maximum SAR values increase with frequency [25]. In the very next year, Hirata et al. published a brief communication on the dominant factors that influence whole body average SAR values in far field exposure scenario specifically near the frequency of whole body resonance and in GHz region. Computational results indicate that electromagnetic absorption rate reaches its peak around the resonance frequency and largely depends upon the tissue dielectric properties – however, the peak SAR value in GHz region is mainly dependent upon the surface area of the biological model [26]. Next, Hirata et al. conservatively estimated whole body averaged SAR values for nine months old infant employing a simple homogeneous phantom model in GHz region – the simulations have been performed over 1 GHz to 6 GHz in far field exposure scenario [27]. In 2008, a novel SAR measurement method has been reported employing a flat solid phantom model with multiple embedded electric field probes. Iyama et al. designed a measurement configuration to attain SAR distributions within 10% error limit both at 900 and 1950 MHz [28]. Wessapan et al. investigated SAR and temperature distributions in human head model due to mobile phone radiation exposure at multiple frequency bands (900 MHz and 1800 MHz) in 2012. In a real like human head model, the contributions of frequency and separation between mobile phone and human head on SAR and temperature profiles have been investigated. It should be noted that the temperature distribution is not directly proportional to the local SAR profile – as reported in this article [29]. In the following year (2013), Wessapan and Rattanadecho reported SAR profile and temperature increase in human eye because of electromagnetic exposure at 900 MHz and 1800 MHz. It was reported that temperature distribution in human eye is not directly proportionate to SAR distribution – as, tissue dielectric and thermal properties, blood perfusion and depth of penetration play important roles. In addition, this investigation demonstrated the influence of exposure time on temperature increment in the eye [30].

It's a fact that, even before ten years from now, SAR values and their spatial distributions have been evaluated using simulations and measurements only for human models [18-30]. However, high dielectric constant ( $\epsilon_r$ ) of fruit / plant tissues along with past developments related to SAR simulations and measurements in human models have significantly motivated to estimate SAR data and their spatial distributions in different fruit and plant models at far field exposure



scenario. As a consequence, rigorous SAR simulations have been performed and reported later in this thesis for various fruit and plant models under different exposure scenarios.

## **2.4 Disagreement among Different Electromagnetic Guidelines**

In the previous section, relevant articles on electromagnetic energy absorption rate (SAR) analyses in different human equivalent phantom models have been reviewed [18-30]. Based on the analyses, significant SAR values have been noted in different human models – in addition, there are a number of published articles that reported electromagnetic irradiation induced biological responses in humans [31-36]. Therefore, rational electromagnetic exposure limits must be prescribed to restrict maximum permissible SAR value in human body based on averaging tissue mass. In this connection, a number of international and national authorities have come up with different electromagnetic exposure regulatory guidelines – these guidelines have been adopted across the world [37-42]. In these electromagnetic exposure guidelines, frequency dependent reference power densities or plane wave equivalent field strengths have been capped for far field exposure scenario – in addition to basic SAR limits for humans [37-42].

However, it is crucial to note that the frequency dependent reference power density or equivalent field strength values for far field exposure have been capped at different limits based on the regulatory guidelines in effect. Thus, even at a particular frequency, prescribed electromagnetic power density levels can differ by factors of 10 to 100, depending upon the adopted electromagnetic regulatory guidelines [37-42]. To be specific, far and wide adopted international electromagnetic regulatory guidelines have been prescribed by two particular international organizations – Federal Communications Commission (FCC) and International Commission on Non-Ionizing Radiation Protection (ICNIRP) [37-38]. In addition, there are some stringent national electromagnetic exposure regulatory standards in countries like India, Switzerland, Russia and Italy etc. [39-42]. In general, stringent national electromagnetic regulatory standards have been followed to address potential health concerns and increasing awareness among general public [31-36].

It should be noted that different international and national electromagnetic regulatory guidelines have been prepared based on significantly diversified geographical locations, technical backgrounds, medical protocols and purposes to protect human lives on earth [37-42, 75-76]. Some of these standards have been prescribed to protect from immediate thermal effects of

microwave irradiation over short duration, few others plan to mitigate non-thermal biological effects over long duration exposure, whereas, the rest have been drafted to ensure enough safety measures against yet unknown health effects in humans. Furthermore, it should be noted that individual electromagnetic regulatory standards are consistent with the course of action promoted by respective governing authorities [76].

However, as discussed earlier in this section, there is a severe lack of harmonization among these international and national electromagnetic regulatory standards. To be a bit specific, it should be noted that FCC and ICNIRP prescribed public electromagnetic exposure standards differ by a narrow margin below 2000 MHz and are exactly identical thereafter – FCC prescribed power density levels are 33% and 8.5% higher (compared to ICNIRP) at 947.5 MHz and 1842.5 MHz respectively (please, refer to Table 2.1). These two international electromagnetic exposure standards are quite relaxed compared to other national electromagnetic exposure standards [37-42, 76]. In contrast, Indian public electromagnetic exposure standards are at moderate levels i.e. the prescribed reference power density levels are at  $1/10^{\text{th}}$  levels compared to ICNIRP standards – please, refer to Table 2.1 [38-39]. The most stringent public electromagnetic exposure standards have been adopted in Switzerland at  $1/100^{\text{th}}$  reference power density levels with respect to ICNIRP guidelines [38-40, 76]. All the above mentioned electromagnetic exposure standards have been prescribed for public exposure only. However, FCC and ICNIRP prescribed occupational exposure power density levels are five times more relaxed compared to respective power density levels for public exposure scenarios [37-38].

Table 2.1 Lack of harmonization among different international and national electromagnetic exposure regulatory standards [37-42, 76]

Frequency of exposure (MHz)	Prescribed power density level ( $W/m^2$ )					
	Occupational Zone			Public Zone		
	FCC	ICNIRP	FCC	ICNIRP	India	Swiss
947.5	31.58	23.69	6.32	4.74	0.47	0.047
1842.5	50	46.06	10	9.21	0.92	0.092
2150	50	50	10	10	1	0.1
2350	50	50	10	10	1	0.1
2450	50	50	10	10	1	0.1

Now, SAR value at a particular point ( $\sigma|E|^2/2\rho$ ) directly depends upon the square of electric field magnitude developed inside biological tissue – where,  $\sigma$  is electrical conductivity of biological tissue,  $E$  is the developed peak electric field strength inside biological tissue and  $\rho$  is biological tissue density [18-30]. Furthermore, this internal electric field strength magnitude develops in direct proportion with the incident electric field strength. Thus, SAR value and its spatial magnitude distribution directly vary with the magnitude of incident plane wave power density. Hence, the lack of harmonization among different international and national electromagnetic regulatory guidelines has prompted to investigate the variation in SAR values among different prototyped fruit, plant and crop structures across geographical boundaries with contrasting electromagnetic exposure regulatory standards [37-42, 76].

## **2.5 Multilayer Tissues Equivalent Homogeneous Phantom Liquid**

It is well known that interaction of living biological objects with electromagnetic energy is unavoidable due to immense utilization of wireless telecommunication infrastructures over a broad frequency spectrum. This interaction mechanism can take place either in near field (e.g. mobile phone emission) or in far field (e.g. mobile tower radiation) of the radiating element based on application [18-30]. Therefore, it is necessary to quantify electromagnetic energy absorption rate (SAR) due to either near field exposure close to the radiating antenna or plane wave incidence in the far field exposure scenario [37-38, 77-78]. It is an established fact that the SAR value is dependent on shape of biological model, number of distinct dielectric tissue layers, complex dielectric constant ( $\epsilon_r$ ) of each tissue layer, tissue density of each layer and incident field strength [18-30, 37-38, 77-78]. The mathematical expression for point SAR is  $\sigma|E|^2/2\rho$  – where,  $\sigma$ ,  $E$  and  $\rho$  represent the respective parameters discussed in the previous section. It is clear that point SAR is dependent on the second degree of peak electric field strength developed inside biological tissue. Therefore, for practical SAR measurement, electric field probing inside prototyped biological model is absolutely necessary. However, invasive techniques that involve inserting electric field probe inside living biological object are avoided due to medical ethical guidelines. Thus, to circumvent this measurement challenge, few rudimentary attempts have been made to formulate and prepare multilayer tissues equivalent homogeneous phantom liquid with predefined dispersive dielectric properties ( $\epsilon_r$ ) [19, 77-83]. At initial phase, human head equivalent homogeneous phantom liquid formulations were proposed to possess average

dielectric properties ( $\epsilon_r$ ) in between grey matter and white matter; after that, those phantom liquids were utilized for frequency dependent practical SAR measurements [19, 79-80]. Later on, a multilayer tissues equivalent homogeneous dielectric liquid recipe was formulated and proposed based on the average permittivity ( $\epsilon_r'$ ) of all tissue layers and further tuning the conductivity ( $\sigma$ ) to match 1g or 10g averaged SAR value in specific phantom model – this research work was reported by Drossos et al. in the year 2000 [81]. In 2002, Monebhurrin et al. proposed a set of head equivalent phantom liquids based on tuning the maximum 10g averaged SAR value with appropriate set of dielectric properties ( $\epsilon_r$ ) [82]. Later in 2010, Monebhurrin confirmed that the SAM phantom with homogeneous liquid and typical frequency dependent dielectric properties ( $\epsilon_r$ ) can provide conservative SAR estimation in child's head model [83].

However, none of the above mentioned techniques attempted to tune and match the electric field or point SAR distributions inside original multilayered tissue model and the equivalent homogeneous phantom liquid [19, 77-83]. Therefore, the above reported articles have motivated to initiate further research on alignment of spatial point SAR distributions between original multilayer tissue model and equivalent homogeneous liquid on three dimensional coordinate bases. Till present time, no generalized and structured framework has been defined to find out equivalent dielectric properties ( $\epsilon_r$ ) of homogeneous phantom liquid based on dielectric properties ( $\epsilon_r$ ), thickness, stacking distribution and geometric shape of original tissue layers – irrespective of far or near field exposure scenarios. Hence, based on the reported articles, a further generalized algorithm has been developed later in this thesis to synthesize permittivity ( $\epsilon_r'$ ) and loss tangent ( $\tan \delta$ ) of the homogeneous phantom liquid equivalent to arbitrary combinations of stacked tissue layers – the work has been performed aiming accurate practical SAR measurement with precise phantom liquid characteristics.

## 2.6 Phantom Liquid Recipes for SAR Measurement

In the second section of this chapter, a thorough literature review on broadband dielectric properties ( $\epsilon_r$ ) i.e. both permittivity ( $\epsilon_r'$ ) and loss tangent ( $\tan \delta$ ) characterization of different plant, fruit and crop specimens have been performed [7-17]. Based on the reported articles in literature, it is noted that plant, fruit and crop tissues possess quite high complex dielectric properties ( $\epsilon_r$ ) over a broad frequency spectrum. Next, in last part of section 2.3, it is also mentioned that SAR analyses should be performed for the prototyped fruit and plant models as

the constituent tissues possess quite high permittivity ( $\epsilon_r'$ ) and loss tangent ( $\tan \delta$ ) [7-17]. The SAR evaluation can be performed either using numerical simulation or employing practical measurement in customized fruit or plant model filled with tissue equivalent liquid – in particular, considering far-field exposure scenario. To this end, SAR simulations along with spatial distributions have been performed for a number of fruit and plant models later in this thesis (Chapter 4) [84]. Plane wave exposure condition and time domain solver have been employed together in CST Microwave Studio (CST MWS) to simulate SAR data for the prototyped models [84-86]. Once SAR simulations have been performed, customized models along with fruit and plant tissue equivalent phantom liquids need to be prepared for practical validation of simulated SAR data. Therefore, fruit and plant tissue equivalent phantom liquid recipes with appropriate dielectric properties ( $\epsilon_r$ ) should be prepared for practical SAR measurements. It should be taken into consideration that prepared phantom liquids must be non-toxic, non-corrosive to the non-resonant electric field probe and phantom shell – in addition, the liquids should have low viscosity for easy movement of the probe [87-88]. In general, standard chemical formulations and frequency specific dielectric properties ( $\epsilon_r$ ) are available for composite human body and head equivalent homogeneous phantom liquids [77-78, 89-90]. Human tissue equivalent phantom liquid recipes can be formulated with sugar, glycol or diacetic acid based solutions based on frequency range, reference permittivity ( $\epsilon_r'$ ) and loss tangent ( $\tan \delta$ ) values. In general, sugar and water based tissue equivalent liquid recipes are formulated at around 900 MHz – whereas, glycol and water based phantom liquid recipes are preferred at 1800 MHz and 2450 MHz [87-88, 91-98].

It's a fact that till now standard phantom liquid recipes have been formulated only for composite human tissues equivalent model [87-98]. Those liquids have been used for SAR measurements in human body or head equivalent phantom models primarily due to near-field exposure from mobile phone or any other near body microwave transmitter [77-78, 89-90]. However, it can be stated that those previous developments related to human body or head equivalent phantom liquids formulation have helped a lot to outline the shape and direction of this thesis – in particular, to formulate the frequency band specific customized phantom liquids for different fruit or plant tissues. Moreover, the dependence of phantom liquid permittivity ( $\epsilon_r'$ ) and loss tangent ( $\tan \delta$ ) on different chemical constituents have been understood from the related literature articles [87-88, 91-98]. This knowledge base is indeed helpful to formulate phantom

liquids for different fruit and plant tissues with diversified complex dielectric properties ( $\epsilon_r$ ) at multiple frequencies of interest.

## **2.7 Electromagnetic Irradiation Induced Responses in Plants**

The ever increasing utilization of different wireless technologies is reported to cause measurable biological responses on wide range of plants and crops – however, all of these research articles have been reported primarily in past two decades [43-47, 71-74, 99-128]. Therefore, it can easily be interpreted that this particular research domain is at an early stage and needs further attention for development and growth.

In 2002, Scialabba and Tamburello reported 10.50 GHz and 12.50 GHz electromagnetic exposure induced effects on germination and subsequent growth of radish seedlings. To be specific, germination of radish seeds was reported to be delayed and reduced due to low power electromagnetic irradiation at the above mentioned frequencies. Moreover, the electromagnetic exposure also reduced hypocotyl growth rate. The reported effects were noted to be increased with rise in electromagnetic power level [99]. In the same year (2002), Tafforeau et al. reported that epidermal meristem production was induced in flax due to low intensity 0.90 GHz electromagnetic irradiation over two hours at non-thermal level using GSM telephone [100]. Later in 2005, Sandu et al. investigated effects of electromagnetic field on chlorophyll contents in black locust leaves. Three months old black locust seedlings were irradiated to 400 MHz electromagnetic radiation at low power density level. After regular irradiations (for 1, 2, 3 and 8 hours per day) over three weeks, chlorophyll A and chlorophyll B levels were reported to be reduced and statistical significances were tested with respect to control specimens using t-tests [101]. Challis reviewed and reported different interaction mechanisms between electromagnetic fields and biological tissue in 2005 [102]. Next year, a chapter entitled ‘Electrical Signals in Plants: Facts and Hypotheses’ was published by Davies in the book ‘Plant Electrophysiology’ [103]. In 2006, Davies and Stankovic published another chapter on ‘Electrical Signals, the Cytoskeleton and Gene Expression: A Hypothesis on the Coherence of the Cellular Responses to Environmental Insult’ in a book entitled ‘Communication in Plants’ [104]. Both of these book chapters are helpful to explain possible disproportion of  $Ca^{2+}$ ,  $K^{1+}$  and  $Na^{1+}$  concentrations in plant cell under electromagnetic irradiation [103-104]. Roux et al. and Vian et al. investigated and reported controlled electromagnetic irradiation (900 MHz) induced molecular responses i.e.

stress-sensitive gene expression alterations in tomato plants [44-45]. In particular, three weeks old tomato plants have been exposed to short-duration, controlled and deterministic electromagnetic fields at 900 MHz inside a Mode Stirred Reverberation Chamber (MSRC). Upregulated expressions of stress-sensitive transcripts (calmodulin, protease inhibitor, chloroplast mRNA-binding protein and bZIP transcription factor) have been noted following the controlled electromagnetic irradiation at 900 MHz [44-45]. Next in 2007, Beaubois et al. reported intercellular communication in tomato plants due to electromagnetic stimulation [71]. Electromagnetic exposure was reported to induce rapid and substantial bZIP mRNA accumulation in terminal leaf of wild-type tomato plant. In spite of just irradiating the oldest leaf, bZIP mRNA accumulation was reported both in the local exposed leaf as well as in the distant unexposed leaf – however, somewhat delayed accumulation was noted in the distant leaf. Moreover, mRNA accumulation level of PIN2 was reported to be less than bZIP – both in the exposed as well as distant leaves with no delay in systemic response [71]. Furthermore, in 2008, Roux et al. reported that short duration and low amplitude electromagnetic field at 900 MHz caused rapid reduction in ATP concentration and Adenylate Energy Charge (AEC) in tomato plants [105]. In the same year, Roux et al. further confirmed that short duration, controlled and deterministic electromagnetic exposure at 900 MHz, 5 V/m can affect transcription, translation, calcium and energy charge in tomato plants [106]. In 2009, Balmori reported effects of electromagnetic pollution on wildlife, trees and plants [46]. In the same year, Ursache et al. reported the effects of electromagnetic exposure on vegetal (maize) organisms [107]. In 2009, Tkalec et al. published an article on electromagnetic field induced effects on onion seed germination and root meristematic cells [108]. Sharma et al. reported that mobile phone radiation induces oxidative stress and inhibits root growth in mung bean – published in 2009 [109]. Later in 2010, Panagopoulos et al. reported biological effects of radiation with respect to field intensity or distance from the transmitting antenna [72]. Furthermore, in 2010, Jangid et al. investigated electromagnetic irradiation induced mutations and gene expression alterations in moth bean [110]. Once again, Sharma et al. investigated and reported that mobile phone emitted radiation causes biochemical alterations and affects early stage growth in mung bean [111]. In 2012, Sivani and Sudarsanam reviewed research work on electromagnetic irradiation induced effect on several biological systems including plants [73]. In the same year, Akbal et al. reported effects of mobile phone radiation on lentil seed germination, root growth and mitotic division of root tip

cell [112]. Singh et al. reported that cell phone radiation (900 MHz) affects rhizogenesis in mung bean through impairing biochemical processes [113]. Next in 2013, Cucurachi et al. reviewed electromagnetic irradiation induced ecological effects on several biological systems including plants [74]. In the same year, Pesnya and Romanovsky investigated cytotoxic and genotoxic effects of GSM 900 MHz mobile phone radiation on onion – results have been further compared with the effects due to plutonium-239 alpha particles. GSM 900 MHz radiation was reported to increase mitotic index, rate of mitotic and chromosome abnormalities and micronucleus frequency in time dependent manner [114]. In 2014, Chen and Chen investigated mobile phone radiation effects on seed germination and initial growth of five bean species – different germination rates were observed among the bean species [115]. In the same year, long duration electromagnetic irradiation induced effects on mRNA expressions of stress related proteins were investigated in *Lycopersicon esculentum* – expressions for proteinase inhibitor (PIN II) and *Lycopersicon esculentum* basic leucine Zipper1 (lebZIP1) were upregulated following the electromagnetic exposure, as reported by Rammal et al. [116]. In 2014, Sharma and Parihar reported mobile phone irradiation induced effects on nodule formation in leguminous plants. The investigation reported that mobile phone radiation interacts with morphological and biochemical processes – thus, further affects growth and nodule formation in leguminous plants. It was reported that more number of nodules developed with increased radiation exposure [117]. In the next year, reduced soybean seedling growth was reported following weak electromagnetic exposure at 900 MHz – as investigated by Halgamuge et al. [118]. In 2015, Racuciu et al. reported inhibited seedling growth in maize due to low intensity electromagnetic irradiation [119]. Once again, in the same year, Kumar et al. further reported 1800 MHz electromagnetic irradiation induced early seedling growth inhibition in maize due to alterations in starch and sucrose metabolism [120]. Later in 2016, Grémiaux et al. reported that low intensity electromagnetic field at 900 MHz inside MSRC induces delayed and reduced growth of *Rosa* hybrid plant [121]. In the same year, Waldmann-Selsam et al. concluded that electromagnetic radiations injure plants and trees near mobile phone base stations. Based on the statistical analyses, it was reported that mobile tower radiation is harmful for plants and trees – in general, radiation evoked damage starts on one side of a tree and then extending further to the whole tree with time [122]. In 2016, Vian et al. further reviewed and summarized a number of articles related to electromagnetic irradiation induced responses in plants, at different frequencies [47].



In the following year (2017), Halgamuge reviewed a number of articles on weak electromagnetic irradiation induced effects on different plant species and summarized the reported findings. Based on the available articles, it was reported that plants do respond significantly following exposure to electromagnetic radiation [123]. Stefi et al. investigated and reported long duration electromagnetic irradiation induced effects on maize plants in controlled laboratory environment – the structural conformation of chloroplasts within bundle sheath cells of the radiation treated leaves were observed to be affected [124]. Later in 2018, Stefi et al. reported that GSM radiation can cause oxidative stress and animal neurotransmitter synthesizing enzyme accumulation in the leaves of wild growing myrtle [125]. Once again, in 2020, Stefi et al. investigated long term non-ionizing electromagnetic irradiation evoked responses in young *Nerium oleander* plants [126]. Under the above mentioned electromagnetic irradiation, *Nerium oleander* plants exhibited significant structural modifications such as flattening of crypts, elimination of trichomes and reduced layers of epidermal cells. Furthermore, considerable amplification in reactive oxygen species has been noted both at roots and above ground parts. Reduced light absorbance by photosynthetic pigments as well as significantly enhanced biosynthesis of L-Dopa decarboxylase (an enzyme helps in catalyzing the production of secondary metabolites that alleviate stress) has been noted due to the above mentioned long duration electromagnetic irradiation. However, the radiation treated plants exhibited larger primary plant productivity – in spite of reduced photosynthetic pigments and oxidative stress [126]. In recent times (2020), Czerwinski et al. reviewed a number of articles and summarized the influence of mobile telephony radiation on plant community as a whole – the possible interaction mechanisms along with potential indicators have also been investigated [127]. In 2021, Kaur et al. reviewed the impact of high frequency electromagnetic radiation on development of plants along with associated physiological, biochemical and molecular processes. They proposed that electromagnetic irradiation evokes increase in reactive oxygen species metabolism and cytosolic calcium in plants – as a consequence, gene expression alterations and enzymatic activities take place and result in either direct cellular alterations or deferred plant growth [128].

Based on the articles available in literature, it is noted that mobile phones have been utilized in a number of experiments to investigate electromagnetic irradiation induced responses in plants – unfortunately, these wireless devices can't produce entirely deterministic and controlled electromagnetic environment in laboratory conditions [109, 112, 114-115, 117-118]. In addition,

mobile phones emit electromagnetic energy with fixed propagation direction and polarization – as a result, plants get exposed to radiation from only one direction with a particular wave polarization. Therefore, it is difficult to interpret dose-dependent effects of electromagnetic radiation with targeted plant responses. In contrast, controlled and deterministic electromagnetic irradiation induced plant responses have been investigated in a limited manner – particularly at physiological and molecular levels [43-45, 47, 71, 105-106, 121]. Hence, based on the reviewed articles, a significant scope has been found to investigate long duration as well as short duration, controlled and deterministic electromagnetic irradiation induced physiological and molecular consequence in plants. Controlled and deterministic electromagnetic irradiation induced effects on seed germination rate, photosynthetic pigment profiles and stress-sensitive gene expressions can be investigated in model plants. Thus, the reviewed articles have indeed assisted to decide research direction and shape the structure of this thesis.

## **2.8 Conclusions**

With the advancement of microwave measurement techniques, researchers and scientists have put their efforts to develop dielectric properties ( $\epsilon_r$ ) measurement techniques, characterize dielectric properties of some crop and fruit specimens (in addition to human tissues), estimate electromagnetic energy absorption rate in several human models, establish distinct electromagnetic exposure regulatory guidelines, prescribe human tissue equivalent phantom liquids for SAR measurement and investigate short duration electromagnetic irradiation induced immediate responses in humans and few plants. However, with the fast deployment of wireless communication systems, major investigations have been carried out on electromagnetic energy absorption rate estimation in human models along with potential biological effects – in contrast, much less attention has been paid to estimate SAR in plant, fruit and crop models along with associated biological responses.

It can be argued that electromagnetic theories and measurement techniques developed to analyze SAR distribution in human models can judiciously be applied to investigate SAR distributions in different fruit and plant models at different electromagnetic exposure scenarios. Moreover, controlled and deterministic electromagnetic irradiation induced plant responses at physiological and molecular levels can also be investigated for better understanding of the interaction mechanisms between electromagnetic energy and plants. Hence, this thesis entitled

“**Investigations on the Effects of Electromagnetic Radiation on Indian Flora**” aims at dielectric properties ( $\epsilon_r$ ) characterization of several fruit, flower and plant tissue specimens, estimating SAR distribution in prototyped fruit and plant models under different electromagnetic exposure scenarios, formulating basis to define multilayer tissues equivalent homogeneous dielectric liquid, standardizing fruit and plant phantom liquid recipes for practical SAR measurement and investigating long duration as well as short duration electromagnetic irradiation induced physiological and molecular responses in plants.

## References

- [1] C. Gabriel, S. Gabriel, and Y. E. Corthout, ‘The Dielectric Properties of Biological Tissues: I. Literature Survey’, *Physics in Medicine & Biology*, Vol. 41, No. 11, pp. 2231-2249, 1996.
- [2] S. Gabriel, R. W. Lau, and C. Gabriel, ‘The Dielectric Properties of Biological Tissues: II. Measurements in the Frequency Range 10 Hz to 20 GHz’, *Physics in Medicine & Biology*, Vol. 41, No. 11, pp. 2251-2269, 1996.
- [3] S. Gabriel, R. W. Lau, and C. Gabriel, ‘The Dielectric Properties of Biological Tissues: III. Parametric Models for the Dielectric Spectrum of Tissues’, *Physics in Medicine & Biology*, Vol. 41, No. 11, pp. 2271-2293, 1996.
- [4] N. E. Bengtsson, and P. O. Risman, ‘Dielectric Properties of Foods at 3 GHz as Determined by a Cavity Perturbation Technique’, *Journal of Microwave Power*, Vol. 6, No. 2, pp. 107-123, 1971.
- [5] M. A. Stuchly, T. W. Athey, G. M. Samaras, and G. E. Taylor, ‘Measurement of Radio Frequency Permittivity of Biological Tissues with an Open-Ended Coaxial Line: Part II - Experimental Results’, *IEEE Transactions on Microwave Theory and Techniques*, Vol. 30, No. 1, pp. 87-92, 1982.
- [6] G. P. De Loor, and F. W. Meijboom, ‘The Dielectric Constant of Foods and Other Materials with High Water Contents at Microwave Frequencies’, *International Journal of Food Science & Technology*, Vol. 1, No. 4, pp. 313-322, 1966.
- [7] S. O. Nelson, ‘Microwave Dielectric Properties of Grain and Seed’, *Transactions of the ASAE*, Vol. 16, No. 5, pp. 902-905, 1973.
- [8] S. O. Nelson, ‘Microwave Dielectric Properties of Fresh Fruits and Vegetables’, *Transactions of the ASAE*, Vol. 23, No. 5, pp. 1314-1317, 1980.

- [9] S. O. Nelson, 'Dielectric Properties of Some Fresh Fruits and Vegetables at Frequencies of 2.45 to 22 GHz', *Transactions of the ASAE*, Vol. 26, No. 2, pp. 613-616, 1983.
- [10] S. O. Nelson, 'Dielectric Properties of Agricultural Products – Measurements and Applications', *IEEE transactions on Electrical Insulation*, Vol. 26, No. 5, pp.845-869, 1991.
- [11] W. Kuang, and S. O. Nelson, 'Dielectric Relaxation Characteristics of Fresh Fruits and Vegetables from 3 to 20 GHz', *Journal of Microwave Power and Electromagnetic Energy*, Vol. 32, No. 2, pp. 114-122, 1997.
- [12] J. N. Ikediala, J. Tang, S. R. Drake, and L. G. Neven, 'Dielectric Properties of Apple Cultivars and Codling Moth Larvae', *Transactions of the ASAE*, Vol. 43, No. 5, pp. 1175-1184, 2000.
- [13] S. O. Nelson, 'Measuring Dielectric Properties of Fresh Fruits and Vegetables', *IEEE Antennas and Propagation Society International Symposium. Digest. Held in conjunction with: USNC/CNC/URSI North American Radio Sci. Meeting (Cat. No. 03CH37450)*, Vol. 4, pp. 46-49, June, 2003.
- [14] S. O. Nelson, 'Dielectric Spectroscopy of Fresh Fruits and Vegetables', *2005 IEEE Instrumentation and Measurement Technology Conference (IMTC)*, pp. 360-364, Ottawa, Canada, May, 2005.
- [15] W. C. Guo, S. O. Nelson, S. Trabelsi, and S. J. Kays, '10–1800-MHz Dielectric Properties of Fresh Apples during Storage', *Journal of Food Engineering*, Vol. 83, No. 4, pp. 562-569, 2007.
- [16] S. O. Nelson, and S. Trabelsi, 'Dielectric Spectroscopy Measurements on Fruit, Meat, and Grain', *Transactions of the ASABE*, Vol. 51, No. 5, pp. 1829-1834, 2008.
- [17] S. O. Nelson, 'Dielectric Properties of Agricultural Products and Some Applications', *Research in Agricultural Engineering*, Vol. 54, No. 2, pp. 104-112, 2008.
- [18] S. S. Stuchly, M. A. Stuchly, A. Kraszewski, and G. Hartsgrove, 'Energy Deposition in a Model of Man: Frequency Effects', *IEEE Transactions on Biomedical Engineering*, Vol. 33, No. 7, 1986.
- [19] K. Meier, V. Hombach, R. Kästle, R. Y. Tay, and N. Kuster, 'The Dependence of Electromagnetic Energy Absorption upon Human-Head Modelling at 1800 MHz', *IEEE Transactions on Microwave Theory and Techniques*, Vol. 45, No. 11, 1997.

- [20] T. Yelkenci, 'Effects of Metallic Objects on Specific Absorption Rate in the Human Head for 915 and 1900 MHz Mobile Phones', *Frequenz*, Vol. 60, No. 3-4, pp. 46-50, 2006.
- [21] O. P. Gandhi, 'Yes the Children are More Exposed to Radiofrequency Energy from Mobile Telephones than Adults', *IEEE Access*, Vol. 3, pp. 985-988, 2015.
- [22] R. Takei, T. Nagaoka, K. Saito, S. Watanabe, and M. Takahashi, 'SAR Variation due to Exposure from a Smartphone Held at Various Positions Near the Torso', *IEEE Transactions on Electromagnetic Compatibility*, Vol. 59, No. 2, pp. 747-753, 2017.
- [23] J. Cooper, B. Marx, J. Buhl, and V. Hombach, 'Determination of Safety Distance Limits for a Human near a Cellular Base Station Antenna, Adopting the IEEE Standard or ICNIRP Guidelines', *Bioelectromagnetics*, Vol. 23, No. 6, pp. 429-443, 2002.
- [24] A. Christ, A. Klingenböck, T. Samaras, C. Goiceanu, and N. Kuster, 'The Dependence of Electromagnetic Far-Field Absorption on Body Tissue Composition in the Frequency Range from 300 MHz to 6 GHz', *IEEE Transactions on Microwave Theory and Techniques*, Vol. 54, No. 5, 2006.
- [25] M. A. A. Karunarathna, and I. J. Dayawansa, 'Energy Absorption by the Human Body from RF and Microwave Emissions in Sri Lanka', *Sri Lankan Journal of Physics*, Vol. 7, pp. 35-47, 2006.
- [26] A. Hirata, S. Kodera, J. Wang, and O. Fujiwara, 'Dominant Factors Influencing Whole-Body Average SAR Due to Far-Field Exposure in Whole-Body Resonance Frequency and GHz Regions', *Bioelectromagnetics*, Vol. 28, No. 6, pp. 484-487, 2007.
- [27] A. Hirata, N. Ito, O. Fujiwara, T. Nagaoka, and S. Watanabe, 'Conservative Estimation of Whole-Body-Averaged SARs in Infants with a Homogeneous and Simple-Shaped Phantom in the GHz Region', *Physics in Medicine and Biology*, Vol. 53, No. 24, pp. 7215-7223, 2008.
- [28] T. Iyama, T. Onishi, Y. Tarusawa, and S. Uebayashi and T. Nojima, 'Novel Specific Absorption Rate (SAR) Measurement Method Using a Flat Solid Phantom', *IEEE Transactions on Electromagnetic Compatibility*, Vol. 50, No. 1, pp. 43-51, 2008.
- [29] T. Wessapan, S. Srisawatdhisukul, and P. Rattanadecho, 'Specific Absorption Rate and Temperature Distributions in Human Head Subjected to Mobile Phone Radiation at Different Frequencies', *International Journal of Heat and Mass Transfer*, Vol. 55, No. 1-3, pp. 347-359, 2012.

- [30] T. Wessapan, and P. Rattanadecho, ‘Specific Absorption Rate and Temperature Increase in the Human Eye due to Electromagnetic Fields Exposure at Different Frequencies’, *International Journal of Heat and Mass Transfer*, Vol. 64, pp. 426-435, 2013.
- [31] R. J. Aitken, L. E. Bennetts, D. Sawyer, A. M. Wiklendt, and B. V. King, ‘Impact of Radio Frequency Electromagnetic Radiation on DNA Integrity in the Male Germline’, *International Journal of Andrology*, Vol. 28, No. 3, pp. 171-179, 2005.
- [32] G. Kumar, ‘*Report on Cell Tower Radiation*’, submitted to the secretary, Department of Telecommunications (DoT), Ministry of Communications, New Delhi, India, 2010.
- [33] BioInitiative Working Group, ‘*BioInitiative 2012: A Rationale for a Biologically-Based Exposure Standards for Low-Intensity Electromagnetic Radiation*’, In C. Sage, and D. O. Carpenter (eds): *The BioInitiative Report 2012*, 2012. [www.bioinitiative.org](http://www.bioinitiative.org) [Last accessed 03 April 2022].
- [34] Y. H. Hao, L. Zhao, and R. Y. Peng, ‘Effects of Microwave Radiation on Brain Energy Metabolism and Related Mechanisms’, *Military Medical Research*, Vol. 2, No. 1, pp. 1-8, 2015.
- [35] V. Franchini, E. Regalbuto, A. D. Amicis, S. D. Sanctis, S. D. Cristofaro, E. Coluzzi, J. Marinaccio, A. Sgura, S. Ceccuzzi, A. Doria, and G. P. Gallerano, ‘Genotoxic Effects in Human Fibroblasts Exposed to Microwave Radiation’, *Health Physics*, Vol. 115, No. 1, pp. 126-139, 2018.
- [36] Y. F. Lai, H. Y. Wang, and R. Y. Peng, ‘Establishment of Injury Models in Studies of Biological Effects Induced by Microwave Radiation’, *Military Medical Research*, Vol. 8, Article No. 12, pp. 1-18, 2021.
- [37] R. F. Cleveland, Jr., D. M. Sylvar, and J. L. Ulcek, ‘*Evaluating Compliance with FCC Guidelines for Human Exposure to Radiofrequency Electromagnetic Fields*’, FCC OET Bulletin, Vol. 65, Edition 97-01, Washington D.C., 1997.
- [38] International Commission on Non-Ionizing Radiation Protection (ICNIRP), ‘Guidelines for Limiting Exposure to Electromagnetic Fields (100 kHz to 300 GHz)’, *Health Physics*, Vol. 118, No. 5, pp. 483-524, 2020.
- [39] Department of Telecommunications (DoT), ‘*A Journey for EMF*’, 2012, [www.dot.gov.in/journey-emf](http://www.dot.gov.in/journey-emf) [Last accessed 03 April 2022].
- [40] Swiss Agency for the Environment, Forests and Landscape (SAEFL), ‘*Electrosmog in the Environment*’, pp. 1-56, Switzerland, 2005.

- [41] Ministry of Health of the Russian Federation, ‘*SanPiN 2.1.8/2.2.4.1190-03: Arrangement and Operation of Land Mobile Radiocommunication Facilities – Hygienic Requirements*’, pp. 1-17, Russia, 2003.
- [42] The President of the Council of Ministers (Italy), ‘*Establishment of Exposure Limits, Attention Values, and Quality Goals to Protect the Population against Electric, Magnetic, and Electromagnetic Field Generated at Frequencies between 100 kHz and 300 GHz*’, unofficial translation by P. Vecchia, pp. 1-6, Italy, 2003.
- [43] A. Vian, C. Faure, S. Girard, E. Davies, F. Hallé, P. Bonnet, G. Ledoigt, and F. Paladian, ‘Plants Respond to GSM-Like Radiations’, *Plant Signaling & Behaviour*, Vol. 2, No. 6, pp. 522-524, 2007.
- [44] D. Roux, A. Vian, S. Girard, P. Bonnet, F. Paladian, E. Davies, and G. Ledoigt, ‘Electromagnetic Fields (900 MHz) Evoke Consistent Molecular Responses in Tomato Plants’, *Physiologia Plantarum*, Vol. 128, No. 2, pp. 283-288, 2006.
- [45] A. Vian, D. Roux, S. Girard, P. Bonnet, F. Paladian, E. Davies, and G. Ledoigt, ‘Microwave Irradiation Affects Gene Expression in Plants’, *Plant Signaling & Behavior*, Vol. 1, No. 2, pp. 67-69, 2006.
- [46] A. Balmori, ‘Electromagnetic Pollution from Phone Masts. Effects on Wildlife’, *Pathophysiology*, Vol. 16, No. 2-3, pp. 191-199, 2009.
- [47] A. Vian, E. Davies, M. Gendraud, and P. Bonnet, ‘Plant Responses to High Frequency Electromagnetic Fields’, *BioMed Research International*, Article ID: 1830262, 2016.
- [48] M. S. Venkatesh, and G. S. V. Raghavan, ‘An Overview of Dielectric Properties Measuring Techniques’, *Canadian Biosystems Engineering*, Vol. 47, No. 7, pp. 15-30, 2005.
- [49] S. N. Jha, K. Narsaiah, A. L. Basediya, R. Sharma, P. Jaiswal, R. Kumar, and R. Bhardwaj, ‘Measurement Techniques and Application of Electrical Properties for Nondestructive Quality Evaluation of Foods – A Review’, *Journal of Food Science and Technology*, Vol. 48, No. 4, pp. 387-411, 2011.
- [50] A. P. Gregory, and R. N. Clarke, ‘A Review of RF and Microwave Techniques for Dielectric Measurements on Polar Liquids’, *IEEE Transactions on Dielectrics and Electrical Insulation*, Vol. 13, No. 4, pp. 727-743, 2006.

- [51] S. O. Nelson, and P. G. Bartley (Jr.), 'Open-Ended Coaxial-Line Permittivity Measurements on Pulverized Materials', *IEEE Transactions on Instrumentation and Measurement*, Vol. 47, No. 1, pp. 133-137, 1998.
- [52] G. Deschamps, 'Impedance of an Antenna in a Conducting Medium', *IRE Transactions on Antennas and Propagation*, Vol. 10, No. 5, pp. 648-650, 1962.
- [53] L. Liu, D. Xu, and Z. Jiang, 'Improvement in Dielectric Measurement Technique of Open-Ended Coaxial Line Resonator Method', *Electronics Letters*, Vol. 22, No. 7, pp. 373-375, 1986.
- [54] D. Xu, L. Liu, and Z. Jiang, 'Measurement of the Dielectric Properties of Biological Substances using an Improved Open-Ended Coaxial Line Resonator Method', *IEEE Transactions on Microwave Theory and Techniques*, Vol. 35, No. 12, pp. 1424-1428, 1987.
- [55] M. A. Stuchly, and S. S. Stuchly, 'Coaxial Line Reflection Method for Measuring Dielectric Properties of Biological Substances at Radio and Microwave Frequencies – A Review', *IEEE Transactions on Instrumentation and Measurement*, Vol. 29, No. 3, pp 176-183, 1980.
- [56] T. W. Athey, M. A. Stuchly, and S. S. Stuchly, 'Measurement of Radio Frequency Permittivity of Biological Tissues with an Open-Ended Coaxial Line: Part I', *IEEE Transactions on Microwave Theory and Techniques*, Vol. 30, No. 1, pp 82-86, 1982.
- [57] D. M. Hagl, D. Popovic, S. C. Hagness, J. H. Booske, and M. Okoniewski, 'Sensing Volume of Open-Ended Coaxial Probes for Dielectric Characterization of Breast Tissue at Microwave Frequencies', *IEEE Transactions on Microwave Theory and Techniques*, Vol. 51, No. 4, pp. 1194-1206, 2003.
- [58] R. Zajíček, J. Vrba, and K. Novotný; 'Evaluation of a Reflection Method on an Open-Ended Coaxial Line and its Use in Dielectric Measurements', *Acta Polytechnica*, Vol. 46, No. 5, pp. 50-54, 2006.
- [59] R. Zajíček, L. Oppl, and J. Vrba, 'Broadband Measurement of Complex Permittivity using Reflection Method and Coaxial Probes', *Radioengineering*, Vol.17, No. 1, pp. 14-19, 2008.
- [60] J. S. Bobowski, and T. Johnson, 'Permittivity Measurements of Biological Samples by an Open-Ended Coaxial Line', *Progress in Electromagnetics Research B*, Vol. 40, pp. 159-183, 2012.
- [61] S. O. Nelson, 'Dielectric Properties Measuring Techniques and Applications', *American Society of Agricultural Engineers*, Vol. 42, No. 2, pp. 523-529, 1999.



- [62] M. Sucher, and J. Fox, '*Handbook of Microwave Measurements*', Vol. 2, Chap. 9, Polytechnic Press, Polytechnic Institute of Brooklyn, New York, 1963.
- [63] D. R. Thompson, and G. L. Zachariah, 'Dielectric Theory and Bioelectrical Measurements (Part I. Theoretical)', *Transactions of the ASAE*, Vol. 14, No. 2, pp. 211-0213, 1971.
- [64] D. R. Thompson, and G. L. Zachariah, 'Dielectric Theory and Bioelectrical Measurements (Part II. Experimental)', *Transactions of the ASAE*, Vol. 14, No. 2, pp. 214-0215, 1971.
- [65] A. C. Metaxas, and R. J. Meredith, '*Industrial Microwave Heating*', No. 4, IET, 1983.
- [66] S. O. Nelson, 'Improved Sample Holder for Q-meter Dielectric Measurements', *Transactions of the ASAE*, Vol. 22, No. 4, pp. 950-954, 1979.
- [67] S. O. Nelson, 'A System for Measuring Dielectric Properties at Frequencies from 8.2 to 12.4 GHz', *Transactions of the ASAE*, Vol. 15, No. 6, pp. 1094-1098, 1972.
- [68] A. Kraszewski, 'Microwave Aquametry – A Review', *Journal of Microwave Power*, Vol. 15, No. 4, pp. 209-220, 1980.
- [69] H. E. Bussey, 'Measurement of RF Properties of Materials - A Survey', *Proceedings of IEEE Conference*, Vol. 55, No. 6, pp. 1046-1053, 1967.
- [70] Keysight Technologies, '*Keysight 85070E Dielectric Probe Kit 200 MHz to 50 GHz – Technical Overview*', Available Online: <https://www.keysight.com/us/en/assets/7018-01196/technical-overviews/5989-0222.pdf> (Accessed on 18 Feb, 2022).
- [71] E. Beaubois, S. Girard, S. Lallechere, E. Davies, F. Paladian, P. Bonnet, G. Ledoigt, and A. Vian, 'Intercellular Communication in Plants: Evidence for Two Rapidly Transmitted Systemic Signals Generated in Response to Electromagnetic Field Stimulation in Tomato', *Plant, Cell and Environment*, Vol. 30, No. 7, pp. 834-844, 2007.
- [72] D. J. Panagopoulos, E. D. Chavdoula, and L. H. Margaritis, 'Bioeffects of Mobile Telephony Radiation in Relation to its Intensity or Distance from the Antenna', *International Journal of Radiation Biology*, Vol. 86, No. 5, pp. 345-357, 2010.
- [73] S. Sivani, and D. Sudarsanam, 'Impacts of Radio-Frequency Electromagnetic Field (RF-EMF) from Cell Phone Towers and Wireless Devices on Biosystem and Ecosystem – A Review', *Biology and Medicine*, Vol. 4, No. 4, pp. 202-216, 2012.
- [74] S. Cucurachi, W. L. Tamis, M. G. Vijver, W. J. Peijnenburg, J. F. Bolte, and G. R. de Snoo, 'A Review of the Ecological Effects of Radiofrequency Electromagnetic Fields (RF-EMF)', *Environment International*, Vol. 51, pp. 116-140, 2013.

- [75] P. Vecchia, 'Radiofrequency Fields: Bases for Exposure Limits', 2 *European IRPA Congress on Radiation Protection – Radiation Protection: From Knowledge to Action*, pp. 1-19, Paris, 2006.
- [76] K. R. Foster, 'Exposure Limits for Radiofrequency Energy: Three Models', *Proceedings of the Eastern European Regional EMF Meeting and Workshop (Criteria for EMF Standards Harmonization)*, pp. 1-6, Varna, Bulgaria, 2001.
- [77] IEC/IEEE, 'IEC/IEEE International Standard – Determining the Peak Spatial-Average Specific Absorption Rate (SAR) in the Human Body from Wireless Communications Devices, 30 MHz to 6 GHz - Part 1: General Requirements for using the Finite-Difference Time-Domain (FDTD) Method for SAR Calculations', *IEC/IEEE 62704-1:2017*, pp. 1-86, 2017, <https://webstore.iec.ch/publication/34411> (subscription required)
- [78] IEC/IEEE, 'IEC/IEEE International Standard – Determining the Peak Spatial-Average Specific Absorption Rate (SAR) in the Human Body from Wireless Communications Devices, 30 MHz To 6 GHz – Part 2: Specific Requirements for Finite Difference Time Domain (FDTD) Modelling of Exposure from Vehicle Mounted Antennas', *IEC/IEEE 62704-2:2017*, pp. 1-112, 2017, <https://webstore.iec.ch/publication/31306> (subscription required)
- [79] V. Hombach, K. Meier, M. Burkhardt, E. Kuhn, and N. Kuster, 'The Dependence of EM Energy Absorption upon Human Head Modeling at 900 MHz', *IEEE Transactions on Microwave Theory and Techniques*, Vol. 44, No. 10, pp. 1865-1873, 1996.
- [80] K. Meier, M. Burkhardt, T. Schmid, and N. Kuster, 'Broadband Calibration of E-field Probes in Lossy Media [Mobile Telephone Safety Application]', *IEEE Transactions on Microwave Theory and Techniques*, Vol. 44, No. 10, pp. 1954-1962, 1996.
- [81] A. Drossos, V. Santomaa, and N. Kuster, 'The Dependence of Electromagnetic Energy Absorption upon Human Head Tissue Composition in the Frequency Range of 300-3000 MHz', *IEEE Transactions on Microwave Theory and Techniques*, Vol. 48, No. 11, pp. 1988-1995, 2000.
- [82] V. Monebhurrin, C. Dale, J. C. Bolomey, and J. Wiart, 'A Numerical Approach for the Determination of the Tissue Equivalent Liquid used During SAR Assessments', *IEEE Transactions on Magnetics*, Vol. 38, No. 2, pp. 745-748, 2002.

- [83] V. Monebhurrin, 'Conservativeness of the SAM Phantom for the SAR Evaluation in the Child's Head', *IEEE Transactions on Magnetics*, Vol. 46, No. 8, pp. 3477-3480, 2010.
- [84] CST Studio Suite, [www.3ds.com/products-services/simulia/products/cst-studio-suite](http://www.3ds.com/products-services/simulia/products/cst-studio-suite) [Last accessed 04 April 2022].
- [85] T. Weiland, 'A Discretization Method for the Solution of Maxwell's Equations for Six-Component Fields', *Electronics and Communications AEU*, Vol. 31, No. 3, pp. 116-120, 1977.
- [86] M. Clemens, and T. Weiland, 'Discrete Electromagnetism with the Finite Integration Technique', *Progress In Electromagnetics Research*, Vol. 32, pp. 65-87, 2001.
- [87] M. Douglas, and C. K. Chou, 'Enabling the Use of Broadband Tissue Equivalent Liquids for Specific Absorption Rate Measurements', *2007 IEEE International Symposium on Electromagnetic Compatibility*, pp. 1-6, Honolulu, Hawaii, 2007.
- [88] K. Fukunaga, S. Watanabe, H. Asou, and K. Sato, 'Dielectric Properties of Non-Toxic Tissue-Equivalent Liquids for Radiowave Safety Tests', *IEEE International Conference on Dielectric Liquids (ICDL)*, pp. 425-428, Portugal, Coimbra, 2005.
- [89] D. L. Means, and K. W. Chan, 'Evaluating Compliance with FCC Guidelines for Human Exposure to Radiofrequency Electromagnetic Fields – Additional Information for Evaluating Compliance of Mobile and Portable Devices with FCC Limits for Human Exposure to Radiofrequency Emissions', Supplement C (Edition 01-01) to FCC OET Bulletin 65 (Edition 97-01), Washington D.C., 2001.
- [90] IEC/IEEE, 'Determining the Peak Spatial-Average Specific Absorption Rate (SAR) in the Human Body from Wireless Communications Devices, 30 MHz to 6 GHz - Part 3: Specific Requirements for using the Finite Difference Time Domain (FDTD) Method for SAR Calculations of Mobile Phones', *IEC/IEEE 62704-3:2017*, pp. 1-76, 2017, <https://webstore.iec.ch/publication/29311> (subscription required)
- [91] A. Surowiec, P. N. Shrivastava, M. Astrahan, and Z. Petrovich, 'Utilization of a Multilayer Polyacrylamide Phantom for Evaluation of Hyperthermia Applicators', *International Journal of Hyperthermia*, Vol. 8, No. 6, pp. 795-807, 1992.
- [92] K. Ito, K. Furuya, Y. Okano, and L. Hamada, 'Development and Characteristics of a Biological Tissue-Equivalent Phantom for Microwaves', *Electronics and Communications in Japan (Part I: Communications)*, Vol. 84, No. 4, pp. 67-77, 2001.

- [93] K. Fukunaga, S. Watanabe, and Y. Yamanaka, 'Dielectric Properties of Tissue-Equivalent Liquids and Their Effects on Specific Absorption Rate', *IEEE Transactions on Electromagnetic Compatibility*, Vol. 46, No. 1, pp. 126-129, 2004.
- [94] T. Onishi, R. Ishido, T. Takimoto, K. Saito, S. Uebayashi, M. Takahashi, and K. Ito, 'Biological Tissue-Equivalent Agar-Based Solid Phantoms and SAR Estimation using the Thermographic Method in the Range of 3-6 GHz', *IEICE Transactions on Communications*, Vol. 88, No. 9, pp. 3733-3741, 2005.
- [95] N. Chahat, M. Zhadobov, and R. Sauleau, 'Broadband Tissue-Equivalent Phantom for BAN Applications at Millimeter Waves', *IEEE Transactions on Microwave Theory and Techniques*, Vol. 60, No. 7, pp. 2259-2266, 2012.
- [96] K. Quelever, T. Coradin, C. Bonhomme, O. Meyer, B. Derat, 'Composition Simulating the Dielectric Properties of the Human Body and Use Thereof for SAR Measurement', *U.S. Patent PCT WO2013079621 (A1)*, 2013.
- [97] R. Mouthaan, and B. Loader, 'Wideband Tissue-Equivalent Liquid for Multiband Specific Absorption Rate Measurements (850 MHz–2.5 GHz)', *Electronics Letters*, Vol. 52, No. 3, pp. 176-177, 2016.
- [98] A. P. Gregory, K. Quéléver, D. Allal, and O. Jawad, 'Validation of a Broadband Tissue-Equivalent Liquid for SAR Measurement and Monitoring of its Dielectric Properties for Use in a Sealed Phantom', *Sensors*, Vol. 20, No. 10, Article No. 2956, pp. 1-13, 2020.
- [99] A. Scialabba, and C. Tamburello, 'Microwave Effects on Germination and Growth of Radish (*Raphanus sativus* L.) Seedlings', *Acta Botanica Gallica*, Vol. 149, No. 2, pp. 113-123, 2002.
- [100] M. Tafforeau, M. C. Verdus, V. Norris, G. White, M. Demarty, M. Thellier, and C. Ripoll, 'SIMS Study of the Calcium-Deprivation Step Related to Epidermal Meristem Production Induced in Flax by Cold Shock or Radiation from a GSM Telephone', *Journal of Trace and Microprobe Techniques*, Vol. 20, No. 4, pp. 611-623, 2002.
- [101] D. D. Sandu, C. Goiceanu, A. Ispas, I. Creanga, S. Miclaus, and D. E. Creanga, 'A Preliminary Study on Ultra High Frequency Electromagnetic Fields Effect on Black Locust Chlorophylls', *Acta Biologica Hungarica*, Vol. 56, No. 1-2, pp. 109-117, 2005.
- [102] L. J. Challis, 'Mechanisms for Interaction between RF Fields and Biological Tissues', *Bioelectromagnetics*, Vol. 26, No. S7, pp. S98-S106, 2005.

- [103] E. Davies, 'Electrical Signals in Plants: Facts and Hypotheses', In A. G. Volkov (eds): *Plant Electrophysiology*, Springer, pp 407-422, Berlin, Germany, 2006.
- [104] E. Davies, and B. Stankovic, 'Electrical Signals, the Cytoskeleton, and Gene Expression: A Hypothesis on the Coherence of the Cellular Responses to Environmental Insult', In F. Baluška, S. Mancuso, D. Volkmann (eds): *Communication in Plants*, Springer. pp 309-320, Berlin, Germany, 2006.
- [105] D. Roux, C. Faure, P. Bonnet, S. Girard, G. Ledoigt, E. Davies, M. Gendraud, F. Paladian, and A. Vian, 'A Possible Role for Extra-Cellular ATP in Plant Responses to High Frequency, Low Amplitude Electromagnetic Field', *Plant Signaling & Behaviour*, Vol. 3, No. 6, pp. 383-385, 2008.
- [106] D. Roux, A. Vian, S. Girard, P. Bonnet, F. Paladian, E. Davies, and G. Ledoigt, 'High Frequency (900MHz) Low Amplitude (5V m<sup>-1</sup>) Electromagnetic Field: A Genuine Environmental Stimulus that Affects Transcription, Translation, Calcium and Energy Charge in Tomato', *Planta*, Vol. 227, No. 4, pp. 883-891, 2008.
- [107] M. Ursache, G. Mindru, D. E. Creangă, F. M. Tufescu, and C. Goiceanu, 'The Effects of High Frequency Electromagnetic Waves on the Vegetal Organisms', *Romanian Journal of Physics*, Vol. 54, No. 1-2, pp. 133-145, 2009.
- [108] M. Tkalec, K. Malarić, M. Pavlica, B. Pevalek-Kozlina, and Ž. Vidaković-Cifrek, 'Effects of Radiofrequency Electromagnetic Fields on Seed Germination and Root Meristematic Cells of *Allium cepa L*', *Mutation Research/Genetic Toxicology and Environmental Mutagenesis*, Vol. 672, No. 2, pp. 76-81, 2009.
- [109] V. P. Sharma, H. P. Singh, R. K. Kohli, and D. R. Batish, 'Mobile Phone Radiation Inhibits *Vigna radiata* (Mung Bean) Root Growth by Inducing Oxidative Stress', *Science of the Total Environment*, Vol. 407, No. 21, pp. 5543-5547, 2009.
- [110] R. K. Jangid, R. Sharma, Y. Sudarsan, S. Eapen, G. Singh, and A. K. Purohit, 'Microwave Treatment Induced Mutations and Altered Gene Expression in *Vigna aconitifolia*', *Biologia Plantarum*, Vol. 54, No. 4, pp. 703-706, 2010.
- [111] V. P. Sharma, H. P. Singh, D. R. Batish, and R. K. Kohli, 'Cell Phone Radiations Affect Early Growth of *Vigna radiata* (Mung Bean) Through Biochemical Alterations', *Zeitschrift für Naturforschung C*, Vol. 65, No. 1-2, pp. 66-72, 2010.

- [112] A. Akbal, Y. Kiran, A. Sahin, D. Turgut-Balik, and H. H. Balik, 'Effects of Electromagnetic Waves Emitted by Mobile Phones on Germination, Root Growth, and Root Tip Cell Mitotic Division of *Lens culinaris* Medik', *Polish Journal of Environmental Studies*, Vol. 21, No. 1, pp. 23-29, 2012.
- [113] H. P. Singh, V. P. Sharma, D. R. Batish, and R. K. Kohli, 'Cell Phone Electromagnetic Field Radiations Affect Rhizogenesis through Impairment of Biochemical Processes', *Environmental Monitoring and Assessment*, Vol. 184, No. 4, pp. 1813-1821, 2012.
- [114] D. S. Pesnya, and A. V. Romanovsky, 'Comparison of Cytotoxic and Genotoxic Effects of Plutonium-239 Alpha Particles and Mobile Phone GSM 900 Radiation in the *Allium cepa* Test', *Mutation Research/Genetic Toxicology and Environmental Mutagenesis*, Vol. 750, No. 1-2, pp. 27-33, 2013.
- [115] Y. C. Chen, and C. Chen, 'Effects of Mobile Phone Radiation on Germination and Early Growth of Different Bean Species', *Polish Journal of Environmental Studies*, Vol. 23, No. 6, pp. 1949-1958, 2014.
- [116] M. Rammal, F. Jebai, H. Rammal, and W. H. Joumaa, 'Effects of Long Term Exposure to RF/MW Radiations on the Expression of mRNA of Stress Proteins in *Lycopersicon esculentum*', *WSEAS Transactions on Biology and Biomedicine*, Vol. 11, pp. 10-14, 2014.
- [117] S. Sharma, and L. Parihar, 'Effect of Mobile Phone Radiation on Nodule Formation in the Leguminous Plants', *Current World Environment*, Vol. 9, No. 1, pp. 145-155, 2014.
- [118] M. N. Halgamuge, S. K. Yak, and J. L. Eberhardt, 'Reduced Growth of Soybean Seedlings After Exposure to Weak Microwave Radiation from GSM 900 Mobile Phone and Base Station', *Bioelectromagnetics*, Vol. 36, No. 2, pp. 87-95, 2015.
- [119] M. Racuciu, C. Iftode, and S. Miclaus, 'Inhibitory Effects of Low Thermal Radiofrequency Radiation on Physiological Parameters of *Zea mays* Seedlings Growth', *Romanian Journal of Physics*, Vol. 60, No. 3-4, pp. 603-612, 2015.
- [120] A. Kumar, H. P. Singh, D. R. Batish, S. Kaur, and R. K. Kohli, 'EMF Radiations (1800 MHz)-Inhibited Early Seedling Growth of Maize (*Zea mays*) Involves Alterations in Starch and Sucrose Metabolism', *Protoplasma*, Vol. 253, No. 4, pp. 1043-1049, 2015.

- [121] A. Grémiaux, S. Girard, V. Guérin, J. Lothier, F. Baluska, E. Davies, P. Bonnet, and A. Vian, 'Low-Amplitude, High-Frequency Electromagnetic Field Exposure Causes Delayed and Reduced Growth in *Rosa hybrida*', *Journal of Plant Physiology*, Vol. 190, pp.44-53, 2016.
- [122] C. Waldmann-Selsam, A. Balmori-de la Puente, H. Breunig, and A. Balmori, 'Radiofrequency Radiation Injures Trees around Mobile Phone Base Stations', *Science of the Total Environment*, Vol. 572, pp. 554-569, 2016.
- [123] M. N. Halgamuge, 'Weak Radiofrequency Radiation Exposure from Mobile Phone Radiation on Plants', *Electromagnetic Biology and Medicine*, Vol. 36, No. 2, pp. 213-235, 2017.
- [124] A. L. Stefi, L. H. Margaritis, and N. S. Christodoulakis, 'The Effect of the Non-Ionizing Radiation on Exposed, Laboratory Cultivated Maize (*Zea mays L.*) Plants', *Flora*, Vol. 233, pp. 22-30, 2017.
- [125] A. L. Stefi, D. Vassilacopoulou, L. H. Margaritis, and N. S. Christodoulakis, 'Oxidative Stress and an Animal Neurotransmitter Synthesizing Enzyme in the Leaves of Wild Growing Myrtle After Exposure to GSM Radiation', *Flora*, Vol. 243, pp. 67-76, 2018.
- [126] A. L. Stefi, K. Mitsigiorgi, D. Vassilacopoulou, and N. S. Christodoulakis, 'Response of Young *Nerium oleander* Plants to Long-Term Non-Ionizing Radiation', *Planta*, Vol. 251, No. 6, Article No. 108, pp. 1-17, 2020.
- [127] M. Czerwinski, L. Januszkiewicz, A. Vian, and A. Lazaro, 'The Influence of Bioactive Mobile Telephony Radiation at the Level of a Plant Community – Possible Mechanisms and Indicators of the Effects', *Ecological Indicators*, Vol. 108, Article No. 105683, pp. 1-11, 2020.
- [128] S. Kaur, A. Vian, S. Chandel, H. P. Singh, D. R. Batish, and R. K. Kohli, 'Sensitivity of Plants to High Frequency Electromagnetic Radiation: Cellular Mechanisms and Morphological Changes', *Reviews in Environmental Science and Bio/Technology*, Vol. 20, No. 1, pp. 55-74, 2021.

# Chapter 3

## Dielectric Properties Characterization and Multilayer Tissue Modeling

---

### Part I: Dielectric Properties Characterization

#### 3.1 Concept of Dielectric Properties

Complex dielectric properties / dielectric constant ( $\epsilon_r$ ) of a material are composed of two associated parameters – the first one is permittivity ( $\epsilon_r'$ ) of the material under consideration and dielectric loss factor ( $\epsilon_r''$ ) of the material is the second one. The permittivity ( $\epsilon_r'$ ) and dielectric loss factor ( $\epsilon_r''$ ) are respective real and imaginary parts of the complex material dielectric properties ( $\epsilon_r$ ), relative to free space,  $\epsilon_r = \epsilon_r' - j\epsilon_r''$  [1-7]. The real part i.e. permittivity ( $\epsilon_r'$ ) of a material is the measure of its ability to polarize and align internal atoms / molecules while an external time-varying electromagnetic field is incident on the same – polarized atoms / molecules realign themselves from their initial equilibrium positions to follow the incident time-varying electric field, and thus, this whole phenomenon results in dielectric polarization. Resultant internal, developed and aligned molecular dipole moments oppose the external incident electric field strength, and thus, reduce the overall electric field strength inside the dielectric material [1-3, 5-6]. Therefore, the real part i.e. permittivity ( $\epsilon_r'$ ) is associated with energy storage potential of the material while an electromagnetic wave gets incident on it. On the other hand, dielectric loss factor ( $\epsilon_r''$ ) signifies energy dissipation / loss within the material that gets converted to heat or any other form [1-7]. Both electrical conductivity ( $\sigma$ ) and loss tangent ( $\tan \delta$ ) of the material can also be calculated from the above mentioned parameters using the following relationships described in Eqs. (3.1) and (3.2) [1, 3, 5].

$$\sigma = \omega \epsilon_0 \epsilon_r'' \quad (3.1)$$

$$\tan \delta = \epsilon_r'' / \epsilon_r' \quad (3.2)$$



Here, angular frequency  $(\omega) = 2\pi f$  where  $f$  represents the frequency of incident electromagnetic field. In addition, the permittivity of free space  $(\epsilon_0) = 8.854 \times 10^{-12}$  F/m.

### 3.1.1 Dipole Moment and Electronic Polarization

In this context, electric dipole moment ( $p$ ) is an important concept – it essentially measures the electrostatic effect of a pair of similar but opposite charges ( $+Q$ ) and ( $-Q$ ) separated by a finite distance ( $a$ ), and is expressed as in Eq. (3.3). The same relation is expressed in Eq. (3.3a) using vector notations – here,  $\vec{a}$  is the distance vector from ( $-Q$ ) to ( $+Q$ ) and  $\vec{p}$  is the electric dipole moment vector [1].

$$p = Qa \quad (3.3)$$

$$\vec{p} = Q\vec{a} \quad (3.3a)$$

In spite of net charge being zero in the atom or molecule, individual electric dipole moment ( $p$ ) gives rise to small local electric field strength inside materials and the same interacts with other electric fields originating from surrounding or external sources – unless, the positive and negative charge centers coincide.

In general, the net charge within a neutral atom or molecule is noted to be zero. Moreover, the center of electrons inside an atom coincides with the center of positive nuclear charges, resulting in zero net dipole moment. However, under externally applied electric field, the light weight electrons get dislocated from their equilibrium positions inside the atom – as a consequence, separation of negative charge center and positive nucleus takes place inside the atom, resulting in an induced dipole moment ( $p_{induced}$ ). This whole phenomenon is called polarization. The induced dipole moment ( $p_{induced}$ ) largely depends on the incident electric field – a new coefficient term ‘polarizability ( $\alpha$ )’ is introduced to define the relation between induced dipole moment ( $p_{induced}$ ) and incident electric field ( $E$ ). The relation is described in Eq. (3.4).

$$p_{induced} = \alpha E \quad (3.4)$$

As polarization of neutral atom takes place due to displacement of light weight electrons, this phenomenon is called electronic polarization with the coefficient known as ‘electronic polarizability ( $\alpha_e$ )’ [1].

In addition, there are some molecules, like water ( $H_2O$ ), that possess permanent dipole moments due to their structural conformations. Thus, the water molecules, in living plant tissues, attempt to follow the externally applied electric field ( $E$ ) due to their permanent dipole moments. As a consequence, frequency dependent complex dielectric properties ( $\epsilon_r$ ) arise due to the orientational polarization of these dipolar molecules [1, 5].

### 3.1.2 Polarization Vector

A material is composed of a large number of atoms and molecules. When the material / substrate is placed in an electric field ( $E$ ), individual atoms and molecules become polarized inside the material / substrate. As a result, a specific distribution of dipole moments is observed inside the material / substrate – directions of all the induced dipole moments are aligned with the applied electric field [1]. If the polarized bulk material is considered, the induced dipoles are aligned head to tail i.e. one after another. As a consequence, each positive charge inside the material has a negative charge next to it and vice versa – thus, there is zero net charge within the bulk material. However, positive charges of the dipoles ( $+Q_p$ ) appearing on one surface are not cancelled due to absence of negative charges at that surface – similarly, negative dipole charges ( $-Q_p$ ) appearing on the opposite surface are also not cancelled by any positive charges. Thus, equal but opposite charges ( $+Q_p$ ) and ( $-Q_p$ ) appear on the two opposite surfaces of a material under the applied electric field ( $E$ ). It should be remembered that these charges are bound to the material and direct result of molecular polarization. The above mentioned bound charges ( $+Q_p$ ) and ( $-Q_p$ ) are known as ‘surface polarization charges’ [1].

Thus, the polarization of a medium is defined by a vector quantity ( $\vec{P}$ ) and the same is mathematically represented as the total dipole moment per unit volume (please refer to Eq. (3.5)).

$$\vec{P} = \frac{1}{\text{volume}} [\vec{p}_1 + \vec{p}_2 + \dots + \vec{p}_N] \quad (3.5)$$

Here,  $\vec{p}_1, \vec{p}_2, \dots, \vec{p}_N$  are induced dipole moments in  $N$  molecules inside the material volume.

For any arbitrary geometry of a substrate, ‘surface polarization charge density ( $\sigma_p$ )’ i.e. the charge per unit surface area appearing on the surface of a polarized medium is equal to the

normal component of polarization vector ( $\vec{P}_{normal}$ ) i.e. normal to the surface – as illustrated in Eq. (3.6).

$$\vec{P}_{normal} = \sigma_P \quad (3.6)$$

### 3.1.3 Electric Susceptibility and Relative Permittivity

The induced polarization in any dielectric substrate depends on the applied electric field strength. To define the dependence of polarization magnitude ( $P$ ) on the magnitude of applied electric field strength ( $E$ ), a new term ‘electric susceptibility ( $\chi_e$ )’ is introduced – as described in Eq. (3.7).

$$P = \chi_e \varepsilon_0 E \quad (3.7)$$

Moreover, a simple relation can be drawn in between  $P$  and  $p_{induced}$  while proceeding from Eq. (3.4) – the same is depicted in Eq. (3.8).

$$P = N p_{induced} = N \alpha_e E \quad (3.8)$$

Here,  $N$  denotes the number of molecules per unit volume of material. Thus, simplifying Eqs. (3.7) and (3.8), a further important relation is illustrated by Eq. (3.9).

$$\chi_e = \frac{1}{\varepsilon_0} N \alpha_e \quad (3.9)$$

Further proceeding with the above equations, an important relation between the microscopic electronic polarization mechanism ( $\alpha_e$ ) and macroscopic material dielectric properties ( $\varepsilon_r$ ) can be deduced – as given in Eq. (3.10). The intermediate calculation steps are available in standard literature [1].

$$\varepsilon_r = 1 + \chi_e = 1 + \frac{N \alpha_e}{\varepsilon_0} \quad (3.10)$$

### 3.1.4 Local Electric Field and Clausius-Mossotti Equation

It should be noted that there is a little approximation in Eq. (3.10) that relates microscopic electronic polarization mechanism ( $\alpha_e$ ) and macroscopic dielectric properties ( $\varepsilon_r$ ) with each other. The approximation is introduced from the assumption that the electric field acting on each

and every atom or molecule is  $E$  itself – which is considered to be uniform near all the individual electric dipoles within the dielectric material. However, in true sense, induced polarization of individual molecule depends on the actual local electric field strength ( $E_{Loc}$ ) experienced by the molecule but not on overall uniform electric field strength ( $E$ ). Molecules are polarized within dielectric material with their positive and negative charge centers separated – as a consequence, the local electric field strength ( $E_{Loc}$ ) at atomic level is not constant at all places within the dielectric medium. The local electric field strength ( $E_{Loc}$ ) experienced by each molecule is different than the overall uniform electric field strength ( $E$ ). The local electric field strength ( $E_{Loc}$ ) is not only dependent on the externally applied uniform electric field strength ( $E$ ) but also on the arrangement of surrounding polarized molecules. In case of a simple dielectric material with cubic crystal structure or a liquid, the local electric field strength ( $E_{Loc}$ ) is observed to be as illustrated in Eq. (3.11) [1].

$$E_{Loc} = E + \frac{1}{3\epsilon_0}P \quad (3.11)$$

The relation illustrated in Eq. (3.11) is known as Lorentz field. Thus, the induced polarization of molecule depends on local electric field strength ( $E_{Loc}$ ) instead of overall uniform electric field strength ( $E$ ) – as given in Eq. (3.12).

$$p_{induced} = \alpha_e E_{Loc} \quad (3.12)$$

However, the basic concept of electric susceptibility remains the same as described in Eq. (3.7) and  $\epsilon_r = 1 + \chi_e$ . The polarization ( $P$ ) is still defined by the equation  $P = Np_{induced}$  but, the modified  $p_{induced}$  is now calculated using Eqs. (3.11) and (3.12).

Next, using the above relations,

$$P = Np_{induced}$$

$$\text{or, } P = N\alpha_e E_{Loc}$$

$$\text{or, } P = N\alpha_e \left( E + \frac{1}{3\epsilon_0} P \right)$$

$$\text{or, } (\epsilon_r - 1)\epsilon_0 E = N\alpha_e \left( E + \frac{1}{3\epsilon_0} ((\epsilon_r - 1)\epsilon_0 E) \right)$$

$$\begin{aligned}
\text{or, } (\epsilon_r - 1)\epsilon_0 E &= \frac{N\alpha_e}{3\epsilon_0} (3\epsilon_0 E + (\epsilon_r - 1)\epsilon_0 E) \\
\text{or, } (\epsilon_r - 1)\epsilon_0 E &= \frac{N\alpha_e}{3\epsilon_0} (3\epsilon_0 E + \epsilon_r \epsilon_0 E - \epsilon_0 E) \\
\text{or, } (\epsilon_r - 1)\epsilon_0 E &= \frac{N\alpha_e}{3\epsilon_0} (\epsilon_r \epsilon_0 E + 2\epsilon_0 E) \\
\text{or, } (\epsilon_r - 1)\epsilon_0 E &= \frac{N\alpha_e}{3\epsilon_0} (\epsilon_r + 2) \epsilon_0 E \\
\text{or, } (\epsilon_r - 1) &= \frac{N\alpha_e}{3\epsilon_0} (\epsilon_r + 2) \\
\text{or, } \frac{(\epsilon_r - 1)}{(\epsilon_r + 2)} &= \frac{N\alpha_e}{3\epsilon_0} \tag{3.13}
\end{aligned}$$

The above mentioned Eq. (3.13) is known as Clausius-Mossotti equation. This equation facilitates to calculate the macroscopic material dielectric properties ( $\epsilon_r$ ) from microscopic electronic polarization mechanism ( $\alpha_e$ ) employing local electric field strength ( $E_{Loc}$ ) [1].

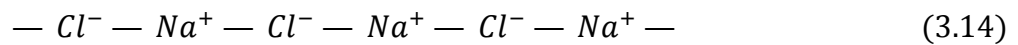
### 3.1.5 Electronic Polarization – Covalent Bond

Under the application of external electric field ( $E$ ), the atoms / molecules in dielectric material become polarized. The center of light weight electron cloud in each atomic structure shifts from the center of positive nucleus – thus, this phenomenon gives rise to electronic polarization. It should be noted that this electronic polarization in atom contributes reasonably less compared to polarization due to the valence electrons in the covalent bond within the dielectric material. Neighboring crystalline silicon atoms share their electrons in covalent bonds – these shared valence electrons form covalent bonds between two neighbor silicon atoms because they are loosely bound to the parent atoms. Thus, in covalent bonds, these shared electrons are not strongly tied with the ionic cores of individual silicon atoms. These electrons belong to the whole silicon crystal as they can relocate from one bond to another and change positions [1].

While an external electric field is applied, the negative charge distribution associated with the valence electrons shifts away from the positively charged silicon ionic cores – as a consequence, the whole silicon crystal becomes polarized. It is reported that only 1 eV to 2 eV energy is sufficient to make a valence electron free from the covalent bond, but more than 10 eV energy is required to free an electron from the ionic silicon core. Thus, the valence electrons in covalent bonds easily get displaced by the applied electric field ( $E$ ) and the consequent electronic polarization contributes to higher dielectric constant of covalent crystal dielectric material ( $\epsilon_{r_{Silicon}} = 11.9$  and  $\epsilon_{r_{Germanium}} = 16$ ) [1].

### 3.1.6 Ionic Polarization Mechanism

Besides electronic polarization, a number of other polarization mechanisms can also be identified and those also contribute to relative dielectric constant ( $\epsilon_r$ ) of materials. Ionic polarization is one of those well known polarization mechanisms. Ionic crystals like  $NaCl$ ,  $KCl$  and  $LiBr$  etc. demonstrate the mechanism of ionic polarization – ionic crystals contain paired ions like  $Na^+$  and  $Cl^-$  and each of such oppositely charged neighboring pairs possess a dipole moment. While the applied electric field ( $E$ ) is absent, the solid crystal possesses no net polarization – as, altering  $Na^+$  and  $Cl^-$  ions stay in a chain formation. Thus, dipole moments of equal magnitudes stay in a chain head-to-head and tail-to-tail, resulting in zero net dipole moment (please refer to Eq. (3.14)).



Thereafter when the electric field ( $E$ ) is applied, the modified opposite dipole moments don't possess equal magnitudes – thus, the net dipole moment becomes non-zero and dependent upon the applied electric field ( $E$ ). To be more precise, the average dipole moment per positive-negative ion pair ( $p_{av}$ ) depends on the applied electric field ( $E$ ). The ionic polarizability ( $\alpha_i$ ) is expressed in terms of the local electric field strength ( $E_{Loc}$ ) – as expressed in Eq. (3.15).

$$p_{av} = \alpha_i E_{Loc} \quad (3.15)$$

In general, ionic polarizability ( $\alpha_i$ ) is much stronger than the electronic polarizability ( $\alpha_e$ ) – at least by a factor of 10 or more. Thus, dielectric materials that possess ionic polarizability ( $\alpha_i$ ) have higher dielectric constants [1, 8].

The polarization ( $P$ ) contributed in ionic material depends upon the number of positive-negative ion pairs ( $N_i$ ) along with average dipole moment per positive-negative ion pair ( $p_{av}$ ) – as expressed in Eq. (3.16).

$$P = N_i p_{av} = N_i \alpha_i E_{Loc} \quad (3.16)$$

Thus further utilizing Eq. (3.16), the Clausius-Mossotti equation can be modified as in Eq. (3.17) – due to ionic polarization.

$$\frac{(\epsilon_r - 1)}{(\epsilon_r + 2)} = \frac{N_i \alpha_i}{3\epsilon_0} \quad (3.17)$$

However, it must be remembered that the electronic polarization gets added upon the ionic polarization – but, the magnitude of electronic polarization remains much smaller [1, 8].

### 3.1.7 Orientational (Dipolar) Polarization Mechanism

A few polar molecules like water ( $H_2O$ ), alcohol, acetone and gaseous  $HCl$  etc. possess permanent dipole moments due to their structural conformation. In water molecule ( $H_2O$ ), the individual dipole moments are originated due to the fact that oxygen atom ( $O$ ) is more electronegative than the hydrogen atom ( $H$ ) – thus, there are two polar  $O - H$  bonds with an intermediate angle of  $104.5^\circ$  ( $H - O - H$ ). As a result, two dipole moments of equal magnitude are originating from the oxygen atom ( $O$ ) to two different hydrogen atoms ( $H$ ) with the intermediate angle of  $104.5^\circ$  ( $H - O - H$ ). The resultant orientational dipole moment ( $p_o$ ) is originating from the oxygen atom ( $O$ ) and direct at  $52.25^\circ$  (i.e.  $104.5^\circ/2$ ) angle from each of hydrogen atoms ( $H$ ).

When there is no applied electric field ( $E$ ), these individual polar molecules orient themselves in random directions due to thermal agitation – as a consequence, net polarization in the dipolar material becomes zero. However when an external electric field ( $E$ ) is applied, all individual dipoles attempt to align themselves parallel to  $E$ . The dipolar molecule experiences a torque

about its center of mass – this torque acts on the dipolar molecule and rotates it to align the orientational dipole moment ( $p_o$ ) with the applied electric field ( $E$ ). In case it is considered that all the molecules rotate and align themselves with the applied electric field ( $E$ ), the total polarization within unit material volume would be as expressed in Eq. (3.18) – where,  $N$  is the number of dipolar molecules per unit material volume [1].

$$P = Np_o \quad (3.18)$$

However, it should be noted that the dipolar molecules attempt to move in random directions due to their thermal energy which varies with the system temperature. Thus, the molecules tend to collide with each other and also with the container walls resulting in random orientations of the molecules – as the system temperature increases. As a consequence, these thermal energy induced molecular collisions somewhat destroy and reduce the overall dipole alignments. Nonetheless, there is a finite net average dipole moment per dipolar molecule and the same is aligned with the applied electric field ( $E$ ) – thus, the overall dipolar material possesses a net orientational / dipolar polarization that further contributes to dielectric constant ( $\epsilon_r$ ) of the material [1-2, 4, 9].

There is a conflict in between the average potential energy of individual molecule ( $E_{dip}$ ) under the applied electric field ( $E$ ) and the average thermal energy of individual molecule ( $\frac{5}{2}kT$ ). In case  $\frac{5}{2}kT > E_{dip}$ , then the thermal energy of the dipolar molecules is sufficiently high to either prevent or destroy dipole alignment with the applied electric field ( $E$ ) and thus the orientational polarization will not take place. On the opposite side, when  $\frac{5}{2}kT < E_{dip}$ , then the thermal energy of the dipolar molecules is insufficient to destroy the dipole alignment and the orientational polarization is conserved within the material. Thus, if the orientational polarization needs to be effective, the average potential energy of individual molecule ( $E_{dip}$ ) must be of greater magnitude compared to the average thermal energy of individual molecule ( $\frac{5}{2}kT$ ) [1, 6, 9].

The orientational polarizability ( $\alpha_d$ ) per dipolar molecule is defined by the following Eq. (3.19).

$$\alpha_d = \frac{1}{3} \frac{p_o^2}{kT} \quad (3.19)$$



It must be noted that the orientational (dipolar) polarization significantly depends upon the temperature – orientational polarizability ( $\alpha_d$ ) reduces with temperature and thus the relative permittivity ( $\epsilon_r'$ ) also reduces with temperature [1, 6, 8-9].

### 3.1.8 Interfacial Polarization Mechanism

In addition to the earlier mentioned polarization mechanisms, an additional interfacial polarization mechanism is exhibited at the interface between two dielectric materials or at dielectric-metal interface, whenever there is an accumulation of interfacial charges. Even in perfect materials, some crystal defects, impurities, mobile charge carriers (like electrons and holes) or impurity ions are always contained. In a particular dielectric material, there are equal numbers of positive and negative ions – either the positive or the negative ions are more mobile depending upon their relative sizes. Now under the application of an external electric field ( $E$ ), either the positive or the negative ions (which are more mobile) reach near the electrode or crystal defect interface. However, these mobile ions near the interface can't leave the dielectric material and enter the metal electrode or crystal defect – rather, those mobile ions simply gather at the interface and give rise to a space charge. These charges near the interface attract more opposite charges on the electrode; thus, this whole phenomenon appears to be an increase in the material dielectric constant ( $\epsilon_r$ ) [1, 8].

The terminology 'interfacial polarization' is conceptualized because the mobile charges (either positive or negative) accumulating near interface and the remaining opposite charges in the bulk dielectric region form dipole moments – these, interfacial dipole moments contribute to the overall polarization vector ( $P$ ). This polarization vector ( $P$ ) is due to all the dipoles per unit volume of the dielectric substrate.

The trapping of electrons or holes at crystal defect surfaces can also lead to interfacial polarization. The grain boundaries in addition to crystal defect boundaries often lead to interfacial polarization as they can trap some charges moving under the influence of an external electric field ( $E$ ). These trapped charges contribute to form dipoles with opposite charges, and result in increased magnitude of polarization vector ( $P$ ) [1].

### 3.1.9 Total Polarization

It should be noted that all the earlier mentioned polarization mechanisms i.e. electronic, ionic and orientational (dipolar) dipole moments come into effect together. Thus, the average dipole moment per molecule consists of cumulative contributions from electronic, ionic and orientational (dipolar) polarization mechanisms – in terms of the local electric field ( $E_{Loc}$ ) [1].

$$p_{av} = \alpha_e E_{Loc} + \alpha_i E_{Loc} + \alpha_d E_{Loc} \quad (3.20)$$

From Eq. (3.20), it is evident that each polarization mechanism contributes in a linear fashion to the cumulative dipole moment per molecule. On contrary, the interfacial polarization mechanism i.e.  $\alpha_{if} E_{Loc}$  can't directly be added to Eq. (3.20) because it is experienced only near the dielectric interfaces. Thus, this interfacial polarization can't simply be added to the average dipole moment per molecule in the bulk dielectric substrate. Furthermore, the local fields are not well defined at the dielectric interfaces. Even, the Lorentz local field approximation can't directly be utilized for dipolar dielectric materials – as a consequence, the Clausius-Mossotti Equation can't be applied in dipolar dielectric materials. However, the relative dielectric constant ( $\epsilon_r$ ) can be calculated under electronic and ionic polarization mechanisms – using Eq. (3.21) [1].

$$\frac{(\epsilon_r - 1)}{(\epsilon_r + 2)} = \frac{1}{3\epsilon_0} (N_e \alpha_e + N_i \alpha_i) \quad (3.21)$$

### 3.1.10 Frequency Dependence: Dielectric Constant and Loss Factor

The static dielectric properties ( $\epsilon_r$ ) account for the polarization effect under dc electric field – however, the polarization of a dielectric medium under ac electric field is generally different than the static condition [1, 9]. In case, orientational polarization is considered for dipolar molecules (for example, water – as it has a significant presence in all plant and fruit tissues), the ac electric field has a sinusoidal variation with continuous time varying magnitude and direction; as a consequence, the molecular dipoles try to follow the variation in applied ac electric field and thus align in one way and then in the other way in alternating cycles.

In an ideal scenario, the instantaneous induced dipole moment ( $p$ ) per molecule can immediately follow the time variation of externally applied field – as in Eq. (3.22).  $\alpha_d$  is at the maximum expected value ( $\frac{1}{3} \frac{p_0^2}{kT}$ ) at static conditions (please refer to earlier Eq. (3.19)).

$$p = \alpha_d E \quad (3.22)$$

However, there are two critical factors opposing the instantaneous dipolar alignment with the applied electric field. The thermal energy of dipolar molecules tries to randomize their orientation – thus, opposes immediate alignment with the time varying electric field. In addition, these dipolar molecules attempt to rotate in a viscous medium due to the interaction with the neighboring molecules – this particular phenomenon somewhat restricts the dipoles to respond immediately to the change in applied field. Because of these two factors, the dipolar molecules can't follow the rapid change in applied field and remain somewhat randomly oriented [1, 9].

Thus, with this physical understanding,  $\alpha_d$  becomes zero at high frequencies as the field can't practically induce a dipole moment. However, at low frequencies,  $\alpha_d$  is at its maximum value because the dipolar molecules can rapidly follow the applied field. In case of static electric field, if the applied field strength is suddenly reduced, the induced dipole moment per molecule must also reduce or relax proportionately. In gaseous or liquid medium, the molecules collide with each other or with the walls of the container – thus, the induced dipole moment per molecule is relaxed. Relaxation time ( $\tau$ ) is the average time between molecular collisions and thus the mean time taken per molecule to randomize the spare induced dipole moment. The orientational (dipolar) polarizability ( $\alpha_d(\omega)$ ) under high frequency ac condition is defined in Eq. (3.23) [1, 9].

$$\alpha_d(\omega) = \frac{\alpha_d(0)}{1 + j\omega\tau} \quad (3.23)$$

As given by Eq. (3.23), frequency dependent orientational polarizability  $\alpha_d(\omega)$  is basically a complex quantity – the same indicates that the induced dipole moment ( $p$ ) and the time harmonic electric field ( $E$ ) are out of phase. As a result, even the polarization per unit volume ( $P = Np$ ) and the alternating electric field ( $E$ ) are out of phase – where,  $N$  is the number of dipolar molecules per unit material volume. As per Eq. (3.23),  $\omega\tau \ll 1$  at low frequency region and as a consequence, the value of  $\alpha_d(\omega)$  is nearly equal to the value of  $\alpha_d(0)$  i.e. induced dipole

moment ( $p$ ) is in proper phase with the time alternating electric field ( $E$ ). At low frequency region, the rate of relaxation ( $\frac{1}{\tau}$ ) is much faster when compared to the frequency ( $\omega$ ) of applied field (or, the rate at which polarization ( $P$ ) is being changed) – thus, induced dipole moment ( $p$ ) can closely follow the time harmonic electric field ( $E$ ). On contrary,  $\omega\tau \gg 1$  at higher frequency region and thus, the rate of relaxation ( $\frac{1}{\tau}$ ) is now much slower compared to the applied frequency ( $\omega$ ). Thus, the induced dipole moment ( $p$ ) can't follow the alternating electric field ( $E$ ) variation [1].

Next, it is possible to calculate the dielectric properties ( $\epsilon_r$ ) from  $\alpha_d(\omega)$  using Eq. (3.10). Thus, it is obvious that the material dielectric properties ( $\epsilon_r$ ) will be complex as  $\alpha_d(\omega)$  itself is complex. As per the convention, complex dielectric constant ( $\epsilon_r$ ) is represented as in Eq. (3.24).

$$\epsilon_r = \epsilon_r' - j\epsilon_r'' \quad (3.24)$$

Here,  $\epsilon_r'$  and  $\epsilon_r''$  are the real and imaginary parts of frequency dependent complex dielectric properties ( $\epsilon_r$ ). The real part ( $\epsilon_r'$ ) reduces from the peak value  $\epsilon_r'(0)$  corresponding to  $\alpha_d(0)$  to 1 at very high frequencies when  $\alpha_d(\omega) = 0$  (please refer to Eq. (3.23)). The imaginary part ( $\epsilon_r''$ ) is near zero at very low frequency region as well as at very high frequency region – however,  $\epsilon_r''$  peaks at  $\omega\tau = 1$  condition i.e. when the condition  $\omega = \frac{1}{\tau}$  is satisfied [1-7, 9].

The real part i.e. permittivity ( $\epsilon_r'$ ) is utilized to calculate the capacitance ( $C$ ) whereas the imaginary part ( $\epsilon_r''$ ) is useful for quantifying the energy loss (or, parallel conductance ( $G_p$ )) in dielectric material. Let's imagine, a sinusoidal voltage is applied across the two electrodes and there is a dielectric material ( $\epsilon_r$ ) in between with cross-sectional area  $A$  and length  $d$ . The admittance ( $Y$ ) is expressed as in Eqs. (3.25) and (3.25a).

$$Y = \frac{j\omega A\epsilon_0\epsilon_r(\omega)}{d} = \frac{j\omega A\epsilon_0\epsilon_r'(\omega)}{d} + \frac{\omega A\epsilon_0\epsilon_r''(\omega)}{d} \quad (3.25)$$

$$\text{or, } Y = j\omega C + G_p \quad (3.25a)$$

$$\text{where, } C = \frac{A\epsilon_0\epsilon_r'(\omega)}{d} \quad \text{and} \quad G_p = \frac{\omega A\epsilon_0\epsilon_r''(\omega)}{d}$$

Thus, admittance ( $Y$ ) of the dielectric medium is a parallel combination of an ideal lossless capacitor ( $C$ ) and a conductance ( $G_p$ ) – as defined in Eq. (3.25a). The conductance ( $G_p$ ) is responsible for real power dissipation. The real dissipated power in the dielectric material is dependent upon  $\varepsilon_r''$  and is maximum when  $\omega = \frac{1}{\tau}$ . In this condition, the energy storage in the dielectric material due to externally applied field and energy loss due to random collisions among the dipolar molecules take place at the same rate – thus, the energy is getting converted to heat in the most efficient way. The maximum value in  $\varepsilon_r''$  versus  $\omega$  plot is known as relaxation peak; at the corresponding frequency ( $\omega$ ) dipole relaxations are at proper rate for the maximum power dissipation – this is known as dielectric resonance [1, 9].

It should be noted that the relative magnitude of  $\varepsilon_r''$  with respect to  $\varepsilon_r'$  is defined as loss tangent ( $\tan \delta$ ) – as illustrated in Eq. (3.2). Thus,  $\varepsilon_r''$  is related to  $\varepsilon_r'$  using a simple relation – as referred in Eq. (3.26). This quantity  $\tan \delta$  peaks in the gigahertz region for most liquid and solid dielectric samples [5].

$$\varepsilon_r'' = \varepsilon_r' \tan \delta \quad (3.26)$$

The power dissipated per unit volume ( $W_{Vol}$ ) of a lossy dielectric material is defined in Eq. (3.27).

$$W_{Vol} = \frac{\text{Power loss}}{\text{Volume}} = \frac{V^2}{R_p} \times \frac{1}{dA} = \frac{V^2}{\frac{1}{G_p}} \times \frac{1}{dA} = \frac{V^2}{\frac{d}{\omega A \varepsilon_0 \varepsilon_r''}} \times \frac{1}{dA} = \frac{V^2}{d^2} \omega \varepsilon_0 \varepsilon_r'' \quad (3.27)$$

Next, employing Eq. (3.26), Eq. (3.27) and  $E = \frac{V}{d}$ , Eq. (3.27a) is derived.

$$W_{Vol} = \omega E^2 \varepsilon_0 \varepsilon_r' \tan \delta \quad (3.27a)$$

Eq. (3.27a) defines how the stored electromagnetic power is dissipated per unit volume of lossy dielectric material due to polarization mechanism. It is evident that the dielectric loss is dependent upon three prime factors viz.  $\omega$ ,  $E$  and  $\tan \delta$  [1, 5].

Although, in the preceding discussion, orientational (dipolar) polarization has been considered – in general, a dielectric material possesses the other polarization mechanisms as well. In general, the interfacial polarization is dominant at low frequency region, whereas the orientational

(dipolar) polarization is dominant at microwave region. The ionic and electronic polarizations lead respectively at infrared and ultraviolet regions [1].

### **3.1.11 Dielectric Properties and Polarizations in Plant Tissues**

In general, different plants, fruits and flowers possess large amount of water and ions – in addition, a number of tissue dielectric interfaces do also exist among them [3-6, 9]. Like most other living biological tissues, there is enormous presence of dipolar water ( $H_2O$ ) molecules in different types of plant tissues – these water ( $H_2O$ ) molecules possess permanent dipole moments due to their structural conformation. As a consequence, the orientational (dipolar) polarization mechanism plays a crucial role and contributes to the complex dielectric properties ( $\epsilon_r$ ) of different plant, fruit and flower tissues (particularly in the microwave region) [1-7, 9]. In addition, large presence of ionic compounds and different ions ( $Ca^{++}$ ,  $Na^+$ , and  $Cl^-$  etc.) contribute to ionic polarization mechanism in plants, fruits and flowers. Thus, this ionic polarization mechanism also contributes to the complex dielectric properties ( $\epsilon_r$ ) of different plant tissues [1-9].

Besides the above discussed polarization mechanisms in various plant tissues, the inherent electronic polarization mechanism is always exhibited due to presence of orbital electron clouds in the atoms, or shared electrons in the covalent bonds [1]. Furthermore, there are tissue dielectric interfaces from one tissue layer to another and small gaps in between tissue layers (acting as defects in tissue dielectrics). As a consequence, the interfacial polarization mechanism becomes significant at those tissue dielectric interfaces and tissue dielectric defects – resulting in contribution to effective dielectric properties ( $\epsilon_r$ ) of plant tissues [1, 8].

Thus, due to the complex compositions of plant tissue dielectrics, all types of polarization mechanisms play their respective roles and contribute to the broadband complex dielectric properties ( $\epsilon_r$ ) of different plant, fruit and flower specimens. In general, it is true that a specific polarization mechanism dominates at a distinct frequency region; however, all these polarization mechanisms still contribute together to the overall broadband complex dielectric properties ( $\epsilon_r$ ) of different plant tissues [1].

Next, to align this discussion with the research objectives, a focused discussion on dielectric properties ( $\epsilon_r$ ) characterization of different plant tissues is absolutely pertinent. It is already

discussed that enormous amount of water content contributes to high permittivity ( $\epsilon_r'$ ) of plant tissues whereas significant dielectric loss factor ( $\epsilon_r''$ ) or equivalent loss tangent ( $\tan \delta$ ) is caused due to the presence of different ions in plant leaves, fruits and flowers [2-7, 9]. Dielectric properties ( $\epsilon_r$ ) of plant tissues are dependent on several physical and physiological factors such as frequency of interest, temperature, tissue variant, ripening stage, water content (moisture), ion contents and so on [2-7, 9-12]. Before proceeding further with complex dielectric properties ( $\epsilon_r$ ) measurement of plant specimens, a comprehensive discussion on different dielectric characterization techniques seems to be much needed – thus, different dielectric measurement techniques are outlined in the following section [11-13]. Afterward, the most appropriate and practiced measurement technique for characterizing dielectric properties ( $\epsilon_r$ ) of different plant specimens is meticulously discussed in the following section [13-23].

### **3.2 Dielectric Characterization Techniques – Special Emphasis on Plant Specimen Measurements**

In general, adoption of suitable dielectric measurement technique depends upon certain parameters such as material type (solid, granular, semi-solid, gel or liquid etc.), electrical nature of material, density of material, particle size, sample shape, surface smoothness, frequency of interest, temperature, required accuracy / precision level, and so on [2-7, 9-13]. Despite the fact that a number of dielectric measuring techniques can be employed, selective dielectric characterization techniques capable of ensuring proper sample holding and reliable characterization of dielectric properties ( $\epsilon_r$ ) at the required frequency region should be adopted. In this context, few critical measurement challenges are appropriate sample holder design and accurate lumped equivalent circuit modeling at microwave frequency range for reliable extraction of dielectric properties ( $\epsilon_r$ ) from the direct measured electromagnetic parameters (such as reflection and transmission coefficients) [11-13, 24]. Once lumped equivalent circuit parameters (impedance or admittance) are calibrated in an accurate manner, the complex dielectric constant ( $\epsilon_r$ ) i.e. both permittivity ( $\epsilon_r'$ ) and dielectric loss factor ( $\epsilon_r''$ ) of material under test can be characterized after solving the lumped equivalent system equations [13-23].

Dielectric characterization techniques can be broadly classified into two segments – reflection or transmission methods using either resonant or non-resonant setups with open / closed material

sensing structures. The characterizing techniques that use waveguides / coaxial transmission lines are closed measurement setups whereas free space transmission technique and open ended coaxial line setup are open sensing structures [11, 25-26]. Either closed resonant cavities or the open resonant structures can be used as two-port devices to measure transmission coefficient or one-port devices to measure reflection coefficient [11, 25].

Complex dielectric properties ( $\epsilon_r$ ) of solid, semi-solid or liquid samples can be measured using several alternative characterization methods like cavity perturbation technique, waveguide / coaxial transmission line technique, free space transmission protocol, microstrip transmission line technique, time domain reflectometry method and the open ended coaxial probe technique [11-13]. A number of dielectric properties ( $\epsilon_r$ ) measurement techniques are available for grains, seeds, fruits and vegetables [27-32]. At low frequency range (50 KHz – 50 MHz), dielectric properties ( $\epsilon_r$ ) of grain and seed samples have been reported to be measured using coaxial line sample holder and Q meter developed based on a resonant circuit [5, 11, 33]. The coaxial line sample holder terminated with open circuit, modeled as transmission line section, was reported to be employed for dielectric measurements with bridge and admittance meter between 50 MHz – 500 MHz [5, 11, 34-35]. In addition, a number of coaxial line / rectangular waveguide sample holder based dielectric measurement techniques (assembled with different microwave components) have been reported to determine dielectric properties ( $\epsilon_r$ ) of seeds, grains, fruits and vegetables in between 1 GHz – 22 GHz [5, 11, 36-39]. The transmission line technique, resonant cavity method and free space technique are some of the widely adopted dielectric characterization schemes beyond 1 GHz [11, 25-26, 40]. However with specific reference to plant specimens (biological specimens in general), a reliable non-destructive dielectric properties ( $\epsilon_r$ ) characterization technique is important so that physical / chemical changes in the plant specimens can be monitored. To this end, open ended coaxial probe technique (one port reflection coefficient measurement system) is the most widely adopted non-destructive dielectric characterization setup for different biological tissues including plant and fruit specimens [14-24]. Thus, a detailed discussion on open ended coaxial probe technique along with background understanding is much needed and useful before proceeding further.



### 3.2.1 Open Ended Coaxial Probe Technique – A Non-Destructive Dielectric Characterization System

The open ended coaxial probe technique for non-destructive dielectric characterization of biological tissues utilizes reflection coefficient data with open material sensing structure – which is a single port measurement system [14-24]. In general, most biological tissues are soft semi-solid, gel or liquid with reasonably high permittivity ( $\epsilon'_r$ ) and loss tangent ( $\tan \delta$ ) over a wide frequency range [2-7, 9]. In most cases, complex dielectric properties ( $\epsilon_r$ ) of different biological tissues need to be measured directly on living biological objects – thus, non-invasive dielectric characterization technique is essential. One particular measurement technique characterizes dielectric properties ( $\epsilon_r$ ) of the Material under Test (MUT) using phase and amplitude of the reflected signal at open end of the coaxial probe pressed against flat smooth surface of MUT sample – however, the open probe is directly immersed inside liquid MUT sample while measuring complex dielectric properties ( $\epsilon_r$ ) of liquid specimens [14-23]. High frequency lumped equivalent circuit for this open ended coaxial probe can be modeled as parallel combination of a fringing capacitance from inner-to-outer conductor through MUT sample, another radiation conductance that signifies wave propagation loss through the MUT sample along with a fringing capacitance from inner-to-outer conductor via the intervening dielectric material within coaxial structure (please refer to Fig. 3.1) [14-23]. For a particular probe with fixed dimensions, respective values of fringing capacitance and radiation conductance are dependent on complex dielectric properties ( $\epsilon_r$ ) of MUT sample and measurement frequency range. The complex input admittance of above mentioned coaxial probe is dependent on radiation conductance and fringing capacitance through MUT sample. The real ( $\epsilon'_r$ ) and

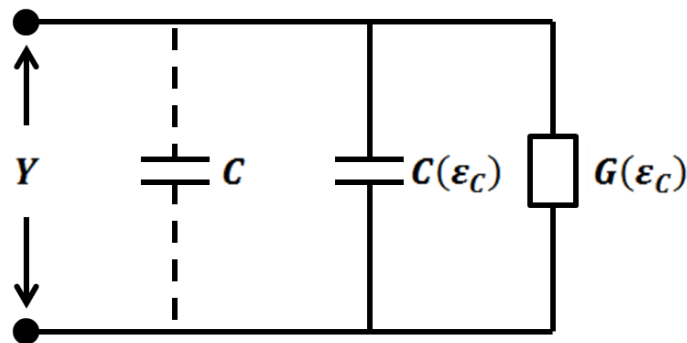


Fig. 3.1: High frequency lumped equivalent circuit for open ended coaxial probe [14-23]

imaginary ( $\epsilon_r''$ ) parts of complex dielectric properties ( $\epsilon_r$ ) of MUT sample can be computed using derived fringing capacitance and radiation conductance of the open ended coaxial probe (while in proper contact with MUT specimen). Detailed physical and mathematical analyses of this dielectric measurement technique are available in literature [14-23].

The input admittance of open ended coaxial probe is expressed as described in Eq. (3.28).

$$Y = G(\epsilon_c, \omega) + j\omega C(\epsilon_c, \omega) \quad (3.28)$$

$$Y_0 = G_0(1, \omega) + j\omega C_0(1, \omega) \quad (3.28a)$$

$Y_0$  = input admittance of the probe in air/ vaccum  
 $G_0$  = conductance while the probe is in air / vaccum  
 $C_0$  = capaticance while the probe is in air/vaccum  
 $\epsilon_c$  = complex permittivity of biological sample  
 $\omega$  = angular frequency

The analytical model for open ended coaxial probe can be represented as an antenna in a lossy dielectric medium.

$$Y(\epsilon_c, \omega) = \sqrt{\epsilon_c} Y_0(1, \omega\sqrt{\epsilon_c}) \quad (3.29)$$

$$Y = j\omega\epsilon_c C_0 + \sqrt{\epsilon_c} G_0 \quad (3.29a)$$

In accordance with Deschamps's theorem, Eq. (3.29) demonstrates that resultant input admittance of the open ended coaxial probe in a dielectric medium with complex permittivity  $\epsilon_c$  and at an angular frequency  $\omega$  is equal to  $\sqrt{\epsilon_c}$  times the input admittance of the same open ended probe in air/vacuum at angular frequency  $\omega\sqrt{\epsilon_c}$  [14].

The capacitance  $C_0$  is considered constant in free space. The value of radiation conductance  $G_0$  while the antenna i.e. open ended coaxial probe is in vacuum is calculated using the formula given by Liu in 1986 (please, refer to Eqs. (3.30) to (3.30c)) [15-16]. The Bessel function can be expanded employing Maclaurin series,

$$G_0 = \left[ \frac{Y_0}{\ln\left(\frac{a}{b}\right)} \right] \int_0^{\pi/2} [J_0(ka \sin \theta) - J_0(kb \sin \theta)]^2 \frac{d\theta}{\sin \theta} \quad (3.30)$$

$$G_0 \approx \left[ \frac{Y_0}{\ln\left(\frac{a}{b}\right)} \right] [G_1(\omega^4) + G_2(\omega^6) + \dots] \quad (3.30a)$$

$$G_0 \approx \left[ \frac{Y_0}{\ln\left(\frac{a}{b}\right)} \right] [G_1(\omega^4)] \quad (\text{N-type/ SMA connectors}) \quad (3.30b)$$

$$G_0 \propto \omega^4 \quad (3.30c)$$

In Eqs. (3.30) to (3.30c),  $J_0(x)$  is Bessel function of order zero whereas  $G_1, G_2, \dots$  etc. are parameters that depend on different antenna dimensions like  $a$  (i.e. inner radius of the outer conductor),  $b$  (i.e. outer radius of the inner conductor) and also on the frequency of operation ( $\omega$ ). Here,  $k$  is equal to  $2\pi/\lambda_0$  where  $\lambda_0$  represents the free space wavelength. It should be noted that the parameter  $G_0$  can be approximated by  $G_1$  for N type and SMA connectors. Thus, the radiation conductance of open ended coaxial probe can be considered to be varying in proportion with  $\omega^4$  [15-16].

Further simplifying Eqs. (3.29) and (3.30), the derived expression for input admittance is illustrated in Eq. (3.30a). Here,  $Y$  is the calculated input admittance of the open ended coaxial probe, whereas the parameters  $C_0$  and  $G_0$  are capacitance and radiation conductance of the probe antenna in free space respectively.

The input admittance of open ended coaxial probe  $Y$  is derived from the measured reflection coefficient  $S_{11}$  data (in linear scale) using Eq. (3.31) [22].

$$Y = Y_0 \frac{1-S_{11}}{1+S_{11}} \quad (3.31)$$

$$Y_0 = 1/50\Omega = 0.02 S$$

$Y_0$  is characteristics admittance of the above mentioned coaxial probe.

The following characterization steps are considered to calculate dielectric properties of MUT sample (biological tissue).

- a. Complex input admittance ( $Y$ ) is calculated from reflection coefficient ( $S_{11}$  in linear scale) data using Eq. (3.31).
- b. Real and imaginary parts of the complex input admittance ( $Y$ ) illustrated in Eq. (3.29a) is separated out.

- c. Thus, two nonlinear equations are derived from Eq. (3.29a) for solving two unknown system parameters i.e.  $C_0$  and  $G_0$ .
- d. To solve for system parameters  $C_0$  and  $G_0$  during calibration, the complex input admittance ( $Y$ ) is derived from reflection coefficient ( $S_{11}$  in linear scale) data for a reference sample (like, distilled water at 25 °C) with known complex dielectric properties ( $\epsilon_r$ ) over broad frequency spectrum.
- e. Next, the derived complex input admittance ( $Y$ ) value and known complex dielectric properties ( $\epsilon_r$ ) of the reference dielectric sample (distilled water at 25 °C) are put in Eq. (3.29a). Thus, the system parameters  $C_0$  and  $G_0$  are solved using Eq. (3.29a) without further effort.
- f. Once  $C_0$  and  $G_0$  are solved during calibration, the complex dielectric properties ( $\epsilon_r$ ) for any unknown MUT sample (biological tissue) can be calculated using the earlier derived values for input admittance ( $Y$ ),  $C_0$  and  $G_0$  in Eq. (3.29a).

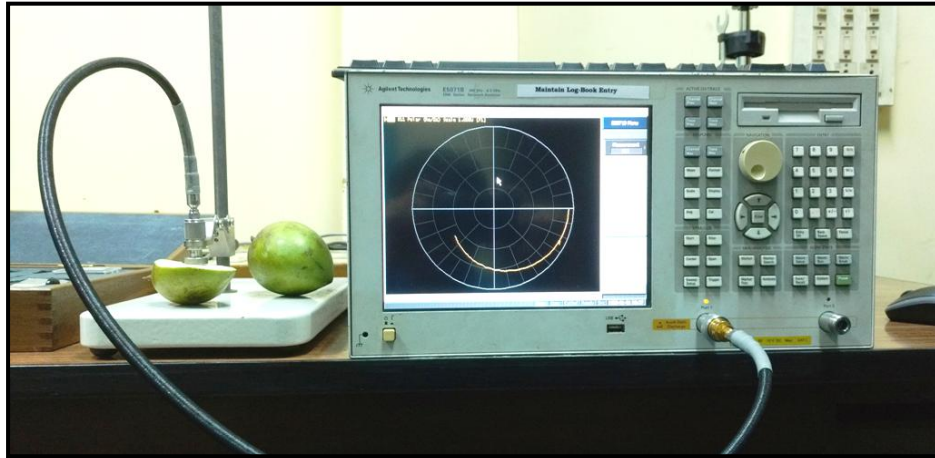
Agilent 85070E open ended coaxial probe kit is the commercial version of the above described dielectric measurement setup. This open ended coaxial probe can withstand high temperature up to 200 °C while measuring real permittivity ( $\epsilon_r'$ ) and loss tangent ( $\tan \delta$ ) of the MUT specimen – please, refer to Fig. 3.2. During dielectric constant ( $\epsilon_r$ ) measurement, amplitude and phase of the reflected electromagnetic wave at flat surface of MUT specimen is employed for reflection coefficient ( $S_{11}$ ) data acquisition. Thus, Agilent Technologies E5071B Vector Network Analyzer



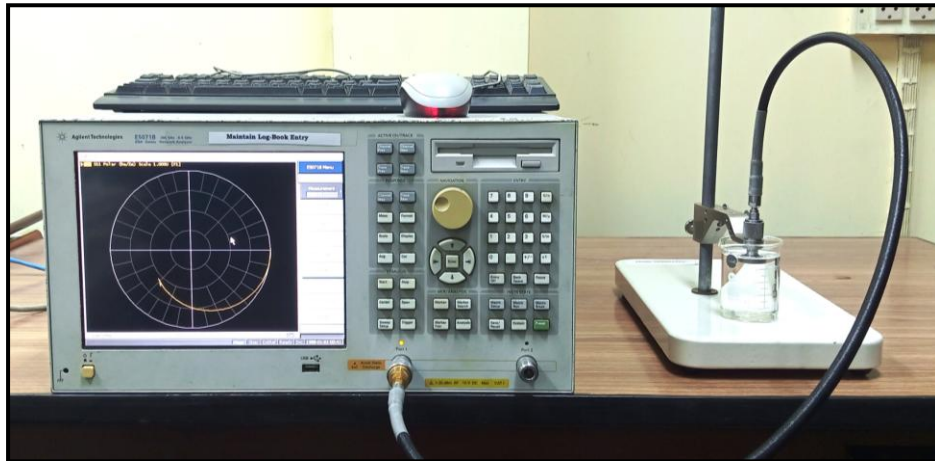
Fig. 3.2: Open ended coaxial probe for broadband dielectric properties measurement [41]

(VNA) is employed with the open ended coaxial probe during open-short-deionized water calibration technique. The diameter of this high temperature open ended coaxial probe is just about 2 cm – thus, MUT specimen diameter should be greater than 2 cm. The above mentioned 85070E dielectric measurement kit is capable of characterizing complex dielectric properties ( $\epsilon_r$ ) up to 20 GHz [41]. However, frequency range of the E5071B VNA is up to 8.5 GHz – thus, the cascaded dielectric characterization setup used can provide measurement data up to 8.5 GHz. The cascaded dielectric properties ( $\epsilon_r$ ) measurement setup is illustrated in Figs. 3.3(a) and (b).

This dielectric characterization setup provides fairly accurate data measurements once system calibration is performed. In this context, it should be noted that there are two types of uncertainty



(a)



(b)

Fig. 3.3: Open ended coaxial probe setup for broadband dielectric properties ( $\epsilon_r$ ) measurements of (a) mango pulp tissue and (b) de-ionized water at 25 °C

factors associated with this dielectric measurement technique – those are random error (Type A) and systematic error (Type B) respectively [42-44]. Random error (Type A) is the primary uncertainty factor – it's essentially associated with sample-to-sample variations in repeated measurements for particular MUT specimen (biological tissue) at fixed temperature and after single system calibration. The typical range of random error (Type A) associated with open ended coaxial measurement technique is observed to be within 4% limit. In addition, there is another uncertainty factor known as systematic error (Type B) – it is associated with open ended coaxial probe calibration technique, calibration in reference liquid specimen, measurement of MUT specimens, VNA drift and movement/bending of coaxial cable. However, all these individual uncertainty factors can precisely be controlled at elemental levels to minimize the cumulative systematic error within 1% limit. Thus, the combined uncertainty limit of measured dielectric parameters is typically observed to be within 5% for different biological specimens [42-44]. Furthermore, MUT specimens (i.e. different plant / fruit specimens) have been cut with a sharp knife to obtain smooth flat surfaces so that there is no air gap between the open ended coaxial probe and MUT specimens for accurate dielectric properties ( $\epsilon_r$ ) measurement. It has been ensured that the entire open ended coaxial probe is covered with electrically large, smooth flat, cut surfaces of MUT specimens (i.e. plant/fruit specimens) during measurement. The radial dimensions as well as dimensions of MUT specimens beneath the coaxial probe have been kept sufficiently large compared to skin depths in respective plant / fruit specimens. Thus, the condition of semi-infinite dimensions of MUT specimens has been satisfied during dielectric properties ( $\epsilon_r$ ) characterization. In addition, optimum pressure has been applied on the flat cut surfaces of MUT specimens with the open ended coaxial probe – as excessive pressure during dielectric measurements could lead to plant/fruit tissue deformation along with subsequent erroneous measurement records. Measured dielectric properties ( $\epsilon_r$ ) of different plant / fruit specimens vary within a fine range. Minor sample-to-sample variation in measured dielectric properties ( $\epsilon_r$ ) of a particular tissue type is fairly reasonable. This variation can be either due to minute difference in percentage of water content along with other tissue constituents (random error (Type A)) or because of other systematic errors (Type B) introduced in the measurement setup [42-44]. It should be noted in this context that internal water content (increases), soluble solid content (increases) and firmness (reduces) etc. alter as fruits mature to ripening phase.

Therefore, the measured dielectric properties ( $\epsilon_r$ ) of different plant / fruit tissues can reasonably vary at different maturation stages with aging [45-47].

### 3.3 Dielectric Properties Characterization of Different Plant Tissues

Broadband dielectric properties ( $\epsilon_r$ ) of a number of fruit, flower and plant tissue specimens have been measured using the 85070E open ended coaxial probe kit along with E5071B VNA – real permittivity ( $\epsilon'_r$ ) and loss tangent ( $\tan \delta$ ) data have been recorded up to 8.5 GHz. Measured dielectric properties ( $\epsilon_r$ ) for the plant tissues have been documented with proper illustrations. Obtained dielectric data points have been plotted using MATLAB R2014a software [48].

#### 3.3.1 Dielectric Properties of Coconut Tissues

Broadband dielectric properties ( $\epsilon_r$ ) of different coconut tissues have been characterized up to 8.5 GHz at 25 °C ambient temperature. Permittivity ( $\epsilon'_r$ ) and loss tangent ( $\tan \delta$ ) data have been measured for coconut's green skin, yellowish pulp and fresh coconut water specimens. The dielectric measurement setup for tissue specimens is illustrated in Figs. 3.4(a) and (b). The open ended coaxial probe is optimally pressed on flat surfaces of coconut green skin and yellowish pulp (in separate measurements) to avoid air gap. The probe is completely immersed inside the coconut water specimen as the same is liquid in nature – formation of air bubbles beneath the probe is strictly avoided. Measured permittivity ( $\epsilon'_r$ ) and loss tangent ( $\tan \delta$ ) data for coconut's green skin, yellowish pulp and fresh coconut water specimens have been plotted in Figs. 3.5(a) and (b) respectively.

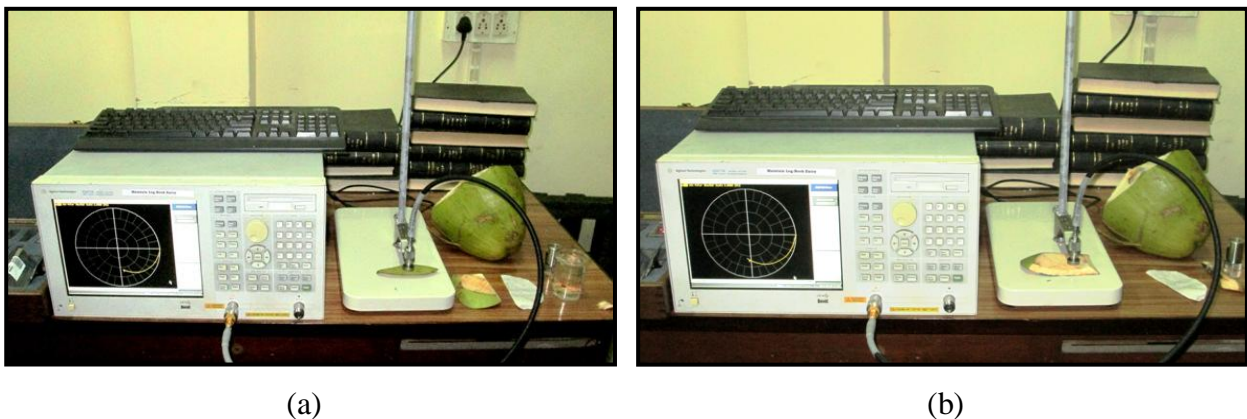
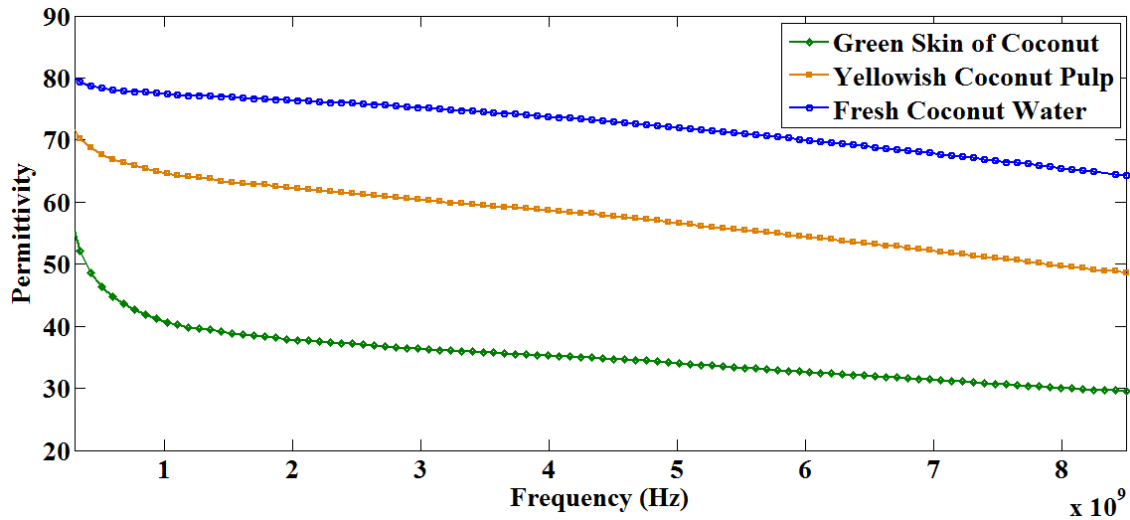
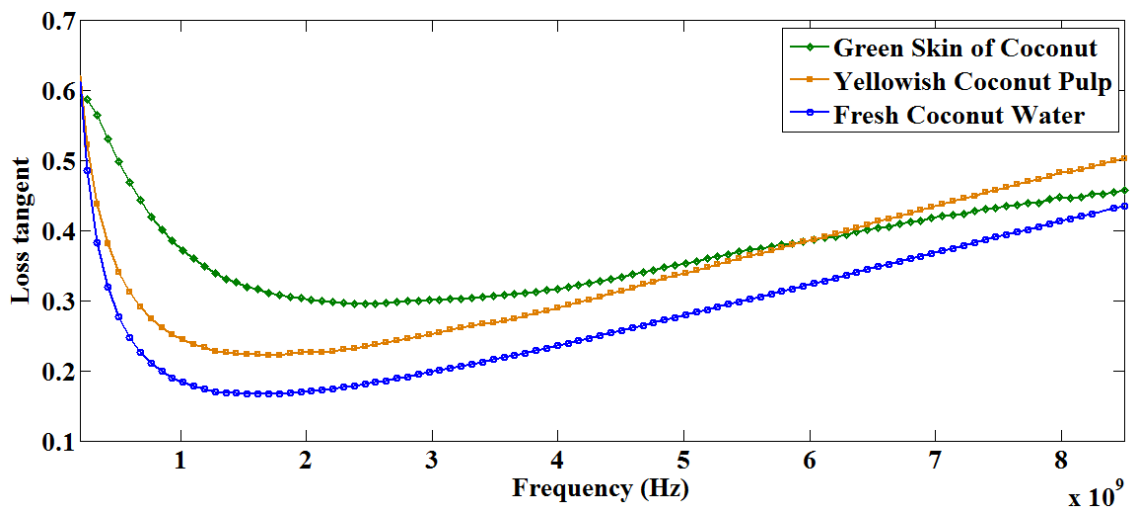


Fig. 3.4: Open ended coaxial probe setup for broadband dielectric properties measurement of coconut tissue specimens (a) green skin, (b) yellowish pulp



(a)



(b)

Fig. 3.5: Broadband dielectric properties of coconut green skin, yellowish pulp and fresh coconut water specimens up to 8.5 GHz (a) permittivity and (b) loss tangent

The highest values of permittivity ( $\epsilon'_r$ ) are noted for coconut water specimen and compared with other coconut tissues – followed by yellowish pulp and green skin of coconut. Please refer to Fig. 3.5(a). It is so because percentage of water content is the highest in fresh coconut water specimen – water percentage reduces in yellowish pulp tissue and the least in coconut green skin specimens. Thus, the observed variations in permittivity ( $\epsilon'_r$ ) data are fairly reasonable. In contrast, the loss tangent ( $\tan \delta$ ) values over a broad frequency spectrum are the minimum for coconut water specimen, moderate for yellowish pulp tissue and the maximum for coconut green



skin specimen – as illustrated in Fig. 3.5(b). However, the loss tangent ( $\tan \delta$ ) of coconut green skin specimen falls below the yellowish pulp tissue beyond 6 GHz. Thus, it is interpreted that availability of free electrons is more in outer tissue layers of green coconut compared to the innermost water content.

### 3.3.2 Dielectric Properties of Mango Tissues

Broadband dielectric properties ( $\epsilon_r$ ) of different green mango fruit and leaf tissues have been characterized up to 8.5 GHz at 25 °C ambient temperature. Permittivity ( $\epsilon_r'$ ) and loss tangent ( $\tan \delta$ ) data have been measured for green mango pulp, seed and leaf specimens. The overall dielectric properties ( $\epsilon_r$ ) measurement setup for a typical mango pulp specimen is illustrated in Fig. 3.6(a) – an enlarged view is illustrated in Fig. 3.6(b). The mango fruits have been cut with a sharp knife to obtain flat specimen surfaces for avoiding air gap beneath the open ended coaxial probe. Next, the probe is pressed on flat surface with optimum pressure for accurate dielectric properties ( $\epsilon_r$ ) measurements. In case of leaf specimens, a number of leaves have been stacked together (without air gap) to provide sufficient tissue thickness beneath the coaxial probe – thus, the condition of infinite sample dimension (thickness > skin depth) is satisfied. The measured permittivity ( $\epsilon_r'$ ) and loss tangent ( $\tan \delta$ ) data for green mango pulp, seed and leaf specimens have been plotted in Figs. 3.7(a) and (b) respectively.

The broadband permittivity ( $\epsilon_r'$ ) values are on the higher side for green mango pulp, in moderate range for mango seed and on the lower side for mango leaves – as plotted in Fig. 3.7(a). These variations in broadband permittivity ( $\epsilon_r'$ ) data are reasonable and maybe linked with the

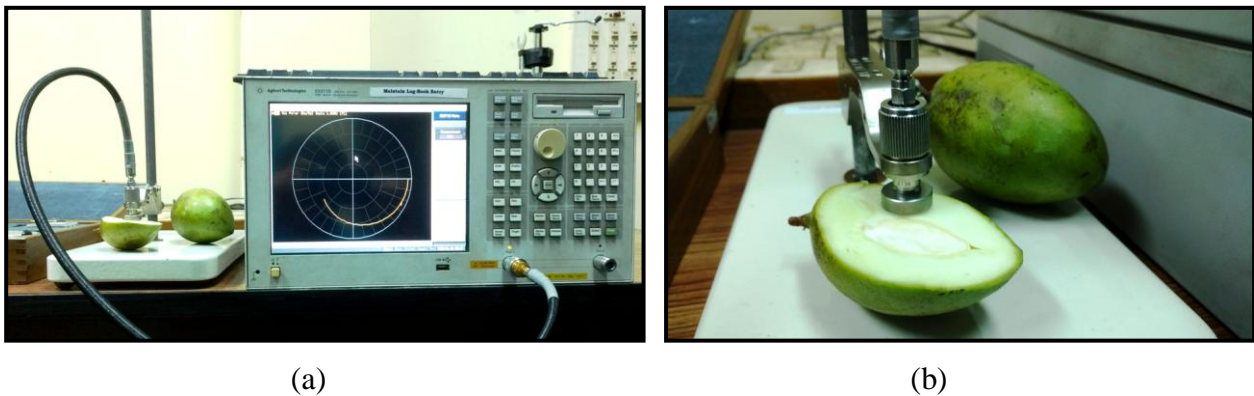
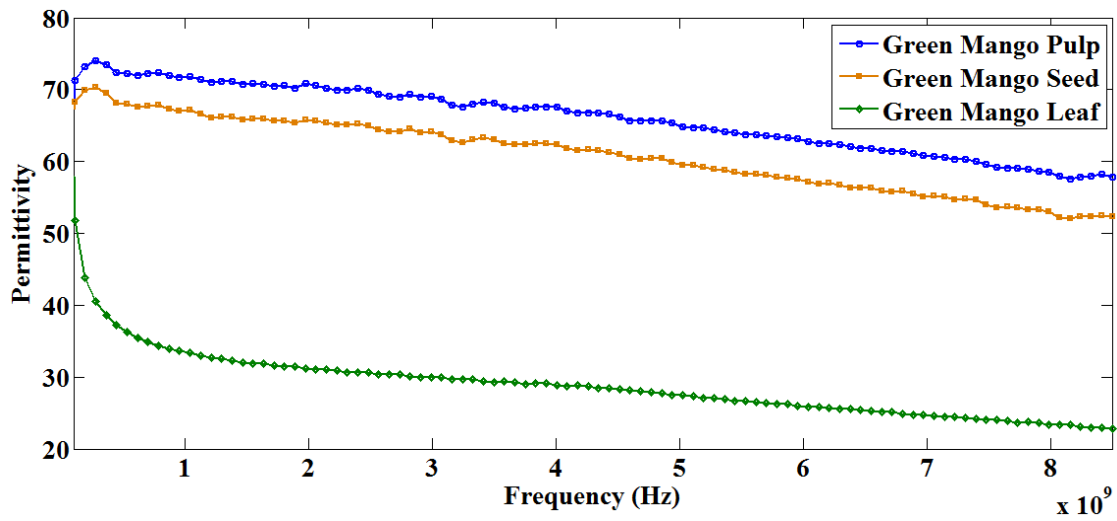
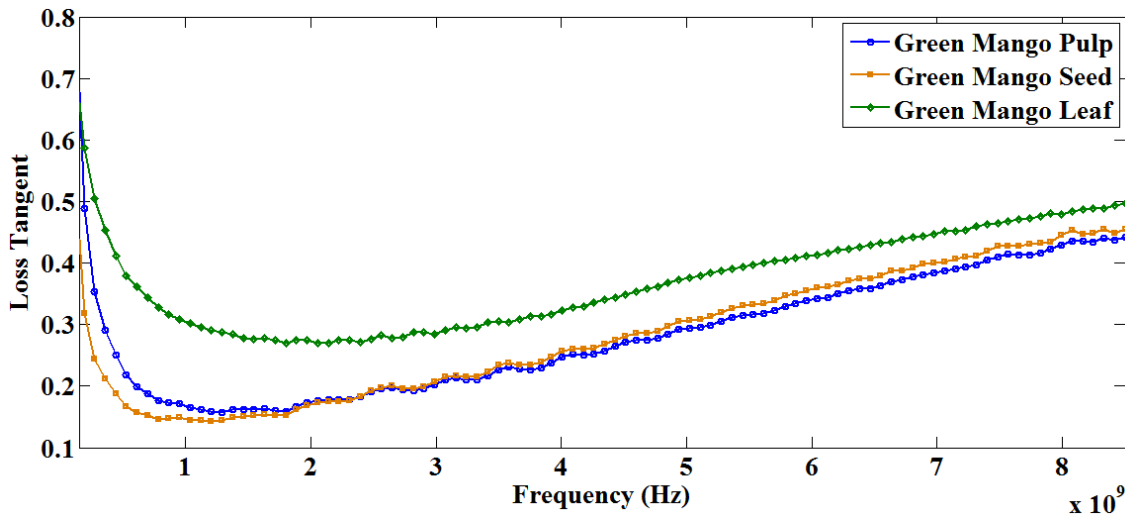


Fig. 3.6: Open ended coaxial probe setup for broadband dielectric properties measurement of mango pulp specimen (a) total measurement setup, (b) close-up view



(a)



(b)

Fig. 3.7: Broadband dielectric properties of green mango pulp, seed and leaf specimens up to 8.5 GHz (a) permittivity and (b) loss tangent

percentage of water content in different mango tissue specimens. In contrast, mango leaf specimens possess higher loss tangent values over broad spectrum up to 8.5 GHz. Mango pulp and seed specimens possess relatively low loss tangent ( $\tan \delta$ ) values – as illustrated in Fig. 3.7(b). Thus, it seems that more free electrons / ions are available in mango leaf tissue to support biophysical transportation activities in plants.

### 3.3.3 Dielectric Properties of Orange Tissues

Broadband dielectric properties ( $\epsilon_r$ ) i.e. permittivity ( $\epsilon'_r$ ) and loss tangent ( $\tan \delta$ ) of ripe orange pulp and peel tissue specimens have been characterized up to 8.5 GHz at 25 °C ambient temperature. The dielectric properties ( $\epsilon_r$ ) measurement setup for typical orange pulp specimen (along with an enlarged view) is illustrated in Figs. 3.8(a) and (b). In addition, the measurement setup for orange peel specimen (along with enlarged view) is illustrated in Figs. 3.8(c) and (d). A number of pulp specimens have been stacked together to ensure sufficient tissue thickness beneath the probe for accurate measurement. Permittivity ( $\epsilon'_r$ ) and loss tangent ( $\tan \delta$ ) data for ripe orange pulp and peel tissue specimens have been plotted in Figs. 3.9(a) and (b) respectively.

As illustrated in Fig. 3.9(a), permittivity ( $\epsilon'_r$ ) of ripe orange pulp is significantly higher than orange peel over the entire frequency range (up to 8.5 GHz) – it's primarily due to the variation in water content. In contrast, the loss tangent ( $\tan \delta$ ) of orange peel is higher than ripe orange pulp over almost the entire frequency range (0.5 GHz to 8.5 GHz). Please, refer to Fig. 3.9(b).

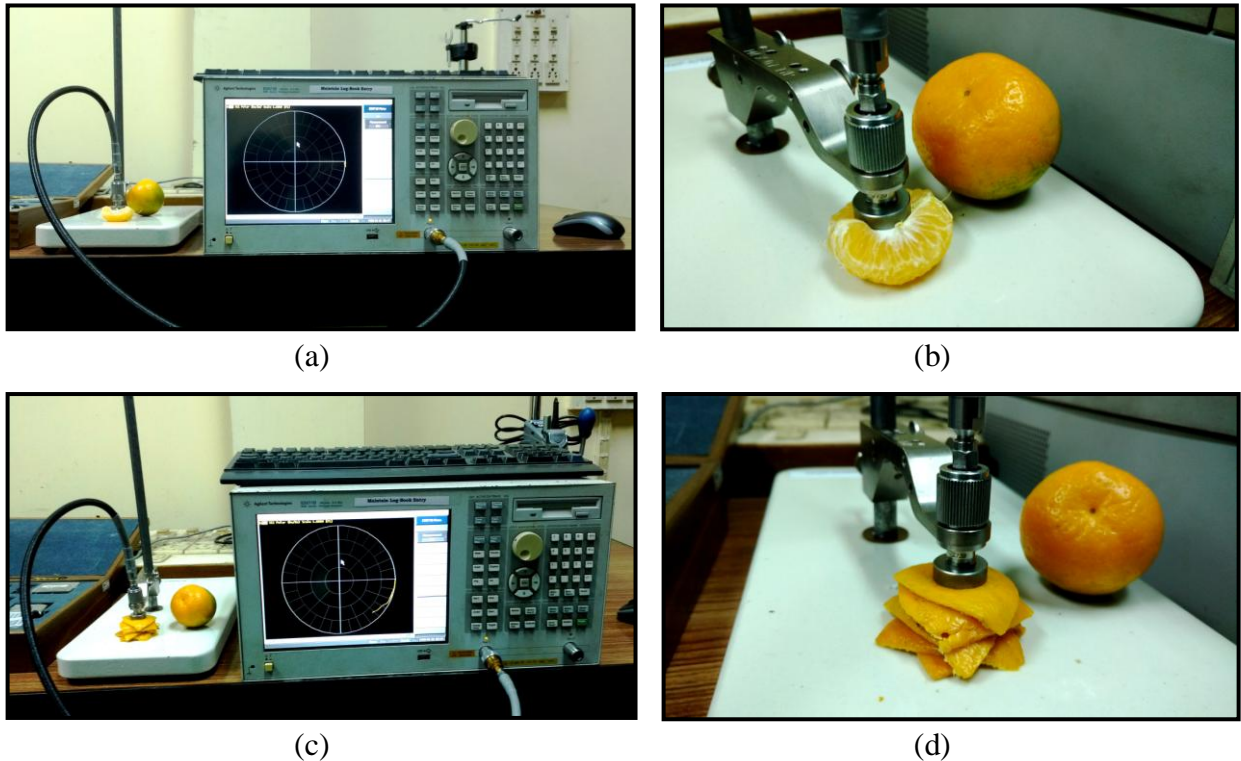
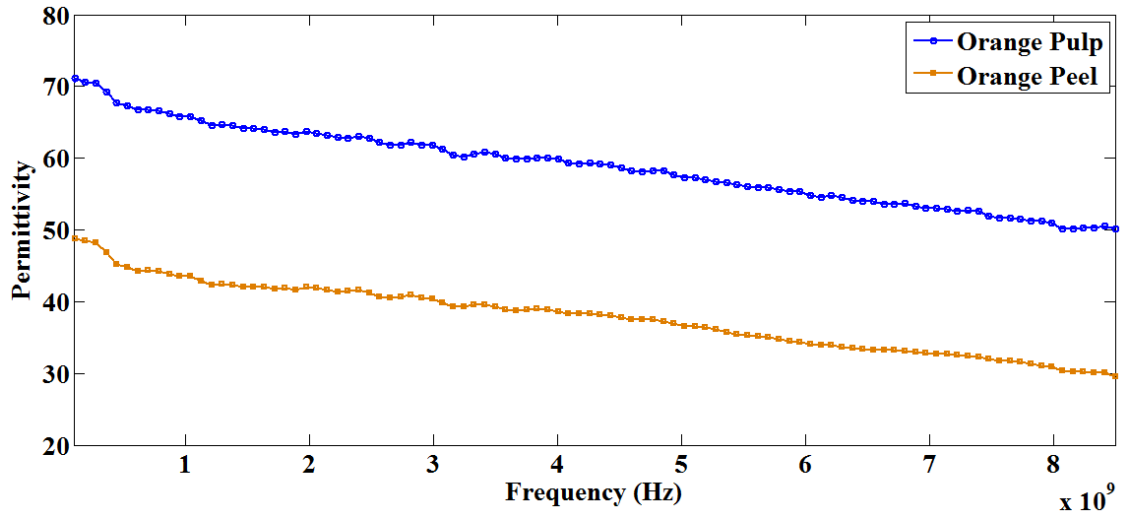
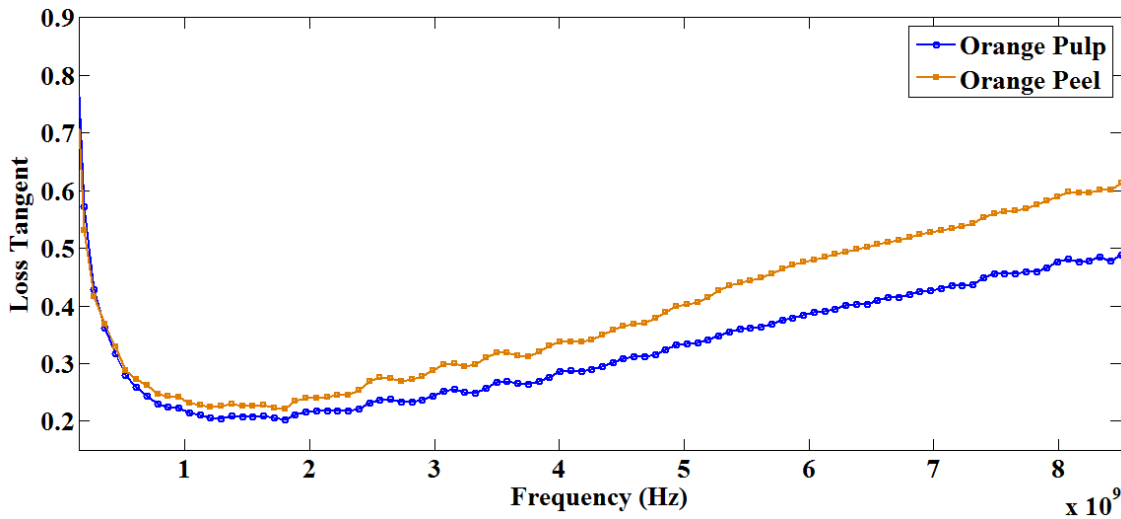


Fig. 3.8: Open ended coaxial probe setup for broadband dielectric properties measurement of orange tissue specimens (a) orange pulp – measurement setup, (b) orange pulp – enlarged view, (c) orange peel – measurement setup and (d) orange peel – enlarged view



(a)



(b)

Fig. 3.9: Broadband dielectric properties of orange pulp and peel specimens up to 8.5 GHz (a) permittivity and (b) loss tangent

### 3.3.4 Dielectric Properties of Water Apple Tissue

Broadband dielectric properties ( $\epsilon_r$ ) i.e. permittivity ( $\epsilon_r'$ ) and loss tangent ( $\tan \delta$ ) of mature water apple specimen have been measured up to 8.5 GHz at 25 °C ambient temperature – the measurement setup and an enlarged view are illustrated in Figs. 3.10(a) and (b) respectively.

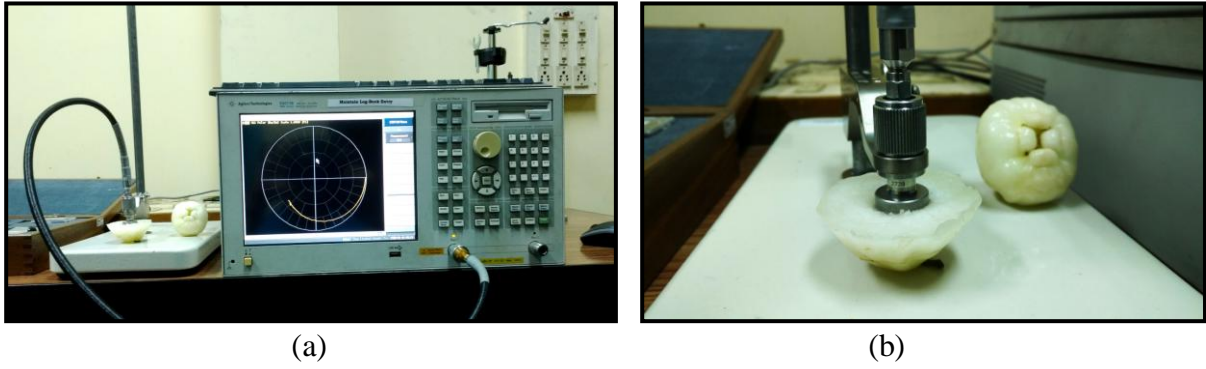


Fig. 3.10: Open ended coaxial probe setup for broadband dielectric properties measurement of water apple tissue specimen (a) total measurement setup, (b) a close-up view

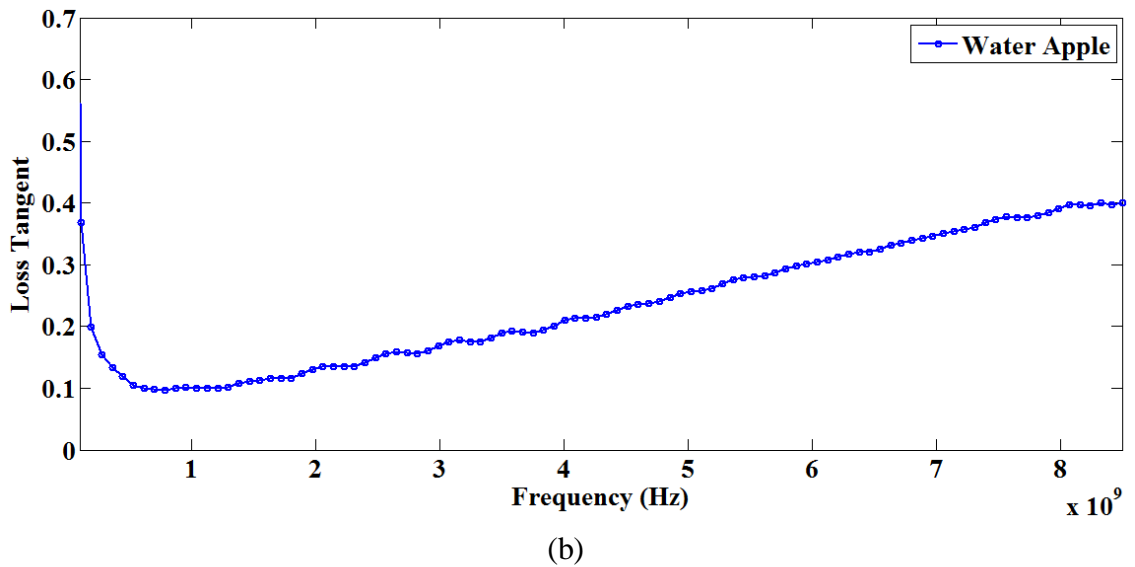
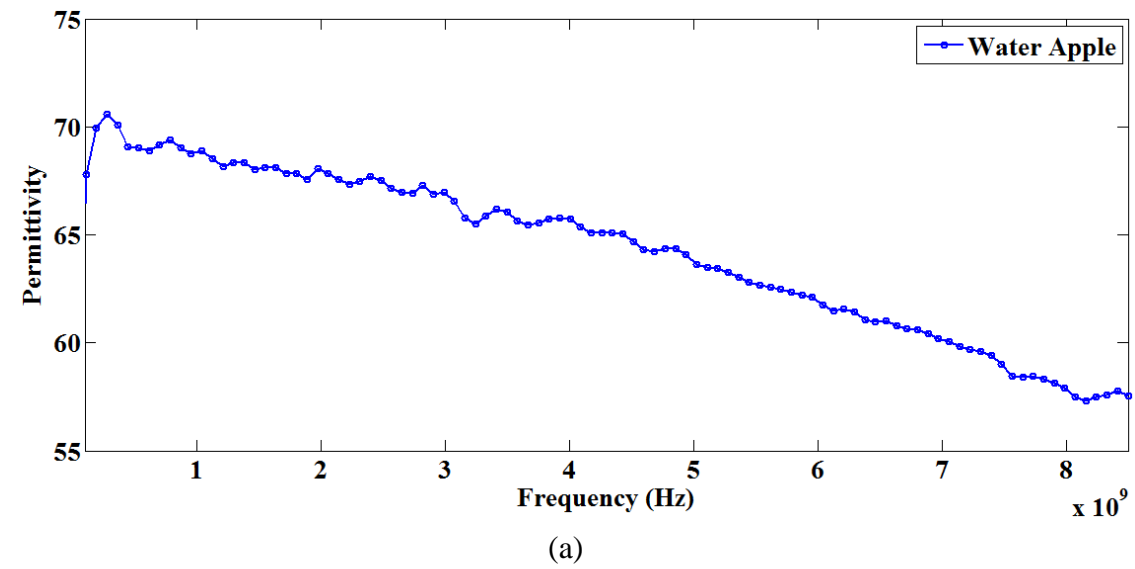


Fig. 3.11: Broadband dielectric properties of water apple specimens up to 8.5 GHz (a) permittivity and (b) loss tangent

Measured permittivity ( $\epsilon_r'$ ) and loss tangent ( $\tan \delta$ ) data for a typical water apple specimen have been plotted in Figs. 3.11(a) and (b) respectively. Reported dielectric properties ( $\epsilon_r$ ) are fairly high due to the presence of sufficient water and ion contents in ripe water apple tissue.

### 3.3.5 Dielectric Properties of Sapodilla Tissues

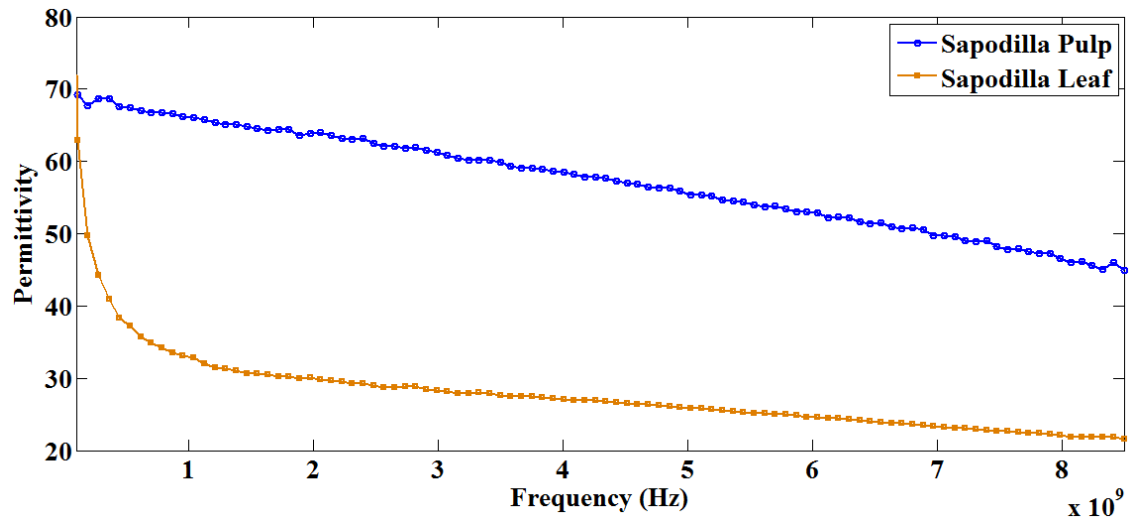
Broadband dielectric properties ( $\epsilon_r$ ) i.e. permittivity ( $\epsilon_r'$ ) and loss tangent ( $\tan \delta$ ) of ripe sapodilla fruit pulp and leaf tissue specimens have been measured up to 8.5 GHz at 25 °C ambient temperature. Photographs of the measurement setup for a typical sapodilla fruit pulp specimen are illustrated in Figs. 3.12(a) and (b). In case of leaf specimens, a number of sapodilla leaves have been stacked together to ensure sufficient thickness without air gap beneath the coaxial probe. Thus, collective MUT thickness turns out to be greater than the skin depth – condition of semi-infinite dimension is fulfilled for accurate dielectric properties ( $\epsilon_r$ ) characterization. Measured permittivity ( $\epsilon_r'$ ) and loss tangent ( $\tan \delta$ ) data for ripe sapodilla fruit pulp and leaf tissue specimens have been plotted in Figs. 3.13(a) and (b) respectively.

As illustrated in Fig. 3.13(a), permittivity ( $\epsilon_r'$ ) of ripe sapodilla fruit pulp is fairly high compared to the respective leaf specimens over the entire frequency spectrum up to 8.5 GHz. Higher water content in ripe fruit pulp predominantly contributes to elevated permittivity ( $\epsilon_r'$ ) value. However, the loss tangent ( $\tan \delta$ ) values of sapodilla leaf tissue are higher than the sapodilla fruit pulp up to 6 GHz – but, the trend alters thereafter at higher frequency region. Please, refer to Fig. 3.13(b).

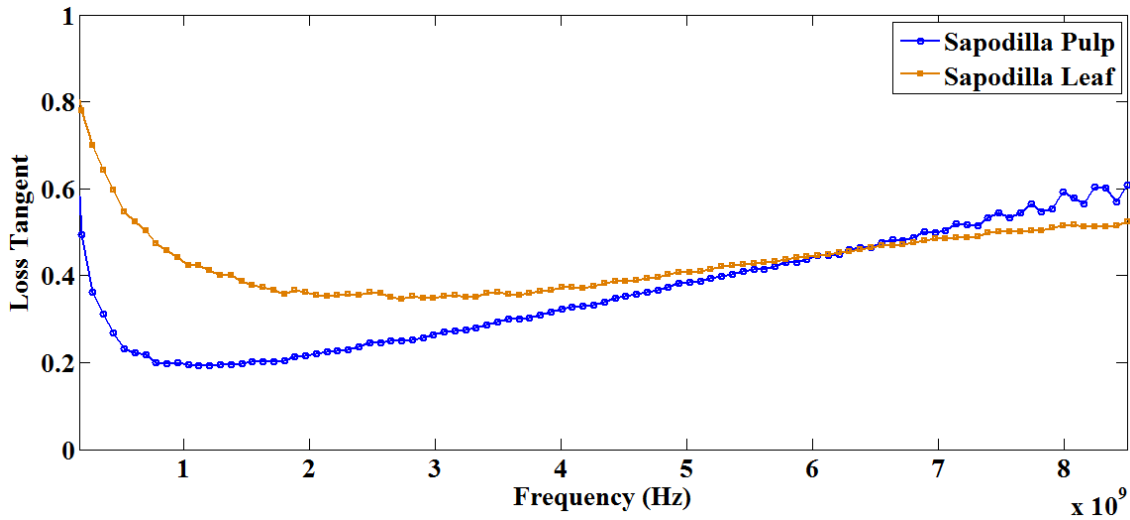


Fig. 3.12: Open ended coaxial probe setup for broadband dielectric properties measurement of sapodilla pulp specimen (a) total measurement setup, (b) close-up view





(a)

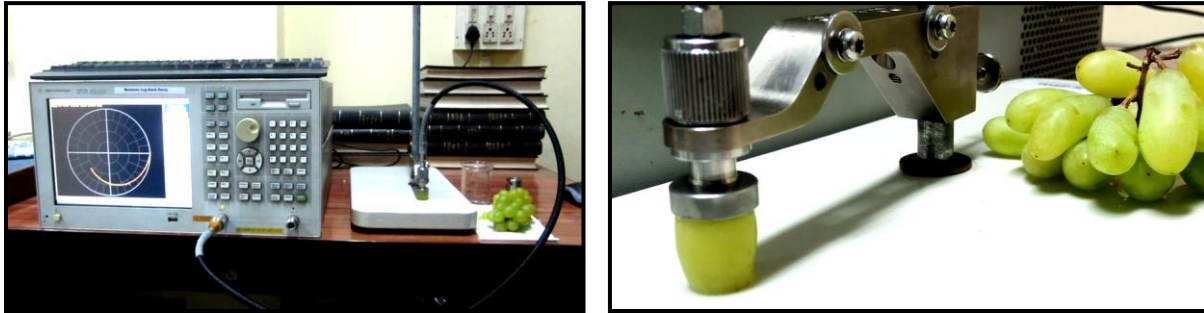


(b)

Fig. 3.13: Broadband dielectric properties of sapodilla pulp and leaf specimens up to 8.5 GHz  
(a) permittivity and (b) loss tangent

### 3.3.6 Dielectric Properties of Grape Tissue

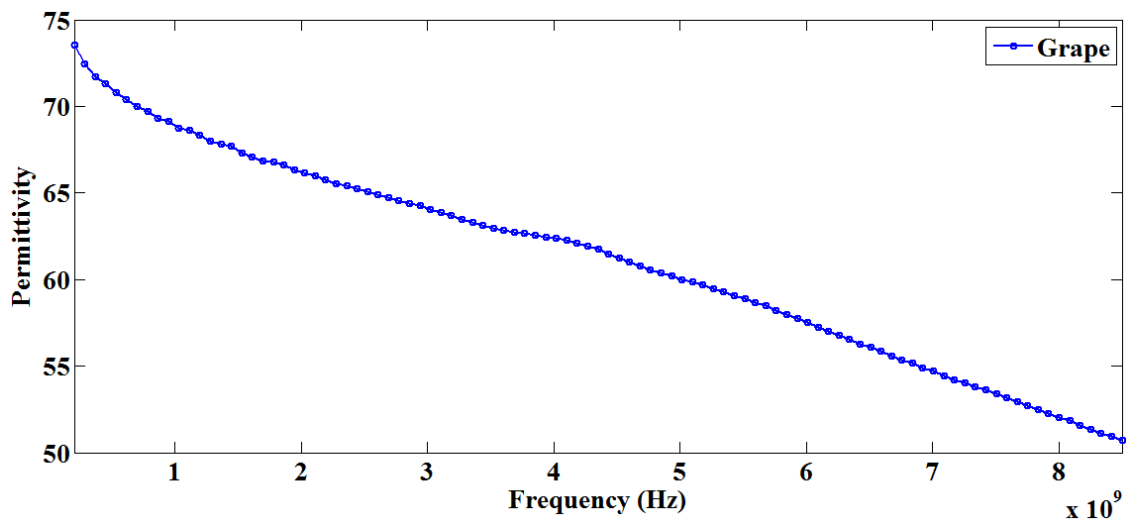
This time, broadband dielectric properties ( $\epsilon_r$ ) of ripe grape fruit pulp specimen have been characterized at 25 °C ambient temperature up to 8.5 GHz. The measurement setup for a typical grape fruit specimen is illustrated in Figs. 3.14(a) and (b).



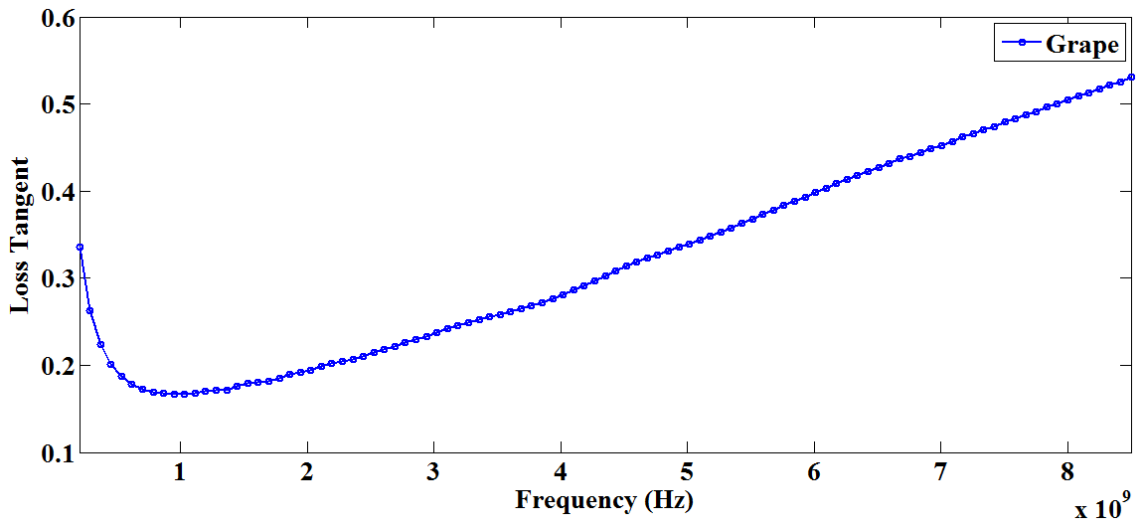
(a)

(b)

Fig. 3.14: Open ended coaxial probe setup for broadband dielectric properties measurement of ripe grape fruit specimen (a) total measurement setup, (b) close-up view



(a)



(b)

Fig. 3.15: Frequency dependent variation in broadband dielectric properties of ripe grape tissue specimen up to 8.5 GHz (a) permittivity and (b) loss tangent



The respective percentages of water and free ion contents are fairly high in ripe grape fruit specimen – thus, the effective skin depth should be reasonably less. Therefore, the condition of semi-infinite MUT thickness can be satisfied even with a single grape fruit beneath the coaxial probe. Measured permittivity ( $\epsilon'_r$ ) and loss tangent ( $\tan \delta$ ) data for ripe grape pulp specimen have been plotted in Figs. 3.15(a) and (b) respectively.

As illustrated in Fig. 3.15(a), permittivity ( $\epsilon'_r$ ) of ripe grape fruit pulp is fairly high over the entire measured spectrum up to 8.5 GHz. As expected, high amount of water content in ripe grape fruit largely contributes to elevated permittivity ( $\epsilon'_r$ ) value. In addition, significant loss tangent ( $\tan \delta$ ) values over a broadband spectrum are caused due to adequate presence of free ions in the ripe grape tissue specimen (please, refer to Fig. 3.15(b)). These free ions possibly take part in different biophysical or transportation activities in plants and fruits.

### 3.3.7 Dielectric Properties of Apple Tissue

Broadband dielectric properties ( $\epsilon_r$ ) of fresh apple fruit tissue have been characterized up to 8.5 GHz at two different temperatures i.e. 25 °C and 16 °C. Prior to performing dielectric measurements, fresh apple fruit specimens have been divided in two sets – one set has been stored at 25 °C ambient temperature and the other at 16 °C ambient temperature for at least 4 hours. Thus, the temperatures of respective apple specimens were made to settle at the desired values i.e. either 25 °C or 16 °C. Next, the temperature dependent variations in permittivity ( $\epsilon'_r$ ) and loss tangent ( $\tan \delta$ ) data have been studied for fresh apple tissue specimens. The overall dielectric properties ( $\epsilon_r$ ) measurement setup for a typical apple fruit specimen is illustrated in Fig. 3.16(a) and an enlarged view is illustrated in Fig. 3.16(b). The apple fruit specimens have been cut with a sharp knife to obtain flat surfaces for avoiding air gap beneath the coaxial probe – thus, an accurate measurement system has been ensured. Measured permittivity ( $\epsilon'_r$ ) and loss tangent ( $\tan \delta$ ) data for the apple specimens at two different temperatures i.e. 25 °C and 16 °C have been plotted in Figs. 3.17(a) and (b) respectively.

The broadband permittivity ( $\epsilon'_r$ ) value for apple fruit specimen reduces with temperature – i.e. the permittivity ( $\epsilon'_r$ ) data are higher at 16 °C and lower at 25 °C over the measured frequency range up to 8.5 GHz (please, refer to Fig. 3.17(a)). In contrast, the broadband loss tangent ( $\tan \delta$ ) / tissue conductivity ( $\sigma$ ) value for apple fruit specimen increases with temperature – as

plotted in Fig. 3.17(b). Observed temperature dependent variations in permittivity ( $\epsilon_r'$ ) and loss tangent ( $\tan \delta$ ) data for the apple fruit tissue are justified and aligned with the previous reported temperature dependent dielectric data available in literature [2-3, 6-7].

To explain temperature dependent complex dielectric properties ( $\epsilon_r$ ) of apple tissue, concepts of ionic and orientational (dipolar) polarization mechanisms should be revisited [1-4, 6-9]. Apple contains enormous ion content – therefore, the ionic polarization dominates over dipolar relaxation at low frequency region and permittivity ( $\epsilon_r'$ ) of apple increases with temperature (typically, up to few tens of MHz) [2-3, 6-7]. However, the same phenomenon is not reflected here in the measured permittivity ( $\epsilon_r'$ ) data for apple because 85070E dielectric measurement kit works from 200 MHz and above [41]. On contrary, permittivity ( $\epsilon_r'$ ) of apple starts decreasing with temperature at higher frequency region where dipolar relaxation mechanism dominates – this phenomenon is observed here (200 MHz to 8.5 GHz) [2-3, 6-7]. As discussed earlier, dipolar molecules tend to move in random directions at higher temperature – thus, the overall alignment of dipolar molecules under external applied electric field gets disturbed at higher temperature and consequently permittivity ( $\epsilon_r'$ ) decreases with temperature [1]. Apple tissue also contains quite high amount of water which is a dipolar molecule – thus, apple exhibits quite strong dipolar relaxation over 200 MHz to 8.5 GHz, and permittivity ( $\epsilon_r'$ ) of apple reduces with temperature [1-3, 6-7]. For every fruit / vegetable, there is a particular frequency point where the permittivity ( $\epsilon_r'$ ) doesn't alter with temperature – ionic polarization dominates below that frequency and dipolar relaxation becomes dominant thereafter. The loss tangent ( $\tan \delta$ ) of apple increases with temperature over entire frequency range – as reported for other fruits as well [2-3, 6-7].

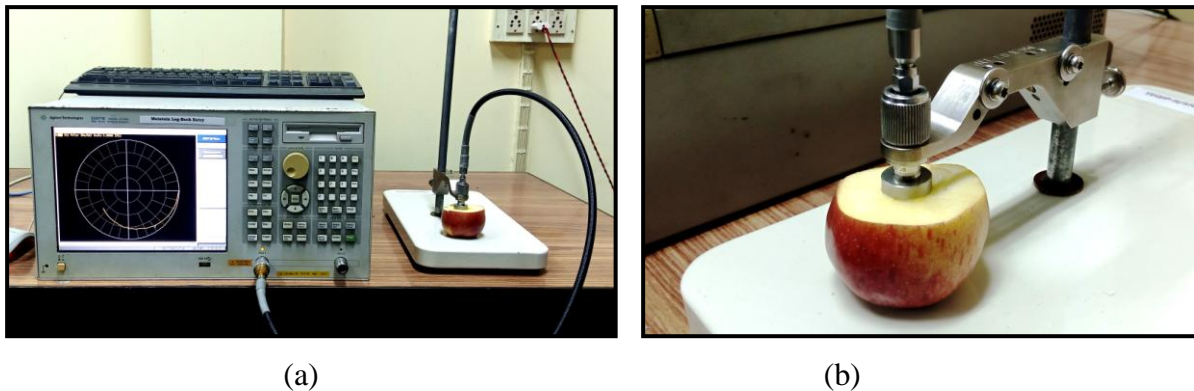


Fig. 3.16: Open ended coaxial probe setup for broadband dielectric properties measurement of apple tissue specimen (a) total measurement setup, (b) a close-up view

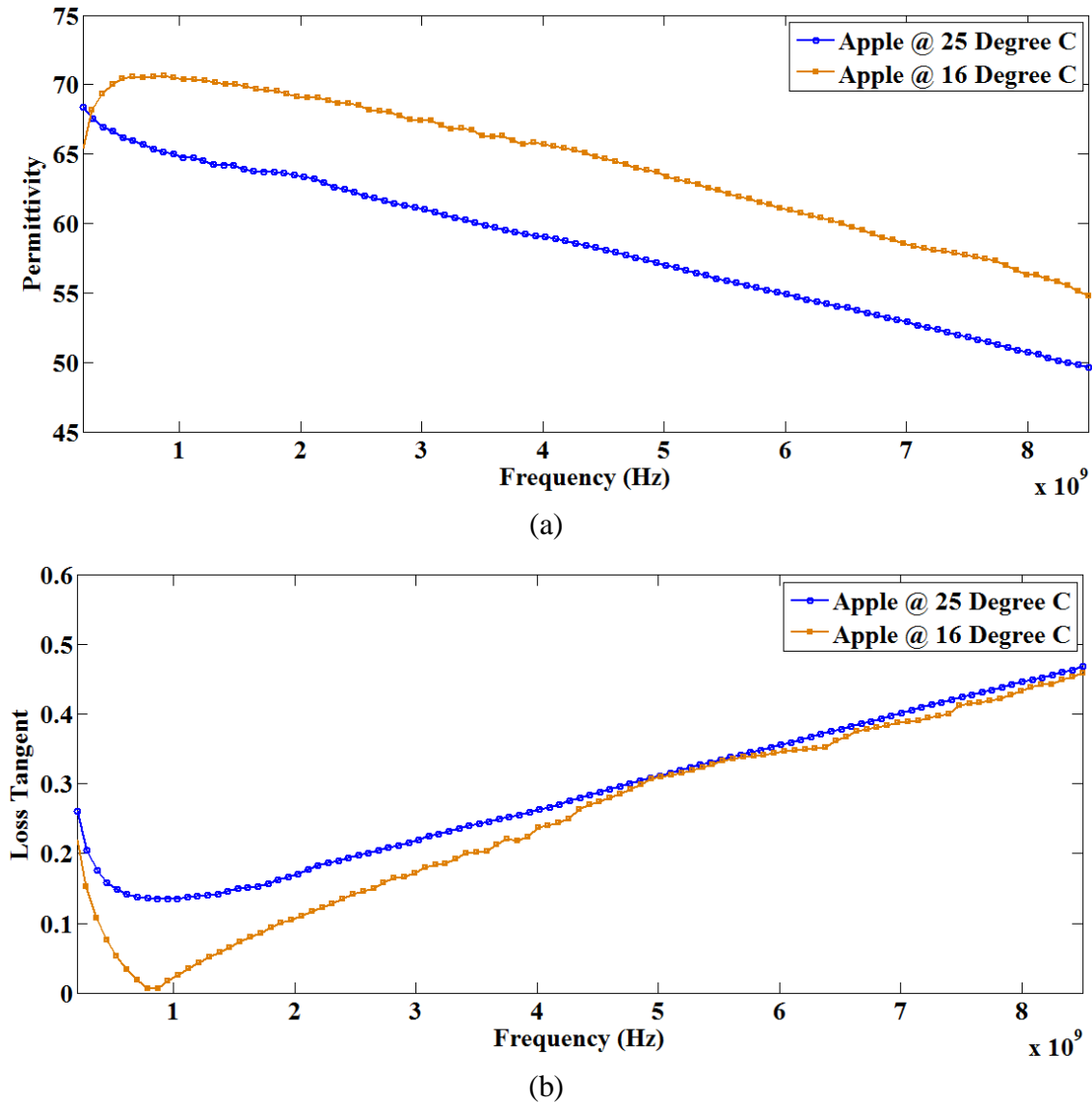


Fig. 3.17: Temperature dependent variations in broadband dielectric properties of apple tissue specimens up to 8.5 GHz (a) permittivity and (b) loss tangent

### 3.3.8 Dielectric Properties of Tomato Tissue

Broadband dielectric properties ( $\epsilon_r$ ) of ripe red tomato tissue have been characterized up to 8.5 GHz at two different temperatures viz. 25 °C and 16 °C. Similar to the apple specimens, fresh red tomato specimens have also been divided in two groups prior to performing measurements – one group has been stored at 25 °C ambient temperature and the other at 16 °C ambient temperature

for at least 4 hours. Subsequently, temperatures of respective tomato specimens settled at the desired values of either 25 °C or 16 °C. Thereafter, temperature dependent variations in permittivity ( $\epsilon_r'$ ) and loss tangent ( $\tan \delta$ ) data have been studied for fresh ripe tomato specimens. The total dielectric properties ( $\epsilon_r$ ) measurement setup and an enlarged view of a typical MUT specimen are illustrated in Figs. 3.18(a) and (b) respectively. The open ended coaxial probe has been optimally pressed against the ripe tomato specimen so that a flat surface can be managed to avoid possible air gap in between – thus, an accurate measurement setup has been established. Characterized permittivity ( $\epsilon_r'$ ) and loss tangent ( $\tan \delta$ ) data for the ripe tomato specimens have been plotted in Figs. 3.19(a) and (b) respectively – at the above mentioned temperatures i.e. 25 °C and 16 °C.

It is observed that broadband permittivity ( $\epsilon_r'$ ) for ripe tomato specimens reduces with temperature – i.e. higher permittivity ( $\epsilon_r'$ ) data have been noted at 16 °C compared to the respective data at 25 °C over the entire measured frequency range up to 8.5 GHz (please, refer to Fig. 3.19(a)). In contrast, noted broadband loss tangent ( $\tan \delta$ ) / tissue conductivity ( $\sigma$ ) data for ripe tomato specimen increase with temperature – as illustrated in Fig. 3.19(b). However, observed temperature dependent variations in dielectric properties ( $\epsilon_r$ ) of ripe red tomato specimens are absolutely justified and aligned with the previous observations for apple specimens. Moreover, research articles indicating similar temperature dependent dielectric variations in fruits and vegetables over the reported frequency span are also available in literature [2-3, 6-7].



Fig. 3.18: Open ended coaxial probe setup for broadband dielectric properties measurement of ripe tomato specimen (a) total measurement setup, (b) a close-up view

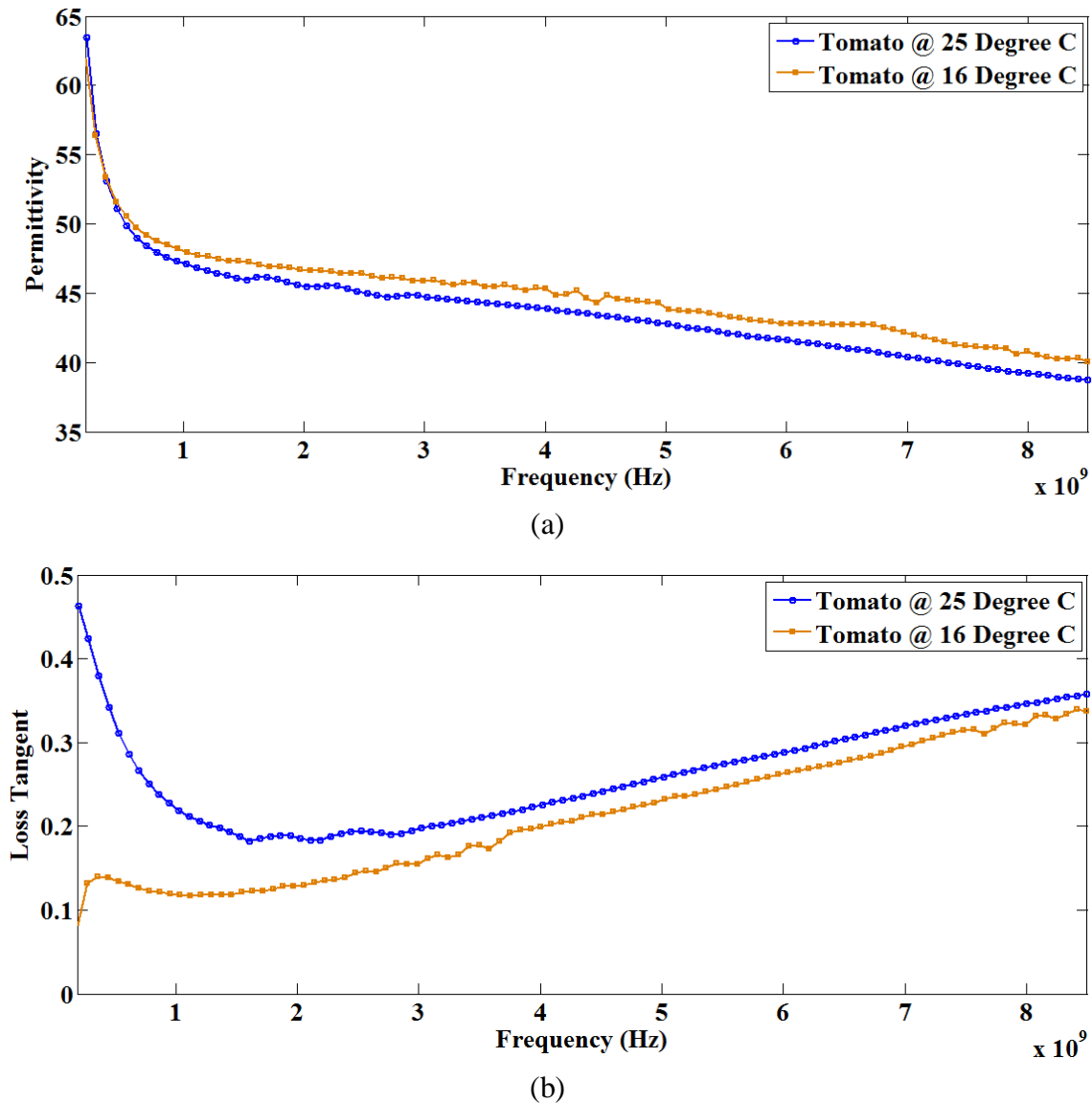


Fig. 3.19: Temperature dependent variations in broadband dielectric properties of ripe tomato tissue specimens up to 8.5 GHz (a) permittivity and (b) loss tangent

### 3.3.9 Dielectric Properties of Brinjal Tissue

Next, broadband dielectric properties ( $\epsilon_r$ ) of mature brinjal tissue have also been characterized up to 8.5 GHz at 25 °C and 16 °C. The brinjal specimens have also been divided in two sets prior to performing dielectric measurements – as performed in cases of apple and tomato specimens. Next, one set has been stored at 25 °C ambient temperature and the other set at 16 °C ambient temperature for at least 4 hours each – thus, the ultimate temperatures of respective brinjal

specimens settled at 25 °C and 16 °C. Subsequently, temperature dependent alterations in dielectric properties ( $\epsilon_r$ ) of mature brinjal specimens have been studied. The overall dielectric properties ( $\epsilon_r$ ) measurement setup and a close-up view of a typical brinjal specimen beneath the coaxial probe are illustrated in Figs. 3.20(a) and (b) respectively. The open ended coaxial probe has been pressed against flat cut plane of the brinjal specimen – thus, air gap has been avoided to obtain accurate measured data. Measured permittivity ( $\epsilon'_r$ ) and loss tangent ( $\tan \delta$ ) data for the brinjal specimens have been plotted in Figs. 3.21(a) and (b) respectively at 25 °C and 16 °C.

The broadband permittivity ( $\epsilon'_r$ ) values for mature brinjal specimens are quite less than other fruit / vegetable specimens – it's primarily due to less water content. Furthermore, the permittivity ( $\epsilon'_r$ ) of mature brinjal specimen reduces with increase in temperature – i.e. higher permittivity ( $\epsilon'_r$ ) data have been measured at 16 °C compared to respective data at 25 °C over the entire range up to 8.5 GHz (please, refer to Fig. 3.21(a)). However, broadband loss tangent ( $\tan \delta$ ) data for the brinjal specimen increase with temperature up to around 3.5 GHz but, the trend reverses thereafter – as illustrated in Fig. 3.21(b). Observed temperature dependent variation in permittivity ( $\epsilon'_r$ ) of mature brinjal specimens is aligned with the previous observations [2-3, 6-7]. In case of loss tangent ( $\tan \delta$ ), the trend is aligned with previous observations up to 3.5 GHz but differs slightly thereafter [2-3, 6-7]. Similar type of trend reversals in temperature dependent dielectric loss factor were reported earlier for navel orange and cucumber specimens around 1 GHz to 2 GHz [6]. On contrary, this trend reversal can also be observed simply due to specimen-to-specimen variation that falls under the category of random error (type A) in the measurement technique [42-44].

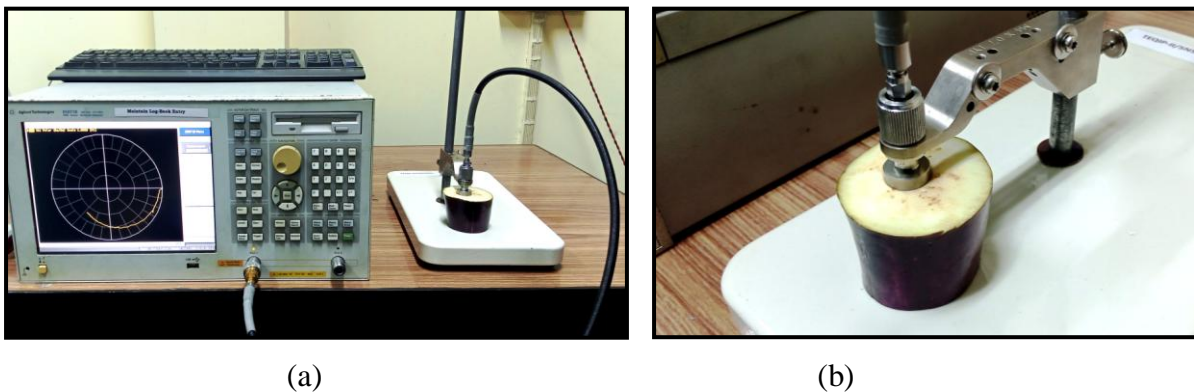


Fig. 3.20: Open ended coaxial probe setup for broadband dielectric properties measurement of mature brinjal specimen (a) total measurement setup, (b) a close-up view

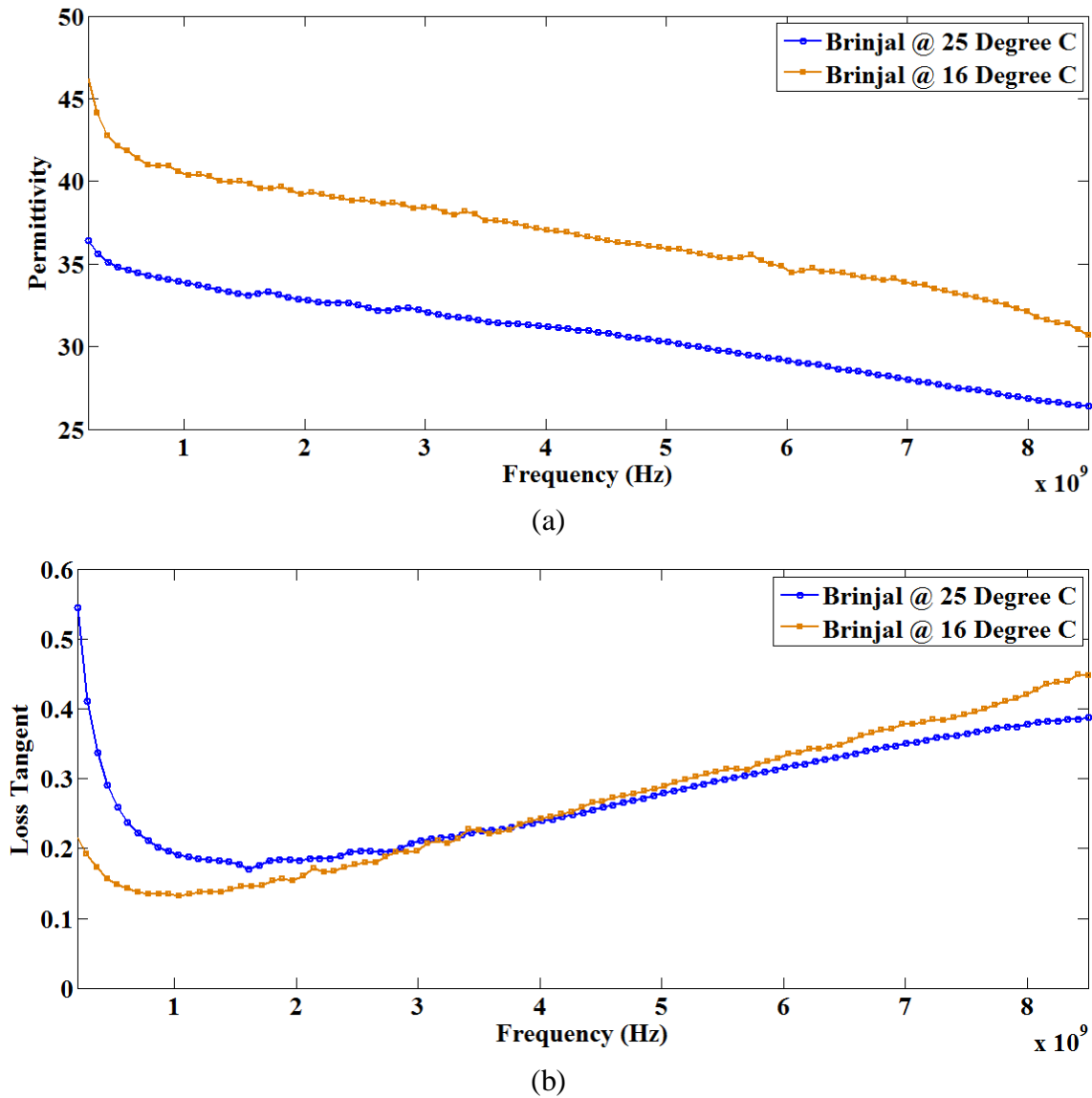


Fig. 3.21: Temperature dependent variations in broadband dielectric properties of mature brinjal tissue specimens up to 8.5 GHz (a) permittivity and (b) loss tangent

### 3.3.10 Dielectric Properties of Guava Tissue

This time, broadband dielectric properties ( $\epsilon_r$ ) of mature guava specimens have been measured up to 8.5 GHz at 25 °C and 16 °C respectively. The fruit specimens (guavas) have been divided in two sets – one set has been stored at 25 °C ambient temperature and the other at 16 °C ambient temperature for at least 4 hours. At subsequent time, the final temperatures of respective guava specimens settled at 25 °C and 16 °C (similar to earlier fruit specimens). Thereafter, temperature



dependent variations in permittivity ( $\epsilon_r'$ ) and loss tangent ( $\tan \delta$ ) properties of mature guava specimens have been studied. The entire dielectric properties ( $\epsilon_r$ ) characterization setup is illustrated in Fig. 3.22(a) – whereas, an enlarged view of a typical guava specimen beneath the open ended coaxial probe is illustrated in Fig. 3.22(b). The open ended coaxial probe has been pressed with optimal pressure on flat cut surface of the guava specimen. This ensures that no air gap is present in between the open end of coaxial probe and the flat cut surface of MUT (guava) specimen for obtaining accurate dielectric data. Finally, measured permittivity ( $\epsilon_r'$ ) and loss tangent ( $\tan \delta$ ) data for the guava specimens have been plotted in Figs. 3.23(a) and (b) respectively at 25 °C and 16 °C.

Permittivity ( $\epsilon_r'$ ) values for mature guava specimens are reasonably high due to sufficient water content – both at 25 °C and 16 °C. However in contrast to the earlier observations, permittivity ( $\epsilon_r'$ ) data for mature guava specimens have been noted to be increased with temperature – i.e. higher permittivity ( $\epsilon_r'$ ) data have been measured at 25 °C compared to 16 °C over the entire measured frequency range up to 8.5 GHz (please, refer to Fig. 3.23(a)). Moreover, broadband loss tangent ( $\tan \delta$ ) data for guava specimen increase with temperature up to 1 GHz – but, the trend has been lost thereafter – as illustrated in Fig. 3.23(b). Thus, the overall temperature dependent variations in dielectric properties ( $\epsilon_r$ ) of mature guava specimens are somewhat misaligned with previous observations [2-3, 6-7]. Observed misalignments in temperature dependent variations in dielectric properties ( $\epsilon_r$ ) of guava specimens seem to be solely due to specimen-to-specimen variation under random error (type A) – possibly, the guava specimen characterized at 25 °C was overripe [42-44].

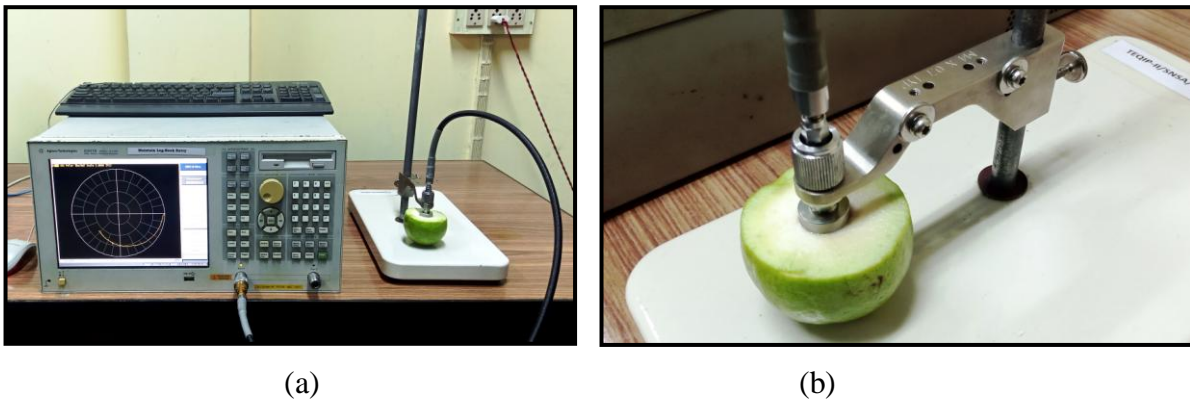


Fig. 3.22: Open ended coaxial probe setup for broadband dielectric properties measurement of mature guava specimen (a) total measurement setup, (b) a close-up view



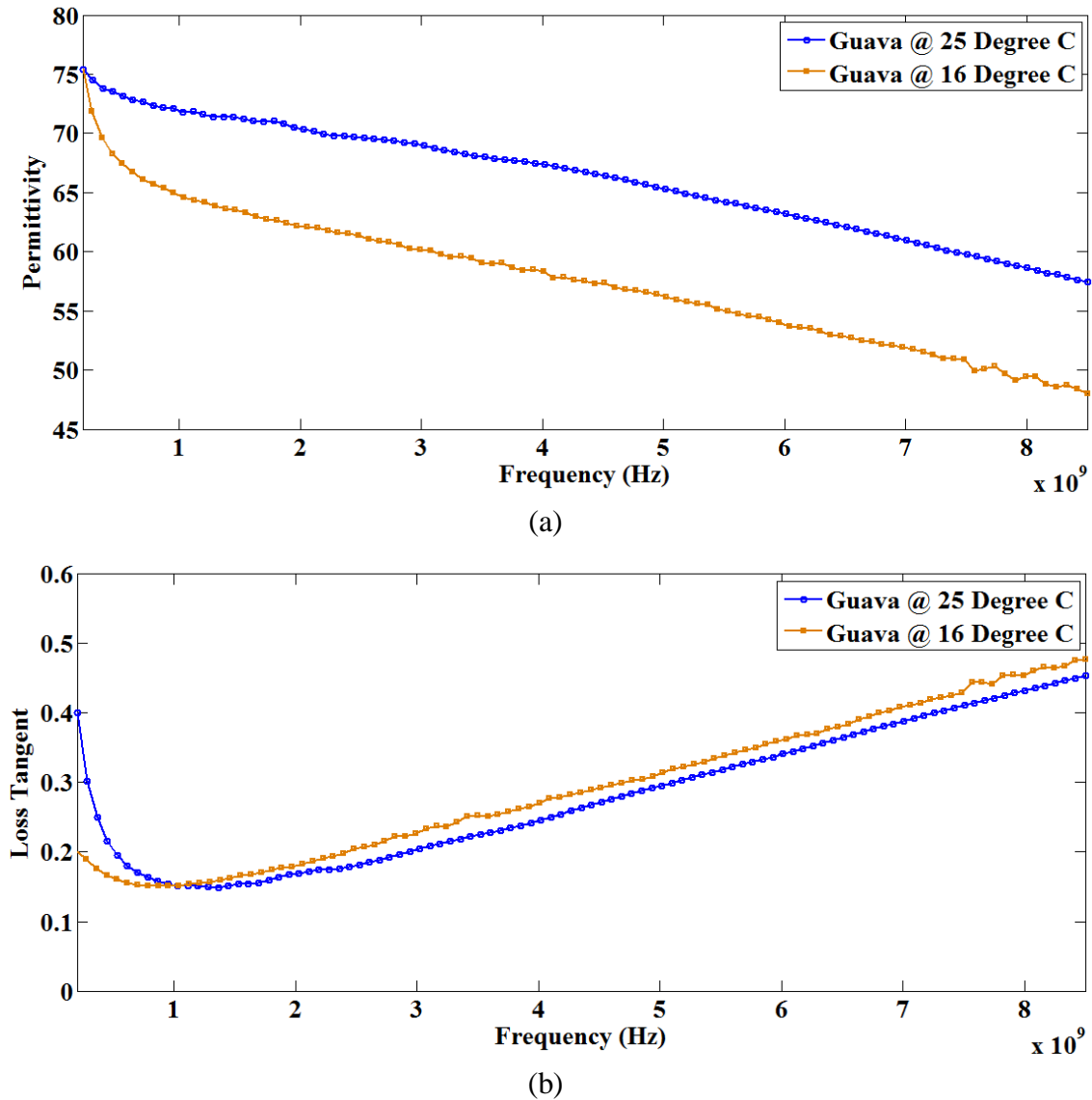


Fig. 3.23: Temperature dependent variations in broadband dielectric properties of mature guava tissue specimens up to 8.5 GHz (a) permittivity and (b) loss tangent

### 3.4 Conclusions

The physics of different polarization phenomenon, contributing to broadband complex dielectric properties ( $\epsilon_r$ ) of different materials, have initially been outlined in the first part of this chapter. In addition, selection of the most suitable non-destructive broadband dielectric properties ( $\epsilon_r$ ) measurement technique (open ended coaxial probe technique) has been justified along with the technical and analytical specifications. Next, measured permittivity ( $\epsilon'_r$ ) and loss tangent ( $\tan \delta$ )

data for numerous plant and fruit specimens have been presented in this part using graphical illustrations – in addition, the temperature dependent variations in complex dielectric properties ( $\epsilon_r$ ) of some fruit specimens have also been studied over the measured frequency range.

Based on the measured data, it is clearly noticed that permittivity ( $\epsilon_r'$ ) of all plant and fruit tissues reduces with frequency i.e. over the span of 200 MHz to 8.5 GHz. It is so because there is a significant presence of water ( $H_2O$ ) in all plant and fruit tissues and the same demonstrates orientational polarization (dipolar molecule). Now, as the frequency increases, the externally applied electric field varies in magnitude with time at a faster rate. As a result, the dipolar molecules in plant and fruit tissues also attempt to follow the fast time variation in applied electric field strength in alternating cycles. But, two prime factors oppose immediate alignment of the dipolar molecules with the applied field at higher frequency range – firstly, the thermal energy of dipolar molecules attempt to destroy their alignment in a particular direction with the applied time varying electric field and randomize their orientation. Over and above, these dipolar molecules rotate in a viscous like medium due to their interactions with adjacent molecules and thus, the dipolar molecules are somewhat restricted to respond immediately to the time varying electric field at higher frequency range. As a consequence of these two phenomena, dipolar molecules in plant and fruit tissues can't follow the rapid time variation in applied electric field at higher frequencies and demonstrate reduced permittivity ( $\epsilon_r'$ ).

In addition, broadband permittivity ( $\epsilon_r'$ ) of different fruit specimens reduces with temperature in general – whereas, loss tangent ( $\tan \delta$ ) increases with temperature. This observation can also be explained with orientational polarization of dipolar molecules in fruit tissues. The thermal energy of dipolar molecules increases with temperature – thus, alignment of dipolar molecules along the direction of applied electric field is furthermore inhibited. Hence, permittivity ( $\epsilon_r'$ ) reduces and loss tangent ( $\tan \delta$ ) increases with temperature.

Reported complex dielectric properties ( $\epsilon_r$ ) of these fruits and plants are indeed useful for 'Specific Absorption Rate (SAR)' estimations in prototyped fruit and plant models in accordance with different electromagnetic regulatory guidelines – as discussed in the next chapter. Moreover, measured dielectric properties ( $\epsilon_r$ ) of these specimens have also been utilized as reference dataset for preparing different fruit and plant tissue equivalent homogeneous phantom liquids for practical SAR measurements (Chapter 5).

## Part II: Multilayer Tissue Modeling

### 3.5 Introduction to Multilayer Tissue Modeling

It's now clear and an established fact that interaction of electromagnetic energy with living biological systems can't be avoided because of the massive utilization of wireless telecommunication systems over a wide spectrum of frequency band. Above said interaction mechanism with biological objects can take place either in far field or in near field of the electromagnetic radiating element – based on the applications [49-58]. Far field plane wave exposure of biological bodies takes place due to mobile tower antenna radiation – whereas, mobile phones and other wireless Body-Area-Network (BAN) devices are the primary reasons for human body exposure to electromagnetic fields near the radiating element [49-58]. As a consequence, it is equally important to quantify electromagnetic energy absorption rate either due to plane wave incidence in far field or very close to the radiating antenna i.e. in near field region. This electromagnetic energy absorption rate is termed as ‘Specific Absorption Rate (SAR)’ in relevant literature [59-63] – SAR is defined as the rate of electromagnetic energy absorption per unit mass of biological tissue while exposed to an external incident electromagnetic field. Magnitude of SAR value in principle depends upon the geometrical shape of living biological object, number of distinguishable tissue layers, complex dielectric properties ( $\epsilon_r$ ) of individual tissue layer, material density of each tissue layer, magnitude of incident electric field, direction of arrival and polarization of incident electric field [55-58]. Therefore, once the above mentioned parameters are known, point SAR value at a particular location can easily be calculated employing any standard electromagnetic solver such as CST Microwave Studio (CST MWS) [64]. The mathematical formulation for point SAR calculation is  $\sigma|E|^2/2\rho$  – where,  $\sigma$  denotes electrical conductivity of the tissue, E represents peak electric field strength developed inside the biological tissue and  $\rho$  represents the density of the biological tissue. Therefore, it is clear that point SAR value significantly depends upon the second degree of peak electric field magnitude (developed inside biological tissue layer) [59-63]. Next, for practical SAR measurement and validation purposes, actual electric field probing and measurement inside the biological model is deemed necessary. However, any invasive technique that involves inserting electric field probes inside living biological tissue layer is completely avoided during

practical SAR measurement – as prescribed by medical ethics. Thus, to overcome this measurement issue, several attempts have been taken to formulate and prepare tissue equivalent homogeneous phantom liquid with dispersive complex dielectric properties ( $\epsilon_r$ ) [59, 61-62, 65-69]. During initial phase, human head equivalent phantom liquid was proposed and formulated by simply considering average dielectric properties ( $\epsilon_r$ ) between the grey and white matters for practical SAR measurement [65-67]. Thereafter, a multilayer tissue equivalent dielectric liquid formula was proposed based on considering the average permittivity ( $\epsilon'_r$ ) of all tissue layers and thereafter adjusting the conductivity ( $\sigma$ ) of that equivalent liquid, so that the original 1g or 10g averaged SAR value in a particular multilayer biological model can be attained [68]. In somewhat similar fashion, another group of researchers formulated a range of head tissue equivalent phantom liquids simply by matching the maximum 10g averaged SAR value with tuned complex dielectric properties ( $\epsilon_r$ ) [69]. Nevertheless, none of the above reported equivalent liquid formulating techniques attempted to replicate either the electric field distribution or the point SAR distribution in original multilayer biological model. Thus, the concerned scientists and researchers are yet to address alignment of point SAR distributions in the original multilayer biological model and the equivalent homogeneous phantom liquid on basis of three dimensional coordinates. In addition, SAR assessment in different prototyped plant and fruit models is another contemporary research theme primarily due to plane wave irradiation in far field region – this research field has been vastly explored in the next part of this thesis. As a consequence, formulation of multilayer plant/fruit tissues equivalent homogeneous dielectric phantom liquid is an added research challenge.

It must be noted that, till date, no generalized and structured framework has been formulated that defines complex dielectric properties ( $\epsilon_r$ ) of the equivalent phantom liquid based on multi-dimensional critical parameters such as dielectric properties ( $\epsilon_r$ ), thickness, stacking sequence and geometrical shape of original biological layers, and also irrespective of far field or near field exposure scenarios. As a consequence, a generalized and structured technique is indeed required on urgent basis to formulate and further synthesize the equivalent homogeneous phantom liquids with customized permittivity ( $\epsilon'_r$ ) and loss tangent ( $\tan \delta$ ) for any random stacked tissue layer combinations in either far or near field exposure scenario. As an accurate SAR measurement is the ultimate objective, any chosen figure of merit for formulating and further synthesizing the

equivalent homogeneous phantom liquid should be defined based on realistic spatial matching of point-wise SAR or internal electric field distributions inside the biological model.

### 3.6 A Brief Outline of the Problem

The work presented in the subsequent part of this chapter aims at formulating and developing a novel, generalized, as well as structured protocol to determine effective complex dielectric properties ( $\epsilon_r$ ) of homogeneous phantom liquid equivalent to any prototyped multilayer tissue model for accurate SAR measurement. In addition, the proposed technique must also be capable of tuning the complex dielectric properties ( $\epsilon_r$ ) of tissue equivalent phantom liquid both in far field due to plane wave exposure as well as in near field i.e. close to the radiating antenna. In this work, electric field distribution as well as point SAR distribution in the original multilayer tissue model has been considered while formulating and developing the basis towards a structured protocol. To address multi-dimensional aspects of the problem, a number of critical parameters such as thickness, relative positioning and geometric shape of each tissue layer have been taken into account while determining the equivalent complex dielectric properties ( $\epsilon_r$ ) of homogeneous phantom liquid. The technique has been proposed to be developed in such a way that the same can work at any particular frequency of interest. Once the proposed protocol is finalized, it can be applied to two specific problems having four tissue layers with different permittivity ( $\epsilon_r'$ ) and loss tangent ( $\tan \delta$ ) values. In one of these two cases, the dielectric tissue layers are of equal thickness – whereas, the dielectric tissue layers are of unequal thickness in the other case. Furthermore, the proposed and developed protocol is applied to the above mentioned multilayer biological tissue prototypes both in plane wave irradiation scenario (far field) as well as in close proximity region to the transmitting antenna (near field) – therefore, the generic nature of this novel protocol is also validated. In the following part, it has been attempted to achieve appropriate permittivity ( $\epsilon_r'$ ) and loss tangent ( $\tan \delta$ ) values of the multilayer tissue equivalent homogeneous phantom liquids for two distinct tissue layer combinations along with two different exposure scenarios (far field and near field).

### 3.7 Multilayer Equivalent Phantom Liquid Formulation Technique

It is already discussed that point SAR at a particular position inside the biological tissue layer at large depends on the magnitude of developed electric field strength at that position ( $|E|$ ), tissue

conductivity ( $\sigma$ ) and tissue density ( $\rho$ ). Thus,  $\sigma$  and  $\rho$  being fixed for a particular type of tissue at a fixed temperature, SAR greatly varies with the squared magnitude of developed electric field strength ( $|E|^2$ ) [59-63]. Hence, there are first and foremost two parameters i.e. internally developed electric field ( $E$ ) and point SAR that can help to formulate an appropriate protocol for defining homogeneous dielectric phantom liquid equivalent to a multilayer biological body (for practical SAR measurement).

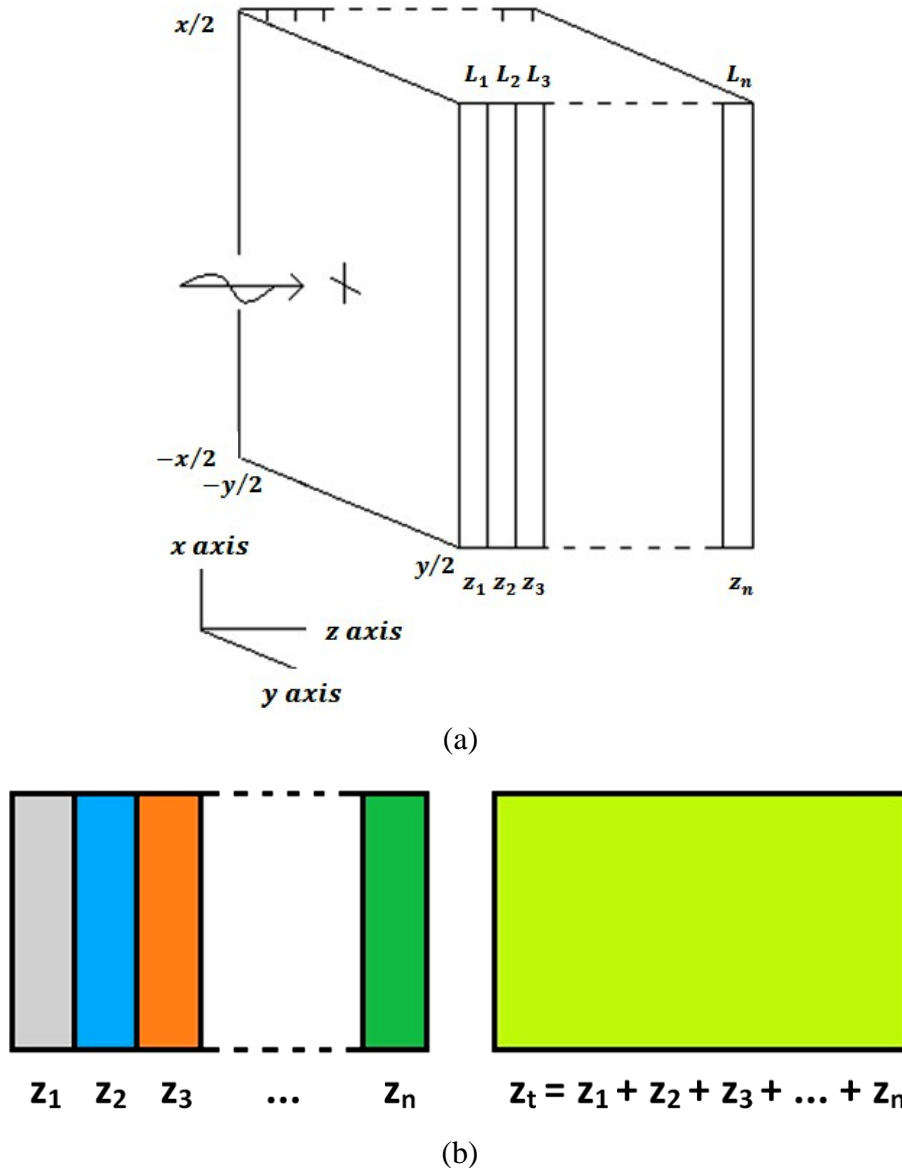


Fig. 3.24: Electromagnetic wave incidence on multilayer tissue model and an equivalent homogeneous phantom formulation (a) a linearly polarized plane wave impinges on the first layer and propagates through all the subsequent layers of  $n$ -layer tissue model, (b) an equivalent homogeneous problem with single phantom dielectric layer of thickness  $z_t$

Fig. 3.24(a) demonstrates the original problem consisting of an n-layer ( $L_1$  to  $L_n$  respectively) biological tissue model – the tissue layer thicknesses and material densities are  $z_1, z_2, z_3, \dots, z_n$  and  $\rho_1, \rho_2, \rho_3, \dots, \rho_n$  respectively. It is important to note that all the tissue layers have equal cross-sectional dimensions along  $x$  ( $-x/2$  to  $+x/2$ ) and  $y$  ( $-y/2$  to  $+y/2$ ) axes – these cross-sectional dimensions are indeed electrically large at the frequency of interest. Thus, the effect of dielectric discontinuities (due to cross-sectional boundaries) can be minimized at the cross-sectional center ( $x = 0, y = 0, z = 0$  to  $z_t$ ) of each tissue layer. At this point, there are two probable exposure scenarios – either, a far field plane wave impinges on the first layer ( $L_1$ ) and passes through all subsequent layers ( $L_2$  to  $L_n$  respectively) of the n-layer tissue model, or, an antenna radiates in close proximity to the first layer ( $L_1$ ) of the same n-layer tissue model and the emitted electromagnetic energy then interacts with the subsequent tissue layers ( $L_2$  to  $L_n$  respectively). In case of far field scenario, a plane wave with linear polarization propagating along  $z$  axis and electric field varying along  $x$  axis impinges on the very first tissue layer ( $L_1$ ) and then propagates through subsequent tissue layers ( $L_2$  to  $L_n$  respectively). In the later case, a simple rectangular microstrip patch antenna radiates in the fundamental mode along  $z$  axis (broadside radiation) in close proximity (near field region) to the very first layer ( $L_1$ ) and the emitted field further interacts with the subsequent dielectric tissue layers i.e.  $L_2$  to  $L_n$  respectively. Fig. 3.24(b) illustrates the equivalent phantom problem with single homogeneous dielectric layer of permittivity ( $\epsilon'_r$ ), loss tangent ( $\tan \delta$ ), thickness ( $z_t$ ) (where,  $z_t = z_1 + z_2 + z_3 + \dots + z_n$ ) and material density ( $\rho_e$ ) (practically,  $\rho_e$  should depend upon choice of equivalent phantom medium based on original multilayer dielectric model – however, in practice,  $\rho_e$  is considered to be  $1000 \text{ kg/m}^3$  for SAR measurements in human tissue equivalent phantom liquid). Now, the prime aim is to determine equivalent  $\epsilon'_r$  and  $\tan \delta$  of the homogeneous phantom liquid so that either electric field distribution or point SAR distribution along the central coordinate points ( $x = 0, y = 0, z = 0$  to  $z_1 + z_2 + z_3 + \dots + z_n$ ) inside the multilayer tissue model and the homogeneous phantom model are spatially similar; however, the exact same electric field or point SAR distribution can never be achieved employing a single-layered homogeneous equivalent liquid particularly at and around the dielectric layer interfaces in original n-layer model.

At initial phase, the maximum difference between two electric field distribution curves from the original n-layer model and the equivalent homogeneous phantom liquid model with varied  $\epsilon'_r$  and  $\tan \delta$  is minimized. A coordinate position dependent ( $z$  dependent) cost function  $f_{i(jk)}$ , computed along cross-sectional central line ( $x = 0, y = 0$ ), is defined as the absolute difference between the two electric field distribution curves in the original n-layer model and the equivalent homogeneous model. This cost function is expressed as described in Eq. (3.32a).

$$f_{i(jk)} = |E_{i(org)} - E_{i(jk)eq}| \quad (3.32a)$$

where,  $i$  varies from 0 to  $z_1 + z_2 + z_3 + \dots + z_n$   
 $j$  represents tuned permittivity value  
 $k$  represents tuned loss tangent value

It should be noted that  $E_{i(org)}$  and  $E_{i(jk)eq}$  are the respective magnitudes of peak electric fields at  $i^{th}$  location in original n-layer tissue model and equivalent single-layered phantom model.

The coordinate location, where  $f_{i(jk)}$  is observed to be maximum, is unique for each combination of permittivity ( $\epsilon'_r$ ) and loss tangent ( $\tan \delta$ ) of the equivalent homogeneous phantom liquid. The maximum value of  $f_{i(jk)}$  is defined as the figure of merit i.e.  $Max(f_{i(jk)})$ .

$$Figure\ of\ merit = Max(f_{i(jk)}) \quad (3.32b)$$

This  $Figure\ of\ merit = Max(f_{i(jk)})$  in Eq. (3.32b) needs to be minimized by tuning the permittivity ( $j$ ) and loss tangent ( $k$ ) of the equivalent homogeneous phantom liquid in an appropriate manner.

In case of the original multilayer (n-layer) problem, it is noted that magnitude of electric field is normally maximum in the first layer ( $L_1$ ) and it is sufficiently high compared to subsequent tissue layers ( $L_2$  to  $L_n$  respectively). As a consequence, the figure of merit defined in Eq. (3.32b) is typically dominated by the very first layer ( $L_1$ ) itself – thus, the equivalent complex dielectric properties ( $\epsilon_r$ ) of the homogeneous phantom liquid are noted to be biased toward  $L_1$  characteristics and very little priority is allotted to the subsequent tissue layers ( $L_2$  to  $L_n$  respectively). To prevail over this issue, a tailored figure of merit is further decided on based on the maximum fractional difference between electric field distribution curves of the original n-



layer model and the equivalent homogeneous phantom model. This particular cost function would stay away from assigning undue priority to the initial tissue layers. Thus, a new  $z$ -coordinate dependent dimensionless cost function  $f'_{i(jk)}$  at  $(x = 0, y = 0)$  is introduced in Eq. (3.33a).

$$f'_{i(jk)} = |(E_{i(org)} - E_{i(jk)eq})/E_{i(org)}| \quad (3.33a)$$

where,  $i$  varies from 0 to  $z_1 + z_2 + z_3 + \dots + z_n$   
 $j$  represents tuned permittivity value  
 $k$  represents tuned loss tangent value

Now, the maximum value of  $f'_{i(jk)}$  is defined as the modified figure of merit i.e.  $Max(f'_{i(jk)})$ .

$$Figure\ of\ merit = Max(f'_{i(jk)}) \quad (3.33b)$$

Subsequently, this cost function is further modified to directly consider the difference in point SAR distribution curves instead of the difference in peak electric field distribution curves. It is already discussed that point SAR value varies with squared magnitude of the developed electric field inside biological tissue layers ( $|E|^2$ ) [59-63] – thus, it can be argued that a cost function formulation based on the difference in point SAR distribution curves is expected to be more appropriate than the earlier ones described in Eqs. (3.32a), (3.32b), (3.33a) and (3.33b) respectively. It is so because SAR is the standard and worldwide accepted metric to directly correlate with electromagnetic energy absorption in different complex biological models. Subsequently, a different coordinate position dependent ( $z$  dependent) cost function  $g_{i(jk)}$ , computed along the cross-sectional central line ( $x = 0, y = 0$ ), is now introduced as the absolute difference between the two point SAR distribution curves from the original  $n$ -layer model and the equivalent homogeneous phantom model. Now, the maximum value of  $g_{i(jk)}$  is defined as the modified figure of merit i.e.  $Max(g_{i(jk)})$  – the same is required to be minimized. These modified cost function i.e.  $g_{i(jk)}$  and the associated figure of merit i.e.  $Max(g_{i(jk)})$  are described in Eqs. (3.34a) and (3.34b) respectively.

$$g_{i(jk)} = |point\ SAR_{i(org)} - point\ SAR_{i(jk)eq}| \quad (3.34a)$$

where,  $i$  varies from 0 to  $z_1 + z_2 + z_3 + \dots + z_n$   
 $j$  represents tuned permittivity value  
 $k$  represents tuned loss tangent value

$$\text{Figure of merit} = \text{Max}(g_{i(jk)}) \quad (3.34b)$$

At the final phase, a further tailored cost function  $g'_{i(jk)}$  is defined based on the fractional difference between two point SAR distribution curves of the original n-layer model and the equivalent homogeneous phantom model. This new z-coordinate dependent dimensionless cost function  $g'_{i(jk)}$  along cross-sectional central coordinates ( $x = 0, y = 0$ ) is introduced in Eq. (3.35a). Next, maximum value of  $g'_{i(jk)}$  is considered as the final figure of merit i.e.  $\text{Max}(g'_{i(jk)})$  – this needs to be minimized. This modified figure of merit i.e.  $\text{Max}(g'_{i(jk)})$  is described in Eq. (3.35b).

$$g'_{i(jk)} = |(\text{point SAR}_{i(org)} - \text{point SAR}_{i(jk)eq}) / \text{point SAR}_{i(org)}| \quad (3.35a)$$

where,  $i$  varies from 0 to  $z_1 + z_2 + z_3 + \dots + z_n$   
 $j$  represents tuned permittivity value  
 $k$  represents tuned loss tangent value

$$\text{Figure of merit} = \text{Max}(g'_{i(jk)}) \quad (3.35b)$$

Herein, it must be noted that the proposed technique for finding out the most appropriate equivalent homogeneous dielectric liquid for SAR measurement, is generic in nature – as, this proposed technique is applicable for any number of tissue dielectric layers, individual tissue layer thickness, dielectric properties ( $\epsilon_r$ ) of individual tissue layer, material density of each tissue layer, frequency of operation, either far field or near field irradiation, magnitude of incident electric field strength and geometrical shape of multilayer biological model.

## **3.8 Multilayer Equivalent Homogeneous Phantom Liquid for Plane Wave Exposure in Far Field Scenario**

### **3.8.1 Plane Wave Exposure – A Typical Four Equal Layer Model**

The proposed technique outlined in the previous section has been applied to a prototyped four tissue layer model ( $L_1$  to  $L_4$ ) with different permittivity ( $\epsilon_r'$ ) and loss tangent ( $\tan \delta$ ) values – it should be noted that all four tissue layers ( $L_1$  to  $L_4$ ) are of identical thickness. In addition, it is considered that all the four layers ( $L_1$  to  $L_4$ ) possess same material density of  $1000 \text{ kg/m}^3$ . A plane wave with linear polarization at  $2.45 \text{ GHz}$  is assumed to impinge on this four equal tissue layers prototype ( $L_1$  to  $L_4$ ). At first, the plane wave impinges on the first tissue layer ( $L_1$ ), with normal incidence to the cross-sectional surface of the biological model, and subsequently propagates through the rest three equal tissue layers ( $L_2$  to  $L_4$ ). The incident plane wave possesses  $27.46 \text{ V/m}$  peak electric field strength as limited for existing Indian public exposure scenario [63]. The cross-sectional dimensions of all four tissue layers ( $L_1$  to  $L_4$ ) are  $50 \text{ cm} \times 50 \text{ cm}$  along with individual layer thickness of  $1 \text{ cm}$  each – as illustrated in Fig. 3.25. Both the peak electric field and the point SAR data are noted along cross-sectional central coordinates of all the tissue layers ( $x = 0, y = 0$  i.e. along  $z$ -axis) so that negligible effects of boundary discontinuity along lateral directions can be ensured in this work. Thickness and dielectric properties ( $\epsilon_r$ ) of individual tissue layers have been outlined in Table 3.1. Then, at first, transient (time domain) simulation is performed in CST MWS 2018 to obtain peak electric field as well as point SAR distributions in the original four equal tissue layers model – along the cross-sectional central coordinates ( $x = 0, y = 0$ ) i.e. for different values of  $z$  coordinate [64]. At subsequent phase, seventy two more transient simulations are performed by systematically tuning the permittivity ( $\epsilon_r'$ ) from 20 to 75, and loss tangent ( $\tan \delta$ ) from 0.10 to 0.35 of the homogeneous phantom liquid while keeping the material density fixed at  $1000 \text{ kg/m}^3$ . At the final phase, the proposed technique outlined in the previous part is applied on step by step basis to derive equivalent complex dielectric properties ( $\epsilon_r$ ) of homogeneous phantom liquid for practical SAR measurement.

Table 3.1 Thickness and dielectric properties ( $\epsilon_r$ ) of four equal tissue layers model

Layer	Permittivity at 2.45 GHz	Loss tangent at 2.45 GHz
$L_1$ : 0 – 1 cm	30	0.30
$L_2$ : 1 – 2 cm	45	0.25
$L_3$ : 2 – 3 cm	60	0.20
$L_4$ : 3 – 4 cm	75	0.15

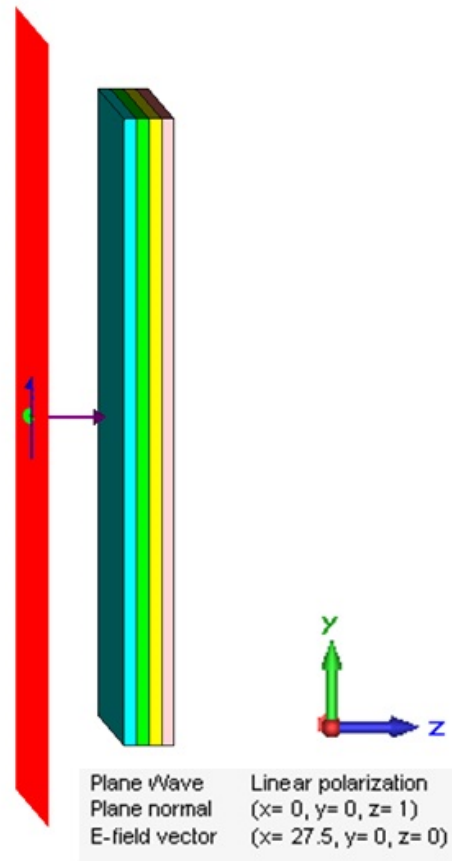


Fig. 3.25: A plane wave with linear polarization at 2.45 GHz impinges on the four equal tissue layers model ( $L_1$  to  $L_4$  respectively) – each tissue layer possesses different dielectric properties but equal thickness (1 cm)

### 3.8.1.1 A Brief Description of the Electromagnetic Simulation Setup

Quite high contrast in complex dielectric properties ( $\epsilon_r$ ) of the adjacent tissue layers ( $L_1$  to  $L_4$  respectively) and low quality factor of the lossy dielectric tissue layers are two fundamental reasons to choose transient solver in CST MWS 2018 for appropriate meshing of the multilayer biological structure as illustrated in Fig. 3.25 [64]. The transient solver available in CST MWS 2018 is developed based on Finite Integration Technique (FIT) computational technique which was conceptualized way back in 1977 [64, 70-71]. In this electromagnetic solver, Maxwell's integral equations are discretized and then solved using numerical technique in the solution space. Thus, this multilayer biological structure ( $L_1$  to  $L_4$  respectively) has been discretized first using hexahedral cells of variable mesh sizes where a wavelength in dielectric tissue layers is subdivided into twenty equal sections. At the structural boundary region, four perfectly matched

layers with 0.0001 reflection coefficient have been set as the electromagnetic absorbing boundary. A steady state energy criterion of  $-40$  dB has been chosen for inverse transformation to observe frequency domain responses.

### 3.8.1.2 Results and Discussion (Plane Wave – Four Equal Layers)

The figures of merit defined in Eqs. (3.32b), (3.33b), (3.34b) and (3.35b) have been employed one at a time to determine permittivity ( $\epsilon'_r$ ) and loss tangent ( $\tan \delta$ ) of the homogeneous phantom liquid equivalent to the four equal tissue layers problem – obviously due to plane wave irradiation with linear polarization at 2.45 GHz. At first, the figure of merit defined in Eqs. (3.32a) and (3.32b) are applied on the four equal tissue layers problem. The  $Max(f_{i(jk)})$  plot for various combinations of permittivity ( $\epsilon'_r$ ) and loss tangent ( $\tan \delta$ ) of the equivalent homogeneous phantom liquid is illustrated in Fig. 3.26(a). Observation indicates that permittivity ( $\epsilon'_r$ ) and loss tangent ( $\tan \delta$ ) combination of (50, 0.20) produces a peak electric field distribution that is the closest replication of peak electric field distribution in the original four equal tissue layers model ( $L_1$  to  $L_4$  respectively). Figs. 3.26(b) and (c) demonstrate the comparison of peak electric field distribution curves and the associated absolute difference plot for (50, 0.20) combination of permittivity ( $\epsilon'_r$ ) and loss tangent ( $\tan \delta$ ) values. A maximum difference of 1.46 V/m between peak electric field distribution curves is observed in the third layer ( $L_3$ ) at coordinate location (0, 0, 2.96 cm).

Next, multilayer equivalent complex dielectric properties ( $\epsilon_r$ ) of the homogeneous phantom liquid have been derived using Eqs. (3.33a) and (3.33b). Fig. 3.26(d) illustrates  $Max(f'_{i(jk)})$  plot for varied permittivity ( $\epsilon'_r$ ) and loss tangent ( $\tan \delta$ ) combinations of homogeneous phantom liquid representing the original four equal layers model ( $L_1$  to  $L_4$  respectively). Complex dielectric properties of (40, 0.35) produce a peak electric field distribution that is closest to the original four equal tissue layers model ( $L_1$  to  $L_4$  respectively) while maximum percentage difference in peak electric field distribution is minimized. Figs. 3.26(e) and (f) demonstrate the comparison of peak electric field distribution curves along with associated absolute peak electric field difference plot for permittivity ( $\epsilon'_r$ ) and loss tangent ( $\tan \delta$ ) combination of (40, 0.35). A maximum absolute difference of 1.91 V/m between the peak electric field distribution curves is observed in the first layer ( $L_1$ ) at coordinate location (0, 0, 0.66 cm).

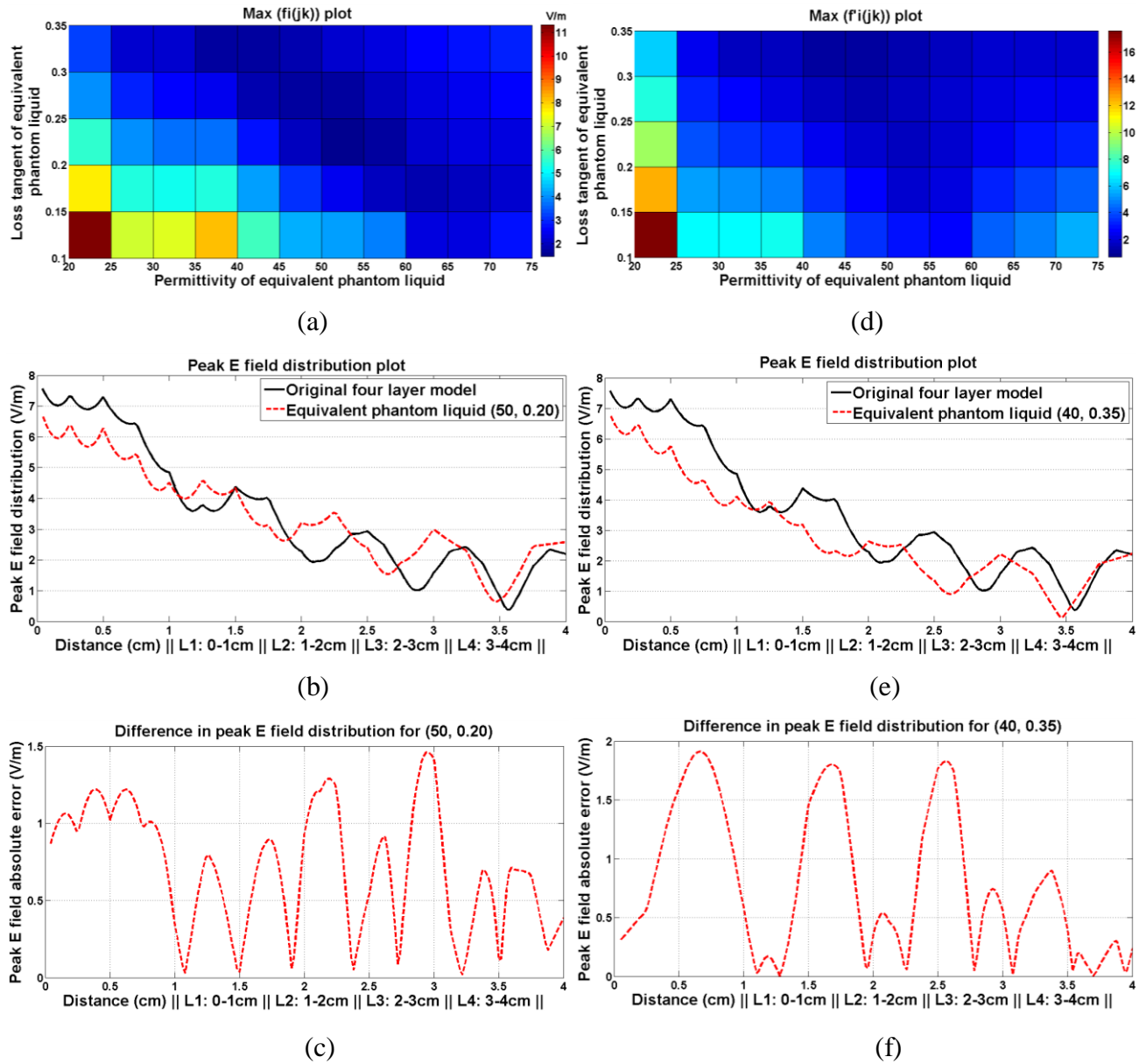


Fig. 3.26: Four equal tissue layers model – plane wave exposure in far field scenario (a)  $Max(f_{i(jk)})$  plot for varied permittivity and loss tangent of equivalent model, (b) comparison of electric field distributions between four equal layers model and equivalent dielectric properties (50, 0.20) that lead to smallest  $Max(f_{i(jk)})$ , (c) difference in peak  $E$  field distribution for equivalent dielectric properties (50, 0.20), (d)  $Max(f'_{i(jk)})$  plot for varied permittivity and loss tangent of equivalent model, (e) comparison of electric field distributions between four equal layers model and equivalent dielectric properties (40, 0.35) that result in smallest  $Max(f'_{i(jk)})$ , (f) difference in peak  $E$  field distribution for equivalent dielectric properties (40, 0.35)

As practical SAR measurement in phantom liquid is our final objective, adopting a cost function developed based upon closely replicating the original SAR distribution in the four equal tissue layers model ( $L_1$  to  $L_4$  respectively), by tuning the dielectric properties ( $\epsilon_r$ ) of the equivalent phantom liquid, seems more logical. To this end, the effective dielectric properties ( $\epsilon_r$ ) of the multilayer ( $L_1$  to  $L_4$  respectively) tissue equivalent liquid have now been attempted to be computed employing the metric defined in Eqs. (3.34a) and (3.34b). In this technique, the absolute maximum difference between the point SAR distributions over the entire cross-sectional central coordinates ( $x = 0, y = 0, z = 0$  to 4 cm) is minimized.

The  $Max(g_{i(jk)})$  plot for varying combinations of permittivity ( $\epsilon_r'$ ) and loss tangent ( $\tan \delta$ ) of the multilayer ( $L_1$  to  $L_4$  respectively) tissue equivalent homogeneous phantom liquid is illustrated in Fig. 3.27(a). It is noted that homogeneous phantom dielectric properties of (25, 0.30) can produce a point SAR distribution closest to the original four equal tissue layers model ( $L_1$  to  $L_4$  respectively). The comparison of point SAR distributions and the associated absolute difference in point SAR plot for (25, 0.30) dielectric combination are illustrated in Figs. 3.27(b) and (c) respectively. It is evident that point SAR distribution inside the derived equivalent homogeneous dielectric liquid (25, 0.30) is best matched in the very first layer ( $L_1$ ) of original four equal tissue layers model ( $L_1$  to  $L_4$  respectively) – as observed in Figs. 3.27(b) and (c). Nevertheless, it should be noted that the obtained difference in overall point SAR distribution is one order down while compared to the original four equal tissue layers model – as seen in Fig. 3.27(c). A maximum absolute difference of  $1.9 \times 10^{-3}$  W/kg in point SAR is noted at the interface of second ( $L_2$ ) and third ( $L_3$ ) tissue layers i.e. at (0, 0, 2 cm) coordinate location.

At last, a final attempt is made to closely replicate the original point SAR distribution not only in the very first tissue layer ( $L_1$ ) but also in the subsequent three tissue layers ( $L_2$  to  $L_4$ ) by minimizing fractional difference in point SAR distribution over the entire cross-sectional central coordinates ( $x = 0, y = 0, z = 0$  to 4 cm). Eqs. (3.35a) and (3.35b) have finally been applied on the raw data sets to minimize the maximum fractional difference in point SAR distribution due to replacing four equal tissue layers model ( $L_1$  to  $L_4$  respectively) with an equivalent homogeneous phantom liquid. Fig. 3.27(d) demonstrates  $Max(g'_{i(jk)})$  plot for varied combinations of permittivity ( $\epsilon_r'$ ) and loss tangent ( $\tan \delta$ ) of the equivalent homogeneous phantom liquid – for accurate SAR measurement. Complex dielectric properties of (40, 0.35) produce a point SAR

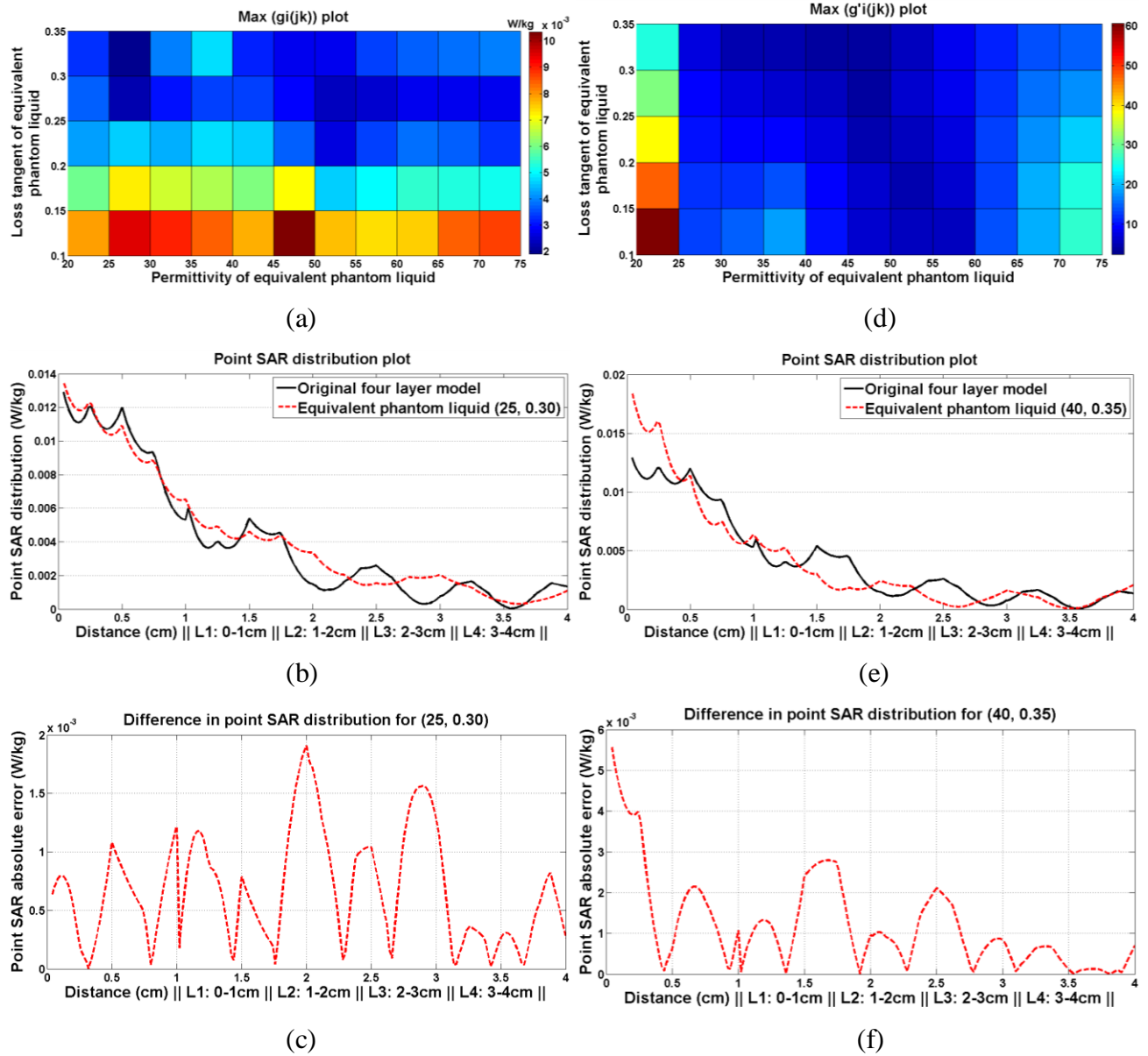


Fig. 3.27: Four equal tissue layers model – plane wave exposure in far field scenario (a)  $Max(g_{i(jk)})$  plot for varied permittivity and loss tangent of equivalent model, (b) comparison of point SAR distributions between four equal layer model and equivalent dielectric properties (25, 0.30) that lead to smallest  $Max(g_{i(jk)})$ , (c) difference in point SAR distribution for equivalent dielectric properties (25, 0.30), (d)  $Max(g'_{i(jk)})$  plot for varied permittivity and loss tangent of equivalent model, (e) comparison of point SAR distributions between four equal layer model and equivalent dielectric properties (40, 0.35) that result in smallest  $Max(g'_{i(jk)})$ , (f) difference in point SAR distribution for equivalent dielectric properties (40, 0.35)



distribution over the entire cross-sectional central coordinates ( $x = 0, y = 0, z = 0$  to 4 cm) that is fairly well replicated and similar to the original four equal tissue layers model ( $L_1$  to  $L_4$  respectively) based on Eqs. (3.35a) and (3.35b). Figs. 3.27(e) and (f) illustrate the comparison of point SAR distributions along with associated difference in point SAR distribution plot for (40, 0.35) dielectric properties combination. It should be taken into note that point SAR distribution inside the derived equivalent homogeneous dielectric liquid (40, 0.35) is matched well over second to fourth tissue layers ( $L_2$  to  $L_4$ ) in addition to the first tissue layer ( $L_1$ ) – please, refer to Figs. 3.27(e) and (f). Observed difference in overall point SAR distribution is still one order down while compared to the original four equal tissue layers model ( $L_1$  to  $L_4$  respectively) – as noted in Fig. 3.27(f). Maximum point SAR difference of  $5.6 \times 10^{-3}$  W/kg is noted at open surface of the first tissue layer ( $L_1$ ) i.e. at (0, 0, 0) coordinate location.

### 3.8.2 Plane Wave Exposure – A Typical Four Unequal Layer Model

All the above mentioned steps along with associated observations have now been repeated for another similar multilayer tissue model with four unequal tissue layers ( $L_1$  to  $L_4$  respectively) – each layer possesses different permittivity ( $\epsilon_r'$ ) and loss tangent ( $\tan \delta$ ). The contrast in dielectric properties ( $\epsilon_r$ ) is exactly alike to that for the previous four equal tissue layers model ( $L_1$  to  $L_4$  respectively) and all the tissue layers possess  $1000 \text{ kg/m}^3$  material density. A plane wave with linear polarization at 2.45 GHz impinges on the first tissue layer ( $L_1$ ) with normal incidence and subsequently propagates through next three tissue layers ( $L_2$  to  $L_4$ ). The incident plane wave possesses peak electric field strength of 27.46 V/m as prescribed for existing Indian scenario [63]. All the four tissue layers possess cross-sectional dimensions of  $50 \text{ cm} \times 50 \text{ cm}$  but with unequal layer thicknesses – individual tissue layer thickness and complex dielectric properties ( $\epsilon_r$ ) have been tabulated in Table 3.2. Next, transient (time domain) simulation has been performed in CST MWS 2018 to note spatial peak electric field and point SAR distributions data in the original four unequal tissue layers ( $L_1$  to  $L_4$  respectively) model along the cross-sectional central coordinates ( $x = 0, y = 0$ ) i.e. for different values of  $z$  coordinate [64]. Peak electric field and point SAR data have been noted at ( $x = 0, y = 0, z = 0$  to 2.5 cm) coordinates of four unequal tissue layers ( $L_1$  to  $L_4$ ) to ensure negligible effect of boundary discontinuity except at tissue layer interfaces. Thereafter, seventy two subsequent simulations have been performed by changing the permittivity ( $\epsilon_r'$ ) from 20 to 75, and loss

Table 3.2 Thickness and dielectric properties ( $\epsilon_r$ ) of four unequal tissue layers model

Layer	Permittivity at 2.45 GHz	Loss tangent at 2.45 GHz
L <sub>1</sub> : 0 – 0.25 cm	30	0.30
L <sub>2</sub> : 0.25 – 0.75 cm	45	0.25
L <sub>3</sub> : 0.75 – 1.50 cm	60	0.20
L <sub>4</sub> : 1.50 – 2.50 cm	75	0.15

tangent ( $\tan \delta$ ) from 0.10 to 0.35 of the homogeneous phantom liquid and keeping the tissue density fixed at 1000 kg/m<sup>3</sup>. At last, the proposed technique has been applied in step by step approach to determine dielectric properties ( $\epsilon_r$ ) of the equivalent homogeneous phantom liquid for practical SAR measurement.

### 3.8.2.1 Results and Discussion (Plane Wave – Four Unequal Layers)

The four cost functions and associated figures of merit defined in Eqs. (3.32a), (3.32b), (3.33a), (3.33b), (3.34a), (3.34b), (3.35a) and (3.35b) have been applied in this problem as well to estimate the permittivity ( $\epsilon'_r$ ) and loss tangent ( $\tan \delta$ ) of proposed equivalent homogeneous liquid – obtained results have been discussed next. At first, Eqs. (3.32a) and (3.32b) have been employed to observe and predict the homogeneous phantom liquid properties by proper tuning of permittivity ( $\epsilon'_r$ ) and loss tangent ( $\tan \delta$ ). Fig. 3.28(a) illustrates  $Max(f_{i(jk)})$  plot for widely varied permittivity ( $\epsilon'_r$ ) and loss tangent ( $\tan \delta$ ) of the equivalent homogeneous phantom liquid. It is observed that permittivity ( $\epsilon'_r$ ) and loss tangent ( $\tan \delta$ ) combination of (55, 0.20) reproduces a peak electric field distribution which is closest to the original four unequal tissue layers model ( $L_1$  to  $L_4$  respectively). Figs. 3.28(b) and (c) respectively demonstrate the comparison of peak electric field distributions along with associated absolute difference plot for (55, 0.20) dielectric properties combination. Noted maximum difference between peak electric field distribution curves is 1.91 V/m in the second tissue layer ( $L_2$ ) at (0, 0, 0.40 cm) coordinate location.

Next, the cost function and associated figure of merit defined in Eqs. (3.33a) and (3.33b) have been employed to solve this problem. Fig. 3.28(d) illustrates  $Max(f'_{i(jk)})$  plot for widely varied permittivity ( $\epsilon'_r$ ) and loss tangent ( $\tan \delta$ ) of the equivalent homogeneous phantom liquid. Complex dielectric properties combination of (60, 0.20) produces a peak electric field

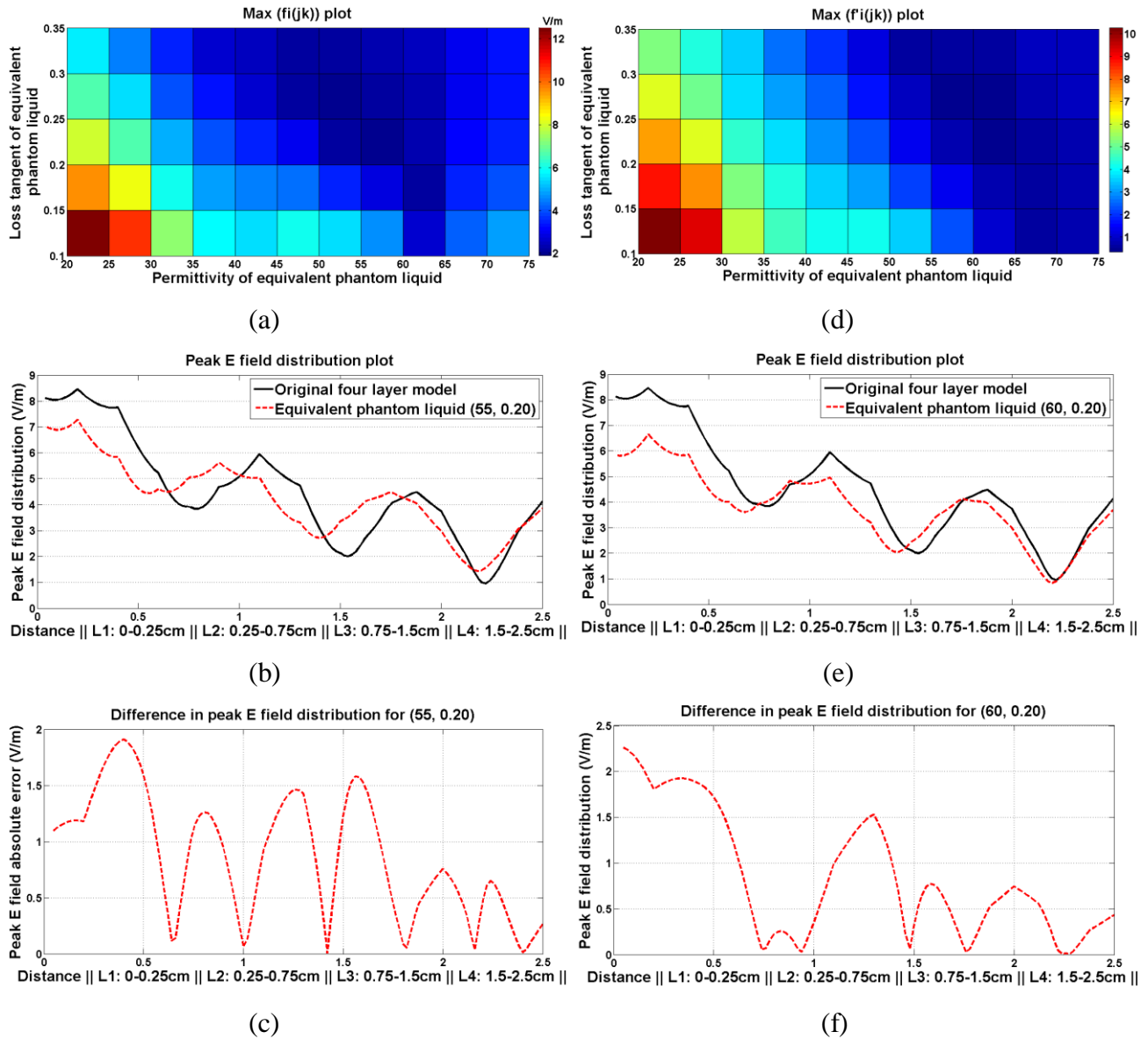


Fig. 3.28: Four unequal tissue layers model – plane wave exposure in far field scenario (a)  $Max(f_{i(jk)})$  plot for varied permittivity and loss tangent of equivalent model, (b) comparison of electric field distributions between four unequal layers model and equivalent dielectric properties (55, 0.20) that lead to smallest  $Max(f_{i(jk)})$ , (c) difference in peak  $E$  field distribution for equivalent dielectric properties (55, 0.20), (d)  $Max(f'_{i(jk)})$  plot for varied permittivity and loss tangent of equivalent model, (e) comparison of electric field distributions between four unequal layers model and equivalent dielectric properties (60, 0.20) that result in smallest  $Max(f'_{i(jk)})$ , (f) difference in peak  $E$  field distribution for equivalent dielectric properties (60, 0.20)

distribution that is closest to the original four unequal tissue layers model ( $L_1$  to  $L_4$  respectively) while minimizing the fractional absolute difference in overall peak electric field distribution. Figs. 3.28(e) and (f) illustrate the comparison of peak electric field distributions along with associated difference plot for (60, 0.20) dielectric combination. A maximum of 2.26 V/m difference in peak electric field distribution is still noted in the first tissue layer ( $L_1$ ) at (0, 0, 0.04 cm) coordinate location.

Then, the figure of merit based on absolute maximum difference in point SAR (Eqs. (3.34a) and (3.34b)) distribution over cross-sectional central coordinate locations ( $x = 0, y = 0, z = 0$  to 2.5 cm) is minimized to obtain the equivalent homogeneous phantom dielectric properties ( $\epsilon_r$ ). Fig. 3.29(a) illustrates  $Max(g_{i(jk)})$  plot for different combinations of permittivity ( $\epsilon_r'$ ) and loss tangent ( $\tan \delta$ ) of the homogeneous phantom liquid equivalent to four unequal tissue layers model ( $L_1$  to  $L_4$  respectively). Equivalent dielectric properties combination of (60, 0.30) reproduces a point SAR distribution closest to the original four unequal tissue layers model based on protocol defined in Eqs. (3.34a) and (3.34b). Figs. 3.29(b) and (c) demonstrate the comparison of point SAR distributions along with associated absolute difference in point SAR for (60, 0.30) dielectric properties combination. It has been observed that point SAR distribution inside equivalent homogeneous dielectric liquid (60, 0.30) is best matched in the very first tissue layer ( $L_1$ ) of the original four unequal layers model ( $L_1$  to  $L_4$  respectively) (please refer to Fig. 3.29(b)). Noted difference in overall point SAR distribution inside equivalent homogeneous phantom liquid is one order down while compared to the original four unequal tissue layers model ( $L_1$  to  $L_4$  respectively) (please refer to Fig. 3.29(c)). Maximum difference of  $4.74 \times 10^{-3}$  W/kg in point SAR is noted in the second tissue layer ( $L_2$ ) at (0, 0, 0.30 cm) coordinate location.

At last, final attempt has been made to determine the complex dielectric properties ( $\epsilon_r$ ) of the homogeneous phantom liquid employing Eqs. (3.35a) and (3.35b). This involves minimization of the maximum fractional point SAR value over entire cross-sectional central coordinate locations ( $x = 0, y = 0, z = 0$  to 2.50 cm). Fig. 3.29(d) illustrates  $Max(g'_{i(jk)})$  plot for different combinations of permittivity ( $\epsilon_r'$ ) and loss tangent ( $\tan \delta$ ) of the equivalent homogeneous phantom liquid. Dielectric properties combination of (60, 0.25) produces a point SAR distribution over entire cross-sectional central coordinate locations ( $x = 0, y = 0, z = 0$  to 2.50 cm) that is closest to the original four unequal tissue layers model ( $L_1$  to  $L_4$

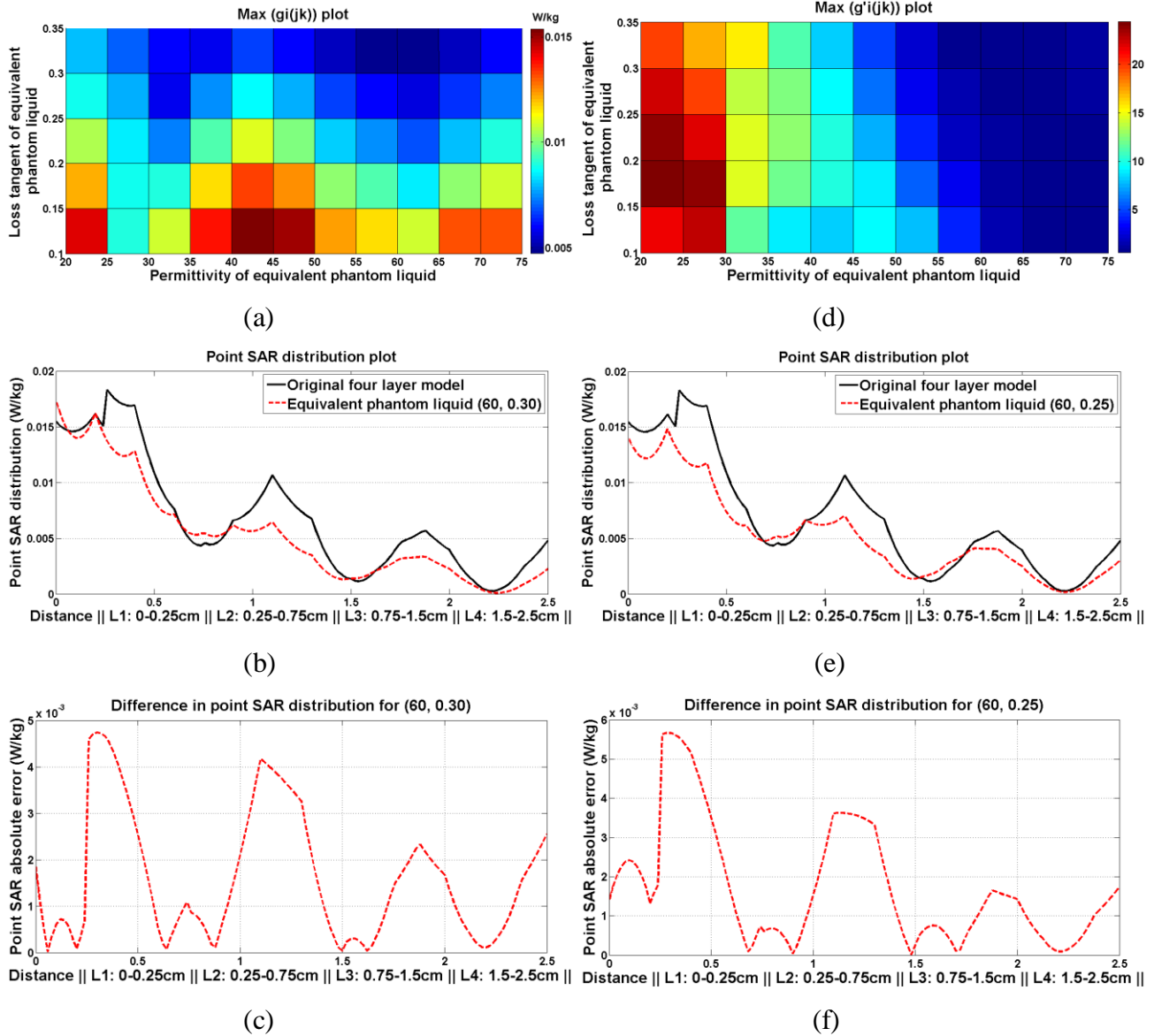


Fig. 3.29: Four unequal tissue layers model – plane wave exposure in far field scenario (a)  $Max(g_{i(jk)})$  plot for varied permittivity and loss tangent of equivalent model, (b) comparison of point SAR distributions between four unequal layer model and equivalent dielectric properties (60, 0.30) that lead to smallest  $Max(g_{i(jk)})$ , (c) difference in point SAR distribution for equivalent dielectric properties (60, 0.30), (d)  $Max(g'_{i(jk)})$  plot for varied permittivity and loss tangent of equivalent model, (e) comparison of point SAR distributions between four unequal layer model and equivalent dielectric properties (60, 0.25) that result in smallest  $Max(g'_{i(jk)})$ , (f) difference in point SAR distribution for equivalent dielectric properties (60, 0.25)

respectively) based on Eqs. (3.35a) and (3.35b). Figs. 3.29(e) and (f) respectively illustrate the comparison of point SAR distributions along with associated difference in point SAR distribution for (60, 0.25) dielectric properties combination. It has been observed that point SAR distribution inside derived equivalent homogeneous liquid (60, 0.25) is better matched over second to fourth tissue layers ( $L_2$  to  $L_4$ ) compared to earlier protocol described above (please refer to Fig. 3.29(e)). In addition, similar to earlier case, absolute difference in overall point SAR distribution is one order down while compared to original unequal tissue layers model ( $L_1$  to  $L_4$  respectively) as visible in Fig. 3.29(f). A maximum point SAR difference of  $5.65 \times 10^{-3}$  W/kg is observed at the beginning of second tissue layer ( $L_2$ ) i.e. at (0, 0, 0.30 cm) coordinate location.

### **3.9 Multilayer Equivalent Homogeneous Phantom Liquid Close to Radiating Antenna in Near Field Scenario**

#### **3.9.1 Antenna Proximity Radiation Exposure – A Typical Four Equal Layer Model**

In this case, a simple rectangular microstrip patch antenna radiates at 2.45 GHz in fundamental mode along z axis (broadside direction) in proximity (near field) to the first tissue layer ( $L_1$ ) of the same four equal tissue layers model ( $L_1$  to  $L_4$  respectively) – the fields further interact with the subsequent tissue layers i.e.  $L_2$  to  $L_4$  (with reference to Fig. 3.30). The earlier proposed technique has been applied once again to the four equal tissue layers model ( $L_1$  to  $L_4$  respectively) and specifications of the individual tissue layers have already been listed earlier (please refer to Table 3.1). The antenna radiated power in near field first impinges on the first tissue layer ( $L_1$ ) with normal incidence and thereafter interacts further with the subsequent tissue layers i.e.  $L_2$  to  $L_4$ . It must be noted that the average input power of this microstrip antenna has been set at 0.50 Watt – thus, the electric field / point SAR values in different tissue layers ( $L_1$  to  $L_4$  respectively) shouldn't be compared with those for the earlier case of plane wave with linear polarization. The peak electric field / point SAR data have been noted along cross-sectional central coordinates ( $x = 0, y = 0, z = 0$  to 4 cm) of the original four equal tissue layers model using transient (time domain) simulation. The same electromagnetic simulation setup has been followed in CST MWS 2018 as stated earlier [64]. Next, seventy two subsequent simulations have been performed with varying permittivity (20 to 75) and loss tangent (0.10 to

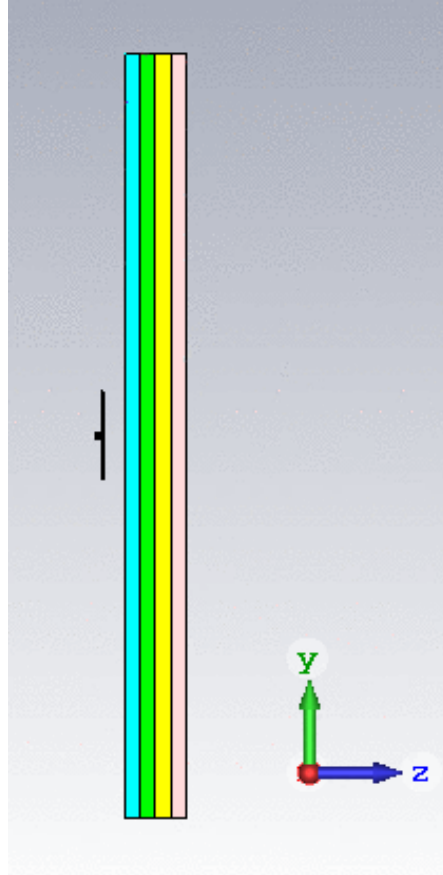


Fig. 3.30: A rectangular microstrip antenna radiates at 2.45 GHz in proximity to the four equal tissue layers model ( $L_1$  to  $L_4$  respectively) – each tissue layer possesses different dielectric properties but equal thickness (1 cm)

0.35) along with a fixed material density of  $1000 \text{ kg/m}^3$  of the equivalent homogeneous phantom liquid. Eventually, the earlier proposed techniques have been applied on the obtained data set to determine complex dielectric properties ( $\epsilon_r$ ) of the closest possible equivalent homogeneous liquid for SAR measurement.

### 3.9.1.1 Results and Discussion (In Close Proximity of Antenna – Four Equal Layers)

This time, cost functions and the associated figures of merit defined in Eqs. (3.32a), (3.32b), (3.33a), (3.33b), (3.34a), (3.34b), (3.35a) and (3.35b) have been employed to determine permittivity ( $\epsilon_r'$ ) and loss tangent ( $\tan \delta$ ) of the equivalent homogeneous phantom liquid – due to 2.45 GHz fields at near field region in proximity to the antenna.

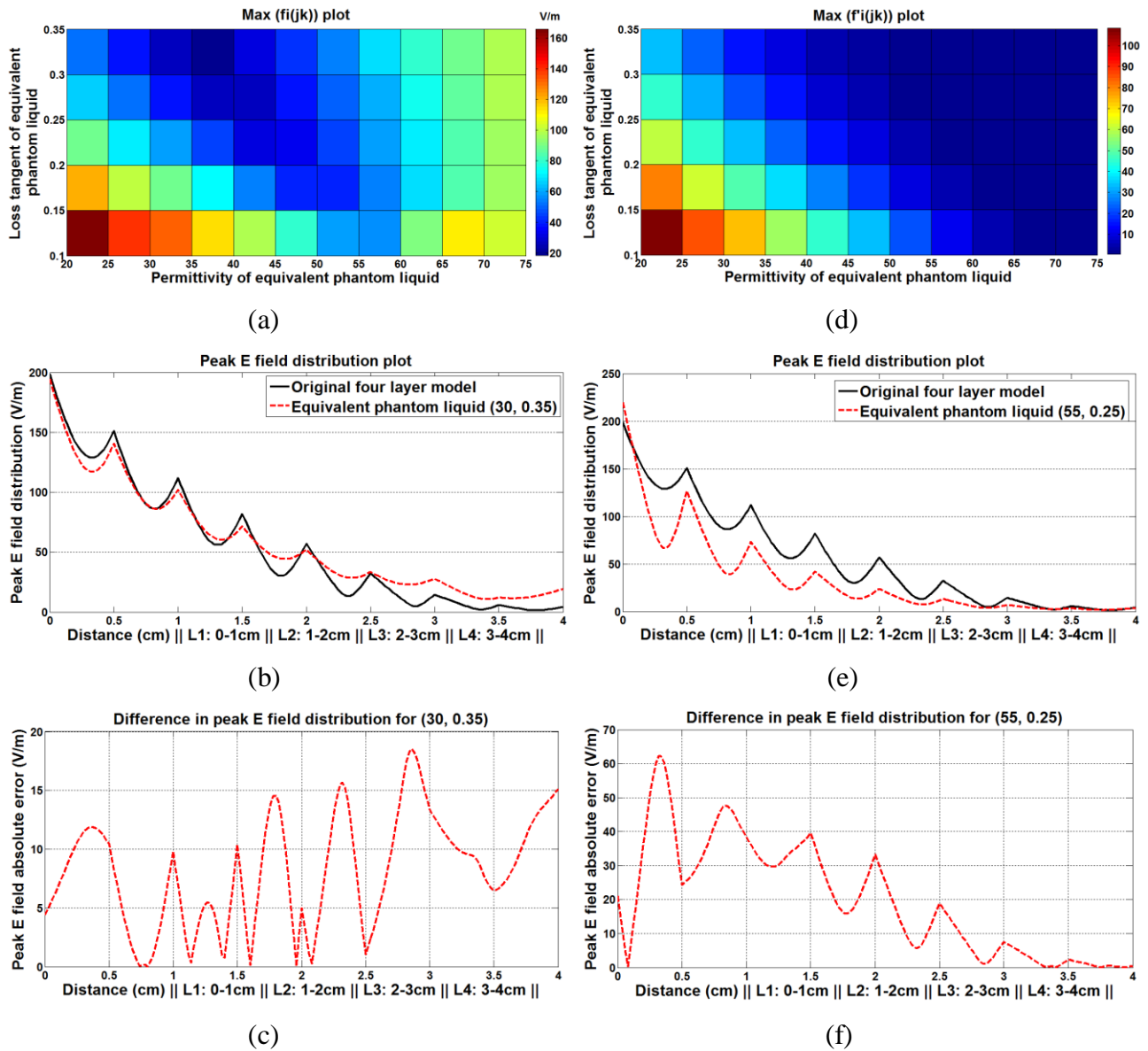


Fig. 3.31: Four equal tissue layers model – close to the radiating antenna in near field scenario (a)  $Max(f_{i(jk)})$  plot for varied permittivity and loss tangent of equivalent model, (b) comparison of electric field distributions between four equal layers model and equivalent dielectric properties (30, 0.35) that lead to smallest  $Max(f_{i(jk)})$ , (c) difference in peak  $E$  field distribution for equivalent dielectric properties (30, 0.35), (d)  $Max(f'_{i(jk)})$  plot for varied permittivity and loss tangent of equivalent model, (e) comparison of electric field distributions between four equal layers model and equivalent dielectric properties (55, 0.25) that result in smallest  $Max(f'_{i(jk)})$ , (f) difference in peak  $E$  field distribution for equivalent dielectric properties (55, 0.25)



Fig. 3.31(a) illustrates  $Max(f_{i(jk)})$  plot for widely varied permittivity ( $\epsilon'_r$ ) and loss tangent ( $\tan \delta$ ) parameters of the equivalent homogeneous phantom liquid – employing the figure of merit defined using Eqs. (3.32a) and (3.32b). It is observed that permittivity ( $\epsilon'_r$ ) and loss tangent ( $\tan \delta$ ) combination of (30, 0.35) produces a peak electric field distribution that is closest to the original four equal tissue layers model ( $L_1$  to  $L_4$  respectively). Figs. 3.31(b) and (c) illustrate the comparison of peak electric field distributions along with associated absolute difference plot for (30, 0.35) dielectric properties combination. A maximum difference of 18.54 V/m between the peak electric field distribution curves is noted in third tissue layer ( $L_3$ ) at (0, 0, 2.86 cm) coordinate location.

At subsequent stage, multilayer equivalent dielectric properties ( $\epsilon_r$ ) of homogeneous phantom liquid have been derived using Eqs. (3.33a) and (3.33b). Fig. 3.31(d) illustrates  $Max(f'_{i(jk)})$  plot for a wide range of permittivity ( $\epsilon'_r$ ) and loss tangent ( $\tan \delta$ ) combinations of the equivalent homogeneous liquid. Finally, dielectric properties combination of (55, 0.25) produces a peak electric field distribution closest to the original four equal tissue layers model ( $L_1$  to  $L_4$  respectively) – while, minimizing the maximum fractional difference over entire cross-sectional central coordinate line ( $x = 0, y = 0, z = 0$  to 4 cm). Figs. 3.31(e) and (f) illustrate the comparison of peak electric field distribution curves and the difference plot for (55, 0.25) dielectric properties combination. This time, a large maximum electric field difference is noted in the first tissue layer ( $L_1$ ) at (0, 0, 0.34 cm) coordinate location.

Next, it is attempted to minimize the maximum absolute difference in point SAR distribution over the entire cross-sectional central coordinates ( $x = 0, y = 0, z = 0$  to 4 cm) employing the cost function and associated figure of merit defined in Eqs. (3.34a) and (3.34b). Fig. 3.32(a) demonstrates  $Max(g_{i(jk)})$  plot for the above mentioned spans of permittivity ( $\epsilon'_r$ ) and loss tangent ( $\tan \delta$ ) of the equivalent homogeneous phantom liquid. Dielectric properties combination of (30, 0.30) produces a point SAR distribution over the cross-sectional central coordinates of the four equal tissue layers ( $x = 0, y = 0, z = 0$  to 4 cm) that closely replicates the point SAR distribution in the original four equal tissue layers model ( $L_1$  to  $L_4$  respectively). Figs. 3.32(b) and (c) illustrate the comparison of point SAR distributions along with associated difference plot in point SAR for (30, 0.30) dielectric properties combination. The obtained point SAR distribution inside derived equivalent homogeneous liquid (30, 0.30) is well matched over

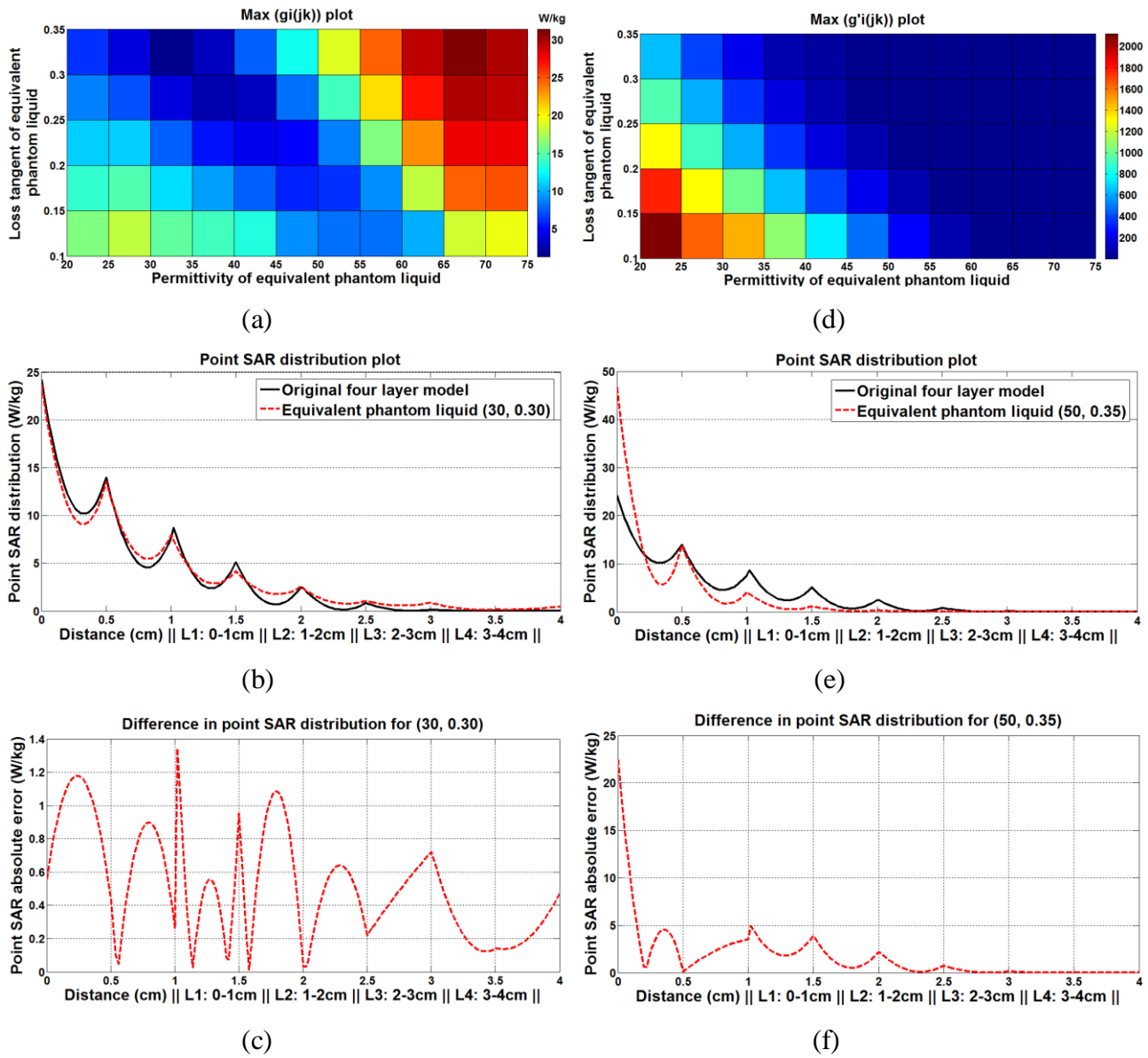


Fig. 3.32: Four equal tissue layers model – close to the radiating antenna in near field scenario (a)  $Max(g_{i(jk)})$  plot for varied permittivity and loss tangent of equivalent model, (b) comparison of point SAR distributions between four equal layers model and equivalent dielectric properties (30, 0.30) that lead to smallest  $Max(g_{i(jk)})$ , (c) difference in point SAR distribution for equivalent dielectric properties (30, 0.30), (d)  $Max(g'_{i(jk)})$  plot for varied permittivity and loss tangent of equivalent model, (e) comparison of point SAR distributions between four equal layers model and equivalent dielectric properties (50, 0.35) that result in smallest  $Max(g'_{i(jk)})$ , (f) difference in point SAR distribution for equivalent dielectric properties (50, 0.35)

all the four equal tissue layers ( $L_1$  to  $L_4$ ) (please refer to Fig. 3.32(b)). Noted difference in overall point SAR distribution is quite negligible while compared to the original four equal tissue layers model ( $L_1$  to  $L_4$  respectively) – as noted in Fig. 3.32(c). A maximum point SAR difference of 1.34 W/kg is noted in the second tissue layer ( $L_2$ ) i.e. at (0, 0, 1.02 cm) coordinate location.

In the final attempt, Eqs. (3.35a) and (3.35b) have been employed to minimize the maximum fractional difference in point SAR distribution along the central coordinates across all four tissue layers ( $L_1$  to  $L_4$  respectively). Thus, it has been attempted to minimize the fractional SAR distribution over coordinate locations ( $x = 0, y = 0, z = 0$  to 4 cm). Fig. 3.32(d) illustrates  $Max(g'_{i(jk)})$  plot for different combinations of permittivity ( $\epsilon_r'$ ) and loss tangent ( $\tan \delta$ ) of the equivalent homogeneous phantom liquid. Dielectric properties combination of (50, 0.35) produces a point SAR distribution closest to the original four equal tissue layers model ( $L_1$  to  $L_4$  respectively). Figs. 3.32(e) and (f) illustrate comparison of point SAR distributions along with their difference plot for (50, 0.35) dielectric properties combination. Point SAR distribution inside the derived equivalent liquid (50, 0.35) is reasonably matched over all four equal tissue layers ( $L_1$  to  $L_4$  respectively) except at the open interface of the very first tissue layer ( $L_1$ ). Please refer to Figs. 3.32(e) and (f).

### 3.9.2 Antenna Proximity Radiation Exposure – A Typical Four Unequal Layer Model

Here, the rectangular microstrip patch antenna radiates at 2.45 GHz fundamental mode along  $z$  axis in close proximity of the first tissue layer ( $L_1$ ) of four unequal tissue layer model ( $L_1$  to  $L_4$  respectively) and the fields further interact with subsequent tissue layers i.e.  $L_2$  to  $L_4$ . The thickness and dielectric properties ( $\epsilon_r$ ) of each layer have already been described in Table 3.2 – in addition, dielectric contrast among four tissue layers is exactly the same as stated earlier and all tissue layers possess  $1000 \text{ kg/m}^3$  material density. Next, the above mentioned steps have been applied once again to the four unequal tissue layers model ( $L_1$  to  $L_4$  respectively). Here also, the average input power of antenna has been kept fixed at 0.50 Watt – the peak electric field / point SAR data have been noted along the cross-sectional central coordinates ( $x = 0, y = 0, z = 0$  to 2.5 cm) of the four unequal tissue layers model. Then, seventy two more simulations

have been performed over wide ranges of permittivity (20 to 75) and loss tangent (0.10 to 0.35) of the equivalent homogeneous phantom liquid. At last, dielectric properties ( $\epsilon_r$ ) of equivalent liquid have been determined for SAR measurement in the four unequal layers model ( $L_1$  to  $L_4$  respectively).

### 3.9.2.1 Results and Discussion (In Close Proximity of Antenna – Four Unequal Layers)

The cost functions and figures of merit defined in Eqs. (3.32a), (3.32b), (3.33a), (3.33b), (3.34a), (3.34b), (3.35a) and (3.35b) have been applied again to estimate complex dielectric properties ( $\epsilon_r$ ) of the equivalent homogeneous phantom liquid – noted results have been discussed in the following section.

Figure of merit defined using Eqs. (3.32a) and (3.32b) has been employed first – consequently, Fig. 3.33(a) demonstrates  $Max(f_{i(jk)})$  plot for wide ranges of permittivity ( $\epsilon_r'$ ) and loss tangent ( $\tan \delta$ ) of the equivalent homogeneous phantom liquid. Specific combination of permittivity ( $\epsilon_r'$ ) and loss tangent (45, 0.20) produces a peak electric field distribution closest to the original four unequal tissue layers model. Figs. 3.33(b) and (c) illustrate comparison of peak electric field distributions and the associated absolute difference plot for (45, 0.20) dielectric properties combination. Noted maximum difference between peak electric field distribution curves is 27.08 V/m near the interface of second ( $L_2$ ) and third ( $L_3$ ) tissue layers at (0, 0, 0.74 cm) coordinate location.

Subsequently, metric defined using Eqs. (3.33a) and (3.33b) has been employed in the next step – Fig. 3.33(d) demonstrates  $Max(f'_{i(jk)})$  plot for the same ranges of permittivity ( $\epsilon_r'$ ) and loss tangent ( $\tan \delta$ ) of the equivalent homogeneous phantom liquid. Dielectric properties combination of (55, 0.35) finally reproduces a peak electric field distribution that is closest to the original four unequal tissue layers model ( $L_1$  to  $L_4$  respectively) while minimizing fractional difference in overall peak electric field distribution. Figs. 3.33(e) and (f) illustrate comparison of peak electric field distributions and the absolute difference plot for (55, 0.35) dielectric properties combination. However, still a significantly large maximum electric field difference is noted in the first tissue layer ( $L_1$ ) at (0, 0, 0.08 cm) coordinate location.

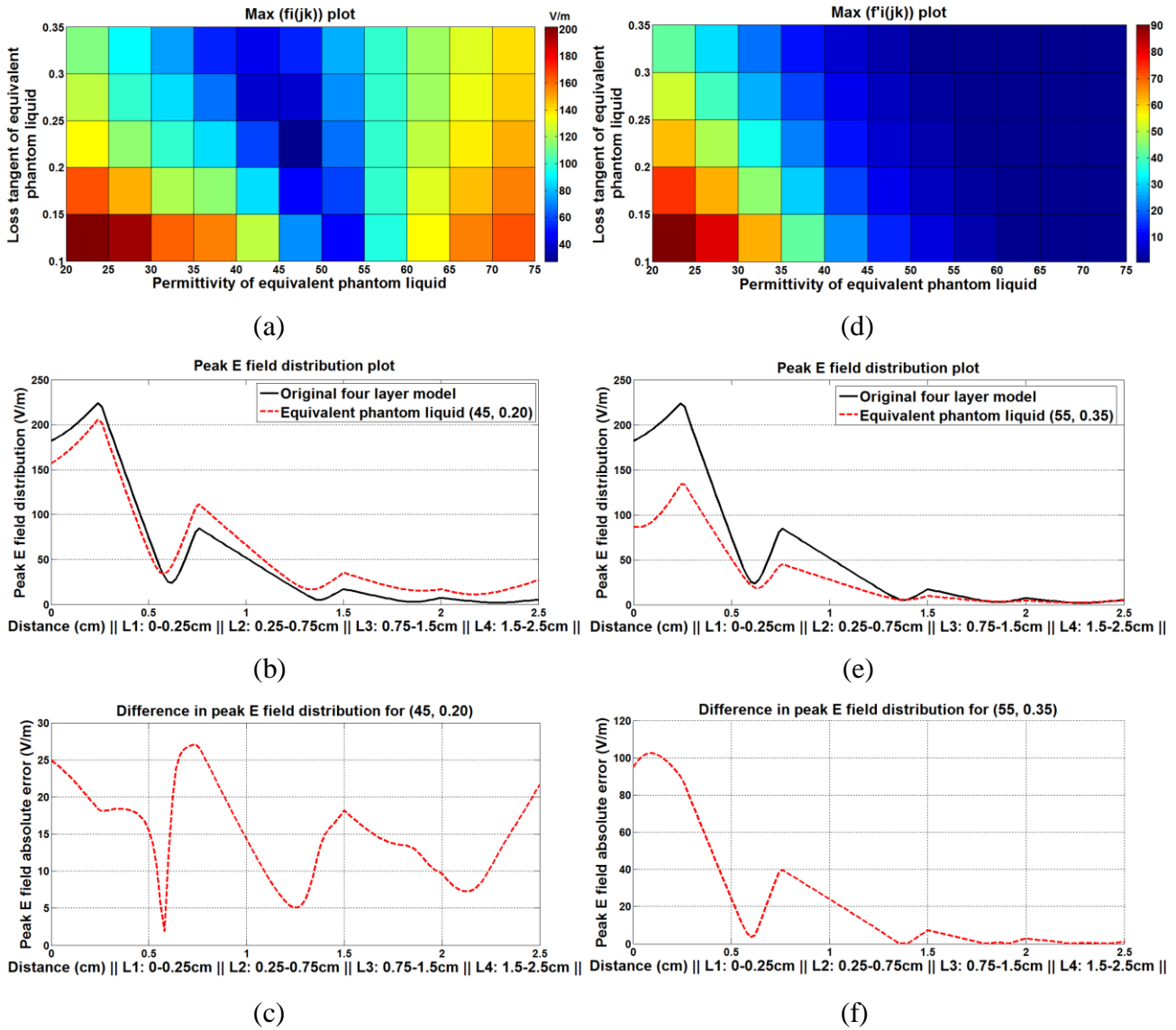


Fig. 3.33: Four unequal tissue layers model – close to the radiating antenna in near field scenario (a)  $Max(f_{i(jk)})$  plot for varied permittivity and loss tangent of equivalent model, (b) comparison of electric field distributions between four unequal layers model and equivalent dielectric properties (45, 0.20) that lead to smallest  $Max(f_{i(jk)})$ , (c) difference in peak  $E$  field distribution for equivalent dielectric properties (45, 0.20), (d)  $Max(f'_{i(jk)})$  plot for varied permittivity and loss tangent of equivalent model, (e) comparison of electric field distributions between four unequal layers model and equivalent dielectric properties (55, 0.35) that result in smallest  $Max(f'_{i(jk)})$ , (f) difference in peak  $E$  field distribution for equivalent dielectric properties (55, 0.35)

Next, it has been attempted to minimize proposed figure of merit based on absolute difference in point SAR distribution (Eqs. (3.34a) and (3.34b)) – Fig. 3.34(a) demonstrates  $Max(g_{i(jk)})$  plot for wide ranges of permittivity ( $\epsilon'_r$ ) and loss tangent ( $\tan \delta$ ) of the equivalent homogeneous phantom liquid for four unequal tissue layers model ( $L_1$  to  $L_4$  respectively). Final equivalent dielectric properties of (45, 0.35) produce a point SAR distribution that is close to the original unequal tissue layers model ( $L_1$  to  $L_4$  respectively). Figs. 3.34(b) and (c) illustrate respectively the comparison of point SAR distributions and the associated absolute point SAR difference plot for (45, 0.35) dielectric properties combination. It is to be noted that point SAR distribution inside the equivalent homogeneous dielectric liquid (45, 0.35) is sensibly matched with the original model ( $L_1$  to  $L_4$  respectively) – however, a reasonable difference is observed at and around the interface of first ( $L_1$ ) and second ( $L_2$ ) tissue layers at (0, 0, 0.26 cm) coordinate location.

At last, Fig. 3.34(d) illustrates  $Max(g'_{i(jk)})$  plot for the wide ranges of permittivity ( $\epsilon'_r$ ) and loss tangent ( $\tan \delta$ ) of equivalent homogeneous phantom liquid employing the metric defined using Eqs. (3.35a) and (3.35b) – it involves minimizing the maximum value of fractional point SAR. Dielectric properties combination of (60, 0.35) produces a point SAR distribution over ( $x = 0, y = 0, z = 0$  to 2.50 cm) coordinates close to the original point SAR distribution in four unequal tissue layers model ( $L_1$  to  $L_4$  respectively). Figs. 3.34(e) and (f) demonstrate comparison of point SAR distributions and their difference for (60, 0.35) combination. It is observed that the nature of point SAR distribution inside the equivalent homogeneous dielectric liquid (60, 0.35) is matched with the original unequal tissue layers model ( $L_1$  to  $L_4$  respectively) (please refer to Figs. 3.34(e) and (f)). However, a considerable difference is still observed in the first ( $L_1$ ) and second ( $L_2$ ) tissue layers with peak near the interface of those two tissue layers at (0, 0, 0.26 cm) coordinate location.

### 3.10 Discussions

It should be noted that minimizing the maximum fractional difference in point SAR distribution provides the appropriate dielectric properties ( $\epsilon_r$ ) of the equivalent homogeneous phantom liquid for most of the multilayer tissue models while targeting overall SAR measurement in all the tissue layers ( $L_1$  to  $L_4$  respectively). Therefore, the overall original SAR distribution along with

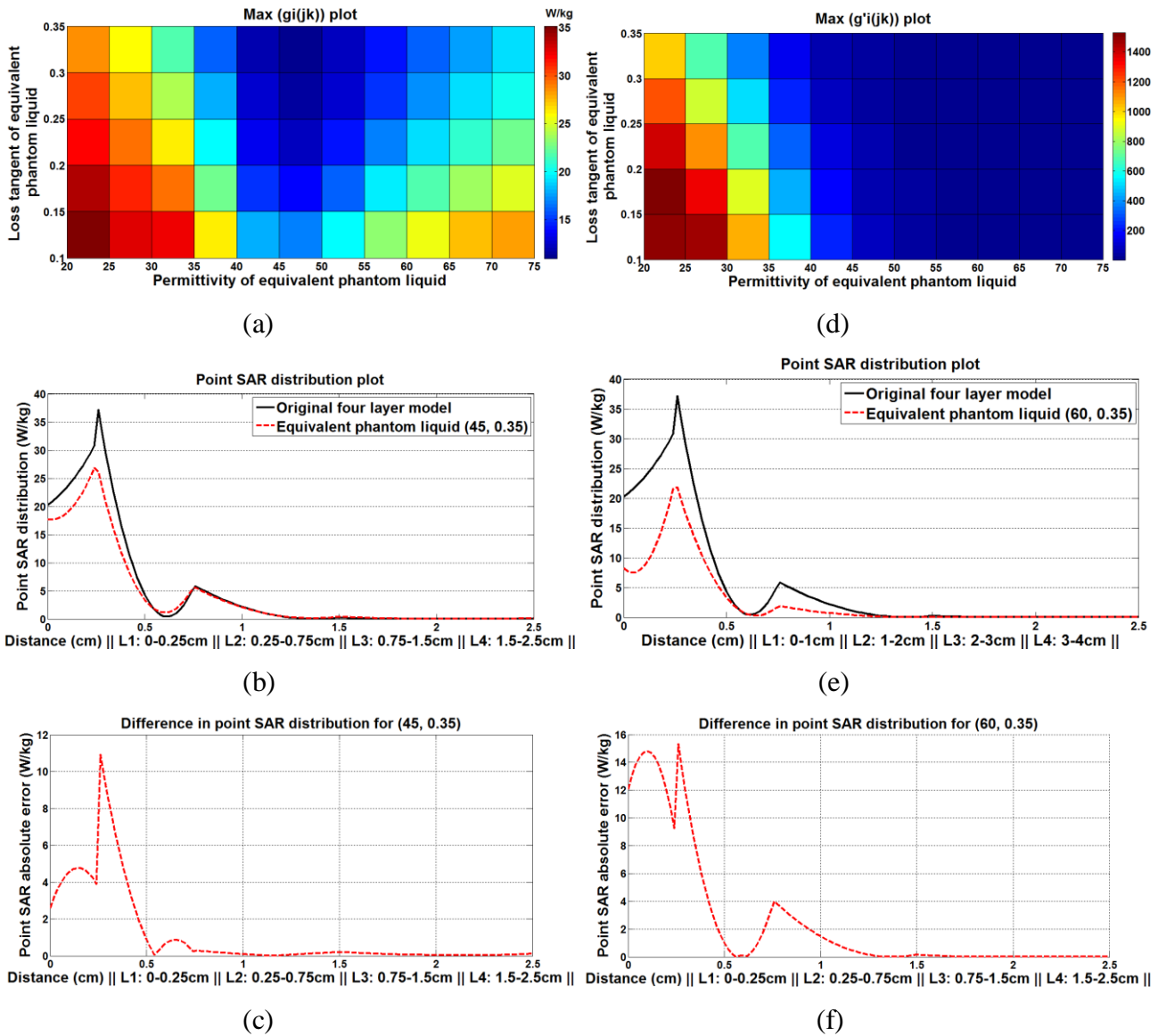


Fig. 3.34: Four unequal tissue layers model – close to the radiating antenna in near field scenario (a)  $Max(g_{i(jk)})$  plot for varied permittivity and loss tangent of equivalent model, (b) comparison of point SAR distributions between four unequal layers model and equivalent dielectric properties (45, 0.35) that lead to smallest  $Max(g_{i(jk)})$ , (c) difference in point SAR distribution for equivalent dielectric properties (45, 0.35), (d)  $Max(g'_{i(jk)})$  plot for varied permittivity and loss tangent of equivalent model, (e) comparison of point SAR distributions between four unequal layers model and equivalent dielectric properties (60, 0.35) that result in smallest  $Max(g'_{i(jk)})$ , (f) difference in point SAR distribution for equivalent dielectric properties (60, 0.35)

SAR values at individual coordinate locations is replicated with minimum possible fractional errors. In some cases, minimizing the maximum absolute point SAR difference results in achieving appropriate equivalent homogeneous phantom liquid for SAR measurement in multilayer tissue models. However, it must also be noted that even the derived equivalent homogeneous liquid to some extent lacks in precisely replicating the original electric field / point SAR distributions near tissue layer interfaces with significant dielectric contrast. This disagreement in electric field / point SAR data near tissue layer interfaces can't be avoided entirely using any homogeneous phantom liquid because the reflection and refraction of electromagnetic wave at layer interfaces can only take place in multilayer models with dielectric discontinuities – these phenomena don't occur in equivalent homogeneous phantom liquid. The proposed technique can more accurately derive the equivalent homogeneous dielectric properties ( $\epsilon_r$ ) of any arbitrary shaped multilayer tissue model in case raw simulation data is available for each and every point inside the tissue layers of that arbitrary shaped model instead of only at cross-sectional central coordinate locations i.e. ( $x = 0, y = 0, z = 0$  to  $z_1 + z_2 + z_3 + \dots + z_n$ ). In addition, special attention should also be drawn on any specific tissue layer (in multilayer model) where the most accurate electric field / SAR measurement is an absolute necessity – dielectric properties ( $\epsilon_r$ ) of the equivalent homogeneous phantom liquid can accordingly be tuned. Thus, the proposed technique to determine equivalent dielectric properties ( $\epsilon_r$ ) of the homogeneous phantom liquid is much improved compared to earlier reported techniques available in literature [59, 65-69].

### 3.11 Conclusions

This work (presented in second part of this chapter) contributes to significant advancement in the domain of formulating equivalent homogeneous phantom liquid properties by developing a novel, generalized and structured technique that does not merely attempt to match the maximum SAR value; rather it attempts to replicate overall geometric peak electric field / point SAR distribution inside the equivalent homogeneous phantom liquid similar to the original multilayer biological model. This is a more appropriate metric than merely matching averaged SAR data over 1 g or 10 g contiguous mass since once point SAR distribution is matched inside equivalent liquid, all other SAR data either averaged over 1 g or 10 g contiguous mass would match well with original multilayer tissue model. As verified for two different four tissue layers models



( $L_1$  to  $L_4$  respectively) both in far-field as well as in proximity to antenna, peak electric field / point SAR distribution inside derived equivalent phantom liquid matches exactly at multiple coordinate locations in different tissue layers and the overall peak electric field or point SAR distribution patterns have also been quite well replicated using the proposed technique (except at tissue layer interfaces). It has been observed that the basis of using fractional difference in point SAR distribution provides the appropriate dielectric properties ( $\epsilon_r$ ) of the homogeneous phantom liquid in most cases of SAR measurements.

It should also be pointed out that exact point by point matching of point SAR distribution across different tissue layers can never be achieved using a single homogeneous equivalent dielectric liquid because of the absence of dielectric discontinuities unlike the original multilayer tissue model. However, the procedure outlined in this work presents an optimal solution as it minimizes the worst case scenario i.e. maximum mismatch between the original problem formulation and the equivalent homogeneous model. Hence, the developed technique can be adopted by international and national electromagnetic exposure regulatory organizations to prescribe equivalent homogeneous dielectric properties ( $\epsilon_r$ ) for customized multilayer biological body during practical SAR measurement.

## References

- [1] S. O. Kasap, *Principles of Electronic Materials and Devices*, McGraw-Hill, New York, Third Ed., 2006.
- [2] S. O. Nelson, and S. Trabelsi, 'Dielectric Spectroscopy Measurements on Fruit, Meat, and Grain', *Transactions of the ASABE*, Vol. 51, No. 5, pp. 1829-1834, 2008.
- [3] S. O. Nelson, 'Dielectric Properties of Agricultural Products and Some Applications', *Research in Agricultural Engineering*, Vol. 54, No. 2, pp. 104-112, 2008.
- [4] W. C. Guo, S. O. Nelson, S. Trabelsi, and S. J. Kays, '10–1800-MHz Dielectric Properties of Fresh Apples during Storage', *Journal of Food Engineering*, Vol. 83, No. 4, pp. 562-569, 2007.
- [5] S. O. Nelson, 'Dielectric Properties of Agricultural Products – Measurements and Applications', *IEEE Transactions on Electrical Insulation*, Vol. 26, No. 5, pp.845-869, 1991.
- [6] S. O. Nelson, 'Dielectric Spectroscopy of Fresh Fruits and Vegetables', *2005 IEEE Instrumentation and Measurement Technology Conference (IMTC)*, pp. 360-364, Ottawa, Canada, May, 2005.

- [7] S. O. Nelson, 'Measuring Dielectric Properties of Fresh Fruits and Vegetables', *IEEE Antennas and Propagation Society International Symposium. Digest. Held in conjunction with: USNC/CNC/URSI North American Radio Sci. Meeting (Cat. No. 03CH37450)*, Vol. 4, pp. 46-49, June, 2003.
- [8] D. Kumar, N. Ahmad, V. Kumar, V. K. Jha, S. Kulshrestha, R. Saini, and M. S. Shekhawat, 'Various Polarization Mechanisms Involved in Ionic Crystals', *AIP Conference Proceedings*, Vol. 2220, No. 1, Article ID. 040036, p. 1-6, May, 2020.
- [9] W. Kuang, and S. O. Nelson, 'Dielectric Relaxation Characteristics of Fresh Fruits and Vegetables from 3 to 20 GHz', *Journal of Microwave Power and Electromagnetic Energy*, Vol. 32, No. 2, pp. 114-122, 1997.
- [10] S. O. Nelson, 'Microwave Dielectric Properties of Fresh Fruits and Vegetables', *Transactions of the ASAE*, Vol. 23, No. 5, pp. 1314-1317, 1980.
- [11] M. S. Venkatesh, and G. S. V. Raghavan, 'An Overview of Dielectric Properties Measuring Techniques', *Canadian Biosystems Engineering*, Vol. 47, No. 7, pp. 15-30, 2005.
- [12] S. N. Jha, K. Narsaiah, A. L. Basediya, R. Sharma, P. Jaiswal, R. Kumar, and R. Bhardwaj, 'Measurement Techniques and Application of Electrical Properties for Nondestructive Quality Evaluation of Foods – A Review', *Journal of Food Science and Technology*, Vol. 48, No. 4, pp. 387-411, 2011.
- [13] A. P. Gregory, and R. N. Clarke, 'A Review of RF and Microwave Techniques for Dielectric Measurements on Polar Liquids', *IEEE Transactions on Dielectrics and Electrical Insulation*, Vol. 13, No. 4, pp. 727-743, 2006.
- [14] G. Deschamps, 'Impedance of an Antenna in a Conducting Medium', *IRE Transactions on Antennas and Propagation*, Vol. 10, No. 5, pp. 648-650, 1962.
- [15] L. Liu, D. Xu, and Z. Jiang, 'Improvement in Dielectric Measurement Technique of Open-Ended Coaxial Line Resonator Method', *Electronics Letters*, Vol. 22, No. 7, pp. 373-375, 1986.
- [16] D. Xu, L. Liu, and Z. Jiang, 'Measurement of the Dielectric Properties of Biological Substances using an Improved Open-Ended Coaxial Line Resonator Method', *IEEE Transactions on Microwave Theory and Techniques*, Vol. 35, No. 12, pp. 1424-1428, 1987.
- [17] M. A. Stuchly, and S. S. Stuchly, 'Coaxial Line Reflection Method for Measuring Dielectric Properties of Biological Substances at Radio and Microwave Frequencies – A Review', *IEEE Transactions on Instrumentation and Measurement*, Vol. 29, No. 3, pp 176-183, 1980.

- [18] T. W. Athey, M. A. Stuchly, and S. S. Stuchly, ‘Measurement of Radio Frequency Permittivity of Biological Tissues with an Open-Ended Coaxial Line: Part I’, *IEEE Transactions on Microwave Theory and Techniques*, Vol. 30, No. 1, pp 82-86, 1982.
- [19] M. A. Stuchly, T. W. Athey, G. M. Samaras, and G. E. Taylor, ‘Measurement of Radio Frequency Permittivity of Biological Tissues with an Open-Ended Coaxial Line: Part II - Experimental Results’, *IEEE Transactions on Microwave Theory and Techniques*, Vol. 30, No. 1, pp. 87-92, 1982.
- [20] D. M. Hagl, D. Popovic, S. C. Hagness, J. H. Booske, and M. Okoniewski, ‘Sensing Volume of Open-Ended Coaxial Probes for Dielectric Characterization of Breast Tissue at Microwave Frequencies’, *IEEE Transactions on Microwave Theory and Techniques*, Vol. 51, No. 4, pp. 1194-1206, 2003.
- [21] R. Zajíček, J. Vrba, and K. Novotný; ‘Evaluation of A Reflection Method on an Open-Ended Coaxial Line and its Use in Dielectric Measurements’, *Acta Polytechnica*, Vol. 46, No. 5, pp. 50-54, 2006.
- [22] R. Zajíček, L. Oppl, and J. Vrba, ‘Broadband Measurement of Complex Permittivity using Reflection Method and Coaxial Probes’, *Radioengineering*, Vol.17, No. 1, pp. 14-19, 2008.
- [23] J. S. Bobowski, and T. Johnson, ‘Permittivity Measurements of Biological Samples by an Open-Ended Coaxial Line’, *Progress in Electromagnetics Research B*, Vol. 40, pp. 159-183, 2012.
- [24] S. O. Nelson, and P. G. Bartley (Jr.), ‘Open-Ended Coaxial-Line Permittivity Measurements on Pulverized Materials’, *IEEE Transactions on Instrumentation and Measurement*, Vol. 47, No. 1, pp. 133-137, 1998.
- [25] S. O. Nelson, ‘Dielectric Properties Measuring Techniques and Applications’, *American Society of Agricultural Engineers*, Vol. 42, No. 2, pp. 523-529, 1999.
- [26] A. Kraszewski, ‘Microwave Aquametry – A Review’, *Journal of Microwave Power*, Vol. 15, No. 4, pp. 209-220, 1980.
- [27] M. Sucher, and J. Fox, ‘*Handbook of Microwave Measurements*’, Vol. 2, Chap. 9, Polytechnic Press, Polytechnic Institute of Brooklyn, New York, 1963.
- [28] G. P. De Loor, and F. W. Meijboom, ‘The Dielectric Constant of Foods and other Materials with High Water Contents at Microwave Frequencies’, *International Journal of Food Science & Technology*, Vol. 1, No. 4, pp. 313-322, 1966.

- [29] N. E. Bengtsson, and P. O. Risman, 'Dielectric Properties of Foods at 3 GHz as Determined by a Cavity Perturbation Technique', *Journal of Microwave Power*, Vol. 6, No. 2, pp. 107-123, 1971.
- [30] D. R. Thompson, and G. L. Zachariah, 'Dielectric Theory and Bioelectrical Measurements (Part I. Theoretical)', *Transactions of the ASAE*, Vol. 14, No. 2, pp. 211-0213, 1971.
- [31] D. R. Thompson, and G. L. Zachariah, 'Dielectric Theory and Bioelectrical Measurements (Part II. Experimental)', *Transactions of the ASAE*, Vol. 14, No. 2, pp. 214-0215, 1971.
- [32] A. C. Metaxas, and R. J. Meredith, '*Industrial Microwave Heating*', No. 4, IET, 1983.
- [33] S. O. Nelson, 'Improved Sample Holder for Q-meter Dielectric Measurements', *Transactions of the ASAE*, Vol. 22, No. 4, pp. 950-954, 1979.
- [34] J. L. Jorgensen, A. R. Edison, S. O. Nelson, and L. E. Stetson, 'Bridge Method for Dielectric Measurements of Grain and Seed in the 50-to 250-MHz Range', *Transactions of the ASAE*, Vol. 13, No. 1, pp. 18-20, 1970.
- [35] L. E. Stetson, and S. O. Nelson, 'A Method for Determining Dielectric Properties of Grain and Seed in the 200- to 500- MHz Range', *Transactions of the ASAE*, Vol. 13, No. 4, pp. 491-495, 1970.
- [36] S. O. Nelson, 'A System for Measuring Dielectric Properties at Frequencies from 8.2 to 12.4 GHz', *Transactions of the ASAE*, Vol. 15, No. 6, pp. 1094-1098, 1972.
- [37] S. O. Nelson, 'Microwave Dielectric Properties of Grain and Seed', *Transactions of the ASAE*, Vol. 16, No. 5, pp. 902-905, 1973.
- [38] S. O. Nelson, 'Microwave Dielectric Properties of Fresh Fruits and Vegetables', *Transactions of the ASAE*, Vol. 23, No. 5, pp. 1314-1317, 1980.
- [39] S. O. Nelson, 'Dielectric Properties of Some Fresh Fruits and Vegetables at Frequencies of 2.45 to 22 GHz', *Transactions of the ASAE*, Vol. 26, No. 2, pp. 613-616, 1983.
- [40] H. E. Bussey, 'Measurement of RF Properties of Materials - A Survey', *Proceedings of IEEE Conference*, Vol. 55, No. 6, pp. 1046-1053, 1967.
- [41] Keysight Technologies, '*Keysight 85070E Dielectric Probe Kit 200 MHz to 50 GHz – Technical Overview*', Available Online: <https://www.keysight.com/us/en/assets/7018-01196/technical-overviews/5989-0222.pdf> (Accessed on 18 Feb, 2022).

- [42] B. N. Taylor, and C. E. Kuyatt, ‘*Guidelines for Evaluating and Expressing the Uncertainty of NIST Measurement Results*’, NIST Technical Note 1297 (1994 edition), National Institute of Standards and Technology, pp. 1-20, USA, 1994.
- [43] C. Gabriel, and A. Peyman, ‘Dielectric Measurement: Error Analysis and Assessment of Uncertainty’, *Physics in Medicine & Biology*, Vol. 51, No. 23, pp. 6033-6046, 2006.
- [44] A. La Gioia, E. Porter, I. Merunka, A. Shahzad, S. Salahuddin, M. Jones, and M. O’Halloran, ‘Open-Ended Coaxial Probe Technique for Dielectric Measurement of Biological Tissues: Challenges and Common Practices’, *Diagnostics*, Vol. 8, No. 2, pp. 40, 2018.
- [45] J. N. Ikediala, J. Tang, S. R. Drake, and L. G. Neven, ‘Dielectric Properties of Apple Cultivars and Codling Moth Larvae’, *Transactions of the ASAE*, Vol. 43, No. 5, pp. 1175-1184, 2000.
- [46] R. Rooban, M. Shanmugam, T. Venkatesan, and C. Tamilmani, ‘Physiochemical Changes During Different Stages of Fruit Ripening of Climacteric Fruit of Mango (*Mangifera indica* L.) and Non-Climacteric of Fruit Cashew Apple (*Anacardium occidentale* L.)’, *Journal of Applied and Advanced Research*, Vol. 1, No. 2, pp. 53-58, 2016.
- [47] T. K. Kataria, J. L. Olvera-Cervantes, A. Corona-Chávez, R. Rojas-Laguna, and M. E. Sosa-Morales, ‘Dielectric Properties of Guava, Mamey Sapote, Prickly Pears, and Nopal in the Microwave Range’, *International Journal of Food Properties*, Vol. 20, No. 12, pp. 2944-2953, 2017.
- [48] The MathWorks, ‘*MATLAB 2014a*’, Natick, 2014.
- [49] S. S. Stuchly, A. Kraszewski, M. A. Stuchly, G. W. Hartsgrove, and R. J. Spiegel, ‘RF Energy Deposition in a Heterogeneous Model of Man: Far-Field Exposures’, *IEEE Transactions on Biomedical Engineering*, Vol. 34, No. 12, pp. 951-957, 1987.
- [50] P. Bernardi, M. Cavagnaro, S. Pisa, and E. PiuZZi, ‘Specific Absorption Rate and Temperature Elevation in a Subject Exposed in the Far-Field of Radio-Frequency Sources Operating in the 10-900-MHz Range’, *IEEE Transactions on Biomedical Engineering*, Vol. 50, No. 3, pp. 295-304, 2003.
- [51] A. Christ, A. Klingenbock, T. Samaras, C. Goiceanu, and N. Kuster, ‘The Dependence of Electromagnetic Far-Field Absorption on Body Tissue Composition in the Frequency Range from 300 MHz to 6 GHz’, *IEEE Transactions on Microwave Theory and Techniques*, Vol. 54, No. 5, pp. 2188-2195, 2006.

- [52] T. Yelkenci, and S. Paker, ‘The Effects of Frequency, Polarization, Direction and Metallic Objects on the SAR Values in a Human Head Model for Plane Wave Exposure (500-2500 MHZ)’, *Frequenz*, Vol. 60, No. 11-12, pp. 215-219, 2006.
- [53] M. A. Stuchly, A. Kraszewski, and S. S. Stuchly, ‘Exposure of Human Models in the Near and Far Field – A Comparison’, *IEEE Transactions on Biomedical Engineering*, Vol. 32, No. 8, pp. 609-616, 1985.
- [54] A. Hirata, ‘Temperature Increase in Human Eyes due to Near-Field and Far-Field Exposures at 900 MHz, 1.5 GHz, and 1.9 GHz’, *IEEE Transactions on Electromagnetic Compatibility*, Vol. 47, No. 1, pp. 68-76, 2005.
- [55] S. S. Stuchly, M. A. Stuchly, A. Kraszewski, and G. Hartsgrove, ‘Energy Deposition in a Model of Man: Frequency Effects’, *IEEE Transactions on Biomedical Engineering*, Vol. 33, No. 7, pp. 702-711, 1986.
- [56] K. Meier, V. Hombach, R. Kästle, R. Y. Tay, and N. Kuster, ‘The Dependence of Electromagnetic Energy Absorption upon Human-Head Modelling at 1800 MHz’, *IEEE Transactions on Microwave Theory and Techniques*, Vol. 45, No. 11, pp. 2058-2062, 1997.
- [57] J. Cooper, B. Marx, J. Buhl, and V. Hombach, ‘Determination of Safety Distance Limits for a Human near a Cellular Base Station Antenna, Adopting the IEEE Standard or ICNIRP Guidelines’, *Bioelectromagnetics* Vol. 23, No. 6, pp. 429-443, 2002.
- [58] A. Christ, A. Klingenböck, T. Samaras, C. Goiceanu, and N. Kuster, ‘The Dependence of Electromagnetic Far-Field Absorption on Body Tissue Composition in the Frequency Range from 300 MHz to 6 GHz’, *IEEE Transactions on Microwave Theory and Techniques*, Vol. 54, No. 5, pp. 2188-2195, 2006.
- [59] D. L. Means, and K. W. Chan, ‘*Evaluating Compliance with FCC Guidelines for Human Exposure to Radiofrequency Electromagnetic Fields - Additional Information for Evaluating Compliance of Mobile and Portable Devices with FCC Limits for Human Exposure to Radiofrequency Emissions: Supplement C Edition 01-01 to OET Bulletin 65 Edition 97-01*’, Office of Engineering and Technology, Federal Communications Commission, 2001. Available Online: <https://transition.fcc.gov/bureaus/oet/info/documents/bulletins/oet65/oet65c.pdf> (Accessed on 18 Feb, 2022).

- [60] International Commission on Non-Ionizing Radiation Protection (ICNIRP), ‘Guidelines for Limiting Exposure to Electromagnetic Fields (100 kHz to 300 GHz)’, *Health Physics*, Vol. 118, No. 5, pp. 483-524, 2020.
- [61] IEC/IEEE, ‘IEC/IEEE International Standard – Determining the Peak Spatial-Average Specific Absorption Rate (SAR) in the Human Body from Wireless Communications Devices, 30 MHz to 6 GHz - Part 1: General Requirements for using the Finite-Difference Time-Domain (FDTD) Method for SAR Calculations’, *IEC/IEEE 62704-1:2017*, pp 1-86, 2017, <https://webstore.iec.ch/publication/34411> (subscription required)
- [62] IEC/IEEE, ‘IEC/IEEE International Standard – Determining the Peak Spatial-Average Specific Absorption Rate (SAR) in the Human Body from Wireless Communications Devices, 30 MHz To 6 GHz – Part 2: Specific Requirements for Finite Difference Time Domain (FDTD) Modelling of Exposure from Vehicle Mounted Antennas’, *IEC/IEEE 62704-2:2017*, pp 1-112, 2017, <https://webstore.iec.ch/publication/31306> (subscription required)
- [63] Department of Telecommunications (DoT), ‘*A Journey for EMF*’, 2012, <https://dot.gov.in/journey-emf> [Last accessed 03 March 2022].
- [64] CST Studio Suite, ‘*CST Microwave Studio 2018*’, 2018, <https://www.3ds.com/products-services/simulia/products/cst-studio-suite> [Last accessed 03 March 2022].
- [65] V. Hombach, K. Meier, M. Burkhardt, E. Kuhn, and N. Kuster, ‘The Dependence of EM Energy Absorption upon Human Head Modeling at 900 MHz’, *IEEE Transactions on Microwave Theory and Techniques*, Vol. 44, No. 10, pp. 1865-1873, 1996.
- [66] K. Meier, M. Burkhardt, T. Schmid, and N. Kuster, ‘Broadband Calibration of E-Field Probes in Lossy Media [Mobile Telephone Safety Application]’, *IEEE Transactions on Microwave Theory and Techniques*, Vol. 44, No. 10, pp. 1954-1962, 1996.
- [67] K. Meier, V. Hombach, R. Kästle, R. Y. Tay, and N. Kuster, ‘The Dependence of Electromagnetic Energy Absorption upon Human-head Modelling at 1800 MHz’, *IEEE Transactions on Microwave Theory and Techniques*, Vol. 45, No. 11, pp. 2058-2062, 1997.
- [68] A. Drossos, V. Santomaa, and N. Kuster, ‘The Dependence of Electromagnetic Energy Absorption upon Human Head Tissue Composition in the Frequency Range of 300-3000 MHz’,

*IEEE Transactions on Microwave Theory and Techniques*, Vol. 48, No. 11, pp. 1988-1995, 2000.

[69] V. Monebhurrun, C. Dale, J. C. Bolomey, and J. Wiart, 'A Numerical Approach for the Determination of the Tissue Equivalent Liquid used during SAR Assessments', *IEEE Transactions on Magnetics*, Vol. 38, No. 2, pp. 745-748, 2002.

[70] T. Weiland, 'A Discretization Method for the Solution of Maxwell's Equations for Six-Component Fields', *Electronics and Communications AEU*, Vol. 31, No. 3, pp. 116-120, 1977.

[71] M. Clemens, and T. Weiland, 'Discrete Electromagnetism with the Finite Integration Technique', *Progress in Electromagnetics Research*, Vol. 32, pp. 65-87, 2001.



# Chapter 4

## Specific Absorption Rate Evaluation for Prototyped Fruit and Plant Models

---

### 4.1 Introduction

Living in this era of 21<sup>st</sup> century, high speed wireless voice and data services are prime need of the hour in current global scenario. For example, people need to work either from home or remote office location and interact via virtual / online meetings, teachers need to teach on virtual platform, students need to interact and learn in digital classroom environment and so on. Therefore, as prerequisite, electromagnetic energy is being utilized extensively over multiple frequency bands with the increasing demand of high speed wireless telecommunication services and other related applications. As a result, all living objects such as humans, animals, plants, fruits and crops are continuously being exposed to simultaneous electromagnetic radiations at multiple frequencies from different sources (transmitting antennas). However, excessive exposure to uncontrolled electromagnetic radiation can possibly lead to either reversible or irreversible biological consequences in humans as well as plants [1-8]. In this connection, to limit electromagnetic exposure of humans, electromagnetic regulatory guidelines have been prescribed by different international and nationalized enforcement organizations [9-16]. Quantifiable metrics like ‘Specific Absorption Rate (SAR)’ and ‘reference power density’ etc. have been prescribed for respective near field and far field exposure scenarios [9-11]. SAR is defined as the rate at which electromagnetic energy is absorbed per unit mass of a living biological object while exposed to an external Radio Frequency (RF) radiation. SAR value at a particular point inside the biological object is defined as  $\sigma|E|^2/2\rho$  – where,  $\sigma$  denotes electrical conductivity of the tissue,  $E$  represents peak electric field strength developed inside the biological tissue and  $\rho$  represents the density of biological tissue. Thus, point SAR is dependent upon reference power density, tissue dielectric properties, geometry of biological object, direction of wave incidence and polarization of incident wave etc. [17-31]. SAR has been employed to quantify electromagnetic energy absorption rate in the near field of transmitter [9-

11, 19-24, 30] – however, recent papers are even reporting SAR estimations in far field exposure scenarios along with its justifications [19, 25, 27-28]. In addition, different international and national electromagnetic regulatory organizations prescribe reference power density limits for far field exposure scenarios just to protect humans from immediate thermal effects [9-16]. However, it is unfortunate that none of these enforcement organizations have considered electromagnetic energy absorption in plants, fruits and crops while preparing the electromagnetic regulatory norms [9-16]. But, most of the plant, fruit and crop tissues possess reasonably high permittivity ( $\epsilon_r'$ ) and electrical conductivity ( $\sigma$ ) – as demonstrated in the previous chapter [32-39]. Thus, investigating electromagnetic energy absorption rates in terms of SAR inside different prototyped plant and fruit models is an absolute necessity in existing electromagnetic exposure scenario. Moreover, the investigated SAR distributions in different plant and fruit models can rationalize further the need to explore electromagnetic irradiation induced physiological and molecular responses in plants [40-48].

As mentioned earlier, evaluated SAR data depends upon squared magnitude of electric field strength developed inside biological tissue – this internal field strength is further dependent upon external incident reference power density or plane wave equivalent incident electric field strength in far field exposure scenario. Thus, the effective electromagnetic regulatory guideline has a significant impact on evaluated SAR data for a particular fruit or plant prototype. Now, it should be noted that a number of international and national electromagnetic exposure regulatory standards are in effect worldwide [9-16] – however, these prescribed standards are quite inconsistent due to development based upon significantly diversified backgrounds, technical specifications, medical inferences and objectives to protect life [16]. Some of these standards prescribe the basic SAR limits along with reference power density limits to protect human health from immediate thermal effects, few others aim at mitigating biological effects of long duration exposure and the rest are prescribed to ensure additional precautions against yet unknown health effects [9-16]. However, these electromagnetic exposure standards prescribed by different international and national organizations are widely inconsistent – prescribed power density limits differ by ten to hundred times due to dissimilarity among these electromagnetic exposure standards [16]. As a consequence, the wide contrast in reference power density limits across geographical boundaries is also expected to be reflected on electromagnetic energy absorption rate in all living biological objects including plants, fruits and crops. In addition, prescribed

reference power density limit also varies with frequency of irradiation [9-16] – thus, electromagnetic energy absorption rates in biological bodies are expected to be dependent upon frequency of irradiation.

Furthermore, in many cases, plant and fruit structures are multilayer and asymmetric in nature – hence, directions of arrival along with polarization of incident electromagnetic wave are also two important factors that play crucial role in determining magnitude of SAR value along with its spatial distribution. Thus, it is obvious that prescribing only the maximum reference power density limits in far field exposure scenario is insufficient without a basic SAR limit. To explore this matter, the dependence of absorbed electromagnetic energy distribution on direction of arrival and polarization of incident wave should also be investigated in homogeneous single layer as well as multilayer fruit models.

Thus, in this particular chapter, Maximum Local Point SAR (MLP SAR), SAR averaged over 1 g of contiguous tissue mass (1g SAR), SAR averaged over 10 g of contiguous tissue mass (10g SAR) and SAR averaged over the entire biological tissue mass i.e. Whole Body Averaged SAR (WBA SAR) along with their respective distributions in the prototyped plant or fruit models have been evaluated in accordance with the existing Indian electromagnetic regulatory guidelines [11]. Next, the contrasts in SAR data have been investigated for some prototyped plant and fruit models due to discrepancy in reference power density limits prescribed by different international and national regulatory organizations [9-12]. At last, frequency, angle of incidence and wave polarization dependent variations in SAR data along with associated spatial distributions have been studied in both homogeneous single layer as well as multilayer fruit models.

## **4.2 SAR Analyses in Different Tropical Fruit Models**

In this section, SAR data along with spatial distributions have been analyzed for a number of multilayer / single layer fruit models such as coconut, apple, guava and grape etc. SAR data have been analyzed in accordance with the Indian public electromagnetic regulatory guidelines prescribed by Department of Telecommunications (DoT), India [11]. It should be noted that Federal Communications Commission (FCC) and International Commission on Non-Ionizing Radiation Protection (ICNIRP) prescribed electromagnetic guidelines are more liberal [9-10] – in contrast, much stricter exposure guidelines have been adopted in Switzerland, Italy, Poland and Luxembourg etc. to avoid possible biological effects of electromagnetic radiation [12-16].

### **4.2.1 SAR Analysis in a Typical Multilayer Coconut Model**

In this work, a realistic multilayer coconut (*Cocos nucifera*) fruit model has been designed in CST Microwave Studio 2010 (CST MWS 2010) electromagnetic simulation platform [49]. Different coconut tissue layers like green skin, yellowish pulp and coconut water along with the connecting twig possess quite high permittivity ( $\epsilon_r'$ ) and electrical conductivity ( $\sigma$ ) values – the same can result in reasonable amount of electromagnetic energy absorption in coconut fruits while maturing in trees. Thus, at first, measured dielectric properties ( $\epsilon_r$ ) for different coconut tissue layers have been reported at specific frequencies of interest – the associated analysis of open ended coaxial probe technique along with broadband dielectric properties ( $\epsilon_r$ ) data have been reported in the last chapter. Next, electromagnetic energy absorption rate (SAR) in a typical twig connected multilayer coconut fruit structure has been reported in context with existing Indian public electromagnetic exposure scenario [11]. SAR data have been evaluated using transient / time domain solver available in CST MWS 2010 platform [49] – the solver has been developed based on Finite Integration Technique (FIT) [50-51]. SAR data and its spatial distribution in the prototyped multilayer coconut fruit model have been evaluated due to linearly polarized plane wave exposure at 947.5 MHz (935-960 MHz downlink band), 1842.5 MHz (1805-1880 MHz downlink band) and 2450 MHz (2400-2500 MHz band) in public exposure scenario. As already known, SAR value is highly dependent upon geometry of the dielectric object – in real scenario, there is a twig, connected to each coconut, which not only contributes to alter SAR distribution but also increases SAR value in the coconut fruit model due to its sharp geometry.

#### **4.2.1.1 Existing Electromagnetic Exposure Standards in India**

In this work, SAR data in the multilayer coconut model and its spatial distribution have been evaluated in accordance with the revised Indian electromagnetic exposure scenario [11]. ICNIRP prescribed electromagnetic exposure regulatory guidelines were in effect in India up to 31<sup>st</sup> August, 2012 along with many other European countries [10]. However, DoT (Govt. of India) has revised the maximum permissible electromagnetic exposure levels to further stringent limits at all frequencies up to 300 GHz [11]. There are mainly three RF exposure zones around a base station transmitting antenna – those are known as excess electromagnetic exposure zone, controlled / occupational electromagnetic exposure zone and public electromagnetic exposure

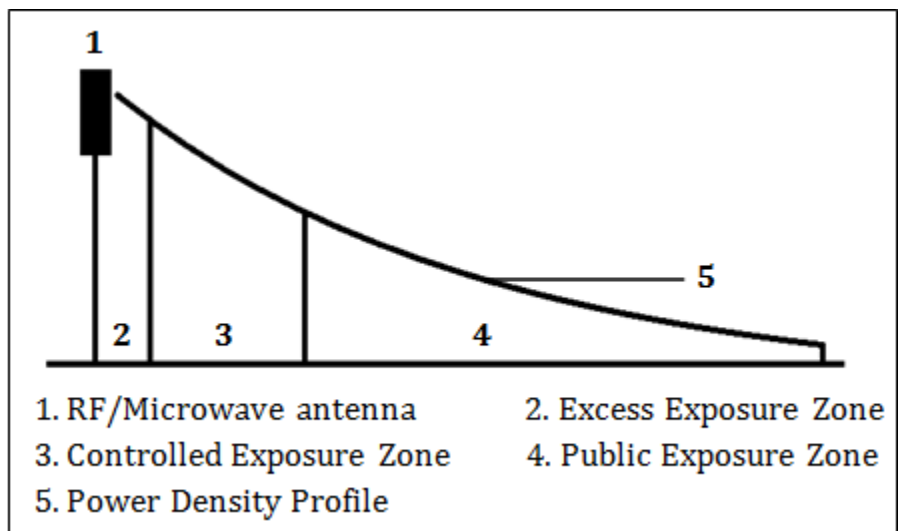


Fig. 4.1: Electromagnetic exposure zones around a base station antenna

Table 4.1 Existing revised Indian public electromagnetic exposure guidelines [11]

Frequency (MHz)	Equivalent Plane Wave Power Density (W/m <sup>2</sup> )	Equivalent Peak Electric Field Strength (V/m)
947.50	0.47375	18.90
1842.50	0.92125	26.36
2450.00	1.00	27.46

zone. All these three electromagnetic exposure zones have been pointed out in Fig. 4.1 along with power density profile. As per the existing Indian electromagnetic exposure standards, maximum permissible electromagnetic power densities at public zone have been reduced to 1/10<sup>th</sup> of ICNIRP regulations – however, no specific information has clearly been mentioned for excess and controlled electromagnetic exposure zones. According to the existing Indian scenario, maximum permissible RF exposure limits for public zone have been tabulated in Table 4.1. In addition to the reference exposure limits, revised Indian electromagnetic exposure standards also include basic restriction on maximum permissible SAR limit for humans up to 1.6 W/kg averaged over 1 g of contiguous tissue [11]. However, it must be noted that all these electromagnetic exposure standards and SAR limit have been prescribed for humans only – these have not been prescribed considering the electromagnetic energy absorption rates and consequent biological effects in plants, fruits and crops.

### 4.2.1.2 Material Density and Dielectric Properties of Coconut

At initial stage, a number of fresh green coconut specimens have been collected – next, random coconut specimens have been chosen for material density ( $\rho$ ) measurements of different tissue layers i.e. green skin (exocarp), yellowish pulp (mesocarp) and coconut water (liquid endosperm). Respective mass and volume of each tissue layer have been measured using electronic balance and a glass beaker (filled with water) respectively for computing the material density ( $\rho$ ). Above mentioned density measurement technique has been repeated for multiple coconut specimens. At last, average tissue densities ( $\rho$ ) for different coconut layers have been tabulated in Table 4.2.

In subsequent stage, broadband dielectric properties ( $\epsilon_r$ ) for the above mentioned coconut tissue layers i.e. green skin, yellowish pulp and coconut water have been measured with Agilent Technologies 85070E open ended coaxial probe kit and Agilent Technologies E5071B bench top VNA. In this connection, it should be noted that the shell (endocarp) around coconut water is so thin in tender coconut fruit that the same can't be characterized as a separate tissue dielectric layer due to difficulties in measuring accurate dielectric properties ( $\epsilon_r$ ) using this open ended coaxial probe technique [52-62]. Thickness of the shell inside tender coconut is insufficient and fails to fulfill the bare minimum tissue layer thickness (based upon the skin depth) for accurate dielectric properties ( $\epsilon_r$ ) measurement. Therefore, the shell has been considered as an integral part together with the yellowish pulp tissue layer. In the previous chapter, comprehensive physical and mathematical analyses of this non-destructive dielectric properties ( $\epsilon_r$ ) measurement technique have been outlined – thus, the same are not repeated here [52-62]. The open ended coaxial probe is capable of measuring complex dielectric properties ( $\epsilon_r$ ) up to 20 GHz and can withstand temperature up to 200 °C. Once system calibration has been performed employing open-short-deionized water, this open ended coaxial probe (along with E5071B VNA) can measure wideband permittivity ( $\epsilon'_r$ ) and loss tangent ( $\tan \delta$ ) data from corresponding reflection coefficient ( $S_{11}$ ) data of the coconut tissue specimens. Due to frequency limitation of the available E5071B VNA, the cascaded system can measure dielectric properties ( $\epsilon_r$ ) up to 8.5 GHz. But, to keep the data consistent with this work, permittivity ( $\epsilon'_r$ ) and loss tangent ( $\tan \delta$ ) data have been tabulated at 947.5 MHz, 1842.5 MHz and 2450 MHz. Complex dielectric properties ( $\epsilon_r$ ) measurement setup employing Agilent Technologies 85070E open ended coaxial

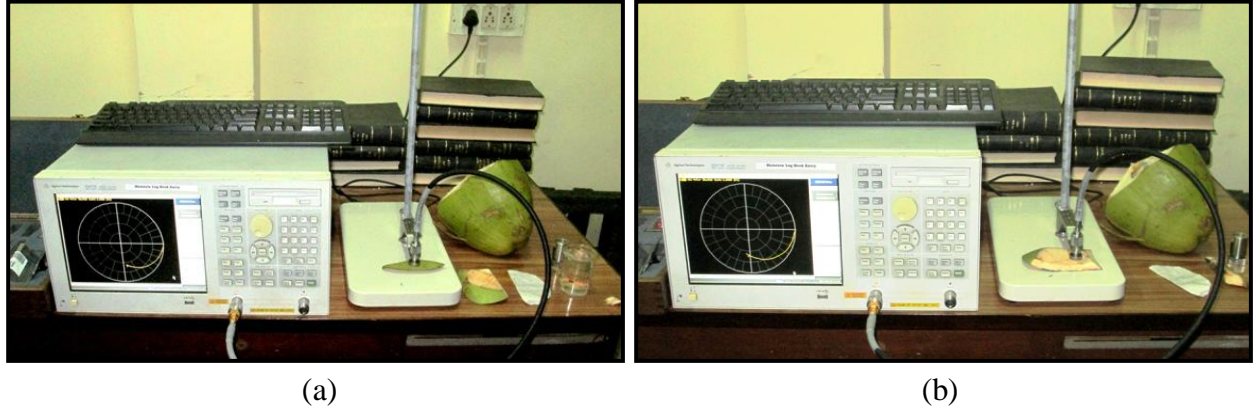


Fig. 4.2: Dielectric properties measurement for coconut layers (a) green skin, (b) yellowish pulp

Table 4.2 Measured material densities ( $\rho$ ) of different coconut layers

Name of coconut layer	Material density ( $\rho$ ) (kg/m <sup>3</sup> )
Green skin	1064
Yellowish pulp	976.5
Coconut water	1013
Twig	1064

Table 4.3 Measured dielectric properties ( $\epsilon_r$ ) of different coconut layers

Name of coconut layer	947.5 MHz		1842.5 MHz		2450 MHz	
	$\epsilon_r'$	$\tan \delta$	$\epsilon_r'$	$\tan \delta$	$\epsilon_r'$	$\tan \delta$
Green skin	41.21	0.385	38.12	0.306	37.14	0.296
Yellowish pulp	65.01	0.251	62.59	0.224	61.46	0.235
Coconut water	77.54	0.190	76.51	0.168	75.91	0.181
Twig <sup>#</sup>	41.21	0.385	38.12	0.306	37.14	0.296

probe kit and Agilent Technologies E5071B bench top VNA has been presented in Figs. 4.2(a) and (b) – those two figures demonstrate respective dielectric properties ( $\epsilon_r$ ) measurements for green coconut skin and yellowish pulp specimens. Measured dielectric properties ( $\epsilon_r$ ) for different coconut tissue layer specimens have been tabulated in Table 4.3.

### 4.2.1.3 A Typical Multilayer Coconut Modeling in CST MWS 2010

At first, a typical standard size fresh green coconut with 1.40 kg mass has been collected to observe shape of the coconut, shape of connecting twig, number of distinguishable tissue layers

in the coconut structure, thickness of each tissue layer along with their inner / outer dimensions etc. Next, observing detailed geometrical shape of the coconut, shape of twig connected to the coconut and size of different sections – three different coconut tissue dielectric layers have been identified from outer to inner direction and named as green skin (exocarp), yellowish pulp (mesocarp) and coconut water (liquid endosperm). Hard shell (endocarp) tissue dielectric layer is so thin that the same couldn't be characterized as a separate tissue dielectric layer due to difficulties in measuring accurate dielectric properties ( $\epsilon_r$ ) using open ended coaxial probe technique that asks for a minimum dielectric thickness (depending upon the skin depth) for accurate measurement [52-62]. Therefore, the hard shell (endocarp) has been taken into consideration together with the yellowish pulp (mesocarp) region. Besides these three tissue layers, the twig connected to the coconut has been considered as a separate section; consideration of twig in the designed coconut structure improves SAR estimation closer to realistic scenario.

The twig connected multilayer coconut structure (three tissue layers) has been modeled in CST MWS 2010 electromagnetic simulator with proper dimensions of each tissue layer [49] – a sharp twig structure has been incorporated for more accurate assessment of SAR data along with associated spatial distributions. Designed typical twig connected multilayer coconut model has been illustrated in Fig. 4.3 along with detailed modeling specifications tabulated in Table 4.4.

#### **4.2.1.4 SAR Computational Technique**

Three coconut tissue layers from outer to inner direction are top most green skin (exocarp), intermediate yellowish pulp region (mesocarp) and inner most coconut water (liquid endosperm) along with a twig structure connected to one pole of the designed coconut structure on green skin – moreover, complex dielectric properties ( $\epsilon_r$ ) and material densities ( $\rho$ ) have also been defined for each dielectric tissue layer. A linearly polarized plane wave impinges on the twig connected coconut structure at each frequency of investigation – the electric field strength of the plane wave alters with frequency of operation as prescribed in the revised Indian electromagnetic exposure regulatory guidelines – please refer to Table 4.1 [11]. The complex geometric structure shown in Fig. 4.3 and the low quality factor due to lossy dielectric tissue layers inside the multilayer coconut structure have led to the choice of transient / time domain solver for achieving a robust mesh distribution. This time domain solver is developed based on a computational numerical method called FIT – it was first introduced way back in 1977 [50-51].



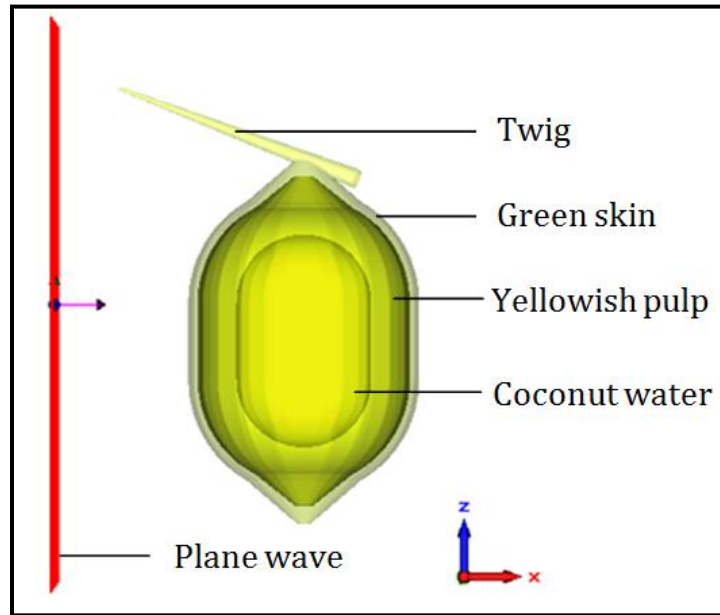


Fig. 4.3: Twig connected multilayer coconut structure modeled in CST MWS 2010 [49]

Table 4.4 Modeling specifications of the twig connected multilayer coconut model

Name of tissue layer	Basic geometrical shapes required to construct tissue layer	Least thickness of tissue layer (cm)	Volume of tissue layer (cm <sup>3</sup> )	Mass of tissue layer (kg)
green skin	cone + sphere + cylinder + sphere + cone	0.5	285.870	0.304166
yellowish pulp	cone + sphere + cylinder + sphere + cone	2.5	745.124	0.727241
coconut water	sphere + cylinder + sphere	3.5	327.801	0.332062
Twig	cone	0.1	4.47086	0.004757

The Maxwell’s integral equations are discretized and solved using numerical techniques inside the prototyped multilayer twig connected coconut model i.e. the desired solution space. The whole prototyped multilayer coconut structure is discretized in space with infinitesimal hexahedral meshes of variable size – one wavelength of spatial distance inside the dielectric tissue layers is subdivided into 20 segments. The typical mesh cell count for the above mentioned multilayer coconut fruit model is observed to be more than a few lakh – moreover, the average mass of individual mesh cell is around 0.0019 g. A typical Gaussian pulse of around 100

ns duration has been used for excitation. Four perfectly matched layers with  $10^{-4}$  reflection coefficient have been used as electromagnetic absorbing boundaries. Distance between the designed coconut structure and the absorbing boundary wall has been set minimal by choosing appropriate boundary conditions – thus, the plane wave can be excited very close to the prototyped structure [49]. The above mentioned multilayer coconut structure has been irradiated with linearly polarized plane waves propagating along  $x$ -axis and electric field variation along the  $z$ -axis – as illustrated in Fig. 4.3. After satisfying the steady state energy criterion, an inverse transformation precision of  $-40$  dB has been preferred in all the time domain simulations to obtain the frequency domain responses [49-51].

MLP SAR, 1g averaged SAR, 10g averaged SAR and WBA SAR data have been simulated in accordance with the revised Indian electromagnetic regulatory standards [11]. All reported SAR data have been evaluated using the most updated IEEE/IEC 62704-1 SAR averaging protocol [17, 49]. As described in this protocol – once the Maxwell's integral equations have been solved and electric field strengths on the edges of a grid cell are known, the average electric fields along all three axes are calculated. Next, the effective electric field at the grid centre is obtained and further utilized to calculate point SAR value ( $\sigma|E|^2/2\rho$ ). Next, a cubical volume is uniformly expanded along all three axes centering a particular grid cell to achieve the desired SAR averaging mass. In few cases, this cubical volume can include at most 10 percent background material near the structural boundaries – but, the background material mass is not taken into consideration to achieve the averaging mass. Thus, 1g or 10g averaged spatial SAR values have been calculated for a particular grid cell – this averaging technique is repeated positioning each valid grid cell at the centre of the averaging cube. Finally, 1g or 10g averaged spatial SAR distributions on and inside the prototyped mango fruits model have been obtained using the earlier calculated spatial averaged SAR data of all individual grid cells in the prototyped structure. This is how spatial SAR averaging has been performed in accordance with the IEEE/IEC 62704-1 SAR averaging protocol – more detailed descriptions are available in literature [17, 49].

#### **4.2.1.5 SAR Results in Twig Connected Coconut Structure**

SAR investigations have been performed for the above mentioned twig connected multilayer coconut structure due to linearly polarized plane wave irradiation at public exposure zone – SAR

data have been evaluated in particular at 947.5 MHz (935-960 MHz downlink band), 1842.5 MHz (1805-1880 MHz downlink band) and 2450 MHz (2400-2500 MHz band) as per the existing Indian electromagnetic exposure regulatory standards [11]. CST MWS 2010 considers peak electric field value for defining plane wave with linear polarization; therefore, peak electric field values have been obtained by multiplying respective unperturbed r. m. s. electric field values with  $\sqrt{2}$  (considering sinusoidal variation) at all three frequencies of interest and further tabulated in Table 4.5. This implies that the modeled multilayer coconut structure has been irradiated with linearly polarized plane wave precisely as per the revised Indian electromagnetic exposure standards at all three frequencies of interest [11]. In real time scenario, plane wave from cell tower antennas and other sources gets radiated 24 hours a day and 365 days a year; thus, the evaluated SAR data would not reduce by averaging over longer time span. SAR data have been calculated over point, 1 g and 10 g contiguous mass of different coconut tissue dielectric layers. A comparative overview of MLP SAR, 1g averaged SAR and 10g averaged SAR data has been illustrated in Table 4.5 and Fig. 4.4 respectively – for this twig connected multilayer coconut model.

It is clearly visible in Fig. 4.4 that SAR data for the twig connected coconut structure cannot be ignored even after revising the Indian electromagnetic exposure standards to much stricter limits [11] – while compared to international standards [9-10]. MLP SAR value is 0.26 W/kg at 947.5 MHz whereas the same increases to 0.69 W/kg and 1.04 W/kg respectively at 1842.5 MHz and 2450 MHz. Later on, it has been clearly observed that MLP SAR values are mostly distributed near and around the twig that connects the multilayer coconut model to the coconut plant. 1g averaged SAR values for the twig connected multilayer coconut structure are 0.07, 0.18 and 0.24 W/kg respectively at 947.5 MHz, 1842.5 MHz and 2450 MHz. SAR values increase at higher frequency bands primarily because of two factors. First of all, the prescribed reference power density level increases at 1842.5 MHz and 2450 MHz (while compared to 947.5 MHz) – thus, the same factor contributes to increased SAR value (at higher frequency) in the designed multilayer coconut model. In addition, there is presence of more number of electric field peaks within the twig connected multilayer coconut structure at higher frequency bands. Free space wavelength ( $\lambda_0$ ) at 1842.5 MHz is 16.28 cm but the wavelength is reduced to only 1.87 cm ( $\approx 16.28/76^{(1/2)}$ ) while considered in coconut water; hence, there is presence of several electric field peaks within the coconut water dielectric layer. It indicates that there is a possibility

Table 4.5 SAR results for twig connected coconut with electric field set as per revised Indian electromagnetic exposure standards [11]

Peak electric field value of the plane wave (V/m)	Frequency of operation (GHz)	SAR Averaging mass (g)	Simulated maximum SAR (W/kg)	WBA SAR (W/kg)
18.90	0.9475	Point	0.260	0.0056
"	"	1	0.072	"
"	"	10	0.024	"
26.36	1.8425	Point	0.689	0.0107
"	"	1	0.184	"
"	"	10	0.084	"
27.46	2.45	Point	1.039	0.0107
"	"	1	0.236	"
"	"	10	0.104	"

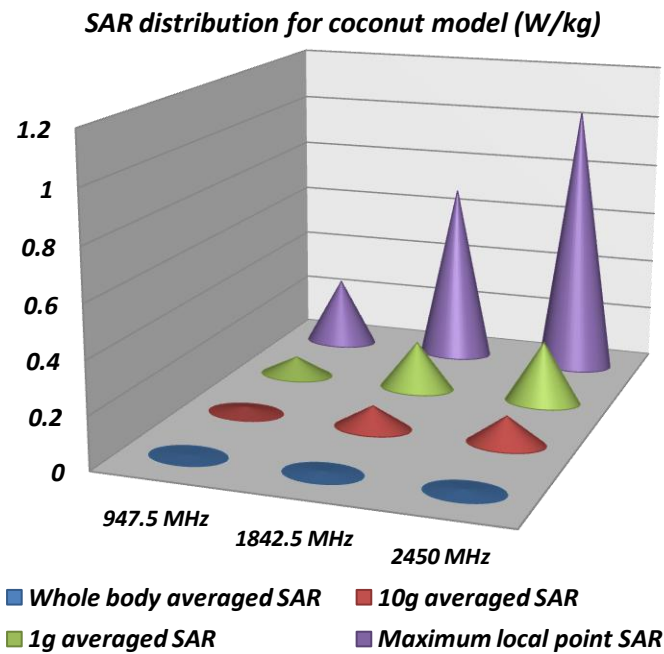


Fig. 4.4: Comparative SAR analysis for the twig connected coconut structure at 947.5 MHz, 1842.5 MHz and 2450 MHz as per the existing electromagnetic standards in India [11]

of local tissue dielectric heating and consequent temperature rise phenomenon near those internal peak electric field regions due to polar nature of coconut water content. Moreover, the aspect of possible physiological and molecular responses in the twig connected multilayer coconut fruit and plant should be investigated in future for better interpretation.

#### 4.2.1.6 SAR Distribution on Surface of the Coconut Model

Three Dimensional (3D) SAR distributions on surface of the twig connected multilayer coconut model have been illustrated in Figs. 4.5 and 4.6. Fig. 4.5(a) illustrates that a plane wave propagating along  $x$ -direction at 2450 MHz (with electric field in  $z$ -direction as per the existing Indian electromagnetic exposure standards) impinges and passes through the twig connected multilayer coconut structure in CST MWS 2010 electromagnetic simulation environment [49]. Corresponding 1g averaged SAR distribution on 3D surface of the twig connected multilayer coconut structure has been illustrated in Fig. 4.5(b). 1g averaged SAR distribution has been illustrated in Fig. 4.5(b) on purpose – because, the existing Indian electromagnetic exposure regulations have been prescribed based upon 1g SAR averaging protocol [11]. It is evident in Fig. 4.5(b) that maximum 1g averaged SAR magnitude is distributed primarily around the twig in the coconut model, whereas, SAR values are extreme less on rest of the coconut surface.

1g averaged SAR distribution has been well illustrated in Figs. 4.6(a) and (b) – these two figures demonstrate respective top view and side view of the twig connected multilayer coconut model. In addition to Fig. 4.5(b), illustrations in Figs. 4.6(a) and (b) validate that 1g averaged maximum SAR distribution is entirely concentrated over a narrow zone around the twig in this prototyped multilayer coconut model. Hence, it is well established that the maximum rate of electromagnetic energy absorption takes place around the junction point where the twig is connected to the typical multilayer coconut model.

#### 4.2.1.7 Conclusions

Evaluated SAR dataset should not be ignored in particular at higher frequencies like 1842.5 MHz and 2450 MHz – the key reasons for elevated SAR values at those frequencies have already been discussed earlier. It is relevant to mention that the twig contributes to significantly higher electromagnetic energy accumulation in the prototyped multilayer coconut structure due to sharp change in geometry near the junction of twig and prototyped coconut model. However while SAR averaging mass is varied from point mass to 1 g and thereafter 10 g, position of maximum 3D SAR slightly relocates around the twig. Maximum 3D SAR positions infer that there is a possibility of local temperature rise near the junction point of twig and prototyped coconut model. This temperature rise can further result in drying out the twig and consequent early fall of

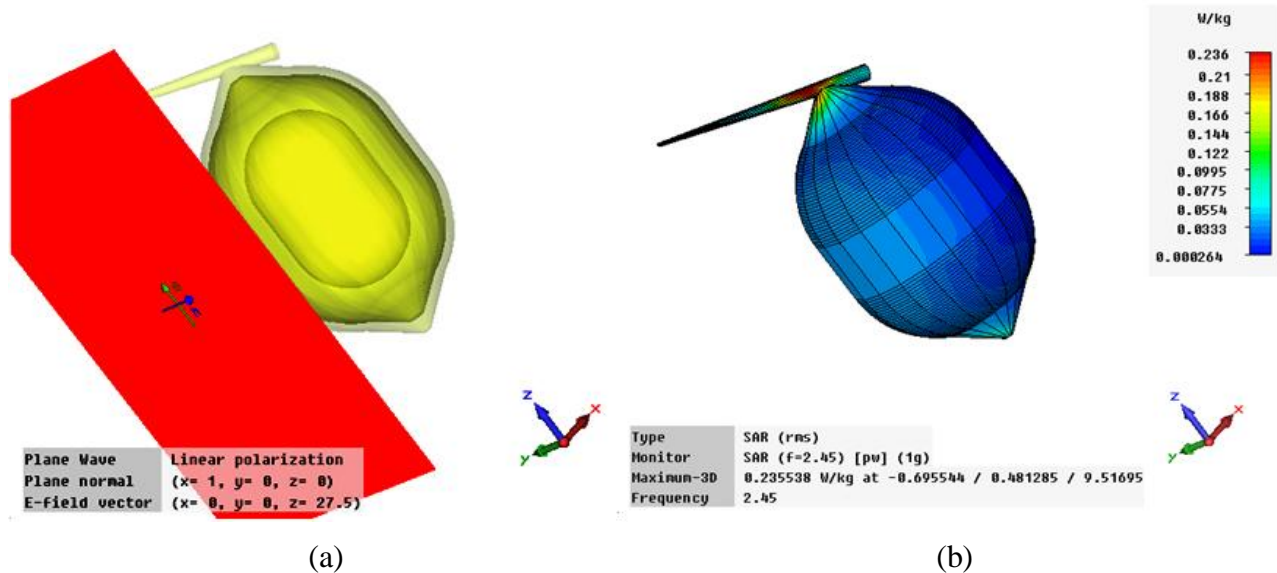


Fig. 4.5: (a) A linearly polarized plane wave at 2450 MHz (with peak electric field 27.46 V/m) impinges on the twig connected multilayer coconut structure, (b) 1g averaged SAR distribution on three dimensional surface of the twig connected multilayer coconut structure at 2450 MHz in Indian scenario

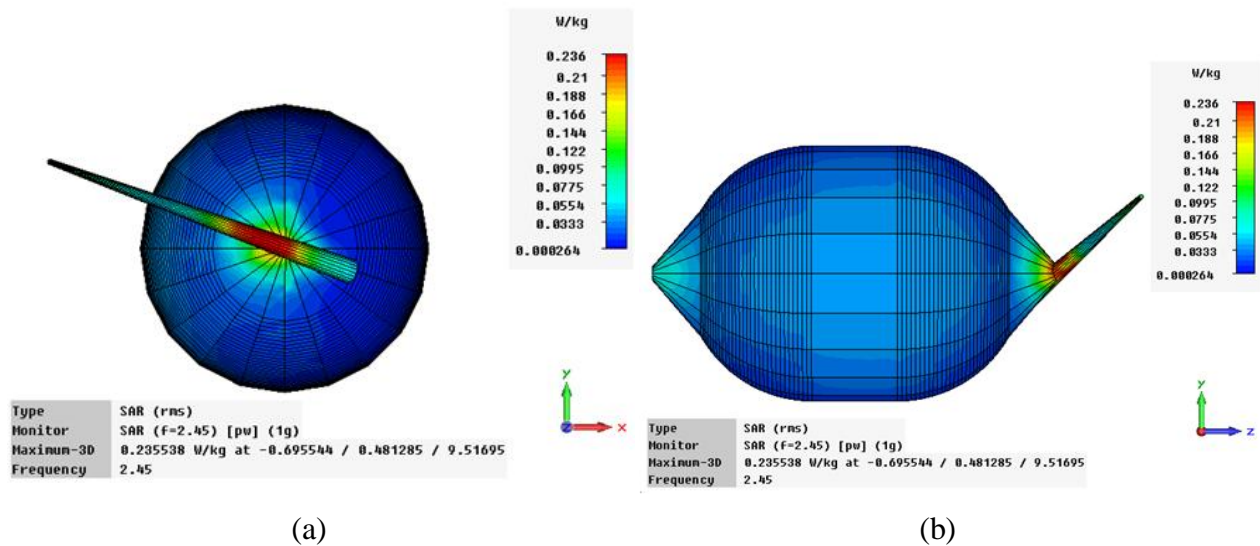


Fig. 4.6: (a) Top view of the twig connected multilayer coconut structure illustrating 1g averaged SAR distribution at 2450 MHz as per the existing Indian electromagnetic exposure scenario, (b) Side view of the twig connected multilayer coconut structure illustrating 1g averaged SAR distribution at 2450 MHz as per the existing Indian electromagnetic exposure scenario

immature green coconuts from plant. All reported SAR data have solely been evaluated for public electromagnetic exposure scenarios – where, the prescribed electromagnetic power densities are sufficiently low. However, evaluated SAR data are expected to be much higher in controlled electromagnetic exposure scenarios near base stations as the prescribed reference power densities have not yet been revised in India [11]. In addition, it should also be noted that SAR is additive in nature over different frequencies of exposure; therefore, cumulative SAR in this twig connected multilayer coconut structure is expected to be much higher due to simultaneous electromagnetic irradiation at multiple frequencies from several sources.

An important aspect should be pointed out that these coconut tissue layers possess moderately high permittivity ( $\epsilon_r'$ ) that contributes to store electromagnetic energy inside the multilayer coconut model rather than supporting radiation from any part of the structure (example twig). Likelihood of radiation further gets minimized due to reasonable conductivity ( $\sigma$ ) of coconut tissue layers; it causes conversion of stored electromagnetic energy to other forms e.g. heat during multiple reflections inside this multilayer structure due to abrupt dielectric discontinuity and contributes to increase in SAR ( $= \sigma|E|^2/2\rho$ ) value.

At last, it should be noted that computation of 3D SAR distribution around the twig of a realistic coconut structure is a significant novel contribution. Further biological investigations can reveal possible physiological and molecular effects of electromagnetic irradiation on plants.

#### **4.2.2 SAR Analysis in Single Apple, Guava and Grape Models**

The prime objective of this work is to investigate electromagnetic energy absorption rate i.e. SAR data in some single and simplified tropical fruit models as per the existing Indian electromagnetic exposure regulatory guidelines – in particular, at 900 MHz, 1800 MHz and 2400 MHz for public exposure scenarios [11]. SAR data have been evaluated for single apple, guava and grape models in public exposure scenarios – at the above mentioned frequencies. At first, shape, mass, volume of typical medium size fruits have been observed and noted down for prototyping three dimensional fruit models in CST MWS 2010 [49]. Next, broadband permittivity ( $\epsilon_r'$ ) and loss tangent ( $\tan \delta$ ) data for the above mentioned fruits have been measured using Agilent Technologies 85070E dielectric probe kit and E5071B VNA – in addition, material density ( $\rho$ ) of those fruit specimens have also been characterized. Thereafter, these measured parameters have been fed into the three dimensional fruit models while using

transient / time domain simulations in CST MWS 2010 [49]. Plane wave with linear polarization has been impinged on individual fruit structures at any particular frequency. MLP SAR, 1g averaged SAR and 10g averaged SAR data have been evaluated for all the prototyped fruit models.

#### 4.2.2.1 Density and Dielectric Properties of Apple, Guava and Grape

Initially, few typical medium sized fresh fruits (apples, guavas and grapes) have been collected. Next, for each type of fruit sample, respective mass and volume have been measured repeatedly. Material density ( $\rho$ ) has been calculated by taking the ratio of mass to volume for each fruit sample. Thereafter, mean material density ( $\rho$ ) value has been recorded for each of three fruit specimens. The above mentioned method has been repeated for all three fruit specimens i.e. apples, guavas and grapes. The finalized mean material densities ( $\rho$ ) of apple, guava and grape specimens have been tabulated in Table 4.6.

The broadband permittivity ( $\epsilon_r'$ ) and loss tangent ( $\tan \delta$ ) parameters for the above mentioned fruit specimens have been measured with Agilent Technologies 85070E coaxial probe kit along with Agilent Technologies E5071B bench top VNA at the Electronics and Telecommunication Engineering department, Jadavpur University. The required physical and mathematical analyses for this non-destructive dielectric measurement technique have already been discussed in the previous chapter [52-62]. The 85070E dielectric probe kit contains a coaxial probe that can measure dielectric properties up to 20 GHz and can withstand temperature up to 200 °C. This 85070E dielectric probe kit needs to be connected with E5071B VNA via coaxial cable for characterizing the broadband permittivity ( $\epsilon_r'$ ) and loss tangent ( $\tan \delta$ ) parameters from respective reflection coefficient data of the fruit specimens – after proper system calibration. However, the frequency range of the available E5071B VNA is limited up to 8.5 GHz – thus, the whole integrated system can measure dielectric properties ( $\epsilon_r$ ) up to 8.5 GHz. But, for keeping the data consistent with this research work, measured permittivity ( $\epsilon_r'$ ) and loss tangent ( $\tan \delta$ ) parameters have precisely been tabulated at 0.9 GHz, 1.8 GHz and 2.4 GHz. Complex dielectric properties ( $\epsilon_r$ ) measurement setup for one apple sample has been illustrated in Fig. 4.7. The permittivity ( $\epsilon_r'$ ) and loss tangent ( $\tan \delta$ ) values for apple, guava and grape specimens have been presented in Table 4.7.





Fig. 4.7: Dielectric properties ( $\epsilon_r$ ) measurement setup for an apple specimen

Table 4.6 Measured material densities ( $\rho$ ) of apple, guava and grape

Name of fruit	Apple	Guava	Grape
Material density ( $\text{kg/m}^3$ )	847.4	887.1	1056.5

Table 4.7 Measured dielectric properties ( $\epsilon_r$ ) of apple, guava and grape

Name of fruit	900 MHz		1800 MHz		2400 MHz	
	$\epsilon'_r$	$\tan \delta$	$\epsilon'_r$	$\tan \delta$	$\epsilon'_r$	$\tan \delta$
Apple	65.03	0.135	63.72	0.156	62.23	0.194
Guava	72.08	0.154	71.05	0.159	69.73	0.179
Grape	69.11	0.167	66.81	0.185	65.27	0.210

#### 4.2.2.2 Modeling of Apple, Guava and Grape in CST MWS 2010

At first, typical modeling of three different fruits i.e. apple, guava and grape is deemed necessary for SAR data evaluations for those fruit specimens. Therefore, three fruit models have been prototyped in their respective closest equivalent shapes utilizing CST MWS 2010 platform [49]. Apple and guava have been modeled to be spherical in shape with equivalent dimensions close to those of the real fruit specimens – whereas the grape has been modeled with one cylinder and two hemi-spheres at the two ends. Thereafter, two small cones have been subtracted from the

Table 4.8 Modeling specifications of apple, guava and grape

Name	Basic shape components	Outer radius of the layers (cm)	Inner radius of the layers (cm)	Volume (cm <sup>3</sup> )	Mass (g)
Apple	Sphere – 2×cone	3.25 (sphere) 0.5 (cone)	0 (sphere) 0 (cone)	139	118
Guava	Sphere	3.20	0	138	122
Grape	Cylinder + 2×(half sphere)	0.5 (cylinder) 0.5 (sphere)	0 (cylinder) 0 (sphere)	5	5.5

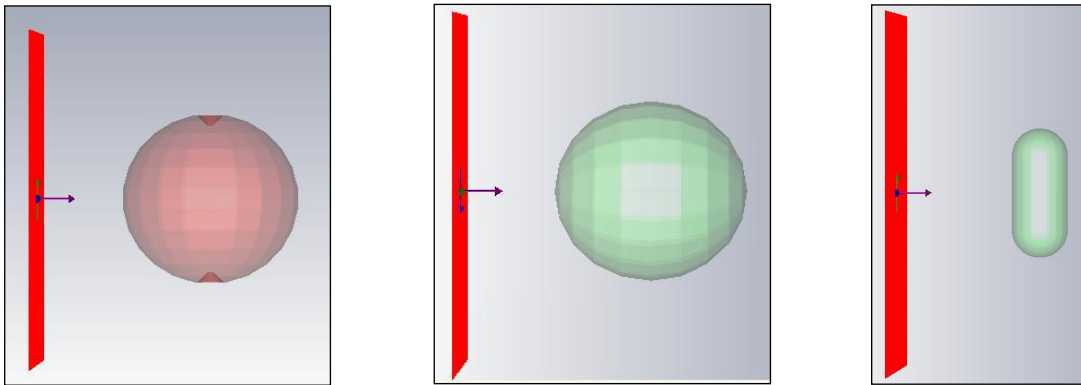


Fig. 4.8: Simplified models of (a) apple, (b) guava and (c) grape fruits

two poles of the apple model to obtain a more realistic shape and further accurate SAR data. Detailed modeling specifications for apple, guava and grape prototypes have been incorporated in Table 4.8 – furthermore, 3D prototyped models for apple, guava and grape specimens have been illustrated in Fig. 4.8(a), (b) and (c) respectively.

#### 4.2.2.3 SAR Computational Technique

SAR simulations for the above mentioned three fruit models have been performed using time domain / transient solver available in CST MWS 2010 [49]. As mentioned earlier, this transient solver has been developed based upon FIT computational technique [50-51]. The detailed SAR simulation setup in CST MWS 2010 transient solver has been discussed earlier in this chapter – almost similar SAR computational protocol has also been utilized in these simulations. Plane waves with linear polarization possessing different electric field strengths have been impinged on

individual fruit models in different electromagnetic simulations. Respective peak electric field values of the linearly polarized plane waves have been defined as per the existing Indian electromagnetic exposure regulatory guidelines – at the frequencies of interest [11]. Four PMLs with 0.0001 reflection coefficient have been utilized as the electromagnetic absorbing boundaries. The separation between individual fruit model and boundary wall has been kept fixed at 3 cm by varying mesh line settings at different frequencies of operation.

#### 4.2.2.4 Indian Electromagnetic Exposure Standards

SAR data have been evaluated for the above mentioned three fruit models (apple, guava and grape) – in accordance with the revised Indian electromagnetic exposure standards prescribed by DoT, Govt. of India [11]. Prior to this, ICNIRP electromagnetic exposure standards were effective in India up to 31<sup>st</sup> August, 2012 [10]. A detailed outline of the revised Indian electromagnetic regulatory standards has already been discussed earlier in this chapter – thus the same is not repeated here. In brief, reference power density limits in India have been brought down to 1/10<sup>th</sup> of ICNIRP limits at all frequencies up to 300 GHz. The revised SAR limit has been cut down to 1.6 W/kg averaged over 1g contiguous human tissue from 2 W/kg averaged over 10g contiguous human tissue. However, it should be noted that there is no existing SAR limit for safety of fruits, crops and plants.

As this work is on SAR evaluations in the prototyped apple, guava and grape models due to plane wave exposure at 900 MHz, 1800 MHz and 2400 MHz as per the revised Indian electromagnetic exposure guidelines, the maximum permissible limits for public exposure to time-varying electric fields as well as reference power densities have been tabulated at those frequencies in Table 4.9 [11].

Table 4.9 Revised Indian electromagnetic exposure guidelines for public scenario [11]

Frequency (MHz)	Equivalent Plane Wave Power Density $S_{eq}$ ( $W/m^2$ )	Unperturbed R.M.S. Electric Field Strength (V/m)	Equivalent Peak Electric Field Strength (V/m)
900	0.45	13.02	18.42
1800	0.90	18.42	26.05
2400	1.00	19.42	27.46

### 4.2.2.5 SAR Computational Results

The prime objective of this work is to investigate SAR data for the prototyped apple, guava and grape models due to far field plane wave irradiation with linear polarization in accordance with the revised Indian public electromagnetic exposure guidelines [11]. Thereafter, comparative analyses of evaluated SAR data for the above mentioned fruit models (apple, guava and grape) have been performed. Thus, in each simulation, individual fruit models have been exposed to linearly polarized plane waves at 900 MHz, 1800 MHz and 2400 MHz with electric field strength defined in accordance with the revised Indian electromagnetic scenario for public exposure [11].

#### A. *Evaluated SAR Data for Apple*

At each of the above specified three frequencies, a plane wave with linear polarization has been impinged on the prototyped apple model in each simulation run. The plane wave with linear polarization possesses peak electric field strength in accordance with the existing Indian electromagnetic regulatory guidelines for public scenario [11]. Respective MLP SAR, 1g averaged SAR, 10g averaged SAR and WBA SAR data for the designed apple model have been noted to be quite less at 900 MHz. However, those SAR values rise in significant manner at 1800 MHz and 2400 MHz. All simulated SAR data for the prototyped apple model have been recorded in Table 4.10 and illustrated in Fig. 4.9.

Table 4.10 SAR data for apple model as per public electromagnetic exposure guidelines in India

Frequency of exposure (GHz)	R. M. S. electric field (V/m)	Equivalent Peak electric field (V/m)	SAR averaging mass (g)	Simulated max SAR (W/kg)	WBA SAR (W/kg)
0.9	13.02	18.42	point	0.049	0.008
			1	0.041	
			10	0.024	
1.8	18.42	26.05	point	0.374	0.025
			1	0.217	
			10	0.096	
2.4	19.42	27.46	point	0.580	0.028
			1	0.275	
			10	0.095	

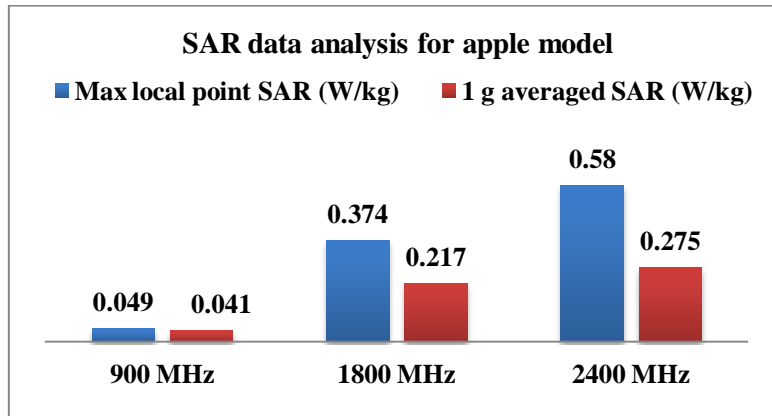


Fig. 4.9: MLP and 1g averaged SAR data analyses for apple model as per public electromagnetic exposure guidelines in India

### B. Evaluated SAR Data for Guava

All SAR data for the prototyped guava model have been evaluated utilizing similar plane wave exposure settings – as in case of the earlier apple model. Thus, MLP SAR, 1g averaged SAR, 10g averaged SAR and WBA SAR data for the guava model have been evaluated in accordance with the revised Indian electromagnetic exposure guidelines for public exposure scenario [11]. All estimated SAR data for the guava model have been tabulated in Table 4.11 and illustrated in Fig. 4.10. This time also, evaluated SAR data for the prototyped guava model have been noted to be quite less at 900 MHz. However, respective SAR data considerably rise at 1800 MHz and 2400 MHz – as visible in Table 4.11 and Fig. 4.10 respectively.

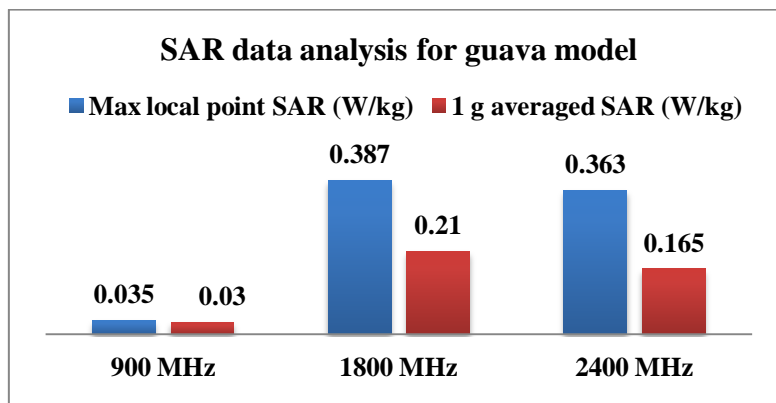


Fig. 4.10: MLP and 1g averaged SAR data analyses for guava model as per public electromagnetic exposure guidelines in India

Table 4.11 SAR data for guava model as per public electromagnetic exposure guidelines in India

Frequency of exposure (GHz)	R. M. S. electric field (V/m)	Equivalent Peak electric field (V/m)	SAR averaging mass (g)	Simulated max SAR (W/kg)	WBA SAR (W/kg)
0.9	13.02	18.42	point	0.035	0.006
			1	0.030	
			10	0.019	
1.8	18.42	26.05	point	0.387	0.022
			1	0.210	
			10	0.077	
2.4	19.42	27.46	point	0.363	0.022
			1	0.165	
			10	0.054	

Table 4.12 SAR data for grape model as per public electromagnetic exposure guidelines in India

Frequency of exposure (GHz)	R. M. S. electric field (V/m)	Equivalent Peak electric field (V/m)	SAR averaging mass (g)	Simulated max SAR (W/kg)	WBA SAR (W/kg)
0.9	13.02	18.42	point	0.013	0.002
			1	0.002	
			2	0.002	
1.8	18.42	26.05	point	0.587	0.140
			1	0.234	
			2	0.195	
2.4	19.42	27.46	point	0.739	0.141
			1	0.255	
			2	0.207	

### C. Evaluated SAR Data for Grape

Adopted SAR data evaluation technique for the prototyped grape model has been similar to the protocol taken up for other two fruit models. Here it must be noted that MLP SAR, 1g averaged SAR and WBA SAR data for the grape model have been evaluated in accordance with the revised Indian electromagnetic exposure guidelines for public exposure scenario [11] – however,

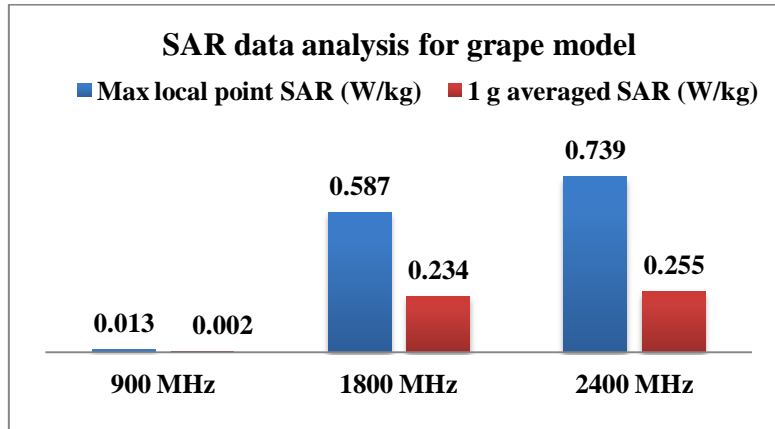


Fig. 4.11: MLP and 1g averaged SAR data analyses for grape model as per public electromagnetic exposure guidelines in India

10g averaged SAR data could not be evaluated as the entire mass of prototyped grape model is 5.5 g only. Thus, 2g averaged SAR data has been estimated in place of 10g averaged SAR data for the prototyped grape model. All estimated SAR data for the grape model have been tabulated in Table 4.12 – whereas, a comparative SAR data analysis has been illustrated in Fig. 4.11. Once again, estimated SAR data for the prototyped grape model have been noted to be considerably less at 900 MHz – but, the respective values significantly rise at 1800 MHz and 2400 MHz.

#### 4.2.2.6 SAR Data Analyses

Before analyzing evaluated SAR data, it must be noted that the maximum prescribed electromagnetic power density is much less for 900 MHz ( $0.45 \text{ W/m}^2$ ) compared to those for 1800 MHz ( $0.90 \text{ W/m}^2$ ) and 2400 MHz ( $1.00 \text{ W/m}^2$ ) (please refer to Table 4.9) [11]. On the other side, respective volume and mass of prototyped apple ( $139 \text{ cm}^3 / 118 \text{ g}$ ) and guava ( $138 \text{ cm}^3 / 122 \text{ g}$ ) models have been noted to be quite similar; but the volume and mass of the grape model ( $5 \text{ cm}^3 / 5.5 \text{ g}$ ) is too small compared to those for the other two fruit models – as observed in Table 4.8. In general, SAR value significantly rises at 1800 MHz and 2400 MHz in each fruit model. It is because of two prime factors – first of all, plane wave equivalent reference power density limit increases at higher frequency (up to 2000 MHz) and thus, the SAR value increases with frequency [11]. In addition, the realized wavelength becomes shorter at higher frequency and more numbers of node and anti-node formations take place within the fruit structures. Moreover, frequency dependent variation in complex dielectric properties ( $\epsilon_r$ ) of fruit specimens

also influences SAR data for the prototyped fruit models. It should be noted that the shapes of individual apple and guava fruit models are almost symmetrical – therefore, the magnitude and spatial distribution of SAR data in individual fruit model are independent of direction of arrival and wave polarization. But, in real scenarios, apple, guava and grape fruits grow in asymmetrical bunches and thus SAR magnitude and spatial distribution significantly depend upon direction of arrival and wave polarization.

#### **4.2.2.7 Conclusions**

SAR data evaluation for the prototyped apple, guava and grape models have been performed in accordance with the existing Indian electromagnetic exposure regulatory guidelines prescribed for public exposure scenarios [11]. Based on evaluated SAR data for the prototyped fruit models, it has been noted that electromagnetic energy absorption rate is quite high in the fruit models in particular at 1800 MHz and 2400 MHz. Fruits and plants get exposed to uninterrupted electromagnetic radiation – hence, the calculated SAR values shouldn't be diluted by averaging over extended averaging time span. It must also be taken into consideration that all SAR data have been evaluated for most simplistic fruit models without any twig or bunch structure – therefore, the recorded SAR data for the prototyped fruit models can increase many folds if twig structures in between the prototyped fruits and the trees are taken into consideration. Local temperature rise due to localized increase in SAR magnitude near the twig structure can result in possible early fall of fruits from the plant at an immature stage. Even in real scenario, apple, guava and grape fruits individually grow in asymmetrical bunches – as a consequence, magnitude and spatial distribution of SAR data depend upon direction of arrival and wave polarization at large. In general, it is true that most of these fruit producing plants are present at public exposure zone – but, there are also a significant number of plants that get exposed to much higher electromagnetic field strength at controlled exposure zones near to the base station antennas. As a consequence, those plants at the controlled exposure zone absorb electromagnetic energy at much significant levels along with associated higher SAR values.

Agriculture being one of the key verticals of Indian economy, it is recommended to investigate SAR data in different fruit, plant and crop models along with associated physiological and molecular responses due to electromagnetic irradiation in accordance with the existing Indian electromagnetic exposure regulatory standards [11].



### 4.2.3 SAR Analysis in a Typical Bunch of Grapes Model

In this work, a typical realistic bunch of grapes model has been prototyped in CST MWS 2010 electromagnetic simulation software [49]. The entire bunch consists of 21 spherical grapes with variable dimensions – the grapes possess reasonably high dielectric properties i.e. permittivity ( $\epsilon_r'$ ) and electrical conductivity ( $\sigma$ ) due to presence of enormous water and ion contents. The dielectric properties for fresh grape samples have been measured with the open ended coaxial probe technique – the associated mathematical and physical analysis of the same along with broadband complex dielectric properties ( $\epsilon_r$ ) data have been reported in the previous chapter. Based on measured dielectric properties ( $\epsilon_r$ ), it has been predicted that the prototyped bunch of grapes can possibly absorb a considerable amount of electromagnetic power while an electromagnetic wave passes through the same and the fact must be investigated for further biophysical and biological inferences. In the previous work, basic SAR estimation in a single homogeneous grape model (along with two other fruits) has already been performed as per the existing Indian electromagnetic exposure regulatory guidelines; however, grapes grow in bunches and thus, this work focuses on more realistic spatial SAR distribution in the prototyped bunch of grapes at 947.5 MHz, 1842.5 MHz and 2450 MHz as per the revised Indian electromagnetic exposure regulatory guidelines [11]. SAR data and their spatial distributions have been analyzed in this typical bunch of grapes due to plane wave electromagnetic exposure at multiple frequencies. All SAR data have been calculated using the transient / time domain solver available in CST MWS 2010 [49] – developed using Finite Integration Technique (FIT) [50-51]. Thereafter, MLP SAR, 1g averaged SAR and also 10g averaged SAR data have been evaluated in the designed bunch of grapes model at each frequency of irradiation in separate electromagnetic simulation environment. In the earlier case, 10g averaged SAR data could not be evaluated for the single grape model due to its smaller mass – however, 10g averaged SAR data have also been evaluated in this realistic bunch of grapes model as the total mass is 23.75 g. SAR data in this typical bunch of grapes are alarming in particular at 1842.5 MHz and 2450 MHz – which require further correlation with biophysical and biological analyses.

#### 4.2.3.1 Indian Electromagnetic Regulatory Guidelines

For the above mentioned bunch of grapes model, all SAR data along with their spatial distributions have been evaluated in accordance with the revised Indian electromagnetic

exposure scenario – as prescribed by DoT, Govt. of India [11]. Detailed discussions on the existing Indian electromagnetic exposure regulatory guidelines have already been carried out in this chapter and thus need not to be repeated here. The reference power density limits along with associated peak electric field strengths have already been tabulated at 947.5 MHz, 1842.5 MHz and 2450 MHz – please, refer to Table 4.1.

#### **4.2.3.2 Material Density and Dielectric Properties of Grapes**

At first, several fresh bunches of grapes have been collected – random samples have been selected from each bunch of grapes. Next, mass and volume of individual grape samples have been measured with an electronic balance and a glass beaker respectively to calculate the material density. This procedure has been repeated for all the grape samples and average material density has been found to be  $1120 \text{ kg/m}^3$ .

Broadband dielectric properties for grape samples have been measured with Agilent Technologies 85070E dielectric properties ( $\epsilon_r$ ) measurement probe kit along with Agilent Technologies E5071B bench top vector network analyzer at Electronics and Telecommunication Engineering department, Jadavpur University. The detailed physical and analytical analyses of this non-destructive dielectric measurement technique have been discussed in the previous chapter [52-62]. Above mentioned dielectric probe is capable of measuring permittivity ( $\epsilon_r'$ ) and electrical conductivity ( $\sigma$ ) up to 20 GHz and can withstand temperature as high as 200 °C. However, the integrated measurement setup demonstrated in Fig. 4.12 can perform dielectric properties ( $\epsilon_r$ ) measurement up to 8.5 GHz which is due to the frequency limitation of E5071B vector network analyzer. As pointed out in the previous chapter, in addition to dependence on frequency, complex dielectric properties ( $\epsilon_r$ ) of any material also vary with temperature. Therefore, it is important to mention that all measurements have been performed at 25 °C ambient temperature. However, the complex dielectric properties ( $\epsilon_r$ ) of grape twig samples could not be measured with Agilent 85070E coaxial dielectric probe (20 mm diameter) as they are of much smaller dimension. Grape twig contains less water than grape fruits and thus, should result in reduced dielectric constant ( $\epsilon_r'$ ) for grape twig samples – those dielectric parameters have been estimated from the measured dielectric properties ( $\epsilon_r$ ) of grape fruits. Broadband permittivity ( $\epsilon_r'$ ) and loss tangent parameters ( $\tan \delta$ ) for grape samples have been once again

plotted in Figs. 4.13(a) and (b) respectively. In addition, dielectric properties ( $\epsilon_r$ ) of grape samples have also been tabulated in Table 4.13 at the frequencies of interest.



Fig. 4.12: Broadband dielectric measurement setup for grape samples at 25 °C using open ended coaxial probe technique

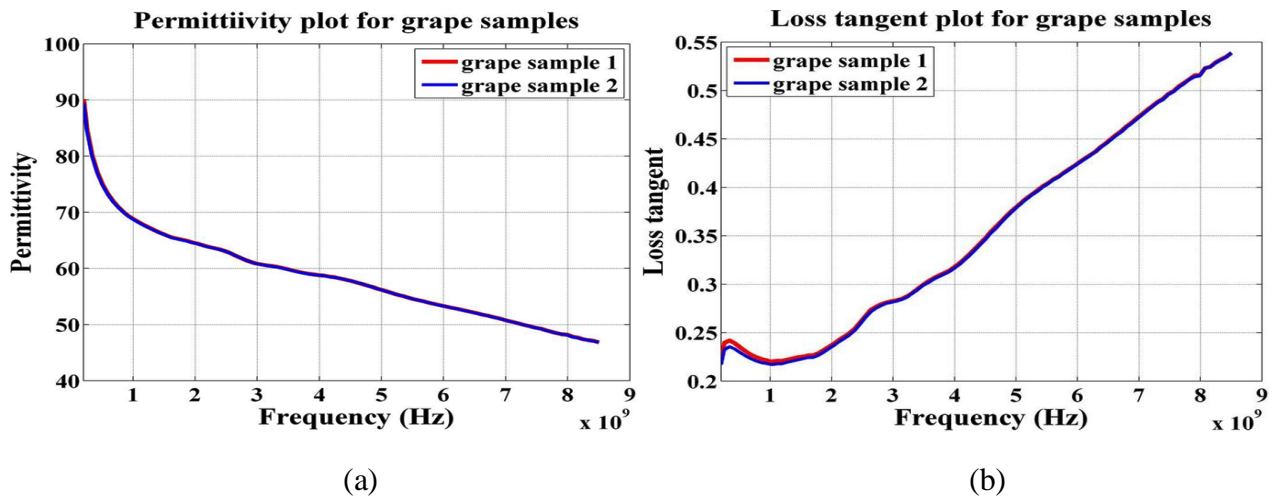


Fig. 4.13: Measured dielectric parameters for two typical grape samples at 25 °C using open ended coaxial probe technique (a) permittivity vs. frequency, (b) loss tangent vs. frequency

Table 4.13 Measured dielectric properties of grape samples

Name	947.5 MHz		1842.5 MHz		2450 MHz	
	$\epsilon_r$	$\tan \delta$	$\epsilon_r$	$\tan \delta$	$\epsilon_r$	$\tan \delta$
Grape	69.28	0.22	64.89	0.23	63.17	0.26
Twig <sup>#</sup>	49.28	0.17	44.89	0.18	43.17	0.21

<sup>#</sup> estimated values.

### 4.2.3.3 A Typical Bunch of Grapes Modeling in CST MWS 2010

A typical bunch of spherical shaped grapes has been prototyped in CST MWS 2010 electromagnetic simulation platform [49]. This typical bunch of grapes model consists of a single twig structure along with twenty one grapes – as illustrated in Figs. 4.14(a) and (b); all grapes are spherical in shape but they are of three different sizes i.e. large, medium and small. Typical modeling specifications for this prototyped bunch of grapes model have been tabulated in Table 4.14. Respective Masses of individual large, medium and small grapes are 1.98 g, 1.05 g and 0.43 g – whereas, the total composite twig structure consists of twenty one cones (with small individual mass) connected to twenty one grapes (one each).

### 4.2.3.4 SAR Computational Scheme

SAR simulations for the above mentioned typical bunch of grapes model has been performed using time domain / transient solver available in CST Microwave Studio 2010 [49] – as discussed earlier, this technique is developed based upon FIT computational scheme [50-51]. A detailed SAR computational technique along with the prerequisite transient / time domain setup in CST MWS 2010 electromagnetic simulator has been outlined earlier in this chapter – a similar SAR computational technique has also been employed in this work [17, 49]. The prototyped bunch of grapes model consists of near about 1,60,000 mesh cells with minimum step size 0.1 cm. A linearly polarized plane wave propagating along  $x$ -direction (with electric field variation along the  $z$ -direction) has been utilized as the incident electromagnetic radiation source. The respective peak electric field strengths of the linearly polarized plane waves have been set in accordance with the existing Indian electromagnetic exposure regulatory guidelines at all three different frequencies [11]. As mentioned earlier, four Perfectly Matched Layers (PMLs) with negligible reflection coefficient have been set as the electromagnetic absorbing boundary – the separation between absorbing boundary and bunch of grapes model has been adjusted to 3 cm.

Table 4.14 Modeling specifications for the bunch of grapes model

<b>Component</b>	<b>Shape</b>	<b>Radius (cm)</b>	<b>Volume (cm<sup>3</sup>)</b>	<b>Mass (g)</b>	<b>Replication</b>
Large grape	sphere	0.75	1.76	1.98	7
Medium grape	sphere	0.60	0.94	1.05	6
Small grape	sphere	0.45	0.38	0.43	8
Twig	21 cones	n/a	0.19	0.21	1

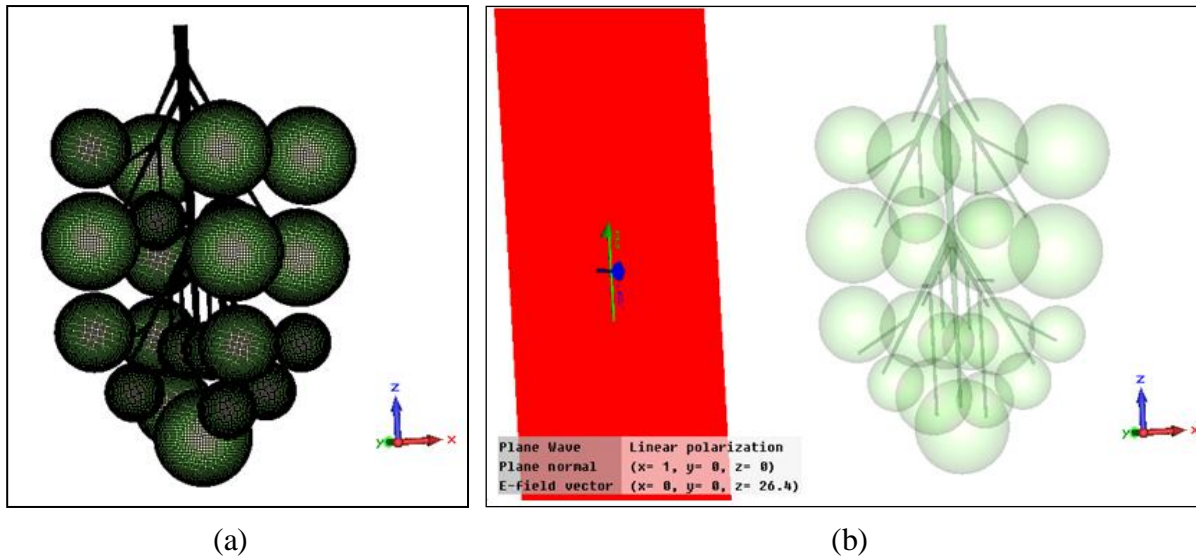


Fig. 4.14: (a) A typical bunch of grapes modeled in CST MWS 2010, (b) The bunch of grapes is exposed to GSM 1842.5 MHz linearly polarized plane wave radiation

#### 4.2.3.5 SAR Results and Discussion

SAR data have been evaluated for the above mentioned bunch of grapes model at 947.5 MHz, 1842.5 MHz and 2450 MHz band as per the revised Indian electromagnetic regulatory guidelines at regions accessible to general public [11]. It is obvious that all measured SAR data have been evaluated in particular at far-field region of the telecom tower antennas considering plane wave incidence – thus, it replicates the real scenario where most of the plants and fruits get exposed to electromagnetic radiation at some distance from the telecom antennas. The maximum permissible electromagnetic field strength increases with frequency of irradiation as indicated in Table 4.15. The bunch of grapes model has been exposed to linearly polarized plane waves for around 100 ns in transient analysis. The peak electric field strengths have been obtained by multiplying  $\sqrt{2}$  to the respective r. m. s. electric field strengths considering sinusoidal variations – as prescribed in the revised Indian public exposure guidelines at all three frequencies [11]. MLP SAR, 1g averaged SAR and 10g averaged SAR data at all three frequencies have been tabulated in Table 4.16 – for the bunch of grapes model illustrated in Fig. 4.14(a). Evaluated SAR (either averaged over point mass or contiguous mass) data have been noted to be quite high at 1842.5 MHz and 2450 MHz (as observed in Table 4.16) while compared to those for 947.5

Table 4.15 Revised Indian electromagnetic regulatory guidelines for public exposure zone

<b>Frequency (MHz)</b>	<b>Equivalent Plane Wave Power Density <math>S_{eq}</math> (W/m<sup>2</sup>)</b>	<b>R. M. S. electric field (V/m)</b>	<b>Peak electric field (V/m)</b>
947.5	0.47	13.31	18.82
1842.5	0.92	18.63	26.35
2450	1.00	19.41	27.46

Table 4.16 SAR data for a typical bunch of grapes model as per the existing Indian electromagnetic regulatory guidelines

<b>Frequency (MHz)</b>	<b>Peak E-field of Plane Wave (V/m)</b>	<b>SAR averaging mass (g)</b>	<b>Simulated Maximum SAR (W/kg)</b>	<b>Whole Body Averaged SAR (W/kg)</b>
947.5	18.82	point	1.520	0.006
"	"	1	0.020	"
"	"	10	0.008	"
1842.5	26.35	point	8.838	0.097
"	"	1	0.440	"
"	"	10	0.143	"
2450	27.46	point	13.61	0.155
"	"	1	0.318	"
"	"	10	0.173	"

MHz. This increment in SAR values takes place due to higher permissible electromagnetic field strength at higher frequency – as visible in Table 4.15 and Table 4.16 [11]. In addition, more numbers of peak electric field hotspots develop within the bunch of grapes model at higher frequencies. It should be noted that SAR values (either averaged over point mass or contiguous mass) in this typical bunch of grapes model are much higher compared to SAR values in a single grape model exposed to similar electromagnetic exposure conditions (as reported earlier). Evaluated SAR values have been noted to be higher in the prototyped bunch of grapes model as

the resultant electric field strength is different than in a single grape model (reported earlier in this chapter). Thus, the shapes of individual grape and overall geometry of the model are two important factors that considerably contribute to SAR data and associated spatial distribution. In addition, measured loss tangent ( $\tan \delta$ ) values of grape samples are slight higher at all three frequencies than the respective values reported earlier in case of single grape model.

The existing Indian electromagnetic exposure regulatory guidelines have been made more stringent than the ICNIRP prescribed electromagnetic exposure guidelines, where it has been instructed to average electromagnetic exposure over 6 minutes of time span [10-11]. However, plane wave gets emitted continuously in far-field region from the wireless communication towers 24×365 hours a year – almost without any break as most TDMA time slots are utilized for voice / data over GSM carriers. Therefore, tabulated SAR data in Table 4.16 would not reduce under any circumstances i.e. averaging over larger time span.

Fig. 4.15(a) demonstrates 1g averaged SAR distribution at 1842.5 MHz on three dimensional surface of the bunch of grapes model; whereas Figs. 4.15(b) and (c) illustrate 1g averaged SAR distributions at 1842.5 MHz on two orthogonal cut-planes in the prototyped bunch of grapes model. It is evident from Figs. 4.15(a), (b) and (c) that the maximum 1g averaged SAR distribution has been noted among those few grapes (in the bunch) on which the plane wave with linear polarization impinges first. This observation indicates that a significant part of electromagnetic energy associated with the plane wave gets absorbed within those few grapes out of the entire model. To support this observation, it should also be noted that the measured permittivity ( $\epsilon'_r$ ) and in particular conductivity ( $\sigma$ ) of grape samples are substantially high compared to several other fruits – as reported earlier; and the same results in huge absorption and energy loss of the plane wave in those grapes through which the plane wave passes first. As observed in Fig. 4.13(b) and Table 4.13, grape samples possess high conductivity ( $\sigma$ ) that results in smaller skin depth and the plane wave loses its maximum energy among the few outer most grapes as observed in Figs. 4.15(a), (b) and (c). Here, it is important to mention that more emphasis has been prioritized on 1g averaged SAR data in the bunch of grapes model – because 1g averaged SAR measurement protocol has been adopted and prescribed in the existing Indian electromagnetic exposure regulatory guidelines [11].

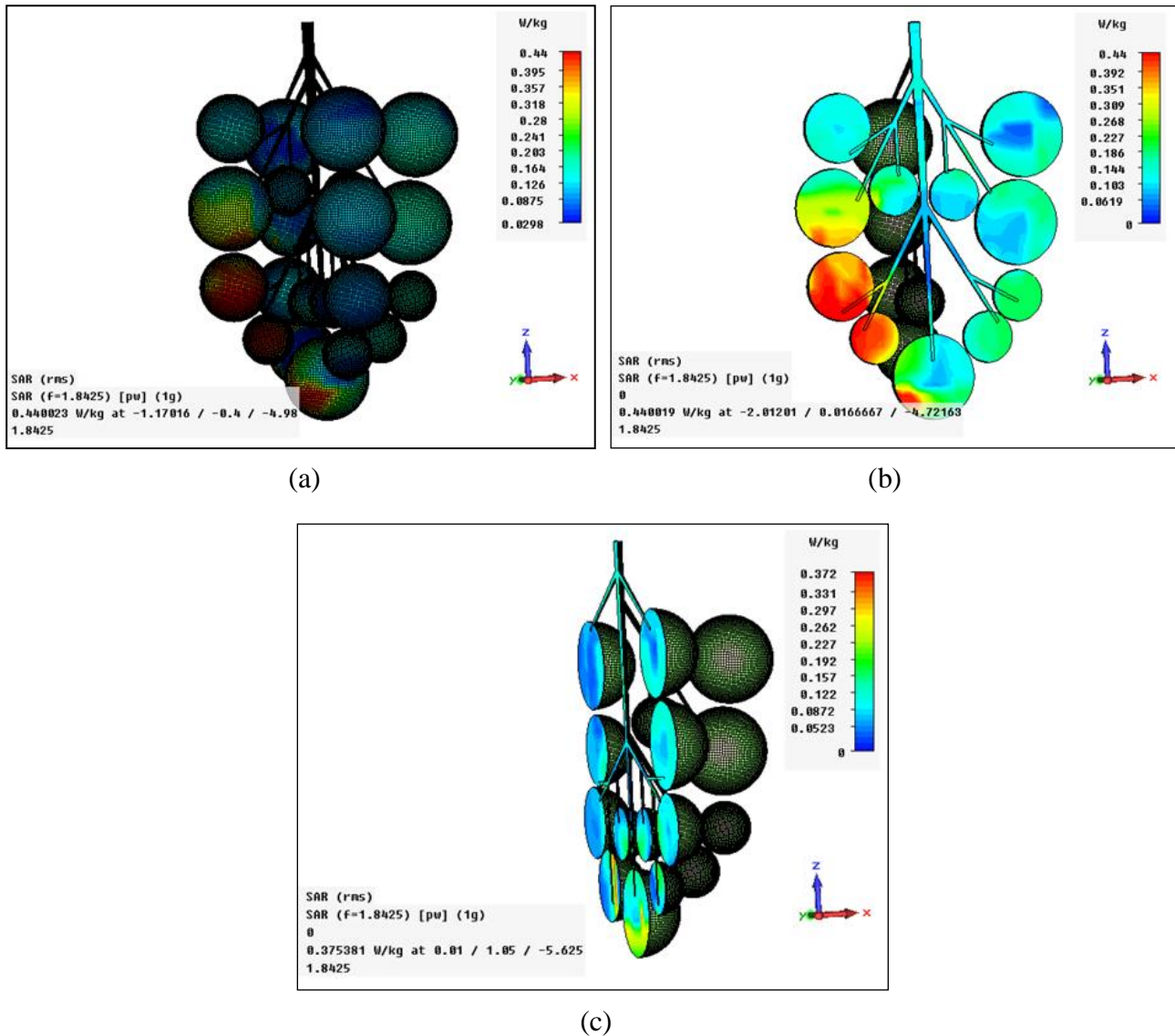


Fig. 4.15: (a) Three dimensional 1g averaged SAR distribution at 1842.5 MHz, (b) Two dimensional 1g averaged SAR distribution on  $x$ - $z$  plane of the prototyped bunch of grapes model at 1842.5 MHz and (c) Two dimensional 1g averaged SAR distribution on  $y$ - $z$  plane of the prototyped bunch of grapes model at 1842.5 MHz

### 4.2.3.6 Conclusions

SAR data have been reported for a typical bunch of grapes model exposed to plane waves with linear polarization in far field region of base station antennas – all SAR simulations have been performed in accordance with the revised Indian public exposure norms [11]. In spite of that, reported SAR values have been noted to be quite alarming; and also, it is obvious that grapes that



grow in controlled electromagnetic exposure zone, i.e. near to the base station antennas, are capable of absorbing much more electromagnetic power even in Indian scenario. ICNIRP and FCC allow much higher electromagnetic field strengths at the mentioned frequencies of interest [9-10]; which can obviously cause more intense electromagnetic energy absorption in the prototyped bunch of grapes model and also in other fruits. However, reported SAR data for the prototyped bunch of grapes model have no relation with the prescribed SAR limits for humans. It is so because human physiological processes are entirely different than plant physiological process, and of course, SAR limits for humans have been prescribed based on immediate thermal effects of electromagnetic radiation on humans only. Therefore, it requires further biological, biochemical and biophysical analyses to comment on potential effects of electromagnetic energy absorption in the bunch of grapes along with its retained food values.

### **4.3 Contrast in SAR Data for Fruit and Plant Specimens – due to Discrepancy among Electromagnetic Regulatory Guidelines**

Seamless connectivity requirements initiated hard challenges for the telecom service providers, who in turn – have exhaustively used up the available bandwidths, leading to continuous electromagnetic emission in nature. As discussed earlier, electromagnetic energy emitted from the cell tower antennas, gets absorbed in biological masses (be it humans or plants) due to reasonably high dielectric properties ( $\epsilon_r$ ) of living tissues [32-39, 63-66]. In this connection, adequate literature is available regarding the electromagnetic energy deposition i.e. SAR estimation in humans [19-31] – moreover, some recent work on plants and fruits have also been reported in this chapter. To gauge and check the maximum permissible SAR limits for humans, several electromagnetic regulatory guidelines are in effect across the globe [9-12]. In addition to the basic SAR limits (for humans), frequency dependent reference electromagnetic field strengths for far field exposures have also been capped at different levels depending upon the regulatory standards in effect, for the concerned geographical regions [9-16]. These guidelines have been prescribed by international electromagnetic exposure regulatory organizations such as FCC, ICNIRP etc. [9-10] – in addition, there are a number of stringent nationalized electromagnetic exposure regulatory guidelines like in India, Switzerland etc. along with few other countries [11-16]. However, no such electromagnetic exposure regulatory guidelines have been adopted for plants, crops or fruits, which too, are at the same time getting exposed to

electromagnetic radiation in a continuous manner throughout their lifespan. On the other hand, significant amount of disparity exists among these different existing electromagnetic exposure regulatory guidelines, in terms of the reference electromagnetic power density levels and the variation lies in the order of as high as ten to hundred folds among the standards [9-16]. As discussed earlier – SAR value extensively depends upon the strength of incident electromagnetic field, in addition to wave polarization, angle of incidence, material properties and geometrical shapes of biological objects. Therefore, the existing disparity among different electromagnetic exposure regulatory standards plays an important role in determining the electromagnetic energy deposition rates, in terms of SAR values of the objects concerned.

Thus, in this section, the contrast in SAR data along with associated spatial distributions in one composite fruits model and a typical plant model have been reported due to existing wide discrepancies among different global and national electromagnetic regulatory standards [9-12].

### **4.3.1 Contrast in SAR Data for a Bunch of Sapodilla Fruits Model**

#### **4.3.1.1 Introduction**

Quantitative estimation of electromagnetic energy absorption rate in composite bunch of fruits structure is less frequently reported. In general, different fruits and plants are of different geometrical shapes and they possess dissimilar dielectric properties ( $\epsilon_r$ ). Consequently, one unique prototype model is neither sufficient nor exhaustive, to conceive the problem and to investigate the phenomenon of electromagnetic energy absorption in fruits and plants respectively. SAR investigations in single fruit models, bunch of fruits model and multilayer fruit model have been reported earlier in this chapter. However, no comparative SAR investigation has been performed in any fruit model based on the existing disparities among different electromagnetic standards [9-12]. Therefore, estimation of SAR levels in a typical bunch of sapodilla fruits model has been presented in this particular work. A detailed discussion on their variations, due to the existing disparity among different international and national electromagnetic regulatory standards has been presented in a quantitative manner [9-12]. The work includes dielectric properties ( $\epsilon_r$ ) characterization of the sapodilla fruit specimen and the modeling of a typical bunch of fruits according to their dielectric properties ( $\epsilon_r$ ) for the simulation-based investigations in order to gauge the SAR levels based on the electromagnetic

exposure standards. A typical geometric shape of the bunch of sapodilla fruits, modeled under the most practical considerations – has also been taken, in order to replicate the exact natural scenario, where the fruits or the other plant tissues are irradiated with electromagnetic exposures from the mobile towers and other electromagnetic energy sources. The variations in the estimated SAR levels calculated under different electromagnetic regulatory standards prescribed globally have been seen to be substantial and the records have been presented in detail herein [9-12]. Rigorous simulation works have been carried out, to ensure accurate comparison between the estimated SAR levels. Two global and two national electromagnetic standards have been taken for the comparisons; both occupational and public exposure standards have been considered [9-12]. Five different frequencies of mobile operations have also been considered as possible electromagnetic exposure sources in this work for the investigations. The variation existing between the estimated SAR levels based on the different electromagnetic standards at each of the frequencies – suggests a critical evaluation of the status quo and calls for the need of maintaining a global homogeneity among the existing electromagnetic exposure regulations considering the effects on plants, fruits and crops.

#### **4.3.1.2 Disparity among Different Electromagnetic Standards**

It is already known that electromagnetic energy absorption rate at a particular point inside biological mass is quantified as  $SAR = \sigma|E|^2/2\rho$ ; where  $\sigma$  is electrical conductivity of biological tissue,  $E$  is peak electric field strength developed inside biological tissue and  $\rho$  is material density of biological tissue. Moreover, 1g averaged SAR, 10g averaged SAR and WBA SAR data are basically averages of local point SAR data over respective contiguous tissue masses [17]. Thus, it is clear that point SAR varies with the squared magnitude of internally developed electric field strength – furthermore, the internal electric field strength magnitude develops in direct proportion with the incident electric field strength on the biological object. Hence, disparity among different international and national electromagnetic regulatory standards plays an important role while investigating SAR magnitudes in a specific biological object at a particular frequency of interest. International electromagnetic standards prescribed by the organizations like FCC, ICNIRP etc. have been adopted over a considerable part of the world to defend against possible health risks [9-10]. But, reference power density levels (below 2000 MHz) for public exposure prescribed by these organizations don't precisely agree with each

Table 4.17 Disparity among different global and national electromagnetic exposure regulatory guidelines [9-12]

Frequency of exposure (MHz)	Prescribed power density level (W/m <sup>2</sup> )					
	Occupational Zone		Public Zone			
	FCC	ICNIRP	FCC	ICNIRP	India	Swiss
947.5	31.58	23.69	6.32	4.74	0.47	0.047
1842.5	50	46.06	10	9.21	0.92	0.092
2150	50	50	10	10	1	0.1
2350	50	50	10	10	1	0.1
2450	50	50	10	10	1	0.1

Table 4.18 Measured material density ( $\rho$ ) of sapodilla fruit, leaf and twig samples

Name of sample	Sapodilla	Leaf	Twig
Material density (kg/m <sup>3</sup> )	1107.8	833.3	1107.8

other. Research outcomes on electromagnetic energy absorption rate in human phantoms along with consequent biological responses have raised concerns among the scientists and general public as well [19-31, 67-73]. In response, competent authorities in nations like India, Switzerland etc. have prescribed stricter national electromagnetic standards [11-12]. However, these global and national electromagnetic regulatory standards are not at par in terms of prescribed reference power density levels – with variations ranging from ten to hundred folds. A comparative overview of these different international and national electromagnetic regulatory guidelines has been tabulated in Table 4.17 [9-12].

### 4.3.1.3 Material Density and Dielectric Properties Characterization

Adequate number of fresh sapodilla fruit samples along with connected leaves has been taken to laboratory for material density measurement and dielectric properties ( $\epsilon_r$ ) characterization. Thereafter, half of the samples have been taken for material density measurement and rest have been utilized in dielectric properties ( $\epsilon_r$ ) characterization.

#### A. Material Density Characterization

For material density characterization, individual mass of sapodilla fruit, leaf and twig specimens has been weighed using a balance. Volume of individual specimen has also been measured.

Thereafter, material densities of sapodilla fruit, leaf and twig specimens have been calculated. Obtained data have been averaged over similar specimens and illustrated in Table 4.18.

### ***B. Dielectric Properties Characterization***

Broadband dielectric properties i.e. real part of complex permittivity ( $\epsilon_r'$ ) and loss tangent ( $\tan \delta$ ) data for sapodilla fruit, leaf and twig specimens have been characterized using 85070E open ended coaxial probe dielectric measurement kit (Agilent Technologies) along with E5071B ENA series VNA (Agilent Technologies). A detailed analysis of this well established non-destructive dielectric properties characterization technique has been outlined in the previous chapter [52-62]. This particular coaxial probe is capable of characterizing permittivity ( $\epsilon_r'$ ) and electrical conductivity ( $\sigma$ ) up to 20 GHz and can also withstand up to 200 °C temperatures. But, the combined measurement set up illustrated in Fig. 4.16(a) is capable of characterizing dielectric properties ( $\epsilon_r$ ) up to 8.5 GHz only – due to frequency limitation of the E5071B VNA. All dielectric properties ( $\epsilon_r$ ) characterizations have been performed at 25 °C ambient temperature. Figs. 4.16(a), (b) and (c) illustrate the actual dielectric properties ( $\epsilon_r$ ) measurement set up for sapodilla fruit and leaf specimens. During dielectric properties ( $\epsilon_r$ ) characterization, adequate numbers of sapodilla leaves have been stacked to ensure negligible contribution from the base material beneath stacked leaves on measured reflection coefficient data at open ended coaxial probe interface. Thickness of stacked sapodilla leaves has been ensured to be more than twice the skin depth to ascertain accurate dielectric properties ( $\epsilon_r$ ) characterization. Dielectric properties ( $\epsilon_r$ ) of sapodilla twig couldn't be characterized separately due to small radial dimension of the twigs compared to diameter of the open ended coaxial probe (2 cm) – thus, the twig has been considered to possess similar dielectric properties to that of sapodilla leaves. Measured dielectric properties ( $\epsilon_r$ ) of sapodilla fruit, leaf and twig (considered) samples have been tabulated in Table 4.19.

#### **4.3.1.4 A Bunch of Sapodilla Fruits Modeling in CST MWS 2014**

A typical three dimensional bunch of sapodilla fruits model along with a leaf structure has been prototyped in CST MWS 2014 [49]. The bunch containing three fruits was weighing 121.16 g and occupying a volume of 109.58 cm<sup>3</sup>. Three sapodilla fruit specimens have been designed as spheres of different radial dimensions. A typical medium sized leaf structure has been first

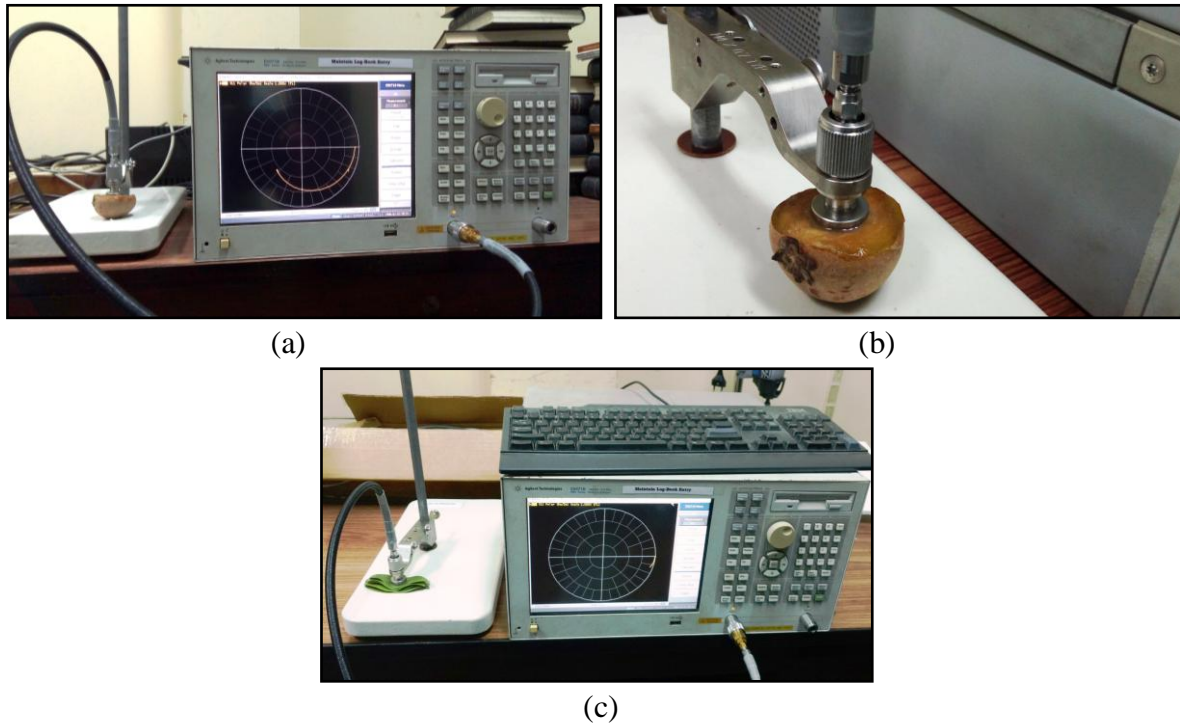


Fig. 4.16: Broadband permittivity and loss tangent measurement setup using Agilent 85070E dielectric measurement kit and E5071B ENA series Vector Network Analyzer (VNA) (a) sapodilla fruit, (b) enlarged view of open ended coaxial probe on flat cut surface of sapodilla fruit and (c) sapodilla leaves

Table 4.19 Measured permittivity and loss tangent of sapodilla fruit, leaf and twig samples

Sample	947.50 MHz		1842.50 MHz		2150 MHz		2350 MHz		2450 MHz	
	$\epsilon'_r$	$\tan \delta$	$\epsilon'_r$	$\tan \delta$	$\epsilon'_r$	$\tan \delta$	$\epsilon'_r$	$\tan \delta$	$\epsilon'_r$	$\tan \delta$
<b>Fruit</b>	66.08	0.222	64.33	0.217	63.30	0.237	62.67	0.239	62.90	0.248
<b>Leaf</b>	33.21	0.438	30.33	0.358	29.72	0.348	29.26	0.358	29.32	0.350
<b>Twig</b>	33.21	0.438	30.33	0.358	29.72	0.348	29.26	0.358	29.32	0.350

outlined on graph paper – then two dimensional coordinates have been imported and extruded to replicate the three dimensional leaf structure with specified thickness. The finalized three dimensional bunch of sapodilla fruits model has been illustrated in Fig. 4.17. In addition, exact geometrical specifications of the prototyped model have been listed in Table 4.20.

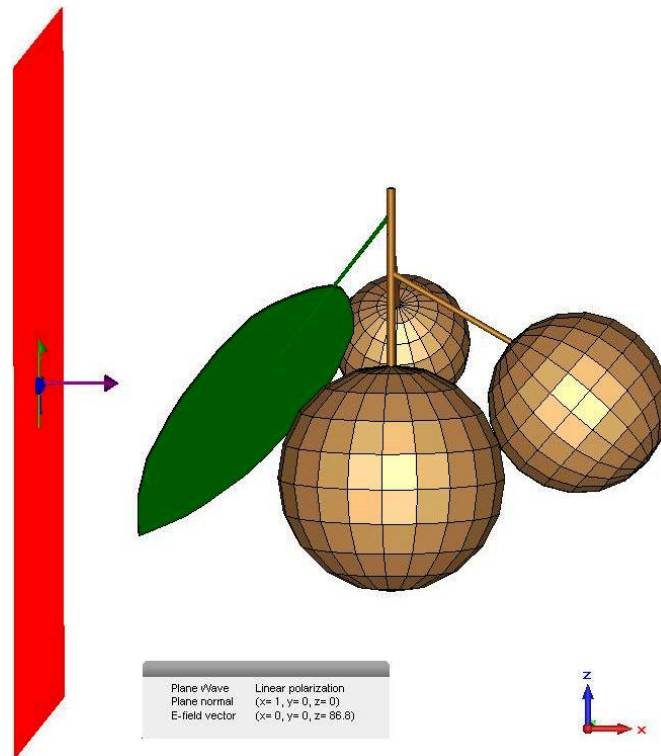


Fig. 4.17: Three dimensional CAD model of the bunch of sapodilla fruits with linearly polarized plane wave at 1842.50 MHz in accordance with FCC public exposure scenario

#### 4.3.1.5 SAR Simulation Setup

The designed bunch of sapodilla fruits model has been irradiated with plane waves as per the contrasting international and national electromagnetic regulatory standards. Linearly polarized plane waves with different electric field strengths, depending upon the frequency of exposure and regulatory standards in effect, have been used as far-field radiation sources. CST MWS 2014 electromagnetic simulator takes into account peak electric field strength as an input for linearly polarized plane wave set up [49]. Hence, prescribed unperturbed r. m. s. electric field strength has been multiplied each time by  $\sqrt{2}$  to obtain the peak electric field strength (considering sinusoidal variation) [9-12]. The transient / time-domain solver available in CST MWS 2014 has been utilized to estimate the SAR values for the prototyped bunch of sapodilla fruits model [49-51]. Total number of mesh cells in the above mentioned prototyped specimen is about 0.25 million in number with an average mesh cell size of 0.004 g. Four PMLs with  $10^{-4}$  reflection

Table 4.20 Modeling specifications of the bunch of sapodilla fruits model

<b>Fruit Sample Specifications</b>				
Sapodilla fruit	Shape	Radius (mm)		
Large	spherical	25		
Medium	spherical	20		
Small	spherical	15		
<b>Leaf Sample Specifications</b>				
Leaf	Shape	Length (mm)	Width (mm)	Thickness (mm)
Leaf blade	Thin planner	80	30	0.5
<b>Twig Sample Specifications</b>				
Twig	Shape	Length (mm)	Radius (mm)	
Primary twig connected to large fruit	cylindrical	40	1	
Secondary twig connected to medium fruit	cylindrical	30	0.7	
Secondary twig connected to small fruit	cylindrical	25	0.7	
Secondary twig connected to leaf blade	cylindrical	20	0.5	

coefficient have been used as electromagnetic absorbing boundaries during simulation. Distance between the bunch of sapodilla fruits and the boundary wall has been kept negligible by choosing appropriate boundary conditions. MLP SAR, 1g averaged SAR, 10g averaged SAR and WBA SAR data have been compared in accordance with the above mentioned electromagnetic exposure regulatory standards [9-12]. SAR data (except point SAR data that don't require averaging) have been averaged using three standard protocols, viz. IEEE C95.3 [74], CST C95.3 [49] and the most recent IEEE/IEC 62704-1 [17] SAR averaging techniques. However, insignificant variations have been noted among the obtained datasets while three different SAR averaging protocols have been adopted. Hence, all SAR data have been reported adopting the most recent IEEE/IEC 62704-1 SAR averaging protocol only [17].



### 4.3.1.6 Comparative SAR Data and Analysis

#### A. SAR Simulation Results

SAR data have been simulated mimicking international occupational as well as public exposure scenarios [9-10]. Moreover, SAR simulations have also been performed in accordance with selected nationalized public exposure scenarios in countries like India and Switzerland [11-12]. SAR data have been estimated at 947.5 MHz, 1842.5 MHz, 2150 MHz, 2350 MHz and 2450 MHz. Earlier, Fig. 4.17 illustrated a typical linearly polarized plane wave impinging on the bunch of sapodilla fruits model at 1842.5 MHz as per FCC public exposure standards [9]. Consequent MLP SAR and 1g averaged SAR distributions have been illustrated in Figs. 4.18(a) and (b) respectively [9]. The contrasts obtained in the comparative SAR datasets for the bunch of sapodilla fruits model at five different frequency bands have been summarized over Table 4.21 to Table 4.25 in sequence with the illustrations in Figs. 4.19(a) to (e). Fig. 4.19(f) depicts the contrast in cumulative SAR data over all the five frequencies for the above mentioned bunch of sapodilla fruits model.

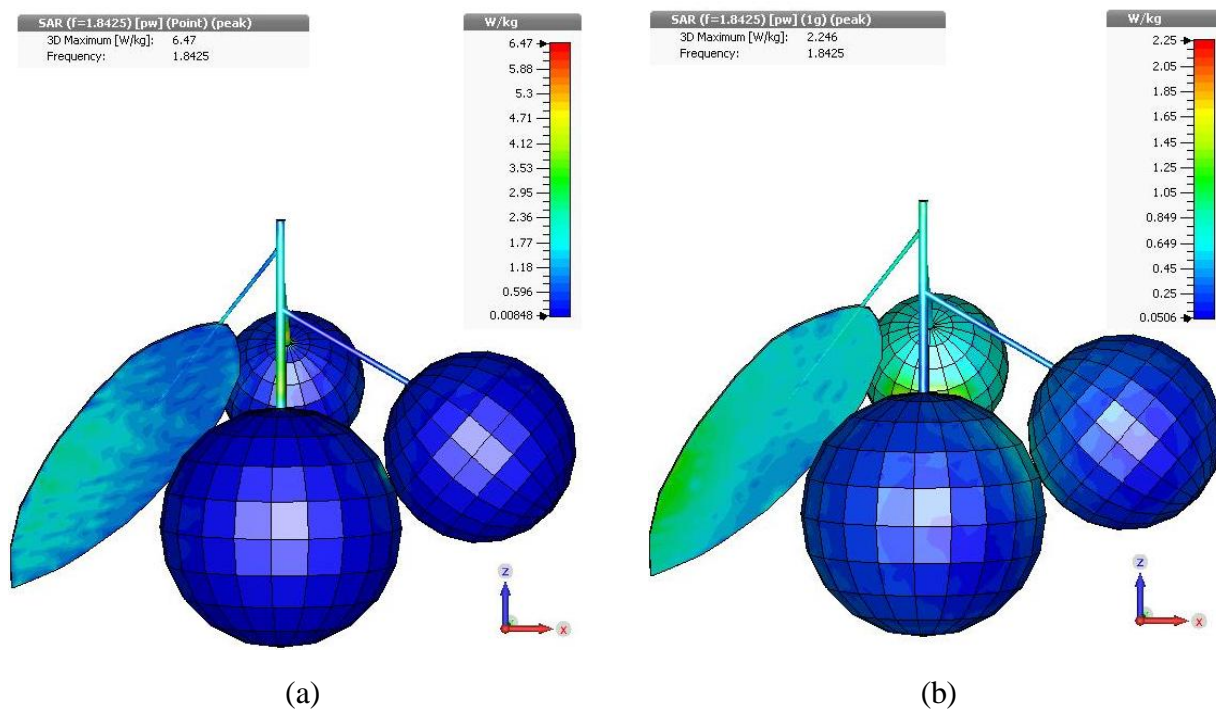


Fig. 4.18: (a) Simulated point SAR profile on surface of sapodilla bunch at 1842.50 MHz in accordance with FCC public exposure scenario and (b) Simulated 1g averaged SAR profile on surface of sapodilla bunch at 1842.50 MHz in accordance with FCC public exposure scenario

Table 4.21 Disparity among SAR data for bunch of sapodilla model at 947.5 MHz as per different global and national electromagnetic standards

Frequency 947.5 MHz						
Exposure Zone	Occupational			Public		
Guidelines	FCC	ICNIRP	FCC	ICNIRP	India	Swiss
<b>Power density (W/m<sup>2</sup>)</b>	31.58	23.69	6.32	4.74	0.47	0.047
<b>Equivalent peak electric field (V/m)</b>	154.3	133.6	69.02	59.77	18.82	5.95
<b>MLP SAR</b>	29.82	22.45	5.96	4.49	0.45	0.045
<b>1g SAR</b>	4.92	3.67	0.98	0.73	0.07	0.007
<b>10g SAR</b>	2.79	2.11	0.56	0.42	0.04	0.004
<b>WBA SAR</b>	1.44	1.08	0.29	0.22	0.02	0.002

SAR is in W/kg

Table 4.22 Disparity among SAR data for bunch of sapodilla model at 1842.5 MHz as per different global and national electromagnetic standards

Frequency 1842.5 MHz						
Exposure Zone	Occupational			Public		
Guidelines	FCC	ICNIRP	FCC	ICNIRP	India	Swiss
<b>Power density (W/m<sup>2</sup>)</b>	50	46.06	10	9.21	0.92	0.092
<b>Equivalent peak electric field (V/m)</b>	194.14	186.33	86.82	83.33	26.35	8.33
<b>MLP SAR</b>	32.35	29.80	6.47	5.96	0.60	0.060
<b>1g SAR</b>	11.23	10.35	2.25	2.07	0.21	0.021
<b>10g SAR</b>	4.60	4.23	0.92	0.85	0.08	0.008
<b>WBA SAR</b>	2.06	1.90	0.41	0.38	0.04	0.004

SAR is in W/kg

Table 4.23 Disparity among SAR data for bunch of sapodilla model at 2150 MHz as per different global and national electromagnetic standards

Frequency 2150 MHz						
Exposure Zone	Occupational		Public			
Guidelines	FCC	ICNIRP	FCC	ICNIRP	India	Swiss
Power density ( $W/m^2$ )	50	50	10	10	1	0.1
Equivalent peak electric field (V/m)	194.14	194.14	86.82	86.82	27.45	8.68
MLP SAR	39.91	39.91	7.98	7.98	0.80	0.08
1g SAR	10.50	10.50	2.10	2.10	0.21	0.021
10g SAR	4.78	4.78	0.96	0.96	0.10	0.01
WBA SAR	2.07	2.07	0.41	0.41	0.04	0.004

SAR is in W/kg

Table 4.24 Disparity among SAR data for bunch of sapodilla model at 2350 MHz as per different global and national electromagnetic standards

Frequency 2350 MHz						
Exposure Zone	Occupational		Public			
Guidelines	FCC	ICNIRP	FCC	ICNIRP	India	Swiss
Power density ( $W/m^2$ )	50	50	10	10	1	0.1
Equivalent peak electric field (V/m)	194.14	194.14	86.82	86.82	27.45	8.68
MLP SAR	35.85	35.85	7.17	7.17	0.72	0.072
1g SAR	10.34	10.34	2.07	2.07	0.21	0.021
10g SAR	4.70	4.70	0.94	0.94	0.09	0.009
WBA SAR	1.99	1.99	0.40	0.40	0.04	0.004

SAR is in W/kg

Table 4.25 Disparity among SAR data for bunch of sapodilla model at 2450 MHz as per different global and national electromagnetic standards

Frequency 2450 MHz						
Exposure Zone	Occupational		Public			
Guidelines	FCC	ICNIRP	FCC	ICNIRP	India	Swiss
Power density ( $\text{W}/\text{m}^2$ )	50	50	10	10	1	0.1
Equivalent peak electric field (V/m)	194.14	194.14	86.82	86.82	27.45	8.68
MLP SAR	38.91	38.91	7.78	7.78	0.78	0.078
1g SAR	11.46	11.46	2.29	2.29	0.23	0.023
10g SAR	4.63	4.63	0.93	0.93	0.09	0.009
WBA SAR	1.96	1.96	0.39	0.39	0.04	0.004

SAR is in W/kg

## B. Result Analysis

It is observed in Figs. 4.18(a) and (b) that SAR distribution increases near the surface with sharp geometries i.e. a surface with higher curvature or smaller radius. Charge density at the locations of greater surface curvature tends to be greater in magnitude. This could also be proved by solving the Poisson's equation on and around the surface of arbitrary shapes [75]. Local electric field due to such non uniform charge densities tends to follow a similar pattern i.e. the electric field near a location with greater charge density is also greater in magnitude [76]. The phenomenon of increased electric field concentration near the sharp edges is not limited to conducting bodies alone [77]. Even in case of a dielectric body with finite conductivity ( $\sigma$ ), similar principle applies. Solution of the scattering problem depicted by the scattering of incident electromagnetic field by the said dielectric object eventually leads to an electric field distribution (or an equivalent induced surface current density) that prefers the sharp edges i.e. the magnitude of the distribution is greater near the regions of greater surface curvature.

Reported data reveal that the SAR value in general increases with frequency of exposure in accordance with any particular electromagnetic regulatory standards [9-12]. It is so because of the following reasons. First of all, the permissible electromagnetic field strength increases with

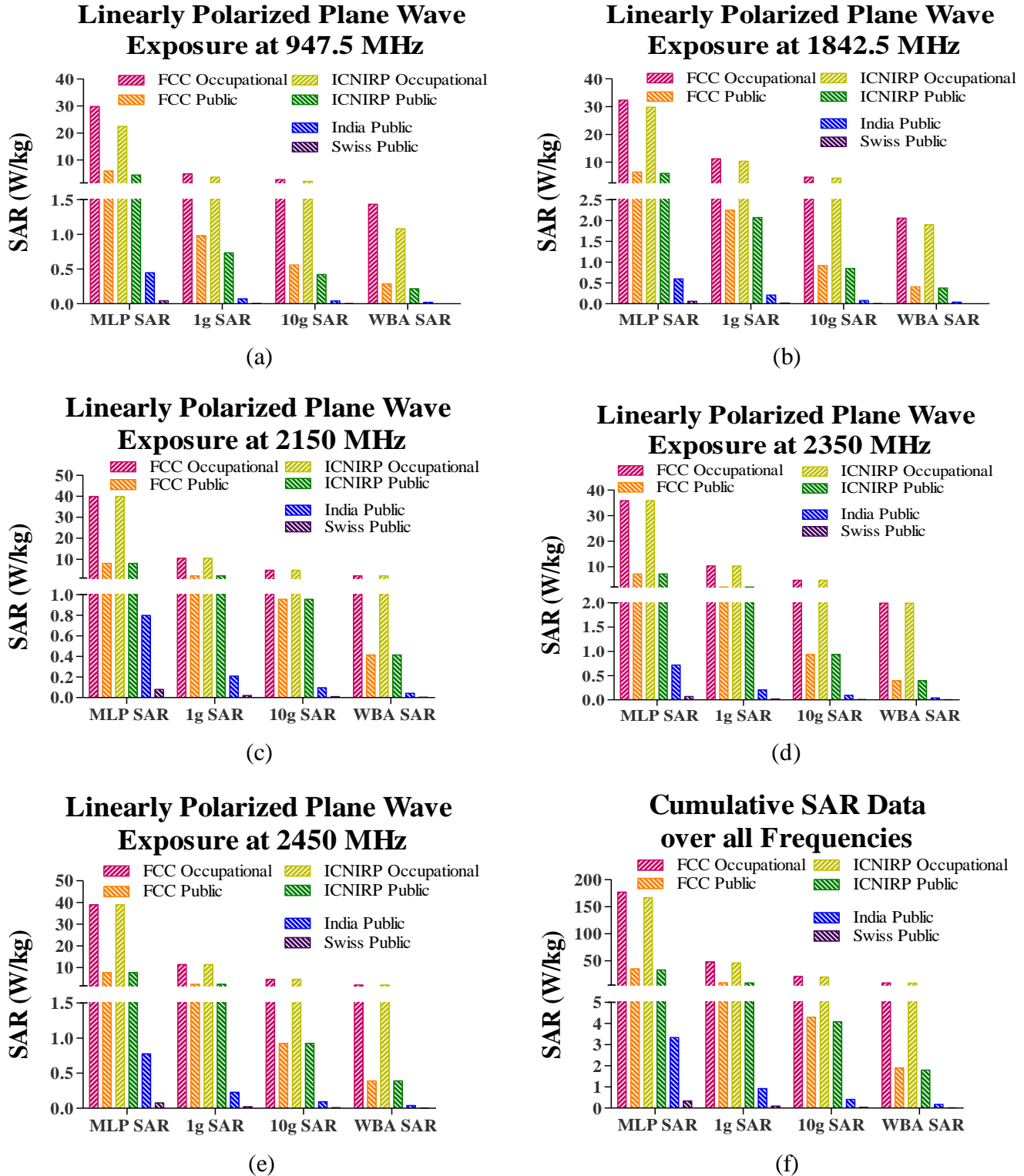


Fig. 4.19: Disparity among SAR data for the bunch of sapodilla model due to variation among different electromagnetic regulatory guidelines (a) 947.5 MHz, (b) 1842.5 MHz, (c) 2150 MHz, (d) 2350 MHz, (e) 2450 MHz and (f) cumulative SAR data over all five frequencies

frequency of exposure up to 2000 MHz in most cases (exception: 1500 MHz in case of the FCC electromagnetic standards) and as a consequence of the same, electric field values inside the bunch of sapodilla model also increase along with the resultant SAR values. Hence, a prominent increment in SAR data has been observed in between 947.5 MHz to 1842.5 MHz. Moreover, the operating wavelength inside the bunch of sapodilla fruits model shortens with an increase in frequency – resulting in more number of hotspots with intense electric field strengths contributing to increased SAR value. In addition, dielectric properties ( $\epsilon_r$ ) of the sapodilla fruit, leaf and twig change with frequency i.e. permittivity ( $\epsilon_r'$ ) to some extent reduces with frequency but loss tangent ( $\tan \delta$ ) increases to a greater extent with frequency above a crucial point in between 1500 MHz to 2500 MHz for plant tissues in general. As a consequence, SAR value also increases with frequency because of the direct and greater dependence of itself on tissue conductivity ( $\sigma$ ) / loss tangent ( $\tan \delta$ ) value. Reported SAR data (be it MLP SAR, 1g SAR, 10g SAR or WBA SAR) are absolutely justified in terms of averaging duration (six or thirty minutes for public exposure [9-12]) – because, plants and fruits are stationary in nature and get exposed to electromagnetic energy throughout their lifespan.

Looking from a different aspect, contrasting SAR data have been noted even at a particular frequency because of disparity among the different electromagnetic standards [9-12] (refer to Table 4.21 to Table 4.25 along with Figs. 4.19(a) to (e)). It should be noted that two reported occupational electromagnetic standards differ by a slight margin below 2000 MHz and match exactly beyond. Both FCC as well as ICNIRP have set down the occupational electromagnetic standards, five folds tolerant compared to the respective public electromagnetic standards [9-10]. SAR ( $= \sigma |E|^2 / 2\rho$ ), being directly dependent upon the square of internal electric field strength magnitude developed inside biological medium i.e. bunch of sapodilla fruits model in this case, varies with the square of incident electric field magnitude / directly with power density of plane wave depending upon electromagnetic standards in effect. In the results, SAR values for the bunch of sapodilla fruits model in the occupational exposure zone are too high in accordance with either FCC or ICNIRP occupational exposure standards. From Table 4.21 and Table 4.22, it is observed that power density levels prescribed in FCC occupational standards (compared to ICNIRP) are 33 percent and 8.5 percent higher at 947.5 MHz and 1842.5 MHz correspondingly. As a consequence, SAR datasets as per FCC standards also differ by respective factors compared to ICNIRP standards; it is so because both incident power density and resultant SAR datasets are

related to the second order of electric field strength magnitude at their respective points of observation. Even in case of public exposure, FCC and ICNIRP prescribed power density levels differ by same folds at 947.5 MHz and 1842.5 MHz along with the resultant SAR values (refer to Table 4.21 and Table 4.22 along with Figs. 4.19(a) and (b) in order). Nationalized public electromagnetic standards in India and Switzerland are ten to hundred folds stricter compared to the global electromagnetic standards [11-12]. As a consequence, SAR values in India and Switzerland are respectively ten to hundred folds lower compared to international standards for public exposure (illustrated in Table 4.21 to Table 4.25). Figs. 4.19(a) to (e) summarize the significant contrast in MLP SAR, 1g SAR, 10g SAR and WBA SAR values as per different electromagnetic standards over 947.5 MHz to 2450 MHz respectively. SAR values are significantly high where FCC or ICNIRP guidelines are in effect; SAR values are moderate in Indian public exposure scenario but strictly less in Swiss public electromagnetic exposure scenario. However, it must be noted that the safe SAR limit for representative sapodilla plant or any other plant is yet unknown. Moreover, simultaneous wireless communications over different frequency bands result in cumulative SAR effects i.e. electromagnetic energy absorption in biological tissue adds up over multiple frequencies of wireless communication as illustrated in Fig. 4.19(f). Cumulative SAR data for the bunch of sapodilla fruits model over all five frequency bands indicate significant disparity among the different global and nationalized electromagnetic standards and seek immediate attention for uniform electromagnetic standards across the globe.

### 4.3.1.7 Conclusions

SAR data for the prototyped bunch of sapodilla fruits model (at a particular frequency) is predominantly dependent on the reference power density prescribed in the electromagnetic regulatory standards in effect. SAR datasets in the occupational zone are quite noticeable as FCC and ICNIRP declare occupational premises based on restricted accessibility to public but not based on the presence of plants [9-10]. Even more, SAR data at public premises have been noted to be varying by ten to hundred folds depending upon the electromagnetic regulatory standards in effect [9-12]. SAR data according to the existing Indian standards have been found to be moderate whereas the same is significantly less in Swiss territory. On contrary, corresponding SAR data in accordance with the global public electromagnetic regulatory standards (i.e. FCC and ICNIRP) are quite high and need to be considered with utmost care. Noted disparity among

the SAR datasets in accordance with the different electromagnetic regulatory guidelines is no different for other biological objects including plants.

Reported SAR data have been recorded due to linearly polarized plane wave (direction of propagation along  $x$ -axis and electric field along  $z$ -axis as illustrated in Fig. 4.17) that impinges from a specific side of the bunch of sapodilla fruits model. It must be noted that the prototyped bunch of sapodilla fruits model is asymmetrical in nature and SAR is highly dependent on geometrical shape of the biological object along with direction and polarization of incident wave. Therefore, absolute value of SAR data can differ for different combinations of plane wave incidence and polarization; however, ratio of SAR values due to the disparity among the different global and nationalized electromagnetic exposure regulatory protocols will remain the same in those cases.

At present, simulated SAR data have been reported and couldn't be extended to practical measurements due to the following reasons. Sapodilla leaf and twig are very thin and precise electric field measurement inside phantom model is difficult due to significant field perturbation using near field probe. In addition, customized non-standard sapodilla phantom model needs to be imported and same would be quite cost involving. Hence, simulated SAR data can be considered for the time being and can be backed by practical measurements in future.

Absence of global or local SAR limit for plants makes the situation complicated to scientifically consider an exposure scenario suitable for sustainable plant growth. Therefore, the biological effects of electromagnetic radiation should be studied over a number of plants and fruits [40-48]. These investigations can further lead to a subsequent uniform electromagnetic standards implementation worldwide along with the explicit SAR limit prescription for plants and the other biological masses concerned.

## **4.3.2 Contrast in SAR Data for a Typical Plant Model**

### **4.3.2.1 Introduction**

Different international and national electromagnetic exposure regulatory standards have been developed based upon significantly diversified premises, developmental backgrounds (such as technical specifications, medical practices etc.) and objectives to safeguard life [9-16]. Some electromagnetic regulatory standards have been developed based on assessing thermal effects of



electromagnetic radiation over short time span, some other standards aim at mitigating non-thermal effects over prolonged exposure duration, whereas the rest are prescribed to take adequate precautions against yet unknown health effects [16]. However, each standard is consistent with the policy promoted by the respective regulatory organization. To name a few organizations who have prescribed global electromagnetic exposure standards, FCC and ICNIRP secure the top ranks in the list [9-10]. In contrast, India, Switzerland, Russia and Italy etc. are among the selected countries to enforce stricter national electromagnetic regulatory standards [11-15]. National electromagnetic exposure regulatory guidelines have been made stricter to address possible health concerns raised by researchers and awareness among common people in selected countries – stricter national protocols have been adopted either based on scientific information or as precautionary measure [16]. However, as discussed earlier in this chapter, there is lack of uniformity among the different global and national electromagnetic exposure standards resulting in ten to hundred fold variations in plane wave equivalent reference power density levels across countries over several telecommunication bands. Let us consider 1842.5 MHz (center frequency of 1805-1880 MHz GSM downlink band) for an example. The plane wave equivalent reference power density levels adopted by FCC, ICNIRP, India and Switzerland are  $10 \text{ W/m}^2$ ,  $9.21 \text{ W/m}^2$ ,  $0.92 \text{ W/m}^2$  and  $0.092 \text{ W/m}^2$  respectively [9-12]. As a consequence, living objects i.e. humans, animals as well as plants are expected to absorb significantly different amount of electromagnetic energy due to mobile tower emitted uninterrupted pulsed microwave radiation depending upon the regulatory standards in effect. Stringent public exposure scenarios in countries like Russia, Italy etc. (fixed at  $0.10 \text{ W/m}^2$  from  $\leq 300 \text{ MHz}$  to  $300 \text{ GHz}$ ) are also at comparable scale to that of Swiss public standard [12-16]. In this connection, it should also be noted that SAR at a point is defined as  $\sigma|E|^2/2\rho$ ; where,  $\sigma$ ,  $E$  and  $\rho$  represent the respective parameters as discussed earlier. For uninterrupted pulsed microwave incidence on biological object, equivalent continuous wave electric field strength can be derived from the duty cycle of the pulse train. Thereafter,  $|E|$  at the point of interest inside biological tissue can be evaluated further to calculate point SAR value.

As reported in Chapter 3, plants, vegetables and fruits also possess dielectric properties ( $\epsilon_r$ ) that indicate a consistent absorption of the RF energy in wireless communication bands. The open ended coaxial probe technique has been primarily reported for dielectric properties ( $\epsilon_r$ ) characterization of different fruit, vegetable and plant samples [32-39]. In recent times, SAR data

have been reported for different fruit models following different electromagnetic exposure standards – as reported earlier in this chapter. However, in spite of lossy dielectric nature of plant tissues, SAR data and its surface distribution for a complete plant model have neither been reported in literature nor been considered while preparing safety standards.

Combining these aspects together, this work aims at highlighting the wide discrepancies among different global and national electromagnetic regulatory standards, characterizing dielectric properties ( $\epsilon_r$ ) of plant samples, investigating SAR distribution in a typical plant model (containing leaves, flower and stem) for plane wave incidence along with analyzing the contrast in SAR data due to discrepancy among different global and national electromagnetic standards over a number of frequency bands [9-12]. To this end, *Catharanthus roseus* plant containing green leaves, green stem and pink flower has been chosen as prototype. Dielectric properties ( $\epsilon_r$ ) of fresh leaf, flower and stem samples have been characterized using open ended coaxial probe technique [32-39]. Next, a typical three dimensional *Catharanthus roseus* plant model has been developed – typical geometric shape of the plant prototype has been modeled considering the most practical scenario. Detailed analyses on variation of SAR levels due to wide discrepancy among the existing electromagnetic regulatory standards have been reported in a quantitative manner. SAR levels have been reported at five different telecommunication bands as per two occupational and four public exposure scenarios. SAR data have been simulated as per established electromagnetic regulatory standards prescribed by ICNIRP (international), FCC (international), India (national) and Switzerland (national) [9-12]. Next, simulated SAR data have been compared at mid frequencies of multiple communication bands like 947.5 MHz (935-960 MHz downlink band), 1842.5 MHz (1805-1880 MHz downlink band), 2150 MHz (2120-2170 MHz downlink band), 2350 MHz (2300-2400 MHz band) and 2450 MHz (2400-2500 MHz band). A total of thirty rigorous simulations have been carried out along with one hundred and twenty SAR data evaluations to ensure accurate comparison among different electromagnetic regulatory standards. Variations among the estimated SAR levels have been noted to be significant and presented in detail in this work. Furthermore, how fixing a global set of criteria for investigating biological effects of electromagnetic radiation can lead to the path of minimizing the existing discrepancies among different electromagnetic standards, has been discussed.

### 4.3.2.2 Disparity among Different Electromagnetic Standards

It has been discussed earlier that different electromagnetic regulatory standards prescribed by FCC, ICNIRP, DoT (India) and Switzerland are extensively inconsistent in terms of plane wave equivalent reference power density limit or equivalent electric field strength limit for public exposure [9-12]. The prescribed plane wave equivalent reference power density levels fluctuate by ten to hundred folds depending upon the electromagnetic regulatory standards in effect. A detailed discussion can be found earlier in this chapter (please refer to Table 4.17) [9-12].

### 4.3.2.3 Material Density and Dielectric Properties Characterization

#### A. Material Density Characterization

Initially, few medium sized fresh *Catharanthus roseus* plants have been collected. Next, mass and volume of leaf, flower and stem samples have been measured – material densities ( $\rho$ ) have been calculated by taking ratio of mass to volume of respective samples. Finally, mean material density ( $\rho$ ) for each type of *Catharanthus roseus* sample has been tabulated in Table 4.26.

#### B. Dielectric Properties Characterization

Real part i.e. permittivity ( $\epsilon'_r$ ) and loss tangent ( $\tan \delta$ ) data for *Catharanthus roseus* leaf, flower and stem samples have been measured using Agilent Technologies 85070E open ended coaxial probe (high temperature probe, – 40 °C to 200 °C, option 020) and Agilent Technologies E5071B VNA. A detailed discussion on this non-destructive dielectric properties ( $\epsilon_r$ ) characterization technique can be found in the previous chapter [52-62]. The dielectric measurement kit consists of a high temperature coaxial probe that can characterize dielectric properties ( $\epsilon_r$ ) up to 20 GHz. This particular probe is capable of characterizing dielectric properties ( $\epsilon_r$ ) for solid (with a smooth flat surface), semi solid and liquid samples possessing relatively high loss tangent (greater than 0.05). Complex dielectric properties ( $\epsilon_r$ ) have been computed from raw reflection coefficient data for the material under test after calibrating measurement setup at 25 °C.

Table 4.26 Measured density ( $\rho$ ) of *Catharanthus roseus* leaf, flower and stem samples

Name of sample	Leaf	Flower	Stem
Material density (kg/m <sup>3</sup> )	717	267.7	774

*Catharanthus roseus* leaves, flowers and green stems consist of soft tissues with significant amount of liquid content. Individual leaf or flower sample being quite thin, sufficient number of leaves or flowers have been stacked and thereafter the coaxial probe is moderately pressed on stacked samples to avoid air gap between leaves or flowers to obtain accurate dielectric properties ( $\epsilon_r$ ). Leaf or flower samples have been stacked to provide sufficient material depth (depending upon skin depth) beneath the coaxial probe for accurate measurement. In case of stem samples, a small amount of air gap couldn't be avoided due to cylindrical shape. Precaution has been taken during measurement because excessive pressure on the plant samples could cause tissue deformation resulting in erroneous measurement data.

Dielectric properties ( $\epsilon_r$ ) for the above mentioned plant samples have been measured from 20 MHz to 8.5 GHz. To keep the data consistent with this work of SAR computation, real part of permittivity ( $\epsilon_r'$ ) and loss tangent ( $\tan \delta$ ) parameters have been tabulated in Table 4.27 at frequencies of interest. Complex dielectric properties ( $\epsilon_r$ ) measurement set up with plant samples has been illustrated in Figs. 4.20(a) and (b).

Table 4.27 Measured dielectric properties of *Catharanthus roseus* leaf, flower and stem

Sample	947.5 MHz		1842.5 MHz		2150 MHz		2350 MHz		2450 MHz	
	$\epsilon_r'$	$\tan \delta$	$\epsilon_r'$	$\tan \delta$	$\epsilon_r'$	$\tan \delta$	$\epsilon_r'$	$\tan \delta$	$\epsilon_r'$	$\tan \delta$
<b>Leaf</b>	57.85	0.501	54.05	0.331	53.53	0.306	53.21	0.295	53.21	0.295
<b>Flower</b>	62.47	0.212	60.53	0.175	60.14	0.182	60.03	0.186	60.04	0.186
<b>Stem</b>	43.26	0.475	40.16	0.326	39.47	0.315	39.29	0.307	39.29	0.307



Fig. 4.20: (a) Entire dielectric properties measurement setup for *Catharanthus roseus* leaf samples, (b) An enlarged view of the coaxial probe with leaf samples

#### 4.3.2.4 *Catharanthus roseus* Plant Modeling in CST MWS 2014

Few typical medium sized *Catharanthus roseus* plants have been collected – thereafter length, width, surface area and radius of plant leaf, flower and stem samples have been measured. Next, two dimensional footprints of leaf and flower samples have been imported and further extruded for making three dimensional models in CST MWS 2014 [49]. Subsequently, the initial three dimensional leaf model has been replicated, scaled and rotated eighteen times around a conical stem at different heights along with a three dimensional flower structure on top of the plant prototype. Detailed specifications of the typical *Catharanthus roseus* plant model (2.70 g mass) have been incorporated in Table 4.28 and designed three-dimensional model is illustrated in Fig. 4.21.

Table 4.28 Modeling specifications of *Catharanthus roseus* leaf, flower and stem

Leaf Samples Specifications			
Leaves from top to bottom	Length along axis (mm)	Thickness of leaves (mm)	Repetition factor
Leaf 1	17.13	0.250	2
Leaf 2	24.56	0.286	2
Leaf 3	32.67	0.330	2
Leaf 4	48.71	0.430	2
Leaf 5	48.80	0.430	2
Leaf 6	51.93	0.450	2
Leaf 7	52.10	0.450	2
Leaf 8	58.89	0.490	2
Leaf 9	63.00	0.545	2

Flower Sample Specifications		
Maximum diagonal length (mm)	Thickness of flower (mm)	Repetition factor
36.23	0.5	1

Stem Sample Specifications			
Vertical length of the cone (mm)	Base radius (mm)	Top radius (mm)	Repetition factor
140.3	2.00	0.50	1

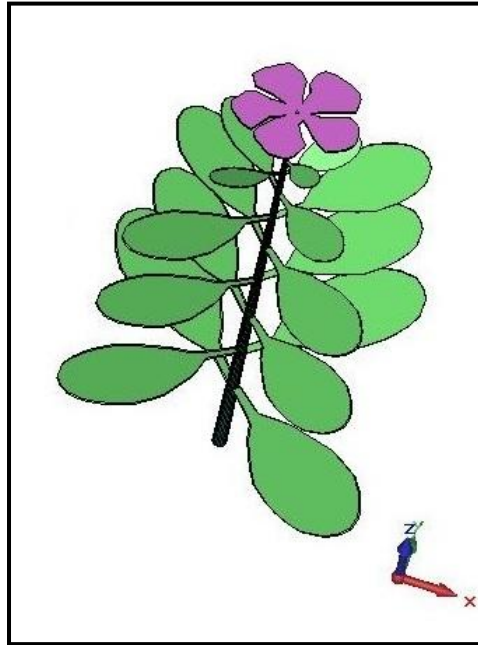


Fig. 4.21: Simplified three dimensional model of *Catharanthus roseus* plant designed in CST MWS 2014 [49]

#### 4.3.2.5 Computational Scheme for SAR Estimation

SAR simulations for *Catharanthus roseus* plant model have been performed using transient solver available in CST MWS 2014 [49]. Complicated nature of the plant structure shown in Fig. 4.21 along with lossy low quality factor of the layer permittivities have led to the choice of time domain / transient solver for a robust meshing. As discussed earlier, the transient solver works based on FIT computational scheme developed in 1977 [50-51]. In this technique, Maxwell's integral equations in the solution space are discretized and solved numerically. Spatial discretizations have been performed with hexahedral meshes of variable sizes and one wavelength of spatial distance is subdivided into 20 parts. Four PMLs with 0.0001 reflection coefficient have been set as electromagnetic boundary at 3 cm distance from the plant structure to bring the plane wave excitation as close as possible. To observe frequency domain characteristics, an inverse transformation accuracy of  $-40$  dB has been chosen that transforms the domain once the steady state energy criterion is met. IEEE/IEC 62704-1 averaging method has been adopted for SAR data calculation with an average mesh cell of 0.00043 g [17]. Once

electric field values on all edges of a particular grid cell are known, electric field values on all edges parallel to a particular axis are averaged; this technique is applied to obtain average electric fields along all three axes and effective electric field strength is calculated at the centre of that grid cell. At last, point SAR is calculated using the standard formula  $\sigma|E|^2/2\rho$ . For SAR averaging, a cubical volume centred at a particular grid cell is expanded evenly in all directions until the target averaging mass is achieved. In special cases, the averaging cube may include partial background material near boundary (maximum 10 percent volume of the cube); however, mass of background material is not considered to achieve the target mass. This is how spatial averaged SAR value is assigned to a particular ‘valid’ grid cell in accordance with IEEE/IEC 62704-1 protocol. Other grid cells encompassed in that averaging cube are flagged as ‘used’ – but, partially covered grid cells are marked as ‘unused’. This technique is repeated keeping every grid cell at the centre and grid cells are flagged as ‘valid’, ‘used’ or ‘unused’. The ‘used’ grid cells that have never been at the centre of a ‘valid’ averaging cube are assigned the highest spatial average SAR value among all averaging cubes in which they were enclosed.

For each ‘unused’ grid cell, six cubical volumes are constructed to achieve the averaging mass by keeping each surface of an ‘unused’ cell at the centre of a surface of those six averaging cubes. Then, those six cubes are expanded until the target mass is achieved regardless the amount of enclosed background material. Spatial average SAR values of cubes whose volume is not greater than 5 percent of the smallest cube are considered – finally, the highest spatial average SAR value among those averaging cubes is assigned to the ‘unused’ cell. Then, spatial averaged SAR distribution on the plant surface is derived from spatial average SAR values of individual grid cells that are lying on surface of the designed plant model. The same technique can also be followed to obtain the spatial averaged SAR distribution on any cut plane inside the plant model. Thus, 1g averaged SAR distribution has been obtained on two dimensional surface of the plant model [17].

#### **4.3.2.6 Computed SAR Data and Analysis**

SAR data along with associated spatial distributions in the *Catharanthus roseus* plant model have been simulated for occupational and public exposure scenarios in accordance with FCC and ICNIRP prescribed global electromagnetic standards [9-10]; moreover, SAR data have also been evaluated as per stricter public exposure standards effective in India and Switzerland [11-12].

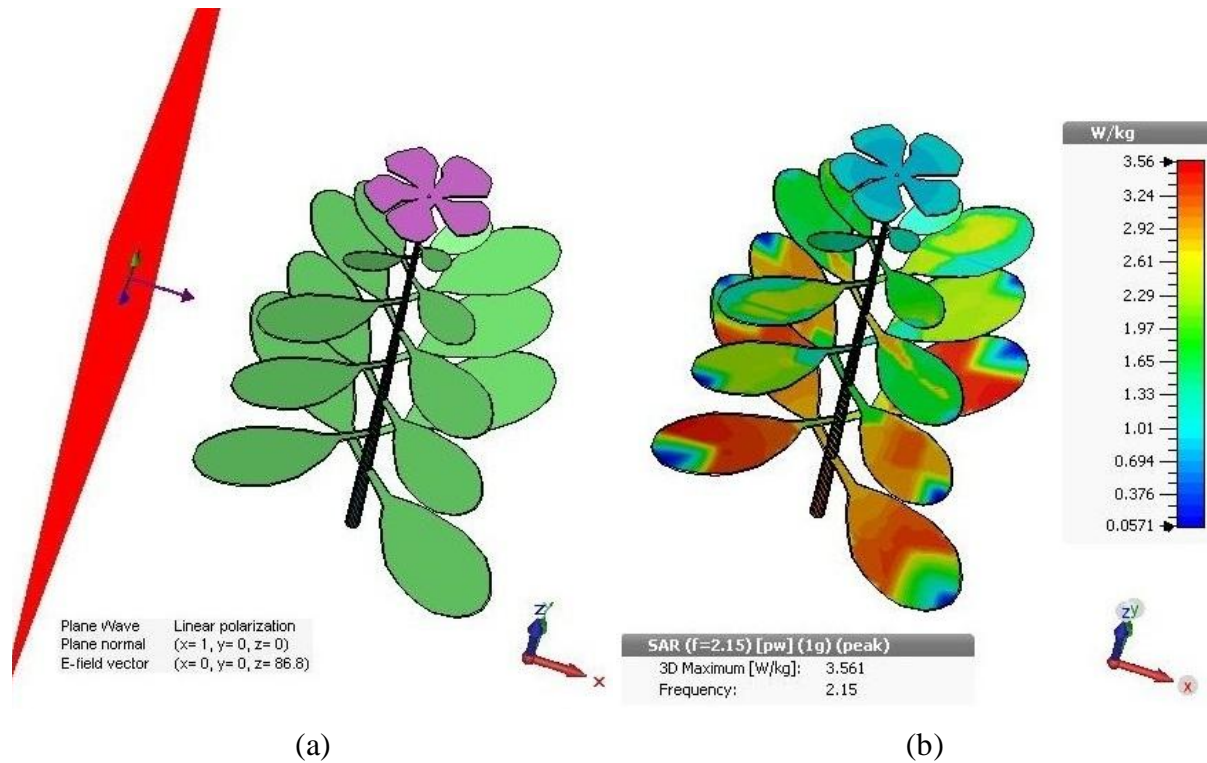


Fig. 4.22: (a) A linearly polarized plane wave passes through *Catharanthus roseus* plant model at 2150 MHz with field strength set as per FCC guidelines for public zone, (b) Evaluated 1g averaged SAR profile on surface of *Catharanthus roseus* model at 2150 MHz

Linearly polarized plane wave (with specified field strength and frequency) impinges on the prototyped plant model in each SAR simulation scenario. MLP SAR, 1g averaged SAR, 2g averaged SAR and WBA SAR data have been simulated for above mentioned plant model at 947.5 MHz, 1842.5 MHz, 2150 MHz, 2350 MHz and 2450 MHz respectively.

Fig. 4.22(a) illustrates a typical simulation setup where a linearly polarized plane wave impinges on the designed *Catharanthus roseus* plant model at 2150 MHz as per FCC public exposure guidelines. Fig. 4.22(b) illustrates consequent 1g averaged SAR distribution profile on surface of the plant model. Elevated SAR distribution levels have been noted among larger leaves at 2150 MHz. It is so because primarily leaves are very thin with sharp edges; moreover, *Catharanthus roseus* leaves possess permittivity ( $\epsilon_r'$ ) of 53.53 at 2150 MHz whereas realized wavelength inside leaf tissue is around  $\frac{13.95}{\sqrt{53.53}}$  cm = 1.9 cm. As a consequence, leaves having dimensions



larger than realized wavelength possess more number of peaks and higher SAR distribution than the rest of the plant structure.

As discussed earlier – charge accumulation on surface area with greater curvature tends to be greater in magnitude; this phenomenon can be proved by solving Poisson's equation on and around the surface of arbitrary shaped structure [75]. Local electric field strength because of such non uniform charge distribution also follows a similar distribution i.e. electric field at points with greater charge density is greater in magnitude [76]. The occurrence of concentrated electric field near sharp edges is not only limited to conducting bodies but also applies to lossy dielectric bodies with finite conductivity ( $\sigma$ ) [77]. Explanation of scattering problem illustrated by scattering of incident electromagnetic field by a lossy dielectric object ultimately leads to an electric field distribution or equivalent induced surface current density that prefers the sharp edges i.e. magnitude of the distribution is greater in close vicinity of greater surface curvature.

Data summarized in Table 4.29 to Table 4.33 indicate that MLP SAR, 1g averaged SAR and WBA SAR values increase with frequency for all electromagnetic regulatory standards. Estimated SAR data increase with frequency primarily because of two factors; first, plane wave equivalent reference power density level increases with increase in frequency of exposure. In addition, effective wavelength within plant dielectric tissue shortens with increase in frequency of exposure; consequently, more numbers of peak electric field point develop within the plant model resulting in increased SAR value for even same magnitude of electromagnetic field. Moreover, dielectric properties ( $\epsilon_r$ ) of plant tissues also vary with frequency which further contributes to alter SAR data. Plants are exposed to mobile tower radiation throughout their lifespan – therefore, simulated SAR data are absolutely pertinent and shouldn't be underestimated further by averaging over six minutes of time span.

Comprehensive analyses of data at any particular frequency reveal that there are wide discrepancies among SAR values depending upon the electromagnetic standards in effect. Six different electromagnetic exposure scenarios have been considered during this comparative study – two are global occupational exposure scenarios and rests are global as well as national public exposure scenarios [9-12]. FCC and ICNIRP prescribed occupational exposure levels are fivefold liberal compared to respective public exposure levels [9-10]. As a consequence, SAR data for the plant model are extremely high in occupational exposure scenarios at all frequencies.

Occupational electromagnetic standards prescribed by FCC and ICNIRP are somewhat different at 900 MHz and 1800 MHz bands; proportionate differences between respective SAR data have also been noted (Table 4.29 and Table 4.30). SAR data rise by 33 percent (947.5 MHz) and 8 percent (1842.5 MHz) as per FCC occupational exposure standards compared to ICNIRP occupational exposure standards.

In public exposure scenario, plane wave equivalent reference power density levels differ by tenfold to hundredfold among different global and national electromagnetic exposure regulatory standards. Resembling occupational exposure scenario, FCC and ICNIRP prescribed public electromagnetic standards are also dissimilar at 900 MHz and 1800 MHz bands; but, national public exposure standards in India and Switzerland are much stricter compared to global scenarios [9-12]. While analyzing, significant disparity in SAR data has been noted under different global and national public exposure scenarios. Similar to occupational exposure scenario at 947.5 MHz and 1842.5 MHz, SAR data differ by same ratio between two global public exposure standards (Table 4.29 and Table 4.30). However compared to global public exposure standards, all SAR values have been reduced by tenfold and hundredfold respectively in India and Switzerland. Fig. 4.23 illustrates severe contrast in 1g averaged SAR data as per different global and national public electromagnetic standards. 1g averaged SAR values at public places have been noted to be extremely high as per FCC and ICNIRP standards, moderate in India and extremely low in Switzerland. Furthermore, it can be noted that SAR values at public places in countries like Russia, Italy etc. would also be very similar to that of Swiss public scenario – as plane wave equivalent reference power density levels are close enough at 947.5 MHz and 1842.5 MHz and exactly similar thereafter [12-16].

Coexistence of several frequency bands results in cumulative SAR effect – base station antennas radiating at different frequencies are operational simultaneously over the years. As a consequence, evaluated SAR data at all frequencies add up and results in cumulative effect in any biological object and this plant model is no exception. Cumulative SAR data over all five frequencies have been illustrated in Fig. 4.24 and resulting curves indicate substantial discrepancies among different global and national electromagnetic exposure guidelines.

Table 4.29 Comparative SAR data for *Catharanthus roseus* plant model at 947.5 MHz as per different global and national electromagnetic regulatory guidelines

Frequency 947.5 MHz						
Exposure Zone	Occupational		Public			
Guidelines	FCC	ICNIRP	FCC	ICNIRP	India	Swiss
Power density (W/m <sup>2</sup> )	31.58	23.69	6.32	4.74	0.47	0.047
Equivalent peak electric field (V/m)	154.3	133.6	69.02	59.77	18.82	5.95
MLP SAR	17.8	13.3	3.56	2.67	0.27	0.027
1g SAR	5.41	4.06	1.08	0.81	0.08	0.008
2g SAR	3.81	2.86	0.76	0.57	0.06	0.006
WBA SAR	3.32	2.49	0.66	0.50	0.05	0.005

SAR is in W/kg

Table 4.30 Comparative SAR data for *Catharanthus roseus* plant model at 1842.5 MHz as per different global and national electromagnetic regulatory guidelines

Frequency 1842.5 MHz						
Exposure Zone	Occupational		Public			
Guidelines	FCC	ICNIRP	FCC	ICNIRP	India	Swiss
Power density (W/m <sup>2</sup> )	50	46.06	10	9.21	0.92	0.092
Equivalent peak electric field (V/m)	194.14	186.33	86.82	83.33	26.35	8.33
MLP SAR	46.28	42.63	9.26	8.53	0.85	0.085
1g SAR	14.34	13.21	2.87	2.64	0.26	0.026
2g SAR	9.83	9.06	1.97	1.81	0.18	0.018
WBA SAR	8.33	7.68	1.67	1.54	0.15	0.015

SAR is in W/kg

Table 4.31 Comparative SAR data for *Catharanthus roseus* plant model at 2150 MHz as per different global and national electromagnetic regulatory guidelines

Frequency 2150 MHz						
Exposure Zone	Occupational		Public			
Guidelines	FCC	ICNIRP	FCC	ICNIRP	India	Swiss
Power density (W/m <sup>2</sup> )	50	50	10	10	1	0.1
Equivalent peak electric field (V/m)	194.14	194.14	86.82	86.82	27.45	8.68
MLP SAR	57.23	57.23	11.44	11.44	1.14	0.114
1g SAR	17.80	17.80	3.56	3.56	0.356	0.036
2g SAR	12.04	12.04	2.41	2.41	0.241	0.024
WBA SAR	10.08	10.08	2.02	2.02	0.202	0.020

SAR is in W/kg

Table 4.32 Comparative SAR data for *Catharanthus roseus* plant model at 2350 MHz as per different global and national electromagnetic regulatory guidelines

Frequency 2350 MHz						
Exposure Zone	Occupational		Public			
Guidelines	FCC	ICNIRP	FCC	ICNIRP	India	Swiss
Power density (W/m <sup>2</sup> )	50	50	10	10	1	0.1
Equivalent peak electric field (V/m)	194.14	194.14	86.82	86.82	27.45	8.68
MLP SAR	66.75	66.75	13.35	13.35	1.34	0.133
1g SAR	20.85	20.85	4.17	4.17	0.417	0.042
2g SAR	13.94	13.94	2.79	2.79	0.279	0.028
WBA SAR	11.59	11.59	2.32	2.32	0.232	0.023

SAR is in W/kg

Table 4.33 Comparative SAR data for *Catharanthus roseus* plant model at 2450 MHz as per different global and national electromagnetic regulatory guidelines

Exposure Zone	Frequency 2450 MHz					
	Occupational		Public			
	FCC	ICNIRP	FCC	ICNIRP	India	Swiss
Guidelines						
Power density ( $W/m^2$ )	50	50	10	10	1	0.1
Equivalent peak electric field (V/m)	194.14	194.14	86.82	86.82	27.45	8.68
MLP SAR	72.76	72.76	14.55	14.55	1.46	0.145
1g SAR	22.63	22.63	4.52	4.52	0.45	0.045
2g SAR	15.05	15.05	3.01	3.01	0.30	0.030
WBA SAR	12.48	12.48	2.50	2.50	0.25	0.025

SAR is in W/kg

### 4.3.2.7 Conclusions

Significant contrast in SAR data has been noted for *Catharanthus roseus* plant model due to lack of uniformity among different global and national electromagnetic regulatory standards [9-12]. SAR data for the plant model reduce by tenfold to hundredfold as per Indian and Swiss public standards respectively compared to other established global electromagnetic standards. It is so because both power density ( $|E_{inc}|^2/2\eta$ ) and SAR ( $\sigma|E|^2/2\rho$ ) vary proportionately with second power of electric field strength;  $|E_{inc}|$  and  $\eta$  respectively stand for maximum amplitude of incident electric field and intrinsic impedance of free space (377 ohm). All SAR data for the designed *Catharanthus roseus* model (stands along z-axis) have been reported due to linearly polarized plane wave incidence with direction of propagation along x-axis and electric field variation along z-axis. However, SAR data are expected to change for different directions of propagation or different axes of electric field variation – as demonstrated later in this chapter. Reported simulation data can be a good reference for validation through practical SAR measurement. *Catharanthus roseus* tissue equivalent phantom liquids are being prepared for the same purpose – those phantom liquid formulae are presented later in this thesis.

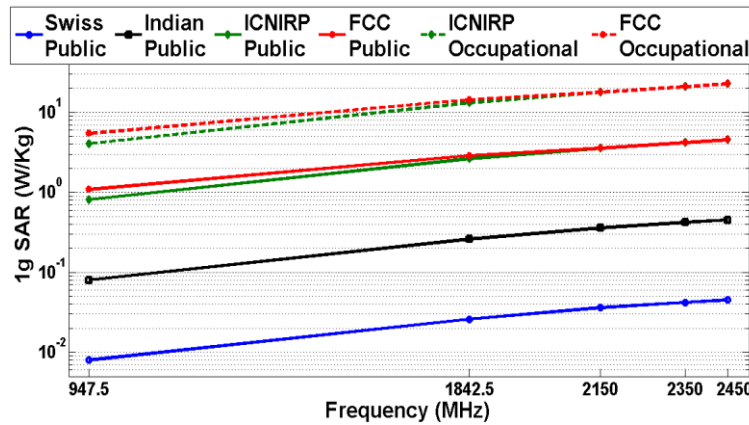


Fig. 4.23: Contrast in 1g averaged SAR data for *Catharanthus roseus* plant model due to variation among different global and national public electromagnetic standards

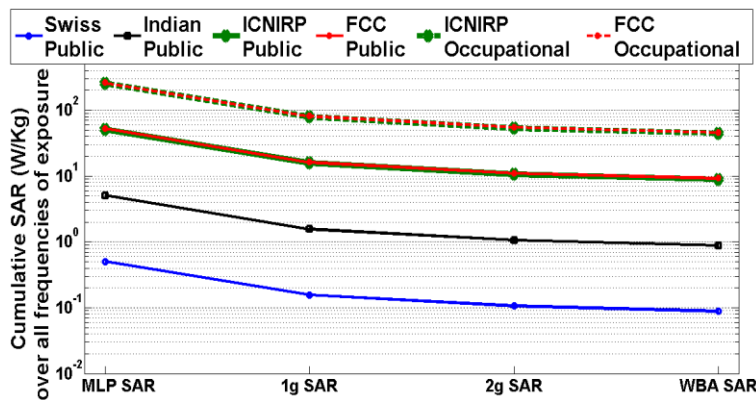


Fig. 4.24: Contrast in cumulative SAR data for *Catharanthus roseus* plant model due to variation among electromagnetic standards prescribed by different global and national organizations

Observed wide variation in SAR data due to lack of uniformity among different electromagnetic standards is not object specific i.e. this contrast in SAR data is applicable for all biological models irrespective of their structures and tissue layer distributions. Hence, introducing uniform electromagnetic regulatory standards worldwide is an absolute necessity considering effects of electromagnetic energy absorption in plants (along with humans). Basis to introduce decisive uniform electromagnetic standards is a trade-off between two factors. Minimum feasible power density (or equivalent electric field strength) sufficient for seamless data and voice connectivity over-the-air is the primary factor. This factor further depends on effective implementation of

smaller cell size and more of frequency reuses; more number of mobile towers should be installed and each mobile tower antenna must emit minimal electromagnetic power to reduce radiated power density in far field. Secondly, further investigations should be carried out to explore the maximum power density levels over different frequency bands that have negligible biological effects on humans as well as plants. Different global and national electromagnetic standards are consistent with their own history, evolution criteria and the policy promoted by the issuing authority. All those regulatory bodies must decide together a standard set of criteria for investigating biological effects of electromagnetic radiation on humans and plants. Scientific publications that report investigations in accordance with those standard set of criteria will only have to be taken into consideration – thus, the regulatory specifications can be harmonized and lead to subsequent introduction of a globally uniform electromagnetic standards [16]. However until biological effects are precisely known, the minimum feasible power density sufficient for seamless data and voice connectivity should be treated as the reference level and lead the path toward uniform electromagnetic regulatory standards worldwide.

#### **4.4 Dependence of SAR Data and Spatial Distribution in Fruit Specimens on Angle of Incidence and Wave Polarization**

The necessity to investigate SAR dataset and their spatial distributions in different fruit and plant models has already been discussed. Thus, SAR is not only dependent upon reference power density and dielectric properties ( $\epsilon_r$ ) of the biological model (example, a bunch of fruits structure) but also on its geometry and polarization of incident wave. Hence, investigating variation in SAR data for any particular plant / bunch of fruits structure due to different combinations of frequency, angle of incidence and wave polarization is much needed in far field exposure scenario. To explore this issue meticulously, SAR dataset have been simulated for two asymmetrical bunches of fruits and their variations due to different combinations of frequency, angle of incidence and wave polarization have also been investigated thereafter. This investigation includes SAR dataset and their spatial distributions in a bunch of single layer fruits model as well as in a bunch of multilayer fruits model. These asymmetrical bunches of fruits models have separately been irradiated with plane wave incidence at five different frequencies i.e. 947.50 MHz, 1842.50 MHz, 2150 MHz, 2350 MHz and 2450 MHz respectively. At a particular frequency of irradiation, SAR data have been simulated for six different combinations

of angle of incidence and wave polarization. Electric field strength at different frequencies has been modified as per the electromagnetic exposure regulatory guidelines in effect. Variations of SAR dataset have been noted down for different exposure scenarios. Recorded data indicate different order of changes in SAR value for different bunches of fruits models due to similar combinations of frequency, power density, angle of incidence and wave polarization.

#### **4.4.1 Dependence of SAR in Homogeneous Fruits Model**

##### **4.4.1.1 Introduction**

In most practical scenarios, plants and bunches of fruits are of asymmetric geometrical shapes and sizes. As a consequence, even at a particular frequency with fixed reference power density, electromagnetic energy absorption rate i.e. SAR value in plants and bunches of fruits is expected to differ depending upon the angle of wave incidence and polarization of incident wave. To address these issues in detail, a typical bunch of three single layered water apples has been prototyped and exposed to plane wave irradiation at five different frequency bands as per the existing Indian electromagnetic regulatory guidelines [11]. Broadband dielectric properties ( $\epsilon_r$ ) of water apple specimens have been measured using open ended coaxial probe technique [32-39]; next, measured dielectric properties ( $\epsilon_r$ ) have been fed into the designed model. At a particular frequency, reasonable variations in magnitude and position of maximum local point SAR, 1g averaged SAR and 10g averaged SAR data have been noted for six different combinations of angle of incidence and wave polarization. This whole course of action is repeated over five different frequencies i.e. at 947.50 MHz, 1842.50 MHz, 2150 MHz, 2350 MHz and 2450 MHz respectively. Moreover, variations in observed SAR data have also been compared with the variations in SAR data for another multilayer fruit structure (discussed later in this chapter). Observations indicate different order of changes in SAR for different fruit structures due to similar combinations of frequency, power density, angle of incidence and wave polarization.

##### **4.4.1.2 Indian Electromagnetic Exposure Guidelines**

For the above mentioned bunch of homogeneous water apples model, all SAR datasets along with their spatial distributions have been evaluated in accordance with the existing Indian electromagnetic exposure regulatory guidelines (as prescribed by DoT, Govt. of India) [11]. A



Table 4.34 Reference power density and equivalent electric field strength in India [11]

Public Electromagnetic Guidelines in India	Frequency (MHz)				
	947.50	1842.50	2150	2350	2450
Power Density (W/m <sup>2</sup> )	0.474	0.948	1.00	1.00	1.00
Peak Electric Field (V/m)	18.90	26.73	27.46	27.46	27.46

detailed discussion on the revised Indian electromagnetic exposure regulatory guidelines has already been carried out earlier in this chapter – therefore, the same is not required to be repeated here. The plane wave equivalent reference power density limits along with equivalent peak electric field strengths have been tabulated in Table 4.34 [11].

#### 4.4.1.3 Dielectric Properties and Material Density of Water Apple

It is now well established that complex dielectric properties ( $\epsilon_r$ ) of different fruit specimens are measured using open ended coaxial probe technique [32-39]. It is so because most fruit tissues are soft solids with high permittivity ( $\epsilon_r'$ ) and loss tangent ( $\tan \delta$ ) – thus, they require non invasive dielectric properties ( $\epsilon_r$ ) characterization technique. This technique characterizes dielectric properties ( $\epsilon_r$ ) using phase and amplitude of reflected signal at open end of the probe pressed against flat surface of samples (in case of liquid samples, the probe is directly immersed inside). The 85070E high temperature open ended coaxial probe works with E5071B VNA to record reflection coefficient data. The cascaded system is calibrated employing open-short-reference liquid method [32-39]. The equivalent circuit model along with detailed mathematical analysis has been outlined in the previous chapter [52-62].

Agilent Technologies 85070E open ended coaxial probe kit has been employed along with Agilent Technologies E5071B VNA for broadband permittivity ( $\epsilon_r'$ ) and loss tangent ( $\tan \delta$ ) measurement of green water apple fruit tissue at 25 °C [32-39]. This setup provides quite accurate measured data after precise system calibration. However, there are two categories of uncertainty factors associated with this measurement technique – random error (Type A) and systematic error (Type B) [78-80]. The random error (Type A) is primarily associated with variations in repeated sample-to-sample measurements for a specific biological tissue – even at a fixed temperature and after single system calibration (within 4% typical limit). In contrast, the

systematic error (Type B) is associated with probe calibration technique, calibration in reference liquid, measurement of fruit specimens, VNA drift and movement / bending of cable – however, these factors can be controlled with precision to minimize systematic error (1%). In general, the combined uncertainty of the measured dielectric data is observed to be within 5% limit for different biological specimens. The water apples have been cut with a sharp knife to obtain flat surfaces for accurate dielectric characterization. The entire open ended coaxial probe has been covered by the large flat cut surfaces of fruit specimens. The fruit specimens' dimensions along the radial directions as well as beneath the coaxial probe were large enough compared to the skin depth – thus, the condition of infinite dimensions of the material under test (water apple) has been satisfied. Optimal pressure has been applied with the open ended coaxial probe on the flat cut surfaces of the water apples during measurement – as extreme pressure could result in tissue deformation and subsequent erroneous measurement records. Dielectric properties ( $\epsilon_r$ ) have been measured for five different green water apples at early maturation stage and data for the fifth water apple have been further utilized for SAR estimation. However, the measured dielectric properties ( $\epsilon_r$ ) for the fruit specimens varied within a narrow range. This limited sample-to-sample variation in measured data is quite reasonable due to minor differences in water content and other tissue constituents (random error (Type A)) along with additional factors contributing to systematic error in the measurement setup (Type B) [78-80]. The cascaded dielectric properties ( $\epsilon_r$ ) measurement setup has been illustrated in Fig. 4.25(a). Measured permittivity ( $\epsilon_r'$ ) and loss tangent ( $\tan \delta$ ) data for water apple fruits have been illustrated respectively in Figs. 4.25(b) and (c) along with summarization in Table 4.35. In this context, it should also be noted that the water content (increases), soluble solid content (increases) and firmness (reduces) etc. change with the fruit maturation / ripening process – as a consequence, the measured dielectric properties ( $\epsilon_r$ ) of water apple can also reasonably change at different growth stages as it progresses to maturation / ripening phase [81-83].

Material density of water apple fruit is also required for SAR calculation. Mass and volume of some green water apples have been measured using balance, beaker and a stone with cotton string. Average material density has been observed to be 833.33 kg/m<sup>3</sup>.

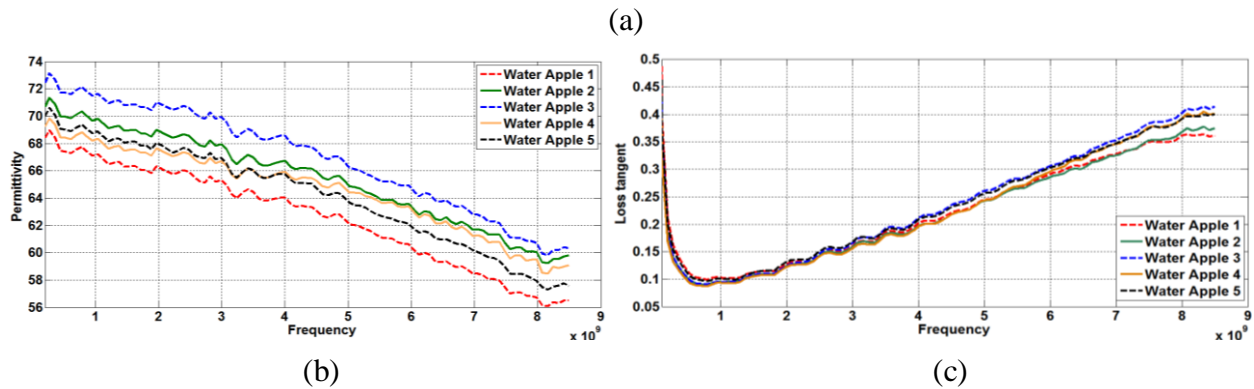
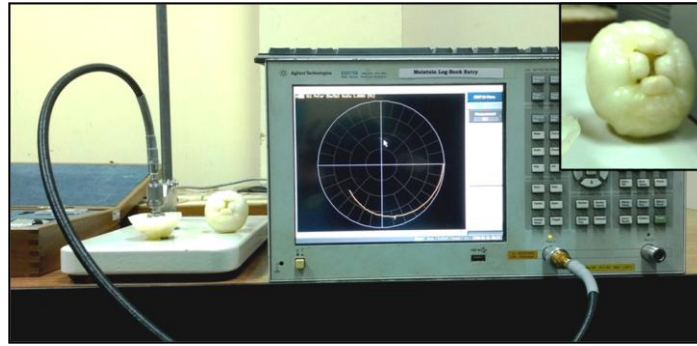


Fig. 4.25: (a) Open ended coaxial probe setup for broadband dielectric properties characterization of water apples, (b) Measured permittivity data for different water apple samples and (c) Measured loss tangent data for different water apple samples

Table 4.35 Measured parameters of water apple tissue

<i>Dielectric Properties</i>	<i>Frequency (MHz)</i>				
	947.50	1842.50	2150	2350	2450
Permittivity	68.75	67.57	67.58	67.68	67.53
Loss Tangent	0.102	0.124	0.136	0.141	0.149

#### 4.4.1.4 Bunch of Water Apples Model and SAR Simulation Setup

A typical bunch of three single layered water apples has been modelled in CST MWS 2016 [49]. The peel of water apple is practically inseparable from the pulp – thus, it has not been considered as a separate dielectric layer in the model. Each individual water apple has been considered to be symmetric along its major axis to reduce the complexity of design. The entire designed prototype is illustrated in Fig. 4.26(a) – where three fruits with different sizes are connected via twigs and

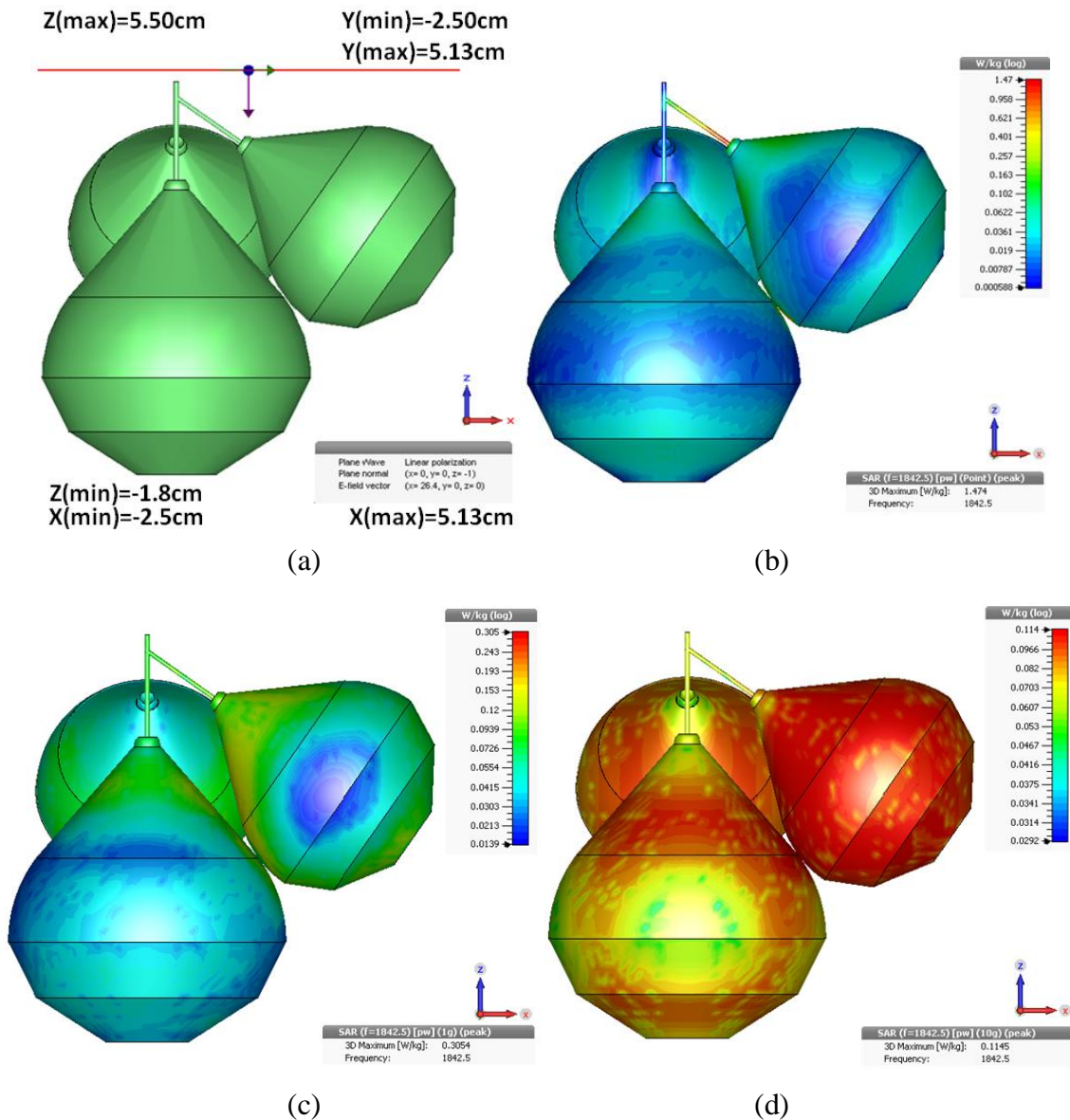


Fig. 4.26: (a) A linearly polarized plane wave incidence on the bunch of water apples [Direction of Propagation (DoP):  $z = -1$ ,  $E$  field:  $x$  axis], (b) MLP SAR distribution at 1842.50 MHz [Direction of Propagation (DoP):  $z = -1$ ,  $E$  field:  $x$  axis], (c) 1g SAR distribution at 1842.50 MHz [Direction of Propagation (DoP):  $z = -1$ ,  $E$  field:  $x$  axis] and (d) 10g SAR distribution at 1842.50 MHz [Direction of Propagation (DoP):  $z = -1$ ,  $E$  field:  $x$  axis]

possess a total mass of 94 g. In the designed prototype, the water apples are inclined to each other – thus, the entire prototype containing three fruits is asymmetric in nature. To achieve a robust meshing of the designed structure – time domain solver has been chosen because of the

complicated geometry of prototyped model and the lossy low quality factor of constituent tissue dielectric layer [49]. As already discussed, this time domain solver in CST MWS 2016 is developed based on FIT computational scheme – the same was first introduced in 1977 [50-51]. In the required solution space, Maxwell’s integral equations are first discretized and then solved using numerical technique in this computational scheme. The prototyped biological model is spatially discretized using hexahedral meshes with flexible size – where one wavelength spatial distance is divided into 20 subsections. Four PMLs have been used as absorbing boundary. Distance of absorbing boundary is kept fixed at 0.10 cm. Inverse transformation accuracy of –40 dB has been chosen as the steady state energy criterion to observe frequency domain characteristics [49]. At a particular frequency, linearly polarized plane waves with six different combinations of direction of propagation and wave polarization have been impinged on the bunch of water apples in six distinct simulations. Then, variations in position and magnitude of maximum SAR data have been recorded. Point SAR at the centre of individual mesh cell is calculated using the formula  $\sigma|E|^2/2\rho$  – where  $\sigma$ , E and  $\rho$  respectively represent electrical conductivity of the biological tissue, developed peak electric field strength at the point of interest and material density of the tissue. The IEEE/IEC 62704-1 SAR averaging protocol available in CST MWS 2016 has been employed to calculate all SAR data – detailed SAR calculation technique and the spatial averaging protocol have already been discussed earlier in this chapter [17, 49]. Simulations have been performed at five different frequency bands of interest (to be precise, 947.50 MHz, 1842.50 MHz, 2150 MHz, 2350 MHz and 2450 MHz) as per the revised Indian electromagnetic regulatory guidelines. MLP SAR, 1g averaged SAR, 10g averaged SAR and WBA SAR data have been recorded at all five frequencies as per the prescribed power density levels in India [11].

#### **4.4.1.5 SAR Results and Discussion**

Observed variations in simulated MLP SAR, 1g SAR, 10g SAR and WBA SAR data for six different combinations of direction of propagation and wave polarization have been tabulated at all five frequencies. Relevant SAR data along with respective positions at 947.50 MHz, 1842.50 MHz, 2150 MHz, 2350 MHz and 2450 MHz have been tabulated respectively in Table 4.36 to Table 4.40. In this connection, MLP SAR, 1g SAR and 10g SAR distributions on three dimensional surfaces of the prototyped bunch of water apples have been illustrated in Figs.

4.26(b), (c) and (d) respectively – specifically at 1842.50 MHz for direction of propagation (plane wave):  $z = -1$  and electric field ( $E$  field):  $x$  axis. Here, it must be noted that higher charge accumulation, consequent local electric field development and equivalent induced surface current density take place near the curved regions on pure conducting bodies as well as lossy dielectric objects [75-77]. Thus, prototyped bunch of water apples contains higher SAR distribution near the curved regions on the fruit surface.

Table 4.36 SAR data for different directions of propagation and wave polarizations at 947.50 MHz

Frequency = 947.50 MHz							
Direction of Propagation & Wave Polarization	MLP SAR (W/kg)	Position [x, y, z] (cm)	1g SAR (W/kg)	Position [x, y, z] (cm)	10g SAR (W/kg)	Position [x, y, z] (cm)	WBA SAR (W/kg)
DoP: $x = 1$ E-field: $y$ axis	<b>1.5005</b>	<b>-0.41625, 1.9266, 1.72001</b>	0.1849	-0.0707107, 2.0625, 1.58667	<b>0.07714</b>	<b>0.183211, 2.80427, 2.40579</b>	0.04536
DoP: $x = 1$ E-field: $z$ axis	0.8532	-0.41625, 1.9266, 1.72001	0.1449	2.0625, -0.0707107, 2.6295	0.08277	2.80427, -0.0707107, 3.31693	0.04016
DoP: $y = 1$ E-field: $x$ axis	1.4908	1.9266, -0.41625, 1.72001	0.1849	2.0625, -0.0707107, 1.58667	0.07716	2.80427, 0.183211, 2.40579	0.04537
DoP: $y = 1$ E-field: $z$ axis	0.8480	1.9266, -0.41625, 1.72001	<b>0.1448</b>	<b>-0.0707107, 2.0625, 2.6295</b>	0.08276	-0.0707107, 2.80427, 3.31693	<b>0.04015</b>
DoP: $z = -1$ E-field: $x$ axis	0.8033	1.7798, 0.0707107, 1.9113	<b>0.1921</b>	<b>2.0625, 0.0707107, 2.40579</b>	<b>0.10592</b>	<b>-0.0707107, 4.17622, 4.6375</b>	<b>0.05341</b>
DoP: $z = -1$ E-field: $y$ axis	<b>0.8026</b>	<b>0.0707107, 1.7798, 1.9113</b>	0.1920	0.0707107, 2.0625, 2.40579	0.10586	4.17622, -0.0707107, 4.6375	0.05339
<b>Max-to-Min SAR Ratio</b>	<b>1.87</b>		<b>1.33</b>		<b>1.37</b>		<b>1.33</b>

Table 4.37 SAR data for different directions of propagation and wave polarizations at 1842.50 MHz

Frequency = 1842.50 MHz							
Direction of Propagation & Wave Polarization	MLP SAR (W/kg)	Position [x, y, z] (cm)	1g SAR (W/kg)	Position [x, y, z] (cm)	10g SAR (W/kg)	Position [x, y, z] (cm)	WBA SAR (W/kg)
DoP: $x = 1$ E-field: $y$ axis	1.1325	-0.0707107, 1.15736, 4.42621	0.27237	0.41625, 3.39399, 2.85807	0.125892	-0.0707107, 3.04446, 2.74335	0.048930
DoP: $x = 1$ E-field: $z$ axis	0.5628	1.7798, -0.0707107, 1.9113	0.24238	0.183211, 0.0707107, 0.286402	0.105029	0.0707107, 0.0707107, 0.515524	0.047632
DoP: $y = 1$ E-field: $x$ axis	1.1329	1.15736, 0.0707107, 4.42621	0.27241	3.39399, 0.41625, 2.85807	<b>0.125896</b>	<b>3.04446, -0.0707107, 2.74335</b>	0.048929
DoP: $y = 1$ E-field: $z$ axis	<b>0.5617</b>	<b>-0.0707107, 1.7798, 1.9113</b>	<b>0.24232</b>	<b>0.0707107, 0.183211, 0.286402</b>	<b>0.105019</b>	<b>0.0707107, 0.0707107, 0.515524</b>	<b>0.047628</b>
DoP: $z = -1$ E-field: $x$ axis	<b>1.4736</b>	<b>1.15736, 0.0707107, 4.42621</b>	0.30543	0.0707107, 0.0707107, 0.515524	0.114452	3.04446, -0.183211, 2.85807	0.061304
DoP: $z = -1$ E-field: $y$ axis	1.4733	-0.0707107, 1.15736, 4.42621	<b>0.30544</b>	<b>0.0707107, 0.0707107, 0.515524</b>	0.114456	-0.183211, 3.04446, 2.85807	<b>0.061310</b>
<b>Max-to-Min SAR Ratio</b>	<b>2.62</b>		<b>1.26</b>		<b>1.20</b>		<b>1.29</b>

Table 4.38 SAR data for different directions of propagation and wave polarizations at 2150 MHz

Frequency = 2150 MHz										
Direction of Propagation & Wave Polarization	MLP SAR (W/kg)	Position [x, y, z] (cm)		1g SAR (W/kg)	Position [x, y, z] (cm)		10g SAR (W/kg)	Position [x, y, z] (cm)		WBA SAR (W/kg)
DoP: x = 1 E-field: y axis	1.4766	-0.0707107, 4.42621	1.15736,	0.21127	0.0707107, 0.400963	0.28875,	<b>0.086005</b>	<b>-0.0707107,</b> <b>0.859207</b>	<b>0.41625,</b>	<b>0.044028</b>
DoP: x = 1 E-field: z axis	1.5689	0.0707107, 3.84605	-0.0707107,	0.18929	0.0707107, 2.74335	3.16456,	<b>0.088682</b>	<b>-0.0707107,</b> <b>0.515524</b>	<b>0.28875,</b>	<b>0.045977</b>
DoP: y = 1 E-field: x axis	1.4769	1.15736, 4.42621	0.0707107,	0.21126	0.28875, 0.400963	0.0707107,	0.086009	0.41625, 0.859207	-0.0707107,	<b>0.044028</b>
DoP: y = 1 E-field: z axis	<b>1.5690</b>	<b>0.0707107,</b> <b>3.84605</b>	<b>-0.0707107,</b>	<b>0.18927</b>	<b>3.16456,</b> <b>2.74335</b>	<b>0.0707107,</b>	0.088680	0.28875, 0.515524	-0.0707107,	<b>0.045977</b>
DoP: z = -1 E-field: x axis	<b>1.1199</b>	<b>1.15736,</b> <b>4.42621</b>	<b>0.0707107,</b>	<b>0.22996</b>	<b>-0.0707107,</b> <b>2.74335</b>	<b>3.28466,</b>	0.087638	-0.183211, 2.68417, 2.28933		0.045340
DoP: z = -1 E-field: y axis	1.1200	-0.0707107, 4.42621	1.15736,	0.22982	3.28466, 2.74335	-0.0707107,	0.087616	2.68417, -0.183211, 2.28933		0.045343
<b>Max-to-Min SAR Ratio</b>	<b>1.40</b>			<b>1.21</b>			<b>1.03</b>			<b>1.04</b>

Table 4.39 SAR data for different directions of propagation and wave polarizations at 2350 MHz

Frequency = 2350 MHz										
Direction of Propagation & Wave Polarization	MLP SAR (W/kg)	Position [x, y, z] (cm)		1g SAR (W/kg)	Position [x, y, z] (cm)		10g SAR (W/kg)	Position [x, y, z] (cm)		WBA SAR (W/kg)
DoP: x = 1 E-field: y axis	1.2237	-0.0707107, 4.42621	1.15736,	0.223071	0.183211, 3.28466, 2.85807		0.093812	-0.0707107, 2.80427, 2.6295		<b>0.044020</b>
DoP: x = 1 E-field: z axis	<b>1.7670</b> <b>(1.60)</b>	<b>0.0707107,</b> <b>3.84605</b>	<b>-0.0707107,</b>	<b>0.214339</b>	<b>0.183211, 3.28466, 2.74335</b>		0.084475	0.0707107, 2.92437, 2.51653		0.045232
DoP: y = 1 E-field: x axis	1.2243	1.15736, 4.42621	0.0707107,	0.223052	3.28466, 0.183211, 2.85807		0.093816	2.80427, -0.0707107, 2.6295		0.044021
DoP: y = 1 E-field: z axis	1.7669	0.0707107, 3.84605	-0.0707107,	0.214343	3.28466, 0.183211, 2.74335		<b>0.084468</b>	<b>2.92437,</b> <b>2.51653</b>	<b>-0.0707107,</b>	0.045230
DoP: z = -1 E-field: x axis	1.1083	1.15736, 4.42621	0.0707107,	<b>0.269293</b>	<b>-0.0707107, 3.28466, 2.6295</b>		<b>0.096274</b> <b>(1.14)</b>	<b>0.183211, 3.04446, 2.74335</b>		0.046575
DoP: z = -1 E-field: y axis	<b>1.1077</b>	<b>-0.0707107,</b> <b>4.42621</b>	<b>1.15736,</b>	0.269167	3.28466, -0.0707107, 2.6295		0.096232	3.04446, 0.183211, 2.74335		<b>0.046578</b>
<b>Max-to-Min SAR Ratio</b>	<b>1.60</b>			<b>1.26</b>			<b>1.14</b>			<b>1.06</b>

Magnitude of MLP SAR varies 1.87, 2.62, 1.40, 1.60 and 1.13 times (i.e. Max-to-Min MLP SAR Ratio) respectively at 947.50 MHz, 1842.50 MHz, 2150 MHz, 2350 MHz and 2450 MHz due to different combinations of direction of arrival and wave polarization. It should be noted that the maximum (or the minimum) SAR values at different frequencies don't happen to occur for unique combination of direction of propagation and wave polarization – it is so because the internally developed electric field distribution alters with frequency and so does the SAR distribution. Even at a particular frequency, positions of MLP SAR, maximum 1g SAR and



Table 4.40 SAR data for different directions of propagation and wave polarizations at 2450 MHz

Frequency = 2450 MHz										
Direction of Propagation & Wave Polarization	MLP SAR (W/kg)	Position [x, y, z] (cm)		1g SAR (W/kg)	Position [x, y, z] (cm)		10g SAR (W/kg)	Position [x, y, z] (cm)	WBA SAR (W/kg)	
DoP: x = 1 E-field: y axis	1.6318	-0.0707107, 4.42621	1.15736,	0.20062	0.28875, 0.400963	0.0707107,	0.084905	-0.183211, 2.80427, 2.51653	0.040987	
DoP: x = 1 E-field: z axis	<b>1.8141</b>	<b>0.0707107,</b> <b>3.84605</b>	<b>-0.0707107,</b>	<b>0.18270</b>	<b>0.0707107,</b> <b>2.74335</b>	<b>3.28466,</b>	0.075784	-0.0707107, 2.92437, 2.40579	0.042298	
DoP: y = 1 E-field: x axis	1.6324	1.15736, 4.42621	0.0707107,	0.20059	0.0707107, 0.400963	0.28875,	<b>0.084910</b>	<b>2.80427, -0.183211, 2.51653</b>	<b>0.040988</b>	
DoP: y = 1 E-field: z axis	<b>1.8141</b>	<b>0.0707107,</b> <b>3.84605</b>	<b>-0.0707107,</b>	0.18270	3.28466, 2.74335	0.0707107,	<b>0.075778</b>	<b>2.92437,</b> <b>2.40579</b>	<b>-0.0707107,</b>	0.042296
DoP: z = -1 E-field: x axis	1.6012	1.15736, 4.42621	0.0707107,	<b>0.23135</b>	<b>-0.0707107, 3.28466, 2.6295</b>		0.082632	0.183211, 3.04446, 2.74335	0.046313	
DoP: z = -1 E-field: y axis	<b>1.6004</b>	<b>-0.0707107,</b> <b>4.42621</b>	<b>1.15736,</b>	0.23125	3.28466, -0.0707107, 2.6295		0.082598	3.04446, 0.183211, 2.74335	<b>0.046316</b>	
<b>Max-to-Min SAR Ratio</b>	<b>1.13</b>			<b>1.27</b>			<b>1.12</b>		<b>1.13</b>	

maximum 10g SAR don't coincide. Figs. 4.27(a) to (e) illustrate variations in position and magnitude of MLP SAR for six different combinations of direction of propagation and wave polarization at five distinct frequencies – wide contrast in spatial coordinates of MLP SAR has been noted in addition to magnitude variation due to alteration in directions of propagation and wave polarizations. However, though significant variations in position of maximum 1g averaged and 10g averaged SAR data have been observed due to different combinations of direction of arrival and wave polarization, magnitudes differ to somewhat extent. Magnitude of maximum 1g averaged SAR varies 1.33, 1.26, 1.21, 1.26 and 1.27 times (i.e. Max-to-Min 1g SAR Ratio) respectively at five frequencies – as illustrated in Figs. 4.28(a) to (e). Likewise, magnitude of maximum 10g averaged SAR varies 1.37, 1.20, 1.03, 1.14 and 1.12 times (i.e. Max-to-Min 10g SAR Ratio) respectively at five frequencies – those have been graphically illustrated in Figs. 4.29(a) to (e). Fig. 4.30 demonstrates that WBA SAR varies 1.33, 1.29, 1.04, 1.06 and 1.13 times (i.e. Max-to-Min WBA SAR Ratio) at five frequencies mentioned earlier.

Water apples are composed of single homogeneous dielectric layer and symmetric over the major axes of individual fruits. Hence, different combinations of direction of arrival and wave polarization have resulted in between 1.13 to 2.62 order of change in MLP SAR. However for multilayer fruit structure, this order of change in MLP SAR can shoot up to a factor of 10 to 13 – as reported later in this chapter. In addition, it is also observed that variation in SAR decreases as



Specific Absorption Rate Evaluation for Prototyped Fruit and Plant Models

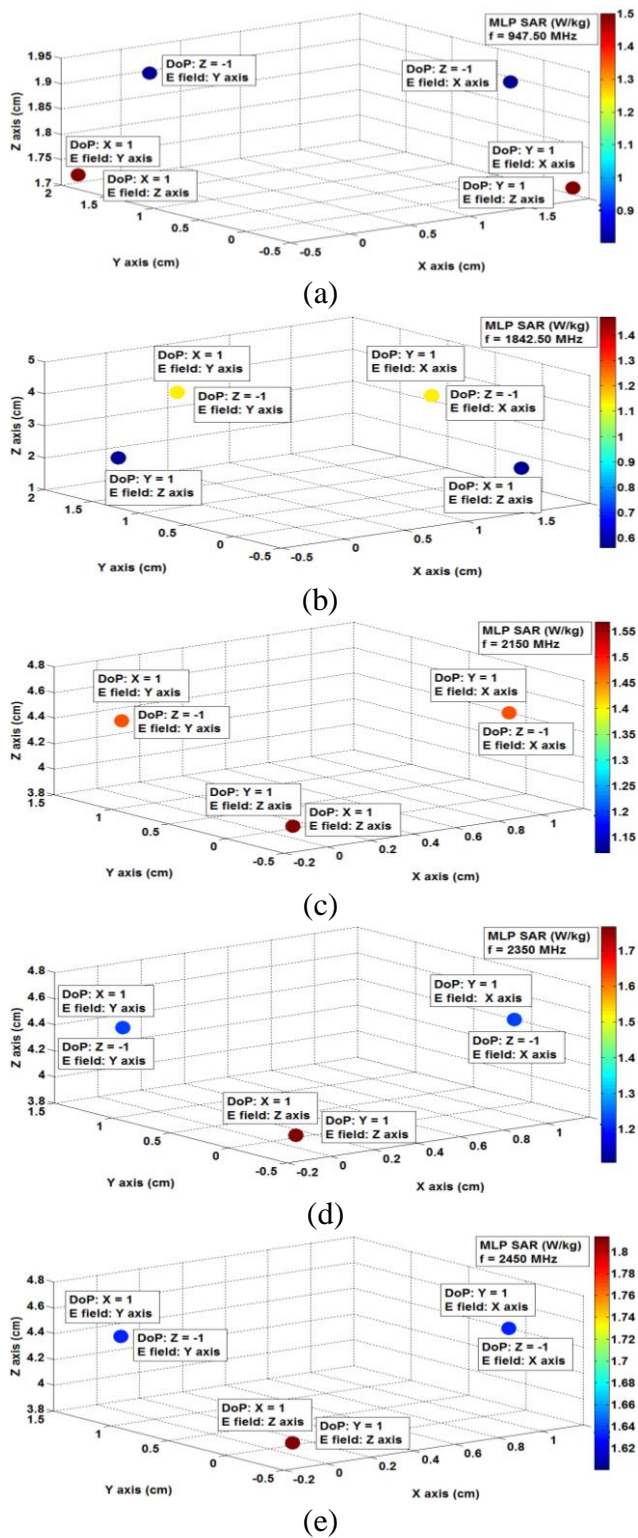


Fig 4.27: (a) to (e) Variations in magnitude and position of MLP SAR for six different combinations of direction of propagation and wave polarization at 947.50 MHz, 1842.50 MHz, 2150 MHz, 2350 MHz and 2450 MHz

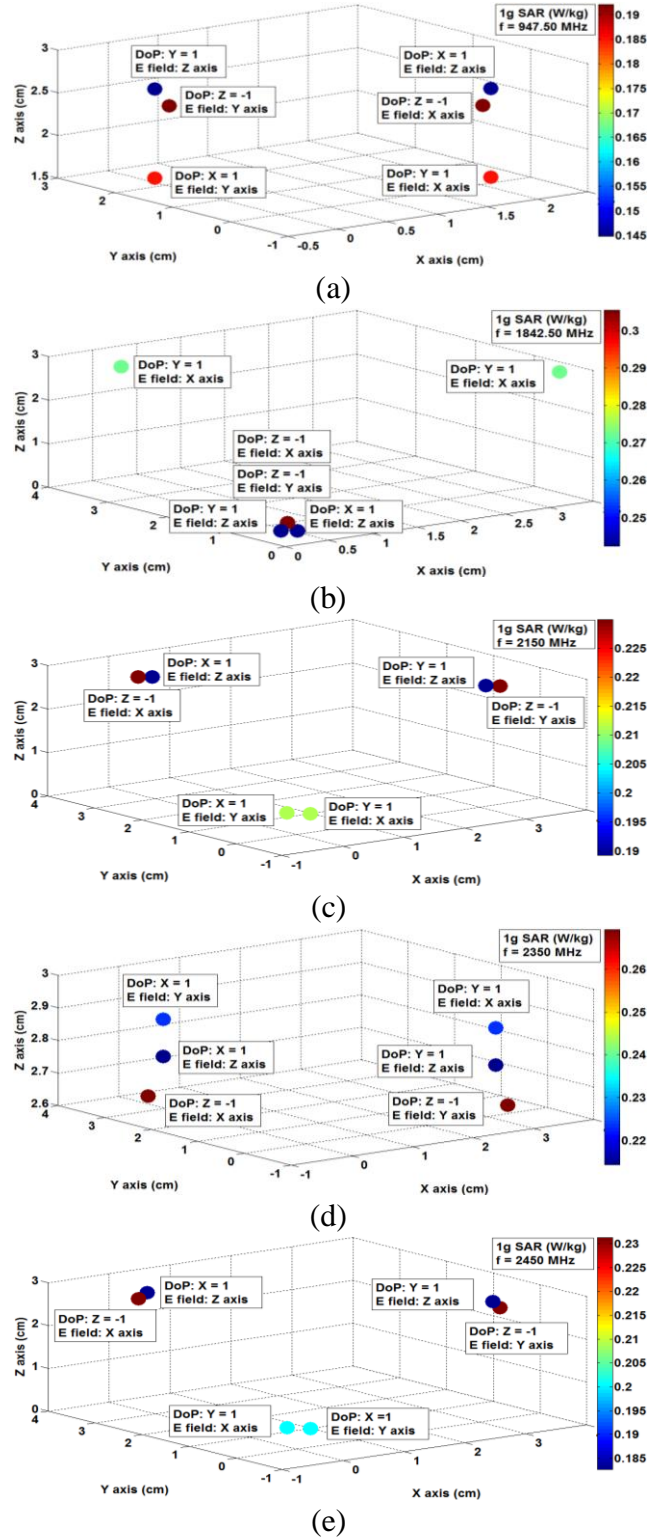


Fig 4.28: (a) to (e) Variation in magnitude and position of 1g averaged SAR for six different combinations of direction of propagation and wave polarization at 947.50 MHz, 1842.50 MHz, 2150 MHz, 2350 MHz and 2450 MHz

## Specific Absorption Rate Evaluation for Prototyped Fruit and Plant Models

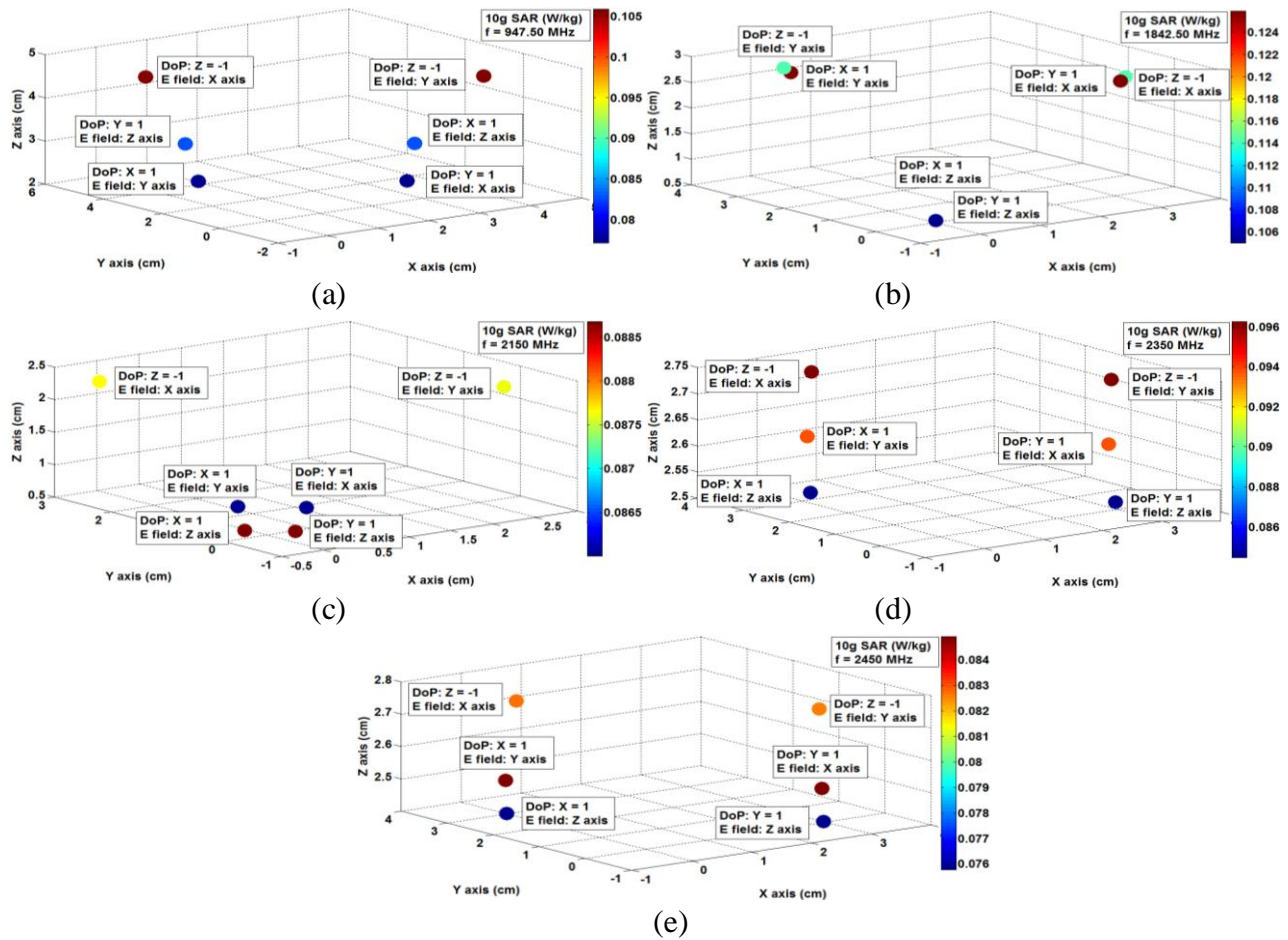


Fig 4.29: (a) to (e) Variation in magnitude and position of 10g averaged SAR for six different combinations of direction of propagation and wave polarization at 947.50 MHz, 1842.50 MHz, 2150 MHz, 2350 MHz and 2450 MHz

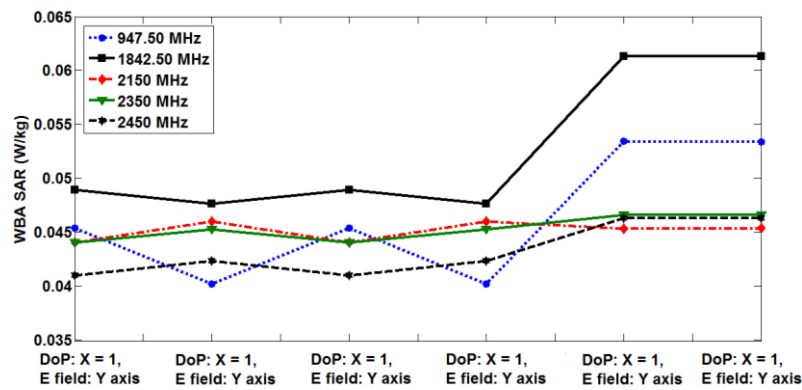


Fig. 4.30: Variation in magnitude of WBA SAR at 947.50 MHz, 1842.50 MHz, 2150 MHz, 2350 MHz and 2450 MHz

the averaging mass increases – the same phenomenon has been observed even for multilayer fruits structure in the later example. Multilayer fruits structure has been reported to have significantly higher order of change even in case of maximum 10g averaged and WBA SAR (2 to 4 times). SAR variation in multilayer fruit model is higher compared to single layer fruit model – it is so because multiple reflections of propagating electromagnetic wave take place at layer interfaces and thus result in local superposition of incident and reflected waves causing elevated SAR in multilayer model – please refer to the next work in this chapter.

#### **4.4.1.6 Conclusions**

Position and magnitude of SAR in fruit models significantly vary with different combinations of frequency, direction of arrival and wave polarization. Moreover, this variation in SAR distribution is also geometry, orientation of fruits, number of dielectric layers and dielectric profile dependent in different models. In addition, the dielectric properties ( $\epsilon_r$ ) of fruits change with maturation process [83] – this factor can further contribute to alter SAR distribution in fruit models. Hence, prescribing reference power density level in far field can't describe the entire electromagnetic energy absorption scenario and fails to reflect comprehensive SAR information in plants and fruits. This particular work has been performed in accordance with the existing Indian electromagnetic guidelines [11] – however, different global and national electromagnetic regulatory guidelines are not uniform with each other and also demand harmonization among themselves [9-16]. Thus, direct adoption of SAR limit for plants and fruits is also required in far field and therefore recommended. SAR limit for plants and fruits should be adopted based upon further investigated outcome of electromagnetic irradiation induced physiological and molecular responses in plants, fruits and crops [40-48].

### **4.4.2 Dependence of SAR in Multilayer Fruits Model**

#### **4.4.2.1 Introduction**

It is already known that a number of diversified international and national electromagnetic regulatory standards have been prescribed across geographical boundaries for limiting electromagnetic radiation – SAR and plane wave equivalent reference power density limits have been prescribed by the international organizations to protect humans from immediate thermal effects [9-16]. However, reference power density limits differ by ten to hundred times across

geographical boundaries depending upon the electromagnetic standards in effect – as discussed earlier in this chapter. Moreover, prescribed reference power density limit also varies with frequency of irradiation. In addition, plants and fruits are primarily asymmetric in nature – therefore, direction of arrival and polarization of incident electromagnetic field are two crucial factors that significantly influence the amplitude and spatial distribution of SAR. Therefore, prescribing only the maximum permissible power density limit in far field seems to be inadequate. To address these issues, SAR data inside a typical multilayer mango fruits model have been estimated at five different frequencies in accordance with four different international and national electromagnetic regulatory standards (with contrasting reference power density limits) [9-12] – the magnitudes and spatial distributions of SAR data have been quantified and reported at different frequencies as well as for distinct averaging techniques. Moreover, the impact of direction of arrival and polarization of incident electromagnetic field on the magnitude and spatial distribution of SAR has also been investigated. A total of one hundred and twenty rigorous simulations has been performed and consequent to it four hundred and eighty SAR data points have been analyzed. Wide disagreement in SAR data has been observed due to variations in four factors mentioned above – i.e. reference power density, frequency, direction of arrival and polarization of incident electromagnetic field. Moreover keeping all the other factors unaltered, SAR can't be directly correlated with the reference power density limit primarily due to non-identical and asymmetric structures of bunch of fruits and plants in most practical scenarios. Thus, observations indicate the necessity of adopting globally harmonized electromagnetic regulatory standards and direct adoption of SAR limit for plants and fruits instead of only the reference power density limits in far field exposure scenario.

#### **4.4.2.2 Dielectric Properties and Material Density of Mango Tissues**

As discussed earlier, the open ended coaxial probe technique is a well established non-invasive method for characterizing dielectric properties of biological tissues [32-39]. The lumped equivalent circuit for open ended coaxial probe along with detailed mathematical analyses has already been discussed in this chapter [52-62]. In this particular work, Agilent Technologies 85070E open ended coaxial dielectric properties measurement probe has been used along with the Agilent Technologies E5071B ENA series vector network analyzer to characterize dielectric properties ( $\epsilon_r$ ) of green mango pulp, seed and leaf samples [32-39]. Dielectric properties ( $\epsilon_r$ ) for

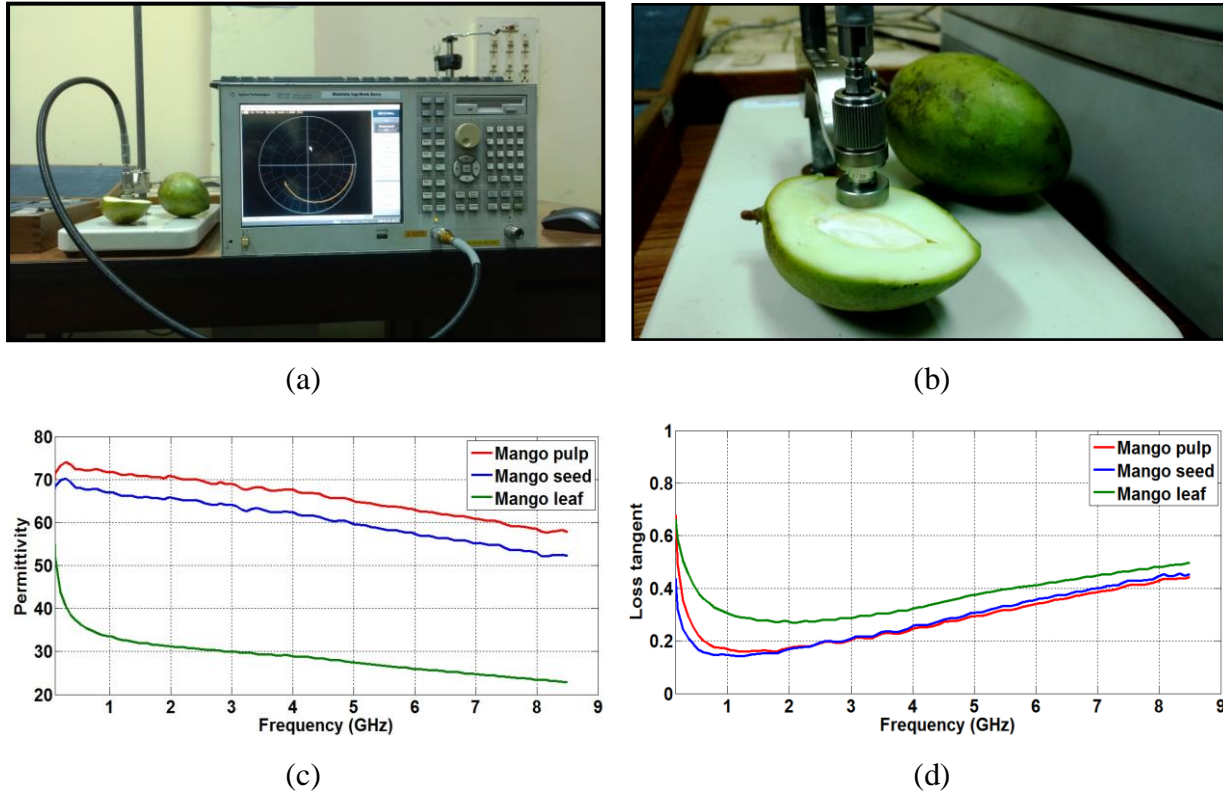


Fig. 4.31: (a) Dielectric properties measurement setup for mango pulp, (b) Close-up view of dielectric properties measurement setup for mango pulp, (c) Measured permittivity for different mango tissues over broad frequency range and (d) Measured loss tangent for different mango tissues over broad frequency range

the above mentioned samples have been measured over 20 MHz to 8.5 GHz frequency spectrum at 25 °C. Dielectric properties ( $\epsilon_r$ ) characterization setup has been illustrated in Figs. 4.31(a) and (b); whereas the measured dielectric properties ( $\epsilon_r$ ) of different mango tissue specimens have been plotted in Figs. 4.31(c) and (d) respectively. Dielectric properties ( $\epsilon_r$ ) have further been summarized in Table 4.41 at the frequencies of interest along with the measured material densities for mango pulp, seed, leaf and twig specimens.

#### 4.4.2.3 Bunch of Mango Fruits and SAR Simulation Setup

An indigenous multilayer prototype for a bunch of two mango fruits has been developed in CST MWS 2014 [49]. The prototyped model is composed of mango pulp, seed, twigs and leaf weighing around 235 g mass along with a volume of 260 cm<sup>3</sup>. As discussed earlier, the complex



Table 4.41 Measured parameters of different mango tissues

<b>Tissue</b>	<b>Pulp</b>		<b>Seed</b>		<b>Leaf &amp; twig</b>	
<b>Density</b>	906.25 kg/m <sup>3</sup>		914.89 kg/m <sup>3</sup>		833.33 kg/m <sup>3</sup>	
<b>Frequency</b>	$\epsilon_r$	$\tan \delta$	$\epsilon_r$	$\tan \delta$	$\epsilon_r$	$\tan \delta$
947.5 MHz	71.72	0.171	67.00	0.148	33.61	0.309
1842.5 MHz	70.59	0.160	65.66	0.152	31.45	0.270
2150 MHz	70.24	0.178	65.32	0.174	31.00	0.270
2350 MHz	70.14	0.182	65.29	0.182	30.67	0.272
2450 MHz	69.88	0.190	65.01	0.192	30.63	0.277

geometric structure shown in Fig. 4.32(a) and the low quality factor due to lossy dielectric layers inside the multilayer fruits model have led to the choice of transient / time domain solver (developed based on FIT) for achieving a robust mesh distribution [50-51]. The Maxwell's integral equations are discretized and solved using numerical techniques inside the prototyped multilayer fruits model i.e. the desired solution space. The whole prototyped multilayer mango fruits model has been discretized in space with infinitesimal hexahedral meshes of variable size – one wavelength of spatial distance inside the dielectric layers has been subdivided into 20 segments. The typical mesh cell count for the above mentioned bunch of mango fruits has been observed to be around 6.5 lakh – moreover, the average mass of individual mesh cell is around 0.0015 g. Four PMLs with  $10^{-4}$  reflection coefficient have been used as the electromagnetic absorbing boundaries. Separation between the prototyped bunch of mango fruits structure and the absorbing boundary wall has been set negligible by choosing appropriate boundary conditions – thus, plane wave is excited very close to the prototyped structure. Next, the above mentioned bunch of mango fruits has been exposed to linearly polarized plane waves with different combinations of directions of propagation and wave polarizations at five different frequencies (refer to Fig. 4.32(b)). After satisfying the steady state energy criterion, an inverse transformation precision of  $-40$  dB has been preferred in all the time domain simulations to obtain the frequency domain responses [49]. MLP SAR, 1g averaged SAR, 10g averaged SAR and WBA SAR data have been simulated in accordance with four different international and national electromagnetic regulatory standards for different directions of incidence and

polarizations of incident field [9-12]. All together, one hundred and twenty electromagnetic simulations have been performed – next, four hundred and eighty SAR data points have been analyzed in subsequent steps. All reported SAR data have been evaluated using the most updated IEEE/IEC 62704-1 SAR averaging protocol [17, 49]. As discussed earlier – once the Maxwell’s integral equations have been solved and electric field strengths on the edges of a grid cell are known, the average electric fields along all three axes are calculated. Next, the effective electric field at the grid centre is obtained and further utilized to calculate point  $SAR = \sigma|E|^2/2\rho$ . Next, a cubical volume is uniformly expanded along all three axes centering a particular grid cell to achieve the desired SAR averaging mass. In few cases, this cubical volume can include at most 10 percent background material near the structural boundaries – but, the background material mass is not taken into consideration to achieve the averaging mass. Thus, 1g or 10g averaged spatial SAR values have been calculated for a particular grid cell – this averaging technique is repeated positioning each valid grid cell at the centre of the averaging cube. Finally, 1g or 10g averaged spatial SAR distributions on and inside the prototyped mango fruits model have been obtained using the earlier calculated spatial averaged SAR data of all individual grid cells in the prototyped structure. This is how spatial SAR averaging has been performed in accordance with the IEEE/IEC 62704-1 SAR averaging protocol – more detailed descriptions are available in literature [17].

#### **4.4.2.4 Contrast among Different Electromagnetic Standards**

SAR value for the designed bunch of mango fruits model is expected to differ with incident electric field strength at any particular frequency. Therefore, the contrasts among different electromagnetic regulatory standards prescribed by FCC, ICNIRP, DoT (India) and Switzerland in terms of plane wave equivalent reference power density limit or equivalent electric field strength limit for public exposure have been outlined earlier in this chapter [9-12]. The plane wave equivalent reference power density limits at public zone differ by ten to hundred times across geographical boundaries based on the regulatory standards in effect (refer to Table 4.17) [9-12, 16]. In addition, the public exposure policies in Russia, Italy etc. are very strict like in Switzerland – thus, those electromagnetic policies haven’t been discussed here separately [12-15].

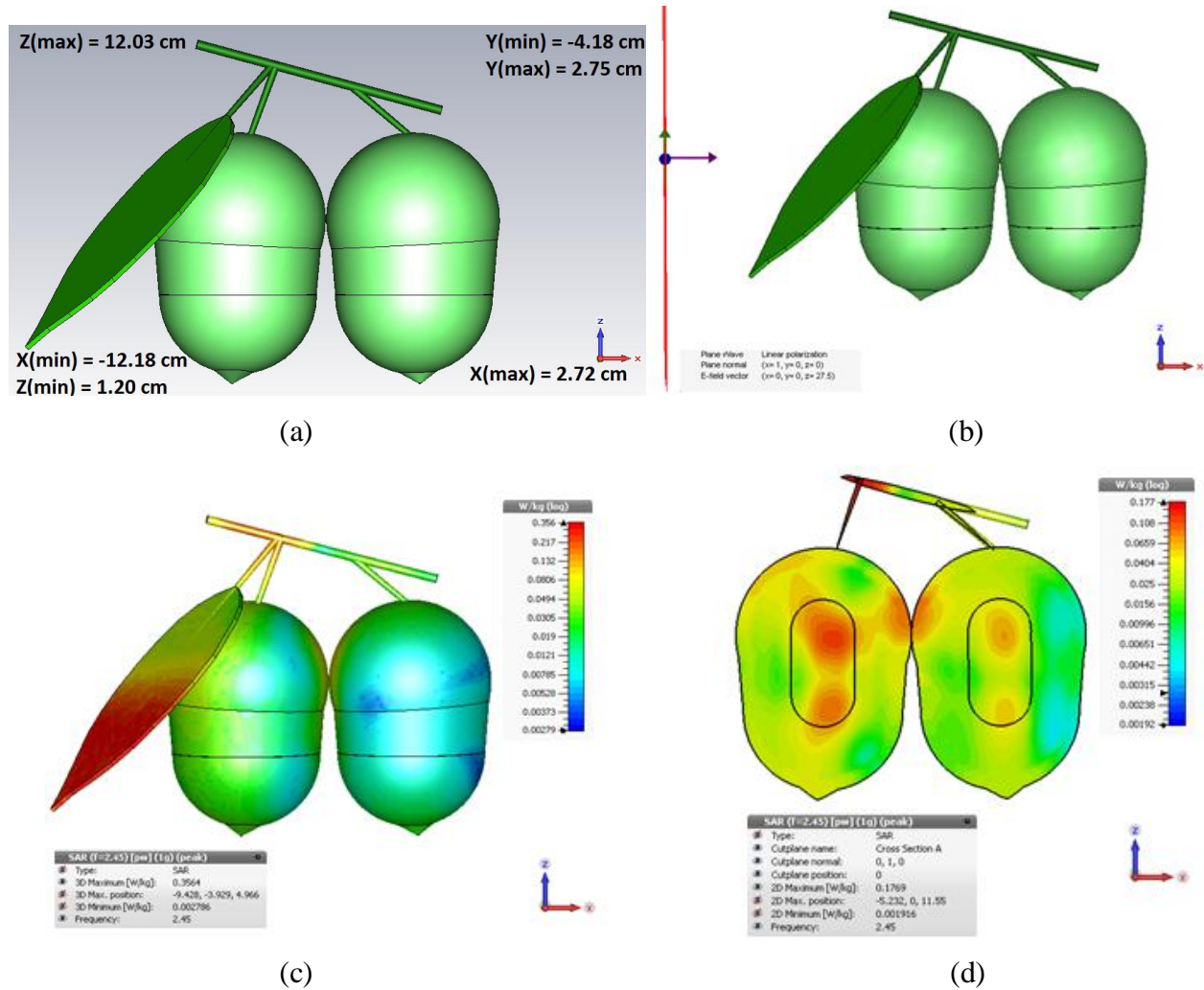


Fig. 4.32: (a) Three dimensional perspective of the designed bunch of mango fruits model with marked coordinates, (b) The bunch of mango fruits model is exposed to a linearly polarized plane wave propagating along  $x$ -axis and electric field along  $z$ -axis, (c) 1g SAR distribution on three dimensional surfaces of the bunch of mango fruits model at 2.45 GHz as per the existing Indian public scenario, (d) 1g SAR distribution on a two dimensional cut plane of the bunch of mango fruits model at 2.45 GHz as per the existing Indian public scenario

#### 4.4.2.5 SAR Data and Analysis

The dependence of SAR magnitude and its distribution inside the typical bunch of mango fruits model on reference power density limit, frequency of irradiation, direction of arrival and wave polarization has been investigated in this work. However, a prior discussion regarding typical SAR distribution on three dimensional external surfaces and on specific internal cut plane of the



Table 4.42 Comparative SAR data at 947.5 MHz for different directions of arrival and polarizations of incident wave

Frequency 947.5 MHz												
Direction and polarization of incident wave	FCC			ICNIRP			India			Swiss		
	MLP	1g	10g	MLP	1g	10g	MLP	1g	10g	MLP	1g	10g
	SAR	SAR	SAR	SAR	SAR	SAR	SAR	SAR	SAR	SAR	SAR	SAR
DoP: y = 1, E-field: z axis	6.97	0.87	0.47	5.22	0.65	0.35	0.52	0.06	0.035	0.05	0.006	0.003
DoP: y = -1, E-field: z axis	7.06	0.87	0.47	5.30	0.65	0.35	0.53	0.06	0.035	0.05	0.006	0.003
DoP: x = 1, E-field: z axis	6.55	1.06	0.61	4.91	0.80	0.46	0.49	0.08	0.046	0.04	0.008	0.004
DoP: x = -1, E-field: z axis	7.34	1.01	0.59	5.51	0.76	0.44	0.55	0.07	0.044	0.05	0.007	0.004
DoP: z = -1, E-field: y axis	1.38	0.41	0.20	1.03	0.31	0.15	0.10	0.03	0.015	0.01	0.003	0.001
DoP: z = -1, E-field: x axis	18.77	3.09	0.93	14.08	2.32	0.70	1.40	0.23	0.070	0.14	0.023	0.007

SAR is in W/kg

Table 4.43 Comparative SAR data at 1842.5 MHz for different directions of arrival and polarizations of incident wave

Frequency 1842.5 MHz												
Direction and polarization of incident wave	FCC			ICNIRP			India			Swiss		
	MLP	1g	10g	MLP	1g	10g	MLP	1g	10g	MLP	1g	10g
	SAR	SAR	SAR	SAR	SAR	SAR	SAR	SAR	SAR	SAR	SAR	SAR
DoP: y = 1, E-field: z axis	6.36	1.84	0.56	5.86	1.69	0.51	0.58	0.16	0.051	0.05	0.016	0.005
DoP: y = -1, E-field: z axis	5.95	1.01	0.46	5.48	0.93	0.43	0.54	0.09	0.043	0.05	0.009	0.004
DoP: x = 1, E-field: z axis	22.23	2.19	0.94	20.48	2.02	0.86	2.04	0.20	0.087	0.20	0.020	0.008
DoP: x = -1, E-field: z axis	22.61	1.90	0.83	20.83	1.75	0.77	2.08	0.17	0.077	0.20	0.017	0.007
DoP: z = -1, E-field: y axis	2.39	1.31	0.63	2.20	1.21	0.58	0.22	0.12	0.058	0.02	0.012	0.005
DoP: z = -1, E-field: x axis	16.11	2.30	1.11	14.84	2.12	1.02	1.48	0.21	0.102	0.14	0.021	0.010

SAR is in W/kg

bunch of mango fruits model is deemed necessary. Figs. 4.32(c) and (d) illustrate 1g averaged SAR distributions respectively on three dimensional surfaces and on specific two dimensional cut planes of prototyped bunch of mango fruits model at 2.45 GHz as per the existing Indian public exposure scenario [11]. The SAR distributions are consequences of linearly polarized plane wave irradiation with direction of propagation along the  $x$ -axis and electric field variation along the  $z$ -axis. It has been observed that the SAR value increases on and around regions with higher curvature or near dielectric boundaries. It is so because magnitude of charge accumulation tends to increase on surface region with greater curvature as obtained by solving Poisson's equation on and around the surface of an arbitrary shaped structure [75]. Local electric field distribution also follows a similar pattern due to such non uniform charge distribution i.e. electric

field strength at regions with greater charge density is greater in magnitude [76]. This phenomenon of concentrated electric field near sharp edges is not only true for conducting bodies but also applies to dielectric objects with reasonably high electrical conductivity / loss tangent [77]. Analysis of the scattering problem i.e. scattering of incident electromagnetic field due to a lossy dielectric body generally leads to an electric field distribution or equivalent induced surface current density that prefers to be in close vicinity of sharp edges – magnitude of surface current distribution is more in close vicinity of greater surface curvature. Hence, increased electromagnetic energy absorption rate near sharp geometries of prototype bunch of mangoes can cause localized effects and the same shouldn't be averaged over nearby masses with less electromagnetic energy absorption rates.

Table 4.44 Comparative SAR data at 2150 MHz for different directions of arrival and polarizations of incident wave

Frequency 2150 MHz												
Direction and polarization of incident wave	FCC			ICNIRP			India			Swiss		
	MLP	1g	10g	MLP	1g	10g	MLP	1g	10g	MLP	1g	10g
	SAR	SAR	SAR	SAR	SAR	SAR	SAR	SAR	SAR	SAR	SAR	SAR
DoP: y = 1, E-field: z axis	6.06	2.55	0.72	6.06	2.55	0.72	0.59	0.25	0.072	0.06	0.025	0.007
DoP: y = -1, E-field: z axis	5.20	1.10	0.46	5.20	1.10	0.46	0.51	0.10	0.046	0.05	0.011	0.004
DoP: x = 1, E-field: z axis	20.53	2.77	0.90	20.53	2.77	0.90	2.06	0.27	0.089	0.20	0.027	0.008
DoP: x = -1, E-field: z axis	18.21	1.54	0.61	18.21	1.54	0.61	1.80	0.15	0.061	0.18	0.015	0.006
DoP: z = -1, E-field: y axis	2.40	1.20	0.45	2.40	1.20	0.45	0.240	0.12	0.045	0.02	0.012	0.004
DoP: z = -1, E-field: x axis	16.42	2.39	1.06	16.42	2.39	1.06	1.62	0.23	0.106	0.16	0.023	0.010

SAR is in W/kg

Table 4.45 Comparative SAR data at 2350 MHz for different directions of arrival and polarizations of incident wave

Frequency 2350 MHz												
Direction and polarization of incident wave	FCC			ICNIRP			India			Swiss		
	MLP	1g	10g	MLP	1g	10g	MLP	1g	10g	MLP	1g	10g
	SAR	SAR	SAR	SAR	SAR	SAR	SAR	SAR	SAR	SAR	SAR	SAR
DoP: y = 1, E-field: z axis	7.40	3.02	0.81	7.40	3.02	0.81	0.71	0.29	0.080	0.07	0.030	0.008
DoP: y = -1, E-field: z axis	6.31	1.00	0.45	6.31	1.00	0.45	0.61	0.10	0.045	0.06	0.010	0.004
DoP: x = 1, E-field: z axis	21.76	3.24	0.89	21.76	3.24	0.89	2.09	0.31	0.088	0.21	0.032	0.008
DoP: x = -1, E-field: z axis	17.87	1.23	0.49	17.87	1.23	0.49	1.73	0.12	0.050	0.17	0.012	0.004
DoP: z = -1, E-field: y axis	2.98	1.51	0.46	2.98	1.51	0.46	0.29	0.14	0.046	0.02	0.015	0.004
DoP: z = -1, E-field: x axis	14.02	2.61	1.07	14.02	2.61	1.07	1.39	0.25	0.106	0.13	0.026	0.010

SAR is in W/kg

Table 4.46 Comparative SAR data at 2450 MHz for different directions of arrival and polarizations of incident wave

Frequency 2450 MHz												
Direction and polarization of incident wave	FCC			ICNIRP			India			Swiss		
	MLP	1g	10g	MLP	1g	10g	MLP	1g	10g	MLP	1g	10g
	SAR	SAR	SAR	SAR	SAR	SAR	SAR	SAR	SAR	SAR	SAR	SAR
DoP: y = 1, E-field: z axis	8.20	3.36	0.87	8.20	3.36	0.87	0.82	0.33	0.087	0.08	0.033	0.008
DoP: y = -1, E-field: z axis	7.81	1.05	0.43	7.81	1.05	0.43	0.78	0.10	0.043	0.07	0.010	0.004
DoP: x = 1, E-field: z axis	24.11	3.56	0.92	24.11	3.56	0.92	2.41	0.35	0.092	0.24	0.035	0.009
DoP: x = -1, E-field: z axis	17.30	1.09	0.44	17.30	1.09	0.44	1.73	0.10	0.044	0.17	0.011	0.004
DoP: z = -1, E-field: y axis	2.97	1.68	0.45	2.97	1.68	0.45	0.29	0.16	0.045	0.03	0.016	0.004
DoP: z = -1, E-field: x axis	15.76	2.69	1.08	15.76	2.69	1.08	1.57	0.26	0.10	0.15	0.026	0.010
												SAR is in W/kg

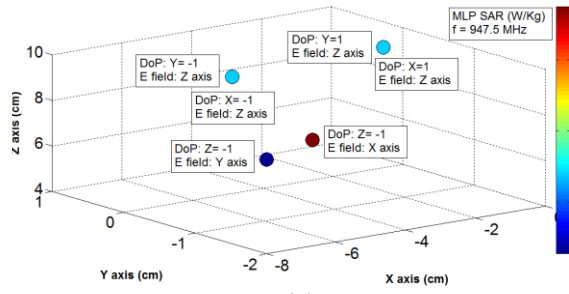
Next, let's consider the effect of reference power density limit which is regulated by the electromagnetic standards in effect; SAR data have been estimated for the prototyped bunch of mango fruits model over five different frequencies in accordance with the FCC and ICNIRP prescribed international public exposure standards [9-10]. In addition, SAR data have also been simulated as per the existing Indian and Swiss national public electromagnetic regulatory policies (refer to Table 4.17) [11-12]. It is noted that for a particular combination of frequency, direction of incidence and wave polarization, SAR values for the bunch of mango fruits model are widely contrasting in nature depending upon the reference power density limit (i.e. the regulatory standards) in effect. Data presented in Table 4.42 to Table 4.46 illustrate that SAR value increases proportionately with the prescribed reference power density limit irrespective of frequency of irradiation. Thus, be it MLP SAR, 1g averaged SAR or 10g averaged SAR, it is always maximum corresponding to public exposure in accordance with the FCC standards [9]; however SAR data are also quite high as per the ICNIRP norms for public exposure (below 1500 MHz) and at par with the FCC standards beyond 1500 MHz [10]. Simulated SAR data in accordance with the existing Indian scenario have been noted to be moderate at 1/10<sup>th</sup> levels of the ICNIRP scenario [10-11]. The most stringent SAR values have been noted as per the Swiss public exposure standards at 1/100<sup>th</sup> levels of the ICNIRP scenario [10, 12]. Both reference power density and SAR value are dependent upon second degree of electric field strength magnitude at their respective points of measurement; hence, contrast in SAR value for the designed bunch of mango fruits model exactly follows contrasting nature of the reference power

density limits as per the above mentioned international and national electromagnetic regulatory standards [9-12].

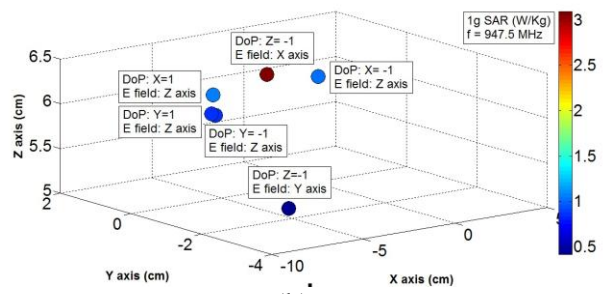
Frequency of irradiation is the second factor that significantly contributes to the SAR magnitude variation along with its distribution in the prototyped bunch of mango fruits model. Keeping all other factors unchanged, SAR magnitude in general varies with the frequency of irradiation as noted in Table 4.42 to Table 4.46. Moreover, the spatial SAR distribution along with the position of maximum SAR shifts inside the prototyped bunch of mango fruits model with frequency of irradiation – as illustrated in Figs. 4.33(a) to (p) and Figs. 4.34(a) to (p). The realized wavelength inside biological tissue layers decreases with increase in frequency of irradiation; as a consequence, more number of peak formations occurs inside the bunch of mango fruits model. Moreover, the maximum permissible reference power density limit increases with frequency of irradiation up to 1500 MHz [9-12]; both these factors influence resultant SAR value. As a consequence, 1g and 10g averaged SAR values increase considerably from 947.5 MHz to 1842.5 MHz (as seen in Table 4.42 to Table 4.43) and thereafter varies at a lower rate with frequency of irradiation.

The magnitude of electromagnetic energy absorption rate and its distribution not only depend upon the reference power density limit and frequency of irradiation – rather, the direction of arrival and polarization of incident wave are also two crucial factors in determining SAR value and its distribution. It is so because plant and fruit structures are mostly asymmetric in nature. Observations in Figs. 4.33(a) to (p), Figs. 4.34(a) to (p) and Tables 4.42-4.47 indicate that the magnitudes of MLP SAR, 1g averaged SAR, 10g averaged SAR and their distributions significantly differ due to six different combinations of direction of arrival and polarization of incident wave. The respective maximum variations in MLP SAR, 1g averaged SAR, 10g averaged SAR and WBA SAR are 9.46 times, 2.27 times, 2.37 times and 1.79 times at 1842.5 MHz due to alterations in direction of arrival and incident wave polarization. Similar variations in electromagnetic energy absorption rate due to different combinations of direction of arrival and polarization of incident wave have been observed at all the other frequencies as well (refer to Table 4.47).

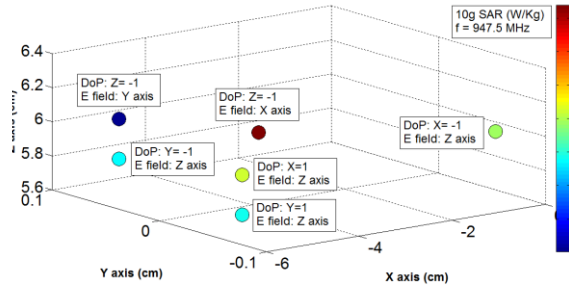
# Specific Absorption Rate Evaluation for Prototyped Fruit and Plant Models



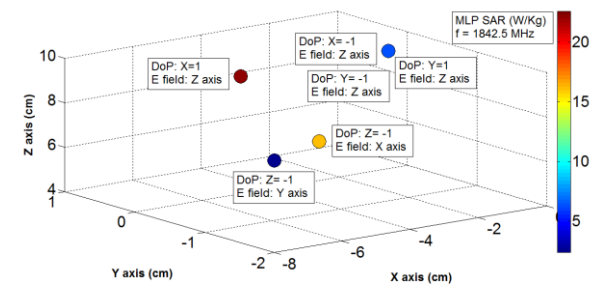
(a)



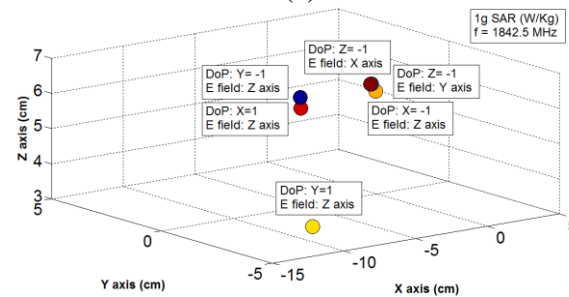
(b)



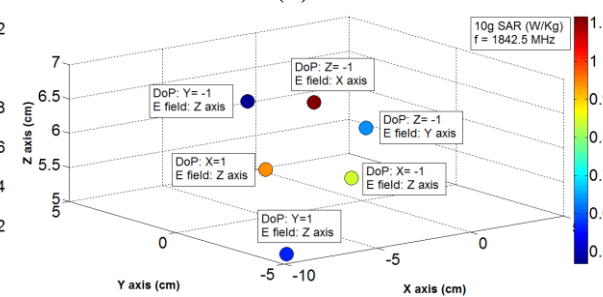
(c)



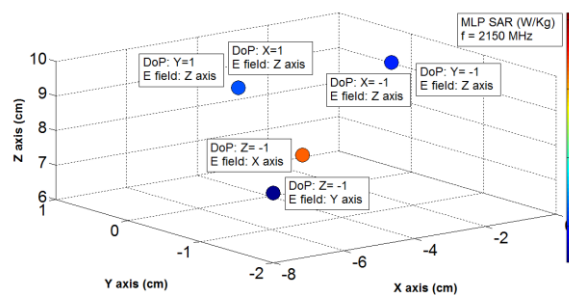
(d)



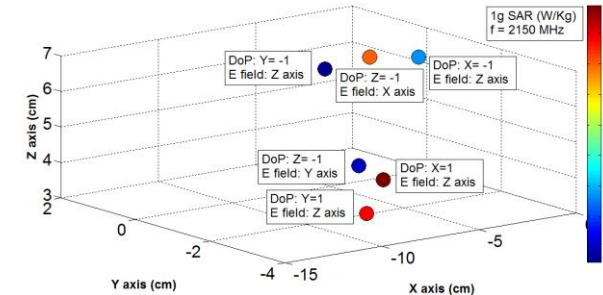
(e)



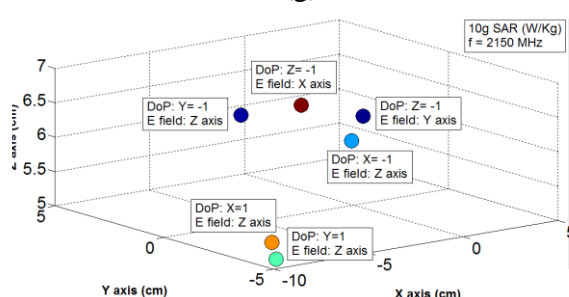
(f)



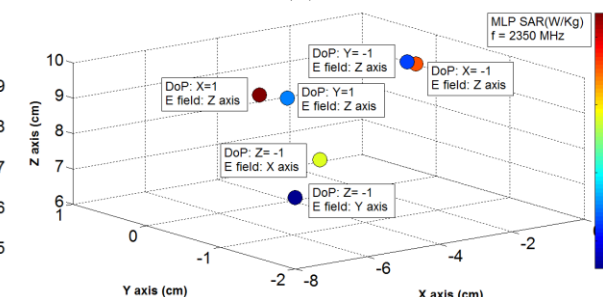
(g)



(h)



(i)



(j)

Continued.

## Specific Absorption Rate Evaluation for Prototyped Fruit and Plant Models

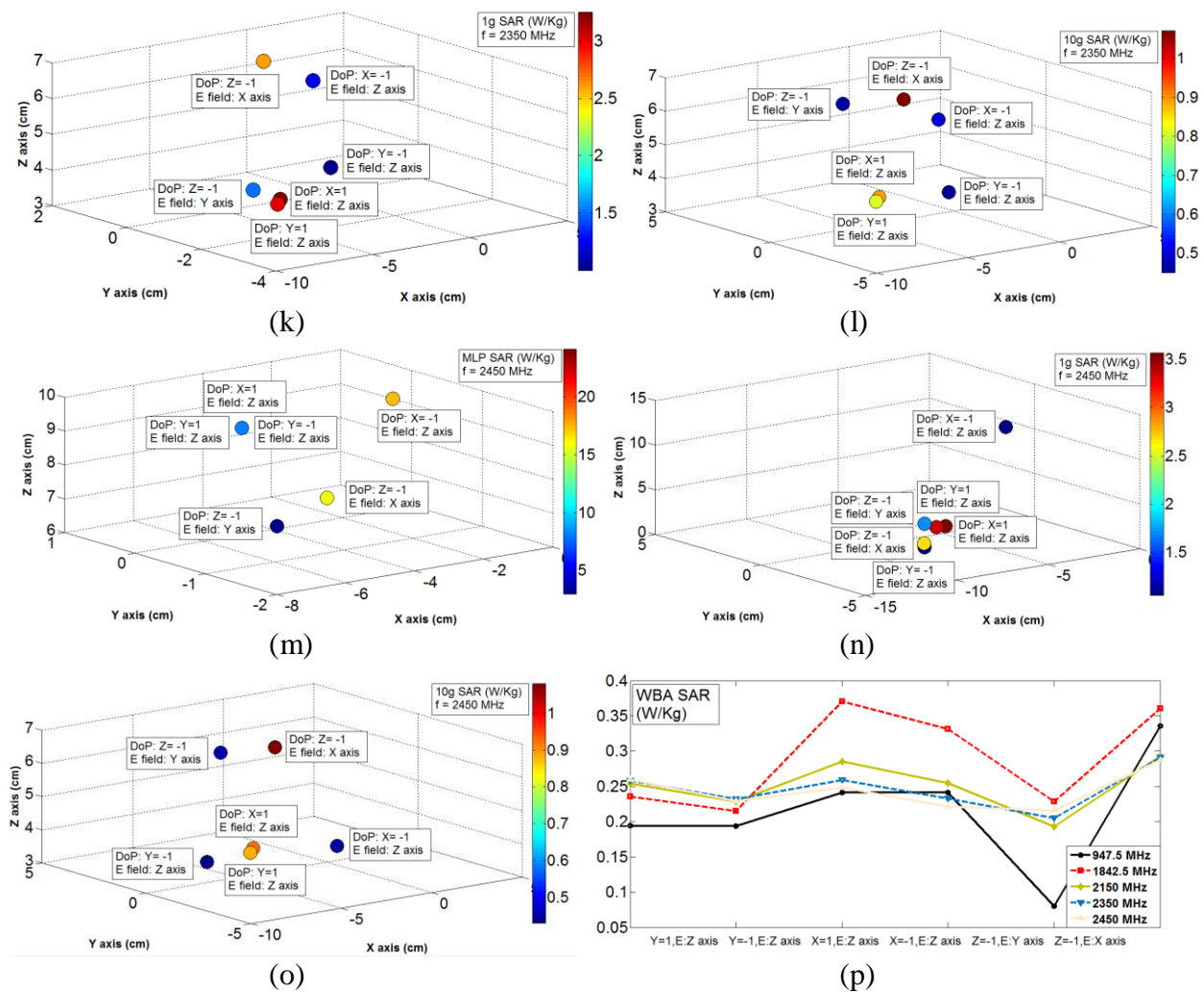
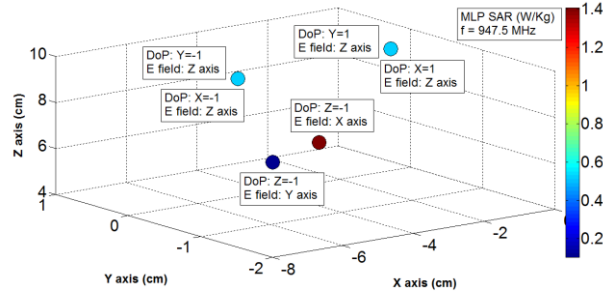
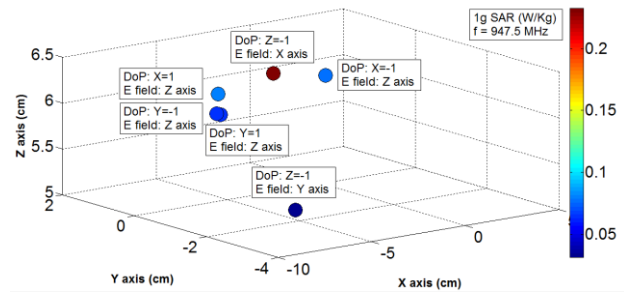


Fig. 4.33: SAR data as per the FCC public electromagnetic standards (a) to (c) MLP SAR, 1g averaged and 10g averaged SAR distribution at 947.5 MHz due to variations in direction of arrival and polarization; (d) to (f) MLP SAR, 1g averaged and 10g averaged SAR distribution at 1842.5 MHz due to variations in direction of arrival and polarization; (g) to (i) MLP SAR, 1g averaged and 10g averaged SAR distribution at 2150 MHz due to variations in direction of arrival and polarization; (j) to (l) MLP SAR, 1g averaged and 10g averaged SAR distribution at 2350 MHz due to variations in direction of arrival and polarization; (m) to (o) MLP SAR, 1g averaged and 10g averaged SAR distribution at 2450 MHz due to variations in direction of arrival and polarization; (p) WBA SAR data over all five frequencies due to variations in direction of arrival and polarization

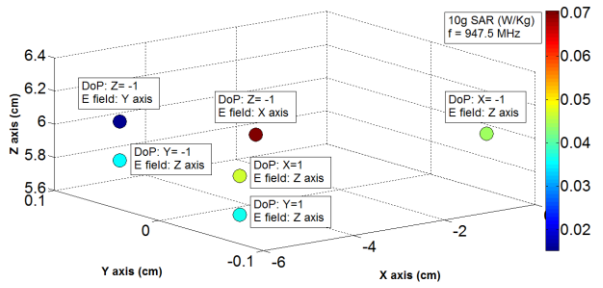
# Specific Absorption Rate Evaluation for Prototyped Fruit and Plant Models



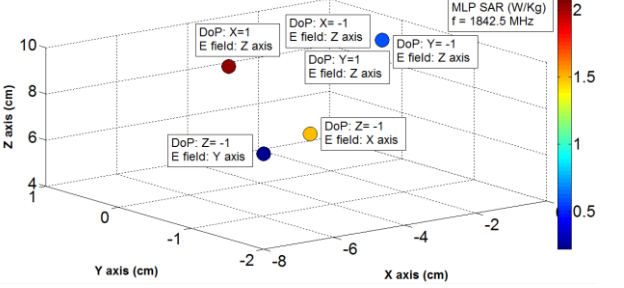
(a)



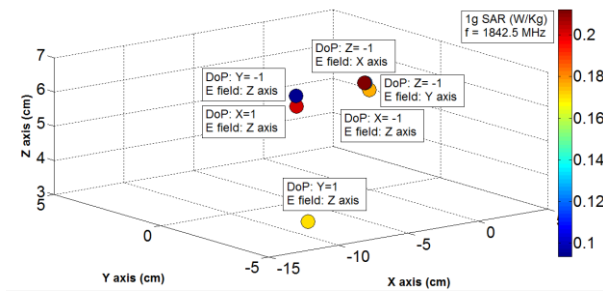
(b)



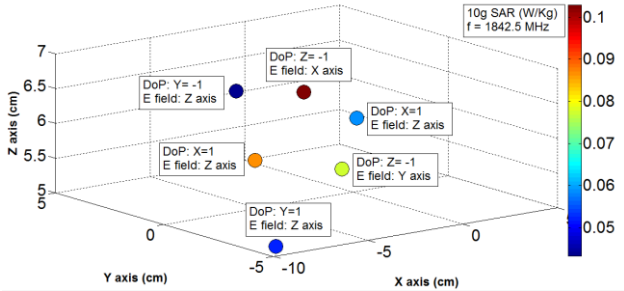
(c)



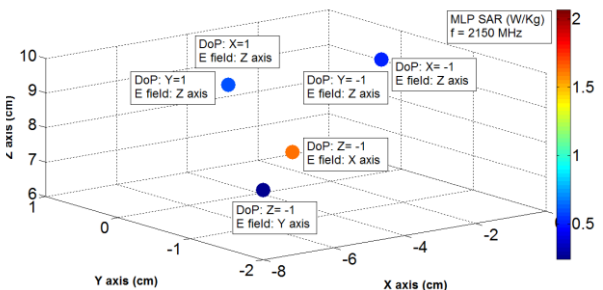
(d)



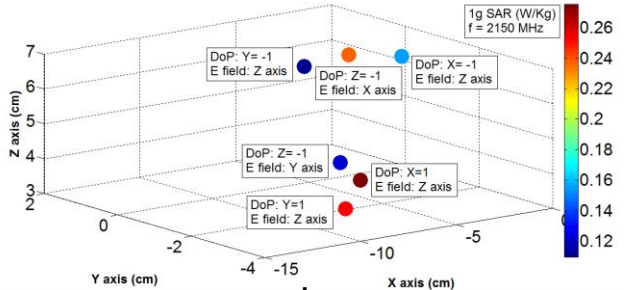
(e)



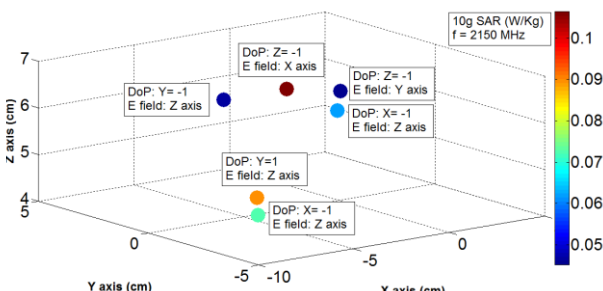
(f)



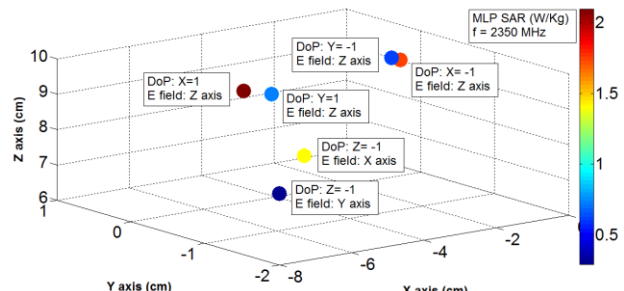
(g)



(h)



(i)



(j)

Continued.



# Specific Absorption Rate Evaluation for Prototyped Fruit and Plant Models

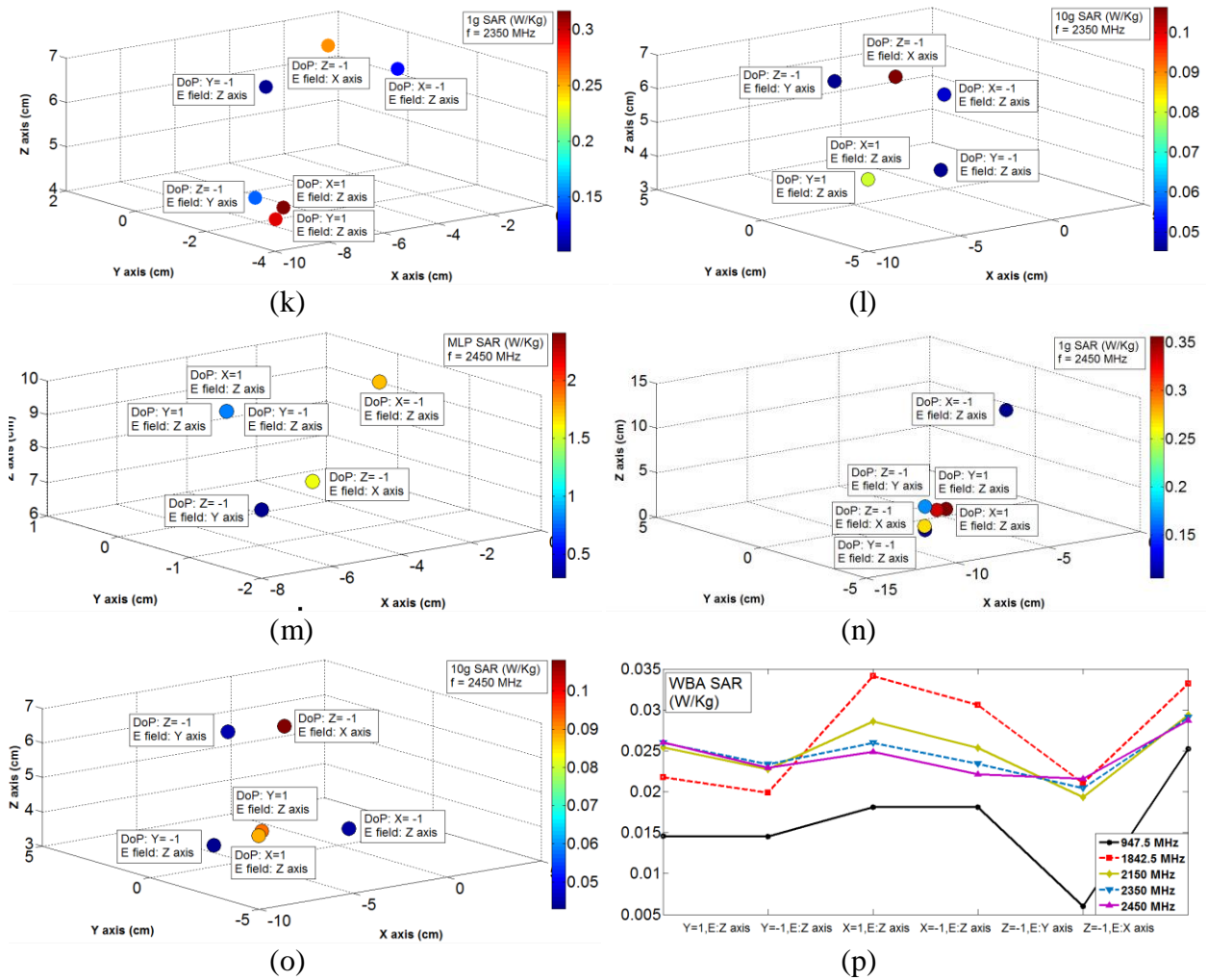


Fig. 4.34: SAR data as per the existing Indian public electromagnetic standards (a) to (c) MLP SAR, 1g averaged and 10g averaged SAR distribution at 947.5 MHz due to variations in direction of arrival and polarization; (d) to (f) MLP SAR, 1g averaged and 10g averaged SAR distribution at 1842.5 MHz due to variations in direction of arrival and polarization; (g) to (i) MLP SAR, 1g averaged and 10g averaged SAR distribution at 2150 MHz due to variations in direction of arrival and polarization; (j) to (l) MLP SAR, 1g averaged and 10g averaged SAR distribution at 2350 MHz due to variations in direction of arrival and polarization; (m) to (o) MLP SAR, 1g averaged and 10g averaged SAR distribution at 2450 MHz due to variations in direction of arrival and polarization; (p) WBA SAR data over all five frequencies due to variations in direction of arrival and polarization



Table 4.47 Typical Max-to-Min SAR ratio for different combinations of direction of arrival and polarization of incident wave

Frequency (MHz)	Typical Max/Min SAR ratio for different combinations of direction of arrival and polarization of incident field			
	MLP SAR	1g SAR	10g SAR	WBA SAR
947.5	13.66	7.48	4.66	4.16
1842.5	9.46	2.27	2.37	1.79
2150	8.55	2.51	2.35	1.52
2350	7.30	3.24	2.37	1.45
2450	8.11	3.39	2.51	1.32

The reported data in Table 4.47 strongly indicate that limiting the reference power density level or the equivalent electric field strength is inadequate to correlate with SAR value and ensure safety of plants, crops and fruits in far field region; because, electromagnetic energy absorption rate in asymmetric bunch of mango fruits model is largely dependent upon the direction of arrival and polarization of incident wave. Hence, direct adoption of basic SAR limit for all living bodies is more logical even in far field.

#### 4.4.2.6 Conclusions

All reported SAR data have been estimated for public exposure in accordance with different international and national electromagnetic regulatory standards. However, it must be noted that the reference power density limits are much liberal in case of occupational exposure scenario; as a consequence, estimated SAR values would increase five times or so for such exposure scenario [9-10]. Furthermore, SAR values are additive in nature over multiple frequency bands of irradiation; hence, restriction should also be imposed to limit the cumulative SAR value instead of SAR estimated for a single frequency of irradiation.

Electromagnetic energy absorption rate inside the prototyped bunch of mango fruits model considerably varies depending upon each of these factors – i.e. reference power density, frequency, direction of arrival and polarization of incident wave. Proportionate disagreement in SAR magnitude due to discrepancy in reference power density limit as per the different

international and national guidelines indicates the need of uniform regulatory guidelines worldwide [16]. In addition, magnitude as well as spatial distribution of SAR varies significantly with frequency of irradiation. In general, SAR magnitude increases with frequency of irradiation because of enhanced reference power density limits (up to 2000 MHz) and increased number of peak formations due to reduced wavelength in biological tissues. Plant and fruit structures are reasonably asymmetric in nature – as a consequence, magnitude and spatial distribution of SAR inside the bunch of mango fruits model crucially vary with direction of arrival and polarization of incident wave. The ratios of maximum SAR magnitude to minimum SAR magnitude at different frequencies have been noted to be quite significant – as reported in Table 4.47. In addition, significant variations in spatial SAR distribution due to different directions of arrival and polarizations of incident wave have also been reported. Hence, uniform electromagnetic regulatory standards should be adopted worldwide – in addition, direct adoption of maximum allowable SAR limits is preferable even for plant and fruit structures as they are quite asymmetric in nature.

## References

- [1] R. J. Aitken, L. E. Bennetts, D. Sawyer, A. M. Wiklendt, and B. V. King, ‘Impact of Radio Frequency Electromagnetic Radiation on DNA Integrity in the Male Germline’, *International Journal of Andrology*, Vol. 28, No. 3, pp. 171-179, 2005.
- [2] E. Beaubois, S. Girard, S. Lallechere, E. Davies, F. Paladian, P. Bonnet, G. Ledoigt, and A. Vian, ‘Intercellular Communication in Plants: Evidence for Two Rapidly Transmitted Systemic Signals Generated in Response to Electromagnetic Field Stimulation in Tomato’, *Plant, Cell and Environment*, Vol. 30, No. 7, pp. 834-844, 2007.
- [3] A. Balmori, ‘Electromagnetic Pollution from Phone Masts. Effects on Wildlife’, *Pathophysiology*, Vol. 16, No. 2-3, pp. 191-199, 2009.
- [4] D. J. Panagopoulos, E. D. Chavdoula, and L. H. Margaritis, ‘Bioeffects of Mobile Telephony Radiation in Relation to its Intensity or Distance from the Antenna’, *International Journal of Radiation Biology*, Vol. 86, No. 5, pp. 345-357, 2010.
- [5] G. Kumar, ‘Report on Cell Tower Radiation’, submitted to the secretary, Department of Telecommunications (DoT), Ministry of Communications, New Delhi, India, 2010.

- [6] BioInitiative Working Group, '*BioInitiative 2012: A Rationale for a Biologically-Based Exposure Standards for Low-Intensity Electromagnetic Radiation*', In C. Sage, and D. O. Carpenter (eds): The BioInitiative Report 2012, 2012. [www.bioinitiative.org](http://www.bioinitiative.org) [Last accessed 03 April 2022].
- [7] S. Sivani, and D. Sudarsanam, 'Impacts of Radio-Frequency Electromagnetic Field (RF-EMF) from Cell Phone Towers and Wireless Devices on Biosystem and Ecosystem – A Review', *Biology and Medicine*, Vol. 4, No. 4, pp. 202-216, 2012.
- [8] S. Cucurachi, W. L. Tamis, M. G. Vijver, W. J. Peijnenburg, J. F. Bolte, and G. R. de Snoo, 'A Review of the Ecological Effects of Radiofrequency Electromagnetic Fields (RF-EMF)', *Environment International*, Vol. 51, pp. 116-140, 2013.
- [9] R. F. Cleveland, Jr., D. M. Sylvar, and J. L. Ulcek, '*Evaluating Compliance with FCC Guidelines for Human Exposure to Radiofrequency Electromagnetic Fields*', FCC OET Bulletin, Vol. 65, Edition 97-01, Washington D.C., 1997.
- [10] International Commission on Non-Ionizing Radiation Protection (ICNIRP), 'Guidelines for Limiting Exposure to Electromagnetic Fields (100 kHz to 300 GHz)', *Health Physics*, Vol. 118, No. 5, pp. 483-524, 2020.
- [11] Department of Telecommunications (DoT), '*A Journey for EMF*', 2012, [www.dot.gov.in/journey-emf](http://www.dot.gov.in/journey-emf) [Last accessed 03 April 2022].
- [12] Swiss Agency for the Environment, Forests and Landscape (SAEFL), '*Electrosmog in the Environment*', pp. 1-56, Switzerland, 2005.
- [13] Ministry of Health of the Russian Federation, '*SanPiN 2.1.8/2.2.4.1190-03: Arrangement and Operation of Land Mobile Radiocommunication Facilities – Hygienic Requirements*', pp. 1-17, Russia, 2003.
- [14] The President of the Council of Ministers (Italy), '*Establishment of Exposure Limits, Attention Values, and Quality Goals to Protect the Population against Electric, Magnetic, and Electromagnetic Field Generated at Frequencies between 100 kHz and 300 GHz*', unofficial translation by P. Vecchia, pp. 1-6, Italy, 2003.
- [15] P. Vecchia, 'Radiofrequency Fields: Bases for Exposure Limits', 2 *European IRPA Congress on Radiation Protection – Radiation Protection: From Knowledge to Action*, pp. 1-19, Paris, 2006.

- [16] K. R. Foster, 'Exposure Limits for Radiofrequency Energy: Three Models', *Proceedings of the Eastern European Regional EMF Meeting and Workshop (Criteria for EMF Standards Harmonization)*, pp. 1-6, Varna, Bulgaria, 2001.
- [17] IEC/IEEE, '*IEC/IEEE International Standard – Determining the Peak Spatial-Average Specific Absorption Rate (SAR) in the Human Body from Wireless Communications Devices, 30 MHz to 6 GHz - Part 1: General Requirements for using the Finite-Difference Time-Domain (FDTD) Method for SAR Calculations*', IEC/IEEE 62704-1:2017, pp 1-86, 2017, <https://webstore.iec.ch/publication/34411> (subscription required)
- [18] IEC/IEEE, '*IEC/IEEE International Standard – Determining the Peak Spatial-Average Specific Absorption Rate (SAR) in the Human Body from Wireless Communications Devices, 30 MHz To 6 GHz – Part 2: Specific Requirements for Finite Difference Time Domain (FDTD) Modelling of Exposure from Vehicle Mounted Antennas*', IEC/IEEE 62704-2:2017, pp 1-112, 2017, <https://webstore.iec.ch/publication/31306> (subscription required)
- [19] S. S. Stuchly, M. A. Stuchly, A. Kraszewski, and G. Hartsgrove, 'Energy Deposition in a Model of Man: Frequency Effects', *IEEE Transactions on Biomedical Engineering*, Vol. 33, No. 7, 1986.
- [20] K. Meier, V. Hombach, R. Kästle, R. Y. Tay, and N. Kuster, 'The Dependence of Electromagnetic Energy Absorption upon Human-Head Modelling at 1800 MHz', *IEEE Transactions on Microwave Theory and Techniques*, Vol. 45, No. 11, 1997.
- [21] T. Yelkenci, 'Effects of Metallic Objects on Specific Absorption Rate in the Human Head for 915 and 1900 MHz Mobile Phones', *Frequenz*, Vol. 60, No. 3-4, pp. 46-50, 2006.
- [22] O. P. Gandhi, 'Yes the Children are More Exposed to Radiofrequency Energy from Mobile Telephones than Adults', *IEEE Access*, Vol. 3, pp. 985-988, 2015.
- [23] R. Takei, T. Nagaoka, K. Saito, S. Watanabe, and M. Takahashi, 'SAR Variation due to Exposure from a Smartphone Held at Various Positions Near the Torso', *IEEE Trans. Electromagnetic Compatibility*, Vol. 59, No. 2, pp. 747-753, 2017.
- [24] J. Cooper, B. Marx, J. Buhl, and V. Hombach, 'Determination of Safety Distance Limits for a Human near a Cellular Base Station Antenna, Adopting the IEEE Standard or ICNIRP Guidelines', *Bioelectromagnetics*, Vol. 23, No. 6, pp. 429-443, 2002.
- [25] A. Christ, A. Klingeböck, T. Samaras, C. Goiceanu, and N. Kuster, 'The Dependence of Electromagnetic Far-Field Absorption on Body Tissue Composition in the Frequency Range

from 300 MHz to 6 GHz', *IEEE Transactions on Microwave Theory and Techniques*, Vol. 54, No. 5, 2006.

[26] M. A. A. Karunarathna, and I. J. Dayawansa, 'Energy Absorption by the Human Body from RF and Microwave Emissions in Sri Lanka', *Sri Lankan Journal of Physics*, Vol. 7, pp. 35-47, 2006.

[27] A. Hirata, S. Kodera, J. Wang, and O. Fujiwara, 'Dominant Factors Influencing Whole-Body Average SAR Due to Far-Field Exposure in Whole-Body Resonance Frequency and GHz Regions', *Bioelectromagnetics*, Vol. 28, No. 6, pp. 484-487, 2007.

[28] A. Hirata, N. Ito, O. Fujiwara, T. Nagaoka, and S. Watanabe, 'Conservative Estimation of Whole-Body-Averaged SARs in Infants with a Homogeneous and Simple-Shaped Phantom in the GHz Region', *Physics in Medicine and Biology*, Vol. 53, No. 24, pp. 7215-7223, 2008.

[29] T. Iyama, T. Onishi, Y. Tarusawa, and S. Uebayashi and T. Nojima, 'Novel Specific Absorption Rate (SAR) Measurement Method Using a Flat Solid Phantom', *IEEE Transactions on Electromagnetic Compatibility*, Vol. 50, No. 1, pp. 43-51, 2008.

[30] T. Wessapan, S. Srisawatdhisukul, and P. Rattanadecho, 'Specific Absorption Rate and Temperature Distributions in Human Head Subjected to Mobile Phone Radiation at Different Frequencies', *International Journal of Heat and Mass Transfer*, Vol. 55, No. 1-3, pp. 347-359, 2012.

[31] T. Wessapan, and P. Rattanadecho, 'Specific Absorption Rate and Temperature Increase in the Human Eye due to Electromagnetic Fields Exposure at Different Frequencies', *International Journal of Heat and Mass Transfer*, Vol. 64, pp. 426-435, 2013.

[32] S. O. Nelson, 'Microwave Dielectric Properties of Fresh Fruits and Vegetables', *Transactions of the ASAE*, Vol. 23, No. 5, pp. 1314-1317, 1980.

[33] W. Kuang, and S. O. Nelson, 'Dielectric Relaxation Characteristics of Fresh Fruits and Vegetables from 3 to 20 GHz', *Journal of Microwave Power and Electromagnetic Energy*, Vol. 32, No. 2, pp. 114-122, 1997.

[34] S. O. Nelson, 'Dielectric Properties of Agricultural Products – Measurements and Applications', *IEEE transactions on Electrical Insulation*, Vol. 26, No. 5, pp.845-869, 1991.

[35] S. O. Nelson, 'Measuring Dielectric Properties of Fresh Fruits and Vegetables', *IEEE Antennas and Propagation Society International Symposium. Digest. Held in conjunction with:*

*USNC/CNC/URSI North American Radio Sci. Meeting (Cat. No. 03CH37450)*, Vol. 4, pp. 46-49, June, 2003.

[36] S. O. Nelson, 'Dielectric Spectroscopy of Fresh Fruits and Vegetables', *2005 IEEE Instrumentation and Measurement Technology Conference (IMTC)*, pp. 360-364, Ottawa, Canada, May, 2005.

[37] W. C. Guo, S. O. Nelson, S. Trabelsi, and S. J. Kays, '10–1800-MHz Dielectric Properties of Fresh Apples during Storage', *Journal of Food Engineering*, Vol. 83, No. 4, pp. 562-569, 2007.

[38] S. O. Nelson, and S. Trabelsi, 'Dielectric Spectroscopy Measurements on Fruit, Meat, and Grain', *Transactions of the ASABE*, Vol. 51, No. 5, pp. 1829-1834, 2008.

[39] S. O. Nelson, 'Dielectric Properties of Agricultural Products and Some Applications', *Research in Agricultural Engineering*, Vol. 54, No. 2, pp. 104-112, 2008.

[40] D. Roux, A. Vian, S. Girard, P. Bonnet, F. Paladian, E. Davies, and G. Ledoigt, 'Electromagnetic Fields (900 MHz) Evoke Consistent Molecular Responses in Tomato Plants', *Physiologia Plantarum*, Vol. 128, No. 2, pp. 283-288, 2006.

[41] A. Vian, D. Roux, S. Girard, P. Bonnet, F. Paladian, E. Davies, and G. Ledoigt, 'Microwave Irradiation Affects Gene Expression in Plants', *Plant Signaling & Behavior*, Vol. 1, No. 2, pp. 67-69, 2006.

[42] A. Vian, C. Faure, S. Girard, E. Davies, F. Hallé, P. Bonnet, G. Ledoigt, and F. Paladian, 'Plants Respond to GSM-Like Radiations', *Plant Signaling & Behaviour*, Vol. 2, No. 6, pp. 522-524, 2007.

[43] D. Roux, C. Faure, P. Bonnet, S. Girard, G. Ledoigt, E. Davies, M. Gendraud, F. Paladian, and A. Vian, 'A Possible Role for Extra-Cellular ATP in Plant Responses to High Frequency, Low Amplitude Electromagnetic Field', *Plant Signaling & Behaviour*, Vol. 3, No. 6, pp. 383-385, 2008.

[44] D. Roux, A. Vian, S. Girard, P. Bonnet, F. Paladian, E. Davies, and G. Ledoigt, 'High Frequency (900MHz) Low Amplitude (5V m<sup>-1</sup>) Electromagnetic Field: A Genuine Environmental Stimulus that Affects Transcription, Translation, Calcium and Energy Charge in Tomato', *Planta*, Vol. 227, No. 4, pp. 883-891, 2008.

- [45] S. Cucurachi, W. L. Tamis, M. G. Vijver, W. J. Peijnenburg, J. F. Bolte, and G. R. de Snoo, 'A Review of the Ecological Effects of Radiofrequency Electromagnetic Fields (RF-EMF)', *Environment International*, Vol. 51, pp. 116-140, 2013.
- [46] M. N. Halgamuge, S. K. Yak, and J. L. Eberhardt, 'Reduced Growth of Soybean Seedlings after Exposure to Weak Microwave Radiation from GSM 900 Mobile Phone and Base Station', *Bioelectromagnetics*, Vol. 36, No. 2, pp. 87-95, 2015.
- [47] A. Grémiaux, S. Girard, V. Guérin, J. Lothier, F. Baluska, E. Davies, P. Bonnet, A. Vian, 'Low-Amplitude, High-Frequency Electromagnetic Field Exposure Causes Delayed and Reduced Growth in *Rosa hybrida*', *Journal of Plant Physiology*, Vol. 190, pp. 44-53, 2016.
- [48] A. Vian, E. Davies, M. Gendraud, and P. Bonnet, 'Plant responses to High Frequency Electromagnetic Fields', *BioMed Research International*, Article ID: 1830262, 2016.
- [49] CST Studio Suite, [www.3ds.com/products-services/simulia/products/cst-studio-suite](http://www.3ds.com/products-services/simulia/products/cst-studio-suite) [Last accessed 04 April 2022].
- [50] T. Weiland, 'A Discretization Method for the Solution of Maxwell's Equations for Six-Component Fields', *Electronics and Communications AEU*, Vol. 31, No. 3, pp. 116-120, 1977.
- [51] M. Clemens, and T. Weiland, 'Discrete Electromagnetism with the Finite Integration Technique', *Progress In Electromagnetics Research*, Vol. 32, pp. 65-87, 2001.
- [52] G. Deschamps, 'Impedance of an Antenna in a Conducting Medium', *IRE Transactions on Antennas and Propagation*, Vol. 10, No. 5, pp. 648-650, 1962.
- [53] L. Liu, D. Xu, and Z. Jiang, 'Improvement in Dielectric Measurement Technique of Open-Ended Coaxial Line Resonator Method', *Electronics Letters*, Vol. 22, No. 7, pp. 373-375, 1986.
- [54] D. Xu, L. Liu, and Z. Jiang, 'Measurement of the Dielectric Properties of Biological Substances using an Improved Open-Ended Coaxial Line Resonator Method', *IEEE Transactions on Microwave Theory and Techniques*, Vol. 35, No. 12, pp. 1424-1428, 1987.
- [55] M. A. Stuchly, and S. S. Stuchly, 'Coaxial Line Reflection Method for Measuring Dielectric Properties of Biological Substances at Radio and Microwave Frequencies – A Review', *IEEE Transactions on Instrumentation and Measurement*, Vol. 29, No. 3, pp 176-183, 1980.
- [56] T. W. Athey, M. A. Stuchly, and S. S. Stuchly, 'Measurement of Radio Frequency Permittivity of Biological Tissues with an Open-Ended Coaxial Line: Part I', *IEEE Transactions on Microwave Theory and Techniques*, Vol. 30, No. 1, pp 82-86, 1982.

- [57] M. A. Stuchly, T. W. Athey, G. M. Samaras, and G. E. Taylor, 'Measurement of Radio Frequency Permittivity of Biological Tissues with an Open-Ended Coaxial Line: Part II - Experimental Results', *IEEE Transactions on Microwave Theory and Techniques*, Vol. 30, No. 1, pp. 87-92, 1982.
- [58] D. M. Hagl, D. Popovic, S. C. Hagness, J. H. Booske, and M. Okoniewski, 'Sensing Volume of Open-Ended Coaxial Probes for Dielectric Characterization of Breast Tissue at Microwave Frequencies', *IEEE Transactions on Microwave Theory and Techniques*, Vol. 51, No. 4, pp. 1194-1206, 2003.
- [59] R. Zajíček, J. Vrba, and K. Novotný; 'Evaluation of A Reflection Method on an Open-Ended Coaxial Line and its Use in Dielectric Measurements', *Acta Polytechnica*, Vol. 46, No. 5, pp. 50-54, 2006.
- [60] R. Zajíček, L. Oppl, and J. Vrba, 'Broadband Measurement of Complex Permittivity using Reflection Method and Coaxial Probes', *Radioengineering*, Vol.17, No. 1, pp. 14-19, 2008.
- [61] J. S. Bobowski, and T. Johnson, 'Permittivity Measurements of Biological Samples by an Open-Ended Coaxial Line', *Progress in Electromagnetics Research B*, Vol. 40, pp. 159-183, 2012.
- [62] S. O. Nelson, and P. G. Bartley (Jr.), 'Open-Ended Coaxial-Line Permittivity Measurements on Pulverized Materials', *IEEE Transactions on Instrumentation and Measurement*, Vol. 47, No. 1, pp. 133-137, 1998.
- [63] H. P. Schwan, 'Alternating Current Spectroscopy of Biological Substances', *Proceedings of the IRE*, Vol. 7, No. 11, pp. 1841-1855, 1959.
- [64] C. Gabriel, S. Gabriel, and E. Corthout, 'The Dielectric Properties of Biological Tissues: I. Literature Survey', *Physics in Medicine & Biology*, Vol. 41, No. 11, pp. 2231-2249, 1996.
- [65] S. Gabriel, R. W. Lau, and C. Gabriel, 'The Dielectric Properties of Biological Tissues: II. Measurements in the Frequency Range 10 Hz to 20 GHz', *Physics in Medicine & Biology*, Vol. 41, No. 11, pp. 2251-2269, 1996.
- [66] S. Gabriel, R. W. Lau, and C. Gabriel, 'The Dielectric Properties of Biological Tissues: III. Parametric Models for the Dielectric Spectrum of Tissues', *Physics in Medicine & Biology*, Vol. 41, No. 11, pp. 2271-2293, 1996.



- [67] S. Lin-Liu, and W. R. Adey, 'Low Frequency Amplitude Modulated Microwave Fields Change Calcium Efflux Rates from Synaptosomes', *Bioelectromagnetics*, Vol. 3, No. 3, pp. 309-322, 1982.
- [68] S. Kwee, and P. Raskmark, 'Changes in Cell Proliferation due to Environmental Non-Ionizing Radiation: 2. Microwave Radiation', *Bioelectrochemistry and Bioenergetics*, Vol. 44, No. 2, pp. 251-255, 1998.
- [69] S. Velizarov, P. Raskmark, and S. Kwee, 'The Effects of Radiofrequency Fields on Cell Proliferation are Non-Thermal', *Bioelectrochemistry and Bioenergetics*, Vol. 48, No. 1, pp. 177-180, 1999.
- [70] E. A. Navarro, J. Segura, M. Portolés, and C. Gómez-Perretta de Mateo, 'The Microwave Syndrome: A Preliminary Study in Spain', *Electromagnetic Biology and Medicine*, Vol. 22, No. 2-3, pp. 161-169, 2003.
- [71] D. Remondini, R. Nylund, J. Reivinen, F. Poullietier de Gannes, B. Veyret, I. Lagroye, E. Haro, M. A. Trillo, M. Capri, C. Franceschi, and K. Schlatterer, 'Gene Expression Changes in Human Cells after Exposure to Mobile Phone Microwaves', *Proteomics*, Vol. 6, No. 17, pp. 4745-4754, 2006.
- [72] H. Hinrikus, M. Bachmann, D. Karai, and J. Lass, 'Mechanism of Low-Level Microwave Radiation Effect on Nervous System', *Electromagnetic Biology and Medicine*, Vol. 36, No. 2, pp. 202-212, 2017.
- [73] D. J. Panagopoulos, M. Cammaerts, D. Favre, and A. Balmori, 'Comments on Environmental Impact of Radiofrequency Fields from Mobile Phone Base Stations', *Critical Reviews in Environmental Science and Technology*, Vol. 46, No. 9, pp. 885-903, 2016.
- [74] Institute of Electrical and Electronics Engineers (IEEE), '*IEEE Recommended Practice for Measurements and Computations of Radio Frequency Electromagnetic Fields with respect to Human Exposure to Such Fields, 100 kHz-300 GHz*', IEEE Std C95.3-2002 (Revision of IEEE Std C95.3-1991), pp. 1-126, 2002. doi: 10.1109/IEEESTD.2002.94226
- [75] K. Bhattacharya, 'On the Dependence of Charge Density on Surface Curvature of an Isolated Conductor', *Physica Scripta*, Vol. 91, No. 3, 035501, 2016.
- [76] E. C. Jordan, and K. G. Balmain, '*Electromagnetic Waves and Radiating Systems (2nd Edition)*', New Jersey, PHI, 2009.

- [77] M. D. Deshpande, C. R. Cockrell, F. B. Beck, E. Vedeler, and M. B. Koch, '*Analysis of Electromagnetic Scattering from Irregularly Shaped, Thin, Metallic Flat Plates*', NASA Technical Paper 3361, 1993.
- [78] B. N. Taylor, and C. E. Kuyatt, '*Guidelines for Evaluating and Expressing the Uncertainty of NIST Measurement Results*', NIST Technical Note 1297 (1994 edition), National Institute of Standards and Technology, pp. 1-20, USA, 1994.
- [79] C. Gabriel, and A. Peyman, 'Dielectric Measurement: Error Analysis and Assessment of Uncertainty', *Physics in Medicine and Biology*, Vol. 51, No. 23, pp. 6033-6046, 2006.
- [80] A. La Gioia, E. Porter, I. Merunka, A. Shahzad, S. Salahuddin, M. Jones, and M. O'Halloran, 'Open-Ended Coaxial Probe Technique for Dielectric Measurement of Biological Tissues: Challenges and Common Practices', *Diagnostics*, Vol. 8, No. 2, pp. 40, 2018.
- [81] J. N. Ikediala, J. Tang, S. R. Drake, and L. G. Neven, 'Dielectric Properties of Apple Cultivars and Codling Moth Larvae', *Transactions of the ASAE*, Vol. 43, No. 5, pp. 1175-1184, 2000.
- [82] R. Rooban, M. Shanmugam, T. Venkatesan, and C. Tamilmani, 'Physiochemical Changes during Different Stages of Fruit Ripening of Climacteric Fruit of Mango (*Mangifera indica L.*) and Non-Climacteric of Fruit Cashew Apple (*Anacardium occidentale L.*)', *Journal of Applied and Advanced Research*, Vol. 1, No. 2, pp. 53-58, 2016.
- [83] T. K. Kataria, J. L. Olvera-Cervantes, A. Corona-Chávez, R. Rojas-Laguna, and M. E. Sosa-Morales, 'Dielectric Properties of Guava, Mamey Sapote, Prickly Pears, and Nopal in the Microwave Range', *International journal of food properties*, Vol. 20, No. 12, pp. 2944-2953, 2017.

# Chapter 5

## Phantom Liquid Preparation for Different Fruit and Plant Samples to Perform Practical Specific Absorption Rate Measurement

---

### 5.1 Introduction

In the previous two chapters, broadband complex dielectric properties ( $\epsilon_r$ ) have been characterized and Specific Absorption Rate (SAR) data have been estimated for a number of fruit and plant specimens. Broadband dielectric properties ( $\epsilon_r$ ) i.e. permittivity ( $\epsilon'_r$ ) and loss tangent ( $\tan \delta$ ) data have been measured using open ended coaxial probe technique over a broad frequency range up to 8.5 GHz [1-11]. Moreover, SAR data and their variations in a number of fruit and plant prototypes due to contrast in electromagnetic regulatory guidelines, angle of wave incidence and polarization have been simulated using the Time Domain (TD) solver available in CST Microwave Studio (CST MWS) [12-14]. Next, to further validate these simulated SAR data, customized fruit and plant phantom models are required. To be specific, three dimensional hollow fruit and plant phantom models need to be manufactured using thin, low permittivity ( $\epsilon'_r$ ) and low lossy ( $\tan \delta$ ) dielectric material – the same needs precise industrial manufacturing support. In addition, different fruit and plant tissue equivalent phantom liquids must also be prepared for practical SAR measurement with appropriate dielectric properties ( $\epsilon_r$ ) i.e. permittivity ( $\epsilon'_r$ ) and loss tangent ( $\tan \delta$ ).

Thus, different fruit and plant tissue equivalent phantom liquids have been prepared for three different frequencies i.e. 947.50 MHz, 1842.50 MHz and 2450 MHz. While preparing the tissue equivalent liquids, it should be taken into consideration that the phantom liquids must be non-toxic, non-corrosive to the measuring electric field probe and phantom shell and of low viscosity to ease the movement of electric field probe [15].

Standard dielectric properties ( $\epsilon_r$ ) and chemical recipes are now available for human body and head equivalent phantom liquids at different frequencies of interest [16]. Biological tissue equivalent phantom liquids can be prepared using sugar, glycol or diacetin based solutions depending upon frequency of operation, required permittivity ( $\epsilon_r'$ ) and loss tangent ( $\tan \delta$ ) parameter values. In general, sugar based solutions are prepared to formulate tissue equivalent liquids at lower frequencies such as 900 MHz – but, glycol based solutions are more preferred at 1800 MHz and 2450 MHz [15].

Keeping all these design and application constraints in vision, frequency dependent phantom liquid recipes have been prepared for twenty fruit and plant tissue layers (from twelve fruit and plant specimens) – targeting proper dielectric properties ( $\epsilon_r$ ) equivalence at around 947.50 MHz, 1842.50 MHz and 2450 MHz.

### **5.2 Phantom Liquid Preparation for Fruit and Plant Specimens**

Different fruit and plant tissue layer equivalent phantom liquids have been prepared for application around 947.50 MHz, 1842.50 MHz and 2450 MHz. All the plant tissue equivalent phantom liquids have been prepared based on De-Ionized (DI) water with 13 M $\Omega$ cm resistivity – sucrose (sugar) based solutions have been prepared primarily at 947.50 MHz, whereas, 98% pure diethylene glycol monobutyl ether (glycol) based solutions have been prepared majorly at 1842.50 MHz and 2450 MHz. In addition, 99.5% pure sodium chloride (NaCl) has been added to tune the electrical conductivity ( $\sigma$ ) / loss tangent ( $\tan \delta$ ) of the phantom liquid solutions.

Individual tissue equivalent phantom liquid recipes have been prepared for twenty tissue layers identified out of twelve fruit and plant specimens – some of the fruit / plant structures are multilayer in nature. As mentioned before, complex dielectric properties ( $\epsilon_r$ ) have been realized at 947.50 MHz and 1842.50 MHz downlink frequencies along with at ISM 2450 MHz. Thus, altogether, sixty (60) phantom liquid recipes have been prepared typically within 5% limit (in most cases) of the target permittivity ( $\epsilon_r'$ ) and loss tangent ( $\tan \delta$ ) values at the frequencies of interest. Customized recipes for fruit and plant tissue equivalent phantom liquids have been prepared in this chapter with different compositions of DI water, sucrose / diethylene glycol monobutyl ether and sodium chloride (NaCl). Next, dielectric properties ( $\epsilon_r$ ) of the custom-made phantom liquids have been measured with high temperature open-ended dielectric probe

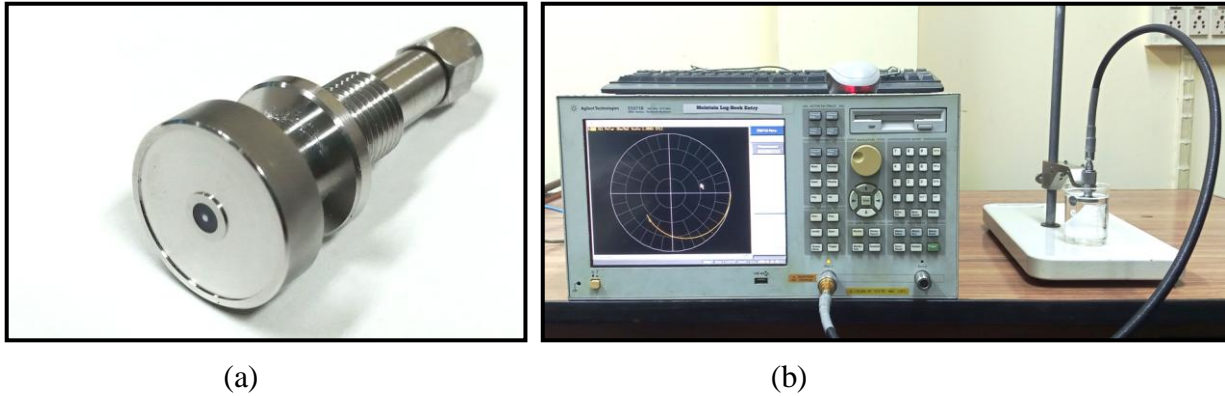


Fig. 5.1: Open-ended coaxial probe and dielectric properties ( $\epsilon_r$ ) measurement setup (a) 85070E high temperature open-ended coaxial dielectric measurement probe, (b) broadband dielectric properties ( $\epsilon_r$ ) measurement setup for characterizing phantom liquids

kit (Agilent Technologies 85070E dielectric measurement kit) and Agilent Technologies E5071B Vector Network Analyzer (VNA) – after proper system calibration at 25 °C. All measured dielectric properties ( $\epsilon_r$ ) i.e. both permittivity ( $\epsilon'_r$ ) and loss tangent ( $\tan \delta$ ) data of the phantom liquids have been plotted using MATLAB software [17]. Figs. 5.1(a) and (b) illustrate 85070E high temperature open-ended coaxial dielectric measurement probe and the entire dielectric properties ( $\epsilon_r$ ) measurement setup for characterizing permittivity ( $\epsilon'_r$ ) and loss tangent ( $\tan \delta$ ) of the prepared phantom liquids [18].

### 5.3 Target Dielectric Properties of Fruit and Plant Specimens

In this section, the measured reference dielectric properties ( $\epsilon_r$ ) for a number of fruit and plant specimens have been tabulated at the frequencies of interest i.e. at 947.50 MHz, 1842.50 MHz and 2450 MHz. Based on these measured dielectric properties ( $\epsilon_r$ ), various fruit / plant tissue equivalent phantom liquid compositions have been proposed at the above mentioned frequencies. The permittivity ( $\epsilon'_r$ ) and loss tangent ( $\tan \delta$ ) data altogether for twenty tissue layers identified out of the twelve fruit and plant specimens have been presented in Table 5.1 – most of these measured data have been taken from the work reported in last two chapters. However, the measured dielectric properties ( $\epsilon_r$ ) for black grape have only been taken from literature [19].

In this connection, it should be noted that broadband complex dielectric properties ( $\epsilon_r$ ) i.e. both permittivity ( $\epsilon'_r$ ) and loss tangent ( $\tan \delta$ ) of different fruit / plant specimens alter with maturation stage. Thus, even these measured reference dielectric properties ( $\epsilon_r$ ) of different fruit

/ plant specimens can be a little different based on the maturation stage – the phantom liquid recipes can also be fine tuned in accordance with the reference values as per requirements.

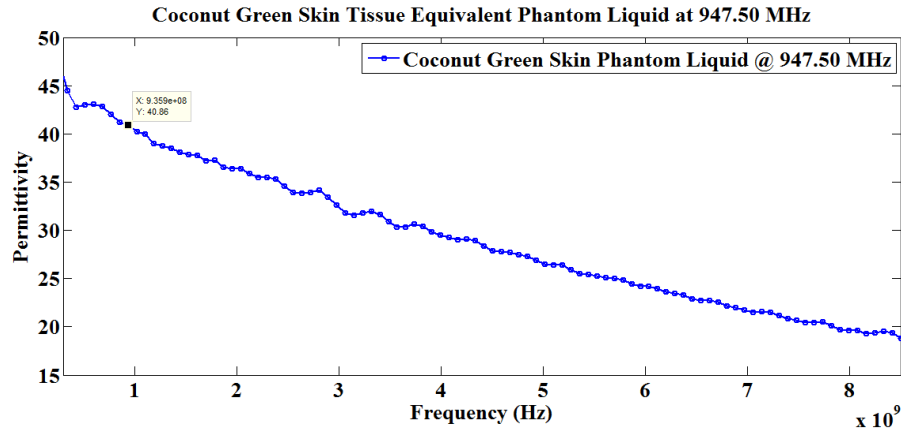
Table 5.1 Measured dielectric properties ( $\epsilon_r$ ) of the targeted fruit and plant specimens

Sl. No.	Fruit / Plant Specimen	947.5 MHz		1842.5 MHz		2450 MHz	
		$\epsilon'_r$	$\tan \delta$	$\epsilon'_r$	$\tan \delta$	$\epsilon'_r$	$\tan \delta$
1	Coconut green skin	41.21	0.385	38.12	0.306	37.14	0.296
	Coconut pulp	65.01	0.251	62.59	0.224	61.46	0.235
	Coconut water	77.54	0.190	76.51	0.168	75.91	0.181
2	Apple	65.03	0.135	63.72	0.156	62.23	0.194
3	Guava	72.08	0.154	71.05	0.159	69.73	0.179
4	Grape	69.11	0.167	66.81	0.185	65.27	0.210
5	Tomato	47.00	0.225	46.00	0.190	45.00	0.200
6	Brinjal	34.00	0.200	33.00	0.185	32.50	0.200
7	Chiku	66.02	0.199	63.65	0.214	62.50	0.245
	Chiku leaf	33.12	0.440	30.28	0.360	28.94	0.360
8	<i>Catharanthus roseus</i> leaf	57.85	0.501	54.05	0.331	53.21	0.295
	<i>Catharanthus roseus</i> flower	62.47	0.212	60.53	0.175	60.04	0.186
	<i>Catharanthus roseus</i> stem	43.26	0.475	40.16	0.326	39.29	0.307
9	Green mango pulp	71.68	0.178	70.54	0.173	70.17	0.197
	Green mango seed	67.59	0.156	65.69	0.168	65.12	0.197
	Green mango leaf	34.03	0.302	31.80	0.268	31.04	0.272
10	Water apple	68.75	0.102	67.57	0.124	67.53	0.149
11	Orange	65.78	0.220	63.35	0.210	62.70	0.230
	Orange peel	43.48	0.240	41.59	0.230	41.26	0.269
12	Black grape	71.25	0.176	68.94	0.202	67.47	0.224

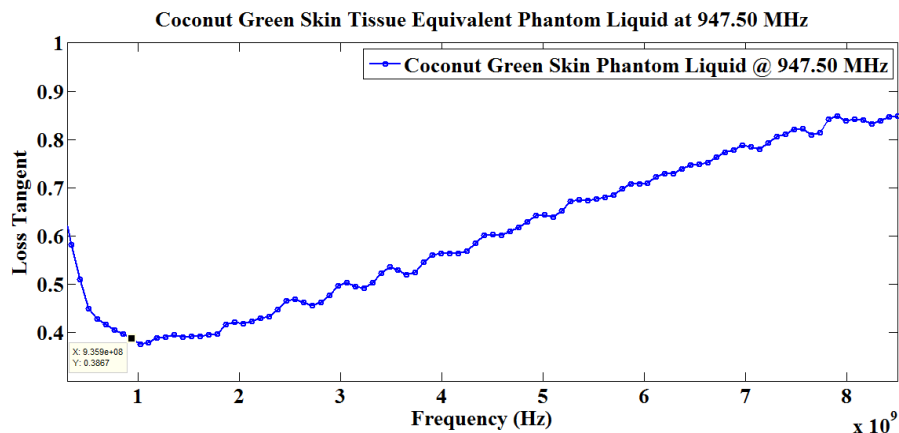
## 5.4 Phantom Liquid Preparation for Fruit and Plant Specimens

### 5.4.1 Phantom Liquids Preparation for Coconut Specimens

Phantom liquids have been prepared for three different tissue layers in green coconut i.e. green skin in coconut, coconut pulp and coconut water. Phantom liquid recipes have been prepared at three different frequencies as stated earlier (947.50 MHz, 1842.50 MHz and 2450.00 MHz respectively). In most scenarios, different compositions of DI water, sucrose / diethylene glycol monobutyl ether and sodium chloride (NaCl) have been employed to achieve the desired permittivity ( $\epsilon_r'$ ) and loss tangent ( $\tan \delta$ ) values of the tissue equivalent phantom liquids at the frequencies of interest.



(a)

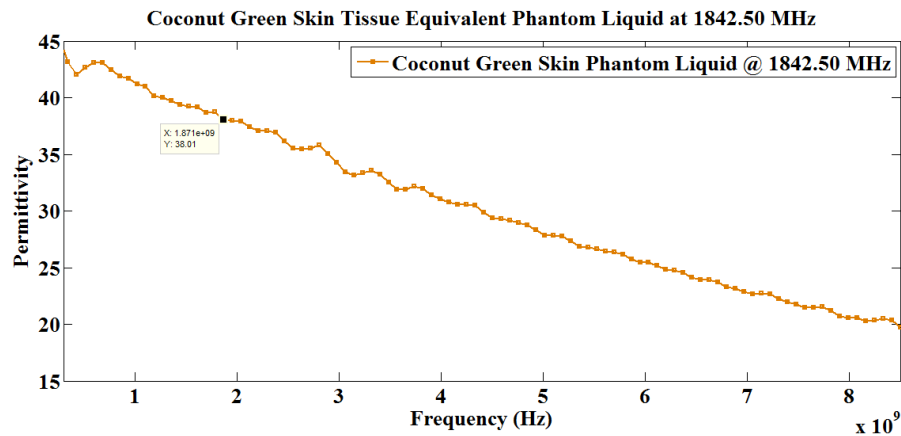


(b)

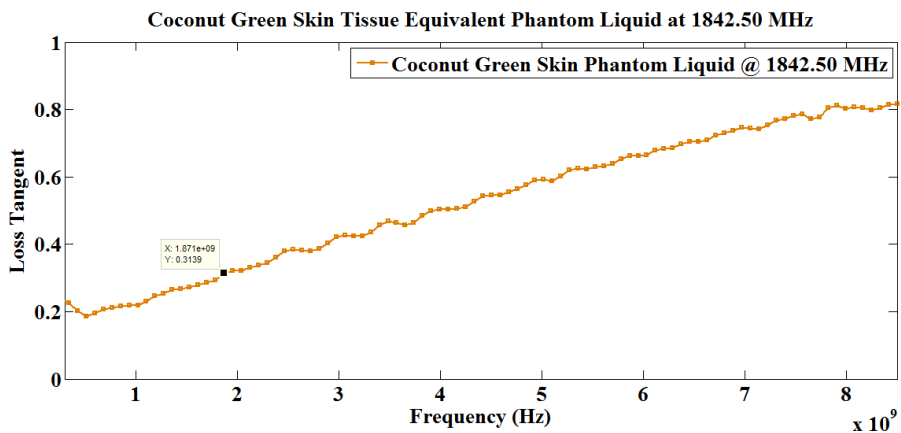
Fig. 5.2: Coconut green skin tissue equivalent phantom liquid at 947.50 MHz (a) permittivity and (b) loss tangent

### 5.4.1.1 Phantom Liquids for Coconut Green Skin

Phantom liquid recipes have been prepared for coconut green skin tissue layer at 947.50 MHz, 1842.50 MHz and 2450.00 MHz respectively. In all scenarios, coconut green skin tissue equivalent phantom liquids (at above mentioned frequencies) have been prepared based on different compositions of DI water (13 M $\Omega$ cm resistivity), diethylene glycol monobutyl ether and sodium chloride (NaCl). In general, diethylene glycol monobutyl ether has been added with DI water in order to bring down the permittivity ( $\epsilon_r'$ ) of the composition – thus, to tune the consequential permittivity ( $\epsilon_r'$ ) close to the reference permittivity ( $\epsilon_r'$ ) of coconut green skin. Furthermore, sodium chloride (NaCl) has been added to the liquid recipes to fine tune the electrical conductivity ( $\sigma$ ) / loss tangent ( $\tan \delta$ ) of the equivalent phantom liquid solutions.



(a)



(b)

Fig. 5.3: Coconut green skin tissue equivalent phantom liquid at 1842.50 MHz (a) permittivity and (b) loss tangent



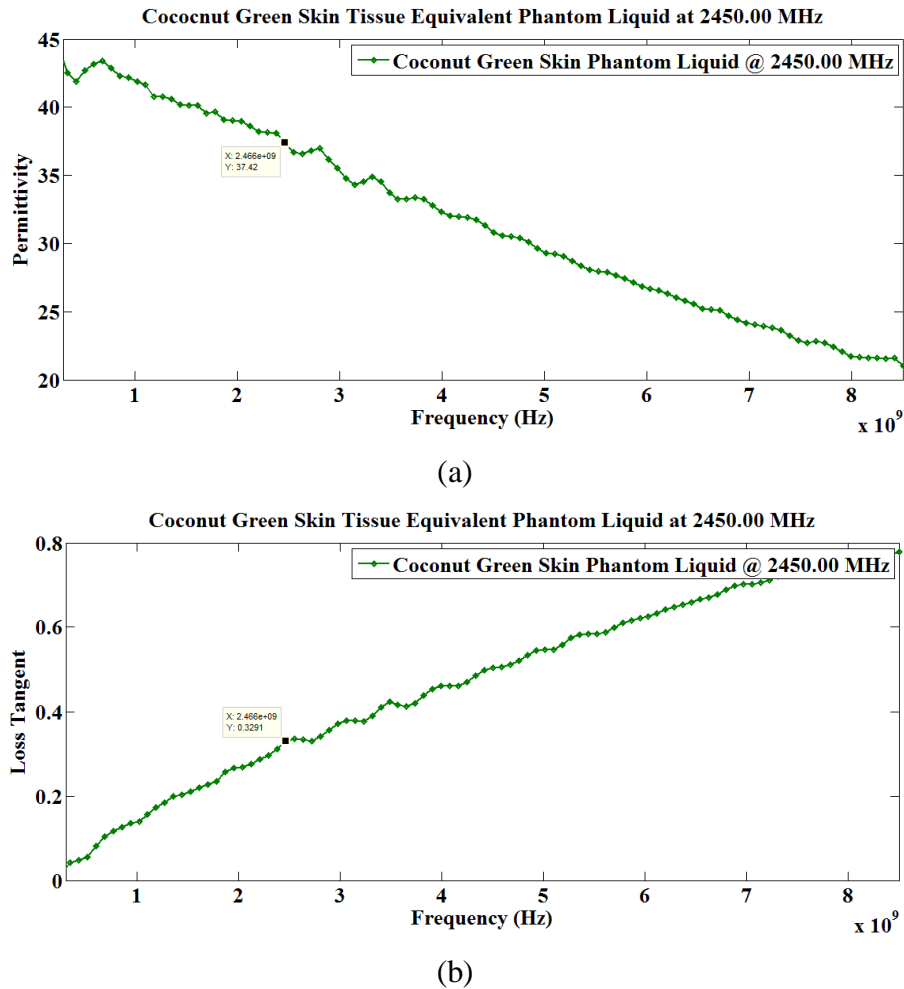


Fig. 5.4: Coconut green skin tissue equivalent phantom liquid at 2450.00 MHz (a) permittivity and (b) loss tangent

To prepare the coconut green skin tissue equivalent phantom liquids, broadband complex dielectric properties ( $\epsilon_r$ ) of pure DI water (13 M $\Omega$ cm resistivity) have been measured at initial phase. The measured permittivity ( $\epsilon_r'$ ) and loss tangent ( $\tan \delta$ ) values of the above mentioned DI water at 25 °C are 78.21, 77.69, 77.20 and 0.045, 0.091, 0.120 respectively at 947.50 MHz, 1842.50 MHz and 2450.00 MHz.

Aiming coconut green skin tissue equivalent phantom liquid at 947.50 MHz, 100 ml diethylene glycol monobutyl ether and 1600 mg sodium chloride (NaCl) have been mixed with 100 ml DI water in order to tune permittivity ( $\epsilon_r'$ ) and loss tangent ( $\tan \delta$ ) of the phantom liquid to values close to the original measured data – please refer to Table 5.2. Final phantom liquid permittivity ( $\epsilon_r'$ ) and loss tangent ( $\tan \delta$ ) values have been achieved within 0.85% and 0.52% limits of the reference values at 947.50 MHz – please refer to Fig. 5.2 and Table 5.3.

Next at 1842.50 MHz, 100 ml diethylene glycol monobutyl ether and 400 mg sodium chloride (NaCl) have been added with 100 ml DI water to tune dielectric properties ( $\epsilon_r$ ) of the resultant phantom liquid close to the original coconut green skin tissue – please refer to Table 5.2. Achieved phantom liquid permittivity ( $\epsilon_r'$ ) and loss tangent ( $\tan \delta$ ) values are within 0.29% and 2.61% limits of the reference values at 1842.50 MHz – please refer to Fig. 5.3 and Table 5.3.

At 2450.00 MHz, 100 ml diethylene glycol monobutyl ether has been added with 100 ml DI water to tune permittivity ( $\epsilon_r'$ ) and loss tangent ( $\tan \delta$ ) of the resultant phantom liquid to values close to the original coconut green skin tissue – please refer to Table 5.2. Achieved phantom liquid permittivity ( $\epsilon_r'$ ) and loss tangent ( $\tan \delta$ ) values are within 0.75% and 11.15% limits of the reference values at 2450.00 MHz – please refer to Fig. 5.4 and Table 5.3. The deviation in loss tangent ( $\tan \delta$ ) can be minimized further using DI water with higher resistivity (>13 M $\Omega$ cm).

Table 5.2 Final compositions of coconut green skin tissue equivalent phantom liquids

Frequency (MHz)	Final composition of phantom liquid
947.50	100 ml DI water, 100 ml DGME & 1600 mg NaCl
1842.50	100 ml DI water, 100 ml DGME & 400 mg NaCl
2450.00	100 ml DI water & 100 ml DGME

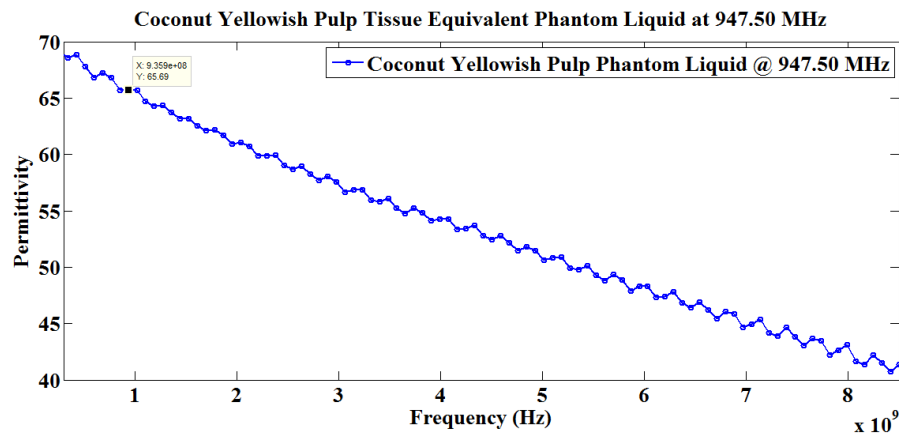
DGME = diethylene glycol monobutyl ether

Table 5.3 Difference between the measured dielectric properties ( $\epsilon_r$ ) of coconut green skin tissue specimen and equivalent phantom liquids

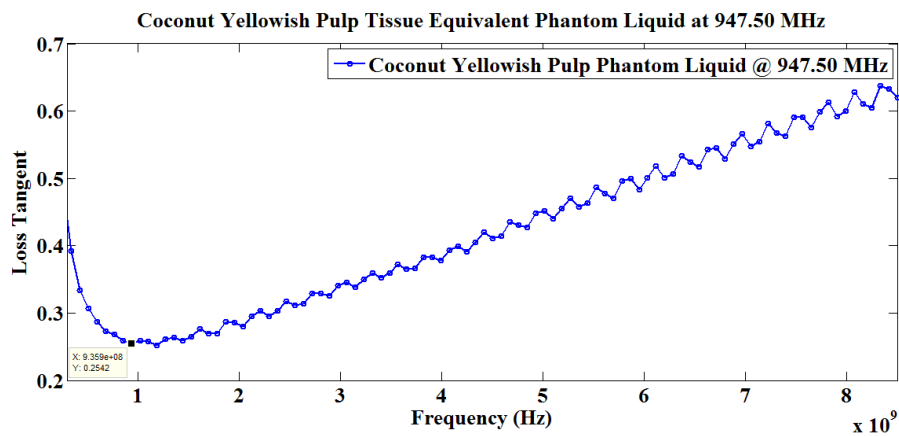
Frequency (MHz)	947.50	Deviation	1842.50	Deviation	2450.00	Deviation
Reference Permittivity ( $\epsilon_r'$ )	41.21		38.12		37.14	
Phantom Liquid Permittivity ( $\epsilon_r'$ )	40.86	0.85%	38.01	0.29%	37.42	0.75%
Reference Loss Tangent ( $\tan \delta$ )	0.385		0.306		0.296	
Phantom Liquid Loss Tangent ( $\tan \delta$ )	0.387	0.52%	0.314	2.61%	0.329	11.15%

### 5.4.1.2 Phantom Liquids for Coconut Pulp

This time, phantom liquids have been formulated for coconut pulp tissue layer at 947.50 MHz, 1842.50 MHz and 2450.00 MHz respectively. Coconut pulp tissue equivalent phantom liquids have been prepared based on different compositions of DI water (13 MΩcm resistivity), sucrose and sodium chloride (NaCl). In general, sucrose has been added with DI water to reduce permittivity ( $\epsilon_r'$ ) of the composition and thus to tune the phantom liquid permittivity ( $\epsilon_r'$ ) close to the reference permittivity ( $\epsilon_r'$ ) values of coconut pulp tissue (original measured data). In addition, sodium chloride (NaCl) has been added to the phantom liquid recipes for fine tuning electrical conductivity ( $\sigma$ ) / loss tangent ( $\tan \delta$ ) of the final equivalent phantom liquids.

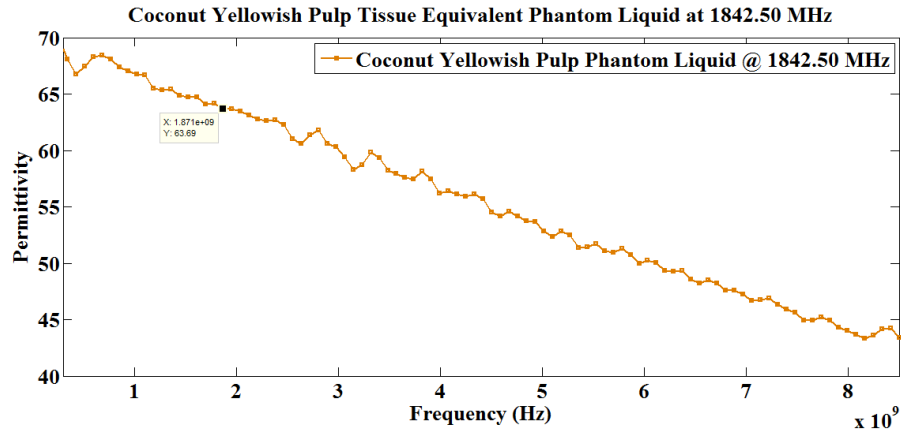


(a)

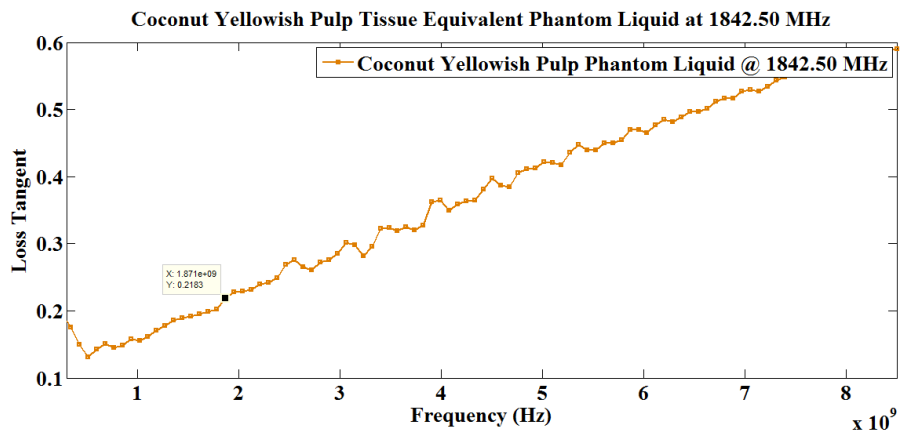


(b)

Fig. 5.5: Coconut pulp tissue equivalent phantom liquid at 947.50 MHz (a) permittivity and (b) loss tangent



(a)

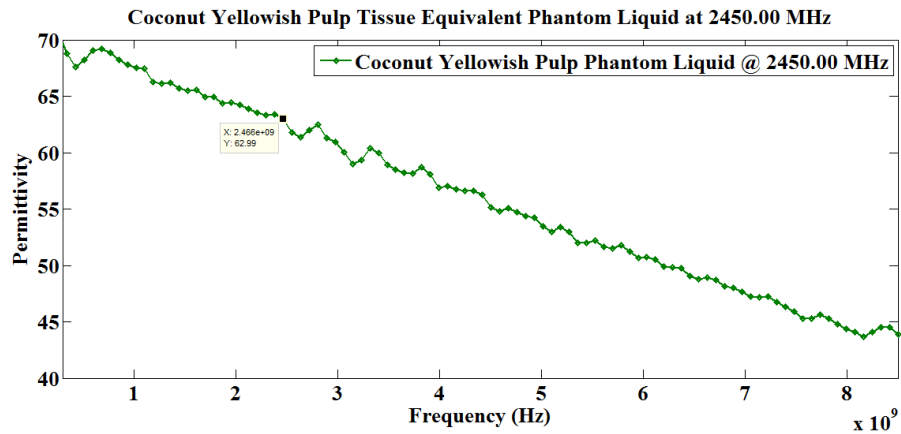


(b)

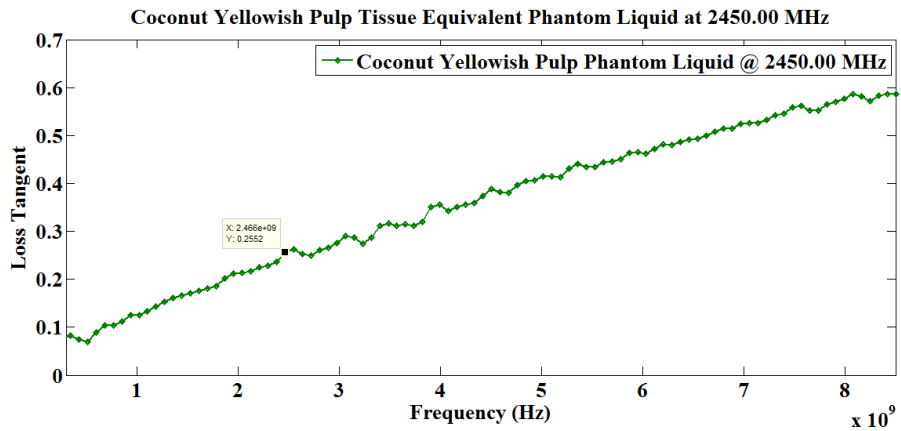
Fig. 5.6: Coconut pulp tissue equivalent phantom liquid at 1842.50 MHz (a) permittivity and (b) loss tangent

Before proceeding with coconut pulp tissue equivalent phantom liquid preparations, broadband complex dielectric properties ( $\epsilon_r$ ) i.e. permittivity ( $\epsilon_r'$ ) and loss tangent ( $\tan \delta$ ) of pure DI water (13 M $\Omega$ cm resistivity) has been measured at initial stage. The frequency dependent permittivity ( $\epsilon_r'$ ) and loss tangent ( $\tan \delta$ ) values of the DI water (13 M $\Omega$ cm resistivity) at 25 °C have already been mentioned earlier and thus not repeated here.

In order to prepare coconut pulp tissue equivalent phantom liquid recipe at 947.50 MHz, 42 g sucrose and 650 mg sodium chloride (NaCl) have been added to 100 ml DI water for tuning permittivity ( $\epsilon_r'$ ) and loss tangent ( $\tan \delta$ ) of the final phantom liquid to values close to the original measured values – please refer to Table 5.4. Final phantom liquid permittivity ( $\epsilon_r'$ ) and



(a)



(b)

Fig. 5.7: Coconut pulp tissue equivalent phantom liquid at 2450.00 MHz (a) permittivity and (b) loss tangent

loss tangent ( $\tan \delta$ ) values have been achieved within 1.05% and 1.18% limits of the reference values at 947.50 MHz – please refer to Fig. 5.5 and Table 5.5.

Next, to formulate coconut pulp tissue equivalent phantom liquid preparation at 1842.50 MHz, 42 g sucrose and 200 mg sodium chloride (NaCl) have been added with 100 ml DI water to tune permittivity ( $\epsilon_r'$ ) and loss tangent ( $\tan \delta$ ) parameters of the consequential phantom liquid close to the original coconut pulp tissue specimen – please refer to Table 5.4. It should be noted that the phantom liquid permittivity ( $\epsilon_r'$ ) and loss tangent ( $\tan \delta$ ) values have been attained within 1.76% and 2.68% limits of the reference values at 1842.50 MHz – please refer to Fig. 5.6 and Table 5.5.

## Phantom Liquid Preparation for Different Fruit and Plant Samples

At final phase, to prepare coconut pulp tissue equivalent phantom liquid recipe at 2450.00 MHz, 42 g sucrose and 50 mg sodium chloride (NaCl) have been added to 100 ml DI water for tuning final dielectric properties ( $\epsilon_r$ ) i.e. permittivity ( $\epsilon_r'$ ) and loss tangent ( $\tan \delta$ ) values of the phantom liquid recipe close to the original coconut pulp tissue specimen – please refer to Table 5.4 for detailed composition. Finalized phantom liquid permittivity ( $\epsilon_r'$ ) and loss tangent ( $\tan \delta$ ) parameter values have been achieved within 2.49% and 8.51% limits of the reference dielectric values at 2450.00 MHz – please refer to Fig. 5.7 and Table 5.5. In this connection, it should be noted that the loss tangent ( $\tan \delta$ ) at 2450.00 MHz has been achieved with 8.51% error – however, the difference in loss tangent ( $\tan \delta$ ) can further be reduced by using DI water with resistivity greater than 13 M $\Omega$ cm.

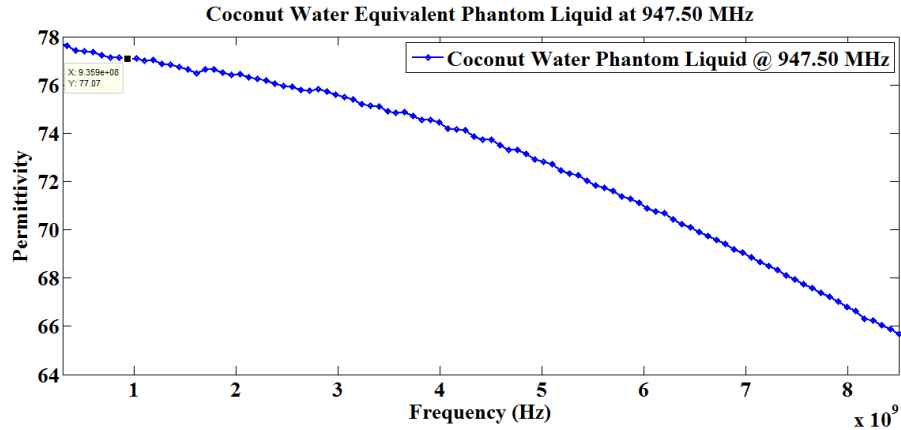
Table 5.4 Final compositions of coconut pulp tissue equivalent phantom liquids

Frequency (MHz)	Final composition of phantom liquid
947.50	100 ml DI water, 42 g sucrose & 650 mg NaCl
1842.50	100 ml DI water, 42 g sucrose & 200 mg NaCl
2450.00	100 ml DI water, 42 g sucrose & 50 mg NaCl

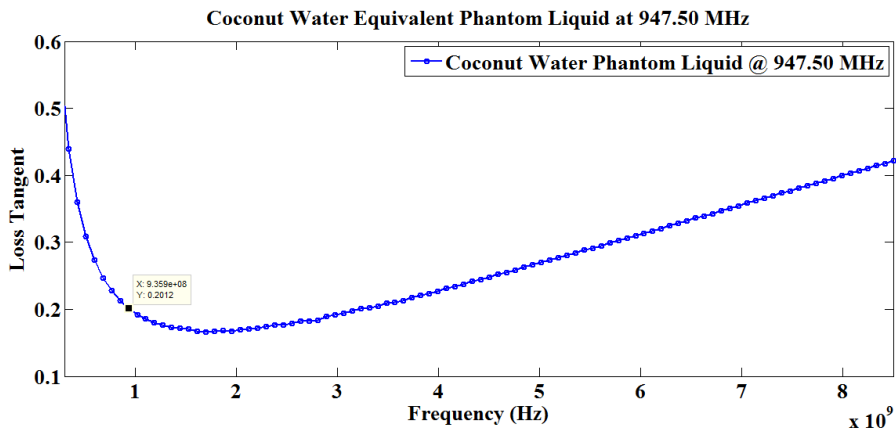
Table 5.5 Difference between the measured dielectric properties ( $\epsilon_r$ ) of coconut pulp tissue specimen and equivalent phantom liquids

Frequency (MHz)	947.50	Deviation	1842.50	Deviation	2450.00	Deviation
Reference Permittivity ( $\epsilon_r'$ )	65.01		62.59		61.46	
Phantom Liquid Permittivity ( $\epsilon_r'$ )	65.69	1.05%	63.69	1.76%	62.99	2.49%
Reference Loss Tangent ( $\tan \delta$ )	0.251		0.224		0.235	
Phantom Liquid Loss Tangent ( $\tan \delta$ )	0.254	1.18%	0.218	2.68%	0.255	8.51%

### 5.4.1.3 Phantom Liquids for Coconut Water



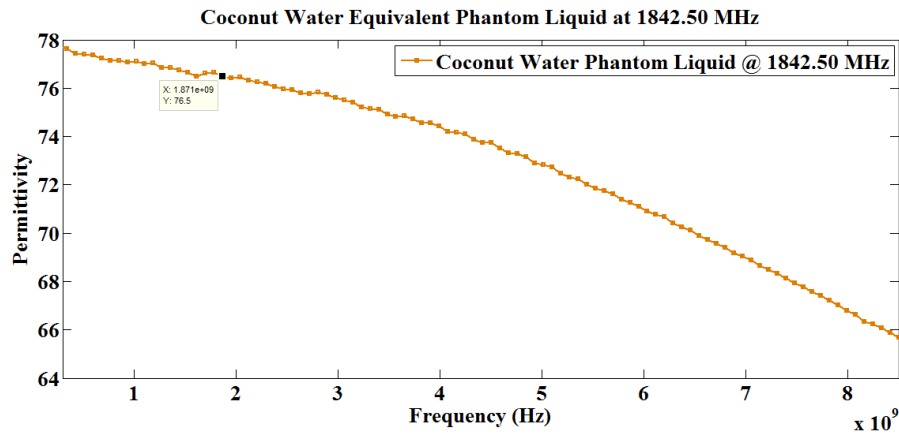
(a)



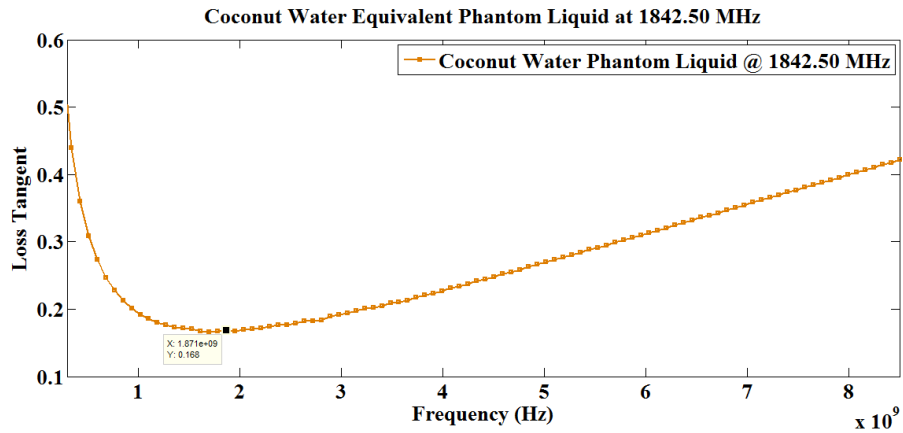
(b)

Fig. 5.8: Coconut water equivalent phantom liquid at 947.50 MHz (a) permittivity and (b) loss tangent

Coconut water equivalent phantom liquid recipe has been prepared to achieve reference permittivity ( $\epsilon_r'$ ) and loss tangent ( $\tan \delta$ ) values at all three frequencies i.e. 947.50 MHz, 1842.50 MHz and 2450.00 MHz. Coconut water equivalent phantom liquid recipe has been formulated based on a single composition of DI water (13 M $\Omega$ cm resistivity) and sodium chloride (NaCl). It is well understood that sodium chloride (NaCl) has been added to DI water for increasing the electrical conductivity ( $\sigma$ ) / loss tangent ( $\tan \delta$ ) of the equivalent phantom liquid to match with coconut water specimen.



(a)



(b)

Fig. 5.9: Coconut water equivalent phantom liquid at 1842.50 MHz (a) permittivity and (b) loss tangent

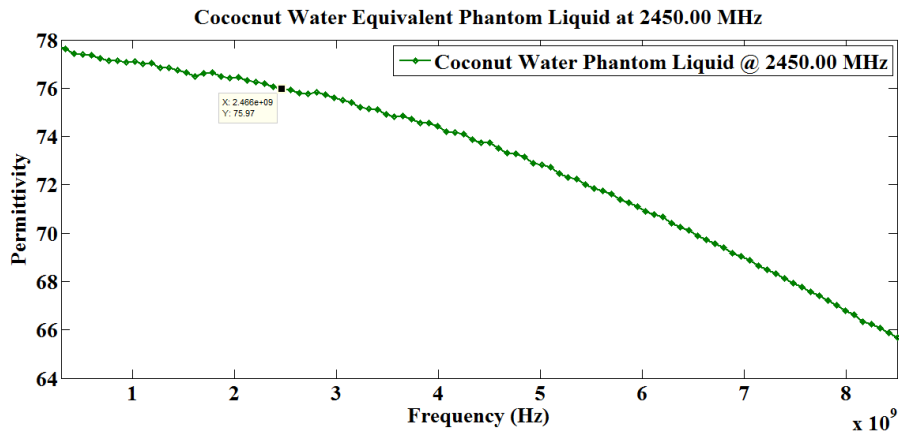
As mentioned earlier, prior to formulate coconut water equivalent phantom liquid recipe, broadband complex dielectric properties ( $\epsilon_r$ ) of pure DI water (13 M $\Omega$ cm resistivity) has been measured and validated. The measured permittivity ( $\epsilon_r'$ ) and loss tangent ( $\tan \delta$ ) values of the DI water (13 M $\Omega$ cm resistivity) at 947.50 MHz, 1842.50 MHz and 2450.00 MHz have been mentioned before in this chapter – thus, not repeated here.

To prepare coconut water equivalent phantom liquid recipe at 947.50 MHz, 300 mg sodium chloride (NaCl) has been added with 100 ml DI water to tune permittivity ( $\epsilon_r'$ ) and loss tangent ( $\tan \delta$ ) of the phantom liquid close to the reference values – please refer to Table 5.6. Final phantom liquid permittivity ( $\epsilon_r'$ ) and loss tangent ( $\tan \delta$ ) values have been achieved within

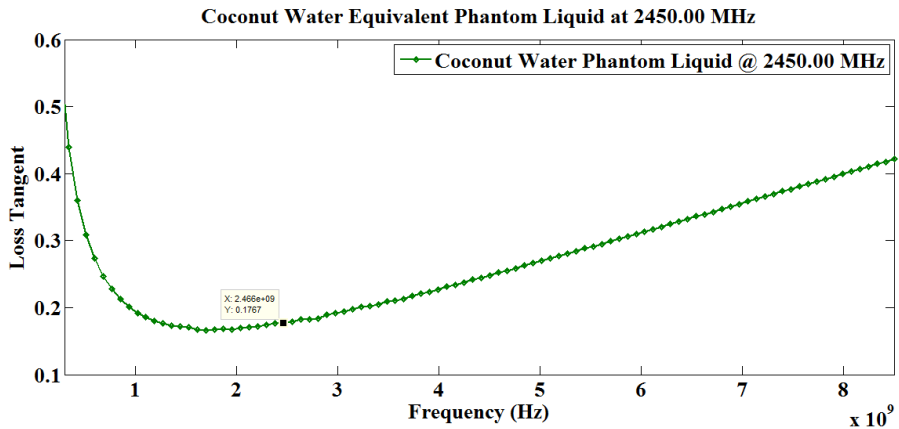


0.61% and 5.79% limits of the reference values at 947.50 MHz – please refer to Fig. 5.8 and Table 5.7. It should be noted that the error limit in loss tangent ( $\tan \delta$ ) at 947.50 MHz can be further brought down by employing DI water with higher resistivity ( $>13 \text{ M}\Omega\text{cm}$ ).

Next, the same composition has been utilized further to achieve permittivity ( $\epsilon_r'$ ) and loss tangent ( $\tan \delta$ ) values of the coconut water equivalent phantom liquid even at 1842.50 MHz and 2450.00 MHz – please refer to Table 5.6. Final phantom liquid permittivity ( $\epsilon_r'$ ) and loss tangent ( $\tan \delta$ ) values have been achieved within 0.01%, 0.08% and 0.00%, 2.21% limits respectively at 1842.50 MHz and 2450 MHz – please refer to Figs. 5.9 and 5.10 along with Table 5.7.



(a)



(b)

Fig. 5.10: Coconut water equivalent phantom liquid at 2450.00 MHz (a) permittivity and (b) loss tangent

Table 5.6 Final compositions of coconut water equivalent phantom liquids

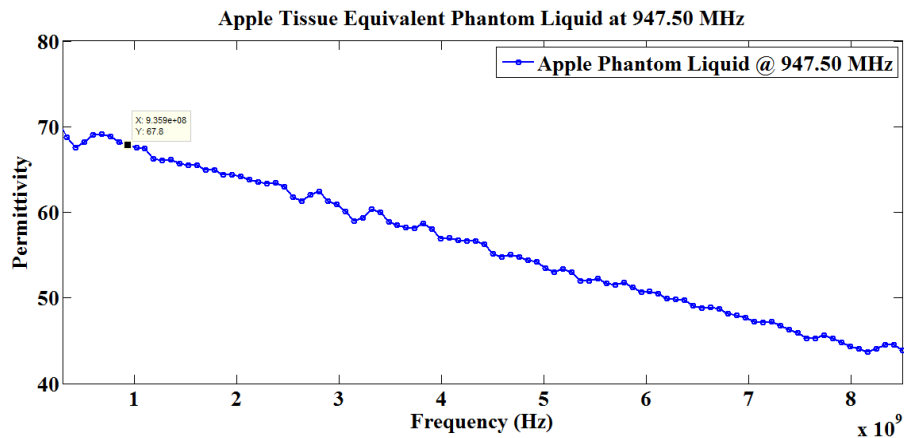
Frequency (MHz)	Final composition of phantom liquid
947.50	100 ml DI water & 300 mg NaCl
1842.50	100 ml DI water & 300 mg NaCl
2450.00	100 ml DI water & 300 mg NaCl

Table 5.7 Difference between the measured dielectric properties ( $\epsilon_r$ ) of coconut water specimen and equivalent phantom liquids

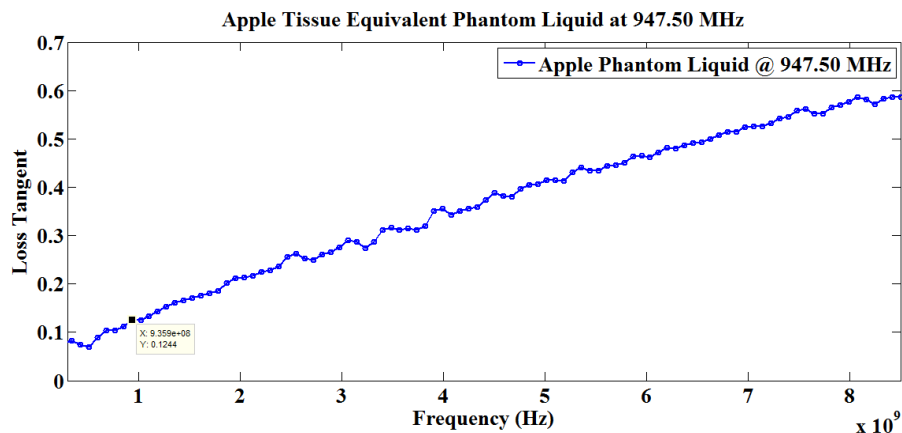
Frequency (MHz)	947.50	Deviation	1842.50	Deviation	2450.00	Deviation
Reference Permittivity ( $\epsilon_r'$ )	77.54		76.51		75.91	
Phantom Liquid Permittivity ( $\epsilon_r'$ )	77.07	0.61%	76.50	0.01%	75.97	0.08%
Reference Loss Tangent ( $\tan \delta$ )	0.190		0.168		0.181	
Phantom Liquid Loss Tangent ( $\tan \delta$ )	0.201	5.79%	0.168	0.00%	0.177	2.21%

### 5.4.2 Phantom Liquids Preparation for Apple Specimen

Phantom liquid recipes have been prepared for apple tissue at 947.50 MHz, 1842.50 MHz and 2450.00 MHz respectively. Apple tissue equivalent phantom liquids have been prepared based on different compositions of DI water (13 M $\Omega$ cm resistivity), sucrose / diethylene glycol monobutyl ether and sodium chloride (NaCl). Based on desired frequency range, sucrose / diethylene glycol monobutyl ether has been added with DI water in order to bring down permittivity ( $\epsilon_r'$ ) of the liquid composition – thus, phantom liquid permittivity ( $\epsilon_r'$ ) is tuned closer to the measured permittivity ( $\epsilon_r'$ ) of apple tissue (reference data). Furthermore, sodium chloride (NaCl) has been added to the phantom liquid preparations to fine tune electrical conductivity ( $\sigma$ ) / loss tangent ( $\tan \delta$ ) of the equivalent phantom liquids.

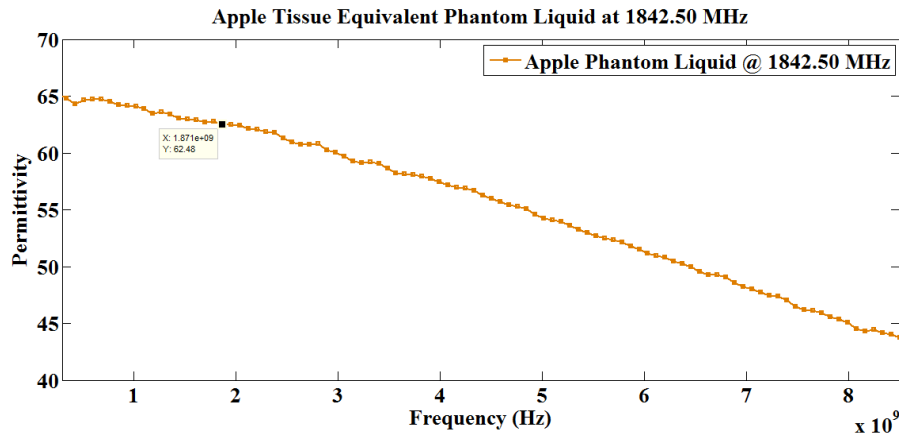


(a)

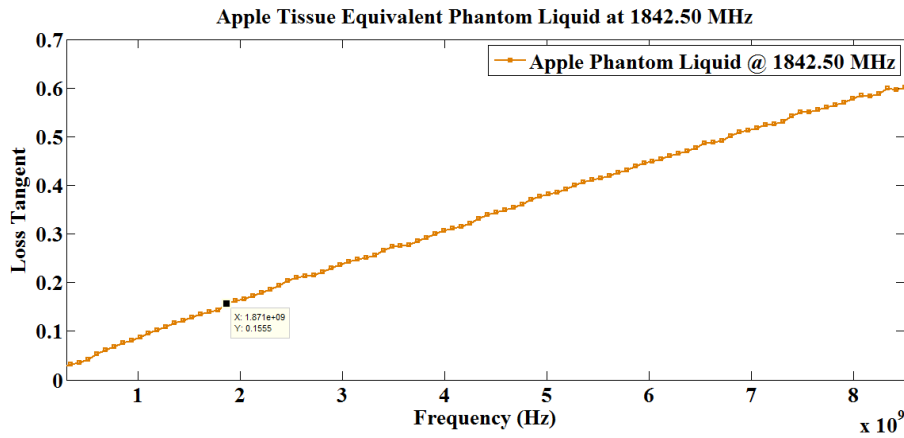


(b)

Fig. 5.11: Apple tissue equivalent phantom liquid at 947.50 MHz (a) permittivity and (b) loss tangent



(a)



(b)

Fig. 5.12: Apple tissue equivalent phantom liquid at 1842.50 MHz (a) permittivity and (b) loss tangent

As stated earlier, broadband dielectric properties ( $\epsilon_r$ ) i.e. permittivity ( $\epsilon_r'$ ) and loss tangent ( $\tan \delta$ ) data for unadulterated DI water (13 M $\Omega$ cm resistivity) have been measured first i.e. ahead of apple tissue equivalent phantom liquids preparation. The dielectric properties ( $\epsilon_r$ ) i.e. permittivity ( $\epsilon_r'$ ) and loss tangent ( $\tan \delta$ ) data for DI water (13 M $\Omega$ cm resistivity) at 25 °C have been discussed earlier at 947.50 MHz, 1842.50 MHz and 2450.00 MHz – therefore, those values are not repeated here.

At first, to formulate apple tissue equivalent phantom liquid preparation at 947.50 MHz, 42 g sucrose and 50 mg sodium chloride (NaCl) have been added to 100 ml DI water for achieving phantom liquid permittivity ( $\epsilon_r'$ ) and loss tangent ( $\tan \delta$ ) values close to the original reference

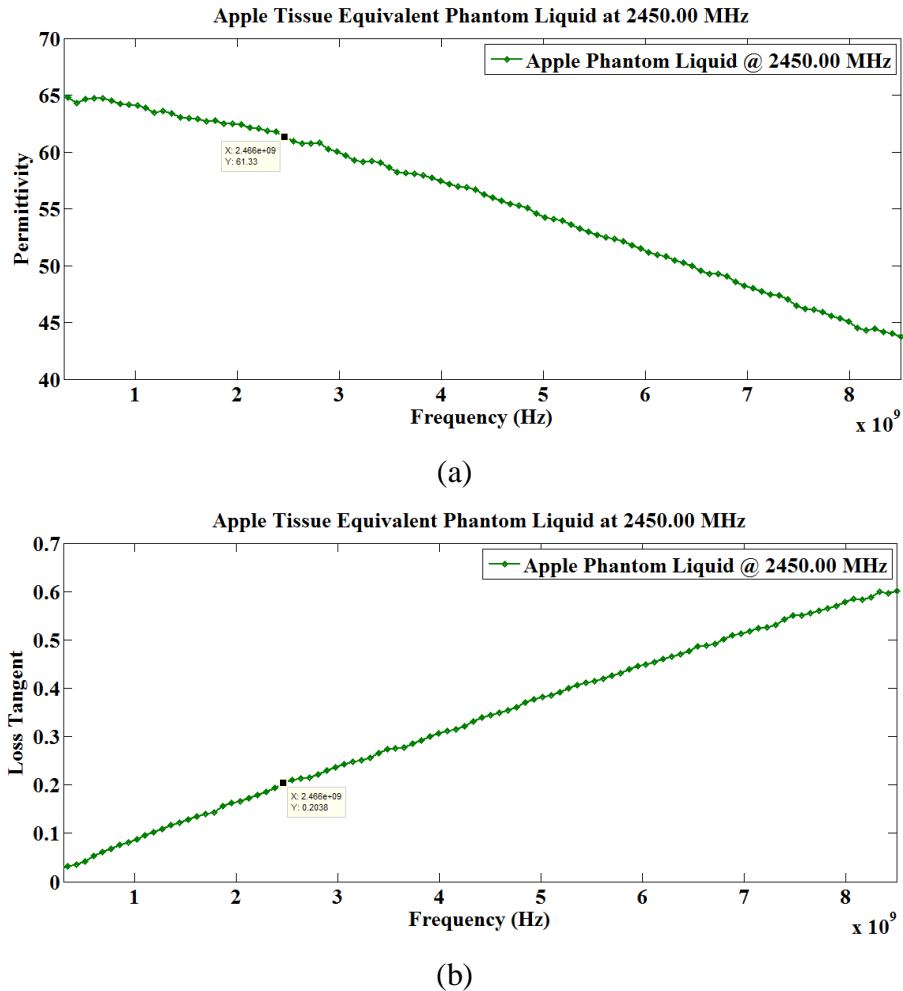


Fig. 5.13: Apple tissue equivalent phantom liquid at 2450.00 MHz (a) permittivity and (b) loss tangent

data for apple specimen (please refer to Table 5.8). The ultimate phantom liquid permittivity ( $\epsilon_r'$ ) and loss tangent ( $\tan \delta$ ) values have been achieved within 4.26% and 8.15% limits of the reference data at 947.50 MHz (please refer to Fig. 5.11 and Table 5.9). It should be noted that the deviation in loss tangent ( $\tan \delta$ ) value can further be brought down by utilizing DI water with resistivity more than 13 M $\Omega$ cm.

Next, to prepare apple tissue equivalent phantom liquid recipe at 1842.50 MHz, 26.32 ml diethylene glycol monobutyl ether has been added with 100 ml DI water (resistivity = 13 M $\Omega$ cm) to tune permittivity ( $\epsilon_r'$ ) and loss tangent ( $\tan \delta$ ) values of the equivalent phantom liquid close to the original apple tissue specimen (please refer to Table 5.8). It should be noted that the final

phantom liquid permittivity ( $\epsilon_r'$ ) value has been achieved within 1.95% limit of the reference value and loss tangent ( $\tan \delta$ ) value exactly matches at 1842.50 MHz – please refer to Fig. 5.12 and Table 5.9.

At final stage, the last mentioned phantom liquid composition i.e. a mixture of 26.32 ml diethylene glycol monobutyl ether and 100 ml DI water (resistivity = 13 M $\Omega$ cm) has been utilized to tune dielectric properties ( $\epsilon_r$ ) i.e. permittivity ( $\epsilon_r'$ ) and loss tangent ( $\tan \delta$ ) values of the liquid formulation close to the original apple tissue specimen at 2450.00 MHz (please refer to Table 5.8 for detailed chemical composition at 25 °C). Finalized phantom liquid permittivity ( $\epsilon_r'$ ) and loss tangent ( $\tan \delta$ ) values have been tuned within 1.45% and 5.15% limits of the reference dielectric properties ( $\epsilon_r$ ) of apple tissue specimen at 2450.00 MHz (please refer to Fig. 5.13 and Table 5.9). Once again, it should be noted that the deviation in loss tangent ( $\tan \delta$ ) at 2450.00 MHz can further be minimized by employing DI water with resistivity more than 13 M $\Omega$ cm.

Table 5.8 Final compositions of apple tissue equivalent phantom liquids

Frequency (MHz)	Final composition of phantom liquid
947.50	100 ml DI water, 42 g sucrose & 50 mg NaCl
1842.50	100 ml DI water & 26.32 ml DGME
2450.00	100 ml DI water & 26.32 ml DGME

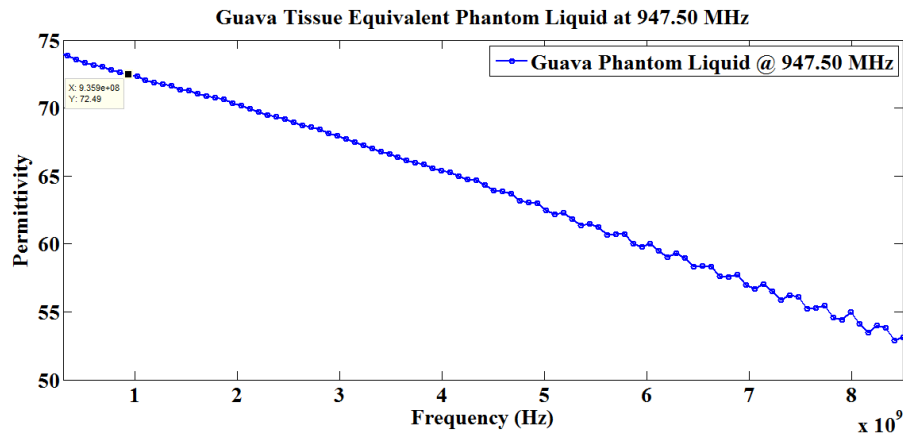
DGME = diethylene glycol monobutyl ether

Table 5.9 Difference between the measured dielectric properties ( $\epsilon_r$ ) of apple tissue specimen and equivalent phantom liquids

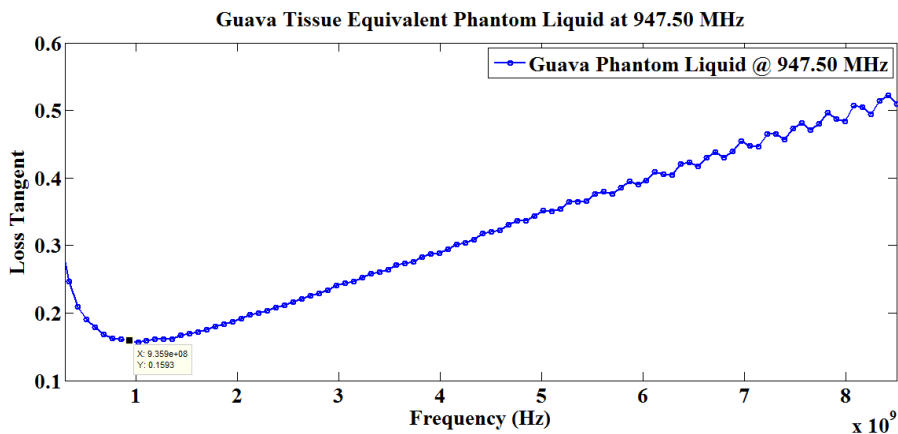
Frequency (MHz)	947.50	Deviation	1842.50	Deviation	2450.00	Deviation
Reference Permittivity ( $\epsilon_r'$ )	65.03		63.72		62.23	
Phantom Liquid Permittivity ( $\epsilon_r'$ )	67.80	4.26%	62.48	1.95%	61.33	1.45%
Reference Loss Tangent ( $\tan \delta$ )	0.135		0.156		0.194	
Phantom Liquid Loss Tangent ( $\tan \delta$ )	0.124	8.15%	0.156	0.00%	0.204	5.15%

### 5.4.3 Phantom Liquids Preparation for Guava Specimen

This time, phantom liquid formulations have been prepared for guava fruit tissue at 947.50 MHz, 1842.50 MHz and 2450.00 MHz. Guava tissue equivalent phantom liquid recipes have been prepared based on different compositions of DI water (resistivity = 13 M $\Omega$ cm), sucrose and sodium chloride (NaCl). At initial phase, certain amount of sucrose has been added to DI water for bringing down the permittivity ( $\epsilon_r'$ ) of phantom liquid composition; in this manner, phantom liquid permittivity ( $\epsilon_r'$ ) is tuned closer to the measured permittivity ( $\epsilon_r'$ ) of guava tissue (original reference data). Thereafter, based on frequency of interest, different amounts of sodium chloride (NaCl) have been added to the above mentioned liquid composition for fine tuning electrical conductivity ( $\sigma$ ) / loss tangent ( $\tan \delta$ ) of the final equivalent phantom liquids.

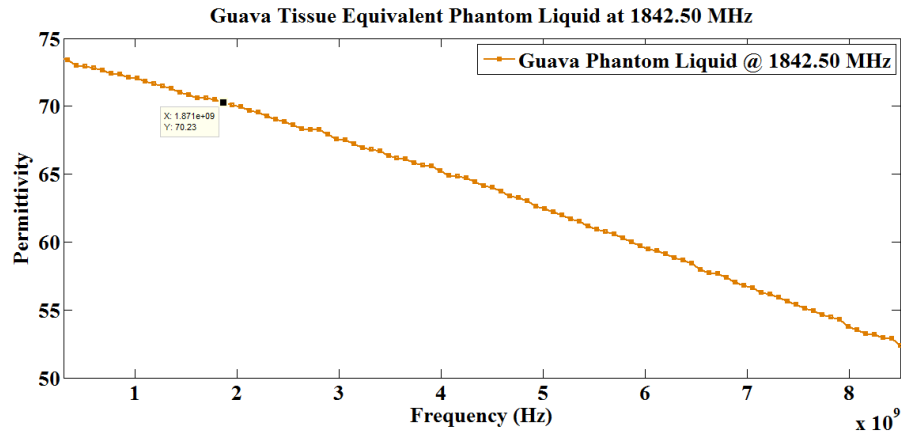


(a)

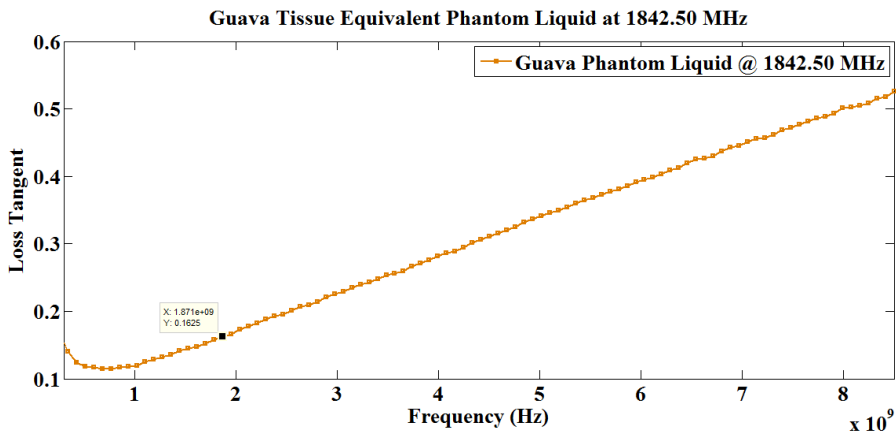


(b)

Fig. 5.14: Guava tissue equivalent phantom liquid at 947.50 MHz (a) permittivity and (b) loss tangent



(a)



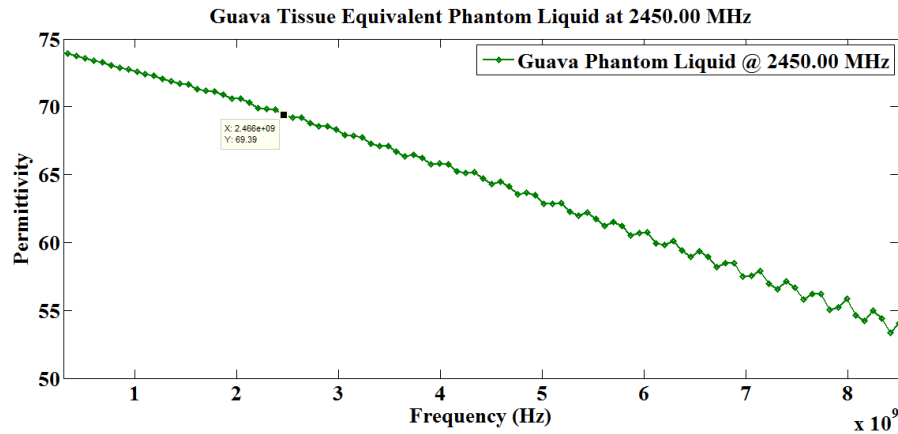
(b)

Fig. 5.15: Guava tissue equivalent phantom liquid at 1842.50 MHz (a) permittivity and (b) loss tangent

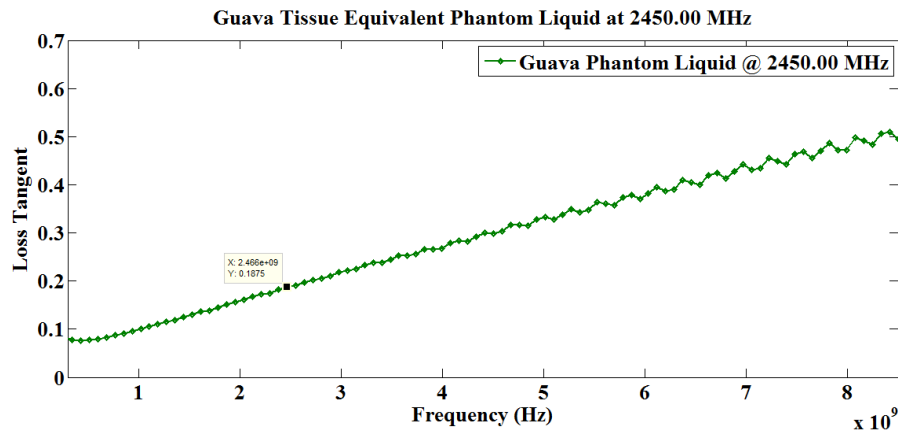
As stated above, initially, complex dielectric properties ( $\epsilon_r$ ) i.e. permittivity ( $\epsilon_r'$ ) and loss tangent ( $\tan \delta$ ) data have been measured for pure DI water (13 M $\Omega$ cm resistivity) at 25 °C – prior to guava tissue equivalent phantom liquid recipes preparation. The measured permittivity ( $\epsilon_r'$ ) and loss tangent ( $\tan \delta$ ) data for the above mentioned DI water have already been discussed earlier at 947.50 MHz, 1842.50 MHz and 2450.00 MHz.

At initial stage, to prepare guava fruit tissue equivalent phantom liquid recipe at 947.50 MHz, 20 g sucrose and 250 mg sodium chloride (NaCl) have been added with 100 ml DI water (13 M $\Omega$ cm resistivity) to attain permittivity ( $\epsilon_r'$ ) and loss tangent ( $\tan \delta$ ) values close to the original measured data for guava specimen (please refer to Table 5.10). The final phantom liquid





(a)



(b)

Fig. 5.16: Guava tissue equivalent phantom liquid at 2450.00 MHz (a) permittivity and (b) loss tangent

permittivity ( $\epsilon'_r$ ) and loss tangent ( $\tan \delta$ ) data have been achieved within 0.57% and 3.25% limits of the reference data at 947.50 MHz (please refer to Fig. 5.14 and Table 5.11).

At subsequent phase, to formulate guava tissue equivalent phantom liquid preparation at 1842.50 MHz, 20 g sucrose and 100 mg sodium chloride (NaCl) have been added with 100 ml DI water (13 M $\Omega$ cm resistivity) to tune permittivity ( $\epsilon'_r$ ) and loss tangent ( $\tan \delta$ ) parameters of equivalent liquid close to the original guava specimen (please refer to Table 5.10). The final equivalent phantom liquid permittivity ( $\epsilon'_r$ ) and loss tangent ( $\tan \delta$ ) values have been achieved within 1.15% and 1.89% limits of the reference values for guava specimen at 1842.50 MHz (please refer to Fig. 5.15 and Table 5.11).

## Phantom Liquid Preparation for Different Fruit and Plant Samples

At last, 20 g sucrose and 50 mg sodium chloride (NaCl) have been added to 100 ml DI water (13 MΩcm resistivity) for fine tuning equivalent phantom liquid permittivity ( $\epsilon_r'$ ) and loss tangent ( $\tan \delta$ ) values close to the original guava specimen at 2450.00 MHz (please refer to Table 5.10 for detailed composition at 25 °C). Final permittivity ( $\epsilon_r'$ ) and loss tangent ( $\tan \delta$ ) values of the equivalent phantom liquid have been tuned within 0.49% and 5.03% limits of the reference dielectric properties ( $\epsilon_r$ ) of original guava specimen at 2450.00 MHz (please refer to Fig. 5.16 and Table 5.11). Here also, it is to be noted that the deviation in loss tangent ( $\tan \delta$ ) data can be further minimized if DI water with resistivity higher than 13 MΩcm is utilized in the equivalent phantom liquid composition.

Table 5.10 Final compositions of guava tissue equivalent phantom liquids

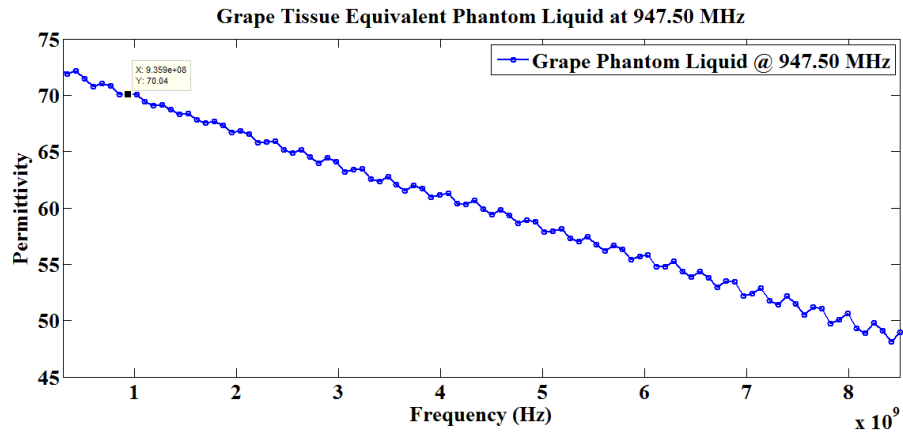
Frequency (MHz)	Final composition of phantom liquid
947.50	100 ml DI water, 20 g sucrose & 250 mg NaCl
1842.50	100 ml DI water, 20 g sucrose & 100 mg NaCl
2450.00	100 ml DI water, 20 g sucrose & 50 mg NaCl

Table 5.11 Difference between the measured dielectric properties ( $\epsilon_r$ ) of guava tissue specimen and equivalent phantom liquids

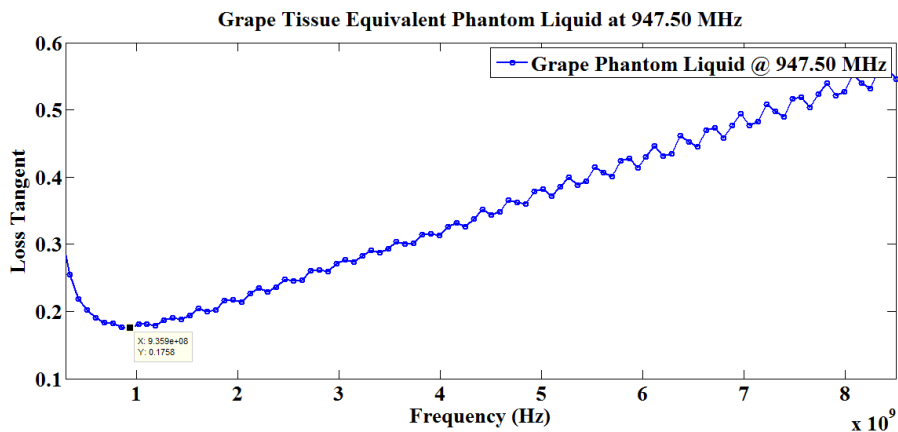
Frequency (MHz)	947.50	Deviation	1842.50	Deviation	2450.00	Deviation
Reference Permittivity ( $\epsilon_r'$ )	72.08		71.05		69.73	
Phantom Liquid Permittivity ( $\epsilon_r'$ )	72.49	0.57%	70.23	1.15%	69.39	0.49%
Reference Loss Tangent ( $\tan \delta$ )	0.154		0.159		0.179	
Phantom Liquid Loss Tangent ( $\tan \delta$ )	0.159	3.25%	0.162	1.89%	0.188	5.03%

### 5.4.4 Phantom Liquids Preparation for Grape Specimen

Phantom liquid compositions have been prepared for grape tissue at 947.50 MHz, 1842.50 MHz and 2450.00 MHz respectively. Grape tissue equivalent liquid recipes have been prepared based on different compositions of DI water (13 M $\Omega$ cm resistivity), sucrose / diethylene glycol monobutyl ether and sodium chloride (NaCl). Based upon the frequency of interest, sucrose / diethylene glycol monobutyl ether has been added with DI water (13 M $\Omega$ cm resistivity) to reduce permittivity ( $\epsilon_r'$ ) of the liquid composition; in this fashion, phantom liquid permittivity ( $\epsilon_r'$ ) is tuned close to the measured permittivity ( $\epsilon_r'$ ) of grape tissue specimen (reference data). Next, sodium chloride (NaCl) has further been added to those liquid preparations for fine tuning electrical conductivity ( $\sigma$ ) / loss tangent ( $\tan \delta$ ) of the equivalent phantom liquids.



(a)



(b)

Fig. 5.17: Grape tissue equivalent phantom liquid at 947.50 MHz (a) permittivity and (b) loss tangent

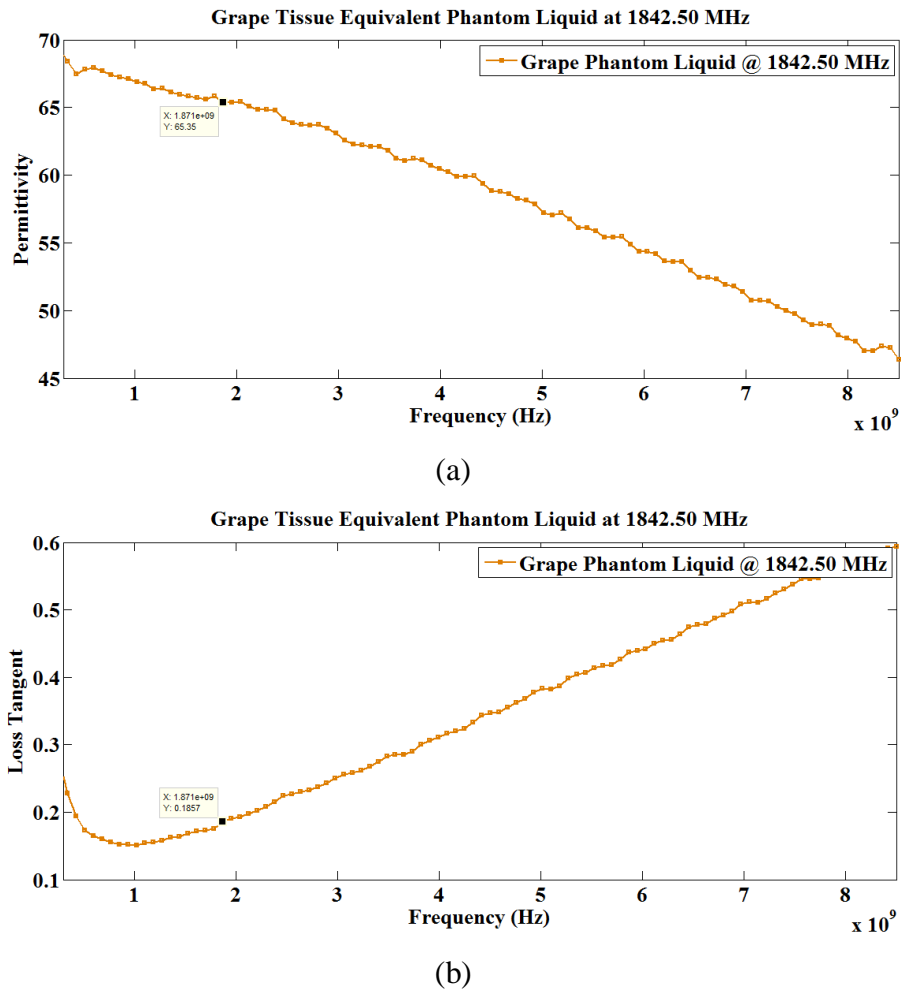
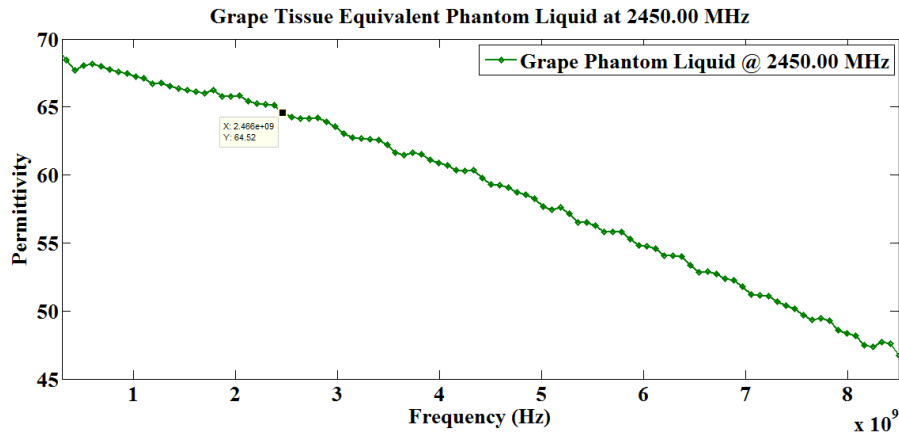


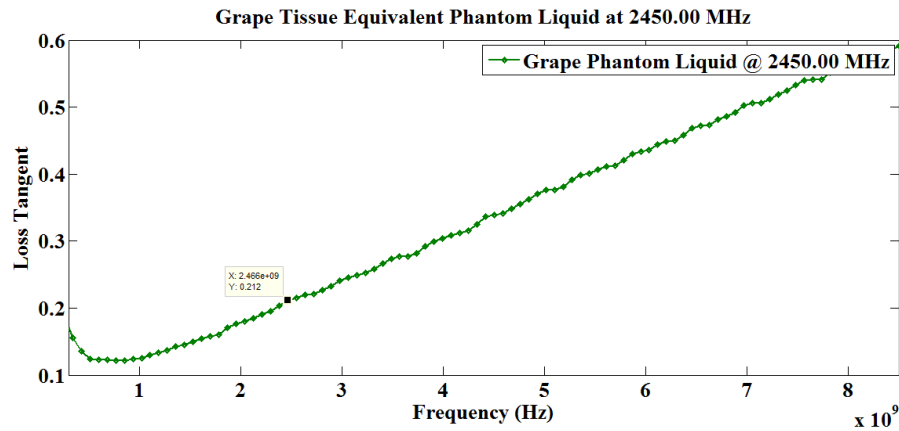
Fig. 5.18: Grape tissue equivalent phantom liquid at 1842.50 MHz (a) permittivity and (b) loss tangent

As noted earlier, complex dielectric properties ( $\epsilon_r$ ) i.e. permittivity ( $\epsilon_r'$ ) and loss tangent ( $\tan \delta$ ) data for pure DI water (13 M $\Omega$ cm resistivity) have been measured at initial stage – before grape tissue equivalent phantom liquids formulation. The complex dielectric properties ( $\epsilon_r$ ) i.e. permittivity ( $\epsilon_r'$ ) and loss tangent ( $\tan \delta$ ) data for DI water at 25 °C have been mentioned earlier at 947.50 MHz, 1842.50 MHz and 2450.00 MHz – hence, those data haven't been repeated here.

At initial phase, in order to prepare grape tissue equivalent phantom liquid formulation at 947.50 MHz, 27 g sucrose and 300 mg sodium chloride (NaCl) have been added to 100 ml DI water (13 M $\Omega$ cm resistivity) for attaining equivalent phantom liquid permittivity ( $\epsilon_r'$ ) and loss tangent ( $\tan \delta$ ) data close to the original reference values for measured grape specimen – please refer to



(a)



(b)

Fig. 5.19: Grape tissue equivalent phantom liquid at 2450.00 MHz (a) permittivity and (b) loss tangent

Table 5.12. The final phantom liquid permittivity ( $\epsilon_r'$ ) and loss tangent ( $\tan \delta$ ) values have been achieved within 1.35% and 5.39% limits of the reference data at 947.50 MHz (please refer to Fig. 5.17 and Table 5.13). It must be noted that the deviation in loss tangent ( $\tan \delta$ ) value can be minimized further by utilizing DI water with resistivity more than 13 M $\Omega$ cm.

Subsequently, to prepare grape tissue equivalent phantom liquid recipe at 1842.50 MHz, 19.23 ml diethylene glycol monobutyl ether and 230.77 mg sodium chloride (NaCl) have been added with 100 ml DI water (resistivity = 13 M $\Omega$ cm) to tune permittivity ( $\epsilon_r'$ ) and loss tangent ( $\tan \delta$ ) parameters of equivalent phantom liquid close to the original grape tissue specimen (please refer to Table 5.12). Final permittivity ( $\epsilon_r'$ ) and loss tangent ( $\tan \delta$ ) values of the equivalent phantom

liquid have been achieved within 2.18% and 0.54% limits of the measured reference values at 1842.50 MHz (please refer to Fig. 5.18 and Table 5.13).

At final phase, 19.23 ml diethylene glycol monobutyl ether and 153.85 mg sodium chloride (NaCl) have been mixed with 100 ml DI water (resistivity = 13 M $\Omega$ cm) to tune permittivity ( $\epsilon_r'$ ) and loss tangent ( $\tan \delta$ ) values of equivalent phantom liquid close to the original grape tissue specimen at 2450.00 MHz (please refer to Table 5.12 for detailed recipe formulation at 25 °C). Finalized phantom liquid permittivity ( $\epsilon_r'$ ) and loss tangent ( $\tan \delta$ ) values have been tuned within 1.15% and 0.95% limits of the reference dielectric properties ( $\epsilon_r$ ) of grape tissue specimen at 2450.00 MHz (please refer to Fig. 5.19 and Table 5.13).

Table 5.12 Final compositions of grape tissue equivalent phantom liquids

Frequency (MHz)	Final composition of phantom liquid
947.50	100 ml DI water, 27 g sucrose & 300 mg NaCl
1842.50	100 ml DI water, 19.23 ml DGME & 230.77 mg NaCl
2450.00	100 ml DI water, 19.23 ml DGME & 153.85 mg NaCl

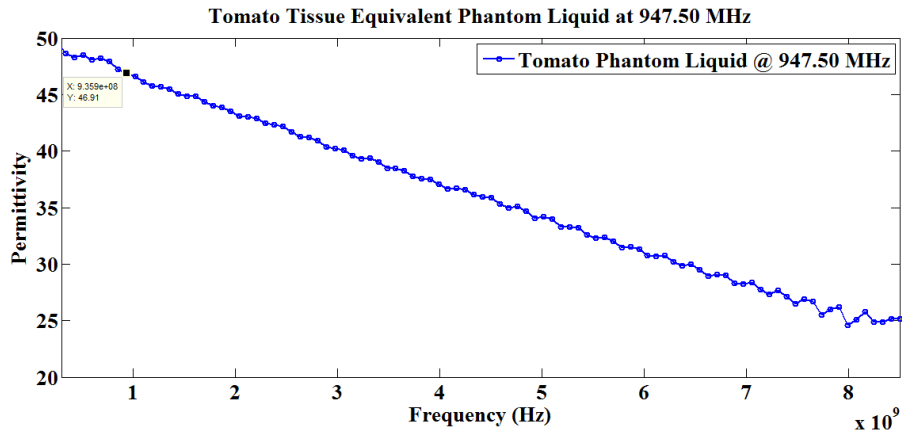
DGME = diethylene glycol monobutyl ether

Table 5.13 Difference between the measured dielectric properties ( $\epsilon_r$ ) of grape tissue specimen and equivalent phantom liquids

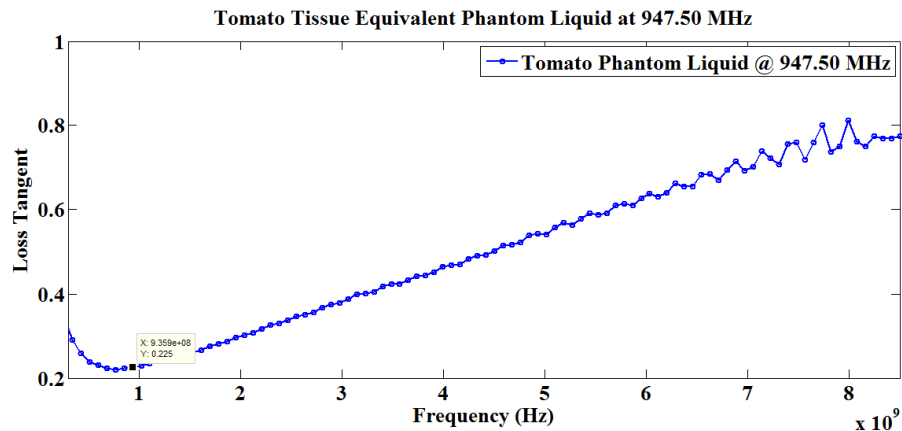
Frequency (MHz)	947.50	Deviation	1842.50	Deviation	2450.00	Deviation
Reference Permittivity ( $\epsilon_r'$ )	69.11		66.81		65.27	
Phantom Liquid Permittivity ( $\epsilon_r'$ )	70.04	1.35%	65.35	2.18%	64.52	1.15%
Reference Loss Tangent ( $\tan \delta$ )	0.167		0.185		0.210	
Phantom Liquid Loss Tangent ( $\tan \delta$ )	0.176	5.39%	0.186	0.54%	0.212	0.95%

### 5.4.5 Phantom Liquids Preparation for Tomato Specimen

Tomato tissue equivalent phantom liquid recipes have been prepared at 947.50 MHz, 1842.50 MHz and 2450.00 MHz respectively. These liquid recipes, equivalent to the measured tomato tissue specimen, have been prepared based on different compositions of DI water (13 M $\Omega$ cm resistivity), diethylene glycol monobutyl ether and sodium chloride (NaCl). In fact, diethylene glycol monobutyl ether has been added with DI water (13 M $\Omega$ cm resistivity) to bring down permittivity ( $\epsilon_r'$ ) of the phantom liquid compositions – thus, equivalent phantom liquid permittivity ( $\epsilon_r'$ ) is tuned close to the measured permittivity ( $\epsilon_r'$ ) of tomato tissue specimen. Thereafter, sodium chloride (NaCl) has been added to those liquid recipes for tuning electrical conductivity ( $\sigma$ ) / loss tangent ( $\tan \delta$ ) of the equivalent phantom liquids.



(a)



(b)

Fig. 5.20: Tomato tissue equivalent phantom liquid at 947.50 MHz (a) permittivity and (b) loss tangent

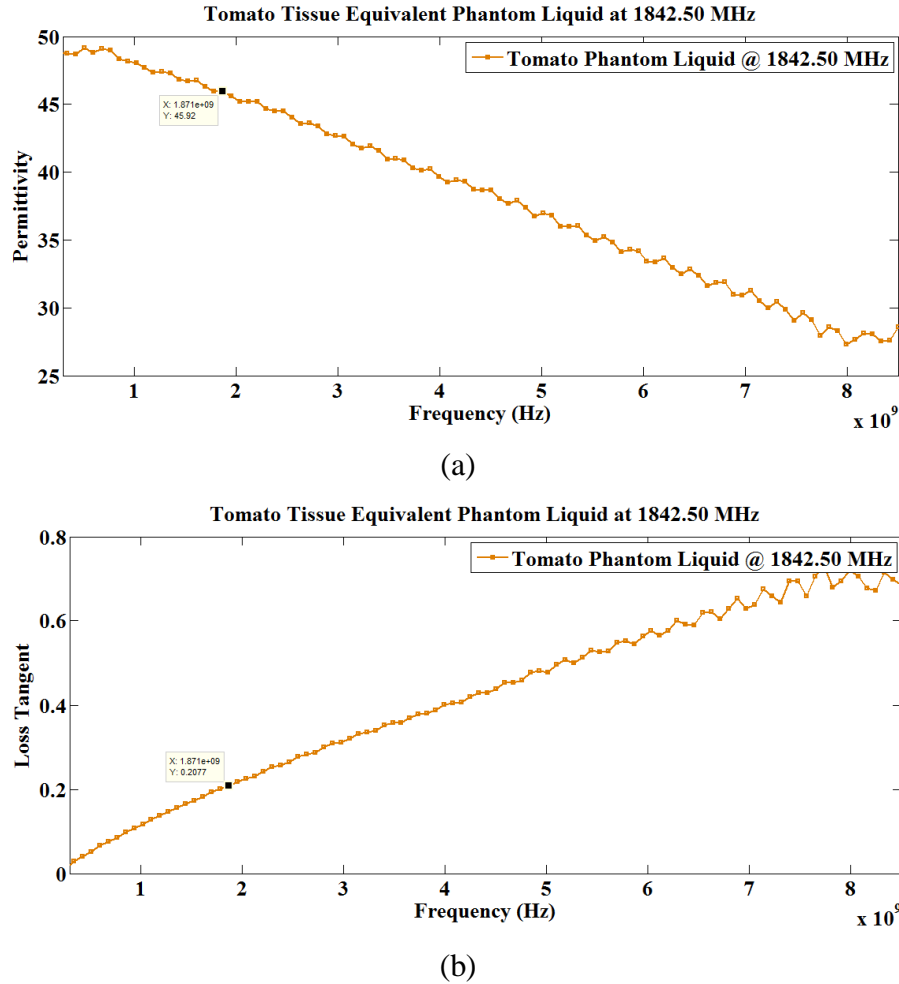
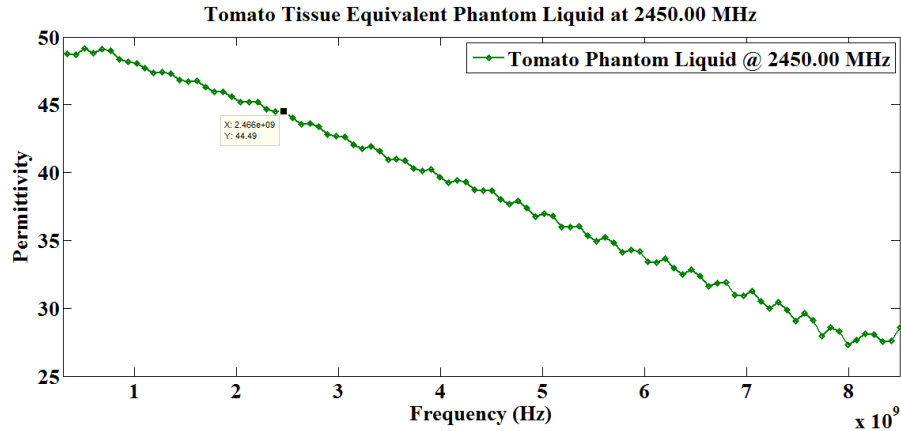


Fig. 5.21: Tomato tissue equivalent phantom liquid at 1842.50 MHz (a) permittivity and (b) loss tangent

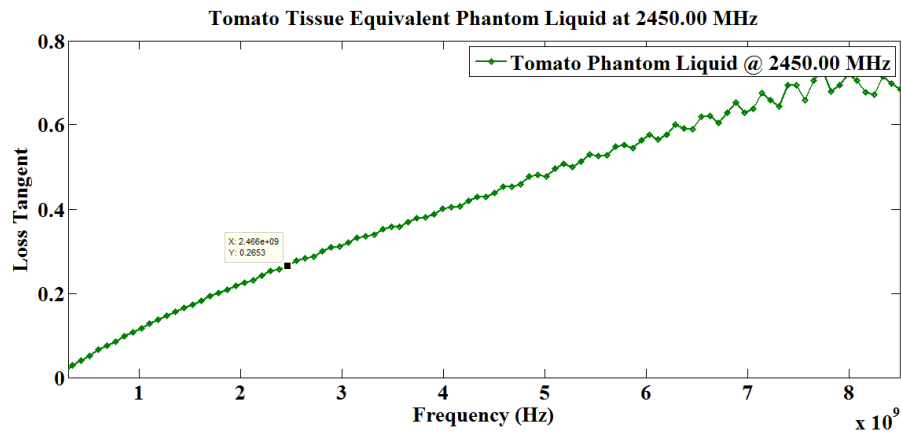
As stated before, permittivity ( $\epsilon_r'$ ) and loss tangent ( $\tan \delta$ ) parameters for pure DI water (13 M $\Omega$ cm resistivity) have been measured at the beginning i.e. even before starting to prepare tomato tissue equivalent phantom liquids at 25 °C. The measured dielectric properties ( $\epsilon_r$ ) i.e. permittivity ( $\epsilon_r'$ ) and loss tangent ( $\tan \delta$ ) data for pure DI water at 25 °C have already been discussed at 947.50 MHz, 1842.50 MHz and 2450.00 MHz.

At first, to prepare tomato tissue equivalent phantom liquid preparation at 947.50 MHz, 71.43 ml diethylene glycol monobutyl ether along with 500 mg sodium chloride (NaCl) has been added with 100 ml DI water (13 M $\Omega$ cm resistivity) for achieving equivalent phantom liquid permittivity ( $\epsilon_r'$ ) and loss tangent ( $\tan \delta$ ) data close to the original measured values for tomato specimen (please refer to Table 5.14). The ultimate equivalent phantom liquid permittivity ( $\epsilon_r'$ )





(a)



(b)

Fig. 5.22: Tomato tissue equivalent phantom liquid at 2450.00 MHz (a) permittivity and (b) loss tangent

value has been achieved within 0.19% limit of the reference value and loss tangent ( $\tan \delta$ ) value exactly matches at 947.50 MHz (please refer to Fig. 5.20 and Table 5.15).

At subsequent stage, to formulate tomato tissue equivalent phantom liquid at 1842.50 MHz, 71.43 ml diethylene glycol monobutyl ether has simply been added with 100 ml DI water (resistivity = 13 M $\Omega$ cm) to tune permittivity ( $\epsilon'_r$ ) and loss tangent ( $\tan \delta$ ) values of equivalent phantom liquid close to the original tomato specimen (please refer to Table 5.14). Final permittivity ( $\epsilon'_r$ ) and loss tangent ( $\tan \delta$ ) values of the equivalent phantom liquid have been achieved within 0.17% and 9.47% limits of the measured reference values at 1842.50 MHz (please refer to Fig. 5.21 and Table 5.15). It should be noted that the deviation in loss tangent

( $\tan \delta$ ) value can be minimized further if DI water with resistivity more than 13 M $\Omega$ cm is utilized.

At final stage, the immediate past liquid composition i.e. 71.43 ml diethylene glycol monobutyl ether with 100 ml DI water (resistivity = 13 M $\Omega$ cm) has been utilized to tune permittivity ( $\epsilon_r'$ ) and loss tangent ( $\tan \delta$ ) data of equivalent phantom liquid close to the reference tomato specimen (please refer to Table 5.14 for the recipe at 25 °C). The final phantom liquid permittivity ( $\epsilon_r'$ ) value has been tuned within 1.13% limit of the reference tomato tissue specimen at 2450.00 MHz (please refer to Fig. 5.22(a) and Table 5.15). However, the reference loss tangent ( $\tan \delta$ ) value for tomato specimen couldn't be achieved with 13 M $\Omega$ cm resistivity DI water at 2450.00 MHz (please refer to Fig. 5.22(b) and Table 5.15). It should be noted that phantom liquid loss tangent ( $\tan \delta$ ) at 2450.00 MHz can be matched with DI water possessing resistivity much greater than 13 M $\Omega$ cm.

Table 5.14 Final compositions of tomato tissue equivalent phantom liquids

Frequency (MHz)	Final composition of phantom liquid
947.50	100 ml DI water, 71.43 ml DGME & 500 mg NaCl
1842.50	100 ml DI water & 71.43 ml DGME
2450.00	100 ml DI water & 71.43 ml DGME

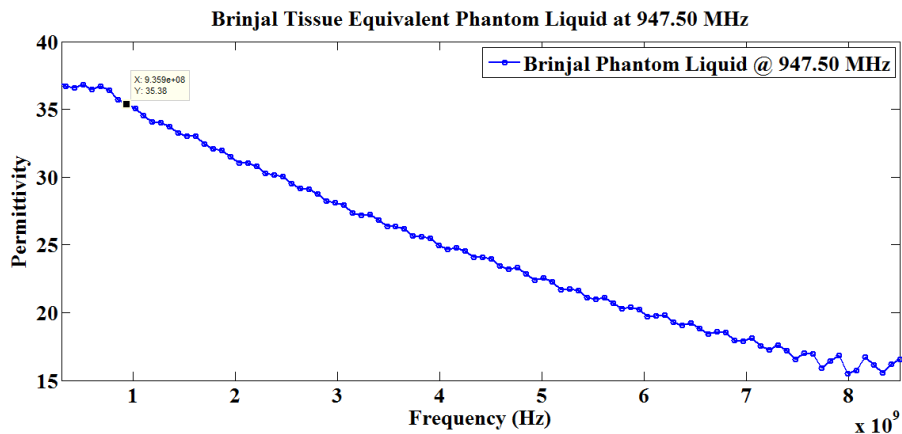
DGME = diethylene glycol monobutyl ether

Table 5.15 Difference between the measured dielectric properties ( $\epsilon_r$ ) of tomato tissue specimen and equivalent phantom liquids

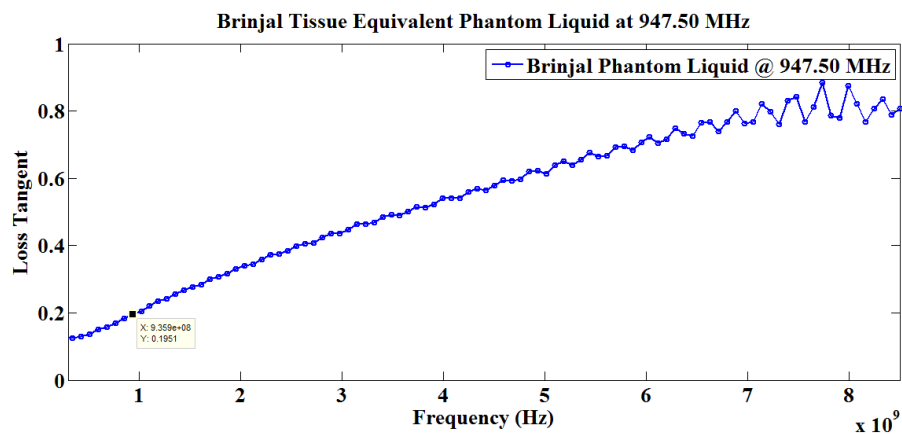
Frequency (MHz)	947.50	Deviation	1842.50	Deviation	2450.00	Deviation
Reference Permittivity ( $\epsilon_r'$ )	47.00		46.00		45.00	
Phantom Liquid Permittivity ( $\epsilon_r'$ )	46.91	0.19%	45.92	0.17%	44.49	1.13%
Reference Loss Tangent ( $\tan \delta$ )	0.225		0.190		0.200	
Phantom Liquid Loss Tangent ( $\tan \delta$ )	0.225	0.00%	0.208	9.47%	0.265	32.50%

### 5.4.6 Phantom Liquids Preparation for Brinjal Specimen

Attempts have been made to prepare brinjal tissue equivalent phantom liquid recipes at 947.50 MHz, 1842.50 MHz and 2450.00 MHz respectively. Phantom liquid recipes, close to the measured brinjal specimen, have been attempted to be prepared based on different compositions of DI water (13 MΩcm resistivity), diethylene glycol monobutyl ether and sodium chloride (NaCl). In fact, diethylene glycol monobutyl ether has been added with DI water (resistivity = 13 MΩcm) to reduce permittivity ( $\epsilon_r'$ ) of the phantom liquid recipes – in this manner, permittivity ( $\epsilon_r'$ ) of the equivalent phantom liquids is tuned close to the original permittivity ( $\epsilon_r'$ ) of brinjal tissue specimen. Furthermore, sodium chloride (NaCl) has been added to the liquid recipe for



(a)



(b)

Fig. 5.23: Brinjal tissue equivalent phantom liquid at 947.50 MHz (a) permittivity and (b) loss tangent

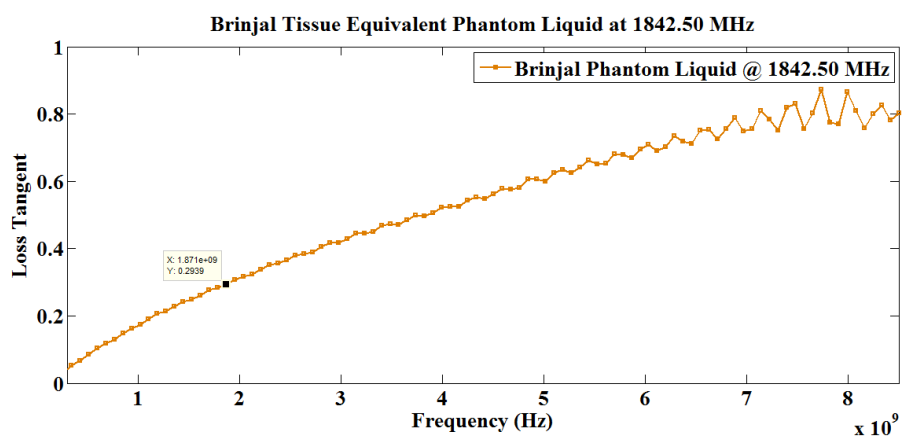
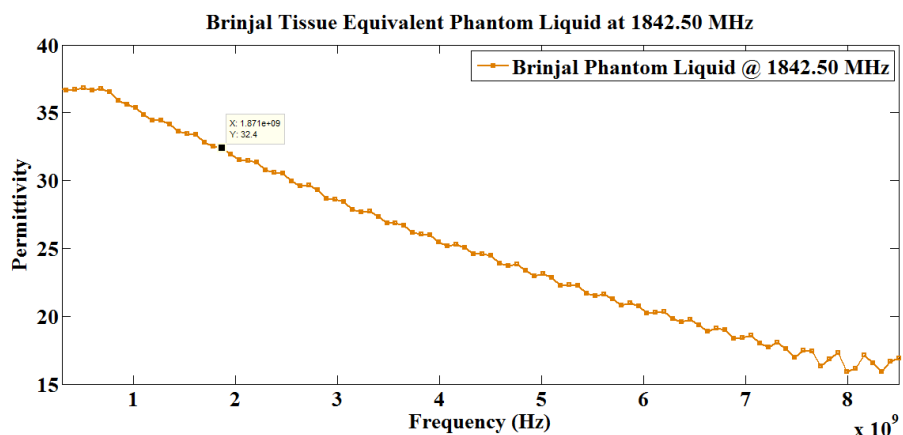
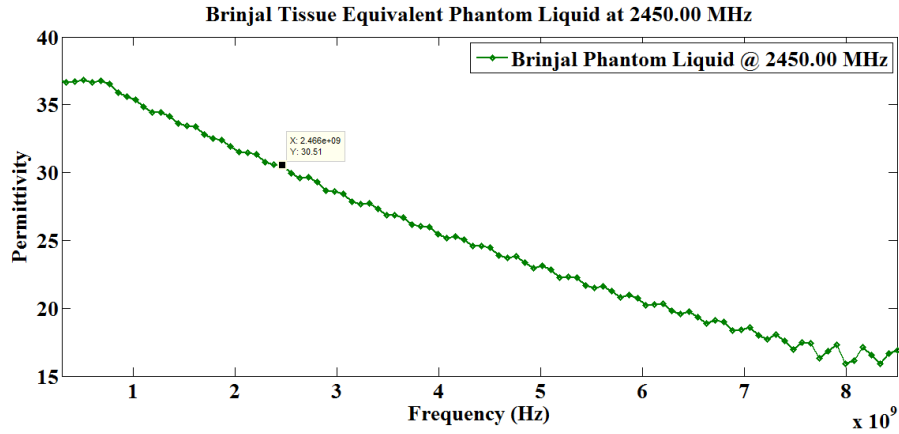


Fig. 5.24: Brinjal tissue equivalent phantom liquid at 1842.50 MHz (a) permittivity and (b) loss tangent

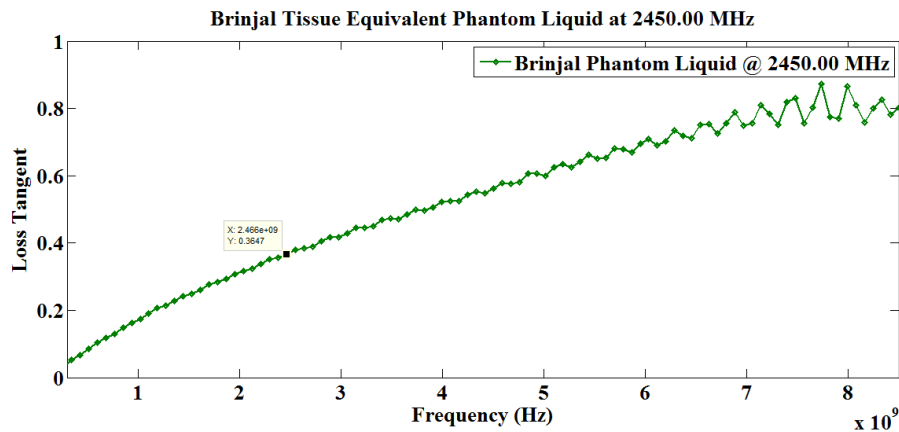
tuning electrical conductivity ( $\sigma$ ) / loss tangent ( $\tan \delta$ ) of the equivalent phantom liquid in particular at 947.50 MHz.

As discussed earlier, complex dielectric properties ( $\epsilon_r$ ) i.e. permittivity ( $\epsilon_r'$ ) and loss tangent ( $\tan \delta$ ) values for pure DI water (resistivity = 13 M $\Omega$ cm) have been measured at the initial stage – prior to preparing brinjal tissue equivalent phantom liquids. Measured permittivity ( $\epsilon_r'$ ) and loss tangent ( $\tan \delta$ ) values for pure DI water have been discussed earlier at 947.50 MHz, 1842.50 MHz and 2450.00 MHz.

In order to prepare brinjal tissue equivalent phantom liquid at 947.50 MHz, 142.86 ml diethylene glycol monobutyl ether and 214.28 mg sodium chloride (NaCl) have been added with 100 ml DI



(a)



(b)

Fig. 5.25: Brinjal tissue equivalent phantom liquid at 2450.00 MHz (a) permittivity and (b) loss tangent

water (resistivity = 13 M $\Omega$ cm) for attaining equivalent phantom liquid permittivity ( $\epsilon_r'$ ) and loss tangent ( $\tan \delta$ ) values close to the original brinjal specimen (please refer to Table 5.16). The equivalent phantom liquid permittivity ( $\epsilon_r'$ ) and loss tangent ( $\tan \delta$ ) values have been achieved within 4.06% and 2.50% limits of the original reference data at 947.50 MHz (please refer to Fig. 5.23 and Table 5.17).

Next, to prepare brinjal tissue equivalent phantom liquid recipe at 1842.50 MHz, 142.86 ml diethylene glycol monobutyl ether has been mixed with 100 ml DI water (resistivity = 13 M $\Omega$ cm) to tune permittivity ( $\epsilon_r'$ ) value of the equivalent phantom liquid close to original brinjal specimen (please refer to Table 5.16). The final permittivity ( $\epsilon_r'$ ) value of the equivalent phantom liquid has been attained within 1.82% limit of the measured brinjal specimen at 1842.50

MHz (please refer to Fig. 5.24(a) and Table 5.17). However, it must be noted that the deviation in loss tangent ( $\tan \delta$ ) value is significantly large at 1842.50 MHz (please refer to Fig. 5.24(b) and Table 5.17) – noted deviation can only be minimized by using DI water with resistivity much greater than 13 M $\Omega$ cm.

At final stage, the above mentioned liquid composition i.e. 142.86 ml diethylene glycol monobutyl ether mixed with 100 ml DI water (resistivity = 13 M $\Omega$ cm) has been employed to tune permittivity ( $\epsilon_r'$ ) of equivalent phantom liquid close to the reference brinjal specimen (please refer to Table 5.16). The final phantom liquid permittivity ( $\epsilon_r'$ ) value has been tuned within 6.12% limit of the reference brinjal specimen at 2450.00 MHz (please refer to Fig. 5.25(a) and Table 5.17). However, once again, it is to be noted that the deviation in loss tangent ( $\tan \delta$ ) value is significantly large even at 2450.00 MHz (please refer to Fig. 5.25(b) and Table 5.17). The deviation in loss tangent ( $\tan \delta$ ) can only be attempted to minimize by utilizing DI water with resistivity much greater than 13 M $\Omega$ cm.

Table 5.16 Final compositions of brinjal tissue equivalent phantom liquids

Frequency (MHz)	Final composition of phantom liquid
947.50	100 ml DI water, 142.86 ml DGME & 214.28 mg NaCl
1842.50	100 ml DI water & 142.86 ml DGME
2450.00	100 ml DI water & 142.86 ml DGME

DGME = diethylene glycol monobutyl ether

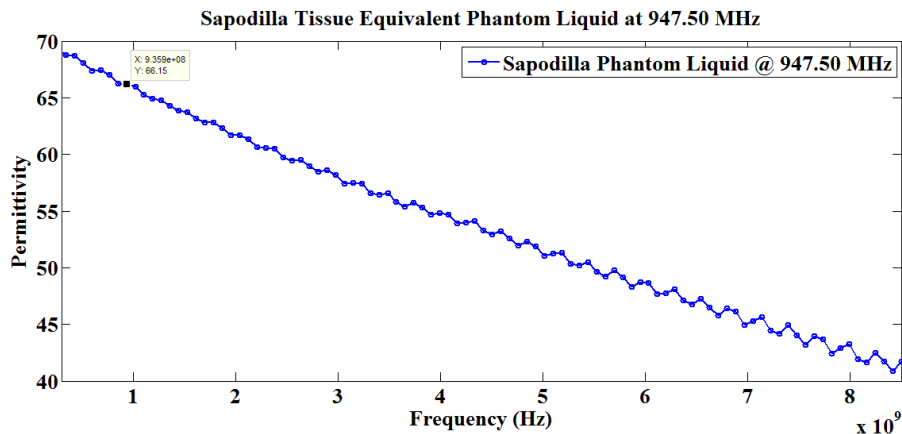
Table 5.17 Difference between the measured dielectric properties ( $\epsilon_r$ ) of brinjal tissue specimen and equivalent phantom liquids

Frequency (MHz)	947.50	Deviation	1842.50	Deviation	2450.00	Deviation
Reference Permittivity ( $\epsilon_r'$ )	34.00		33.00		32.50	
Phantom Liquid Permittivity ( $\epsilon_r'$ )	35.38	4.06%	32.40	1.82%	30.51	6.12%
Reference Loss Tangent ( $\tan \delta$ )	0.200		0.185		0.200	
Phantom Liquid Loss Tangent ( $\tan \delta$ )	0.195	2.50%	0.294	58.92%	0.365	82.50%

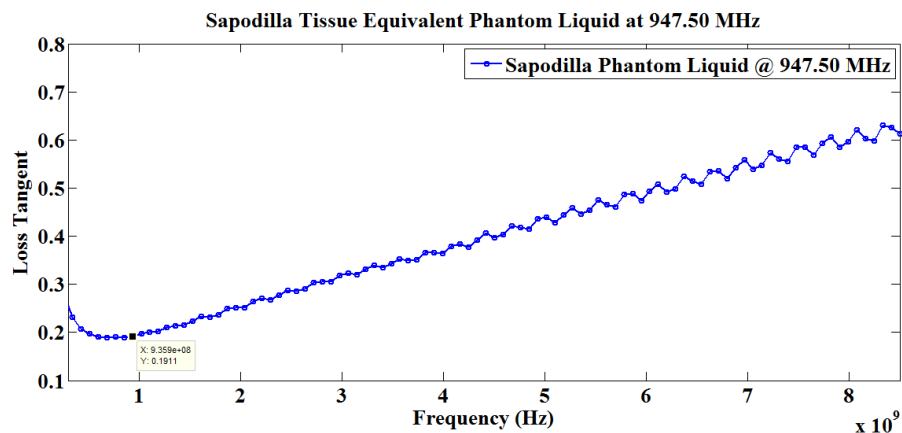
## 5.4.7 Phantom Liquids Preparation for Sapodilla Specimens

### 5.4.7.1 Phantom Liquids Preparation for Sapodilla Fruit Specimen

Phantom liquid compositions have been prepared for sapodilla fruit tissue specimen at 947.50 MHz, 1842.50 MHz and 2450.00 MHz. Sapodilla fruit tissue equivalent liquid preparations have been formulated based on different compositions of DI water (resistivity = 13 MΩcm), sucrose / diethylene glycol monobutyl ether and sodium chloride (NaCl). Based on frequency of interest, either sucrose or diethylene glycol monobutyl ether has been added with DI water (resistivity = 13 MΩcm) to bring down permittivity ( $\epsilon_r'$ ) of the phantom liquid composition – thus, phantom liquid permittivity ( $\epsilon_r'$ ) value is tuned close to the measured permittivity ( $\epsilon_r'$ ) of sapodilla fruit

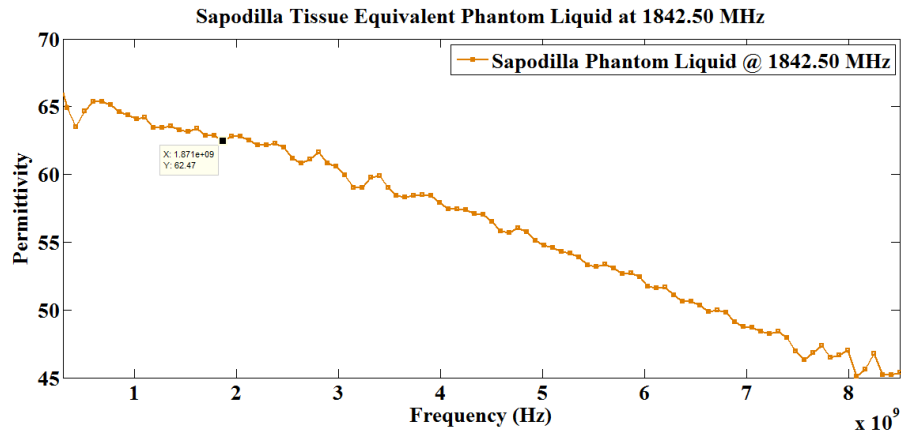


(a)

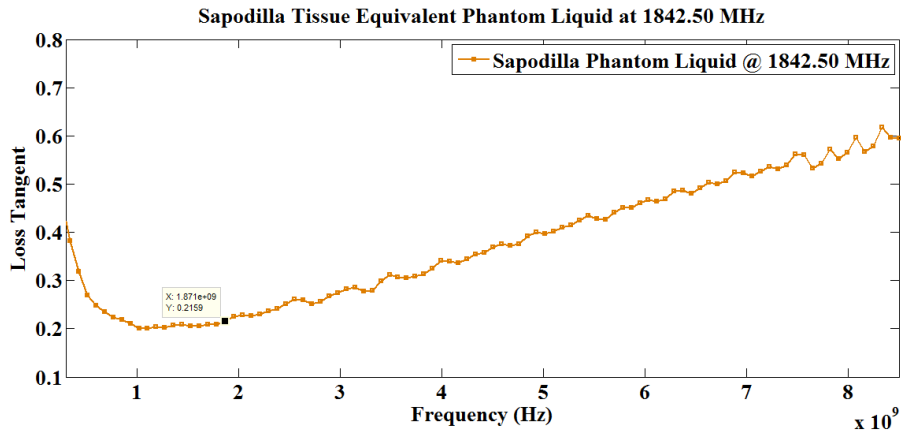


(b)

Fig. 5.26: Sapodilla fruit tissue equivalent phantom liquid at 947.50 MHz (a) permittivity and (b) loss tangent



(a)



(b)

Fig. 5.27: Sapodilla fruit tissue equivalent phantom liquid at 1842.50 MHz (a) permittivity and (b) loss tangent

tissue specimen. Thereafter, sodium chloride (NaCl) has further been added to those compositions for fine tuning electrical conductivity ( $\sigma$ ) / loss tangent ( $\tan \delta$ ) of the final equivalent phantom liquids.

As already noted, dielectric properties ( $\epsilon_r$ ) i.e. permittivity ( $\epsilon_r'$ ) and loss tangent ( $\tan \delta$ ) data for pure DI water (resistivity = 13 M $\Omega$ cm) have been measured prior to sapodilla fruit tissue equivalent phantom liquids preparation. The complex dielectric properties ( $\epsilon_r$ ) i.e. permittivity ( $\epsilon_r'$ ) and loss tangent ( $\tan \delta$ ) data for DI water at 25 °C have earlier been mentioned at 947.50 MHz, 1842.50 MHz and 2450.00 MHz – thus, those values aren't repeated here.



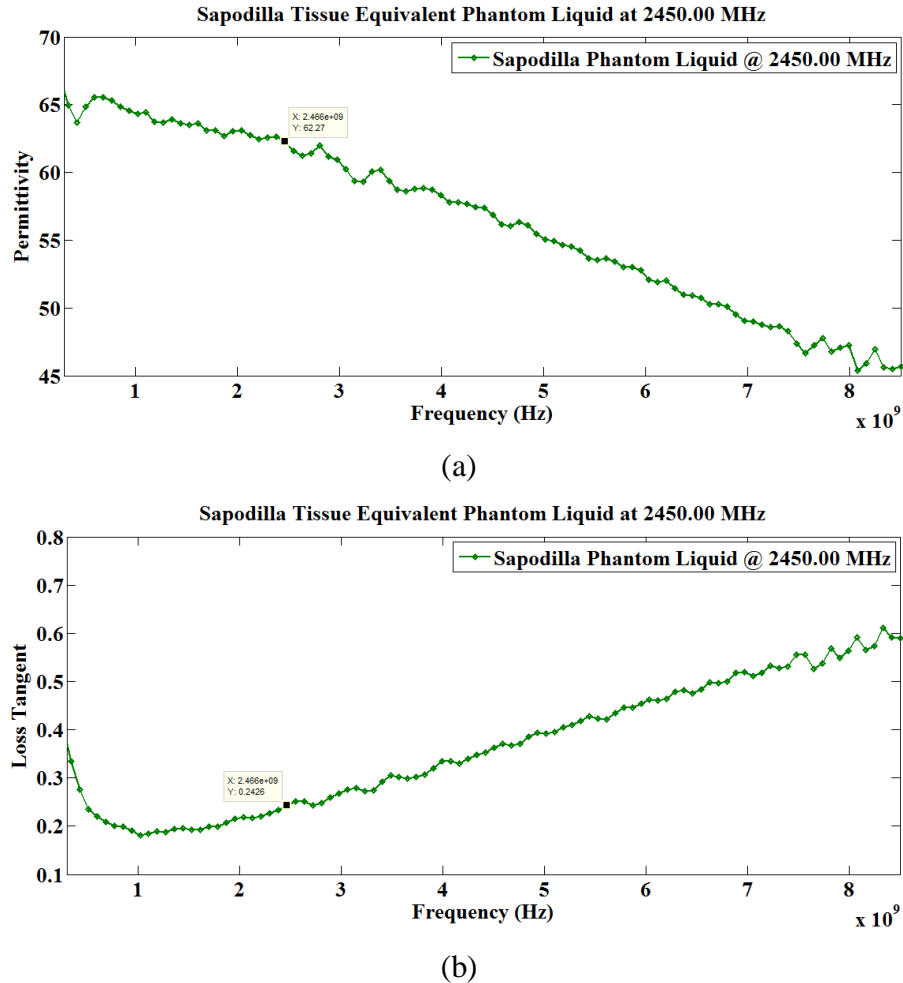


Fig. 5.28: Sapodilla fruit tissue equivalent phantom liquid at 2450.00 MHz (a) permittivity and (b) loss tangent

At first, to formulate sapodilla fruit tissue equivalent phantom liquid at 947.50 MHz, 42 g sucrose and 350 mg sodium chloride (NaCl) have been added with 100 ml DI water (resistivity = 13 M $\Omega$ cm) to achieve equivalent phantom liquid permittivity ( $\epsilon_r'$ ) and loss tangent ( $\tan \delta$ ) values close to the measured data for sapodilla fruit specimen (please refer to Table 5.18). The final phantom liquid permittivity ( $\epsilon_r'$ ) and loss tangent ( $\tan \delta$ ) values have been achieved within 0.20% and 4.02% limits of the reference data at 947.50 MHz (please refer to Fig. 5.26 and Table 5.19).

At subsequent stage, to prepare sapodilla fruit tissue equivalent phantom liquid recipe at 1842.50 MHz, 23.81 ml diethylene glycol monobutyl ether and 380.95 mg sodium chloride (NaCl) have been mixed with 100 ml DI water (resistivity = 13 M $\Omega$ cm) for tuning permittivity ( $\epsilon_r'$ ) and loss

tangent ( $\tan \delta$ ) values of equivalent phantom liquid close to the original sapodilla fruit tissue specimen (please refer to Table 5.18). Final permittivity ( $\epsilon_r'$ ) and loss tangent ( $\tan \delta$ ) values of the equivalent phantom liquid have been achieved within 1.85% and 0.93% limits of the original reference values at 1842.50 MHz (please refer to Fig. 5.27 and Table 5.19).

At last, 23.81 ml diethylene glycol monobutyl ether and 333.33 mg sodium chloride (NaCl) have been mixed with 100 ml DI water (resistivity = 13 M $\Omega$ cm) to tune permittivity ( $\epsilon_r'$ ) and loss tangent ( $\tan \delta$ ) parameters of equivalent phantom liquid close to the original sapodilla fruit specimen at 2450.00 MHz (please refer to Table 5.18 for detailed recipe at 25 °C). The finalized phantom liquid permittivity ( $\epsilon_r'$ ) and loss tangent ( $\tan \delta$ ) values have been tuned within 0.37% and 0.82% limits of the measured dielectric properties ( $\epsilon_r$ ) of sapodilla fruit specimen at 2450.00 MHz (please refer to Fig. 5.28 and Table 5.19).

Table 5.18 Final compositions of sapodilla fruit tissue equivalent phantom liquids

Frequency (MHz)	Final composition of phantom liquid
947.50	100 ml DI water, 42 g sucrose & 350 mg NaCl
1842.50	100 ml DI water, 23.81 ml DGME & 380.95 mg NaCl
2450.00	100 ml DI water, 23.81 ml DGME & 333.33 mg NaCl

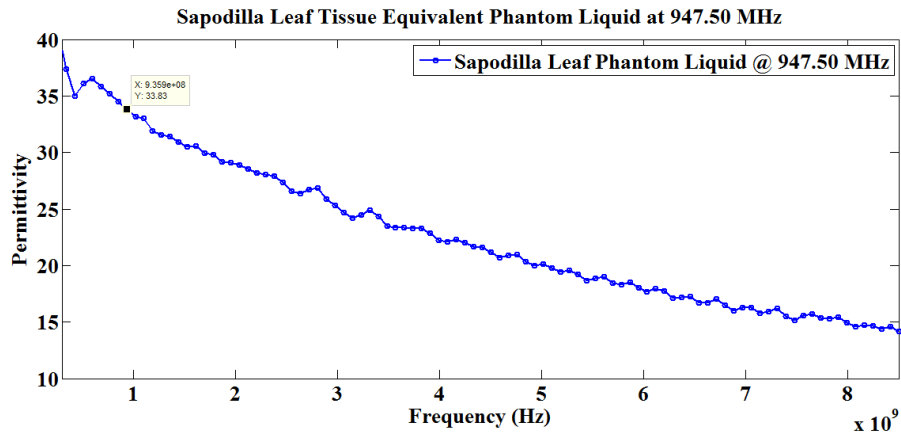
DGME = diethylene glycol monobutyl ether

Table 5.19 Difference between the measured dielectric properties ( $\epsilon_r$ ) of sapodilla fruit tissue specimen and equivalent phantom liquids

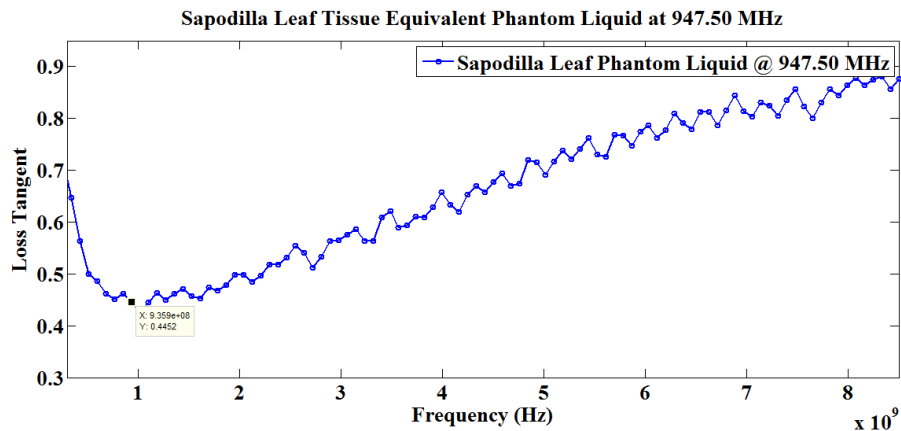
Frequency (MHz)	947.50	Deviation	1842.50	Deviation	2450.00	Deviation
Reference Permittivity ( $\epsilon_r'$ )	66.02		63.65		62.50	
Phantom Liquid Permittivity ( $\epsilon_r'$ )	66.15	0.20%	62.47	1.85%	62.27	0.37%
Reference Loss Tangent ( $\tan \delta$ )	0.199		0.214		0.245	
Phantom Liquid Loss Tangent ( $\tan \delta$ )	0.191	4.02%	0.216	0.93%	0.243	0.82%

### 5.4.7.2 Phantom Liquids Preparation for Sapodilla Leaf Specimen

This time, phantom liquid compositions have been prepared for sapodilla leaf tissue specimen at 947.50 MHz, 1842.50 MHz and 2450.00 MHz. Sapodilla leaf tissue equivalent liquid recipes have been prepared based on different compositions of DI water (resistivity = 13 MΩcm), diethylene glycol monobutyl ether and sodium chloride (NaCl). Depending on frequency range, different amount of diethylene glycol monobutyl ether has been added with DI water (resistivity = 13 MΩcm) to considerably reduce permittivity ( $\epsilon_r'$ ) of the phantom liquid – in this manner, phantom liquid permittivity ( $\epsilon_r'$ ) is tuned closer to the measured permittivity ( $\epsilon_r'$ ) of sapodilla leaf tissue specimen. Furthermore, sodium chloride (NaCl) has been added to the liquid recipe to fine tune electrical conductivity ( $\sigma$ ) / loss tangent ( $\tan \delta$ ) of the final equivalent phantom liquid.



(a)



(b)

Fig. 5.29: Sapodilla leaf tissue equivalent phantom liquid at 947.50 MHz (a) permittivity and (b) loss tangent

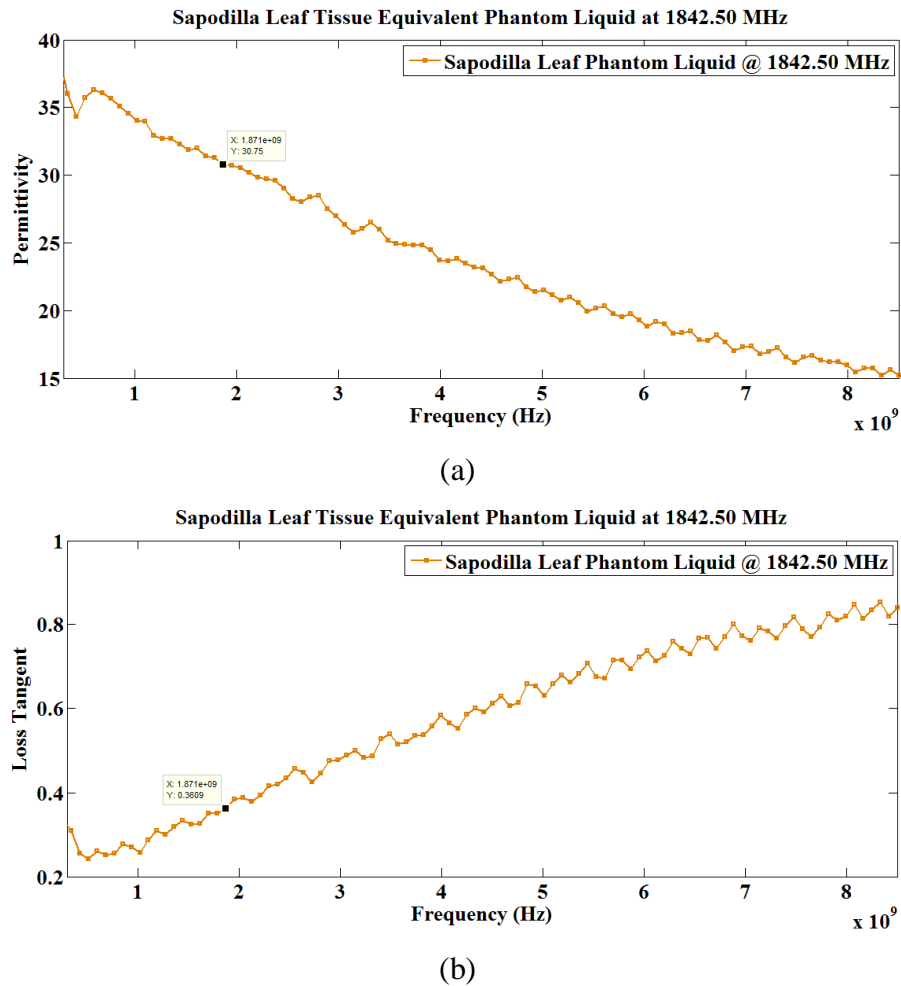


Fig. 5.30: Sapodilla leaf tissue equivalent phantom liquid at 1842.50 MHz (a) permittivity and (b) loss tangent

As discussed before, complex dielectric properties ( $\epsilon_r$ ) i.e. permittivity ( $\epsilon_r'$ ) and loss tangent ( $\tan \delta$ ) data for DI water (resistivity = 13 M $\Omega$ cm) have been measured prior to sapodilla leaf tissue equivalent phantom liquids preparation at different frequencies. Measured permittivity ( $\epsilon_r'$ ) and loss tangent ( $\tan \delta$ ) data for DI water at 25 °C have earlier been discussed at 947.50 MHz, 1842.50 MHz and 2450.00 MHz – thus, those data haven't been repeated here.

At initial stage, to prepare sapodilla leaf tissue equivalent phantom liquid recipe at 947.50 MHz, 143.75 ml diethylene glycol monobutyl ether and 2.56 g sodium chloride (NaCl) have been mixed with 100 ml DI water (resistivity = 13 M $\Omega$ cm) to attain phantom liquid permittivity ( $\epsilon_r'$ ) and loss tangent ( $\tan \delta$ ) data close to the original values of sapodilla leaf specimen – please

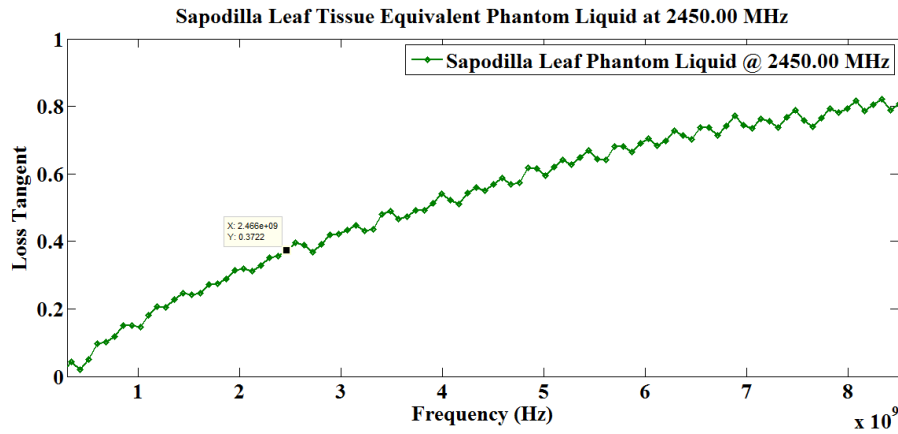
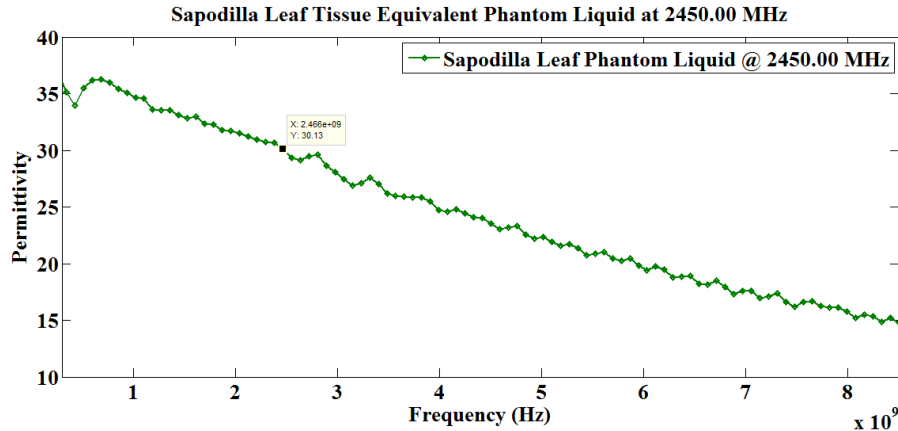


Fig. 5.31: Sapodilla leaf tissue equivalent phantom liquid at 2450.00 MHz (a) permittivity and (b) loss tangent

refer to Table 5.20. The ultimate phantom liquid permittivity ( $\epsilon_r'$ ) and loss tangent ( $\tan \delta$ ) values have been achieved within 2.14% and 1.14% limits of the reference data at 947.50 MHz (please refer to Fig. 5.29 and Table 5.21).

Next, to achieve sapodilla leaf tissue equivalent phantom liquid recipe at 1842.50 MHz, 133.33 ml diethylene glycol monobutyl ether and 888.89 mg sodium chloride (NaCl) have been mixed with 100 ml DI water (resistivity = 13 M $\Omega$ cm) to tune permittivity ( $\epsilon_r'$ ) and loss tangent ( $\tan \delta$ ) values of equivalent phantom liquid close to the original sapodilla leaf tissue specimen (please refer to Table 5.20). Final permittivity ( $\epsilon_r'$ ) and loss tangent ( $\tan \delta$ ) values of the equivalent

phantom liquid have been attained within 1.55% and 0.28% limits of the reference values at 1842.50 MHz (please refer to Fig. 5.30 and Table 5.21).

At final stage, 133.33 ml diethylene glycol monobutyl ether has been mixed with 100 ml DI water (resistivity = 13 MΩcm) to tune permittivity ( $\epsilon_r'$ ) and loss tangent ( $\tan \delta$ ) values of equivalent phantom liquid close to the original sapodilla leaf specimen at 2450.00 MHz (please refer to Table 5.20 for the composition at 25 °C). The final phantom liquid permittivity ( $\epsilon_r'$ ) and loss tangent ( $\tan \delta$ ) values have been tuned within 4.11% and 3.33% limits of the measured dielectric properties ( $\epsilon_r$ ) of sapodilla leaf specimen at 2450.00 MHz (please refer to Fig. 5.31 and Table 5.21).

Table 5.20 Final compositions of sapodilla leaf tissue equivalent phantom liquids

Frequency (MHz)	Final composition of phantom liquid
947.50	100 ml DI water, 143.75 ml DGME & 2.56 g NaCl
1842.50	100 ml DI water, 133.33 ml DGME & 888.89 mg NaCl
2450.00	100 ml DI water & 133.33 ml DGME

DGME = diethylene glycol monobutyl ether

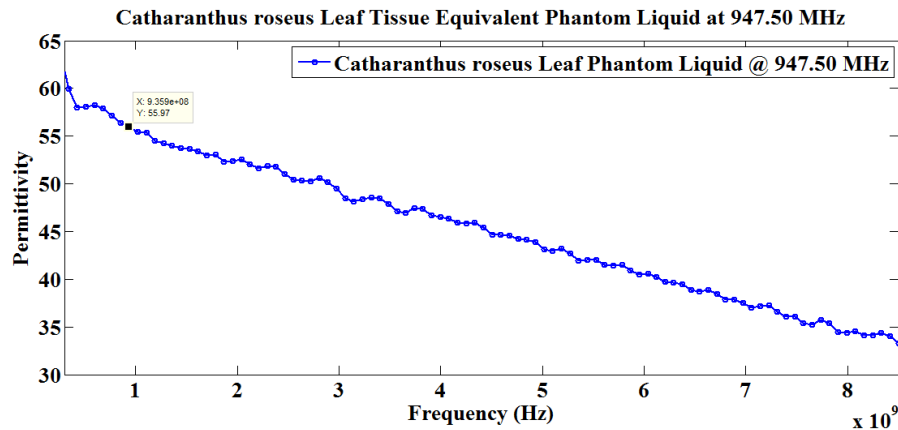
Table 5.21 Difference between the measured dielectric properties ( $\epsilon_r$ ) of sapodilla leaf tissue specimen and equivalent phantom liquids

Frequency (MHz)	947.50	Deviation	1842.50	Deviation	2450.00	Deviation
Reference Permittivity ( $\epsilon_r'$ )	33.12		30.28		28.94	
Phantom Liquid Permittivity ( $\epsilon_r'$ )	33.83	2.14%	30.75	1.55%	30.13	4.11%
Reference Loss Tangent ( $\tan \delta$ )	0.440		0.360		0.360	
Phantom Liquid Loss Tangent ( $\tan \delta$ )	0.445	1.14%	0.361	0.28%	0.372	3.33%

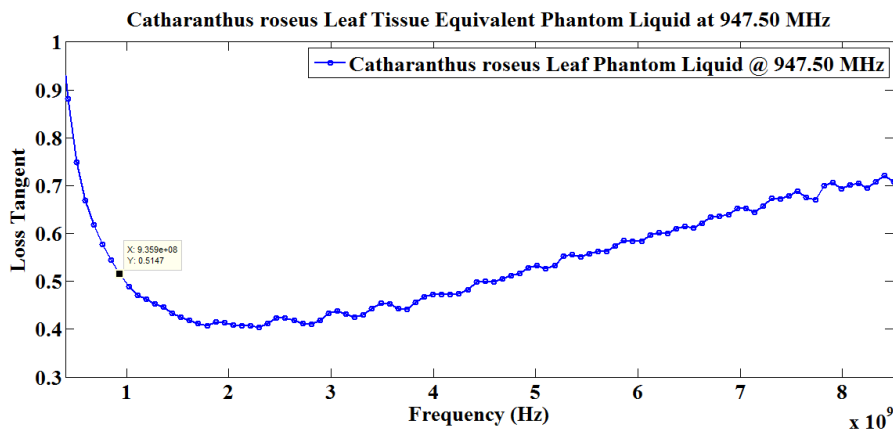
## 5.4.8 Phantom Liquids Preparation for *Catharanthus roseus* Specimens

### 5.4.8.1 Phantom Liquids Preparation for *Catharanthus roseus* Leaf Specimen

Phantom liquid recipes have been prepared for *Catharanthus roseus* leaf tissue specimen at 947.50 MHz, 1842.50 MHz and 2450.00 MHz. *Catharanthus roseus* leaf tissue equivalent phantom liquid recipes have been prepared based on different compositions of DI water (resistivity = 13 M $\Omega$ cm), diethylene glycol monobutyl ether and sodium chloride (NaCl). Depending on frequency of interest, different concentrations of diethylene glycol monobutyl ether have been added with DI water (resistivity = 13 M $\Omega$ cm) to bring down permittivity ( $\epsilon_r'$ ) of

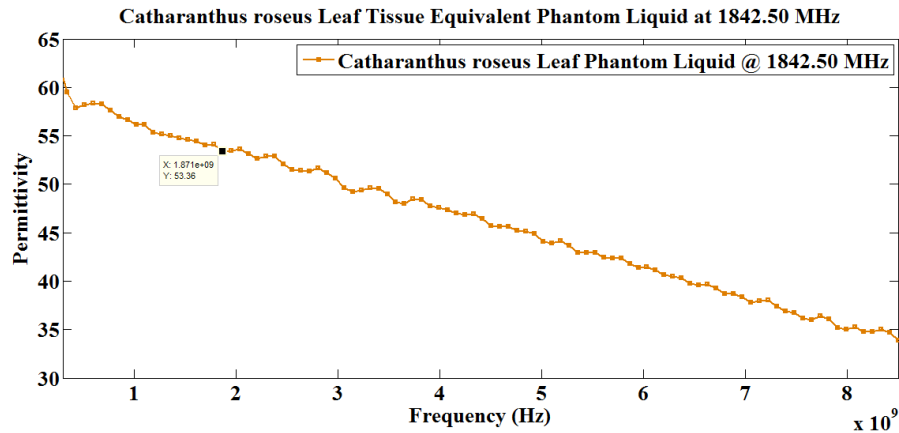


(a)

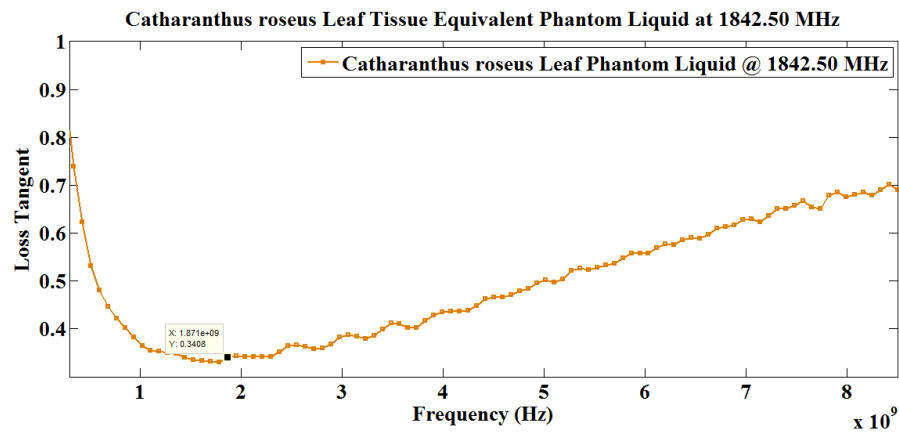


(b)

Fig. 5.32: *Catharanthus roseus* leaf tissue equivalent phantom liquid at 947.50 MHz (a) permittivity and (b) loss tangent



(a)



(b)

Fig. 5.33: *Catharanthus roseus* leaf tissue equivalent phantom liquid at 1842.50 MHz (a) permittivity and (b) loss tangent

the phantom liquids – thus, permittivity ( $\epsilon_r'$ ) of phantom liquids are tuned closer to *Catharanthus roseus* leaf tissue specimen. In addition, sodium chloride (NaCl) has further been added to the liquid preparation for fine tuning electrical conductivity ( $\sigma$ ) / loss tangent ( $\tan \delta$ ) of the final equivalent phantom liquid.

As mentioned before, permittivity ( $\epsilon_r'$ ) and loss tangent ( $\tan \delta$ ) values for DI water (resistivity = 13 M $\Omega$ cm) have been measured prior to *Catharanthus roseus* leaf tissue equivalent phantom liquids preparation. Measured permittivity ( $\epsilon_r'$ ) and loss tangent ( $\tan \delta$ ) parameters for pure DI water at 25 °C have already been discussed at 947.50 MHz, 1842.50 MHz and 2450.00 MHz – thus, those data haven't been mentioned here again.



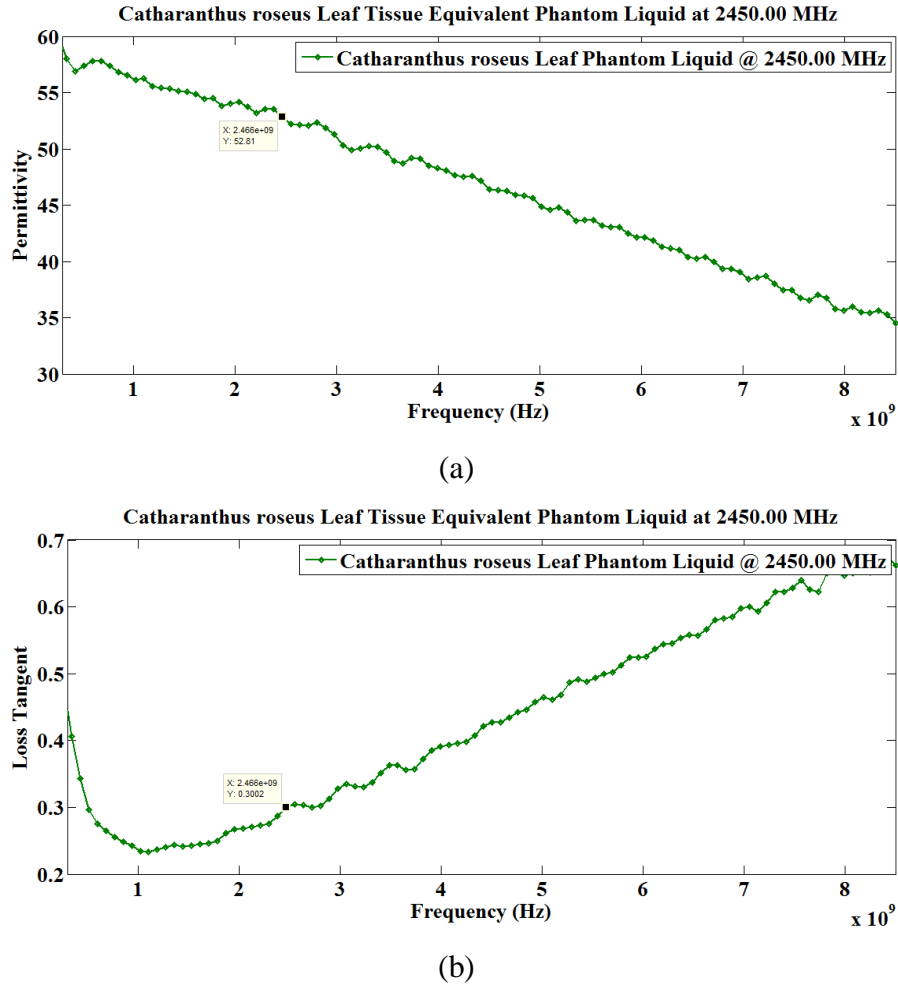


Fig. 5.34: *Catharanthus roseus* leaf tissue equivalent phantom liquid at 2450.00 MHz (a) permittivity and (b) loss tangent

At first, to prepare *Catharanthus roseus* leaf tissue equivalent phantom liquid formulation at 947.50 MHz, 42.86 ml diethylene glycol monobutyl ether and 1.71 g sodium chloride (NaCl) have been added with 100 ml DI water (resistivity = 13 M $\Omega$ cm) to achieve equivalent liquid permittivity ( $\epsilon_r'$ ) and loss tangent ( $\tan \delta$ ) values close to the original *Catharanthus roseus* leaf specimen (please refer to Table 5.22). The final phantom liquid permittivity ( $\epsilon_r'$ ) and loss tangent ( $\tan \delta$ ) values have been achieved within 3.25% and 2.79% limits of the reference data at 947.50 MHz (please refer to Fig. 5.32 and Table 5.23).

At subsequent stage, to achieve *Catharanthus roseus* leaf tissue equivalent phantom liquid preparation at 1842.50 MHz, 42.86 ml diethylene glycol monobutyl ether and 1.14 g sodium chloride (NaCl) have been added with 100 ml DI water (resistivity = 13 M $\Omega$ cm) to attain

permittivity ( $\epsilon_r'$ ) and loss tangent ( $\tan \delta$ ) parameters of equivalent phantom liquid close to the original *Catharanthus roseus* leaf tissue specimen (please refer to Table 5.22). Resultant permittivity ( $\epsilon_r'$ ) and loss tangent ( $\tan \delta$ ) values of the equivalent phantom liquid have been achieved within 1.28% and 3.02% limits of the reference values at 1842.50 MHz (please refer to Fig. 5.33 and Table 5.23).

At last, 42.86 ml diethylene glycol monobutyl ether and 571.43 mg sodium chloride (NaCl) have been added with 100 ml DI water (resistivity = 13 M $\Omega$ cm) to tune permittivity ( $\epsilon_r'$ ) and loss tangent ( $\tan \delta$ ) data of equivalent phantom liquid close to the original *Catharanthus roseus* leaf specimen at 2450.00 MHz (please refer to Table 5.22 for the liquid composition at 25 °C). The phantom liquid permittivity ( $\epsilon_r'$ ) and loss tangent ( $\tan \delta$ ) parameters have been tuned within 0.75% and 1.69% limits of the measured dielectric properties ( $\epsilon_r$ ) of *Catharanthus roseus* leaf specimen at 2450.00 MHz (please refer to Fig. 5.34 and Table 5.23).

Table 5.22 Final compositions of *Catharanthus roseus* leaf tissue equivalent phantom liquids

Frequency (MHz)	Final composition of phantom liquid
947.50	100 ml DI water, 42.86 ml DGME & 1.71 g NaCl
1842.50	100 ml DI water, 42.86 ml DGME & 1.14 g NaCl
2450.00	100 ml DI water, 42.86 ml DGME & 571.43 mg NaCl

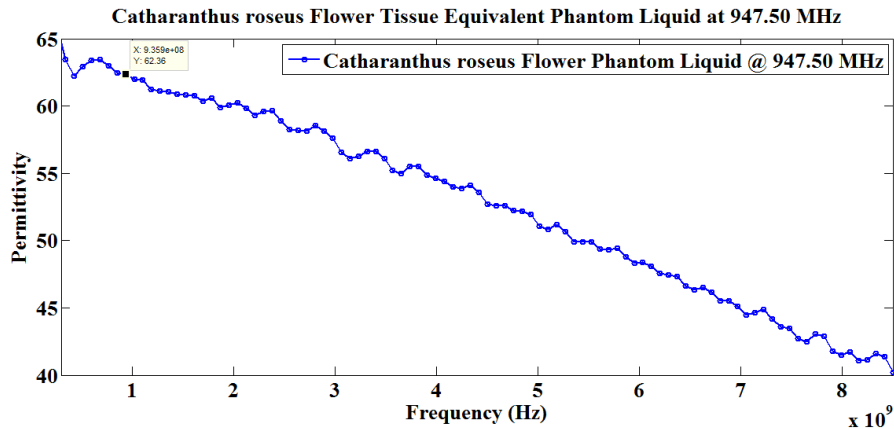
DGME = diethylene glycol monobutyl ether

Table 5.23 Difference between the measured dielectric properties ( $\epsilon_r$ ) of *Catharanthus roseus* leaf tissue specimen and equivalent phantom liquids

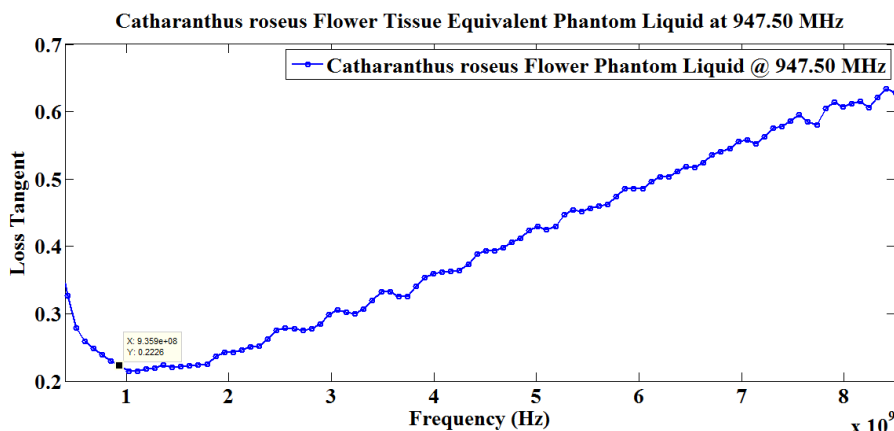
Frequency (MHz)	947.50	Deviation	1842.50	Deviation	2450.00	Deviation
Reference Permittivity ( $\epsilon_r'$ )	57.85		54.05		53.21	
Phantom Liquid Permittivity ( $\epsilon_r'$ )	55.97	3.25%	53.36	1.28%	52.81	0.75%
Reference Loss Tangent ( $\tan \delta$ )	0.501		0.331		0.295	
Phantom Liquid Loss Tangent ( $\tan \delta$ )	0.515	2.79%	0.341	3.02%	0.300	1.69%

### 5.4.8.2 Phantom Liquids Preparation for *Catharanthus roseus* Flower Specimen

This time, phantom liquid formulations have been prepared for *Catharanthus roseus* flower specimen at 947.50 MHz, 1842.50 MHz and 2450.00 MHz. *Catharanthus roseus* flower tissue equivalent phantom liquid preparations have been formulated based on different compositions of DI water (resistivity = 13 MΩcm), diethylene glycol monobutyl ether and sodium chloride (NaCl). In fact, based on frequency of interest, different amount of diethylene glycol monobutyl ether has been mixed with DI water (resistivity = 13 MΩcm) to reduce permittivity ( $\epsilon_r'$ ) of the equivalent phantom liquids – in this way, permittivity ( $\epsilon_r'$ ) of the phantom liquids have been tuned close to *Catharanthus roseus* flower tissue specimen. Moreover, sodium chloride (NaCl)

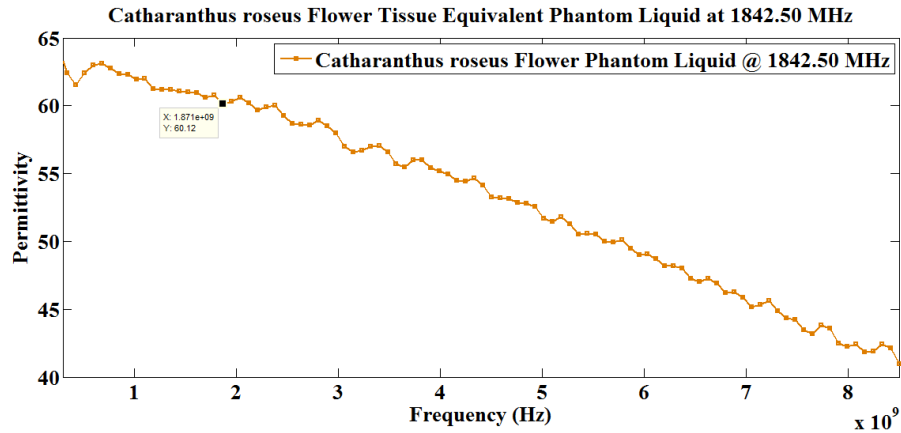


(a)

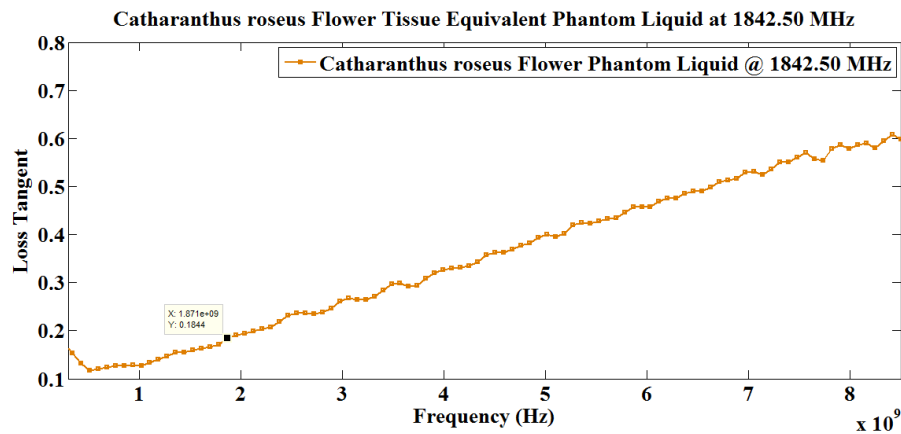


(b)

Fig. 5.35: *Catharanthus roseus* flower tissue equivalent phantom liquid at 947.50 MHz (a) permittivity and (b) loss tangent



(a)



(b)

Fig. 5.36: *Catharanthus roseus* flower tissue equivalent phantom liquid at 1842.50 MHz (a) permittivity and (b) loss tangent

has been added to the liquid recipe for fine tuning electrical conductivity ( $\sigma$ ) / loss tangent ( $\tan \delta$ ) of the final equivalent phantom liquid.

As discussed earlier, broadband permittivity ( $\epsilon_r'$ ) and loss tangent ( $\tan \delta$ ) parameters for DI water (resistivity = 13 M $\Omega$ cm) have been measured before initiating preparations for *Catharanthus roseus* flower tissue equivalent phantom liquids. Measured permittivity ( $\epsilon_r'$ ) and loss tangent ( $\tan \delta$ ) data for pure DI water have been discussed earlier at 947.50 MHz, 1842.50 MHz and 2450.00 MHz – hence, those data aren't repeated here.

At initial stage, to formulate *Catharanthus roseus* flower tissue equivalent phantom liquid recipe at 947.50 MHz, 29.41 ml diethylene glycol monobutyl ether and 470.59 mg sodium chloride (NaCl) have been added with 100 ml DI water (resistivity = 13 M $\Omega$ cm) to attain phantom liquid

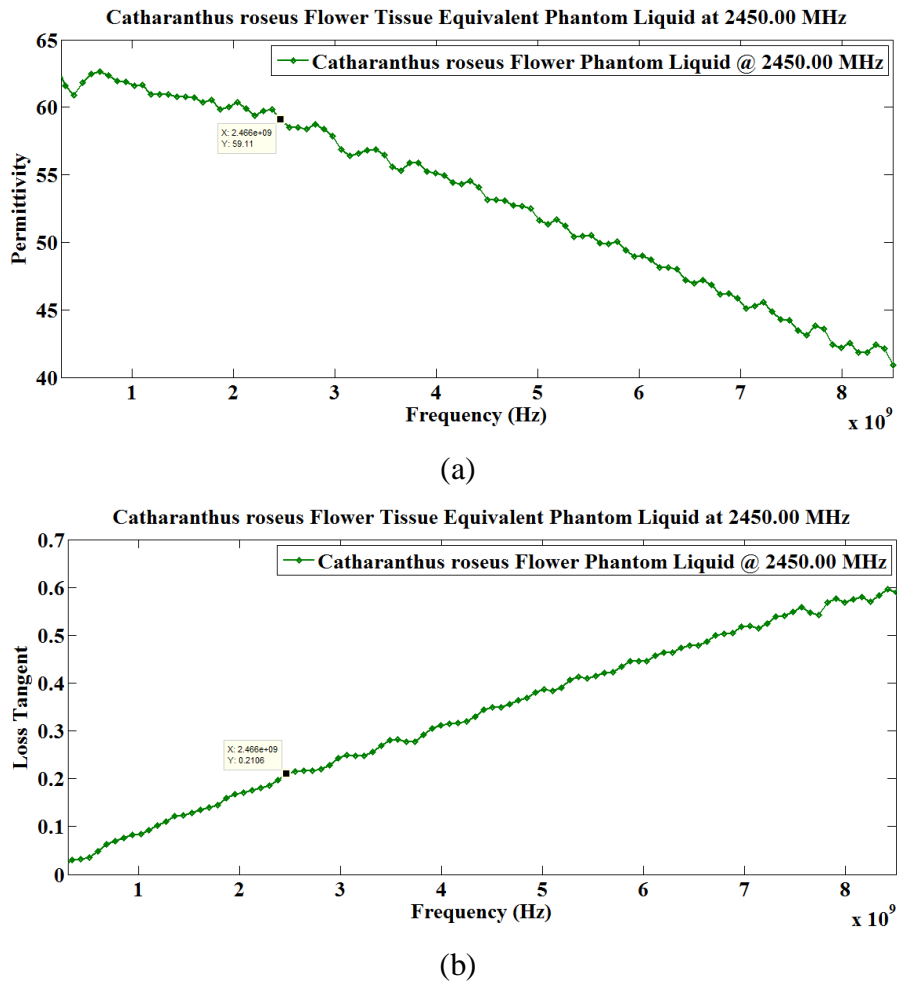


Fig. 5.37: *Catharanthus roseus* flower tissue equivalent phantom liquid at 2450.00 MHz (a) permittivity and (b) loss tangent

permittivity ( $\epsilon'_r$ ) and loss tangent ( $\tan \delta$ ) values close to the reference *Catharanthus roseus* flower specimen (please refer to Table 5.24). The resultant phantom liquid permittivity ( $\epsilon'_r$ ) and loss tangent ( $\tan \delta$ ) values have been achieved within 0.18% and 5.19% limits of the reference data at 947.50 MHz (please refer to Fig. 5.35 and Table 5.25). It should be noted that the deviation in loss tangent ( $\tan \delta$ ) could be minimized further by utilizing DI water with resistivity higher than 13 M $\Omega$ cm.

Next, to formulate *Catharanthus roseus* flower tissue equivalent phantom liquid preparation at 1842.50 MHz, 29.41 ml diethylene glycol monobutyl ether and 117.65 mg sodium chloride (NaCl) have been mixed with 100 ml DI water (resistivity = 13 M $\Omega$ cm) to achieve permittivity

( $\epsilon_r'$ ) and loss tangent ( $\tan \delta$ ) values of equivalent phantom liquid close to the reference *Catharanthus roseus* flower tissue specimen (please refer to Table 5.24). Final permittivity ( $\epsilon_r'$ ) and loss tangent ( $\tan \delta$ ) values of the equivalent liquid have been attained within 0.68% and 5.14% limits of the reference data at 1842.50 MHz (please refer to Fig. 5.36 and Table 5.25).

At final phase, a mixture of 29.41 ml Diethylene glycol monobutyl ether and 100 ml DI water has been prepared to tune permittivity ( $\epsilon_r'$ ) and loss tangent ( $\tan \delta$ ) data of equivalent phantom liquid close to the original *Catharanthus roseus* flower specimen at 2450.00 MHz (please refer to Table 5.24 for the liquid composition at 25 °C). Final permittivity ( $\epsilon_r'$ ) and loss tangent ( $\tan \delta$ ) values of the prepared phantom liquid have been tuned within 1.55% and 13.44% limits of the measured reference data for *Catharanthus roseus* flower specimen at 2450.00 MHz (please refer to Fig. 5.37 and Table 5.25). It is to be noted that the deviation in loss tangent ( $\tan \delta$ ) data can be minimized further by employing DI water with resistivity much greater than 13 M $\Omega$ cm.

Table 5.24 Final compositions of *Catharanthus roseus* flower tissue equivalent phantom liquids

Frequency (MHz)	Final composition of phantom liquid
947.50	100 ml DI water, 29.41 ml DGME & 470.59 mg NaCl
1842.50	100 ml DI water, 29.41 ml DGME & 117.65 mg NaCl
2450.00	100 ml DI water & 29.41 ml DGME

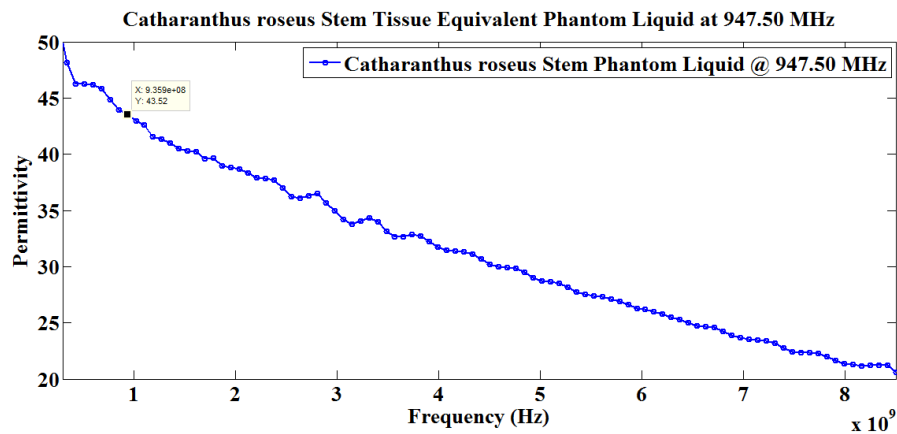
DGME = diethylene glycol monobutyl ether

Table 5.25 Difference between the measured dielectric properties ( $\epsilon_r$ ) of *Catharanthus roseus* flower tissue specimen and equivalent phantom liquids

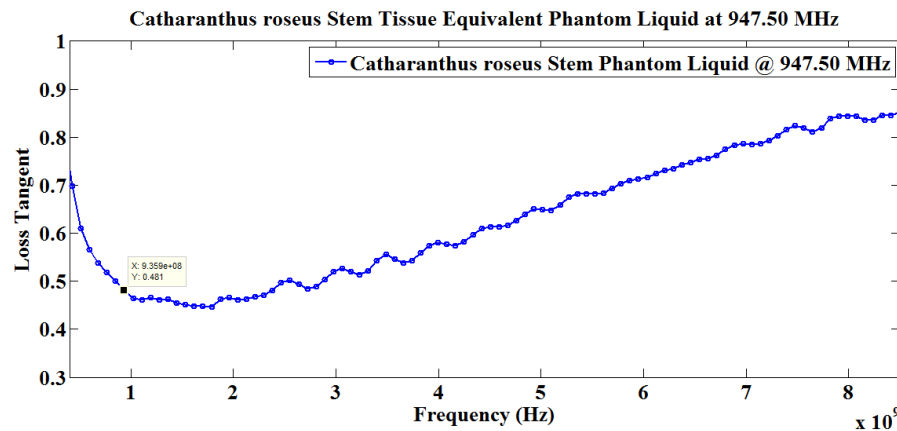
Frequency (MHz)	947.50	Deviation	1842.50	Deviation	2450.00	Deviation
Reference Permittivity ( $\epsilon_r'$ )	62.47		60.53		60.04	
Phantom Liquid Permittivity ( $\epsilon_r'$ )	62.36	0.18%	60.12	0.68%	59.11	1.55%
Reference Loss Tangent ( $\tan \delta$ )	0.212		0.175		0.186	
Phantom Liquid Loss Tangent ( $\tan \delta$ )	0.223	5.19%	0.184	5.14%	0.211	13.44%

### 5.4.8.3 Phantom Liquids Preparation for *Catharanthus roseus* Stem Specimen

Phantom liquid recipes have been prepared for *Catharanthus roseus* stem specimen at 947.50 MHz, 1842.50 MHz and 2450.00 MHz. *Catharanthus roseus* stem tissue equivalent phantom liquid recipes have been prepared based on different compositions of DI water (resistivity = 13 MΩcm), diethylene glycol monobutyl ether and sodium chloride (NaCl). In fact, different amount of diethylene glycol monobutyl ether is mixed with DI water (resistivity = 13 MΩcm) to bring down permittivity ( $\epsilon_r'$ ) of the phantom liquids (depending on frequency of interest). In this manner, permittivity ( $\epsilon_r'$ ) values of the phantom liquids have been tuned close to *Catharanthus roseus* stem tissue specimen. Furthermore, sodium chloride (NaCl) has been added to the liquid



(a)



(b)

Fig. 5.38: *Catharanthus roseus* stem tissue equivalent phantom liquid at 947.50 MHz (a) permittivity and (b) loss tangent

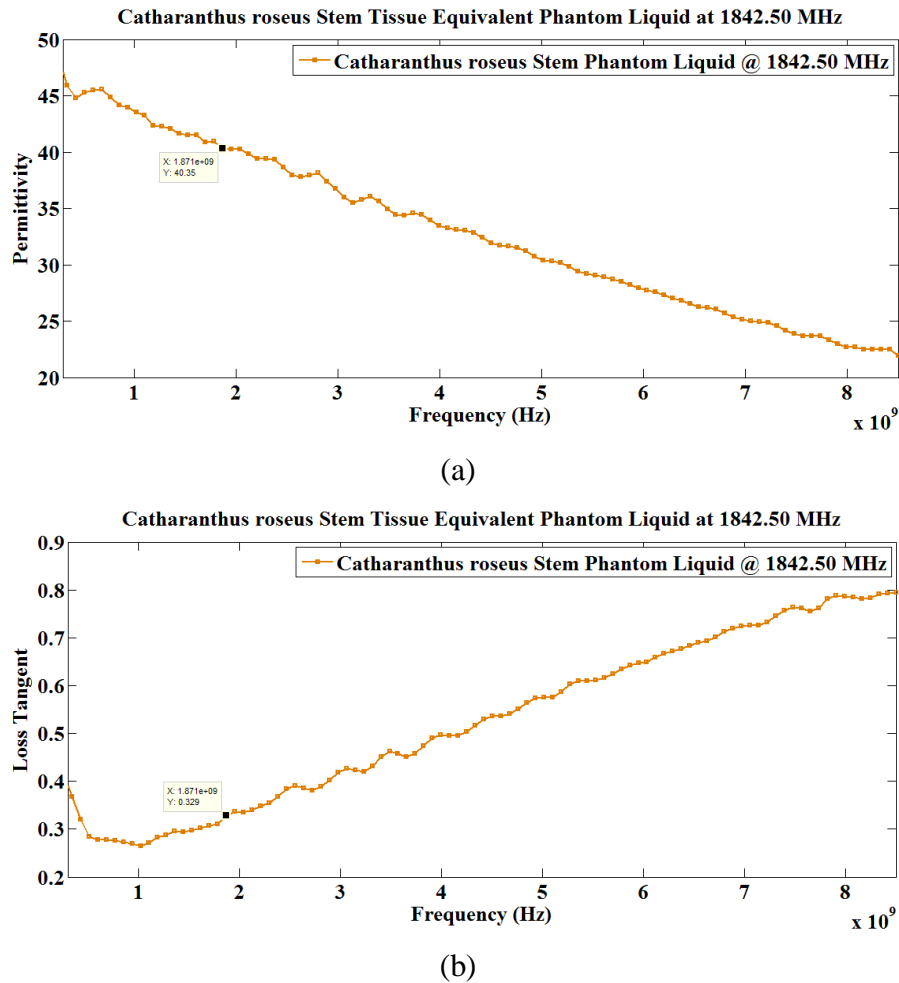


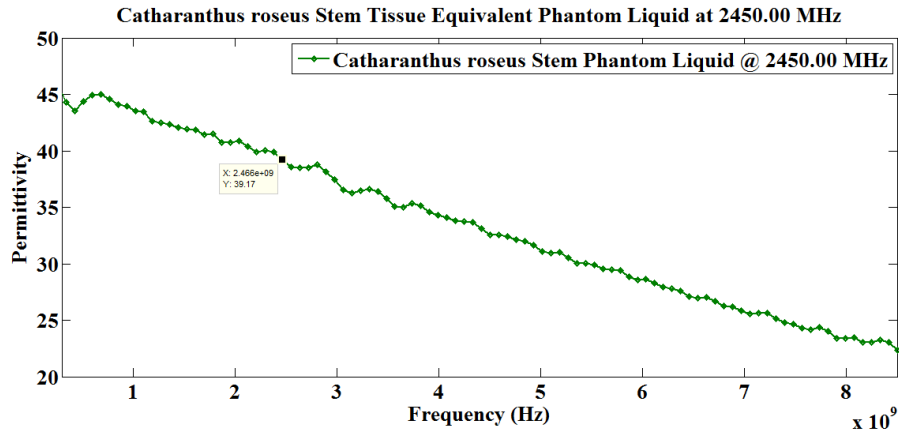
Fig. 5.39: *Catharanthus roseus* stem tissue equivalent phantom liquid at 1842.50 MHz (a) permittivity and (b) loss tangent

recipes to fine tune electrical conductivity ( $\sigma$ ) / loss tangent ( $\tan \delta$ ) of the final equivalent phantom liquids.

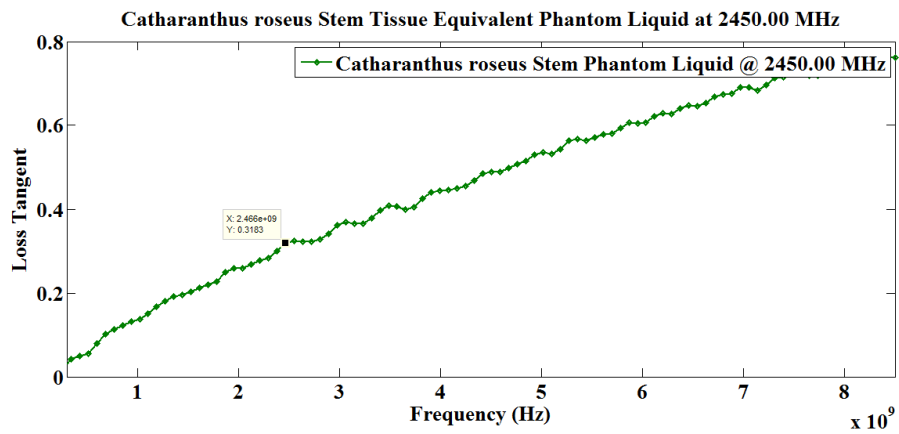
As discussed before, broadband complex dielectric properties ( $\epsilon_r$ ) i.e. permittivity ( $\epsilon_r'$ ) and loss tangent ( $\tan \delta$ ) values for pure DI water (resistivity = 13 M $\Omega$ cm) at 25 °C have been measured – prior to preparing *Catharanthus roseus* stem tissue equivalent phantom liquids. Measured permittivity ( $\epsilon_r'$ ) and loss tangent ( $\tan \delta$ ) data for the DI water have already been discussed at 947.50 MHz, 1842.50 MHz and 2450.00 MHz.

At first, to prepare *Catharanthus roseus* stem tissue equivalent liquid recipe at 947.50 MHz, 90 ml diethylene glycol monobutyl ether and 2.20 g sodium chloride (NaCl) have been added with





(a)



(b)

Fig. 5.40: *Catharanthus roseus* stem tissue equivalent phantom liquid at 2450.00 MHz (a) permittivity and (b) loss tangent

100 ml DI water (resistivity = 13 M $\Omega$ cm) for achieving phantom liquid permittivity ( $\epsilon_r'$ ) and loss tangent ( $\tan \delta$ ) data close to the reference *Catharanthus roseus* stem tissue specimen (please refer to Table 5.26). The final phantom liquid permittivity ( $\epsilon_r'$ ) and loss tangent ( $\tan \delta$ ) data have been attained within 0.60% and 1.26% limits of the reference values at 947.50 MHz (please refer to Fig. 5.38 and Table 5.27).

At subsequent stage, to prepare *Catharanthus roseus* stem tissue equivalent phantom liquid formulation at 1842.50 MHz, 90 ml diethylene glycol monobutyl ether and 0.80 g sodium chloride (NaCl) have been added with 100 ml DI water (resistivity = 13 M $\Omega$ cm) to realize permittivity ( $\epsilon_r'$ ) and loss tangent ( $\tan \delta$ ) values of equivalent phantom liquid close to the

reference *Catharanthus roseus* stem tissue specimen (please refer to Table 5.26). Resultant permittivity ( $\epsilon_r'$ ) and loss tangent ( $\tan \delta$ ) parameters of the equivalent phantom liquid have been realized within 0.47% and 0.92% limits of the original measured data at 1842.50 MHz (please refer to Fig. 5.39 and Table 5.27).

At last, a recipe of 90 ml diethylene glycol monobutyl ether and 100 ml DI water has been prepared to tune permittivity ( $\epsilon_r'$ ) and loss tangent ( $\tan \delta$ ) data of equivalent phantom liquid close to the original *Catharanthus roseus* stem tissue specimen at 2450.00 MHz (please refer to Table 5.26 for detailed composition at 25 °C). Permittivity ( $\epsilon_r'$ ) and loss tangent ( $\tan \delta$ ) parameters of the final phantom liquid have been tuned within 0.30% and 3.58% limits of the reference data for *Catharanthus roseus* stem specimen at 2450.00 MHz – please refer to Fig. 5.40 and Table 5.27.

Table 5.26 Final compositions of *Catharanthus roseus* stem tissue equivalent phantom liquids

Frequency (MHz)	Final composition of phantom liquid
947.50	100 ml DI water, 90 ml DGME & 2.20 g NaCl
1842.50	100 ml DI water, 90 ml DGME & 0.80 g NaCl
2450.00	100 ml DI water & 90 ml DGME

DGME = diethylene glycol monobutyl ether

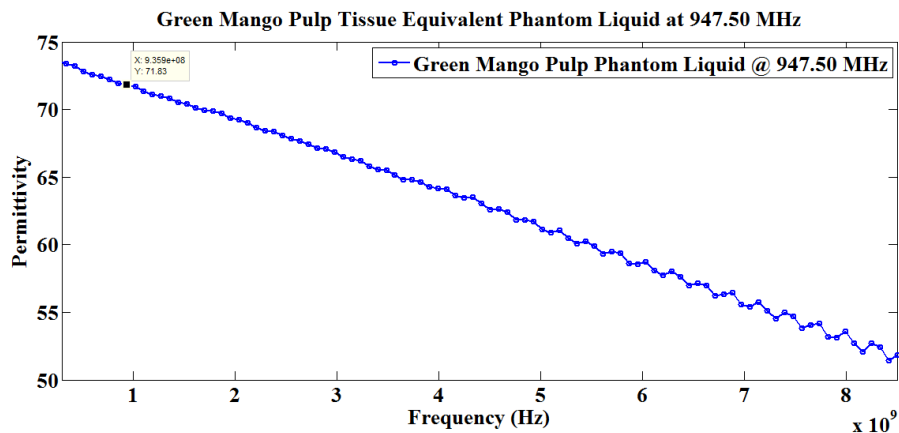
Table 5.27 Difference between the measured dielectric properties ( $\epsilon_r$ ) of *Catharanthus roseus* stem tissue specimen and equivalent phantom liquids

Frequency (MHz)	947.50	Deviation	1842.50	Deviation	2450.00	Deviation
Reference Permittivity ( $\epsilon_r'$ )	43.26		40.16		39.29	
Phantom Liquid Permittivity ( $\epsilon_r'$ )	43.52	0.60%	40.35	0.47%	39.17	0.30%
Reference Loss Tangent ( $\tan \delta$ )	0.475		0.326		0.307	
Phantom Liquid Loss Tangent ( $\tan \delta$ )	0.481	1.26%	0.329	0.92%	0.318	3.58%

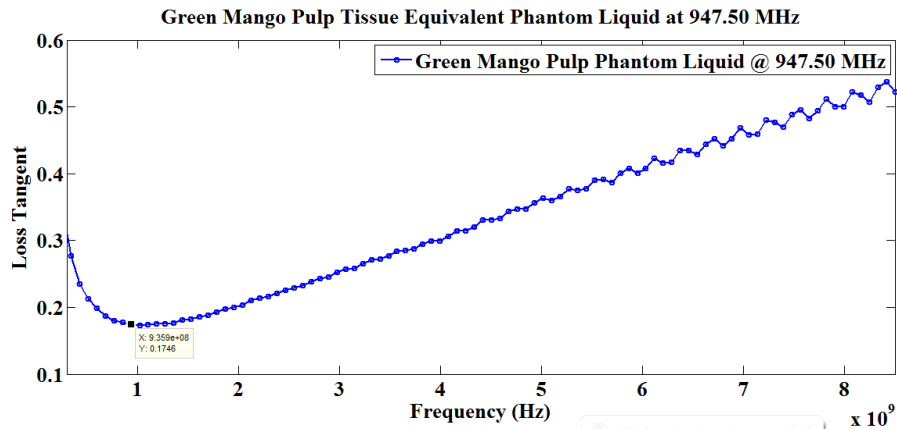
## 5.4.9 Phantom Liquids Preparation for Green Mango Specimens

### 5.4.9.1 Phantom Liquids Preparation for Green Mango Pulp Specimen

Phantom liquid compositions have been prepared for green mango pulp tissue specimen at 947.50 MHz, 1842.50 MHz and 2450.00 MHz. Green mango pulp tissue equivalent phantom liquids have been prepared based on different compositions of DI water (resistivity = 13 M $\Omega$ cm), sucrose and sodium chloride (NaCl). In fact, different amount of sucrose has been added with DI water (resistivity = 13 M $\Omega$ cm) in order to reduce permittivity ( $\epsilon_r'$ ) of the phantom liquids (based on frequency of interest) – thus, permittivity ( $\epsilon_r'$ ) values of the phantom liquid recipes have been

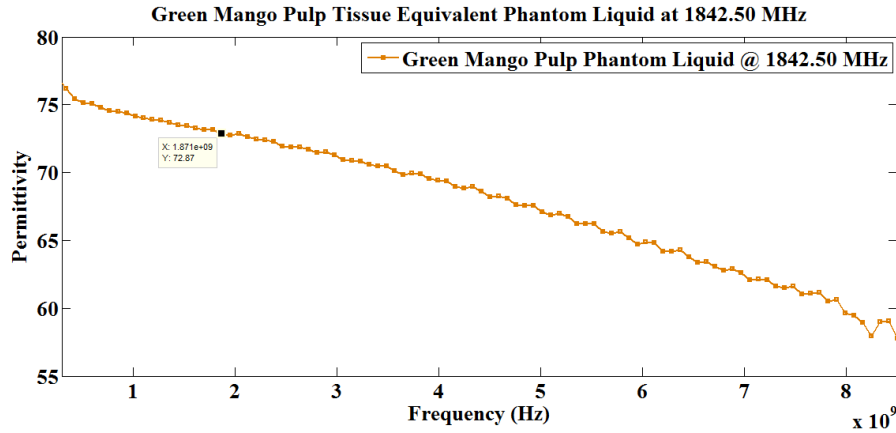


(a)

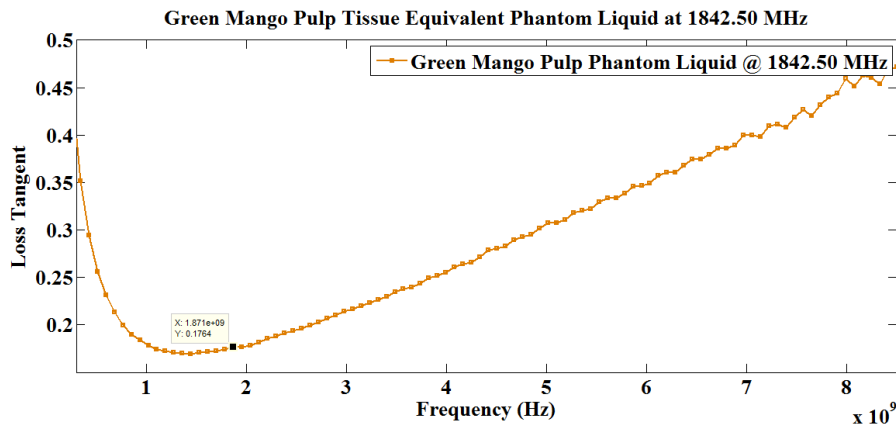


(b)

Fig. 5.41: Green mango pulp tissue equivalent phantom liquid at 947.50 MHz (a) permittivity and (b) loss tangent



(a)

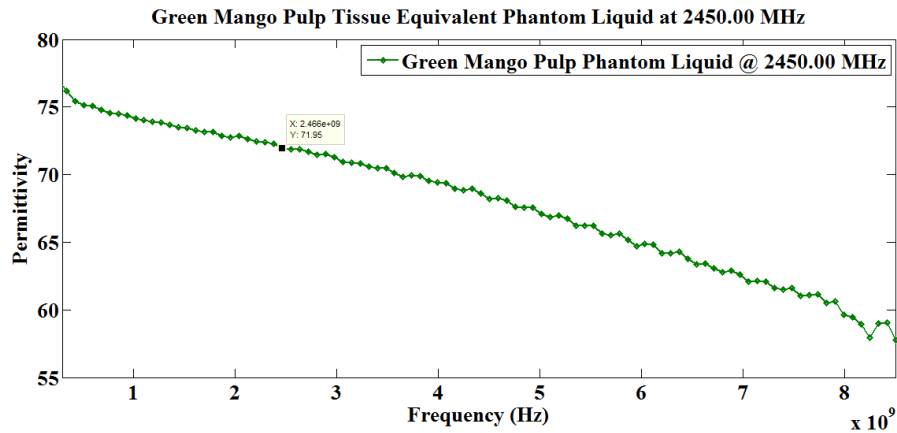


(b)

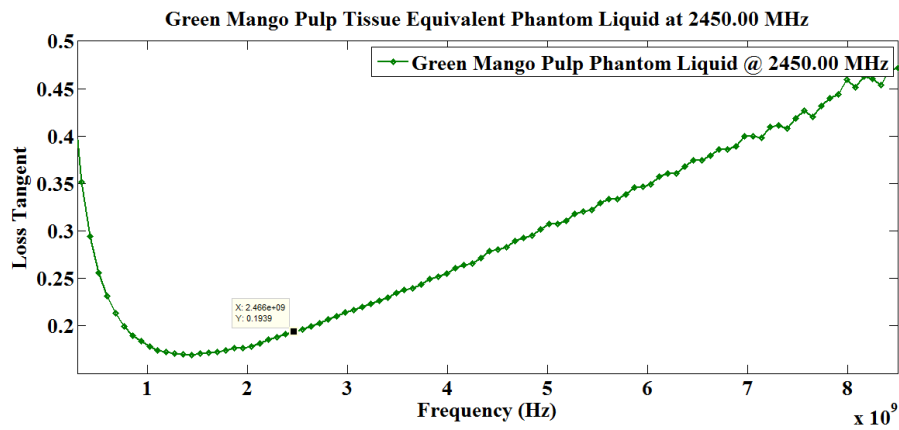
Fig. 5.42: Green mango pulp tissue equivalent phantom liquid at 1842.50 MHz (a) permittivity and (b) loss tangent

tuned close to green mango pulp tissue specimen. In addition, sodium chloride (NaCl) has further been added to the liquid recipes for fine tuning electrical conductivity ( $\sigma$ ) / loss tangent ( $\tan \delta$ ) of the final equivalent phantom liquids.

As mentioned earlier, broadband dielectric properties ( $\epsilon_r$ ) i.e. permittivity ( $\epsilon_r'$ ) and loss tangent ( $\tan \delta$ ) data for DI water (resistivity = 13 M $\Omega$ cm) at 25 °C have been measured at initial stage – permittivity ( $\epsilon_r'$ ) and loss tangent ( $\tan \delta$ ) data for the DI water have been discussed earlier at 947.50 MHz, 1842.50 MHz and 2450.00 MHz. Therefore, the obtained dielectric values ( $\epsilon_r$ ) haven't been repeated here.



(a)



(b)

Fig. 5.43: Green mango pulp tissue equivalent phantom liquid at 2450.00 MHz (a) permittivity and (b) loss tangent

At first stage, to formulate green mango pulp tissue equivalent phantom liquid recipe at 947.50 MHz, 22 g sucrose and 300 mg sodium chloride (NaCl) have been mixed with 100 ml DI water (resistivity = 13 M $\Omega$ cm) to realize phantom liquid permittivity ( $\epsilon_r'$ ) and loss tangent ( $\tan \delta$ ) data close to the reference green mango pulp tissue specimen (please refer to Table 5.28). The final phantom liquid permittivity ( $\epsilon_r'$ ) and loss tangent ( $\tan \delta$ ) data have been achieved within 0.21% and 1.68% limits of the reference values at 947.50 MHz (please refer to Fig. 5.41 and Table 5.29).

At subsequent stage, 10 g sucrose and 300 mg sodium chloride (NaCl) have been mixed with 100 ml DI water (resistivity = 13 M $\Omega$ cm) to realize permittivity ( $\epsilon_r'$ ) and loss tangent ( $\tan \delta$ )

values of equivalent phantom liquid close to the reference green mango pulp tissue specimen at 1842.50 MHz (please refer to Table 5.28). Final permittivity ( $\epsilon_r'$ ) and loss tangent ( $\tan \delta$ ) values of the equivalent phantom liquid have been achieved within 3.30% and 1.73% limits of the original data for green mango pulp tissue specimen at 1842.50 MHz (please refer to Fig. 5.42 and Table 5.29).

At final stage, the last recipe i.e. 10 g sucrose and 300 mg sodium chloride (NaCl) mixed with 100 ml DI water (resistivity = 13 M $\Omega$ cm), has been prepared to tune permittivity ( $\epsilon_r'$ ) and loss tangent ( $\tan \delta$ ) data of equivalent phantom liquid close to the original green mango pulp tissue specimen at 2450.00 MHz (please refer to Table 5.28 for the composition at 25 °C). Permittivity ( $\epsilon_r'$ ) and loss tangent ( $\tan \delta$ ) values of the final phantom liquid have been tuned within 2.54% and 1.52% limits of the original data for green mango pulp tissue specimen at 2450.00 MHz (please refer to Fig. 5.43 and Table 5.29).

Table 5.28 Final compositions of green mango pulp tissue equivalent phantom liquids

Frequency (MHz)	Final composition of phantom liquid
947.50	100 ml DI water, 22 g sucrose & 300 mg NaCl
1842.50	100 ml DI water, 10 g sucrose & 300 mg NaCl
2450.00	100 ml DI water, 10 g sucrose & 300 mg NaCl

Table 5.29 Difference between the measured dielectric properties ( $\epsilon_r$ ) of green mango pulp tissue specimen and equivalent phantom liquids

Frequency (MHz)	947.50	Deviation	1842.50	Deviation	2450.00	Deviation
Reference Permittivity ( $\epsilon_r'$ )	71.68		70.54		70.17	
Phantom Liquid Permittivity ( $\epsilon_r'$ )	71.83	0.21%	72.87	3.30%	71.95	2.54%
Reference Loss Tangent ( $\tan \delta$ )	0.178		0.173		0.197	
Phantom Liquid Loss Tangent ( $\tan \delta$ )	0.175	1.68%	0.176	1.73%	0.194	1.52%

### 5.4.9.2 Phantom Liquids Preparation for Green Mango Seed Specimen

This time, phantom liquid preparations have been realized for green mango seed specimen at 947.50 MHz, 1842.50 MHz and 2450.00 MHz. Green mango seed tissue equivalent phantom liquids have been prepared based on different compositions of DI water (resistivity = 13 M $\Omega$ cm), sucrose / diethylene glycol monobutyl ether and sodium chloride (NaCl). In fact, different amount of sucrose / diethylene glycol monobutyl ether has been added with DI water (resistivity = 13 M $\Omega$ cm) to reduce permittivity ( $\epsilon_r'$ ) of the phantom liquids (based on the frequency of interest). In this way, permittivity ( $\epsilon_r'$ ) values of the phantom liquids have been tuned close to original green mango seed tissue specimen. In addition, sodium chloride (NaCl) has further been

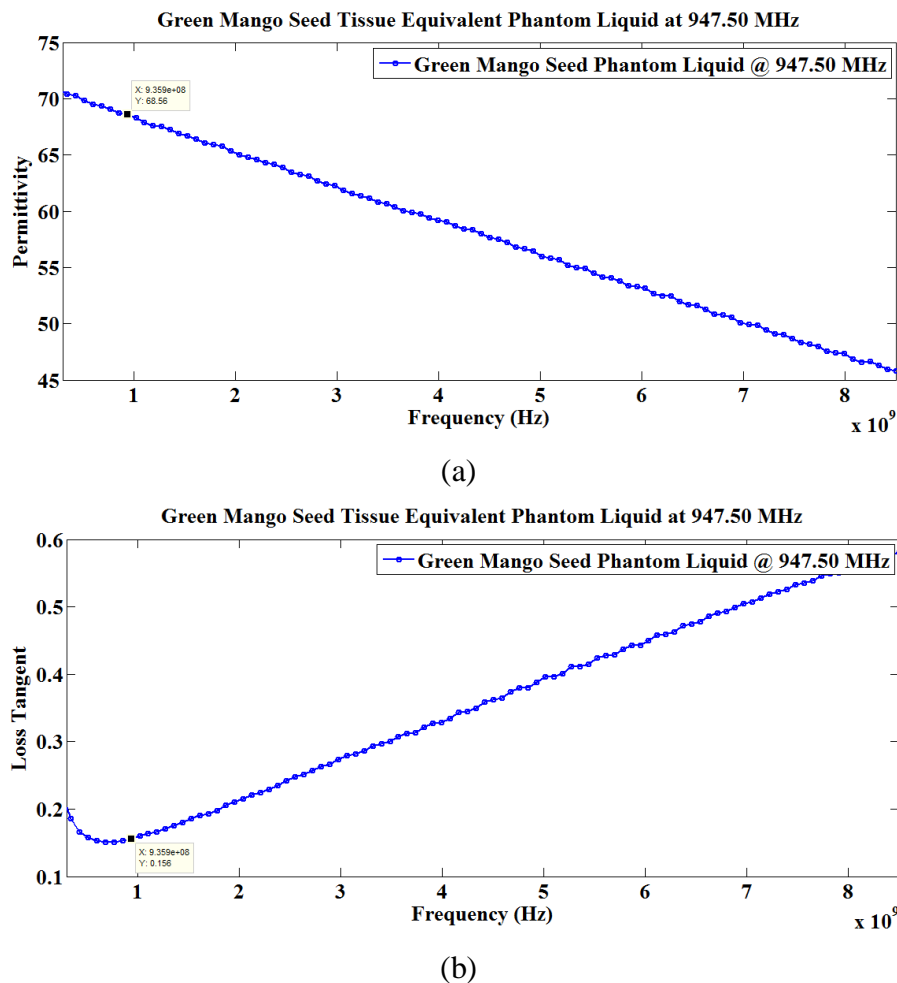
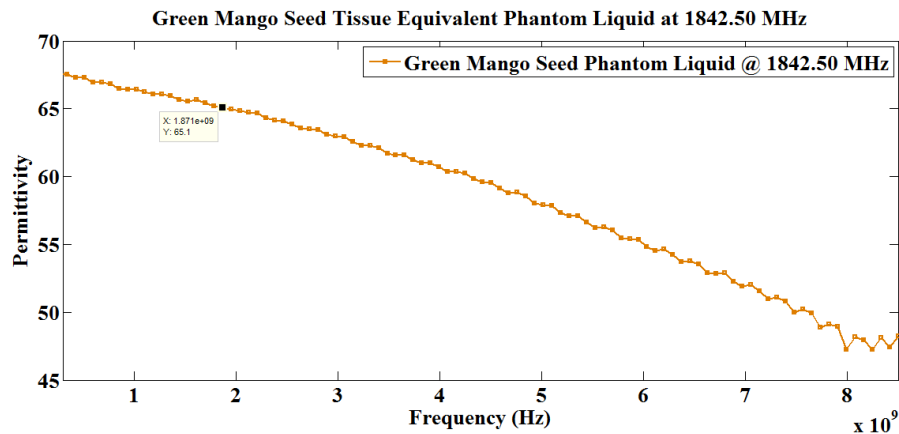
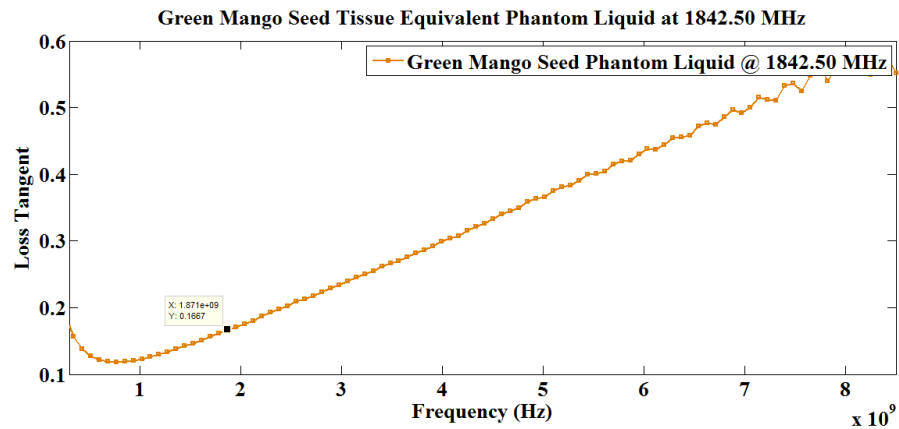


Fig. 5.44: Green mango seed tissue equivalent phantom liquid at 947.50 MHz (a) permittivity and (b) loss tangent



(a)



(b)

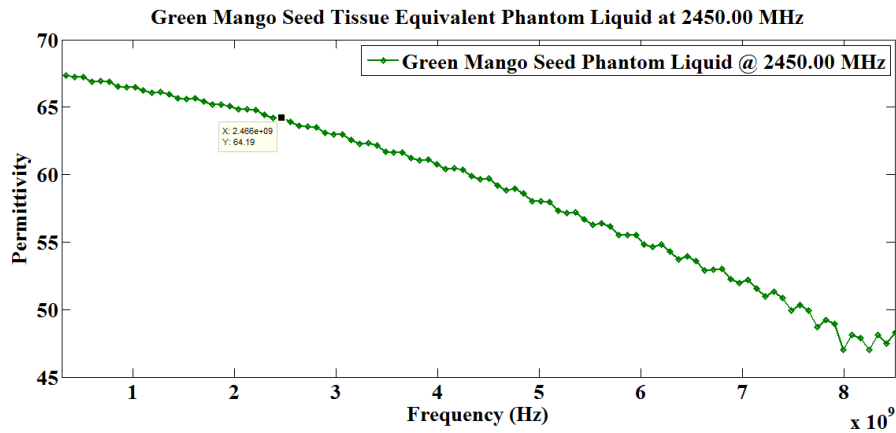
Fig. 5.45: Green mango seed tissue equivalent phantom liquid at 1842.50 MHz (a) permittivity and (b) loss tangent

added to the liquid recipes to fine tune electrical conductivity ( $\sigma$ ) / loss tangent ( $\tan \delta$ ) of the final tissue equivalent phantom liquids.

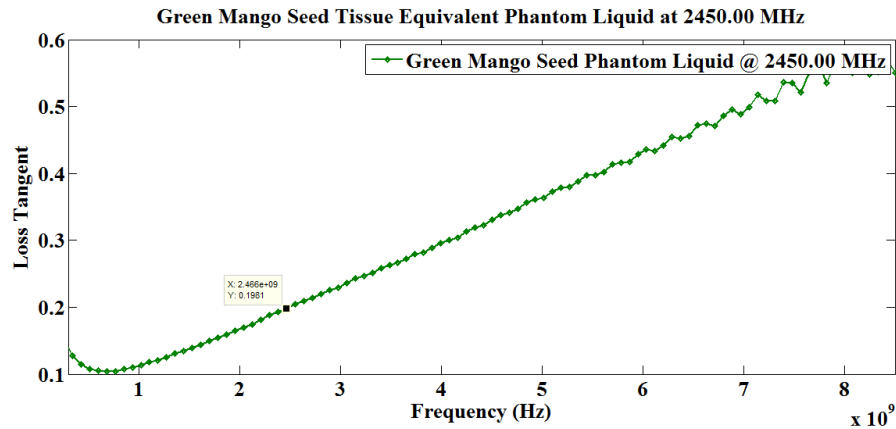
As mentioned earlier, complex dielectric properties ( $\epsilon_r$ ) i.e. permittivity ( $\epsilon_r'$ ) and loss tangent ( $\tan \delta$ ) data for pure DI water (resistivity = 13 M $\Omega$ cm) at 25 °C have been measured at first (prior to preparing green mango seed tissue equivalent phantom recipes). Measured permittivity ( $\epsilon_r'$ ) and loss tangent ( $\tan \delta$ ) data for the DI water have been discussed earlier at 947.50 MHz, 1842.50 MHz and 2450.00 MHz – thus, those data haven't been discussed anymore.

At the initial phase, in order to realize green mango seed tissue equivalent liquid recipe at 947.50 MHz, 35 g sucrose and 200 mg sodium chloride (NaCl) have been added with 100 ml DI water





(a)



(b)

Fig. 5.46: Green mango seed tissue equivalent phantom liquid at 2450.00 MHz (a) permittivity and (b) loss tangent

(resistivity = 13 M $\Omega$ cm) to realize equivalent phantom liquid permittivity ( $\epsilon'_r$ ) and loss tangent ( $\tan \delta$ ) data close to the original green mango seed specimen – please refer to Table 5.30. The final phantom liquid permittivity ( $\epsilon'_r$ ) and loss tangent ( $\tan \delta$ ) data have been achieved within 1.44% and 0.00% limits of the reference values at 947.50 MHz (please refer to Fig. 5.44 and Table 5.31).

At a subsequent stage, to prepare green mango seed tissue equivalent phantom liquid recipe at 1842.50 MHz, 20.83 ml diethylene glycol monobutyl ether and 125 mg sodium chloride (NaCl) have been added with 100 ml DI water (resistivity = 13 M $\Omega$ cm) for achieving permittivity ( $\epsilon'_r$ ) and loss tangent ( $\tan \delta$ ) data of phantom liquid close to the original green mango seed tissue

specimen (please refer to Table 5.30). Final permittivity ( $\epsilon_r'$ ) and loss tangent ( $\tan \delta$ ) data of the equivalent phantom liquid have been realized within 0.90% and 0.60% limits of the original measured values at 1842.50 MHz (please refer to Fig. 5.45 and Table 5.31).

At the final phase, a liquid preparation of 20.83 ml diethylene glycol monobutyl ether, 83.33 mg sodium chloride (NaCl) and 100 ml DI water has been realized to tune permittivity ( $\epsilon_r'$ ) and loss tangent ( $\tan \delta$ ) data of equivalent phantom liquid close to the original green mango seed tissue specimen at 2450.00 MHz (please refer to Table 5.30 for the composition at 25 °C). Permittivity ( $\epsilon_r'$ ) and loss tangent ( $\tan \delta$ ) values of the final phantom liquid have been tuned within 1.43% and 0.51% limits of the reference data for green mango seed tissue specimen at 2450.00 MHz (please refer to Fig. 5.46 and Table 5.31).

Table 5.30 Final compositions of green mango seed tissue equivalent phantom liquids

Frequency (MHz)	Final composition of phantom liquid
947.50	100 ml DI water, 35 g sucrose & 200 mg NaCl
1842.50	100 ml DI water, 20.83 ml DGME & 125 mg NaCl
2450.00	100 ml DI water, 20.83 ml DGME & 83.33 mg NaCl

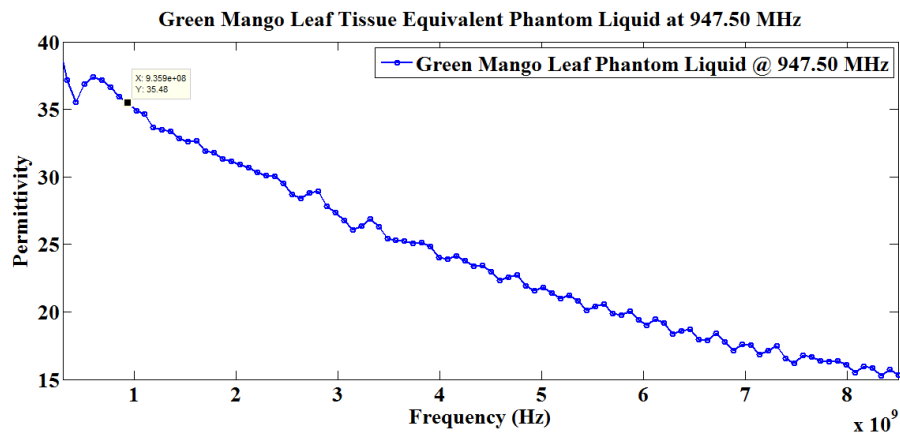
DGME = diethylene glycol monobutyl ether

Table 5.31 Difference between the measured dielectric properties ( $\epsilon_r$ ) of green mango seed tissue specimen and equivalent phantom liquids

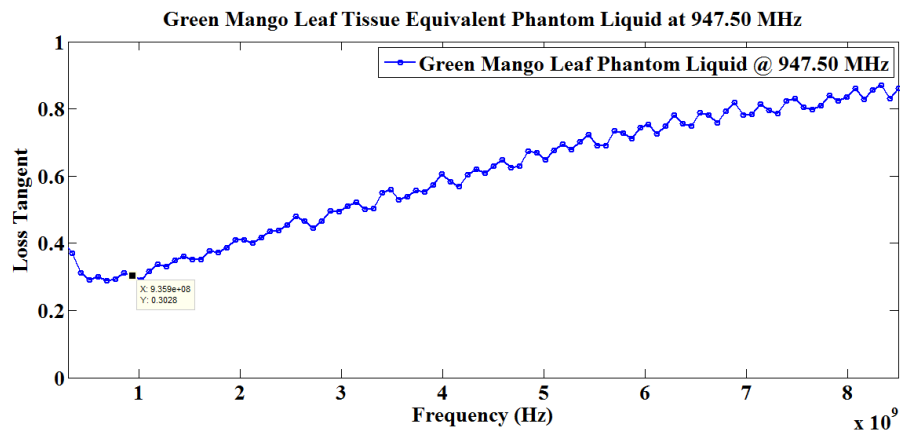
Frequency (MHz)	947.50	Deviation	1842.50	Deviation	2450.00	Deviation
Reference Permittivity ( $\epsilon_r'$ )	67.59		65.69		65.12	
Phantom Liquid Permittivity ( $\epsilon_r'$ )	68.56	1.44%	65.10	0.90%	64.19	1.43%
Reference Loss Tangent ( $\tan \delta$ )	0.156		0.168		0.197	
Phantom Liquid Loss Tangent ( $\tan \delta$ )	0.156	0.00%	0.167	0.60%	0.198	0.51%

### 5.4.9.3 Phantom Liquids Preparation for Green Mango Leaf Specimen

Phantom liquid recipes have been prepared for green mango leaf specimen at 947.50 MHz, 1842.50 MHz and 2450.00 MHz. Green mango leaf tissue equivalent phantom liquid formulations have been prepared based on different compositions of DI water (resistivity = 13 M $\Omega$ cm), diethylene glycol monobutyl ether and sodium chloride (NaCl). Different amounts of diethylene glycol monobutyl ether have been added with DI water (resistivity = 13 M $\Omega$ cm) to bring down permittivity ( $\epsilon_r'$ ) of the phantom liquids (depending upon frequency of interest). As a consequence, permittivity ( $\epsilon_r'$ ) values of the prepared phantom liquids have been tuned close to original green mango leaf tissue specimen. Furthermore, sodium chloride (NaCl) has been added



(a)



(b)

Fig. 5.47: Green mango leaf tissue equivalent phantom liquid at 947.50 MHz (a) permittivity and (b) loss tangent

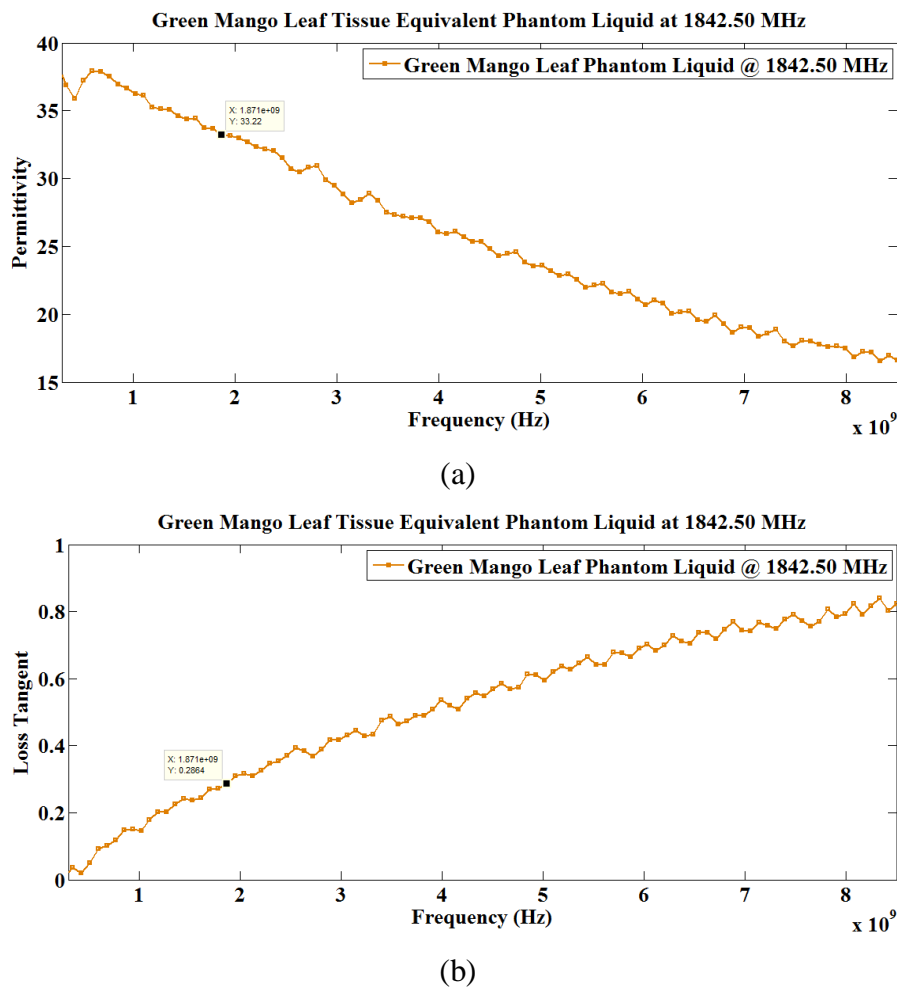
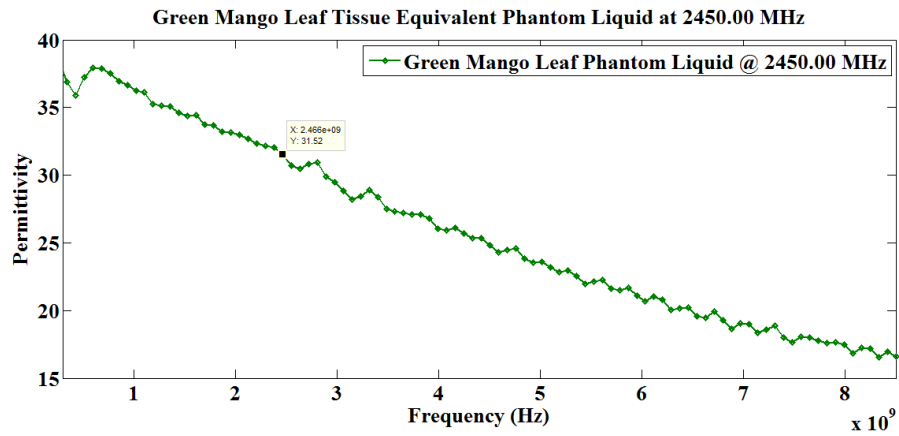


Fig. 5.48: Green mango leaf tissue equivalent phantom liquid at 1842.50 MHz (a) permittivity and (b) loss tangent

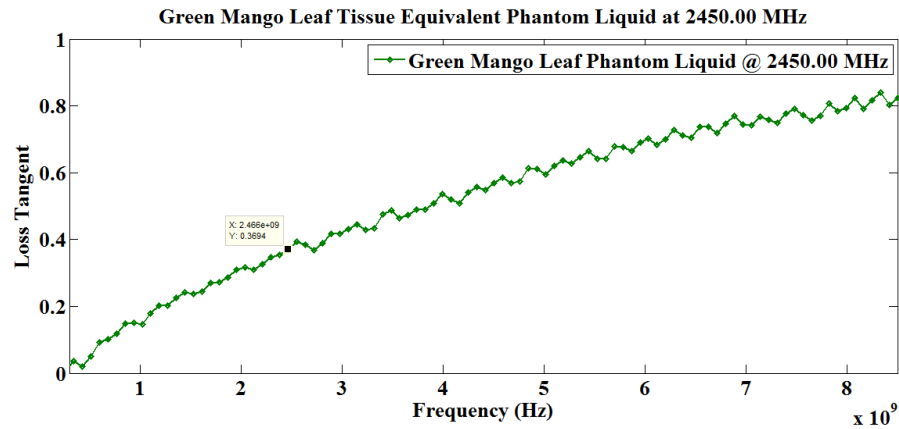
to selected liquid recipe (as and where required) to fine tune electrical conductivity ( $\sigma$ ) / loss tangent ( $\tan \delta$ ) of the final tissue equivalent phantom liquid (primarily at 947.50 MHz).

As discussed before, both permittivity ( $\epsilon'_r$ ) and loss tangent ( $\tan \delta$ ) values for DI water (resistivity = 13 M $\Omega$ cm) have been measured at 25 °C (prior to preparing green mango leaf tissue equivalent phantom liquids). Measured permittivity ( $\epsilon'_r$ ) and loss tangent ( $\tan \delta$ ) data for DI water have already been discussed before at 947.50 MHz, 1842.50 MHz and 2450.00 MHz – hence, those values haven't been mentioned here.

At first, to prepare green mango leaf tissue equivalent liquid recipe at 947.50 MHz, 137.50 ml diethylene glycol monobutyl ether and 1125 mg sodium chloride (NaCl) have been mixed with



(a)



(b)

Fig. 5.49: Green mango leaf tissue equivalent phantom liquid at 2450.00 MHz (a) permittivity and (b) loss tangent

100 ml DI water (resistivity = 13 M $\Omega$ cm) to realize phantom liquid permittivity ( $\epsilon'_r$ ) and loss tangent ( $\tan \delta$ ) data close to the original green mango leaf specimen (please refer to Table 5.32). Final phantom liquid permittivity ( $\epsilon'_r$ ) and loss tangent ( $\tan \delta$ ) data have been achieved within 4.62% and 0.33% limits of the respective original values at 947.50 MHz (please refer to Fig. 5.47 and Table 5.33).

Next, at 1842.50 MHz, 131.25 ml diethylene glycol monobutyl ether has been mixed with 100 ml DI water (resistivity = 13 M $\Omega$ cm) to attain permittivity ( $\epsilon'_r$ ) and loss tangent ( $\tan \delta$ ) values of equivalent phantom liquid close to the original green mango leaf tissue specimen (please refer to Table 5.32). Final permittivity ( $\epsilon'_r$ ) and loss tangent ( $\tan \delta$ ) data of equivalent phantom liquid

have been achieved within 4.46% and 6.72% limits of the reference values at 1842.50 MHz (please refer to Fig. 5.48 and Table 5.33). It should be noted that the deviation in loss tangent ( $\tan \delta$ ) can be minimized further by using DI water with resistivity higher than 13 M $\Omega$ cm.

At last, the above mentioned liquid composition i.e. mixture of 131.25 ml diethylene glycol monobutyl ether and 100 ml DI water (resistivity = 13 M $\Omega$ cm) has been utilized to tune permittivity ( $\epsilon_r'$ ) and loss tangent ( $\tan \delta$ ) data of equivalent phantom liquid close to original green mango leaf tissue specimen at 2450.00 MHz (please refer to Table 5.32). Permittivity ( $\epsilon_r'$ ) and loss tangent ( $\tan \delta$ ) data of the final phantom liquid have been tuned within 1.55% and 35.66% limits of the respective original measured values for green mango leaf specimen at 2450.00 MHz (please refer to Fig. 5.49 and Table 5.33). Here, it must be noted that the deviation in loss tangent ( $\tan \delta$ ) is significantly large at 2450.00 MHz – the same can be minimized by utilizing DI water with resistivity much higher than 13 M $\Omega$ cm.

Table 5.32 Final compositions of green mango leaf tissue equivalent phantom liquids

Frequency (MHz)	Final composition of phantom liquid
947.50	100 ml DI water, 137.50 ml DGME & 1125 mg NaCl
1842.50	100 ml DI water & 131.25 ml DGME
2450.00	100 ml DI water & 131.25 ml DGME

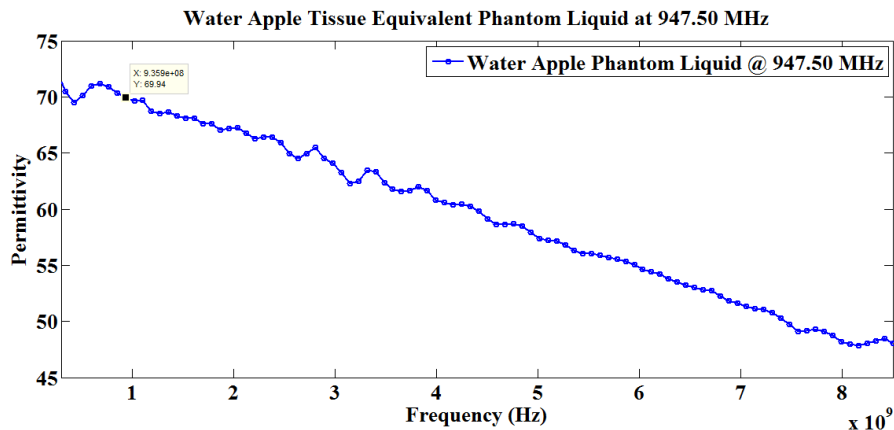
DGME = diethylene glycol monobutyl ether

Table 5.33 Difference between the measured dielectric properties ( $\epsilon_r$ ) of green mango leaf tissue specimen and equivalent phantom liquids

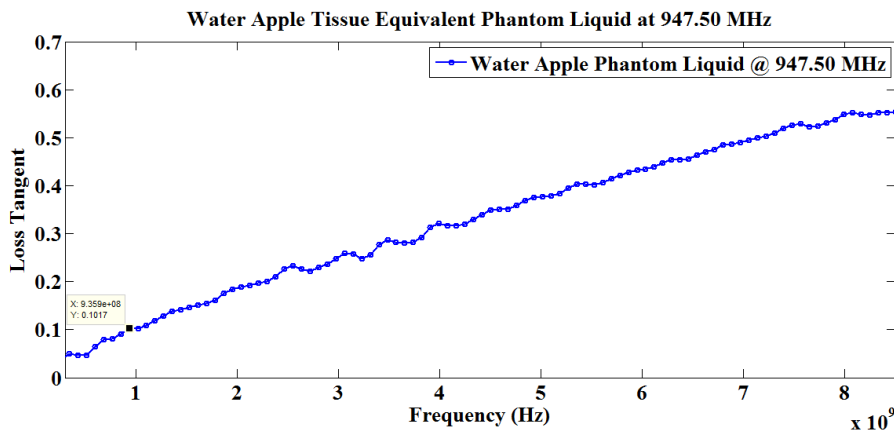
Frequency (MHz)	947.50	Deviation	1842.50	Deviation	2450.00	Deviation
Reference Permittivity ( $\epsilon_r'$ )	34.03		31.80		31.04	
Phantom Liquid Permittivity ( $\epsilon_r'$ )	35.48	4.62%	33.22	4.46%	31.52	1.55%
Reference Loss Tangent ( $\tan \delta$ )	0.302		0.268		0.272	
Phantom Liquid Loss Tangent ( $\tan \delta$ )	0.303	0.33%	0.286	6.72%	0.369	35.66%

### 5.4.10 Phantom Liquids Preparation for Water Apple Specimen

Phantom liquid preparations have been formulated for water apple tissue specimen at 947.50 MHz, 1842.50 MHz and 2450.00 MHz. Water apple tissue equivalent phantom liquid recipes have been formulated based on different compositions of DI water (resistivity = 13 M $\Omega$ cm) and sucrose / diethylene glycol monobutyl ether. Different amounts of sucrose / diethylene glycol monobutyl ether have been added with DI water (resistivity = 13 M $\Omega$ cm) primarily to reduce permittivity ( $\epsilon_r'$ ) of the equivalent phantom liquids (based on frequency of interest) – thus, permittivity ( $\epsilon_r'$ ) values of the prepared phantom liquids have been tuned close to the original water apple tissue specimen. However, it should be noted that the electrical conductivity ( $\sigma$ ) / loss tangent ( $\tan \delta$ ) values of the phantom liquids have already been tuned close to original



(a)



(b)

Fig. 5.50: Water apple tissue equivalent phantom liquid at 947.50 MHz (a) permittivity and (b) loss tangent

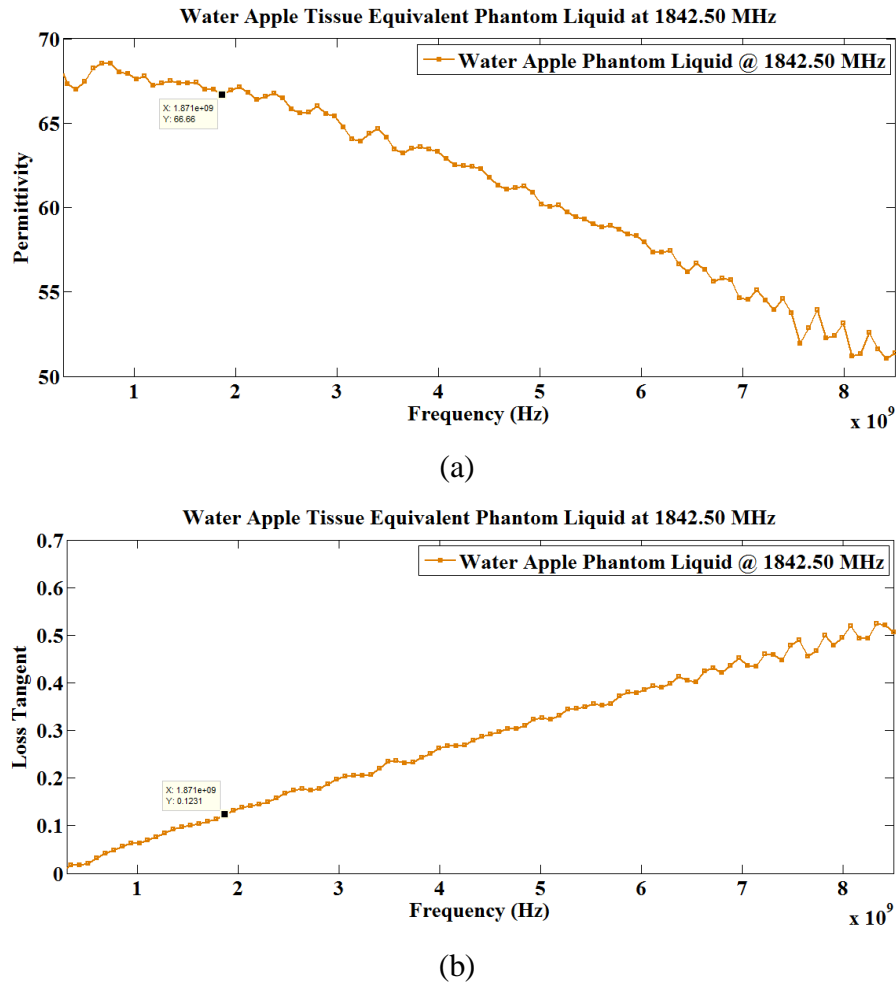


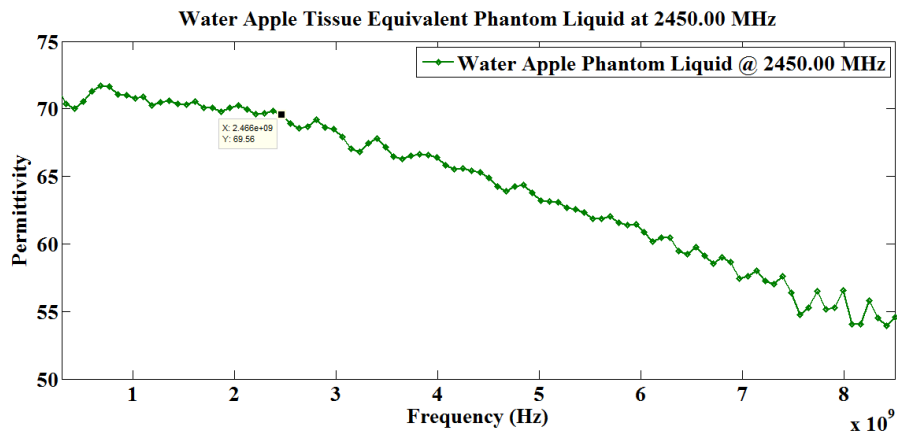
Fig. 5.51: Water apple tissue equivalent phantom liquid at 1842.50 MHz (a) permittivity and (b) loss tangent

water apple tissue specimen without adding sodium chloride (NaCl).

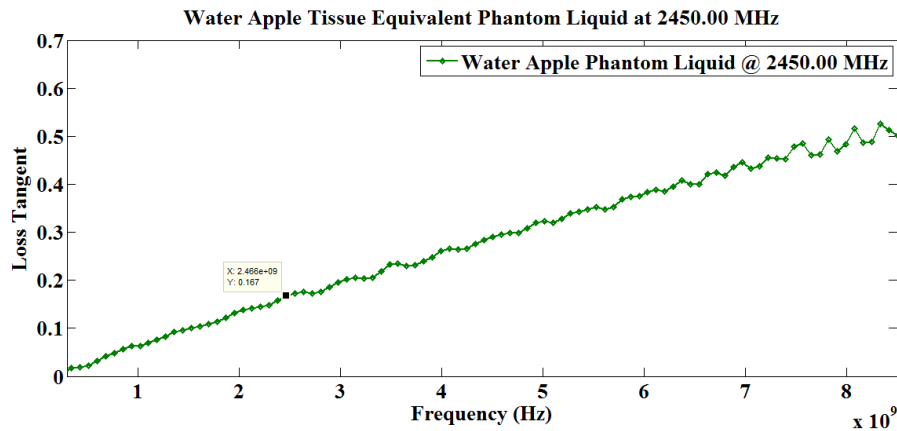
As mentioned earlier, complex dielectric properties ( $\epsilon_r$ ) i.e. both permittivity ( $\epsilon_r'$ ) and loss tangent ( $\tan \delta$ ) values for DI water (resistivity = 13 M $\Omega$ cm) have been measured at first stage. Those measured permittivity ( $\epsilon_r'$ ) and loss tangent ( $\tan \delta$ ) values for DI water at 25 °C have been discussed earlier at 947.50 MHz, 1842.50 MHz and 2450.00 MHz – thus, those values aren't repeated here again.

At initial stage, to formulate water apple tissue equivalent phantom liquid preparation at 947.50 MHz, 32 g sucrose has been mixed with 100 ml DI water (resistivity = 13 M $\Omega$ cm) to realize equivalent liquid permittivity ( $\epsilon_r'$ ) and loss tangent ( $\tan \delta$ ) values near the original water apple





(a)



(b)

Fig. 5.52: Water apple tissue equivalent phantom liquid at 2450.00 MHz (a) permittivity and (b) loss tangent

tissue specimen (please refer to Table 5.34). The resultant phantom liquid permittivity ( $\epsilon'_r$ ) and loss tangent ( $\tan \delta$ ) values have been realized within 1.73% and 0.00% limits of the respective reference dielectric data ( $\epsilon_r$ ) at 947.50 MHz (please refer to Fig. 5.50 and Table 5.35).

Next, at the subsequent stage, 15 ml Diethylene glycol monobutyl ether has been mixed with 100 ml DI water (resistivity = 13 M $\Omega$ cm) to achieve permittivity ( $\epsilon'_r$ ) and loss tangent ( $\tan \delta$ ) values of the resultant phantom liquid close to the original water apple tissue specimen (please refer to Table 5.34). Final permittivity ( $\epsilon'_r$ ) and loss tangent ( $\tan \delta$ ) values of the equivalent phantom liquid have been achieved within 1.35% and 0.81% limits of the reference dielectric data ( $\epsilon_r$ ) at 1842.50 MHz (please refer to Fig. 5.51 and Table 5.35).

At the last stage, the above mentioned liquid composition i.e. a mixture of 13.04 ml diethylene glycol monobutyl ether and 100 ml DI water (resistivity = 13 MΩcm) has been realized to tune permittivity ( $\epsilon_r'$ ) and loss tangent ( $\tan \delta$ ) data of equivalent phantom liquid close to original water apple tissue specimen at 2450.00 MHz (please refer to Table 5.34). Final permittivity ( $\epsilon_r'$ ) and loss tangent ( $\tan \delta$ ) data of the equivalent phantom liquid have been tuned within 3.01% and 12.08% limits of the respective reference measured values for water apple specimen at 2450.00 MHz (please refer to Fig. 5.52 and Table 5.35). It is to be taken into note that the deviation in loss tangent ( $\tan \delta$ ) is significant at 2450.00 MHz and the same can be minimized using DI water with resistivity greater than 13 MΩcm.

Table 5.34 Final compositions of water apple tissue equivalent phantom liquids

Frequency (MHz)	Final composition of phantom liquid
947.50	100 ml DI water & 32 g sucrose
1842.50	100 ml DI water & 15 ml DGME
2450.00	100 ml DI water & 13.04 ml DGME

DGME = diethylene glycol monobutyl ether

Table 5.35 Difference between the measured dielectric properties ( $\epsilon_r$ ) of water apple tissue specimen and equivalent phantom liquids

Frequency (MHz)	947.50	Deviation	1842.50	Deviation	2450.00	Deviation
Reference Permittivity ( $\epsilon_r'$ )	68.75		67.57		67.53	
Phantom Liquid Permittivity ( $\epsilon_r'$ )	69.94	1.73%	66.66	1.35%	69.56	3.01%
Reference Loss Tangent ( $\tan \delta$ )	0.102		0.124		0.149	
Phantom Liquid Loss Tangent ( $\tan \delta$ )	0.102	0.00%	0.123	0.81%	0.167	12.08%

## 5.4.11 Phantom Liquids Preparation for Orange Specimens

### 5.4.11.1 Phantom Liquids Preparation for Orange Pulp Specimen

Phantom liquid preparations have been formulated for orange pulp tissue specimen at 947.50 MHz, 1842.50 MHz and 2450.00 MHz. Orange pulp tissue equivalent phantom liquid recipes have been prepared based on different compositions of DI water (resistivity = 13 M $\Omega$ cm), sucrose / diethylene glycol monobutyl ether and sodium chloride (NaCl). Different amounts of sucrose / diethylene glycol monobutyl ether have been mixed with DI water (resistivity = 13 M $\Omega$ cm) to reduce permittivity ( $\epsilon_r'$ ) of the phantom liquids based on frequency of interest. In this manner, permittivity ( $\epsilon_r'$ ) values of the phantom liquids have been tuned close to original orange pulp tissue specimen. Furthermore, sodium chloride (NaCl) has been added to the liquid recipes

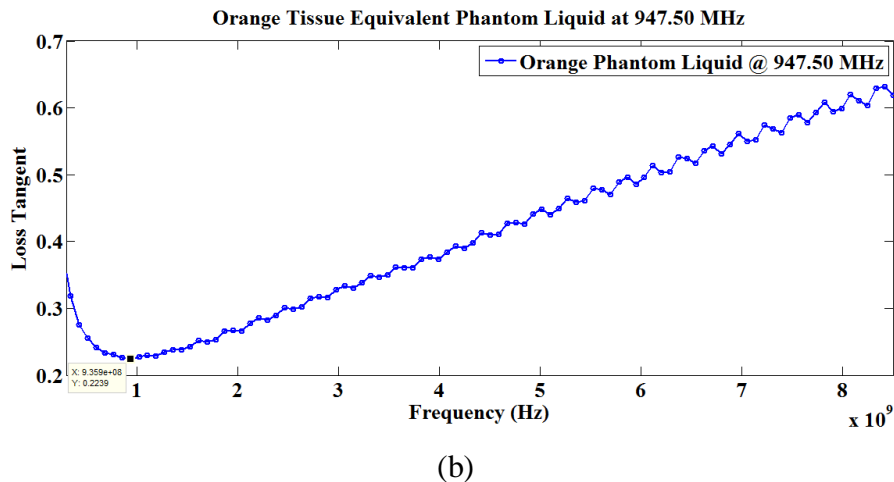
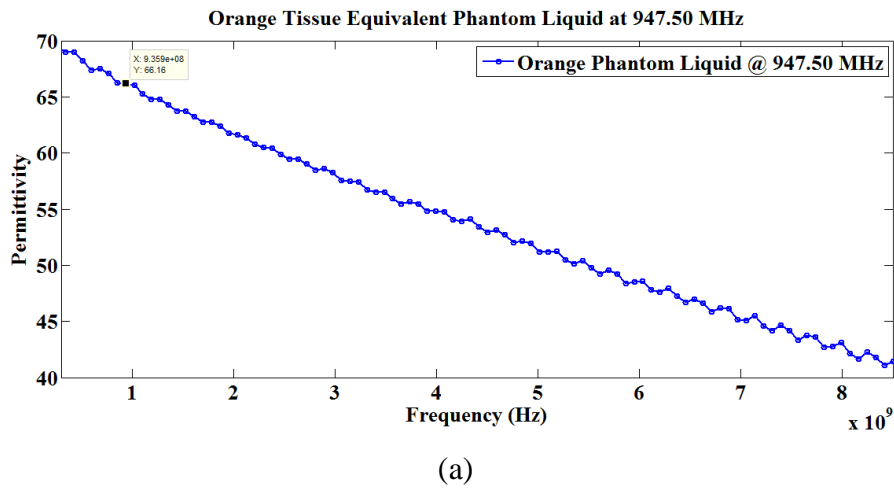


Fig. 5.53: Orange pulp tissue equivalent phantom liquid at 947.50 MHz (a) permittivity and (b) loss tangent

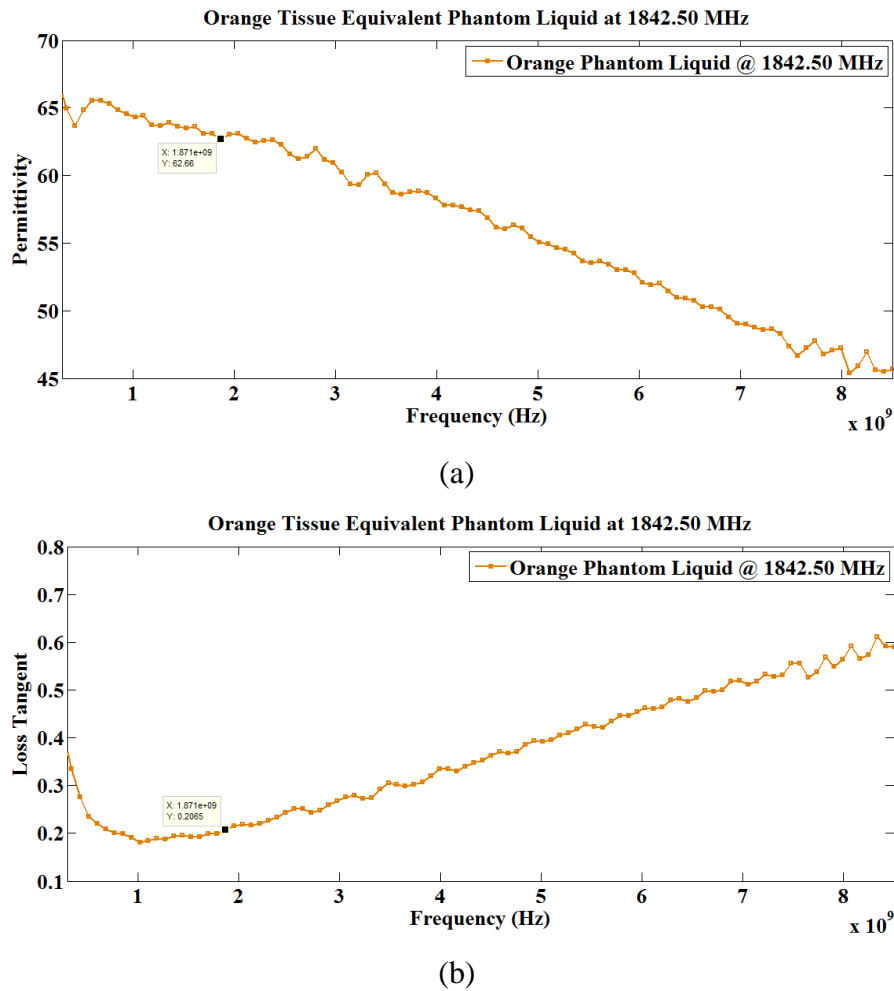


Fig. 5.54: Orange pulp tissue equivalent phantom liquid at 1842.50 MHz (a) permittivity and (b) loss tangent

for fine tuning electrical conductivity ( $\sigma$ ) / loss tangent ( $\tan \delta$ ) values of the final tissue equivalent phantom liquids.

As discussed before, prior to realizing orange pulp tissue equivalent phantom liquid recipes, both permittivity ( $\epsilon_r'$ ) and loss tangent ( $\tan \delta$ ) data for DI water (resistivity = 13 M $\Omega$ cm) have been measured at 25 °C. Obtained permittivity ( $\epsilon_r'$ ) and loss tangent ( $\tan \delta$ ) data for the DI water have earlier been discussed at 947.50 MHz, 1842.50 MHz and 2450.00 MHz – thus, not repeated here again.

At first, in order to prepare orange pulp tissue equivalent phantom liquid at 947.50 MHz, 42 g sucrose and 500 mg sodium chloride (NaCl) have been mixed with 100 ml DI water (resistivity =

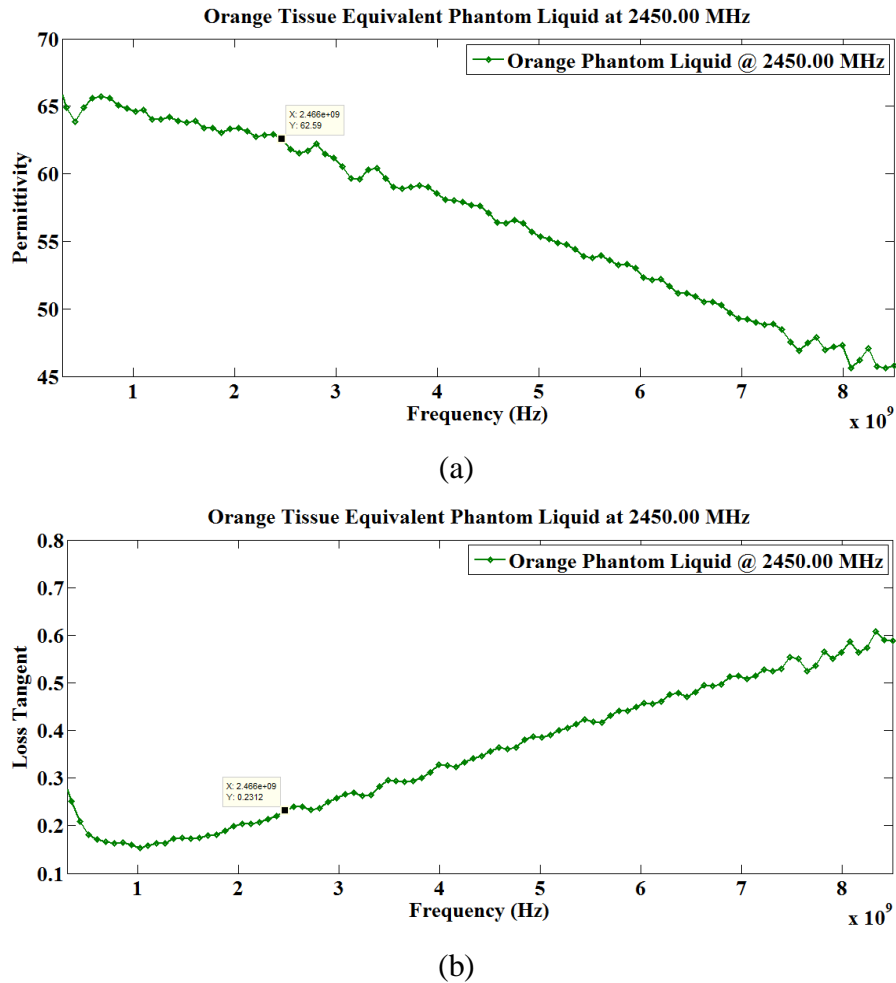


Fig. 5.55: Orange pulp tissue equivalent phantom liquid at 2450.00 MHz (a) permittivity and (b) loss tangent

13 M $\Omega$ cm) to achieve phantom liquid permittivity ( $\epsilon_r'$ ) and loss tangent ( $\tan \delta$ ) data close to original orange pulp specimen (please refer to Table 5.36). Final phantom liquid permittivity ( $\epsilon_r'$ ) and loss tangent ( $\tan \delta$ ) data have been realized within 0.58% and 1.82% limits of the respective original values at 947.50 MHz (please refer to Fig. 5.53 and Table 5.37).

Next, at 1842.50 MHz, 23.81 ml diethylene glycol monobutyl ether and 333.33 mg sodium chloride (NaCl) have been mixed with 100 ml DI water (resistivity = 13 M $\Omega$ cm) to achieve equivalent phantom liquid permittivity ( $\epsilon_r'$ ) and loss tangent ( $\tan \delta$ ) values close to the original orange pulp tissue specimen (please refer to Table 5.36). Final permittivity ( $\epsilon_r'$ ) and loss tangent

( $\tan \delta$ ) data of the equivalent phantom liquid recipe have been achieved within 1.09% and 1.90% limits of the reference values at 1842.50 MHz (please refer to Fig. 5.54 and Table 5.37).

At last, 23.81 ml diethylene glycol monobutyl ether and 238.10 mg sodium chloride (NaCl) have been added with 100 ml DI water (resistivity = 13 M $\Omega$ cm) to tune permittivity ( $\epsilon_r'$ ) and loss tangent ( $\tan \delta$ ) data of equivalent phantom liquid close to the original orange pulp tissue specimen at 2450.00 MHz (please refer to Table 5.36). Permittivity ( $\epsilon_r'$ ) and loss tangent ( $\tan \delta$ ) values of final phantom liquid have been tuned within 0.18% and 0.43% limits of the respective measured values for orange pulp tissue specimen at 2450.00 MHz (please refer to Fig. 5.55 and Table 5.37).

Table 5.36 Final compositions of orange pulp tissue equivalent phantom liquids

Frequency (MHz)	Final composition of phantom liquid
947.50	100 ml DI water, 42 g sucrose & 500 mg NaCl
1842.50	100 ml DI water, 23.81 ml DGME & 333.33 mg NaCl
2450.00	100 ml DI water, 23.81 ml DGME & 238.10 mg NaCl

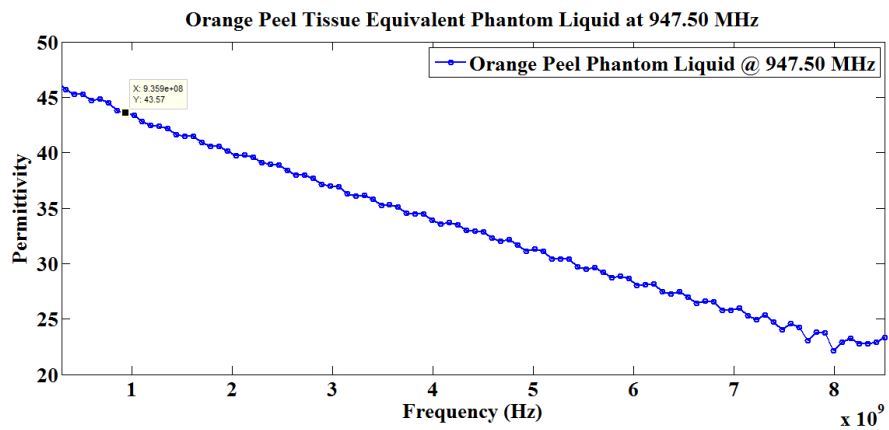
DGME = diethylene glycol monobutyl ether

Table 5.37 Difference between the measured dielectric properties ( $\epsilon_r$ ) of orange pulp tissue specimen and equivalent phantom liquids

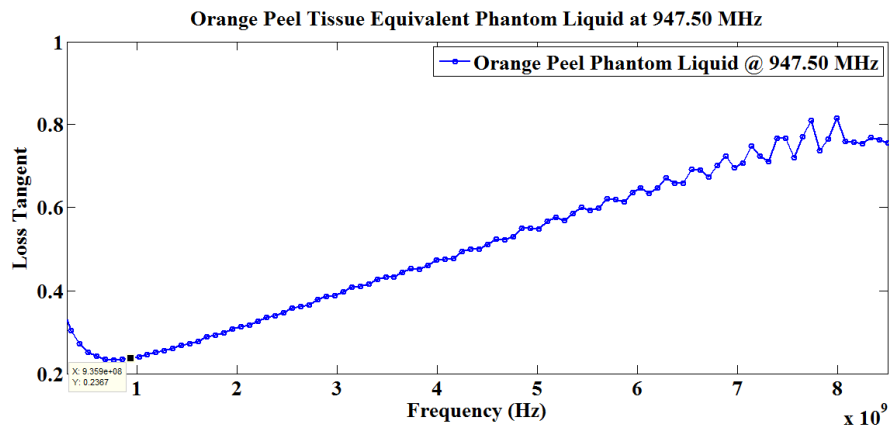
Frequency (MHz)	947.50	Deviation	1842.50	Deviation	2450.00	Deviation
Reference Permittivity ( $\epsilon_r'$ )	65.78		63.35		62.70	
Phantom Liquid Permittivity ( $\epsilon_r'$ )	66.16	0.58%	62.66	1.09%	62.59	0.18%
Reference Loss Tangent ( $\tan \delta$ )	0.220		0.210		0.230	
Phantom Liquid Loss Tangent ( $\tan \delta$ )	0.224	1.82%	0.206	1.90%	0.231	0.43%

### 5.4.11.2 Phantom Liquids Preparation for Orange Peel Specimen

Phantom liquid recipes have been prepared for orange peel tissue specimen at 947.50 MHz, 1842.50 MHz and 2450.00 MHz. Orange peel tissue equivalent phantom liquid formulations have been prepared based on different compositions of DI water (resistivity = 13 M $\Omega$ cm), diethylene glycol monobutyl ether and sodium chloride (NaCl). Depending on frequency range, different amount of diethylene glycol monobutyl ether has been added with DI water (resistivity = 13 M $\Omega$ cm) to decrease permittivity ( $\epsilon_r'$ ) of the phantom liquids. Thus, permittivity ( $\epsilon_r'$ ) values of the prepared phantom liquids have been tuned close to original orange peel tissue specimen. In addition, sodium chloride (NaCl) has further been added to selected liquid recipe for fine tuning electrical conductivity ( $\sigma$ ) / loss tangent ( $\tan \delta$ ) value of the final tissue equivalent phantom liquid (in particular, at 947.50 MHz).

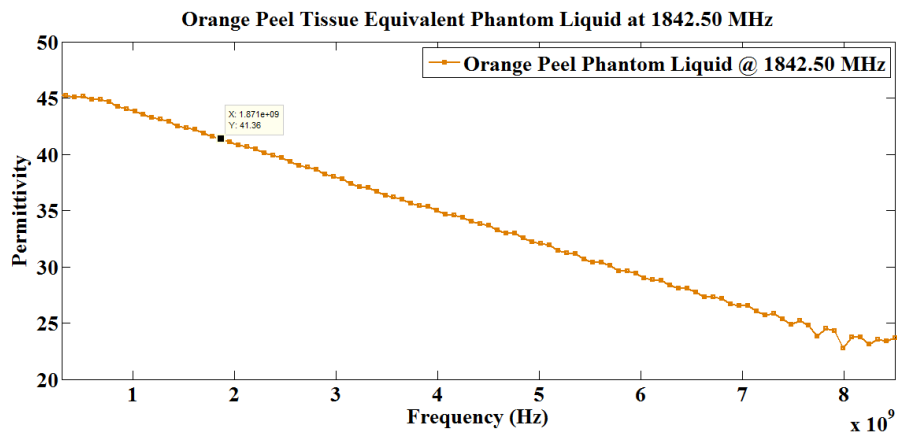


(a)

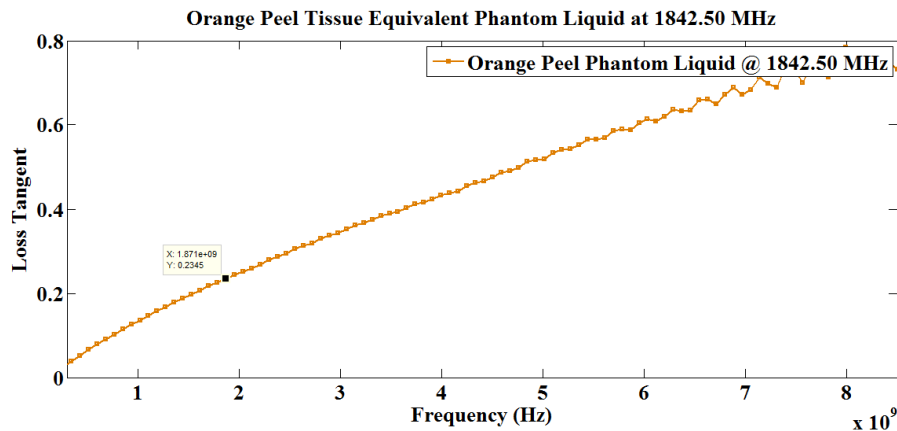


(b)

Fig. 5.56: Orange peel tissue equivalent phantom liquid at 947.50 MHz (a) permittivity and (b) loss tangent



(a)



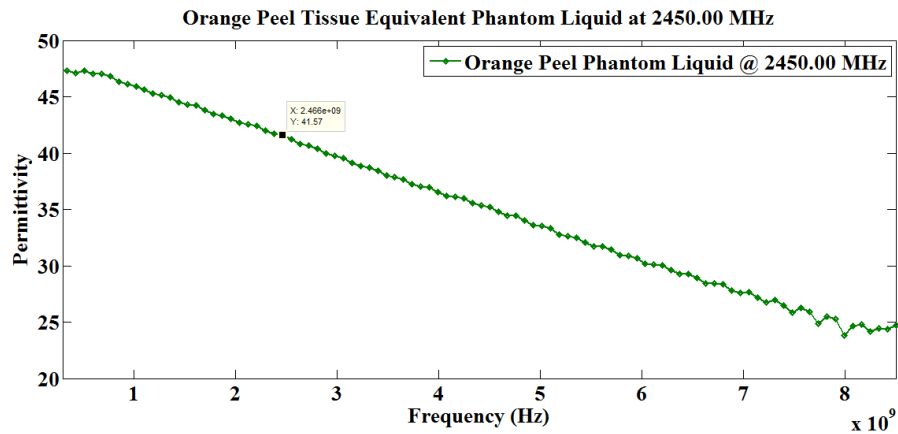
(b)

Fig. 5.57: Orange peel tissue equivalent phantom liquid at 1842.50 MHz (a) permittivity and (b) loss tangent

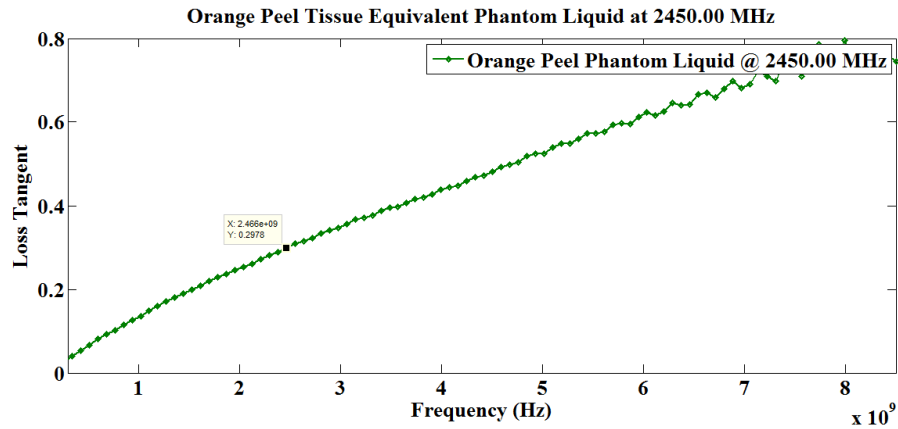
Prior to start preparing orange peel tissue equivalent phantom liquid recipes, complex dielectric properties ( $\epsilon_r$ ) i.e. both permittivity ( $\epsilon_r'$ ) and loss tangent ( $\tan \delta$ ) values of pure DI water (resistivity = 13 M $\Omega$ cm) have been measured at 25 °C for reference check. Measured permittivity ( $\epsilon_r'$ ) and loss tangent ( $\tan \delta$ ) values of DI water have already been mentioned earlier at 947.50 MHz, 1842.50 MHz and 2450.00 MHz – thus, those data aren't repeated here.

At the first stage, in order to prepare orange peel tissue equivalent phantom liquid recipe at 947.50 MHz, 90 ml diethylene glycol monobutyl ether and 600 mg sodium chloride (NaCl) have been added with 100 ml DI water (resistivity = 13 M $\Omega$ cm) for attaining phantom liquid permittivity ( $\epsilon_r'$ ) and loss tangent ( $\tan \delta$ ) data close to original orange peel tissue specimen





(a)



(b)

Fig. 5.58: Orange peel tissue equivalent phantom liquid at 2450.00 MHz (a) permittivity and (b) loss tangent

(please, refer to Table 5.38). Ultimate phantom liquid permittivity ( $\epsilon_r'$ ) and loss tangent ( $\tan \delta$ ) values have been achieved within 0.21% and 1.25% limits of the respective reference data at 947.50 MHz (please refer to Fig. 5.56 and Table 5.39).

Thereafter, at 1842.50 MHz, 90 ml diethylene glycol monobutyl ether has been mixed with 100 ml DI water (resistivity = 13 M $\Omega$ cm) in order to attain equivalent phantom liquid permittivity ( $\epsilon_r'$ ) and loss tangent ( $\tan \delta$ ) values close to the original orange peel tissue specimen (please refer to Table 5.38). Final permittivity ( $\epsilon_r'$ ) and loss tangent ( $\tan \delta$ ) values of the equivalent phantom liquid preparation have been realized within 0.55% and 1.74% limits of the reference values at 1842.50 MHz (please refer to Fig. 5.57 and Table 5.39).

## Phantom Liquid Preparation for Different Fruit and Plant Samples

At the last stage, 78.57 ml diethylene glycol monobutyl ether has been mixed with 100 ml DI water (resistivity = 13 MΩcm) for tuning permittivity ( $\epsilon_r'$ ) and loss tangent ( $\tan \delta$ ) parameters of equivalent phantom liquid close to the original orange peel specimen at 2450.00 MHz (please, refer to Table 5.38). Final permittivity ( $\epsilon_r'$ ) and loss tangent ( $\tan \delta$ ) values of phantom liquid have been tuned within 0.75% and 10.78% limits of the respective values of original orange peel specimen at 2450.00 MHz (please refer to Fig. 5.58 and Table 5.39). It should be noted that the deviation in loss tangent ( $\tan \delta$ ) is considerable at 2450.00 MHz – however, the same can be minimized employing DI water with resistivity greater than 13 MΩcm.

Table 5.38 Final compositions of orange peel tissue equivalent phantom liquids

Frequency (MHz)	Final composition of phantom liquid
947.50	100 ml DI water, 90 ml DGME & 600 mg NaCl
1842.50	100 ml DI water & 90 ml DGME
2450.00	100 ml DI water & 78.57 ml DGME

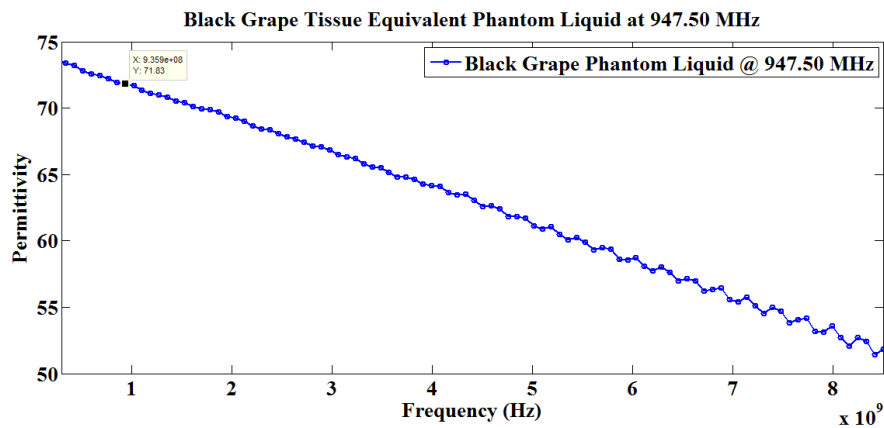
DGME = diethylene glycol monobutyl ether

Table 5.39 Difference between the measured dielectric properties ( $\epsilon_r$ ) of orange peel tissue specimen and equivalent phantom liquids

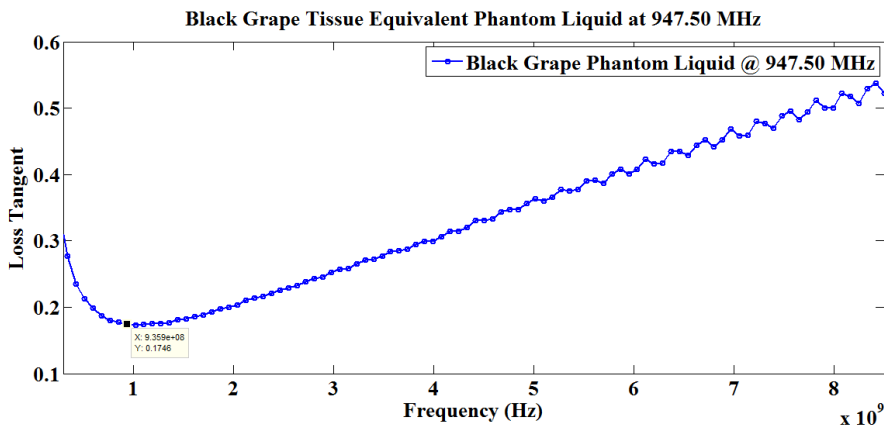
Frequency (MHz)	947.50	Deviation	1842.50	Deviation	2450.00	Deviation
Reference Permittivity ( $\epsilon_r'$ )	43.48		41.59		41.26	
Phantom Liquid Permittivity ( $\epsilon_r'$ )	43.57	0.21%	41.36	0.55%	41.57	0.75%
Reference Loss Tangent ( $\tan \delta$ )	0.240		0.230		0.269	
Phantom Liquid Loss Tangent ( $\tan \delta$ )	0.237	1.25%	0.234	1.74%	0.298	10.78%

### 5.4.12 Phantom Liquids Preparation for Black Grape Specimen

This time, phantom liquid recipes have been prepared for black grape tissue specimen at 947.50 MHz, 1842.50 MHz and 2450.00 MHz. Black grape tissue equivalent phantom liquid preparations have been realized based on different compositions of DI water (resistivity = 13 M $\Omega$ cm), sucrose / diethylene glycol monobutyl ether and sodium chloride (NaCl). In fact, based on the frequency range, different amounts of sucrose / diethylene glycol monobutyl ether have been added with DI water (resistivity = 13 M $\Omega$ cm) to bring down permittivity ( $\epsilon_r'$ ) of the prepared phantom liquids. In this manner, permittivity ( $\epsilon_r'$ ) values of the resultant phantom liquids have been tuned close to original black grape tissue specimen. Moreover, sodium chloride (NaCl) has been added further to fine tune electrical conductivity ( $\sigma$ ) / loss tangent ( $\tan \delta$ ) values of the final tissue equivalent phantom liquids.



(a)



(b)

Fig. 5.59: Black grape tissue equivalent phantom liquid at 947.50 MHz (a) permittivity and (b) loss tangent

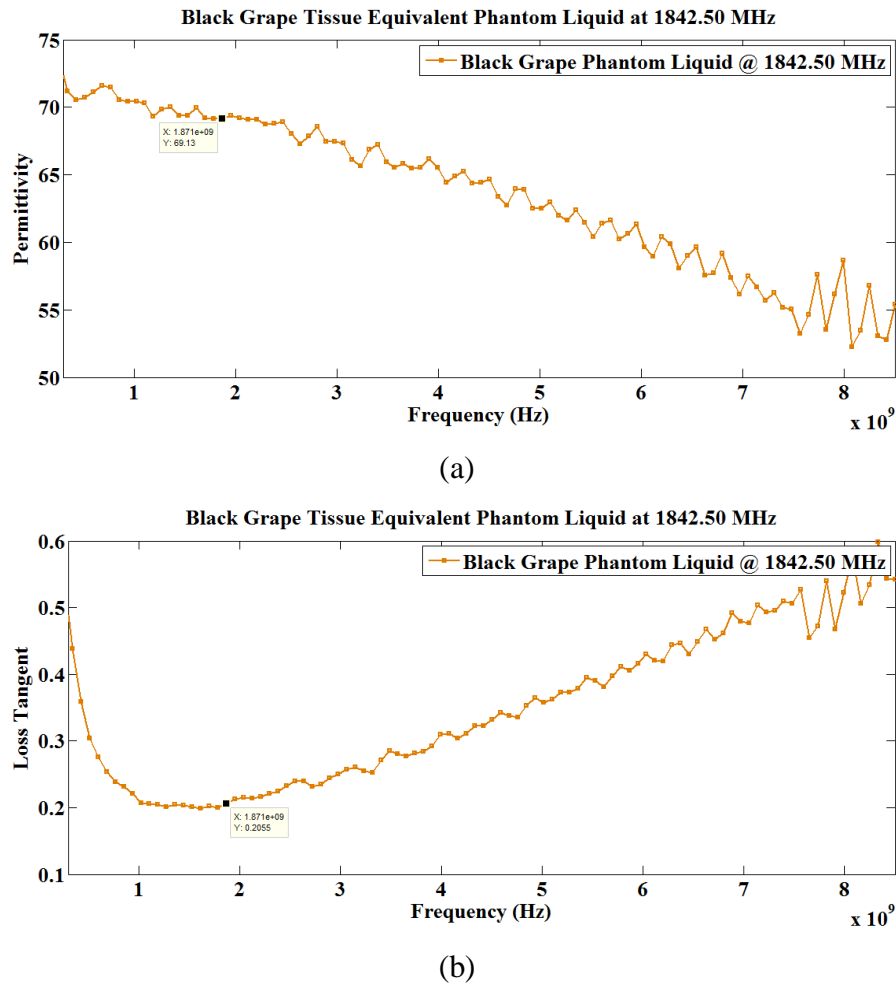


Fig. 5.60: Black grape tissue equivalent phantom liquid at 1842.50 MHz (a) permittivity and (b) loss tangent

As discussed before, prior to preparing black grape tissue equivalent phantom liquids, broadband dielectric properties ( $\epsilon_r$ ) i.e. both permittivity ( $\epsilon_r'$ ) and loss tangent ( $\tan \delta$ ) values of DI water (resistivity = 13 M $\Omega$ cm) have been measured at 25 °C for reference check. Obtained permittivity ( $\epsilon_r'$ ) and loss tangent ( $\tan \delta$ ) data for DI water have been mentioned earlier at 947.50 MHz, 1842.50 MHz and 2450.00 MHz – thus, those are not repeated here again.

Next, for preparing black grape tissue equivalent phantom liquid at 947.50 MHz, 22 g sucrose and 300 mg sodium chloride (NaCl) have been mixed with 100 ml DI water (resistivity = 13 M $\Omega$ cm) to attain phantom liquid permittivity ( $\epsilon_r'$ ) and loss tangent ( $\tan \delta$ ) values close to original black grape tissue specimen (please, refer to Table 5.40). Final phantom liquid

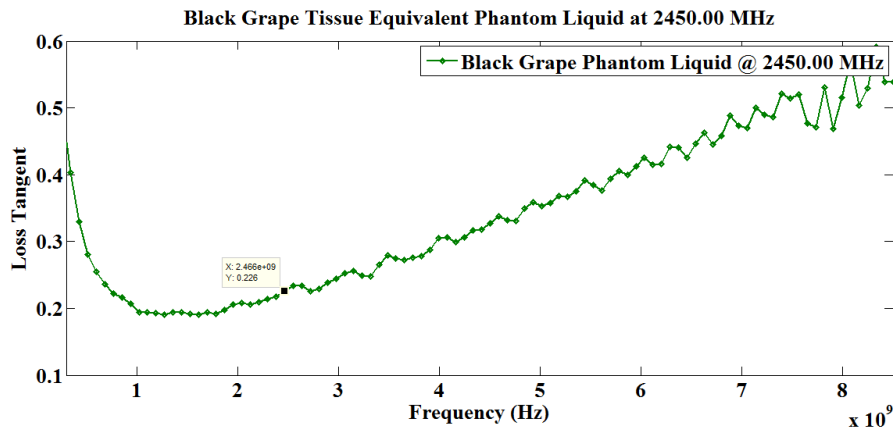
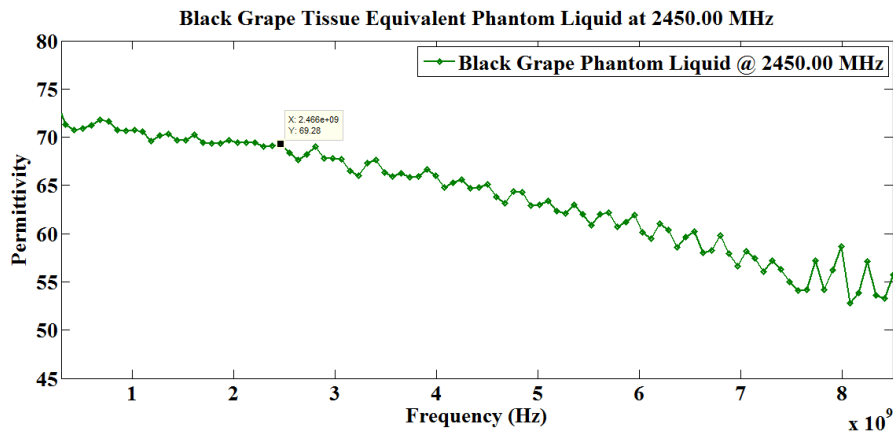


Fig. 5.61: Black grape tissue equivalent phantom liquid at 2450.00 MHz (a) permittivity and (b) loss tangent

permittivity ( $\epsilon_r'$ ) and loss tangent ( $\tan \delta$ ) values have been realized within 0.81% and 0.57% limits of the respective reference data at 947.50 MHz (please refer to Fig. 5.59 and Table 5.41).

Subsequently, at 1842.50 MHz, 13.04 ml diethylene glycol monobutyl ether and 391.30 mg sodium chloride (NaCl) have been added with 100 ml DI water (resistivity = 13 M $\Omega$ cm) in order to realize equivalent phantom liquid permittivity ( $\epsilon_r'$ ) and loss tangent ( $\tan \delta$ ) values close to the original black grape tissue specimen (please refer to Table 5.40). Final permittivity ( $\epsilon_r'$ ) and loss tangent ( $\tan \delta$ ) values of the equivalent phantom liquid have been achieved within 0.28% and 1.98% limits of the respective reference data at 1842.50 MHz (please refer to Fig. 5.60 and Table 5.41).

At last, 13.04 ml diethylene glycol monobutyl ether and 347.83 mg sodium chloride (NaCl) have been mixed with 100 ml DI water (resistivity = 13 MΩcm) in order to tune permittivity ( $\epsilon_r'$ ) and loss tangent ( $\tan \delta$ ) of equivalent phantom liquid close to the original black grape specimen at 2450.00 MHz (please refer to Table 5.40). Final permittivity ( $\epsilon_r'$ ) and loss tangent ( $\tan \delta$ ) values of prepared phantom liquid have been tuned within 2.68% and 0.89% limits of the respective reference data for black grape specimen at 2450.00 MHz (please refer to Fig. 5.61 and Table 5.41).

Table 5.40 Final compositions of black grape tissue equivalent phantom liquids

Frequency (MHz)	Final composition of phantom liquid
947.50	100 ml DI water, 22 g sucrose & 300 mg NaCl
1842.50	100 ml DI water, 13.04 ml DGME & 391.30 mg NaCl
2450.00	100 ml DI water, 13.04 ml DGME & 347.83 mg NaCl

DGME = diethylene glycol monobutyl ether

Table 5.41 Difference between the measured dielectric properties ( $\epsilon_r$ ) of black grape tissue specimen and equivalent phantom liquids

Frequency (MHz)	947.50	Deviation	1842.50	Deviation	2450.00	Deviation
Reference Permittivity ( $\epsilon_r'$ )	71.25		68.94		67.47	
Phantom Liquid Permittivity ( $\epsilon_r'$ )	71.83	0.81%	69.13	0.28%	69.28	2.68%
Reference Loss Tangent ( $\tan \delta$ )	0.176		0.202		0.224	
Phantom Liquid Loss Tangent ( $\tan \delta$ )	0.175	0.57%	0.206	1.98%	0.226	0.89%

## 5.5 Discussions

In total, phantom liquids have been prepared for twenty fruit / plant tissue layers chosen out of twelve fruit / plant specimens – some fruit / plant specimens are multilayer in nature and rest possess homogeneous tissue layers. It should be noted, tissue equivalent liquids have been prepared at three frequencies of interest i.e. 947.50 MHz, 1842.50 MHz and 2450.00 MHz – thus, altogether, sixty liquid recipes have been prescribed.

In general, DI water (resistivity = 13 MΩcm), sucrose and sodium chloride (NaCl) based liquid compositions have been prepared primarily at 947.50 MHz; however, these sucrose based preparations possess high electrical conductivity ( $\sigma$ ) / loss tangent ( $\tan \delta$ ) values at 1842.50 MHz and 2450.00 MHz – thus, aren't suitable at those higher frequencies (except few scenarios). Therefore, at higher frequencies, DI water (resistivity = 13 MΩcm), diethylene glycol monobutyl ether and sodium chloride (NaCl) based liquid preparations have been formulated to realize tissue equivalent phantom liquids in order to precisely tune electrical conductivity ( $\sigma$ ) / loss tangent ( $\tan \delta$ ) values. In fact, at any particular frequency, diethylene glycol monobutyl ether possesses lower electrical conductivity ( $\sigma$ ) / loss tangent ( $\tan \delta$ ) compared to DI water and sucrose solution. However, in few cases, even plain mixtures of DI water (resistivity = 13 MΩcm) and diethylene glycol monobutyl ether go beyond the electrical conductivity ( $\sigma$ ) / loss tangent ( $\tan \delta$ ) values of targeted fruit / plant tissue layers. In those scenarios, difference in loss tangent ( $\tan \delta$ ) values (at 1842.50 MHz and 2450.00 MHz) can considerably be minimized with high resistivity DI water (resistivity > 13 MΩcm).

## 5.6 Conclusions

Prepared phantom liquid recipes are indeed useful for practical SAR measurement in different fruit / plant prototypes at 947.50 MHz, 1842.50 MHz and 2450.00 MHz. These fruit / plant tissue equivalent liquids can be poured inside customized fruit / plant phantom models for accurate SAR measurements. Described phantom liquid recipes can instantly be prepared just before practical SAR measurements and the complex dielectric properties ( $\epsilon_r$ ) can be verified using open ended coaxial probe technique [1-11, 18]. In addition, preparing different compositions of DI water (resistivity = 13 MΩcm), sucrose / diethylene glycol monobutyl ether and sodium chloride (NaCl) for attaining a wide range of permittivity ( $\epsilon_r'$ ) and loss tangent ( $\tan \delta$ ) values

have facilitated to identify the contributions of individual elements in tuning complex dielectric properties ( $\epsilon_r$ ) of phantom liquids. Thus, in future, customized tissue equivalent phantom liquid recipe can be prepared for any other fruit / plant or even human tissue specimen. These fruit / plant tissue equivalent phantom liquid preparations can be considered as an advancement in the direction of practical SAR measurement in prototyped fruit / plant models and furthermore, in quantifying electromagnetic energy absorption rates in fruit / plant models to limit electromagnetic exposure for ensuring safety of fruits, crops and plants.

## References

- [1] G. Deschamps, 'Impedance of an Antenna in a Conducting Medium', *IRE Transactions on Antennas and Propagation*, Vol. 10, No. 5, pp. 648-650, 1962.
- [2] L. Liu, D. Xu, and Z. Jiang, 'Improvement in Dielectric Measurement Technique of Open-Ended Coaxial Line Resonator Method', *Electronics Letters*, Vol. 22, No. 7, pp. 373-375, 1986.
- [3] D. Xu, L. Liu, and Z. Jiang, 'Measurement of the Dielectric Properties of Biological Substances using an Improved Open-Ended Coaxial Line Resonator Method', *IEEE Transactions on Microwave Theory and Techniques*, Vol. 35, No. 12, pp. 1424-1428, 1987.
- [4] M. A. Stuchly, and S. S. Stuchly, 'Coaxial Line Reflection Method for Measuring Dielectric Properties of Biological Substances at Radio and Microwave Frequencies – A Review', *IEEE Transactions on Instrumentation and Measurement*, Vol. 29, No. 3, pp 176-183, 1980.
- [5] T. W. Athey, M. A. Stuchly, and S. S. Stuchly, 'Measurement of Radio Frequency Permittivity of Biological Tissues with an Open-Ended Coaxial Line: Part I', *IEEE Transactions on Microwave Theory and Techniques*, Vol. 30, No. 1, pp 82-86, 1982.
- [6] M. A. Stuchly, T. W. Athey, G. M. Samaras, and G. E. Taylor, 'Measurement of Radio Frequency Permittivity of Biological Tissues with an Open-Ended Coaxial Line: Part II - Experimental Results', *IEEE Transactions on Microwave Theory and Techniques*, Vol. 30, No. 1, pp. 87-92, 1982.
- [7] D. M. Hagl, D. Popovic, S. C. Hagness, J. H. Booske, and M. Okoniewski, 'Sensing Volume of Open-Ended Coaxial Probes for Dielectric Characterization of Breast Tissue at Microwave Frequencies', *IEEE Transactions on Microwave Theory and Techniques*, Vol. 51, No. 4, pp. 1194-1206, 2003.



- [8] R. Zajíček, J. Vrba, and K. Novotný, 'Evaluation of a Reflection Method on an Open-Ended Coaxial Line and its Use in Dielectric Measurements', *Acta Polytechnica*, Vol. 46, No. 5, pp. 50-54, 2006.
- [9] R. Zajíček, L. Oppl, and J. Vrba, 'Broadband Measurement of Complex Permittivity using Reflection Method and Coaxial Probes', *Radioengineering*, Vol.17, No. 1, pp. 14-19, 2008.
- [10] J. S. Bobowski, and T. Johnson, 'Permittivity Measurements of Biological Samples by an Open-Ended Coaxial Line', *Progress in Electromagnetics Research B*, Vol. 40, pp. 159-183, 2012.
- [11] S. O. Nelson, and P. G. Bartley (Jr.), 'Open-Ended Coaxial-Line Permittivity Measurements on Pulverized Materials', *IEEE Transactions on Instrumentation and Measurement*, Vol. 47, No. 1, pp. 133-137, 1998.
- [12] CST Studio Suite, [www.3ds.com/products-services/simulia/products/cst-studio-suite](http://www.3ds.com/products-services/simulia/products/cst-studio-suite) [Last accessed 04 April 2022].
- [13] T. Weiland, 'A Discretization Method for the Solution of Maxwell's Equations for Six-Component Fields', *Electronics and Communications AEU*, Vol. 31, No. 3, pp. 116-120, 1977.
- [14] M. Clemens, and T. Weiland, 'Discrete Electromagnetism with the Finite Integration Technique', *Progress In Electromagnetics Research*, Vol. 32, pp. 65-87, 2001.
- [15] M. Douglas, and C. K. Chou, 'Enabling the Use of Broadband Tissue Equivalent Liquids for Specific Absorption Rate Measurements', *2007 IEEE International Symposium on Electromagnetic Compatibility*, pp. 1-6, Honolulu, Hawaii, 2007.
- [16] D. L. Means, and K. W. Chan, 'Evaluating Compliance with FCC Guidelines for Human Exposure to Radiofrequency Electromagnetic Fields – Additional Information for Evaluating Compliance of Mobile and Portable Devices with FCC Limits for Human Exposure to Radiofrequency Emissions', Supplement C (Edition 01-01) to FCC OET Bulletin 65 (Edition 97-01), Washington D.C., 2001.
- [17] The MathWorks, 'MATLAB 2014a', Natick, 2014.
- [18] Keysight Technologies, 'Keysight 85070E Dielectric Probe Kit 200 MHz to 50 GHz – Technical Overview', Available Online: <https://www.keysight.com/us/en/assets/7018-01196/technical-overviews/5989-0222.pdf> (Accessed on 18 Feb, 2022).
- [19] Sriparna De, 'Study on Phantom Model for SAR Measurement', ME Thesis, Electronics and Telecommunication Engineering Department, Jadavpur University, Kolkata, India, 2016.

# Chapter 6

## Electromagnetic Propagation Loss due to Plants and Initial Responses under Long Duration Cell Phone Irradiation

---

### **Part I: Electromagnetic Propagation Loss due to Plants – A Preliminary Investigation**

#### **6.1 Introduction**

Plants are often considered to be one of the natural shielding materials for electromagnetic wave propagation and a concern for wireless communication coverage failure [1-5]. It is so because most plants, fruits and flower tissues possess considerably high dielectric properties ( $\epsilon_r$ ) i.e. permittivity ( $\epsilon'_r$ ) and electrical conductivity ( $\sigma$ ) / loss tangent ( $\tan \delta$ ) [6-16] – thus, they are capable of absorbing a reasonable amount of incident electromagnetic energy that impinges on them (as discussed in Chapter 4). In addition, depending on frequency of operation and length of individual plant leaf, a considerable part of the incident electromagnetic energy can also be scattered in random directions. Consequently, the likelihood of plants being affected due to electromagnetic energy absorption also needs to be investigated. Hence, it is important from both perspectives to investigate electromagnetic propagation loss / attenuation due to presence of single / multiple plants – while, electromagnetic wave propagates through them. As discussed earlier, this propagation loss / attenuation is in principal composed of two parts – electromagnetic energy absorption in plants (discussed in Chapter 4) and electromagnetic energy scattering due to leaves and other parts of plants. Thus, cumulative electromagnetic propagation loss / attenuation due to presence of plants should be investigated for analyzing overall absorption and scattering contribution. Later on, measured propagation loss / attenuation data may be correlated with potential physiological and molecular effects on plants.

## 6.2 Research Statement

In this preliminary investigation, three Chinese *Tabernaemontana divaricata* plants have been chosen (one such plant is illustrated in Fig. 6.1) to examine electromagnetic propagation loss / attenuation at 1.73 GHz, 1.75 GHz and 1.77 GHz. Two half-wave dipole antennas have been placed 1.50 m apart at transmitting and receiving sides to ensure far-field scenario – next, *Tabernaemontana divaricata* plants have been placed in between the half-wave dipole antennas one by one to measure propagation loss / attenuation due to a single plant as well as all three plants. Microwave power at the receiving antenna side has been measured with a Handheld Spectrum Analyzer (HSA) (make: Agilent Technologies, up to 13.6 GHz) – both, in absence and presence of the Chinese *Tabernaemontana divaricata* plants. Considerable and consistent drop in received power has been noted due to presence of Chinese *Tabernaemontana divaricata* plants in Line-of-Sight (LOS) propagation channel between the transmitting and receiving antennas.

## 6.3 Materials and Equipment

The following plant specimens, microwave instruments and measuring accessories have been utilized to investigate electromagnetic propagation loss / attenuation due to presence of single / multiple plants.

Three Chinese *Tabernaemontana divaricata* plants have been utilized in this investigation – please refer to Fig. 6.1 and Table 6.1 for dimensions of individual plant specimens. In addition, two half-wave dipole antennas with center frequencies around 1.75 GHz have been used as the transmitting and receiving antennas during measurement. Measured reflection coefficient ( $S_{11}$ ) data for these two antennas have been illustrated in Fig. 6.2. The reflection coefficient characteristics for the half-wave dipole antennas have been measured with Agilent Technologies E5071B ENA series Vector Network Analyzer (VNA). Microwave power at 1.73 GHz, 1.75 GHz and 1.77 GHz has been fed to the transmitting half-wave dipole antenna from a benchtop signal generator with variable power output (make: Rohde & Schwarz). One HSA (make: Agilent Technologies, up to 13.6 GHz) has been connected to the other half-wave dipole antenna via coaxial cable for measuring received power at the above mentioned frequencies. High frequency low loss coaxial cables and connectors have been used at transmitting and receiving antenna terminals. The entire investigation has been conducted inside a semi-anechoic chamber.



Fig. 6.1: A typical Chinese *Tabernaemontana divaricata* plant ( $L_1$ ,  $L_2$ ,  $S$  and  $T$  represent height of foliage, width of foliage, height of stem and height of earthen pot respectively)

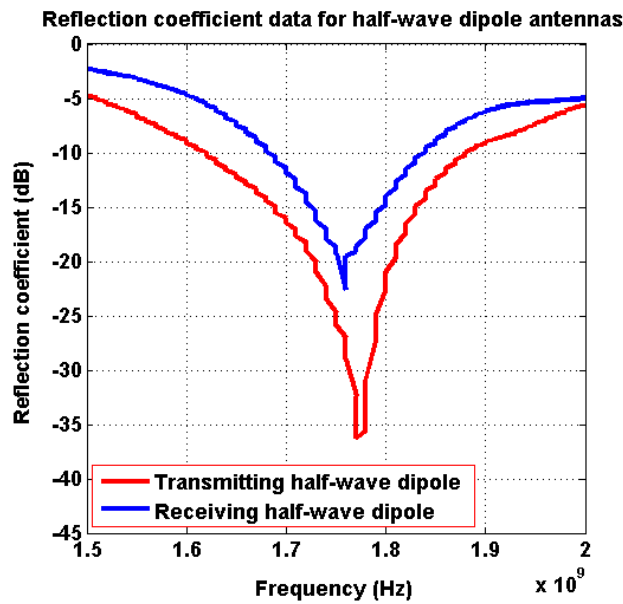


Fig. 6.2: Reflection coefficients ( $S_{11}$ ) for transmitting and receiving half-wave dipole antennas

Table 6.1 Dimensions of three *Tabernaemontana divaricata* plants (refer to Fig. 6.1)

Serial Number	$L_1$ (cm)	$L_2$ (cm)	$S^{\#}$ (cm)	$T$ (cm)
First Plant	21	32	10	15
Second Plant	19	28	10	13
Third Plant	19	30	7	14

<sup>#</sup>All stem ( $S$ ) diameters are less than 1 cm

## 6.4 Investigation Technique

At initial stage, two half-wave dipole antennas have been fabricated at center frequency 1.75 GHz i.e. at the middle of 1800 MHz uplink band (1710 MHz – 1785 MHz). This frequency band is dedicated for uplink communication from several low power devices (such as cell phones or tablets) to base station antennas. The microwave source available at Electronics and Telecommunication Engineering department, Jadavpur University can deliver 0 dBm to 25 dBm output power (make: Rohde & Schwarz) – this range matches well with power emitted from a cell phone / tablet. Next, the reflection coefficients ( $S_{11}$ ) have been measured with a VNA for both half-wave dipole antennas. At subsequent stage, one of the half-wave dipole antennas has



Fig. 6.3: (a) Experimental setup inside semi-anechoic chamber for measuring propagation loss due to presence of the plants, (b) Microwave signal generator with the transmitting half-wave dipole antenna at 1.75 GHz and (c) HSA connected with the receiving half-wave dipole antenna

been connected with a microwave power source at the transmitting side – whereas, the receiving half-wave dipole antenna has been positioned 1.50 m apart from the transmitting antenna inside a semi-anechoic chamber. One HSA (noise floor below  $-120$  dBm) has been connected with the receiving half-wave dipole antenna via low loss coaxial cable.

Next, antenna received power data have been measured with the HSA for specific combinations of operating frequency and input power level at the transmitting dipole antenna side in absence of *Tabernaemontana divaricata* plants. Next, Chinese *Tabernaemontana divaricata* plants have been placed one by one in between the transmitting and receiving half-wave dipole antennas – consequently, second dipole antenna received power levels have been recorded using the HSA. This process has been repeated at three different frequencies (1.73 GHz, 1.75 GHz and 1.77 GHz) and for six different input power levels (0 dBm to 25 dBm at intervals of 5 dBm) at the transmitting dipole antenna side. Figs. 6.3(a), (b) and (c) illustrate the practical measurement setup inside semi-anechoic chamber.

## 6.5 Results and Analyses

Fig. 6.4(a) illustrates decline in 2<sup>nd</sup> half-wave dipole antenna received power at 1.73 GHz due to propagation loss / attenuation in Chinese *Tabernaemontana divaricata* plants placed in between the transmitting and receiving antennas.

Analyses reveal that approximately 0.66 dB (averaged over six different power levels) propagation loss / attenuation has been noted at 1.73 GHz due to presence of a single *Tabernaemontana divaricata* plant in between the two half-wave dipole antennas. It is also to be noted that on an average 2.91 dB and 5.50 dB (averaged over six different power levels) cumulative propagation losses / attenuations have been observed due to respective presence of two and three *Tabernaemontana divaricata* plants in between the antennas at 1.73 GHz.

Next, operating frequency of the microwave source has been set to 1.75 GHz and above mentioned measurement technique has been repeated. This time, measured propagation loss / attenuation data have been illustrated in Fig. 6.4(b) – it illustrates relative drop in 2<sup>nd</sup> half-wave dipole antenna received power at 1.75 GHz due to presence of the Chinese *Tabernaemontana divaricata* plant specimens. The entire measurement process has been repeated for six different input power levels (0 dBm to 25 dBm at intervals of 5 dBm) at 1.75 GHz.



Based on measured data analyses, about 1.24 dB (averaged over six different input power levels) propagation loss / attenuation has been observed due to presence of a single *Tabernaemontana divaricata* plant in between the transmitting and receiving half-wave dipole antennas at 1.75 GHz; whereas, on an average 2.87 dB and 5.90 dB cumulative propagation losses have been noted due to respective presence of two and three plants at 1.75 GHz.

At the final stage, frequency of operation has been tuned to 1.77 GHz and the entire measurement procedure has been repeated again. Fig. 6.4(c) demonstrates relative drop in antenna received power and cumulative propagation loss / attenuation due to presence of chinese *Tabernaemontana divaricata* plants for six different input power levels at 1.77 GHz.

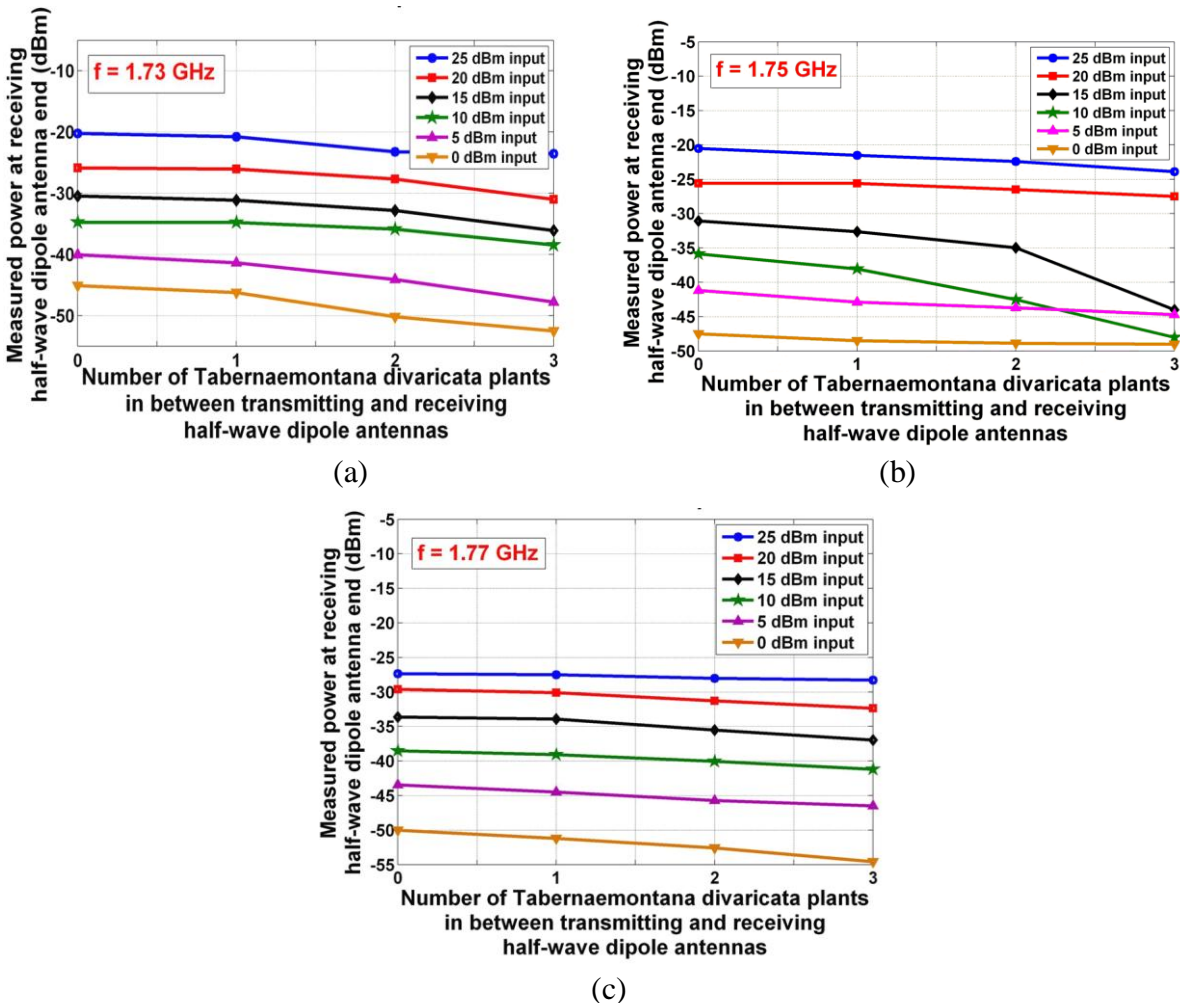


Fig. 6.4: Decline in half-wave dipole antenna received power due to propagation loss / attenuation in Chinese *Tabernaemontana divaricata* plants present in between the transmitting and receiving antennas (a) at 1.73 GHz, (b) at 1.75 GHz and (c) at 1.77 GHz

Based on result analyses, an average of 0.62 dB propagation loss has been noted due to presence of a single *Tabernaemontana divaricata* plant whereas 1.76 dB and 2.89 dB cumulative attenuation losses have been observed respectively for two and three *Tabernaemontana divaricata* plants at 1.77 GHz. Above data have been reported after analyzing results over six different input power levels at the transmitting half-wave dipole antenna.

## 6.6 Discussions

Detailed analyses of measured data demonstrate significant propagation loss / attenuation due to presence of single as well as multiple Chinese *Tabernaemontana divaricata* plant specimens. A significant part of the propagation loss is expected due to absorption in the plants because of high tissue dielectric properties ( $\epsilon_r$ ) [6-16] – whereas, scattering of electromagnetic energy should also be taken into consideration. In general, propagation loss / attenuation is high enough at 1.73 GHz (5.50 dB) and at 1.75 GHz (5.90 dB) when three chinese *Tabernaemontana divaricata* plants have been placed on LOS – however, the measured propagation loss has been noted to be reduced at 1.77 GHz possibly due to change in orientation of plants while repeating the experiment. It should be noted that the transmitting and receiving antennas have been positioned 30 cm above the ground – thus, the foliage of three plants have fallen on LOS in between the antennas. In addition, it is also to be noted that a part of the reported propagation loss / attenuation has been contributed by soil in earthen pots in addition to plant foliage – as half-wave dipole antennas posses flat beam width.

Obtained results demonstrate that three Chinese *Tabernaemontana divaricata* plants with 30 cm foliage diameter and 20 cm foliage height are capable of introducing significant propagation loss around 1.75 GHz. The cumulative foliage depth is less than a meter ( $3 \times 30$  cm) and the same has introduced almost 5 dB attenuation (on average) near 1800 MHz band. Therefore, attention should be paid to investigate physiological and molecular effects of electromagnetic irradiation on plants and crops.

## 6.7 Conclusions

Fairly significant propagation loss / attenuation has been observed in Chinese *Tabernaemontana divaricata* plant specimens. Measured propagation loss / attenuation data and dielectric properties ( $\epsilon_r$ ) of different plant tissues indicate that a significant part of the loss is possibly due



to considerable water and ion contents in leaves, flowers and stems [6-16]; an accurate dielectric properties ( $\epsilon_r$ ) measurement of *Tabernaemontana divaricata* plant leaf, flower and stem specimens along with subsequent Specific Absorption Rate (SAR) evaluation can help to quantify accurate electromagnetic energy absorption in the above mentioned plants. Thereafter, simulated SAR data can be correlated further with measured propagation loss / attenuation data in above mentioned plant structures. Furthermore, physiological and molecular effects on plants can be investigated due to short duration as well as long duration electromagnetic irradiation.

## **Part II: Initial Plant Responses under Long Duration Cell Phone Irradiation**

### **6.8 Introduction**

Electromagnetic radiations over a wide spectrum of frequencies are present in the environment – some of these radiations are natural while others are manmade / technology based [17]. In general, natural electromagnetic radiations are low enough with respect to Radio Frequency (RF) radiations utilized for technological development. All living objects including humans, animals and plants are exposed to prolonged electromagnetic radiation in open environment. Such prolonged electromagnetic irradiation might have some measurable impact on humans as well as plants – because dielectric tissue heating in living objects is an important phenomenon [18-25]. Modern wireless communication systems utilize electromagnetic radiation in multiple frequency bands. Extensive use of electromagnetic energy over wireless communication bands has reported human health implications [18-22] – thus, similar investigations i.e. electromagnetic irradiation induced responses should also be studied in plants and crops [23-30]. In this connection, it should be noted that several international and national electromagnetic exposure regulatory guidelines and Specific Absorption Rate (SAR) limits have been prescribed worldwide to minimize associated human health risks [17, 31-34] – however, no such precautionary guidelines have been prescribed yet to protect plants and crops.

Plants are continuously exposed to electromagnetic radiation at multiple frequencies from mobile tower antennas – 24 hours a day and 365 days a year. In current situation, there is no guideline to limit electromagnetic exposure on plants from shared telecom tower antennas and other radiating

elements. As a consequence, plants are often exposed to intense electromagnetic radiations throughout their lifespan. As reported in literature, electromagnetic radiation does affect plant seed germination rate, subsequent sapling growth and plant health [23-30].

This particular investigation deals with *Capsicum annuum* (commonly known as Chilli) which is cultivated all over in India. *Capsicum annuum* (Chilli pepper) seeds have been chosen because of its wide availability, low cost, faster germination and subsequent sapling growth rate in all seasons. Hundred such healthy and viable *Capsicum annuum* seeds (collected from Chillies grown in same plant) have been equally divided into two six inch diameter earthen pots with fertilized soil as illustrated in Figs. 6.5(a) and (b) respectively – i.e. fifty *Capsicum annuum* seeds have been sown in each earthen pot for germination and subsequent growth. The first earthen pot has been kept in natural low electromagnetic environment while the 2<sup>nd</sup> one has been placed next to a GSM cell phone with 10g averaged SAR value of 1.48 W/kg (measured in human head phantom model) [35-36]. Initial plant responses such as seed germination rate and subsequent sapling growth rate have been studied for both sets of *Capsicum annuum* (Chilli pepper) specimens over a span of 50 days duration. A significant reduction has been noted in number of germinated *Capsicum annuum* saplings in the earthen pot placed next to GSM cell phone compared to sham-exposed earthen pot kept in natural low electromagnetic environment.

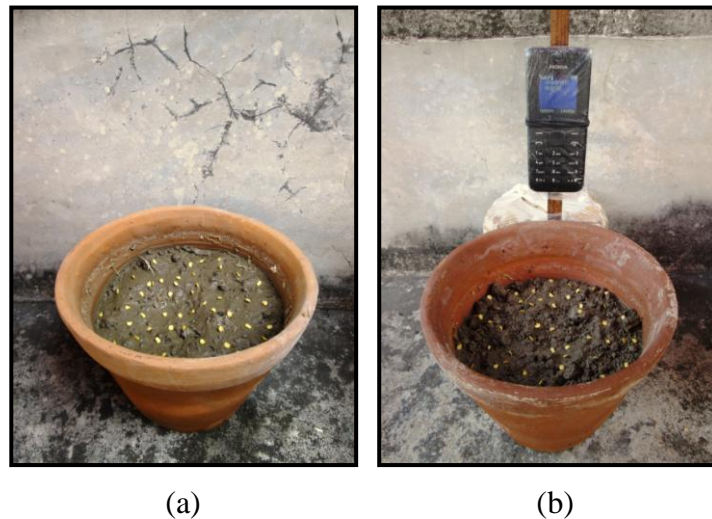


Fig. 6.5: (a) Fifty *Capsicum annuum* seeds have been spread in the 1<sup>st</sup> earthen pot (kept in natural environment) and (b) Fifty *Capsicum annuum* seeds have been spread in the 2<sup>nd</sup> earthen pot (exposed to GSM cell phone radiation)

## 6.9 Materials, Equipment and Experimental Method

### 6.9.1 Materials and Equipment

In order to perform this investigation, hundred healthy viable *Capsicum annuum* seeds, two six inch diameter earthen pots and fertilized soil have been utilized – the earthen pots have been filled with fertilized soil. All hundred *Capsicum annuum* seeds have been collected from dried Chilli peppers that were grown in a single plant. Two identical GSM cell phones with 10g averaged SAR value 1.48 W/kg (in human head model) have been used to irradiate target *Capsicum annuum* seeds and subsequent saplings in the 2<sup>nd</sup> earthen pot [35-36]. A wooden stand has been utilized to hold one cell phone next to the 2<sup>nd</sup> earthen pot containing *Capsicum annuum* seeds / saplings. Electric power line and power adapters have been used to keep the cell phones switched on over 50 days duration. Furthermore, RF power measuring device i.e. handheld electromagnetic power meter (up to 6 GHz) and a half-wave dipole antenna designed at 1.75 GHz (center frequency) have been employed to characterize cell phone emitted frequency and exposure levels. One measuring tape and a couple of fiber scales have also been used to measure the growth of *Capsicum annuum* sapling specimens over the stipulated investigation duration.

### 6.9.2 Experimental Method

This experiment has been performed to investigate effects of electromagnetic irradiation on *Capsicum annuum* seed germination and subsequent sapling growth – as, electromagnetic radiation has been reported to be a stress factor for plants [24, 26, 28-30]. Detailed experimental protocol to investigate electromagnetic irradiation induced responses at initial stages of *Capsicum annuum* plant growth has been discussed in the following section.

At first, two six inch diameter earthen pots have been filled with fertilized soil and placed in similar natural electromagnetic environment. Next, a few dried red Chilli peppers have been chosen out of several similar specimens that were collected from a single *Capsicum annuum* plant. All seeds have been collected from those few selected Chilli peppers and compiled together. At subsequent stage, hundred healthy and viable *Capsicum annuum* seeds have equally been distributed in two earthen pots in a systematic approach as illustrated in Figs. 6.5(a) and (b). One GSM cell phone has been fixed on a thin wooden stand and placed in close vicinity of the 2<sup>nd</sup> earthen pot as depicted in Fig. 6.5(b). This particular GSM cell phone has been equipped with

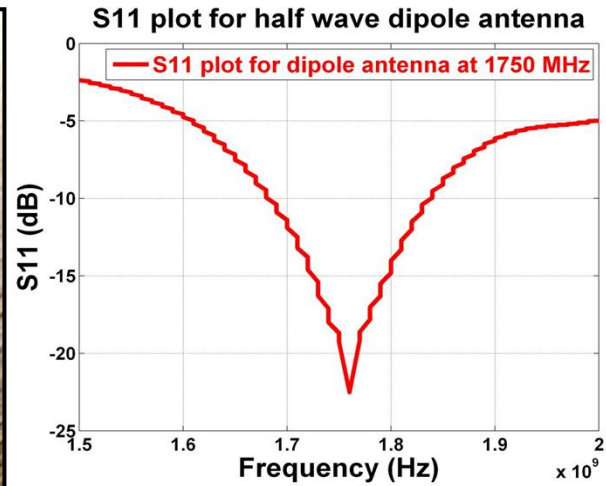
a GSM Subscriber Identity Module (SIM) having unlimited on-network call subscription – the same equipment has been used as the non-ionizing electromagnetic radiation source at GSM 1.8 GHz uplink band [37-38]. The other cell phone (kept at a far distance inside room) also contained a GSM SIM card from same service provider and has been used to receive calls initiated from the 1<sup>st</sup> cell phone. All calls have been initiated from the cell phone placed in close vicinity of 2<sup>nd</sup> earthen pot with an average collective call duration of 5 h and 41 min per day. During rest of the time, the transmitting cell phone has been kept in standby mode (switched on) close to the 2<sup>nd</sup> earthen pot. A half-wave dipole antenna has been fabricated in GSM 1.8 GHz uplink band with center frequency at 1.75 GHz – the same antenna has been employed along with a handheld power meter to compare electromagnetic power densities near the 1<sup>st</sup> (placed in natural environment) and 2<sup>nd</sup> (next to the GSM cell phone) earthen pots. Two earthen pots each containing fifty *Capsicum annuum* seeds have been kept under observation – relevant data have been noted at regular intervals. Significant physiological responses such as seed germination, subsequent sapling growth, largest and average sapling lengths, largest leaf length and wrinkled leaves etc. have been noted down over 50 days duration.

## 6.10 Antenna Received Power Measurement

As discussed above, the 1<sup>st</sup> earthen pot has been placed in natural environment with low electromagnetic field strength – whereas, the 2<sup>nd</sup> earthen pot has been kept in close vicinity of a GSM cell phone with 10g averaged SAR value of 1.48 W/kg (in human head equivalent model) [35-36]. It is important to note that GSM mobile phones transmit electromagnetic energy both in 900 MHz uplink band (890 MHz – 915 MHz) and 1800 MHz uplink band (1710 MHz – 1785 MHz). Therefore, it is obvious that *Capsicum annuum* seeds and subsequent germinated saplings in the 2<sup>nd</sup> earthen pot have been exposed to higher electromagnetic field strength compared to the sham-exposed (control) 1<sup>st</sup> earthen pot. A half-wave dipole antenna has been fabricated at 1750 MHz i.e. at the centre frequency of GSM 1800 MHz uplink band (1710 MHz – 1785 MHz) and connected with a handheld power meter for measuring antenna received power in surrounding areas of 1<sup>st</sup> and 2<sup>nd</sup> earthen pots. Fabricated half-wave dipole and its reflection coefficient ( $S_{11}$ ) characteristics have been illustrated in Figs. 6.6(a) and (b) respectively. The handheld RF power meter has been shown in Figs. 6.7(a) and (b) along with the half wave dipole antenna.



(a)



(b)

Fig. 6.6: (a) Half-wave dipole antenna at 1750 MHz with SMA to coaxial N-type adapter and (b) Measured reflection coefficient ( $S_{11}$ ) characteristics of the fabricated half-wave dipole antenna



(a)



(b)

Fig. 6.7: (a) Handheld power meter along with fabricated half-wave dipole antenna at 1750 MHz and (b) Half-wave dipole antenna received power measurement in close vicinity of the 2<sup>nd</sup> earthen pot placed next to GSM cell phone

Table 6.2 Comparison of half-wave dipole antenna received power data next to 1<sup>st</sup> earthen pot (natural low electromagnetic environment) and the 2<sup>nd</sup> earthen pot (beside GSM mobile phone)

Half-wave dipole antenna received power measurement using handheld RF power meter at around 1750 MHz	Peak Instantaneous Received RF power at around 1750 MHz (dBm)		Average saturated Received RF power at around 1750 MHz (dBm)	
	<i>Half-wave dipole placed in vertical plane</i>	<i>Half-wave dipole placed in horizontal plane</i>	<i>Half-wave dipole placed in vertical plane</i>	<i>Half-wave dipole placed in horizontal plane</i>
Near 1 <sup>st</sup> earthen pot in natural environment	-39.0	-41.0	-39.0	-41.0
Near 2 <sup>nd</sup> earthen pot during call setup mode	+1.06	-3.00	-3.00	-7.00
Near 2 <sup>nd</sup> earthen pot during ringing mode	-8.00	-19.0	-13.0	-22.0
Near 2 <sup>nd</sup> earthen pot during call ongoing mode	-16.0	-26.0	-19.0	-30.0
Near 2 <sup>nd</sup> earthen pot during standby mode	-39.0	-41.0	-39.0	-41.0

Table 6.3 Radiation exposure duration of *Capsicum annuum* seeds and subsequent saplings in the 2<sup>nd</sup> earthen pot over 50 days duration

<b>Mobile operating modes next to 2<sup>nd</sup> earthen pot</b>	<b>Time duration (min)</b>
Cell phone in standby mode (switched on)	54818
Cell phone in call ongoing mode	17046
Cell phone in ringing mode	126
Cell phone in call setup mode	10 (304 calls)
<b>Total</b>	<b>72000 (50 days)</b>

The half-wave dipole antenna received power data have been measured over entire 1800 MHz uplink band both in natural low electromagnetic environment next to the 1<sup>st</sup> earthen pot and in close vicinity of GSM cell phone next to the 2<sup>nd</sup> earthen pot. Measured power data for different

modes of GSM cell phone operation have been tabulated in Table 6.2. Antenna received power data have been measured with handheld power meter in natural environment, as well as in vicinity of GSM cell phone during call set up, ringing, call ongoing mode and standby mode.

On an average, approximately 35 dB higher electromagnetic power has been received by the half-wave dipole antenna around the 2<sup>nd</sup> earthen pot adjacent to GSM phone in call set up mode – while, compared to natural environment near the 1<sup>st</sup> earthen pot. It has been further observed that GSM mobile phone transmits less power once the call has been established – please, refer to Table 6.2. During call ongoing mode, the half-wave dipole antenna received power near the GSM cell phone (i.e. adjacent to 2<sup>nd</sup> earthen pot) has been noted to be about 20 dB higher in comparison to natural electromagnetic environment (1<sup>st</sup> earthen pot). In standby mode, GSM cell phones emit high amplitude short duration pulses; but, the power meter couldn't record those – instead, a spectrum analyzer could have been employed. As a consequence, very low power level has been detected around the cell phone (near 2<sup>nd</sup> earthen pot) in standby mode.

As reported in Table 6.2, half-wave dipole antenna received electromagnetic power adjacent to the 2<sup>nd</sup> earthen pot is quite significant in call ongoing mode while compared to natural electromagnetic scenario next to the 1<sup>st</sup> earthen pot. It should also be noted that the GSM phone was in call ongoing mode around 5 h and 41 min per day – please refer to Table 6.3. For rest of the day i.e. around 18 hours and 16 minutes, the cell phone has been kept in standby mode while radiated power level was much less – please refer to Table 6.2 and Table 6.3. For remaining 3 minutes, the phone was either in call setup mode or in ringing mode. Hence, it is obvious that resultant electromagnetic field strength near the 2<sup>nd</sup> earthen pot was much less than the maximum permissible limits prescribed in existing Indian exposure guidelines [32]. The GSM cell phones operate at around 1750 MHz i.e. in 1800 MHz uplink band next to the 1800 MHz downlink band (1805 MHz to 1880 MHz) – thus, the physiological plant responses in this investigation can be corroborated to the potential plant responses under 1800 MHz cell tower radiation.

## **6.11 Radiation Effects on Seed Germination and Sapling Growth**

*Capsicum annuum* seed germination rate and subsequent sapling growth have been observed over duration of 50 days – both, in 1<sup>st</sup> sham-exposed earthen pot (kept in natural environment) and also in 2<sup>nd</sup> earthen pot next to the GSM mobile phone. At initial stage, reduced number of germinated *Capsicum annuum* seeds has been observed in GSM phone radiation treated 2<sup>nd</sup>

earthen pot compared to the 1<sup>st</sup> earthen pot (sham-exposed). The difference in number of germinated seeds between the two earthen pots increased to a significant level with time. However, during the last three weeks of this investigation, higher sapling growth rate and wrinkled leaves have been observed among saplings in the 2<sup>nd</sup> earthen pot next to the GSM mobile phone.

### **6.11.1 Reduced Seed Germination**

At initial stage, hundred healthy viable *Capsicum annuum* seeds have equally been distributed between the 1<sup>st</sup> (kept in natural environment) and 2<sup>nd</sup> (treated under cell phone radiation) earthen pots – as illustrated in Figs. 6.5(a) and (b). Thereafter, *Capsicum annuum* seed germination rate and subsequent sapling growth have been observed at regular intervals to note possible variations due to electromagnetic irradiation.

A difference has been noted in germinated *Capsicum annuum* seed count on the 6<sup>th</sup> day of observation. Six *Capsicum annuum* seeds have germinated in the 1<sup>st</sup> sham-exposed earthen pot whereas four *Capsicum annuum* seeds have germinated in the 2<sup>nd</sup> earthen pot next to GSM cell phone. Detailed data have been tabulated in Table 6.4. The reduction in number of germinated *Capsicum annuum* saplings under cell phone irradiation has become significant with time – as visible in Table 6.4, Figs. 6.8(a) and (b) respectively.

On 22<sup>nd</sup> day of observation, forty five *Capsicum annuum* saplings have been visible in the 1<sup>st</sup> earthen pot (sham exposed / control) – while, only twenty seven saplings have been observed in the 2<sup>nd</sup> earthen pot in close vicinity of the GSM mobile phone. Pictorial descriptions have been illustrated in Figs. 6.9(a) and (b) along with data in Table 6.4. At final stage, thirty eight *Capsicum annuum* saplings have been visible in 1<sup>st</sup> sham-exposed earthen pot – in contrast, only twenty five *Capsicum annuum* saplings have been observed in the 2<sup>nd</sup> earthen pot (next to the GSM mobile phone). Pictures taken on 50<sup>th</sup> day have been depicted in Figs. 6.10(a) and (b) respectively. Data demonstrate that 76% *Capsicum annuum* seeds survived to produce subsequent saplings in sham-exposed 1<sup>st</sup> earthen pot – whereas, only 50% seeds survived to produce saplings in radiation treated 2<sup>nd</sup> earthen pot next to the GSM mobile phone.



Table 6.4 Germinated sapling count and mean sapling height over 50 days

Day	Number of germinated seedlings		Mean sapling height (cm)	
	<i>In 1<sup>st</sup> earthen pot (sham-exposed)</i>	<i>In 2<sup>nd</sup> earthen pot (next to the mobile phone)</i>	<i>In 1<sup>st</sup> earthen pot (sham-exposed)</i>	<i>In 2<sup>nd</sup> earthen pot (next to the mobile phone)</i>
1	0	0	0.00	0.00
6	6	4	0.10	0.40
10	19	6	-	-
15	36	22	4.00	3.50
22	45	27	5.25	5.50
36	39	27	7.50	9.00
42	38	27	8.50	9.50
50	38	25	11.7	14.0



(a)

(b)

Fig. 6.8: Observation on 15<sup>th</sup> day (a) thirty six saplings in the 1<sup>st</sup> earthen pot kept in natural environment and (b) twenty two saplings in the 2<sup>nd</sup> earthen pot next to GSM mobile phone



(a)

(b)

Fig. 6.9: Observation on 22<sup>nd</sup> day (a) forty five saplings in the 1<sup>st</sup> earthen pot kept in natural environment and (b) twenty seven saplings in the 2<sup>nd</sup> earthen pot next to GSM mobile phone



(a)

(b)

Fig. 6.10: Observation on 50<sup>th</sup> day (a) thirty eight saplings in the 1<sup>st</sup> earthen pot kept in natural environment and (b) twenty five saplings in the 2<sup>nd</sup> earthen pot next to GSM mobile phone

### 6.11.2 Increased Sapling Height and Leaf Length

Reduction in seed germination and subsequent sapling counts is not the only observation while *Capsicum annuum* specimens have been exposed under mobile phone radiation. In addition, increased *Capsicum annuum* sapling height and larger leaves have also been seen among saplings in the 2<sup>nd</sup> earthen pot following GSM mobile phone irradiation (while compared to the 1<sup>st</sup> earthen pot) – exception on 15<sup>th</sup> day of observation. Supportive statistical data have been presented in Table 6.4. Data presented in Table 6.5 illustrate that the largest sapling length is much higher in the 2<sup>nd</sup> earthen pot (treated with GSM mobile phone radiation) while compared to the sham-exposed pot. In addition, the largest leaf length among electromagnetic irradiation treated saplings in the 2<sup>nd</sup> earthen pot is consistently high compared to the 1<sup>st</sup> earthen – please refer to Table 6.5.

### 6.11.3 Wrinkled Top Leaves

Few wrinkled top leaves have been observed among saplings in the 2<sup>nd</sup> earthen pot treated under GSM mobile phone radiation (after 35 days of observation). In contrary, no such wrinkled leaves have been seen among the sham-exposed saplings in the 1<sup>st</sup> earthen pot – rather, glowing healthy leaves have been observed. Please, refer to Figs. 6.11(a) and (b) for pictorial illustrations. This particular observations raise legitimate question regarding potential effects of electromagnetic radiation on plants.

Table 6.5 Comparison of largest sapling height and largest leaf length between the 1<sup>st</sup> and 2<sup>nd</sup> earthen pots

Day	Largest sapling height (cm)		Largest leaf length (cm)	
	<i>Among saplings in untreated reference 1<sup>st</sup> earthen pot</i>	<i>Among saplings in GSM mobile phone radiation treated 2<sup>nd</sup> earthen pot</i>	<i>Among saplings in untreated reference 1<sup>st</sup> earthen pot</i>	<i>Among saplings in GSM mobile phone radiation treated 2<sup>nd</sup> earthen pot</i>
42	13.00	14.00	5.00	6.50
50	14.50	20.00	5.80	8.20

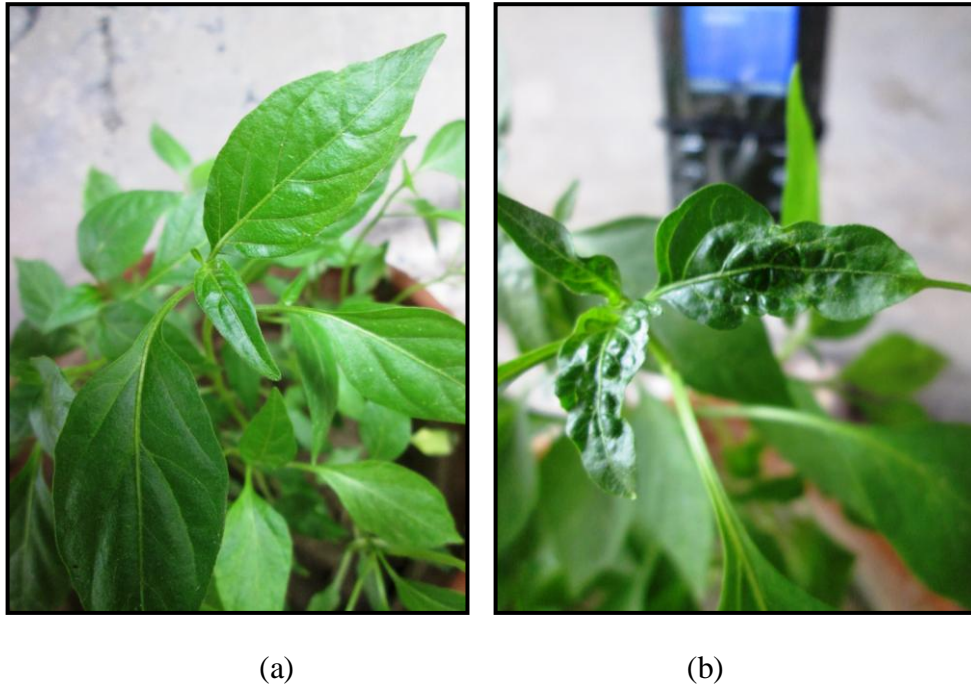


Fig. 6.11: Observation on 50<sup>th</sup> day (a) healthy glowing leaves in the 1<sup>st</sup> earthen pot kept in natural environment and (b) wrinkled leaves in the 2<sup>nd</sup> earthen pot next to GSM mobile phone

## 6.12 Discussions and Conclusions

The outcome of this investigation clearly indicates that GSM mobile phone radiation causes significant reduction in *Capsicum annuum* seed germination. It is also important to note that number of *Capsicum annuum* saplings is consistently less in the 2<sup>nd</sup> earthen pot (mobile phone radiation treated) while compared to the other sham-exposed earthen pot – please refer to Figs. 6.8 to 6.10. GSM mobile phones transmit in uplink bands that are adjacent to corresponding downlink bands – as a consequence, effects would be quite similar even under cell tower radiation. It is also evident that GSM mobile phone radiation stimulates growth of *Capsicum annuum* saplings. Thus, further investigations should be carried out at physiological and molecular levels to explore potential correlation related to electromagnetic irradiation evoked growth stimulation in plants. Wrinkled top leaves among mobile phone radiation treated saplings (in 2<sup>nd</sup> earthen pot) indicate possibly towards dielectric tissue heating – else, electromagnetic radiation is perceived by plants as a stress factor [24, 26, 28]. SAR simulation can be performed for the *Capsicum annuum* saplings to investigate dielectric tissue heating (as reported earlier in Chapter 4). The stress conditions can further be investigated at physiological and molecular



levels [24, 26, 28]. Please note that no pest infection has been observed among saplings in the 2<sup>nd</sup> earthen pot that can cause wrinkled leaves.

It is important to note that minimum electromagnetic power density required for establishing mobile communication is much less than the respective prescribed limits in international and national electromagnetic exposure regulatory guidelines [17, 31-34]. Until electromagnetic irradiation induced plant responses at physiological and molecular levels are completely known, more number of mobile towers should be installed with each antenna emitting minimal power. In addition, sharing of mobile towers among several service providers should be restricted to further bring down the cumulative electromagnetic field strength. These initiatives can make significant contributions to protect plants and humans from potential effects of electromagnetic radiation hazards.

## References

- [1] M. O. Al-Nuaimi, and A. M. Hammoudeh, 'Measurements and Predictions of Attenuation and Scatter of Microwave Signals by Trees', *IEE Proceedings - Microwaves, Antennas and Propagation*, Vol. 141, No. 2, pp. 70-76, 1994.
- [2] Y. H. Lee, and Y. S. Meng, 'VHF and UHF Propagation through a Coconut Plantation', *International Symposium on Antennas and Propagation (ISAP) 2006*, pp. 1-4, Singapore, November, 2006.
- [3] D. L. Ndzi, L. M. Kamarudin, E. A. A. Mohammad, A. Zakaria, R. B. Ahmad, M. M. A. Fareq, A. Y. M. Shakaff, and M. N. Jafaar, 'Vegetation Attenuation Measurements and Modeling in Plantations for Wireless Sensor Network Planning', *Progress in Electromagnetics Research B*, Vol. 36, pp. 283-301, 2012.
- [4] F. Ali, and S. Ray, 'Study of EM Wave Absorption and Shielding Characteristics for a Bonsai Tree for GSM-900 Band', *Progress in Electromagnetics Research C*, Vol. 49, pp. 149-157, 2014.
- [5] F. Ali, S. B. Belamgi, and S. Ray, 'A Study of Specific Absorption Rate and Shielding Effectiveness for Money Plant at 2.4 GHz', *Microwave Review*, Vol. 21, No. 2, pp. 02-06, 2015.
- [6] S. O. Nelson, 'Microwave Dielectric Properties of Fresh Fruits and Vegetables', *Transactions of the ASAE*, Vol. 23, No. 5, pp. 1314-1317, 1980.

- [7] S. O. Nelson, 'Dielectric Properties of Agricultural Products – Measurements and Applications', *IEEE transactions on Electrical Insulation*, Vol. 26, No. 5, pp.845-869, 1991.
- [8] S. O. Nelson, 'Measurement and Applications of Dielectric Properties of Agricultural Products', *IEEE Transactions on Instrumentation and Measurement*, Vol. 41, No. 1, pp. 116-122, 1992.
- [9] W. Kuang, and S. O. Nelson, 'Dielectric Relaxation Characteristics of Fresh Fruits and Vegetables from 3 to 20 GHz', *Journal of Microwave Power and Electromagnetic Energy*, Vol. 32, No. 2, pp. 114-122, 1997.
- [10] S. O. Nelson, 'Measuring Dielectric Properties of Fresh Fruits and Vegetables', *IEEE Antennas and Propagation Society International Symposium. Digest. Held in conjunction with: USNC/CNC/URSI North American Radio Sci. Meeting (Cat. No. 03CH37450)*, Vol. 4, pp. 46-49, June, 2003.
- [11] O. Sipahioglu, and S. A. Barringer, 'Dielectric Properties of Vegetables and Fruits as a Function of Temperature, Ash, and Moisture Content', *Journal of Food Science*, Vol. 68, No. 1, pp. 234-239, 2003.
- [12] S. O. Nelson, 'Dielectric Spectroscopy of Fresh Fruits and Vegetables', *2005 IEEE Instrumentation and Measurement Technology Conference (IMTC)*, pp. 360-364, Ottawa, Canada, May, 2005.
- [13] S. O. Nelson, 'Agricultural Applications of Dielectric Measurements', *IEEE Transactions on Dielectrics and Electrical Insulation*, Vol. 13, No. 4, pp. 688-702, 2006.
- [14] W. C. Guo, S. O. Nelson, S. Trabelsi, and S. J. Kays, '10–1800-MHz Dielectric Properties of Fresh Apples during Storage', *Journal of Food Engineering*, Vol. 83, No. 4, pp. 562-569, 2007.
- [15] S. O. Nelson, and S. Trabelsi, 'Dielectric Spectroscopy Measurements on Fruit, Meat, and Grain', *Transactions of the ASABE*, Vol. 51, No. 5, pp. 1829-1834, 2008.
- [16] S. O. Nelson, 'Dielectric Properties of Agricultural Products and Some Applications', *Research in Agricultural Engineering*, Vol. 54, No. 2, pp. 104-112, 2008.
- [17] International Commission on Non-Ionizing Radiation Protection (ICNIRP), 'Guidelines for Limiting Exposure to Electromagnetic Fields (100 kHz to 300 GHz)', *Health Physics*, Vol. 118, No. 5, pp. 483-524, 2020.

- [18] J. C. Lin, 'Safety Standards for Human Exposure to Radio Frequency Radiation and Their Biological Rationale', *IEEE Microwave Magazine*, Vol.4, No.4, pp. 22-26, December, 2003.
- [19] C. Buccella, V. D. Santis, and M. Feliziani, 'Prediction of Temperature Increase in Human Eyes Due to RF Sources', *IEEE Transactions on Electromagnetic Compatibility*, Vol. 49, No. 4, pp. 825-833, November, 2007.
- [20] J. C. Lin, 'Risk of Human Exposure to Cellular Mobile Communication Radiation', *IEEE Microwave Magazine*, Vol. 2, No. 2, pp. 36-40, June, 2001.
- [21] T. Samaras, A. Christ, A. Klingenbock, and N. Kuster, 'Worst Case Temperature Rise in a One-Dimensional Tissue Model Exposed to Radiofrequency Radiation', *IEEE Transactions on Biomedical Engineering*, Vol. 54, No. 3, pp. 492-496, March, 2007.
- [22] L. S. Xu, M. Q. H. Meng, and C. Hu, 'Effects of Dielectric Values of Human Body on Specific Absorption Rate following 430, 800, and 1200 MHz RF Exposure to Ingestible Wireless Device', *IEEE Transactions on Information Technology in Biomedicine*, Vol.14, No.1, pp.52-59, January, 2010.
- [23] M. Tkalec, K. Malarić, and B. Pevalek-Kozlina, 'Influence of 400, 900, and 1900 MHz Electromagnetic Fields on *Lemna minor* Growth and Peroxidase Activity', *Bioelectromagnetics*, Vol. 26, No. 3, pp. 185-193, April, 2005.
- [24] D. Roux, A. Vian, S. Girard, P. Bonnet, F. Paladian, E. Davies, and G. Ledoigt, 'High Frequency (900MHz) Low Amplitude (5V m<sup>-1</sup>) Electromagnetic Field: A Genuine Environmental Stimulus that Affects Transcription, Translation, Calcium and Energy Charge in Tomato', *Planta*, Vol. 227, No. 4, pp. 883-891, 2008.
- [25] M. Ursache, G. Mindru, D. E. Creangă, F. M. Tufescu, and C. Goiceanu, 'The Effects of High Frequency Electromagnetic Waves on the Vegetal Organisms', *Romanian Journal of Physics*, Vol. 54, No. 1-2, pp. 133-145, 2009.
- [26] D. Roux, A. Vian, S. Girard, P. Bonnet, F. Paladian, E. Davies, and G. Ledoigt, 'Electromagnetic Fields (900 MHz) Evoke Consistent Molecular Responses in Tomato Plants', *Physiologia Plantarum*, Vol. 128, No. 2, pp. 283-288, 2006.
- [27] A. Scialabba, and C. Tamburello, 'Microwave Effects on Germination and Growth of Radish (*Raphanus sativus* L.) Seedlings', *Acta Botanica Gallica*, Vol. 149, No. 2, pp. 113-123, 2002.

- [28] A. Vian, D. Roux, S. Girard, P. Bonnet, F. Paladian, E. Davies, and G. Ledoigt, 'Microwave Irradiation Affects Gene Expression in Plants', *Plant Signaling & Behavior*, Vol. 1, No. 2, pp. 67-69, 2006.
- [29] A. Vian, C. Faure, S. Girard, E. Davies, F. Hallé, P. Bonnet, G. Ledoigt, and F. Paladian, 'Plants Respond to GSM-Like Radiations', *Plant Signaling & Behaviour*, Vol. 2, No. 6, pp. 522-524, 2007.
- [30] A. Vian, E. Davies, M. Gendraud, and P. Bonnet, 'Plant Responses to High Frequency Electromagnetic Fields', *BioMed Research International*, Article ID: 1830262, 2016.
- [31] R. F. Cleveland, Jr., D. M. Sylvar, and J. L. Ulcek, 'Evaluating Compliance with FCC Guidelines for Human Exposure to Radiofrequency Electromagnetic Fields', FCC OET Bulletin, Vol. 65, Edition 97-01, Washington D.C., 1997.
- [32] Department of Telecommunications (DoT), 'A Journey for EMF', 2012, Available Online: [www.dot.gov.in/journey-emf](http://www.dot.gov.in/journey-emf) [Last accessed 03 April 2022].
- [33] Swiss Agency for the Environment, Forests and Landscape (SAEFL), 'Electrosmog in the Environment', pp. 1-56, Switzerland, 2005.
- [34] Ministry of Health of the Russian Federation, 'SanPiN 2.1.8/2.2.4.1190-03: Arrangement and Operation of Land Mobile Radiocommunication Facilities – Hygienic Requirements', pp. 1-17, Russia, 2003.
- [35] Nokia, 'Nokia 105 User Guide', Available Online: [www.download.fdsncom.nokia.com/supportFiles/phones/files/pdf\\_guides/devices/105/Nokia\\_105\\_UG\\_en\\_IN.pdf](http://www.download.fdsncom.nokia.com/supportFiles/phones/files/pdf_guides/devices/105/Nokia_105_UG_en_IN.pdf) [Last accessed Dec 2015].
- [36] S21, 'SAR Values', Available Online: [www.s21.com/sar.php](http://www.s21.com/sar.php) [Last accessed 30 Jun 2022].
- [37] Telecom Regulatory Authority of India, 'Consultation Paper on Valuation and Reserve Price of Spectrum', 2013, Available Online: [www.trai.gov.in/WriteReaddata/ConsultationPaper/Document/Consultation%20paper%2023.07.2013\\_Final.pdf](http://www.trai.gov.in/WriteReaddata/ConsultationPaper/Document/Consultation%20paper%2023.07.2013_Final.pdf) [Last accessed Dec 2015].
- [38] Telecom Regulatory Authority of India, 'Consultation Paper on Auction of Spectrum', New Delhi, March, 2012, Available Online: [www.trai.gov.in/WriteReaddata/ConsultationPaper/Document/consultation%20paper%20spectrum%20of%20auction.pdf](http://www.trai.gov.in/WriteReaddata/ConsultationPaper/Document/consultation%20paper%20spectrum%20of%20auction.pdf) [Last accessed Dec 2015].



# Chapter 7

## Periodic and Controlled Electromagnetic Irradiation Evoked Physiological and Molecular Responses in Plants

---

### 7.1 Introduction

The expanding use of non-ionizing electromagnetic radiation over a large number of frequency bands revolutionized the modern wireless telecommunication systems. Be it high speed data transmission or clear voice transmission over wireless media, broadcast of microwave energy over multiple frequency bands is the only mode available. However, the increased use of wireless technology devices is reported to have slow but measurable impact on wide range of biological systems [1-15]. Different biological tissues in humans and plants possess reasonably high dielectric properties ( $\epsilon_r$ ) as reported in several studies [16-24]. In this context, measured broadband dielectric properties ( $\epsilon_r$ ) of several plant tissues have also been reported in Chapter 3. Humans, plants and common crops absorb quite high amount of electromagnetic energy at multiple radio frequency bands simultaneously [25-39] – electromagnetic energy absorption rates have been assessed for a number of realistic fruit and plant models in Chapter 4. Electromagnetic energy absorption rate in biological tissue is defined in terms of ‘Specific Absorption Rate (SAR)’ which is the rate of electromagnetic energy absorption per unit mass of biological tissue while microwave radiation impinges on it. Although SAR analyses in different human phantom models have been performed over last three decades, available SAR data for realistic plant and fruit models are very limited [25-39] – hence, SAR estimations for a number of practical fruit and plant models have been discussed in Chapter 4. In fact, in the BioInitiative report 2012, most of it was focused on investigating biological effects of electromagnetic radiation on mammals (humans and animals) compared to plants [40]. However, several reports suggested that living organisms do not respond biologically in a different way with respect to the sham-exposed (control) samples, while exposed to non-ionizing microwave radiation [41-48]. This could be primarily due to lack of controlled and consistent electromagnetic stimulating environment. Use

of mobile phone devices or transverse electromagnetic cells couldn't simulate a controlled electromagnetic stimulation in laboratory conditions and therefore it remained impossible to address the effects on target host response. Moreover, these devices emitted microwave energy with fixed direction of propagation and polarization; consequently living objects were irradiated from one direction with fixed polarization. In contrast, electromagnetic exposure inside a reverberation chamber is known to recreate absolutely controlled stimulation with electromagnetic irradiation on living objects from several directions with different polarization. Roux et al. and Vian et al. pioneered the use of Mode Stirred Reverberation Chamber (MSRC) to comprehensively study the effects of electromagnetic irradiation on whole plant and also demonstrated detailed utilities of MSRC functionalities in bio-electromagnetic experiments [7, 13-15, 49-51].

Being immobile with high dielectric properties ( $\epsilon_r$ ), plants are more susceptible to electromagnetic irradiation compared to humans or animals. Therefore, an effect of minor environmental variations (including electromagnetic irradiation) should fairly be measurable in case of plants over animals or humans. Humans and animals absorb and release substances through interior tubes with minimal surface to volume ratio; whereas plants maximize the surface to volume ratio for absorbing more water, minerals through roots, gases and light through leaves – allowing them to have more interactions with electromagnetic energy over broader frequency spectrum [14]. In spite of such advantages, use of plant as a model to study the interaction with non-ionizing electromagnetic energy along with consequent effects remained quite limited [2, 7-8, 13-15, 52-53].

Previous studies indicated significant physiological or morphological changes in plants due to electromagnetic irradiation of duration up to 13 weeks [54]. Some studies endorsed effects of long duration but uncontrolled electromagnetic exposure on seed germination rate and chlorophyll contents [2, 8, 11, 52-53, 55]. Significant reduction in seed germination rate was reported following four hours exposure to radiation from mobile phone at 900 MHz, 8.55  $\mu\text{W}/\text{cm}^2$  [56]; more such observations were reported for various plant seeds at different exposure setup [57-58]. Reduction in photosynthetic pigment concentrations due to electromagnetic irradiation at 1 GHz in 12-days-old maize was reported [59]; Chlorophyll A concentration dropped by 80% after 7 h of electromagnetic exposure. A significant reduction in Chlorophyll content was also observed followed by 4 h exposure in maize due to 1800 MHz,

332±10.36 mW/m<sup>2</sup> power density and SAR of 1.69±0.0×10<sup>-1</sup> W/kg [60]. Furthermore, short duration controlled electromagnetic stimulation has been previously categorized as a factor that can elicit stress – as seen in case of leaf flaming, insect bite or electrical stimulation [7, 13, 51]. Three weeks old whole tomato plants have been reported to be irradiated with 2-10 min short duration isotropic homogeneous electric field of 5 V/m at 900 MHz inside MSRC. Choice of whole tomato plant was preferred to maintain full potential for signal perception, transduction and response [7]. Relative expressions of stress-related transcripts like calmodulin-N6, calcium-dependent protein kinase (CDPK), chloroplast mRNA-binding protein (CMBP), proteinase inhibitor (PIN2) and basic leucine-zipper transcription factor (lebZIP1) were found to be upregulated due to above mentioned stimulation [7, 13, 15, 51, 61]. Similar stimulation has also triggered reduced Adenosine Triphosphate (ATP) and Adenylate Energy Charge (AEC) levels that are good markers of cell energy status [50-51]. Rammal et al. independently replicated similar experiment to investigate the effects of 10 days long continuous electromagnetic exposure at 1250 MHz, 6 V/m on proteinase inhibitor 2 (PIN2) and lebZIP1 expressions and also found to be upregulated; however, this experiment couldn't ensure strictly controlled electromagnetic environment [62]. Moreover, short duration high power (800 W/cm<sup>2</sup>) electromagnetic irradiation at 2450 MHz was able to modify the gene expression in seven-eight days old *Vigna aconitifolia* seedlings; however, due to high power density inside microwave oven, reported changes couldn't exclude the possibility of causing thermal effects of electromagnetic irradiation [63]. However, many of the above investigations were conducted at different growth stages following one time electromagnetic irradiations for few minutes to few hours. In fact, majority of such studies couldn't even ensure a controlled and reproducible electromagnetic stimulation. In contrast, the role of periodic as well as controlled electromagnetic irradiation on plants particularly with respect to possible changes in physiological and molecular responses remained undetermined. Rice, being the staple food crop in Asia, is widely cultivated in rural open fields and gets exposed to uninterrupted mobile tower radiations throughout the lifespan. Therefore, it was hypothesized that controlled and periodic electromagnetic irradiation could alter seed germination rate, photosynthetic pigment concentrations and selected stress-sensor gene expressions in rice (*Oryza sativa*).

Rice is a model crop with smallest genome size (389 Mb) and detailed genomic information is available [64-65]. Rice is also a synteny crop with other major cereals like wheat and maize; thus

any information generated in this study can be easily corroborated with those crops. To this end, the present study aimed at investigating long term periodic and controlled 1837.50 MHz, 2.75 mW/m<sup>2</sup> electromagnetic irradiation mediated physiological and molecular responses in two photoperiod insensitive rice variants *Satabdi* and *Swarnaprabha* at different stages starting from germination to middle of vegetative growth, inside a simple reverberation chamber.

It should be noted that present investigation has been performed at 1837.50 MHz, 2.75 mW/m<sup>2</sup> treatment level and this exposure level is far below the standards as prescribed by the international electromagnetic regulations [66-67]. Moreover, the same is somewhat different from most of the previously reported electromagnetic stimulation levels [7, 13, 50-51, 55, 68-75]. All together, this investigation has a direct link with the human food habits, farmers and agricultural economy of several countries.

## 7.2 Electromagnetic Reverberation Chamber

### 7.2.1 A Brief Theoretical Description

Reverberation chamber is an electrically large cavity made of conducting walls through which electromagnetic waves cannot penetrate resulting in high quality factor and effective shielding [76]. Unlike anechoic chamber, electromagnetic signal generated inside reverberation chamber reflects back and forth multiple times and simulates multipath effect similar to real time scenario; as a consequence, an object inside reverberation chamber is expected to be irradiated with electromagnetic waves from different directions along with dissimilar polarizations. This measurement facility was first conceptualized by H.A. Mendes way back in 1968 [76]. At initial stage i.e. during installation, a mode stirred reverberation chamber must be analyzed, tested and calibrated before actual deployment. A rectangular reverberation chamber can be analyzed using fundamentals of rectangular cavity model – a well researched classical area of electromagnetic theory. It is well established that a hollow metallic rectangular cavity is resonant when its dimensions (a, b and c) satisfy the following relations prescribed in Eqs. (7.1) to (7.3) [77-79]:

$$k_{mnp}^2 = (m\pi/a)^2 + (n\pi/b)^2 + (p\pi/c)^2 \quad (7.1)$$

where,  $k = 2\pi/\lambda$

$\lambda$  = wavelength

$m, n, p$  = integer numbers that represent one half

wavelength variation along each of the three dimensions

$$k_{mnp}^2 = k_x^2 + k_y^2 + k_z^2 \quad (7.2)$$

where,  $k_x = (m\pi/a)$ ,  $k_y = (n\pi/b)$ ,  $k_z = (p\pi/c)$

$$f_{mnp} = \frac{1}{2\sqrt{\mu\varepsilon}} \sqrt{\left(\frac{m}{a}\right)^2 + \left(\frac{n}{b}\right)^2 + \left(\frac{p}{c}\right)^2} \quad (7.3)$$

where,  $\mu$  = absolute permeability of medium inside cavity

$\varepsilon$  = absolute permittivity of medium inside cavity

In this connection, the lowest usable frequency is an important parameter for a reverberation chamber. The lowest usable frequency is considered to be the frequency from and above which a reverberation chamber can be operated in an appropriate manner. In literature, different estimations are available for deciding the lowest usable frequency of a reverberation chamber [80-81]. In practical scenario, the lowest usable frequency is much higher than the cutoff frequency of fundamental mode inside rectangular reverberation chamber – at this particular frequency 60 to 100 modes are present above cutoff inside reverberation chamber as well as at least 1.5 modes / MHz [80-81].

Next, the number of modes present inside the rectangular cavity is estimated using the following methods [78-79]. First one is mode counting i.e. counting repeated solutions of Eq. (7.1) for both TE and TM modes; results in total number of modes present with eigenvalues less than or equal to  $k$  (a practical limit for the propagation of modes). Second method is by estimation using Weyl's formula valid for cavities of general shape – as illustrated in Eq. (7.4) [78-79].

$$N = \frac{8\pi}{3} (a \times b \times c) \frac{f^3}{v^3} \quad (7.4)$$

where,  $N$  = number of modes

$f$  = frequency in Hz

$v$  = speed of electromagnetic wave in cavity medium

The final estimation is an extension to Weyl's formula with specific reference to rectangular cavities as prescribed in Eq. (7.5) [78-79].

$$N = \frac{8\pi}{3} (a \times b \times c) \frac{f^3}{v^3} - (a + b + c) + \frac{1}{2} \quad (7.5)$$

Once total number of modes calculation is completed – next, the Quality Factor (Q factor) of the reverberation chamber needs to be evaluated at the frequency of interest. Q factor is defined as the ability of a reverberation chamber to store electromagnetic energy. In general, unloaded reverberation chamber possesses very high Q factor due to low losses through metallic walls (i.e. very high conductivity of the walls). High unloaded Q factor of reverberation chamber results in strong shielding effectiveness and consequent high electric field strength inside for a specified input power fed to radiating antenna. It is known that the walls of reverberation chamber are not made of Perfect Electric Conductor (PEC) but with metallic sheet (for example, Aluminum) with finite high conductivity – as a consequence, ohmic loss takes place. Thus, the unloaded Q factor accounts for the ohmic losses in the actual metallic walls; however, in reverberation chambers, the medium is air in general and thus, dielectric losses need not to be considered in unloaded Q factor. To calculate unloaded quality factor of any rectangular parallelepiped reverberation chamber, different TE and TM modes near to the desired frequency of operation are identified – next, the individual unloaded quality factors for all those TE and TM modes are calculated using the standard formulae given by R.F. Harrington [77]. Finally, the composite unloaded Q factor of the reverberation chamber is calculated by taking average of individual Q factors for all possible TE and TM modes. This composite Q factor of the unloaded rectangular parallelepiped reverberation chamber can also be well estimated with a simplified formula – as given in Eq. (7.6) [82].

$$Q = \frac{3V}{2\mu_r \delta_s A} \frac{1}{\left[1 + \frac{3\lambda}{16} \left(\frac{1}{a} + \frac{1}{b} + \frac{1}{c}\right)\right]} \quad (7.6)$$

where,  $V$  = volume of chamber

$A$  = inner surface area of chamber

$$\text{Skin depth of metal } (\delta_s) = \frac{1}{\sqrt{\pi f \mu \sigma}}$$

However, the loaded Q factor significantly reduces due to additional loss factors; Hill et al. defined some different loss factors that crucially affect the overall loaded Q factor of the

reverberation chamber – those take into account losses due to aperture leakage, losses due to absorption in any loading object, antenna loss factor and losses due to absorption in water vapor (> 18 GHz) in addition to the losses through walls (considered in unloaded Q factor) [83]. Different mode stirring techniques are employed to establish statistically uniform and isotropic field distribution over a period of time at each and every point in the working volume of the reverberation chamber. However, Statistical uniformity of field can't be maintained near metallic walls, where boundary conditions must be satisfied – thus, those regions fall outside the working volume of the mode stirred reverberation chamber. Associated advantage is that there is no requirement of positioning the subject under test (in the working volume of reverberation chamber) whose characteristics is to be determined. The following techniques are employed to stir the modes inside the reverberation chamber – mechanical stirring, polarization stirring, platform / position stirring and frequency stirring [79].

In spite of possessing advantages like lower realization cost (compared to anechoic chamber), statistical control over direction as well as polarization of incident wave, measurement reproducibility and high quality factor, this measurement facility is yet to receive its due recognition in wide areas of electromagnetic research. Reverberation chamber has wide applications like figuring out radiated emission and electromagnetic immunity of electronic devices as well as shielding effectiveness of absorbers, calibrating radio frequency probes, characterizing antenna efficiency, dielectric heating and investigating biological effects of electromagnetic radiation. Roux et al. and Vian et al. first utilized the MSRC to investigate electromagnetic stimulation induced gene expression alterations and other molecular responses in plants [7, 13-15].

### **7.2.2 A Simple Custom-Made Reverberation Chamber**

A simple customized electromagnetic reverberation chamber (3.60 m × 1.95 m × 3.00 m) with thick Aluminum walls was built in containing two sections – rectangular parallelepiped electromagnetic irradiation zone (2.25 m × 1.95 m × 3.00 m) and electromagnetic quiet zone (1.35 m × 1.95 m × 3.00 m) for sham-exposure (control). The resonant frequency of fundamental mode inside the rectangular parallelepiped electromagnetic irradiation zone was far below 1837.50 MHz (around 20 times). In the experimental setup, the simple electromagnetic reverberation chamber (without any mechanical stirrers) could ensure a controlled and

reproducible electromagnetic field distribution inside – but was unable to produce statistically homogeneous electromagnetic environment all over the space unlike in MSRC (as demonstrated by Roux et al. and Vian et al.) [7, 13-15]. Controlled and reproducible electromagnetic power density particularly on the target rice seeds / subsequent saplings / plants was ensured by keeping position, type and input power of the transmitting antenna fixed along with preset position of the target rice seeds / subsequent saplings / plants. Metallic walls almost entirely reflect electromagnetic waves – consequently, unwanted electromagnetic signals from open space can't enter inside this simple reverberation chamber. Moreover, antenna transmitted desired electromagnetic wave reflects back and forth multiple times inside the rectangular parallelepiped irradiation zone of the reverberation chamber due to presence of metallic walls; hence, target seeds / saplings / plants (positioned at certain preselected location) were irradiated with electromagnetic waves from multiple directions – thus, this simple reverberation chamber could somewhat replicate the practical electromagnetic scenario with numerous reflecting walls. Aluminum walls of the rectangular parallelepiped electromagnetic irradiation zone possess large but finite conductivity ( $3.7 \times 10^7$  S/m). Thus, the unloaded Q factors for different TE or TM modes around 1837.50 MHz account for ohmic loss in walls inside the rectangular parallelepiped electromagnetic irradiation zone [77]. The calculated average unloaded Q factor at 1837.50 MHz (averaged over different combinations of directions of propagation, TE and TM modes) was found to be around 3,00,000 – calculated unloaded Q factor matches well with the simplified Q factor estimation for electromagnetic reverberation chamber [82]. However, the loaded Q factor reduced significantly due to additional dielectric losses in rice seeds / saplings / plants and wet soil inside the earthen pot while conducting the electromagnetic irradiation experiment. The electromagnetic stimulation setup inside this simple reverberation chamber consisted of a portable microwave signal generator BPSG4 (Aaronia, Strickscheid, Germany), one customized rectangular patch antenna at 1837.50 MHz (bandwidth: 1826 MHz – 1842 MHz), one Radio Frequency (RF) cable ULC-6FT-SMSM+ (Mini-Circuits, Brooklyn, NY) having 1.47 dB loss and one laptop computer. The output power of BPSG4 was set at 15 dBm (31.6 mW) and fed to the input of ULC-6FT-SMSM+ RF cable – the same cable was connected with the patch antenna at the other end. Schematic diagram of the simple reverberation chamber and the actual electromagnetic transmitting system are illustrated in Figs. 7.1(a) and (b) respectively.



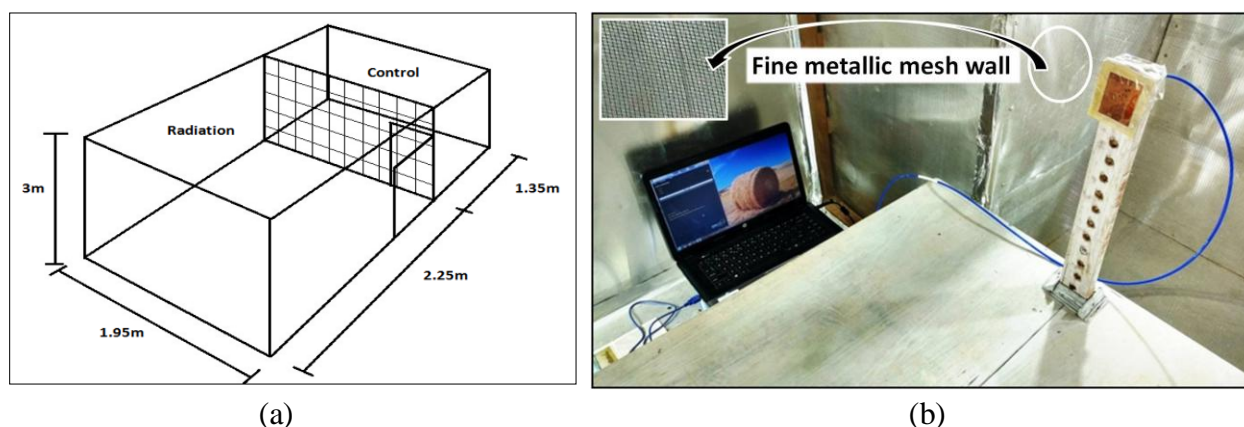


Fig. 7.1: Simple electromagnetic reverberation chamber and transmitting system (a) schematic representation of the simple reverberation chamber, (b) transmitting system inside the simple reverberation chamber

Few selected positions had been pre-identified inside the electromagnetic irradiation zone to treat the target rice seeds / saplings / plants (as per the experimental plan) with desired electromagnetic radiation at 1837.50 MHz. Calibrated rectangular patch antenna (linearly polarized with 2.41 dBi measured gain) received RF power data were measured with a handheld spectrum analyzer N9343C (Keysight Technologies, Santa Rosa, CA) at those pre-identified positions in three orthogonal axes. Subsequently, three respective orthogonal components of electric field (at a particular position) were computed from the antenna received power data in three orthogonal axes. The resultant total electric field value at a particular pre-identified position was computed using the norm of orthogonal electric field components at that point. Afterwards, typical equivalent radiated power density data was calculated using a standard technique – the resultant value was observed to be  $2.75 \text{ mW/m}^2$ . No electromagnetic signal strength was detected using the spectrum analyzer (up to 3 GHz) inside both the sections of this simple reverberation chamber while the 1837.50 MHz electromagnetic transmitting system was kept in switched off mode – thus, perfect electromagnetic shielding effectiveness was ensured inside the custom-made simple reverberation chamber. Once the RF transmitting system was switched on, measured electromagnetic power density at a pre-selected position inside the irradiation zone was noted to be  $2.75 \text{ mW/m}^2$  at 1837.50 MHz – but,  $0.07 \text{ mW/m}^2$  (40 times less) power density was observed in electromagnetic quiet zone (isolated with dense metallic mesh). Potential factors like Photosynthetically Active Radiation (PAR) and air temperature in both sections were kept

under control to avoid non-uniform secondary stress on the seeds, saplings and plants. Moreover, cool daylighting arrangements (6500 K) with  $400 \mu\text{mol m}^{-2} \text{s}^{-1}$  PAR were set up inside both sections of the simple reverberation chamber.

### **7.3 Periodic EM Irradiation Evoked Responses in *Satabdi* Rice Plant**

In this investigation, controlled and periodic (6 h per day) electromagnetic irradiation (1837.50 MHz,  $2.75 \text{ mW/m}^2$ ) evoked physiological and molecular responses have been investigated on a popular rice variety (var. *Satabdi*). At first, the effects of long term periodic (6 h per day) electromagnetic irradiation on initial seed germination rate and photosynthetic pigment profiles (chlorophyll A, chlorophyll B and carotenoids) in 32 days old *Satabdi* rice variant have been investigated. *Satabdi* is a widely cultivated early maturing (<115 days) semi-dwarf (<110 cm) high yielding variety developed from a cross between two parents and one of the parents, CR10 14, was originated from a crossing between tropical *japonica* and *indica*. Thus this long slender grain variety carries allelic set from both the *japonica* and *indica* rice. Photoperiod insensitive *Satabdi* rice was chosen as this study involved indoor environment inside simple electromagnetic reverberation chamber with additional supplementary lighting arrangement. Following it, gene expression profiles of periodically irradiated plants have been studied in 12 days as well as 32 days old *Satabdi* rice plants. Selected stress-sensitive genes with known functions had been pre-identified as established molecular markers to assess the effects of controlled electromagnetic radiation on rice with respect to sham-exposed samples. Figures 7.2(a), (b) and (c) schematically illustrate the seed germination, photosynthetic pigments profiling and gene expression studies at different growth stages under periodic electromagnetic irradiation.

#### **7.3.1 Plant culture and growth conditions**

Viable seeds of *Satabdi* rice (*Oryza sativa*) have been chosen as prototype to investigate the effect of electromagnetic irradiation on seed germination rates. Rice seedlings grown from the irradiated seeds (after germination) have been cultivated to study the effects of this prolonged periodic irradiation on photosynthetic pigment concentrations and expression profiles of selected known stress-responsive genes. The entire investigation has been conducted during the wet season at the main campus of Indian Institute of Science Education and Research Kolkata

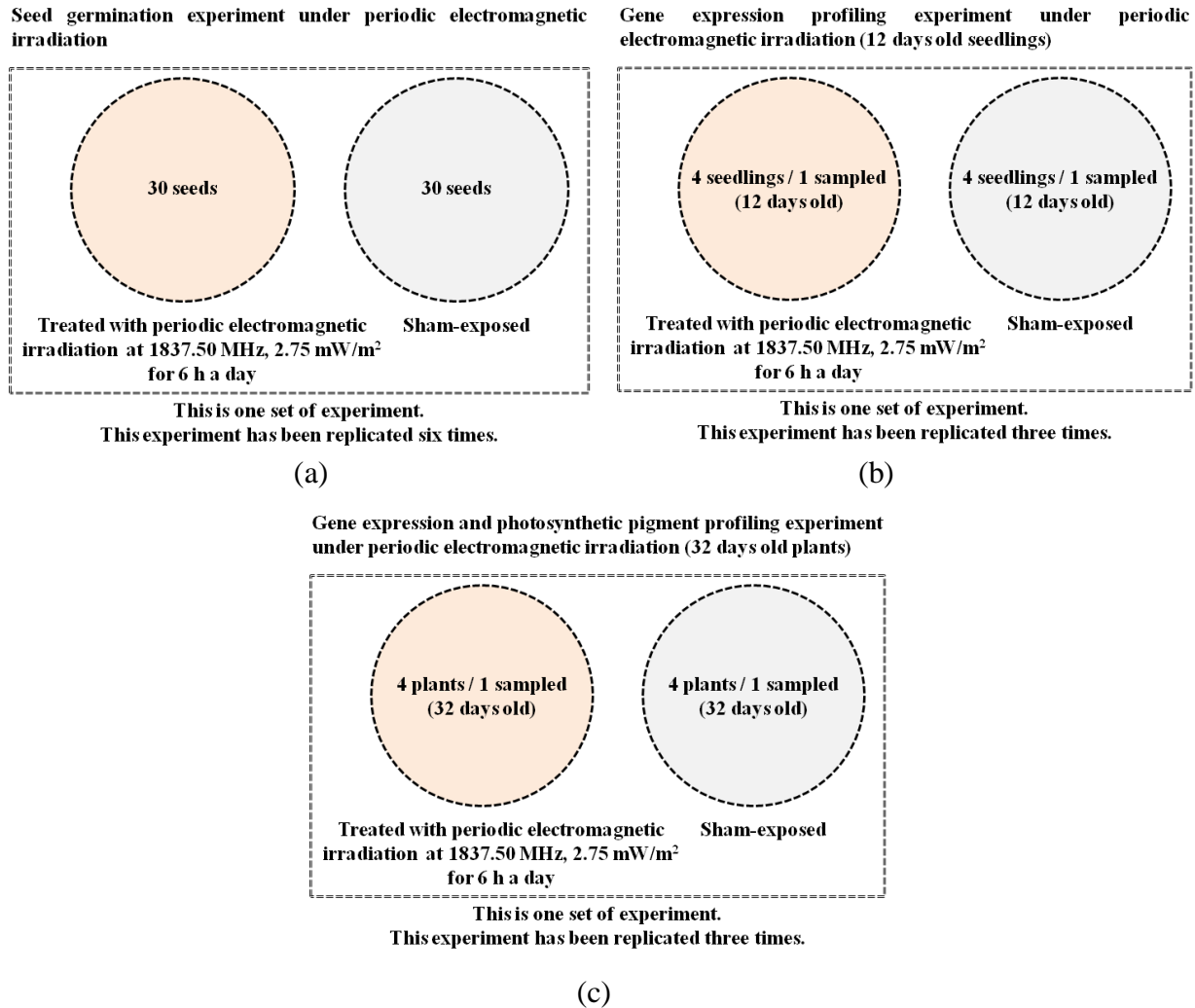


Fig. 7.2: Graphical schemes of seed germination, photosynthetic pigment profiling and gene expression profiling experiments in *Satabdi* rice under periodic electromagnetic irradiation (a) seed germination experiment, (b) gene expression profiling experiment in 12 days old *Satabdi* rice seedlings and (c) photosynthetic pigment profiling and gene expression profiling experiment in 32 days old *Satabdi* rice plants

(22.9638° N, 88.5245° E), West Bengal, India where air temperature typically varied around 32 °C during day time and 27 °C at night. To assess the effects of long term periodic electromagnetic irradiation, 30 seeds of *Satabdi* variety have been soaked in water for germination under periodic electromagnetic irradiation for 6 h per day at 1837.50 MHz, 2.75 mW/m<sup>2</sup> in the electromagnetic irradiation zone. At the same time, equal rice seeds have been germinated under identical conditions except electromagnetic irradiation in the electromagnetic

quiet zone for sham-exposure (control samples). Water has been changed on a regular basis and all seeds have been kept in dark until germination i.e. for the initial four days. Thereafter, seed germination rates have been calculated for both electromagnetic radiation treated batch along with the sham-exposed batch – this experiment is illustrated in Figure 7.2(a).

Once the germination rates have been calculated, four germinated seeds exposed to periodic electromagnetic irradiation have directly been seeded into each 25.4 cm diameter earthen pot with parallel sham-exposed samples. Calendar age of rice seedlings has been counted from the day of direct seeding in earthen pots. Thereafter, the earthen pots containing germinated seeds and subsequent seedlings have been kept inside Faraday cages made of metallic mesh in daylight with  $800 \mu\text{mol m}^{-2} \text{s}^{-1}$  to  $900 \mu\text{mol m}^{-2} \text{s}^{-1}$  PAR during Monsoon for the entire day (12 h 30 min) to retain sufficient sunlight required for uninterrupted photosynthesis process. The Faraday cages have been made of metallic mesh to isolate the electromagnetic quiet zone inside. This concept has been followed to ascertain that the target rice seedlings get exposed only to desired 1837.50 MHz electromagnetic irradiation for 6 h a day and sham-exposed seedlings grow in an absolute electromagnetic radiation free zone. During night, earthen pots containing seedlings have been transferred to respective sections of the simple electromagnetic reverberation chamber. The photoperiod of 14 h (light): 10 h (dark) has been managed with additional supplementary cool day lighting arrangement (colour temperature 6500 K with  $400 \mu\text{mol m}^{-2} \text{s}^{-1}$  PAR) during evening inside the simple electromagnetic reverberation chamber. Rice seedlings have not been transplanted to avoid unnecessary stress.

## **7.3.2 Intermediate Protocols to Inspect Plant Responses**

### **7.3.2.1 Seed Germination Rate Inspection**

The number of germinated seeds has been counted in periodic electromagnetic irradiation treated batch (out of 30 seeds) along with the sham-exposed batch after four days from initial soaking into water – respective seed germination rates have been calculated and recorded.

### **7.3.2.2 Photosynthetic Pigment Concentrations Estimation**

Youngest leaf samples have been collected from 32 days old rice plants to investigate the effects of periodic electromagnetic irradiation on chlorophyll A, chlorophyll B and carotenoids (please

refer to Fig. 7.2(c)). All leaf samples have been stored in black polythene bags immediately after collection for preventing further exposure to natural light. Fresh leaf subsample of 100 mg has been separated out from each sample and sliced into small pieces within 20 min after collection. Immediately, sliced pieces have been poured in a test tube containing 25 ml acetone (80%) and wrapped with silver paper to prevent evaporation of acetone solution and exposure to light. All test tubes have been stored at 4 °C for 48 h before further measurements.

### **7.3.2.3 Spectrophotometric Analysis of Photosynthetic Pigments**

To quantify the concentrations of chlorophyll A, chlorophyll B and carotenoids, solution containing leaves in acetone has been poured in an optically transparent cuvette to measure absorbance at 663 nm, 645 nm and 470 nm using spectrophotometer – as standardized by Lichtenthaler [84]. All absorbance data have been normalized against blank measurement using 80% acetone solution. Finally, absorbance data for each sample have been further processed to calculate chlorophyll A, chlorophyll B and carotenoids profiles (mg/g FW of leaf) [84].

### **7.3.2.4 Periodic EM Irradiation Induced Gene Expressions**

#### ***A. Plant Sample Preparation for RNA Extraction***

To investigate the effect of periodic electromagnetic irradiation on gene expression profiles, samples have been collected at two growth stages i.e. 12 days and 32 days after germination. Plant samples have been collected following 10 h from the last electromagnetic irradiation so that the transient effect of electromagnetic irradiation weakens enough. Respective top-most first leaves of target and sham-exposed rice plants have been sampled and chopped into smallest possible slices at both stages; sliced leaf samples have been kept in RNAlater solution at –20 °C till further use. Tissue samples have also been collected from the basal region of leaf sheaths from 32 days old rice plants. Schematic representations of these experiments have been illustrated in Figs. 7.2(b) and (c) respectively.

#### ***B. RNA Extraction and cDNA Synthesis***

Total RNA has been isolated from the plant leaf and basal region of stem samples kept in RNAlater solution using ‘HiPurA Plant and Fungal RNA Miniprep Purification Kit’ (Himedia, Mumbai, India) and further treated with RNase free DNase I. Next, ‘Super Reverse Transcriptase

(MuLV) Kit' (BioBharati, Kolkata, India) has been used for immediate cDNA synthesis according to manufacturer's instructions. Finally, obtained cDNA has been stored at  $-20^{\circ}\text{C}$  till further use.

### ***C. Quantitative Real Time PCR (qRT-PCR) Analysis***

At the outset, few rice genes have been selected based on their functions under different stress conditions which include calmodulin, proteinase inhibitor (PIN), basic leucine zipper (bZIP1), calcium-dependent protein kinase 1 (CDPK1), phytochrome B, phytochrome C and teosinte branched 1 (TB1). Forward and reverse primers have been designed and commercially synthesized (IDT, Coralville, IA). Relative expressions of the genes have been quantified using 48-well plate. Relative quantification of the gene expression has been performed in 20  $\mu\text{l}$  reaction volume containing 2  $\mu\text{l}$  single stranded-cDNA, 0.75  $\mu\text{l}$  of 10  $\mu\text{M}$  gene specific forward and reverse primer each, 10  $\mu\text{l}$  2x SYBR Green master mix (Applied Biosystems, Foster City, CA) along with 6.5  $\mu\text{l}$  RNase-free water using Step One qRT-PCR thermo-cycler instrument (Applied Biosystems, Foster City, CA). Conditions for the PCR have been set as follows: preheating at  $95^{\circ}\text{C}$  (5 min), followed by 40 cycles each composed of denaturation at  $95^{\circ}\text{C}$  (30 s), annealing at  $56^{\circ}\text{C}$  (45 s) and extension at  $72^{\circ}\text{C}$  (1 min) along with one melting cycle of  $95^{\circ}\text{C}$  (30 s) and  $56^{\circ}\text{C}$  (45 s). All relative gene expression levels have been normalized against the housekeeping gene (actin) in order to counter variation among different samples during RNA isolation. In addition, target gene expression levels among 1837.50 MHz EM irradiation treated rice plant samples have been set relative to respective sham-exposed plant samples. Accession numbers for the housekeeping and target genes are as follows – actin: OsAB047313 (NCBI), calmodulin: OsX65016 (NCBI), proteinase inhibitor PIN: OsU76004.1 (NCBI), basic leucine zipper bZIP1: Os01t0174000-01 (RAP-DB), calcium-dependent protein kinase 1 CDPK1: Os01t0622600 (RAP-DB), phytochrome B: Os03t0309200 (RAP-DB), phytochrome C: Os03t0752100 (RAP-DB) and teosinte branched 1 TB1: Os03g0706500 (RAP-DB). Primer sequences have been illustrated in Table 7.1.

### ***D. Statistical Analysis***

The seed germination experiment has been independently repeated six times – each experiment consisted of 30 seeds treated under periodic electromagnetic irradiation along with 30 sham-

Table 7.1 Primer information for rice (*Oryza sativa*) housekeeping and target genes

Rice Genes	Primer Sequences	
	Forward (5'-3')	Reverse (5'-3')
actin	TACCTCTTCTAGACCGTAGTG	GTCTCAAACATGATCTGGGTC
calmodulin	GTCTAGCGGCTCAAGTTCCT	ACCTCGTTGATCATGTCCTG
PIN	TGTTCTACTTGGGCGGCT	TAGTTCTCCGCTCGGGGTTT
bZIP1	GGCGGTAGCTCCTCATGAAA	AGCGACGATAGCAAGCTGTT
CDPK1	TGTGACCGAACTTCCCAAGG	CGTTCACAGGGGTTGTGGAT
phytochrome B	GGTCGGTGAGGTCTTTGGTA	TCCATTCTGCTCCTCGTGTT
phytochrome C	TGGTGAGGTGATTGCTGAGT	GGTGCCCTGAGAGAGTAGATCC
TB1	CAAGAAATCTCGGCGGCTAG	CGAATTGGCGTAGACGAC

exposed seeds. In case of photosynthetic pigments profiling and gene expressions investigations, samples from one random electromagnetic irradiation treated rice seedling / plant in pair with one random sham-exposed seedling / plant have been used at each time point of a particular experiment. All photosynthetic pigment estimations and gene expression experiments have been independently replicated three times. All plants used in these experiments have been discarded immediately after tissue collection. Statistical significance has been analyzed using two-tailed paired t-test and respective *p-values* have been indicated wherever applicable. All data have been plotted using the statistical analyzer and graphing software package GraphPad Prism 5 (GraphPad Software, San Diego, CA). Data have been represented herein as mean value  $\pm$  SEM from at least three independent experiments.

### 7.3.3 Physiological Responses in *Satabdi* Rice Plant

#### 7.3.3.1 Effect on Seed Germination Rate

Mean germination percentage was 76.67% for the irradiated rice seeds and 83.90% for the sham-exposed seeds. Periodic electromagnetic irradiation evoked significant reduction in germination rate of rice variety *Satabdi* (*p-value* = 0.03). The data mentioned above have been illustrated in Fig. 7.3(a).

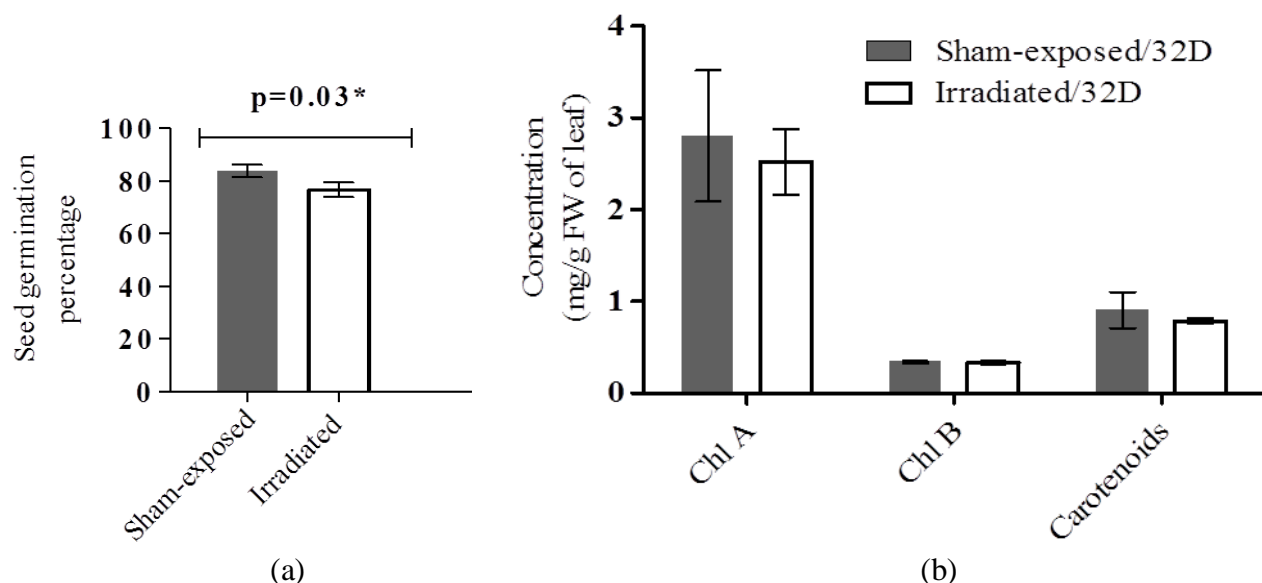


Fig. 7.3: Effect of periodic electromagnetic irradiation on seed germination rate and photosynthetic pigment concentrations (data represent mean value  $\pm$  SEM from at least three independent experiments) (a) significant reduction in *Satabdi* seed germination rate due to 1837.50 MHz periodic electromagnetic irradiation, (b) marginal reduction in photosynthetic pigment concentration levels among 32 days old *Satabdi* rice plants due to periodic electromagnetic exposure at 1837.50 MHz

### 7.3.3.2 Effect on Photosynthetic Pigment Profile

In line with significantly reduced seed germination rate, periodic electromagnetic irradiation also evoked reduction in photosynthetic pigment concentrations among 32 days old *Satabdi* plants. Though not statistically significant, mean concentration levels of chlorophyll A and carotenoids were reduced to some extent as illustrated in Fig. 7.3(b) – chlorophyll A/B ratio also decreased.

### 7.3.4 Molecular Responses in *Satabdi* Rice Plant

Relative gene expressions fold change data shown in Figs. 7.4(a) and (b) describe controlled and periodic electromagnetic irradiation (6 h a day) induced responses respectively among 12 days old and 32 days old *Satabdi* rice plants. It should be noted that TB1 gene expression has been investigated only among the 32 days old *Satabdi* rice plants under periodic electromagnetic irradiation.



Among 12 days old *Satabdi* rice seedlings, the periodic electromagnetic irradiation has evoked upregulation of PIN (1.53 fold) and CDPK1 (1.60 fold) gene expressions. However, statistically significant upregulation of phytochrome B and phytochrome C gene expressions have been noted at respective  $p$ -value = 0.045 (10.60 fold) and  $p$ -value = 0.039 (6.09 fold) under exactly the same dose of treatment i.e. at 1837.50 MHz, 2.75 mW/m<sup>2</sup> for 6 h a day (please refer to Fig. 7.4(a)).

Among 32 days old *Satabdi* rice plants, relative gene expression for PIN has been observed to be unaltered due to periodic electromagnetic irradiation. But, expressions for calmodulin (2.35 fold), CDPK1 (7.34 fold), phytochrome B (1.17 fold) and phytochrome C (2.59 fold) have clearly been upregulated and expressions for bZIP1 (2 fold) and TB1 (4.63 fold) genes have been downregulated under periodic electromagnetic irradiation. Periodic electromagnetic irradiation has resulted in upregulation of calmodulin and phytochrome C gene expressions significant at  $p$ -value = 0.041 and  $p$ -value = 0.05 respectively. In addition, periodic electromagnetic irradiation induced downregulation of bZIP1 gene has been observed to be significant at  $p$ -value = 0.016 (please refer to Fig. 7.4(b)).

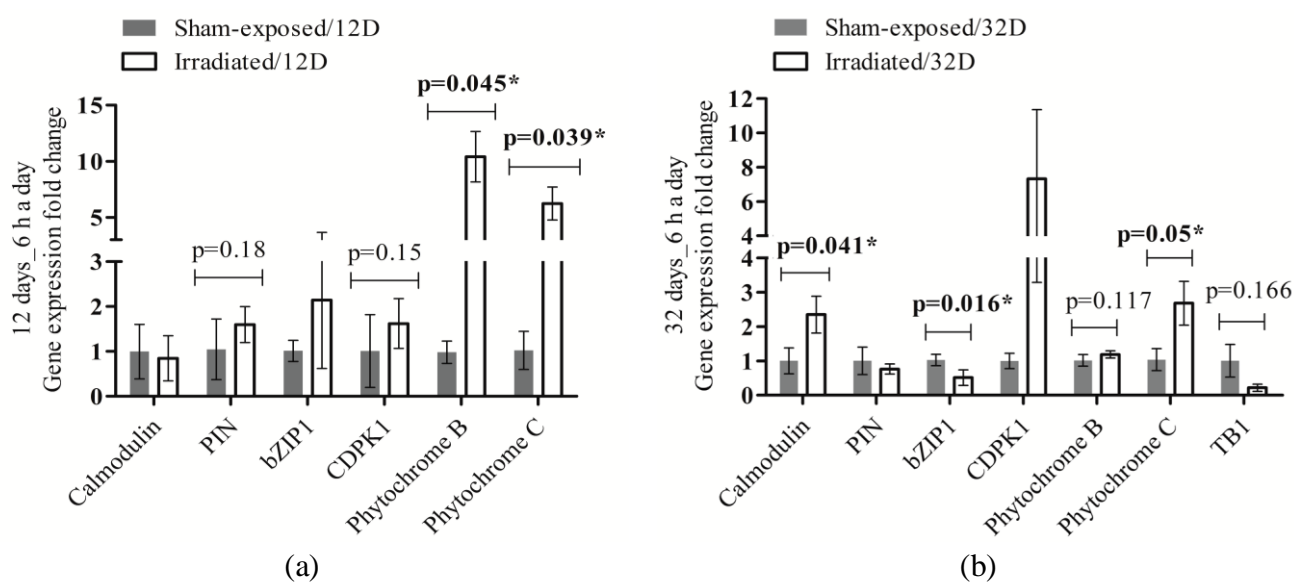


Fig. 7.4: Effect of periodic electromagnetic irradiation on relative gene expression levels (data represent mean value  $\pm$  SEM from three independent experiments) (a) comparison of relative gene expression levels among 12 days old *Satabdi* rice variant due to periodic electromagnetic exposure at 1837.50 MHz, (b) comparison of relative gene expression levels among 32 days old *Satabdi* rice variant due to periodic electromagnetic exposure at 1837.50 MHz

### 7.3.5 Discussions

The ability of a medium to store electromagnetic energy is characterized by its permittivity ( $\epsilon_r'$ ) whereas electrical conductivity ( $\sigma$ ) of that medium contributes to the conversion of the stored energy to other forms (predominantly heat energy). Different parts of plant tissues maintain a large amount of water molecules which contribute to a high permittivity ( $\epsilon_r'$ ) while ionized particles account for reasonably high electrical conductivity ( $\sigma$ ) [19-24]. Moreover, plants maximize their surface to volume ratio for absorbing more light, gases through leaves, water and minerals through roots [14]. As a result, the exposure to electromagnetic energy over a larger surface area is reasonably higher in the case of plants with relatively less tissue mass to dissipate the same. Dielectric tissue heating due to electromagnetic energy absorption in different plant and fruit models has already been discussed in Chapter 3.

Herein, it is found that controlled and periodic (6 h a day) electromagnetic exposure at 1837.50 MHz has resulted significant reduction in *Satabdi* rice seed germination rate. Seed germination starts after a certain period of imbibition and involves a series of metabolic changes which lead to the emergence of radicle and plumule. Thus, 1837.50 MHz periodic electromagnetic irradiation possibly has some detrimental role in presence of a sufficient amount of moisture during the seed imbibition and germination process, which leads to a significant reduction in germination rate. This observation is in accordance with a previous publication where significantly reduced seed germination rates were reported in radish following electromagnetic irradiation [8].

In addition to physiological effects, present investigation has demonstrated noticeable changes in relative gene expressions for calmodulin, phytochrome B and phytochrome C in *Satabdi* rice plant when exposed to periodic electromagnetic irradiation. The genes considered in this investigation are already known for their responsiveness to various environmental stimuli like abiotic stresses and electromagnetic radiation [7, 13, 51]. Phytochrome B and phytochrome C are chromoprotein producing genes which have shown upregulation under periodic electromagnetic irradiation. Depending on wavelength of the irradiance received by plant leaves, phytochromes change their conformation by absorbing red or far-red light. Far-red light absorbing phytochromes enter inside the nucleus and interact with Phytochrome Interacting Factors (PIFs) – thus, they modulate several abiotic or thermo-sensing genes.

Rice phytochromes also regulate seed germination, de-etiolation, plant architecture development, thermal-sensitivity and flowering initiation [85]. Plants with null phytochrome B and phytochrome C alleles induce early flowering [86] – thus, plants with induced expression may also delay flowering in *Satabdi* rice plant under above mentioned periodic electromagnetic irradiation. Therefore, it can be presumed that 1837.50 MHz periodic electromagnetic irradiation has evoked some signals in rice to upregulate transcriptional profiles of phytochrome B and phytochrome C genes. Both phytochrome B and phytochrome C have shown high upregulation in 12 days old seedlings compared to 32 days old plants. This observation suggests that longer time of periodic electromagnetic irradiation helps plants to adapt the stress-like situation mainly by its developmental plasticity. Old tissues with less responsiveness to environmental stimuli may be another reason behind reduced upregulated expressions in case of 32 days old *Satabdi* rice plants. With the maturation, plants probably somewhat acclimatize to the effect of electromagnetic radiation emitted from different wireless communication systems. However, outcomes of this investigation are in line with previous investigations – where electromagnetic irradiation was reported to be a stress factor for plants that resulted in changes in expression profiles of several stress related genes [7, 13, 51]. Moreover, electromagnetic stimulation was reported to trigger reduced ATP and AEC levels that are markers of cell energy level [50-51]. Therefore, the observed changes in gene expression profiles strongly indicate towards the possible contribution of non-ionizing electromagnetic radiation in affecting plants at different growth stages.

The net surface potential of cell membrane is negative at neutral pH primarily due to presence of negatively charged phospholipids. Cell membranes attract cations and repel anions – divalent cations such as calcium ( $Ca^{2+}$ ) are preferred over mono-valent cations like sodium ( $Na^{1+}$ ) or potassium ( $K^{1+}$ ). The ions or  $Ca^{2+}$  stabilize the structure of plasma membrane and serve as cofactors for enzymes. Moreover, they also modulate the surface potential of cell membranes [87]. In fact,  $Ca^{2+}$  ions also contribute in balancing inorganic and organic anions present in plant vacuoles and facilitate activation of different signalling pathways [88]. Cell membranes act like thin capacitive layers and electromagnetic energy induced alternating currents can pass through them – allowing effective interaction at the cellular levels. In addition, electromagnetic radiation induced alternating electric currents can displace  $Ca^{2+}$  from cell membranes and nearby  $Na^{1+}$  or  $K^{1+}$  ions can replace some of those on cell membrane – leading to membrane

leakage. A slight change in the membrane permeability due to such leakage can allow unwanted substances along with large influx of  $Ca^{2+}$  ions in the cytoplasm. Upregulation of stress-sensor genes such as calmodulin under periodic electromagnetic irradiation in 32 days old *Satabdi* rice plant strongly suggests early variations of  $Ca^{2+}$  concentration in cytoplasm and neighbouring locations [7, 13, 89]. Thus, possible disproportion of  $Ca^{2+}$ ,  $K^{1+}$  and  $Na^{1+}$  concentrations inside the plant cell due to electromagnetic irradiation cannot be overruled [90-94]. Moreover, the increase in  $Ca^{2+}$  ions concentration in the cytoplasm often gets sensed by a series of cytosolic enzymes [95]. Therefore, the likelihood of electromagnetic irradiation to trigger alteration in stress sensor gene expressions in plants to activate required defense mechanisms is reasonably high.

One major upshot of this investigation lies in the fact that observed molecular responses under long term periodic (6 h per day) electromagnetic irradiation are fairly consistent at different growth stages of *Satabdi* rice. Moreover, the observed differences in plant responses such as seed germination rate and selected gene expressions at 1837.50 MHz, 2.75 mW/m<sup>2</sup> electromagnetic irradiation level with respect to the sham-exposure power density level of 0.07 mW/m<sup>2</sup>, is in fact novel. In most of the earlier cases, electromagnetic stimulation induced plant responses were reported at somewhat different power density levels [7, 13, 50-51, 55, 68-75]. Reported physiological and molecular changes in *Satabdi* rice plants have been observed much below the international electromagnetic exposure regulatory limits [66-67].

#### **7.4 Periodic EM Irradiation Evoked Responses in *Swarnaprabha* Rice Plant**

In this part of the investigation, similar controlled and periodic (6 h a day) electromagnetic irradiation (1837.50 MHz, 2.75 mW/m<sup>2</sup>) induced physiological and molecular responses in *Swarnaprabha* rice variant have been investigated – *Swarnaprabha* is another photoperiod insensitive rice variant of West Bengal, India. Similar to the *Satabdi* rice variant – in the beginning, periodic (6 h a day) and controlled electromagnetic irradiation (1837.50 MHz, 2.75 mW/m<sup>2</sup>) induced alterations in seed germination rate and photosynthetic pigment profiles i.e. chlorophyll A, chlorophyll B and carotenoids in 32 days old *Swarnaprabha* rice plants have been studied. Photoperiod insensitive *Swarnaprabha* rice variant has been chosen due to involvement of indoor environment inside the simple electromagnetic reverberation chamber with artificial

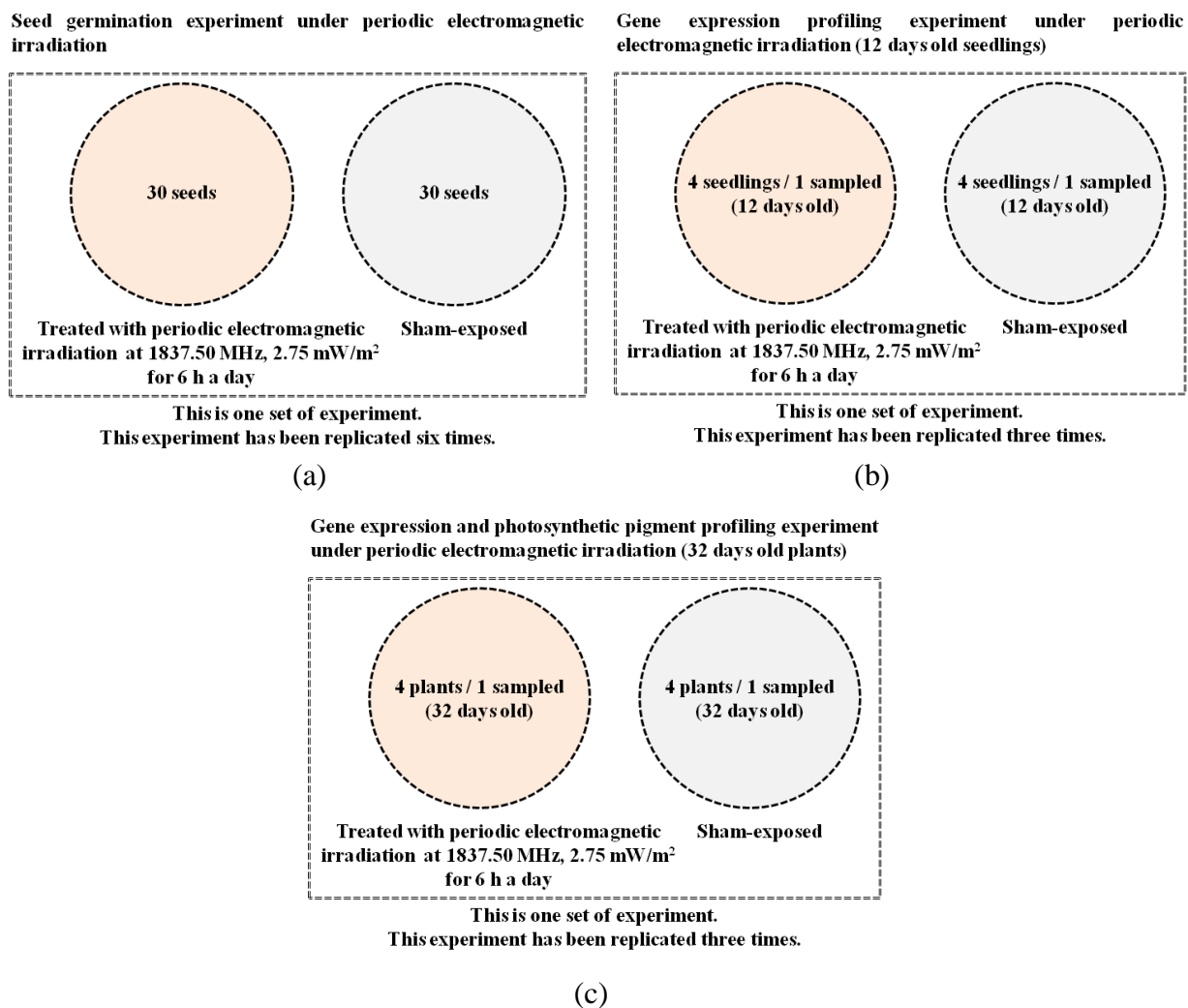


Fig. 7.5: Graphical schemes of seed germination, photosynthetic pigment profiling and gene expression profiling experiments in *Swarnaprabha* rice under periodic electromagnetic irradiation (a) seed germination experiment, (b) gene expression profiling experiment in 12 days old *Swarnaprabha* rice seedlings and (c) photosynthetic pigment profiling and gene expression profiling experiment in 32 days old *Swarnaprabha* rice plants

supplementary lighting arrangement – as discussed earlier. At last, alterations in stress-sensitive gene expression profiles have been studied in 12 days old as well as 32 days old *Swarnaprabha* rice plants under periodic electromagnetic irradiation with respect to sham-exposed specimens. Similar to *Satabdi* rice, the seed germination, photosynthetic pigments profiling and gene expression experiments at different growth stages of *Swarnaprabha* rice under periodic electromagnetic irradiation have been illustrated in Figs. 7.5(a), (b) and (c) respectively.

### **7.4.1 Plant culture and growth conditions**

*Swarnaprabha* seeds, subsequent saplings and plants have been cultured following the exactly similar growth conditions as in case of *Satabdi* rice variant – thus, the growth conditions are not repeated here.

### **7.4.2 Intermediate Protocols to Inspect Plant Responses**

The seed germination rate inspection, photosynthetic pigment concentration profiling (32 days old plants), spectrophotometric analyses of photosynthetic pigments (32 days old plants), plant sample preparation for RNA extraction (12 days old and 32 days old plants), RNA extraction and cDNA synthesis (12 days old and 32 days old plants), quantitative Real Time PCR (qRT-PCR) to analyze pre-selected stress responsive gene expressions (12 days old and 32 days old plants) and statistical data analyses for *Swarnaprabha* rice variant have been performed following similar protocols as in case of *Satabdi* rice variant. Forward and reverse primer sequences for the pre-selected housekeeping (actin) and stress-responsive target genes (calmodulin, proteinase inhibitor PIN, basic leucine zipper bZIP1, calcium-dependent protein kinase 1 CDPK1, phytochrome B, phytochrome C and teosinte branched 1 TB1) have been illustrated earlier in Table 7.1.

### **7.4.3 Physiological Responses in *Swarnaprabha* Rice Plant**

#### **7.4.3.1 Effect on Seed Germination Rate**

No significant difference in *Swarnaprabha* rice seed germination rate has been noted under periodic (6 h a day) electromagnetic irradiation (1837.50 MHz, 2.75 mW/m<sup>2</sup>) (please refer to Fig. 7.6(a)). Respective germination rates have been observed to be 95.55% and 96.67% among the electromagnetic irradiation treated and sham-exposed *Swarnaprabha* rice seeds.

#### **7.4.3.2 Effect on Photosynthetic Pigment Profile**

Above mentioned periodic electromagnetic irradiation (1837.50 MHz, 2.75 mW/m<sup>2</sup>) has induced fairly significant reduction in photosynthetic pigment concentrations in 32 days old *Swarnaprabha* rice plants compared to sham-exposed counterparts. The mean concentration level of chlorophyll A has been noted to be reduced to 2.84 mg/g FW of leaf tissue in periodic

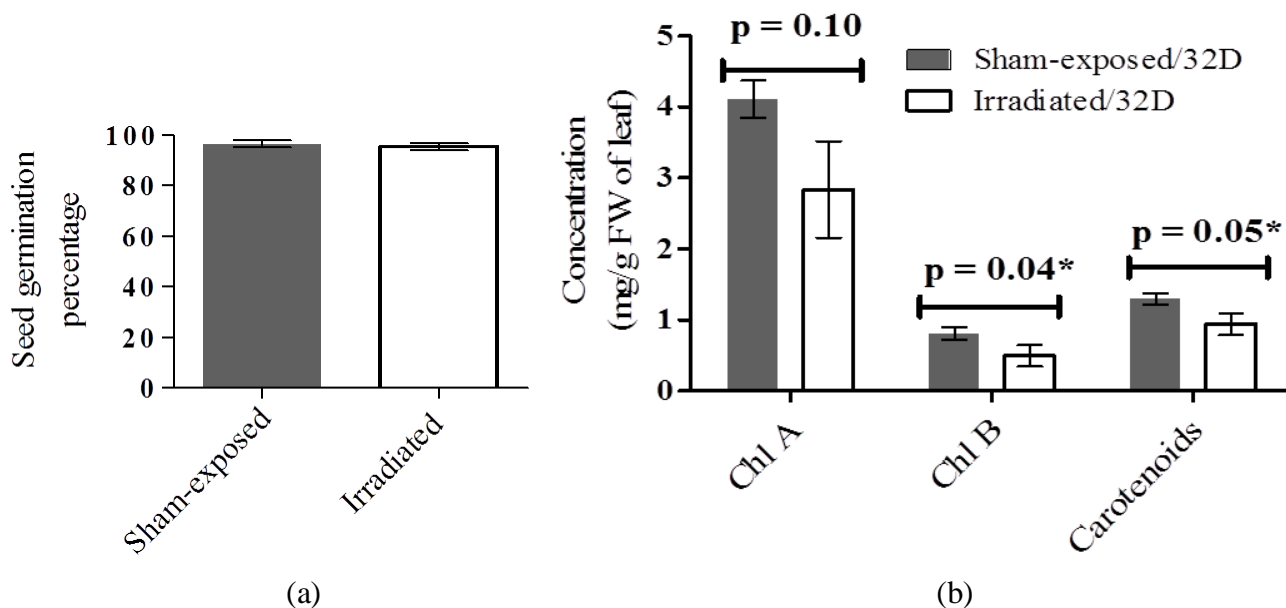


Fig. 7.6: Effect of periodic electromagnetic irradiation on seed germination rate and photosynthetic pigment concentrations (data represent mean value  $\pm$  SEM from at least three independent experiments) (a) no such alteration in *Swarnaprabha* seed germination rate due to 1837.50 MHz periodic electromagnetic irradiation, (b) significant reduction in photosynthetic pigment concentration levels among 32 days old *Swarnaprabha* rice plants due to periodic electromagnetic exposure at 1837.50 MHz

electromagnetic irradiation treated group with respect to 4.11 mg/g FW of leaf tissue in sham-exposed group – the respective *p*-value is 0.10. The same periodic irradiation treatment has significantly reduced (*p*-value = 0.04) the chlorophyll B concentration in targeted group at 0.50 mg/g FW of leaf tissue compared to 0.81 mg/g FW of leaf tissue in sham-exposed group. Furthermore, the carotenoids concentration has been significantly reduced (*p*-value = 0.05) to 0.94 mg/g FW of radiation treated leaf tissue compared to 1.29 mg/g FW of leaf tissue in sham-exposed group. The reported photosynthetic pigment concentrations have been illustrated in Fig. 7.6(b).

#### 7.4.4 Molecular Responses in *Swarnaprabha* Rice Plant

Periodic and controlled electromagnetic irradiation (6 h a day) induced alterations in stress-responsive gene expressions among 12 days old and 32 days old *Swarnaprabha* rice plants have been illustrated in Figs. 7.7(a) and (b) respectively. As discussed earlier, the relative expression

for TB1 gene has been investigated only among the 32 days old *Swarnaprabha* rice plants under above mentioned periodic electromagnetic irradiation.

As illustrated in Fig. 7.7(a), above mentioned periodic electromagnetic irradiation (1837.50 MHz, 2.75 mW/m<sup>2</sup> for 6 h per day) has evoked upregulation trend in PIN (1.69 fold), bZIP1 (4.96 fold), CDPK1 (1.71 fold), phytochrome B (72.50 fold) and phytochrome C (4.03 fold) gene expressions among 12 days old *Swarnaprabha* rice plants. However, statistically significant upregulation has only been noted in CDPK1 gene expression (1.71 fold) under the same dose of treatment at *p-value* = 0.016.

In case of 32 days old *Swarnaprabha* rice plants, relative gene expressions for most of the targeted genes have been noted to be unaltered under above mentioned periodic electromagnetic irradiation. However, relative expressions for bZIP1 (52.94 fold) and CDPK1 (16.30 fold) have shown upregulation trends – though, not at statistical significant levels. Please, refer to Fig. 7.7(b).

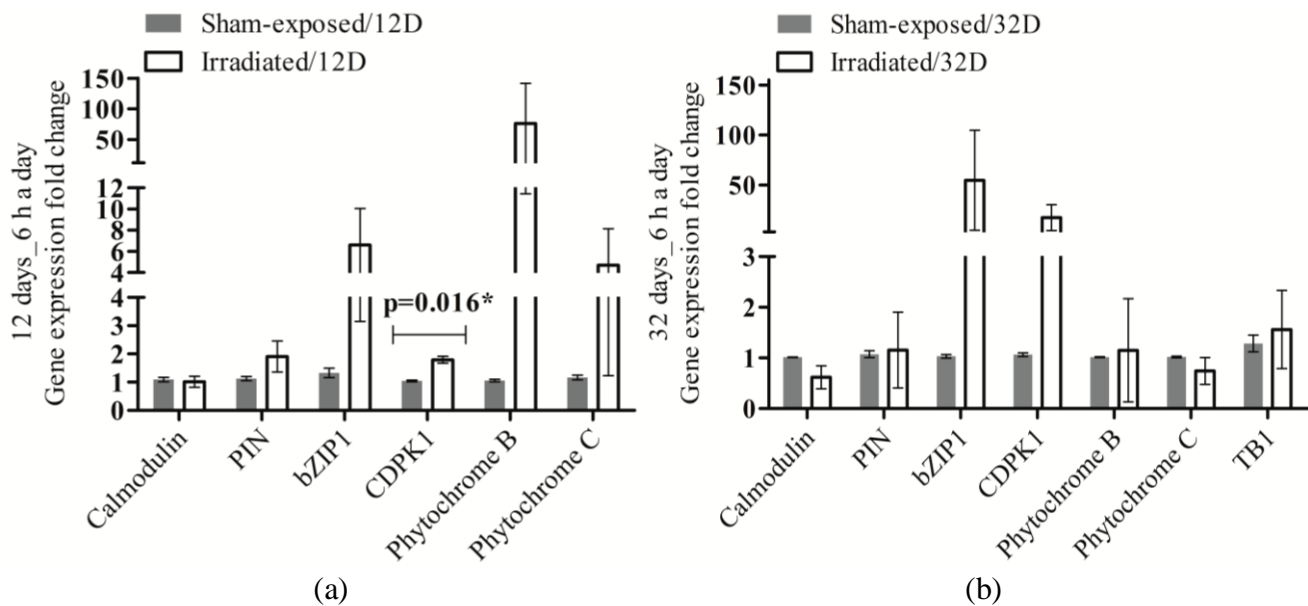


Fig. 7.7: Effect of periodic electromagnetic irradiation on relative gene expression levels (data represent mean value  $\pm$  SEM from three independent experiments) (a) comparison of relative gene expression levels among 12 days old *Swarnaprabha* rice variant due to periodic electromagnetic exposure at 1837.50 MHz, (b) comparison of relative gene expression levels among 32 days old *Swarnaprabha* rice variant due to periodic electromagnetic exposure at 1837.50 MHz



### 7.4.5 Discussions

As noted, above mentioned controlled and periodic (6 h a day) electromagnetic irradiation at 1837.50 MHz, 2.75 mW/m<sup>2</sup> has induced significant reduction in most photosynthetic pigment concentrations among 32 days old *Swarnaprabha* rice plants compared to sham-exposed counterparts. It should be noted that similar trend of electromagnetic irradiation induced reduction in chlorophylls and carotenoids has already been reported in maize seedlings [53, 59-60]. Above mentioned controlled and periodic electromagnetic irradiation induced reduction in chlorophylls and carotenoids can have further impacts on photosynthesis, plant nutrition and health. However, no such significant difference in *Swarnaprabha* rice seed germination rate has been observed under the periodic electromagnetic irradiation.

The above mentioned periodic electromagnetic irradiation has induced significant upregulation only in CDPK1 gene expression ( $p$ -value = 0.016) under the periodic electromagnetic irradiation among 12 days old *Swarnaprabha* rice seedlings. In addition, upregulation trends in bZIP1, phytochrome B and phytochrome C gene expressions have also been noted among 12 days old *Swarnaprabha* rice seedlings. In case of 32 days old *Swarnaprabha* plants, no significant alterations in targeted gene expressions have been noted – though, upregulation trends have been noted for bZIP1 and CDPK1 gene expressions under the same treatment. As discussed earlier, these pre-identified genes are already known for their sensitivity to various abiotic stresses and electromagnetic radiation [7, 13, 51].

CDPK genes encode calcium-binding proteins and are upregulated under wound like stress situations at normal calcium level in plants [51]. CDPKs are major molecular decoders of calcium ion in plant [96]. In general, CDPKs take part in various physiological processes including accumulation of storage starch and protein in immature rice seeds and they help in tolerating different stress conditions in rice plant [96-98]. Thus, significant upregulation of CDPK1 gene expression in 12 days old *Swarnaprabha* rice seedlings is expected to facilitate in tolerating electromagnetic exposure stress condition. In particular, the importance of calcium in establishing plant response under electromagnetic irradiation (a stress like stimulus) is endorsed by the significant upregulation in CDPK1 gene expression among 12 days old *Swarnaprabha* rice seedlings [7, 15, 51]. Though upregulation of other genes have not been noted to be statistically significant, a brief outline on the possible impacts can add value to this discussion. It

should be noted that G-box binding Transcription Factors (TFs) are produced by bZIP1 gene – these TFs take control of several stress-responsive gene expressions under adverse abiotic conditions such as salinity, drought and electromagnetic irradiation. Over and above, the periodic electromagnetic irradiation evoked transcript accumulation of bZIP1 gene can possibly cause rice yield reduction [99]. The consequences of upregulation in phytochrome B and phytochrome C gene expressions have already been discussed in this chapter – those are not repeated here [85-86].

It is to be noted that for all these stress-sensitive genes, higher upregulation trends have been noted in 12 days old *Swarnaprabha* seedlings compared to 32 days old *Swarnaprabha* plants. This observation once again suggests that rice plants attempt to adapt under the stress like electromagnetic stimulation due to their developmental plasticity – as noted earlier in case of *Satabdi* rice variant. In addition, old plant tissues possibly respond less to environmental abiotic stimuli – the same can be another reason behind reduced gene expression upregulation trends in 32 days old *Swarnaprabha* rice plants. Although statistically weak – gene upregulation trends in *Swarnaprabha* rice plant under electromagnetic irradiation are in line with previous investigations in *Satabdi* rice and tomato plants [7, 13, 51]. Thus, there is an indication that periodic electromagnetic radiation possibly affects *Swarnaprabha* rice plants at different stages.

## 7.5 Conclusions

Based on the available knowledge, data presented here seem to be the first report to point out that controlled and periodic electromagnetic exposure even at far lower level than the international regulatory standards, significantly alters either physiological or molecular responses in rice plants – irrespective of variant and growth stage [66-67]. It's true that upregulated stress-sensitive gene expressions have prominently been observed in *Satabdi* rice variant while compared to *Swarnaprabha* variant; however, the upregulation trends in selected stress-sensitive gene expressions in *Swarnaprabha* variant are also aligned with *Satabdi* variant. In addition, the controlled and periodic electromagnetic irradiation induced reduction in photosynthetic pigment concentrations have been noted in both the rice variants – however, the reduction has been observed to be statistically significant in *Swarnaprabha* rice plants but marginal in *Satabdi* plants. Thus, in general, rice plants perceive periodic electromagnetic irradiation as an abiotic stress irrespective of variant or growth stage. In general, either upregulated stress-sensitive gene

expressions or similar upregulation trends have been noted in rice variants – but, these molecular responses somewhat acclimatize with time and plant growth. In conclusion, data presented here indicate towards the possible need for readdressing global electromagnetic regulatory standards to protect plants, crops and fruits in addition to humans.

## References

- [1] R. J. Aitken, L. E. Bennetts, D. Sawyer, A. M. Wiklendt, and B. V. King, ‘Impact of Radio Frequency Electromagnetic Radiation on DNA Integrity in the Male Germline’, *International Journal of Andrology*, Vol. 28, No. 3, pp. 171-179, 2005.
- [2] A. Balmori, ‘Electromagnetic Pollution from Phone Masts. Effects on Wildlife’, *Pathophysiology*, Vol. 16, No. 2-3, pp. 191-199, 2009.
- [3] B. J. Houston, B. Nixon, B. V. King, G. N. De Iuliis, and R. J. Aitken, ‘The Effects of Radiofrequency Electromagnetic Radiation on Sperm Function’, *Reproduction*, Vol. 152, No. 6, pp. R263-R276, 2016.
- [4] K. Liu, Y. Li, G. Zhang, J. Liu, J. Cao, L. Ao, and S. Zhang, ‘Association Between Mobile Phone Use and Semen Quality: A Systemic Review and Meta-Analysis’, *Andrology*, Vol. 2, No. 4, pp. 491-501, 2014.
- [5] M. Mailankot, A. P. Kunnath, H. Jayalekshmi, B. Koduru, and R. Valsalan, ‘Radio Frequency Electromagnetic Radiation (RF-EMR) from GSM (0.9/1.8 GHz) Mobile Phones Induces Oxidative Stress and Reduces Sperm Motility in Rats’, *Clinics*, Vol. 64, No. 6, pp. 561-565, 2009.
- [6] S. N. Narayanan, R. S. Kumar, B. K. Potu, S. Nayak, P. G. Bhat, and M. Mailankot, ‘Effect of Radio-Frequency Electromagnetic Radiations (RF-EMR) on Passive Avoidance Behaviour and Hippocampal Morphology in Wistar Rats’, *Upsala Journal of Medical Sciences*, Vol. 115, No. 2, pp. 91-96, 2010.
- [7] D. Roux, A. Vian, S. Girard, P. Bonnet, F. Paladian, E. Davies, and G. Ledoigt, ‘Electromagnetic Fields (900 MHz) Evoke Consistent Molecular Responses in Tomato Plants’, *Physiologia Plantarum*, Vol. 128, No. 2, pp. 283-288, 2006.
- [8] A. Scialabba, and C. Tamburello, ‘Microwave Effects on Germination and Growth of Radish (*Raphanus sativus* L.) Seedlings’, *Acta Botanica Gallica*, Vol. 149, No. 2, pp. 113-123, 2002.

- [9] S. Sharma, and L. Parihar, 'Effect of Mobile Phone Radiation on Nodule Formation in the Leguminous Plants', *Current World Environment*, Vol. 9, No. 1, pp. 145-155, 2014.
- [10] A. L. Stefi, D. Vassilacopoulou, L. H. Margaritis, and N. S. Christodoulakis, 'Oxidative Stress and an Animal Neurotransmitter Synthesizing Enzyme in the Leaves of Wild Growing Myrtle After Exposure to GSM Radiation', *Flora*, Vol. 243, pp. 67-76, 2018.
- [11] A. L. Stefi, K. Mitsigiorgi, D. Vassilacopoulou, and N. S. Christodoulakis, 'Response of Young *Nerium oleander* Plants to Long-Term Non-Ionizing Radiation', *Planta*, Vol. 251, No. 6, Article No. 108, pp. 1-17, 2020.
- [12] M. Tkalec, K. Malarić, M. Pavlica, B. Pevalek-Kozlina, and Ž. Vidaković-Cifrek, 'Effects of Radiofrequency Electromagnetic Fields on Seed Germination and Root Meristematic Cells of *Allium cepa L'*', *Mutation Research/Genetic Toxicology and Environmental Mutagenesis*, Vol. 672, No. 2, pp. 76-81, 2009.
- [13] A. Vian, D. Roux, S. Girard, P. Bonnet, F. Paladian, E. Davies, and G. Ledoigt, 'Microwave Irradiation Affects Gene Expression in Plants', *Plant Signaling & Behavior*, Vol. 1, No. 2, pp. 67-69, 2006.
- [14] A. Vian, C. Faure, S. Girard, E. Davies, F. Hallé, P. Bonnet, G. Ledoigt, and F. Paladian, 'Plants Respond to GSM-Like Radiations', *Plant Signaling & Behaviour*, Vol. 2, No. 6, pp. 522-524, 2007.
- [15] A. Vian, E. Davies, M. Gendraud, and P. Bonnet, 'Plant Responses to High Frequency Electromagnetic Fields', *BioMed Research International*, Article ID: 1830262, 2016.
- [16] C. Gabriel, S. Gabriel, and E. Corthout, 'The Dielectric Properties of Biological Tissues: I. Literature Survey', *Physics in Medicine & Biology*, Vol. 41, No. 11, pp. 2231-2249, 1996.
- [17] S. Gabriel, R. W. Lau, and C. Gabriel, 'The Dielectric Properties of Biological Tissues: II. Measurements in the Frequency Range 10 Hz to 20 GHz', *Physics in Medicine & Biology*, Vol. 41, No. 11, pp. 2251-2269, 1996.
- [18] S. Gabriel, R. W. Lau, and C. Gabriel, 'The Dielectric Properties of Biological Tissues: III. Parametric Models for the Dielectric Spectrum of Tissues', *Physics in Medicine & Biology*, Vol. 41, No. 11, pp. 2271-2293, 1996.
- [19] S. O. Nelson, 'Microwave Dielectric Properties of Fresh Fruits and Vegetables', *Transactions of the ASAE*, Vol. 23, No. 5, pp. 1314-1317, 1980.

- [20] W. Kuang, and S. O. Nelson, ‘Dielectric Relaxation Characteristics of Fresh Fruits and Vegetables from 3 to 20 GHz’, *Journal of Microwave Power and Electromagnetic Energy*, Vol. 32, No. 2, pp. 114-122, 1997.
- [21] S. O. Nelson, ‘Dielectric Properties of Agricultural Products – Measurements and Applications’, *IEEE transactions on Electrical Insulation*, Vol. 26, No. 5, pp.845-869, 1991.
- [22] W. C. Guo, S. O. Nelson, S. Trabelsi, and S. J. Kays, ‘10–1800-MHz Dielectric Properties of Fresh Apples during Storage’, *Journal of Food Engineering*, Vol. 83, No. 4, pp. 562-569, 2007.
- [23] S. O. Nelson, and S. Trabelsi, ‘Dielectric Spectroscopy Measurements on Fruit, Meat, and Grain’, *Transactions of the ASABE*, Vol. 51, No. 5, pp. 1829-1834, 2008.
- [24] S. O. Nelson, ‘Dielectric Properties of Agricultural Products and Some Applications’, *Research in Agricultural Engineering*, Vol. 54, No. 2, pp. 104-112, 2008.
- [25] S. S. Stuchly, M. A. Stuchly, A. Kraszewski, and G. Hartsgrrove, ‘Energy Deposition in a Model of Man: Frequency Effects’, *IEEE Transactions on Biomedical Engineering*, Vol. 33, No. 7, 1986.
- [26] K. Meier, V. Hombach, R. Kästle, R. Y. Tay, and N. Kuster, ‘The Dependence of Electromagnetic Energy Absorption upon Human-Head Modelling at 1800 MHz’, *IEEE Transactions on Microwave Theory and Techniques*, Vol. 45, No. 11, 1997.
- [27] T. Yelkenci, ‘Effects of Metallic Objects on Specific Absorption Rate in the Human Head for 915 and 1900 MHz Mobile Phones’, *Frequenz*, Vol. 60, No. 3-4, pp. 46-50, 2006.
- [28] O. P. Gandhi, ‘Yes the Children are More Exposed to Radiofrequency Energy from Mobile Telephones than Adults’, *IEEE Access*, Vol. 3, pp. 985-988, 2015.
- [29] R. Takei, T. Nagaoka, K. Saito, S. Watanabe, and M. Takahashi, ‘SAR Variation due to Exposure from a Smartphone Held at Various Positions Near the Torso’, *IEEE Trans. Electromagnetic Compatibility*, Vol. 59, No. 2, pp. 747-753, 2017.
- [30] J. Cooper, B. Marx, J. Buhl, and V. Hombach, ‘Determination of Safety Distance Limits for a Human near a Cellular Base Station Antenna, Adopting the IEEE Standard or ICNIRP Guidelines’, *Bioelectromagnetics*, Vol. 23, No. 6, pp. 429-443, 2002.
- [31] A. Christ, A. Klingenböck, T. Samaras, C. Goiceanu, and N. Kuster, ‘The Dependence of Electromagnetic Far-Field Absorption on Body Tissue Composition in the Frequency Range

from 300 MHz to 6 GHz', *IEEE Transactions on Microwave Theory and Techniques*, Vol. 54, No. 5, 2006.

[32] M. A. A. Karunarathna, and I. J. Dayawansa, 'Energy Absorption by the Human Body from RF and Microwave Emissions in Sri Lanka', *Sri Lankan Journal of Physics*, Vol. 7, pp. 35-47, 2006.

[33] A. Hirata, S. Kodera, J. Wang, and O. Fujiwara, 'Dominant Factors Influencing Whole-Body Average SAR Due to Far-Field Exposure in Whole-Body Resonance Frequency and GHz Regions', *Bioelectromagnetics*, Vol. 28, No. 6, pp. 484-487, 2007.

[34] A. Hirata, N. Ito, O. Fujiwara, T. Nagaoka, and S. Watanabe, 'Conservative Estimation of Whole-Body-Averaged SARs in Infants with a Homogeneous and Simple-Shaped Phantom in the GHz Region', *Physics in Medicine and Biology*, Vol. 53, No. 24, pp. 7215-7223, 2008.

[35] T. Iyama, T. Onishi, Y. Tarusawa, and S. Uebayashi and T. Nojima, 'Novel Specific Absorption Rate (SAR) Measurement Method using a Flat Solid Phantom', *IEEE Transactions on Electromagnetic Compatibility*, Vol. 50, No. 1, pp. 43-51, 2008.

[36] T. Wessapan, S. Srisawatdhisukul, and P. Rattanadecho, 'Specific Absorption Rate and Temperature Distributions in Human Head Subjected to Mobile Phone Radiation at Different Frequencies', *International Journal of Heat and Mass Transfer*, Vol. 55, No. 1-3, pp. 347-359, 2012.

[37] T. Wessapan, and P. Rattanadecho, 'Specific Absorption Rate and Temperature Increase in the Human Eye due to Electromagnetic Fields Exposure at Different Frequencies', *International Journal of Heat and Mass Transfer*, Vol. 64, pp. 426-435, 2013.

[38] N. Mukherjee, A. Kundu, B. Gupta, and M. Mitra, 'Specific Absorption Rate Estimation for a Typical Hibiscus Flower Model as per ICNIRP Electromagnetic Guidelines', *2020 IEEE Calcutta Conference (CALCON)*, pp. 240-243, Kolkata, India, February, 2020.

[39] N. Mukherjee, A. Kundu, B. Gupta, and M. Mitra, 'Assessment of Electromagnetic Energy Absorption Rate in Hibiscus Flower Model at 947.50 MHz and 1842.50 MHz', *2021 IEEE International IOT, Electronics and Mechatronics Conference (IEMTRONICS)*, pp. 1-4, Toronto, Canada, April, 2021.

[40] BioInitiative Working Group, 'BioInitiative 2012: A Rationale for a Biologically-Based Exposure Standards for Low-Intensity Electromagnetic Radiation', In C. Sage, and D. O.

Carpenter (eds): The BioInitiative Report 2012, 2012. [www.bioinitiative.org](http://www.bioinitiative.org) [Last accessed 03 April 2022].

[41] A. Besset, F. Espa, Y. Dauvilliers, M. Billiard, and R. De Seze, 'No Effect on Cognitive Function from Daily Mobile Phone Use', *Bioelectromagnetics*, Vol. 26, No. 2, pp. 102-108, 2005.

[42] S. Dasdag, M. Zulkuf Akdag, F. Aksen, F. Yılmaz F, Bashan M, Mutlu Dasdag M, Salih Celik M. 'Whole Body Exposure of Rats to Microwaves Emitted from a Cell Phone Does Not Affect the Testes', *Bioelectromagnetics*, Vol. 24, No. 3, pp. 182-188, 2003.

[43] R. de Seze, P. Fabbro-Peray, and L. Miro, 'GSM Radiocellular Telephones Do Not Disturb the Secretion of Antepituitary Hormones in Humans', *Bioelectromagnetics*, Vol. 19, No. 5, pp. 271-278, 1998.

[44] J. M. Elwood, 'Epidemiological Studies of Radio Frequency Exposures and Human Cancer', *Bioelectromagnetics*, Vol. 24, pp. S63-S73, 2003.

[45] P. Gos, B. Eicher, J. Kohli, and W. D. Heyer, 'No Mutagenic or Recombinogenic Effects of Mobile Phone Fields at 900 MHz Detected in the Yeast *Saccharomyces cerevisiae*', *Bioelectromagnetics*, Vol. 21, No. 7, pp. 515-523, 2000.

[46] C. Haarala, L. Björnberg, M. Ek, M. Laine, A. Revonsuo, M. Koivisto, H. Hämäläinen, 'Effect of a 902 MHz Electromagnetic Field Emitted by Mobile Phones on Human Cognitive Function: A Replication Study', *Bioelectromagnetics*, Vol. 24, No. 4, pp. 283-288, 2003.

[47] M. Hietanen, A. M. Hämäläinen, and T. Husman, 'Hypersensitivity Symptoms Associated with Exposure to Cellular Telephones: No Causal Link', *Bioelectromagnetics*, Vol. 23, No. 4, pp. 264-270, 2002.

[48] Z. J. Sienkiewicz, R. P. Blackwell, R. G. Haylock, R. D. Saunders, and B. L. Cobb, 'Low-level Exposure to Pulsed 900 MHz Microwave Radiation Does Not Cause Deficits in the Performance of a Spatial Learning Task in Mice', *Bioelectromagnetics*, Vol. 21, No. 3, pp. 151-158, 2000.

[49] International Electrotechnical Commission (IEC), '*IEC 61000-4-21 (2011) Electromagnetic Compatibility (EMC) – Part 4-21: Testing and Measurement Techniques – Reverberation Chamber Test Methods*', International Electrotechnical Commission, Geneva, 2011. [www.webstore.iec.ch/publication/4191](http://www.webstore.iec.ch/publication/4191) (subscription required) [Last accessed 01 December 2020]

- [50] D. Roux, C. Faure, P. Bonnet, S. Girard, G. Ledoigt, E. Davies, M. Gendraud, F. Paladian, and A. Vian, 'A Possible Role for Extra-Cellular ATP in Plant Responses to High Frequency, Low Amplitude Electromagnetic Field', *Plant Signaling & Behaviour*, Vol. 3, No. 6, pp. 383-385, 2008.
- [51] D. Roux, A. Vian, S. Girard, P. Bonnet, F. Paladian, E. Davies, and G. Ledoigt, 'High Frequency (900MHz) Low Amplitude (5V m<sup>-1</sup>) Electromagnetic Field: A Genuine Environmental Stimulus that Affects Transcription, Translation, Calcium and Energy Charge in Tomato', *Planta*, Vol. 227, No. 4, pp. 883-891, 2008.
- [52] D. D. Sandu, C. Goiceanu, A. Ispas, I. Creanga, S. Miclaus, and D. E. Creanga, 'A Preliminary Study on Ultra High Frequency Electromagnetic Fields Effect on Black Locust Chlorophylls', *Acta Biologica Hungarica*, Vol. 56, No. 1-2, pp. 109-117, 2005.
- [53] M. Ursache, G. Mindru, D. E. Creangă, F. M. Tufescu, and C. Goiceanu, 'The Effects of High Frequency Electromagnetic Waves on the Vegetal Organisms', *Romanian Journal of Physics*, Vol. 54, No. 1-2, pp. 133-145, 2009.
- [54] M. N. Halgamuge, 'Weak Radiofrequency Radiation Exposure from Mobile Phone Radiation on Plants', *Electromagnetic Biology and Medicine*, Vol. 36, No. 2, pp. 213-235, 2017.
- [55] A. L. Stefi, L. H. Margaritis, and N. S. Christodoulakis, 'The effect of the Non-Ionizing Radiation on Exposed, Laboratory Cultivated Maize (*Zea mays L.*) Plants', *Flora*, Vol. 233, pp. 22-30, 2017.
- [56] V. P. Sharma, H. P. Singh, D. R. Batish, and R. K. Kohli, 'Cell Phone Radiations Affect Early Growth of *Vigna radiate* (Mung Bean) Through Biochemical Alterations', *Zeitschrift für Naturforschung C*, Vol. 65, No. 1-2, pp. 66-72, 2010.
- [57] A. Akbal, Y. Kiran, A. Sahin, D. Turgut-Balik, and H. H. Balik, 'Effects of Electromagnetic Waves Emitted by Mobile Phones on Germination, Root Growth, and Root Tip Cell Mitotic Division of *Lens culinaris* Medik', *Polish Journal of Environmental Studies*, Vol. 21, No. 1, pp. 23-29, 2012.
- [58] Y. C. Chen, and C. Chen, 'Effects of Mobile Phone Radiation on Germination and Early Growth of Different Bean Species', *Polish Journal of Environmental Studies*, Vol. 23, No. 6, pp. 1949-1958, 2014.



- [59] M. Racuciu, C. Iftode, and S. Miclaus, 'Inhibitory Effects of Low Thermal Radiofrequency Radiation on Physiological Parameters of *Zea mays* Seedlings Growth', *Romanian Journal of Physics*, Vol. 60, No. 3-4, pp. 603-612, 2015.
- [60] A. Kumar, H. P. Singh, D. R. Batish, S. Kaur, and R. K. Kohli, 'EMF Radiations (1800 MHz)-Inhibited Early Seedling Growth of Maize (*Zea mays*) Involves Alterations in Starch and Sucrose Metabolism', *Protoplasma*, Vol. 253, No. 4, pp. 1043-1049, 2015.
- [61] E. Beaubois, S. Girard, S. Lallechere, E. Davies, F. Paladian, P. Bonnet, G. Ledoigt, and A. Vian, 'Intercellular Communication in Plants: Evidence for Two Rapidly Transmitted Systemic Signals Generated in Response to Electromagnetic Field Stimulation in Tomato', *Plant, Cell and Environment*, Vol. 30, No. 7, pp. 834-844, 2007.
- [62] M. Rammal, F. Jebai, H. Rammal, and W. H. Joumaa, 'Effects of Long Term Exposure to RF/MW Radiations on the Expression of mRNA of Stress Proteins in *Lycopersicon esculentum*', *WSEAS Transactions on Biology and Biomedicine*, Vol. 11, pp. 10-14, 2014.
- [63] R. K. Jangid, R. Sharma, Y. Sudarsan, S. Eapen, G. Singh, and A. K. Purohit, 'Microwave Treatment Induced Mutations and Altered Gene Expression in *Vigna aconitifolia*', *Biologia Plantarum*, Vol. 54, No. 4, pp. 703-706, 2010.
- [64] The National Center for Biotechnology Information (NCBI), [www.ncbi.nlm.nih.gov](http://www.ncbi.nlm.nih.gov) [Last accessed on 28 April 2022].
- [65] The Rice Annotation Project Database (RAP-DB), [rapdb.dna.affrc.go.jp](http://rapdb.dna.affrc.go.jp) [Last accessed on 28 April 2022].
- [66] R. F. Cleveland, Jr., D. M. Sylvar, and J. L. Ulcek, 'Evaluating Compliance with FCC Guidelines for Human Exposure to Radiofrequency Electromagnetic Fields', FCC OET Bulletin, Vol. 65, Edition 97-01, Washington D.C., 1997.
- [67] International Commission on Non-Ionizing Radiation Protection (ICNIRP), 'Guidelines for Limiting Exposure to Electromagnetic Fields (100 kHz to 300 GHz)', *Health Physics*, Vol. 118, No. 5, pp. 483-524, 2020.
- [68] E. Beaubois, S. Girard, S. Lallechere, E. Davies, F. Paladian, P. Bonnet, G. Ledoigt, A. Vian, 'Intercellular Communication in Plants: Evidence for Two Rapidly Transmitted Systemic Signals Generated in Response to Electromagnetic Field Stimulation in Tomato', *Plant, Cell and Environment*, Vol. 30, No. 7, pp. 834-844, 2007.

- [69] M. Czerwinski, L. Januszkiewicz, A. Vian, and A. Lazaro, 'The Influence of Bioactive Mobile Telephony Radiation at the Level of a Plant Community – Possible Mechanisms and Indicators of the Effects', *Ecological Indicators*, Vol. 108, Article No. 105683, pp. 1-11, 2020.
- [70] A. Grémiaux, S. Girard, V. Guérin, J. Lothier, F. Baluska, E. Davies, P. Bonnet, and A. Vian, 'Low-Amplitude, High-Frequency Electromagnetic Field Exposure Causes Delayed and Reduced Growth in *Rosa hybrida*', *Journal of Plant Physiology*, Vol. 190, pp.44-53, 2016.
- [71] M. N. Halgamuge, S. K. Yak, and J. L. Eberhardt, 'Reduced Growth of Soybean Seedlings After Exposure to Weak Microwave Radiation from GSM 900 Mobile Phone and Base Station', *Bioelectromagnetics*, Vol. 36, No. 2, pp. 87-95, 2015.
- [72] D. S. Pesnya, and A. V. Romanovsky, 'Comparison of Cytotoxic and Genotoxic Effects of Plutonium-239 Alpha Particles and Mobile Phone GSM 900 Radiation in the *Allium cepa* Test', *Mutation Research/Genetic Toxicology and Environmental Mutagenesis*, Vol. 750, No. 1-2, pp. 27-33, 2013.
- [73] V. P. Sharma, H. P. Singh, R. K. Kohli, and D. R. Batish, 'Mobile Phone Radiation Inhibits *Vigna radiata* (Mung Bean) Root Growth by Inducing Oxidative Stress', *Science of the Total Environment*, Vol. 407, No. 21, pp. 5543-5547, 2009.
- [74] H. P. Singh, V. P. Sharma, D. R. Batish, and R. K. Kohli, 'Cell Phone Electromagnetic Field Radiations Affect Rhizogenesis through Impairment of Biochemical Processes', *Environmental Monitoring and Assessment*, Vol. 184, No. 4, pp. 1813-1821, 2012.
- [75] C. Waldmann-Selsam, A. Balmori-de la Puente, H. Breunig, and A. Balmori, 'Radiofrequency Radiation Injures Trees around Mobile Phone Base Stations', *Science of the Total Environment*, Vol. 572, pp. 554-569, 2016.
- [76] H. A. Mendes, 'A New Approach to Electromagnetic Field Strength Measurements in Shielded Enclosures', *Wescon Technical Papers, Western Electronic Show and Convention*, pp. 20-23, LA, California, Aug, 1968.
- [77] R. F. Harrington, '*Time-Harmonic Electromagnetic Fields*', Wiley IEEE Press, pp. 1-496, New York, 2001.
- [78] D. A. Hill, '*Electromagnetic Fields in Cavities: Deterministic and Statistical Theories*', John Wiley & Sons, 2009.

- [79] S. J. Boyes, ‘*Reverberation Chambers and the Measurement of Antenna Characteristics*’, Doctoral dissertation, University of Liverpool, 2013.
- [80] International Electrotechnical Commission (IEC), ‘*CISPR/A and IEC SC 77B, IEC 61000-4-21 – Electromagnetic Compatibility (EMC) - Part 4-21: Testing and Measurement Techniques – Reverberation Chamber Test Methods*’, International Electrotechnical Commission (IEC) International standard, Aug, 2003.
- [81] C. Bruns, ‘*Three-Dimensional Simulation and Experimental Verification of a Reverberation Chamber*’, Doctoral dissertation, ETH Zurich, 2005.
- [82] B. H. Liu, D. C. Chang, and M. T. Ma, ‘*Eigenmodes and the Composite Quality Factor of a Reverberating Chamber*’, U.S. National Bureau of Standards Technical Note 1066, 1983.
- [83] D. A. Hill, M. T. Ma, A. R. Ondrejka, B. F. Riddle, M. L. Crawford, and R. T. Johnk, ‘*Aperture Excitation of Electrically Large, Lossy Cavities*’, *IEEE Transactions on Electromagnetic Compatibility*, Vol. 36, No. 3, pp. 169-178, 1994.
- [84] H. K. Lichtenthaler, ‘*Chlorophylls and Carotenoids: Pigments of Photosynthetic Biomembranes*’, *Methods in Enzymology*, Vol. 148, pp. 350-382, 1987.
- [85] J. H. Jung, M. Domijan, C. Klose, S. Biswas, D. Ezer, M. Gao, A. K. Khattak, M. S. Box, V. Charoensawan, S. Cortijo, and M. Kumar, ‘*Phytochromes Function as Thermosensors in Arabidopsis*’, *Science*, Vol. 354, No. 6314, pp. 886-889, 2016.
- [86] M. Takano, N. Inagaki, X. Xie, N. Yuzurihara, F. Hihara, T. Ishizuka, M. Yano, M. Nishimura, A. Miyao, H. Hirochika, and T. Shinomura, ‘*Distinct and Cooperative Functions of Phytochromes A, B, and C in the Control of Deetiolation and Flowering in Rice*’, *The Plant Cell*, Vol. 17, No. 12, pp. 3311-3325, 2005.
- [87] C. Larsson, I. M. Møller, and S. Widell, ‘*Introduction to the Plant Plasma Membrane – Its Molecular Composition and Organization*’, In *The Plant Plasma Membrane*, Springer, pp. 1-15, Berlin, Germany, 1990.
- [88] P. J. White, and M. R. Broadley, ‘*Calcium in Plants*’, *Annals of Botany*, Vol. 92, No. 4, pp. 487-511, 2003.

- [89] M. Tafforeau, M. C. Verdus, V. Norris, G. White, M. Demarty, M. Thellier, and C. Ripoll, 'SIMS Study of the Calcium-Deprivation Step Related to Epidermal Meristem Production Induced in Flax by Cold Shock or Radiation from a GSM Telephone', *Journal of Trace and Microprobe Techniques*, Vol. 20, No. 4, pp. 611-623, 2002.
- [90] L. J. Challis, 'Mechanisms for Interaction between RF Fields and Biological Tissues', *Bioelectromagnetics*, Vol. 26, No. S7, pp. S98-S106, 2005.
- [91] S. Cucurachi, W. L. Tamis, M. G. Vijver, W. J. Peijnenburg, J. F. Bolte, and G. R. de Snoo, 'A Review of the Ecological Effects of Radiofrequency Electromagnetic Fields (RF-EMF)', *Environment International*, Vol. 51, pp. 116-140, 2013.
- [92] E. Davies, 'Electrical Signals in Plants: Facts and Hypotheses', In A. G. Volkov (eds): *Plant Electrophysiology*, Springer, pp 407-422, Berlin, Germany, 2006.
- [93] E. Davies, and B. Stankovic, 'Electrical Signals, the Cytoskeleton, and Gene Expression: A Hypothesis on the Coherence of the Cellular Responses to Environmental Insult', In F. Baluška, S. Mancuso, D. Volkmann (eds): *Communication in Plants*, Springer. pp 309-320, Berlin, Germany, 2006.
- [94] M. Levin, 'Bioelectromagnetics in Morphogenesis', *Bioelectromagnetics*, Vol. 24, No. 5, pp. 295-315, 2003.
- [95] A. Goldsworthy, 'The Biological Effects of Weak Electromagnetic Fields: Problems and Solutions', 2012, [www.ecfsapi.fcc.gov/file/7022311211.pdf](http://www.ecfsapi.fcc.gov/file/7022311211.pdf) [Last accessed on 30 September 2020]
- [96] M. Nakata, T. Yuasa, Y. Takahashi, and S. Ishida, 'CDPK1, A Calcium-Dependent Protein Kinase, Regulates Transcriptional Activator RSG in Response to Gibberellins', *Plant Signaling & Behavior*, Vol. 4, No. 5, pp. 372-374, 2009.
- [97] T. Asano, N. Kunieda, Y. Omura, H. Ibe, T. Kawasaki, M. Takano, M. Sato, H. Furuhashi, T. Mujin, F. Takaiwa, and C. Y. Wu, 'Rice SPK a Calmodulin-Like Domain Protein Kinase is Required for Storage Product Accumulation during Seed Development: Phosphorylation of Sucrose Synthase is a Possible Factor', *Plant Cell*, Vol. 14, No. 3, pp. 619-628, 2002.

[98] Y. Saijo, S. Hata, J. Kyojuka, K. Shimamoto, and K. Izui, 'Overexpression of a Single  $\text{Ca}^{2+}$ -dependent Protein Kinase Confers both Cold and Salt/Drought Tolerance on Rice Plants', *The Plant Journal*, Vol. 23, No. 3, pp. 319-327, 2000.

[99] M. Obertello, G. Krouk, M. S. Katari, S. J. Runko, and G. M. Coruzzi, 'Modeling the Global Effect of the Basic-Leucine Zipper Transcription Factor 1 (bZIP1) on Nitrogen and Light Regulation in Arabidopsis', *BMC Systems Biology*, Vol. 4, No. 1, pp. 1-11, 2010.

# Chapter 8

## One-Time Controlled Electromagnetic Irradiation Evoked Molecular Responses in Plants

---

### 8.1 Introduction

Electromagnetic energy is utilized over multiple frequency bands to provide seamless wireless communication services. Non-motile plants contain tissues with reasonably high permittivity ( $\epsilon_r'$ ) and electrical conductivity ( $\sigma$ ) primarily due to the presence of sufficient water and ions respectively [1-2] – thus, plants can well perceive electromagnetic energy present in open environment. Moreover, higher surface-to-volume ratio of plant structure facilitates increased interaction with the incident electromagnetic waves [3]. In this connection, electromagnetic energy absorption rates along with associated spatial distributions have already been reported for a number of fruit and plant prototypes in Chapter 4. Despite such advantages as a prototype, molecular responses in plants following deterministic electromagnetic exposure have not been studied sufficiently [3-8]. To date, few well-designed studies have been conducted inside controlled electromagnetic reverberation chambers to investigate either short duration-low amplitude or long duration-periodic electromagnetic irradiation induced molecular responses in plants [3-8] – the long duration-periodic electromagnetic irradiation induced molecular responses in rice plants have been reported in the last chapter. Vian et al. and Roux et al. first utilized the Mode Stirred Reverberation Chamber (MSRC) to investigate plants' responses in an entirely controlled electromagnetic environment [3-9]. This particular controlled electromagnetic environment was designed on purpose to produce isotropic as well as homogeneous electromagnetic field inside to irradiate target plants from all directions and with random polarizations (mimicking the natural electromagnetic environment) [3-9]. The electromagnetic reverberation chamber is made of metallic walls that can reflect desired electromagnetic wave inside resulting in multiple reflections; it also ensures isolation of target and sham-exposed (control) plant samples from unwanted electromagnetic frequencies present in Open Area Test

Site (OATS). Vian et al. and Roux et al. reported more than a single investigation demonstrating short-duration electromagnetic irradiation induced molecular alterations (upregulated gene expressions) in plants [3-8]. Three weeks old tomato plants were irradiated with statistically uniform electromagnetic field at 900 MHz, 5 V/m inside the MSRC [5]. Several stress-related transcripts i.e. calmodulin-N6, calcium-dependent protein kinase (CDPK), chloroplast mRNA-binding protein (CMBP), proteinase inhibitor (PIN 2) and basic leucine-zipper transcription factor (leZIP1) were upregulated following exposure to the controlled electromagnetic irradiation at 900 MHz [4-5, 7-8, 10]. Furthermore, reduced Adenosine Triphosphate (ATP) and Adenylate Energy Charge (AEC) levels were also noted following similar controlled electromagnetic stimulation in tomato plants [6-7]. In this connection, short-span electromagnetic exposure has been categorized as a stress factor similar to leaf flaming, electrical stimulation etc. after analyzing stress-responsive gene expression profiles [4-5, 7]. In the last chapter i.e. Chapter 7, periodic electromagnetic irradiation induced physiological and molecular responses in rice plants have been reported at different growth stages. The investigations have been conducted at certain fixed positions inside a simple electromagnetic reverberation chamber without mechanical stirrers. This setup could produce controlled and reproducible electromagnetic environment at each position inside provided position, type and input power to the transmitting antenna along with positions of the plants were kept fixed – however, statistically homogeneous electromagnetic field at all positions inside the chamber couldn't be ensured.

However, as far as known, studies investigating molecular responses particularly at the mid-vegetative stage in plants following one-time (hours-long) electromagnetic irradiation have not been reported earlier. Hence, the studies reported in this chapter have aimed at investigating molecular responses in 40 days old (*Swarnaprabha*) rice plants in addition to 12 days old (*Satabdi*) rice seedlings following one-time 1837.50 MHz, 2.75 mW/m<sup>2</sup> electromagnetic irradiation of 2 h 30 min duration. Controlled electromagnetic irradiation inside the simple reverberation chamber has been ensured to achieve pure electromagnetic environment at 1837.50 MHz with deterministic electromagnetic power density at selected position. *Satabdi* and *Swarnaprabha* rice variants have been chosen for this investigation since these rice varieties are widely cultivated and consumed in Indian subcontinents. Subsequent alterations in some selected stress-sensitive gene expressions have been assayed using real-time quantitative PCR technique.

These investigations have been purposefully focused on subsequent molecular responses immediately following electromagnetic irradiation so that the possible effects of secondary stimulations can be avoided. Employed electromagnetic irradiation level i.e. 1837.50 MHz, 2.75 mW/m<sup>2</sup> is far below that specified by the existing international regulations [11-12]. Moreover, the same is somewhat different from most of the previously reported electromagnetic stimulation levels except in last chapter [4-7, 10, 13-20].

## 8.2 Electromagnetic Reverberation Chamber

A brief theoretical outline of general electromagnetic reverberation chambers has already been discussed in Chapter 7. In addition, a detailed description of the custom-made simple electromagnetic reverberation chamber (3.60 m × 1.95 m × 3.00 m) has been outlined in the same chapter – the reverberation chamber contains two sections i.e. rectangular parallelepiped electromagnetic irradiation zone (2.25 m × 1.95 m × 3.00 m) and electromagnetic quiet zone (1.35 m × 1.95 m × 3.00 m) for sham-exposure. Inside the electromagnetic irradiation zone, mechanical stirrers have not been installed – thus, a controlled and reproducible electromagnetic field distribution has been ensured; however, statistically homogeneous electromagnetic field distribution all over the space couldn't be achieved unlike in MSRC [3-8]. As stated earlier in Chapter 7, controlled and reproducible electromagnetic power density 2.75 mW/m<sup>2</sup> (at 1837.50 MHz) has been ensured to irradiate target rice plants – by fixing position, type and input power to the transmitting antenna along with preset position for the target rice plants. The transmitting microstrip patch antenna (measured center frequency at 1837.50 MHz, bandwidth = 1826 MHz to 1842 MHz) has been designed using CST Microwave Studio 2014 with realized gain of 4.47 dBi [21]. The antenna illustrated in Fig. 8.1(a) has been fabricated using ultraviolet photolithography technique on dielectric substrate ( $\epsilon_r' = 4.3$ ,  $\tan \delta = 0.003$ ). Reflection coefficient ( $S_{11}$ ) of the fabricated patch antenna has been characterized using vector network analyzer (E5071B ENA Series, 300 KHz to 8.5 GHz, Agilent Technologies); the same has been depicted in Fig. 8.1(b). Observed data confirms that the antenna radiates in 1805 MHz – 1880 MHz downlink band that is dedicated for mobile tower antennas to ground level communication. The entire electromagnetic stimulation setup inside the customized simple reverberation chamber has been outlined in Chapter 7 – the same infrastructure has been utilized here to investigate one-time controlled electromagnetic irradiation induced molecular responses in rice plants.



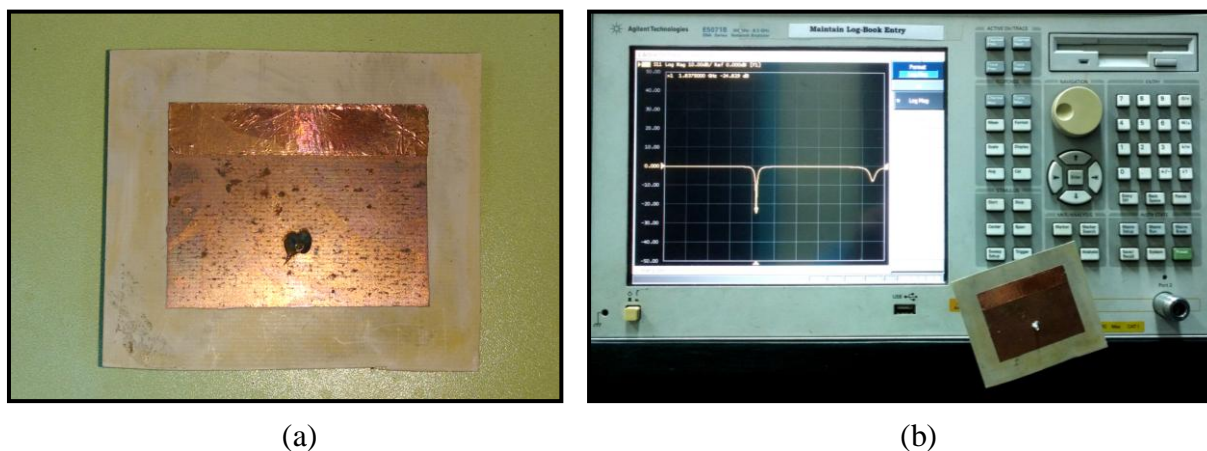


Fig. 8.1: Fabricated transmitting antenna and its reflection coefficient ( $S_{11}$ ) measurement (a) microstrip patch antenna designed at 1837.50 MHz, (b) reflection coefficient ( $S_{11}$ ) measurement

### 8.3 One-Time Controlled Electromagnetic Irradiation Evoked Molecular Responses in *Satabdi* Rice Plant

Rice is a model crop with smallest genome size (389 Mb) and detailed genomic information is also available [22-23]. Rice is a synteny crop like other cereal crops (wheat, maize etc.) – thus, any information generated in this investigation can easily be corroborated with those cereal crops as well as other rice variants. Therefore, this study aimed at investigating immediate molecular responses in 12 days old *Satabdi* rice seedlings following short duration one-time electromagnetic irradiation (2 h 30 min). *Satabdi* is a widely cultivated early maturing (<115 days) semi-dwarf (<110 cm) high yielding variety developed from a cross between two parents and one of the parents, CR10 14, was originated from a crossing between tropical *japonica* and *indica*. Thus, this long slender grain variety carries allelic set from both the *japonica* and *indica* rice. Photoperiod insensitive *Satabdi* rice has been chosen because this investigation involves indoor environment inside the reverberation chamber. Instantaneous molecular responses due to one-time (2 h 30 min) electromagnetic irradiation on relative expressions of pre-selected stress-sensitive genes have been investigated in 12 days old *Satabdi* rice seedlings. The transient gene expression profiling experiment due to one-time electromagnetic irradiation has been illustrated using a graphical scheme in Fig. 8.2. Stress-responsive genes with known functionalities have been pre-identified as molecular markers to investigate one-time electromagnetic irradiation induced molecular responses in 12 days old *Satabdi* rice seedlings.

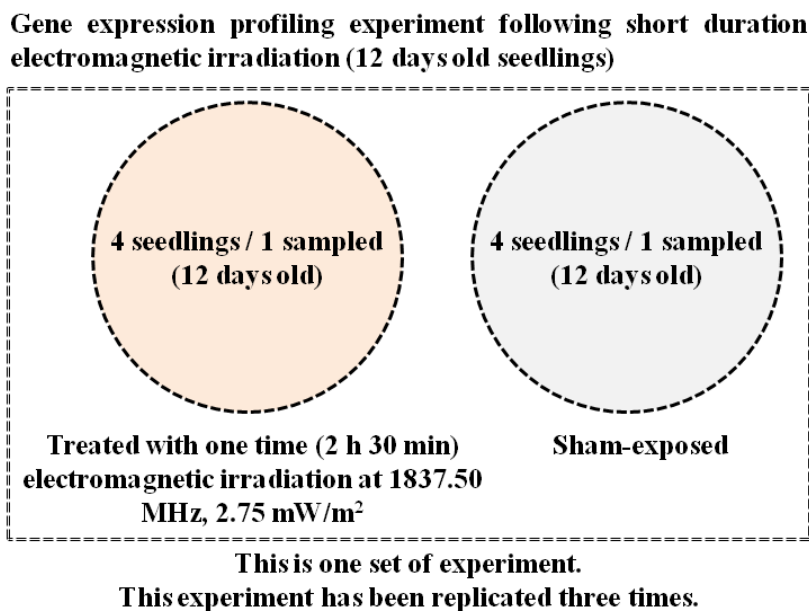


Fig. 8.2: Graphical scheme of gene expression profiling experiment in 12 days old *Satabdi* rice seedlings following one-time electromagnetic irradiation

### 8.3.1 Plant culture and growth conditions

Viable seeds of *Satabdi* rice (*Oryza sativa*) variant have been chosen to investigate 2 h 30 min long 1837.50 MHz, 2.75 mW/m<sup>2</sup> electromagnetic irradiation induced molecular responses in 12 days old seedlings. The investigation has been conducted during the wet season at Indian Institute of Science Education and Research Kolkata (22.9638° N, 88.5245° E), West Bengal, India with typical air temperature range: 32 °C during daytime and 27 °C at night. At first, 30 healthy and viable *Satabdi* seeds have been soaked in water for germination inside the electromagnetic quiet zone of the simple reverberation chamber i.e. without any electromagnetic radiation. Those seeds have been kept in dark and water has been changed on a regular basis for four days. Next, after rice seed germination, eight healthy and viable germinated seeds have been chosen and immediately seeded in two earthen pots (25.4 cm diameter) – four germinated seeds in each earthen pot. Thereafter, these two earthen pots with *Satabdi* rice seedlings have been placed together inside a Faraday cage with metallic mesh walls under natural sunlight (800 μmol m<sup>-2</sup> s<sup>-1</sup> to 900 μmol m<sup>-2</sup> s<sup>-1</sup> photosynthetically active radiation for 12 h 30 min during daytime). This setup has been able to provide sufficient sunlight for photosynthesis along with isolation

from unintended electromagnetic radiations present in the open environment. *Satabdi* seedlings in both the earthen pots have been grown for 12 days inside the electromagnetic quiet zone (Faraday cage) before proceeding with the experimental procedures and subsequent investigations.

### **8.3.2 Electromagnetic Irradiation on *Satabdi* Rice Plant**

One earthen pot containing four 12 days old *Satabdi* rice seedlings have been transferred to rectangular parallelepiped electromagnetic irradiation zone of the custom-made simple reverberation chamber – the other earthen pot containing four similar *Satabdi* rice seedlings has been transferred to the electromagnetic quiet zone for sham-exposure. All rice seedlings have been transferred to the respective sections of the simple reverberation chamber after sunset and also 10 h before the electromagnetic irradiation experiment in dark (during predawn hours). Thus, any possibility of non-uniform secondary stress generated on the seedlings due to this transfer procedure has strictly been avoided. After that, targeted *Satabdi* rice seedlings have been exposed to 1837.50 MHz, 2.75 mW/m<sup>2</sup> electromagnetic radiation for 2 h 30 min, whereas the rice seedlings for sham-exposure have been kept in electromagnetic quiet zone during the same time period. The schematic description of this experiment is illustrated in Fig. 8.2.

Right after the controlled electromagnetic irradiation for 2 h 30 min duration, top-most first leaf of the 12 days old target and sham-exposed *Satabdi* rice seedlings have been collected, sliced into smallest possible pieces and stored in RNAlater solution at –20 °C till further use.

### **8.3.3 Plant RNA Extraction and cDNA Synthesis (*Satabdi*)**

Total RNA has been extracted from the sliced leaf samples (12 days old *Satabdi* seedlings) using ‘HiPurA Plant and Fungal RNA Miniprep Purification Kit’ (Himedia, India) followed by treatment with RNase free DNase I. Next, cDNA has been synthesized using ‘Super Reverse Transcriptase (MuLV) Kit’ (BioBharati, India) as per the manufacturer’s protocol. cDNA has been stored at –20 °C for further use.

### **8.3.4 Quantitative Real-Time PCR (qRT-PCR)**

Selection of key stress-sensitive plant genes such as calmodulin, proteinase inhibitor (PIN), basic leucine zipper (bZIP1), calcium-dependent protein kinase 1 (CDPK1), phytochrome B and

phytochrome C has been performed based on their established roles under electromagnetic irradiation and some other stress inducible conditions [3-5, 7-8, 10]. For each individual gene, forward and reverse primers have been commercially synthesized based on designed sequences (IDT, Coralville, IA) – those primer sequences have been tabulated in Table 8.1. Relative expressions of the selected set of stress-responsive genes have been quantified using 48-well plate in qRT-PCR technique following the conditions reported in Chapter 7. Relative quantifications of the targeted gene expressions have been performed in 20  $\mu$ l reaction volume using the Step One qRT-PCR thermo-cycler instrument (Applied Biosystems) – 2  $\mu$ l single stranded cDNA, 0.75  $\mu$ l of 10  $\mu$ M gene-specific forward primer, 0.75  $\mu$ l of 10  $\mu$ M gene-specific reverse primer, 10  $\mu$ l 2x SYBR Green master mix (Applied Biosystems, Foster City, CA) and 6.5  $\mu$ l RNase-free water. The specific conditions for qRT-PCR technique are as follows: preheating at 95 °C (5min), followed by 40 cycles each consisting of denaturation at 95 °C (30 s), annealing at 56 °C (45 s) and extension at 72 °C (1 min) along with one final melting cycle of 95 °C (30 s) and 56 °C (45 s).

Relative expressions for all the targeted stress-sensitive genes have been normalized with respect to the housekeeping gene (actin) so as to counter variation among the samples during RNA isolation. Moreover, relative gene expression levels in 1837.50 MHz, 2.75 mW/m<sup>2</sup> electromagnetic irradiation treated 12 days old *Satabdi* rice seedlings have been set relative to the respective gene expressions in the sham-exposed rice seedlings. Public domain genome database accession numbers of the target and housekeeping genes are calmodulin: OsX65016 (NCBI), proteinase inhibitor PIN: OsU76004.1 (NCBI), basic leucine zipper bZIP1: Os01t0174000-01 (RAP-DB), calcium-dependent protein kinase 1 CDPK1: Os01t0622600 (RAP-DB), phytochrome B: Os03t0309200 (RAP-DB), phytochrome C: Os03t0752100 (RAP-DB) and actin: OsAB047313 (NCBI) [22-23].

### 8.3.5 Statistical Analysis

At each time instant of a particular experiment, leaf samples have been collected from a randomly selected single electromagnetic irradiation treated 12 days old *Satabdi* rice seedling in pair with one random sham-exposed rice seedling. All the experiments have been repeated three times under identical conditions ( $n = 3$ ). Rice seedlings used in this investigation have been discarded immediately after leaf sampling. Statistical significances of observed relative gene

expression data have been analyzed using two-tailed paired t-tests and the levels of significance (p-values) are indicated with asterisk mark (\*) wherever applicable. All relative gene expression data have been plotted using GraphPad Prism 5 software (GraphPad Software, San Diego, CA). Data represent mean  $\pm$  standard error of the mean (SEM) from three independent experiments.

Table 8.1 Primer information for rice (*Oryza sativa*) housekeeping and target genes

Rice Genes	Primer Sequences	
	Forward (5'-3')	Reverse (5'-3')
actin	TACCTCTTCTAGACCGTAGTG	GTCTCAAACATGATCTGGGTC
calmodulin	GTCTAGCGGCTCAAGTTCCT	ACCTCGTTGATCATGTCCTG
PIN	TGTTCTACTTGGGCGGCT	TAGTTCTCCGCTCGGGGTTT
bZIP1	GCGGTAGCTCCTCATGAAA	AGCGACGATAGCAAGCTGTT
CDPK1	TGTGACCGAACTTCCCAAGG	CGTTCACAGGGGTTGTGGAT
phytochrome B	GGTCGGTGAGGTCTTTGGTA	TCCATTCTGCTCCTCGTGTT
phytochrome C	TGGTGAGGTGATTGCTGAGT	GGTGCCCTGAGAGAGTAGATCC

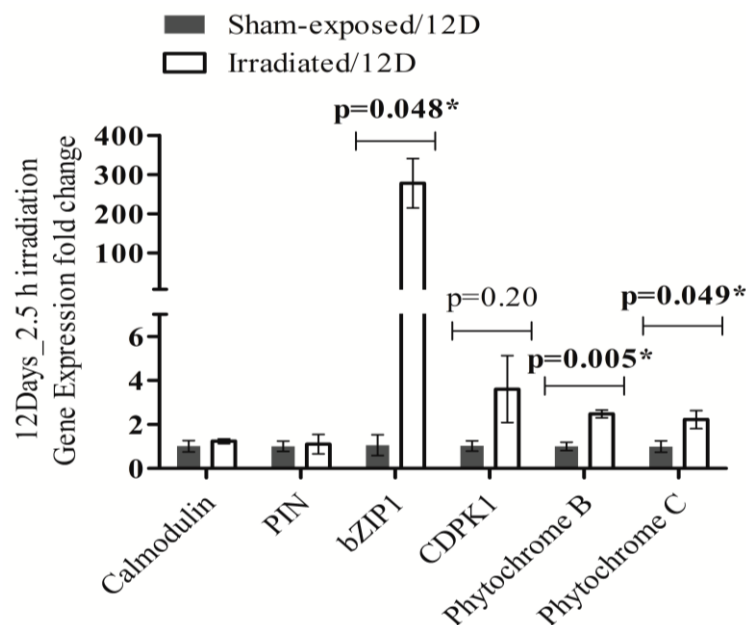


Fig. 8.3: Comparison of relative gene expression levels in 12 days old *Satabdi* rice seedlings following one-time electromagnetic irradiation at 1837.50 MHz, 2.75 mW/m<sup>2</sup> for 2 h 30 min (data represent mean value  $\pm$  SEM from three independent experiments)

### 8.3.6 Molecular Responses in *Satabdi* Rice Plant

In 12 days old *Satabdi* rice seedlings, relative gene expressions for stress-responsive bZIP1 (262.88 fold), CDPK1 (3.53 fold), Phytochrome B (2.48 fold) and Phytochrome C (2.23 fold) genes have clearly been upregulated following the one-time controlled electromagnetic irradiation (2 h 30 min – 1837.50 MHz, 2.75 mW/m<sup>2</sup>). After performing two tailed paired t-tests, upregulations in bZIP1, Phytochrome B and Phytochrome C gene expressions have been noted to be statistically significant at  $p\text{-value} = 0.048$ ,  $p\text{-value} = 0.005$  and  $p\text{-value} = 0.049$  respectively. However, relative expressions for calmodulin and PIN genes have been observed to be unaltered following the same dose of treatment. The normalized fold changes in relative expressions of the stress-sensitive genes have been illustrated in Fig. 8.3 – respective  $p\text{-values}$  have also been indicated wherever applicable.

### 8.3.7 Discussions

The above mentioned one-time controlled electromagnetic irradiation (2 h 30 min – 1837.50 MHz, 2.75 mW/m<sup>2</sup>) has evoked significant upregulation in stress-responsive bZIP1, phytochrome B and phytochrome C gene expressions in 12 days old *Satabdi* rice seedlings. These genes are already known for their responsiveness to different environmental stimuli / abiotic stresses [4-5, 7]. As discussed in the last chapter (Chapter 7), phytochrome B and phytochrome C are chromoprotein producing genes – these two genes have shown upregulation following the one-time flash electromagnetic irradiation. Based on the wavelength of irradiance received by plant leaves, phytochromes alter their conformation by either absorbing red or far-red light. Far-red light absorbing phytochromes reach inside the nucleus and then, act together with Phytochrome Interacting Factors (PIFs) – as a consequence, they modulate a number of abiotic or thermo-sensing genes. In addition, rice phytochromes control seed germination, de-etiolation, plant architecture development, thermal-sensitivity and flowering initiation [24]. As reported in literature, plants with null phytochrome B and phytochrome C alleles induce early flowering initiation [25]; as a consequence, it is interpreted that induced upregulation in phytochrome B and phytochrome C gene expressions in rice can delay flowering stage. In this connection, it should be recollected (based on the findings reported in Chapter 7) that rice plants somewhat adapt under long-term

periodic electromagnetic irradiation mainly by their developmental plasticity – matured old tissues possess less responsiveness to incident electromagnetic radiation.

Gene with leucine-rich zipper (bZIP1), in chromosome1, produces G-box binding Transcription Factors (TFs) that regulate multiple stress tolerance gene expressions like under salinity, drought etc. Here, more than 250 fold upregulation is probably due to immediate extraction of RNA just after 2 h 30 min flash irradiation [26]. Actually, very low bZIP1 expression has been observed in 12 days old sham-exposed *Satabdi* seedlings as reflected by high Cycle Threshold (CT) value (37-39) where the house-keeping actin gene has given CT at 27-28 both in irradiated and sham-exposed *Satabdi* seedlings – thus, the possibilities of poor quality of RNA or sampling error has been eliminated. Upregulation of stress-induced abscisic acid-responsive bZIP1 expression may cut rice-yield [27]. Upregulated expressions of the above mentioned stress-responsive genes in 12 days old *Satabdi* rice seedlings are in line with previously reported investigations – where, electromagnetic radiation has been reported to be a stress factor for plants [4-5, 7].

## **8.4 One-Time Controlled Electromagnetic Irradiation Evoked Molecular Responses in *Swarnaprabha* Rice Plant**

*Swarnaprabha* is one of the major photoperiod insensitive variants of rice. It is primarily grown in wet season when majority of rice variants is cultivated in India. *Swarnaprabha* rice plants mature by 125 to 130 days with typical yield potentiality around 6.5 to 7.0 ton/ha – these resemble well with the mean maturity duration and yield potentiality of popular wet-season rice variants. Therefore, it is an ideal prototype for studying the effect of one-time controlled electromagnetic irradiation on subsequent molecular responses in plants inside a simple reverberation chamber. In this research experiment, one-time (2 h 30 min) controlled EM irradiation (1837.50 MHz, 2.75 mW/m<sup>2</sup>) induced molecular responses have been investigated in 40-day-old *Swarnaprabha* rice plants and relative expression profiles of pre-selected stress-responsive genes have been studied following 2 h 30 min electromagnetic irradiation. A schematic of the experimental model is presented in Fig. 8.4.

### **8.4.1 Plant culture and growth conditions**

*Swarnaprabha* rice (*Oryza sativa*) variant has been chosen to investigate 2 h 30 min long 1837.50 MHz, 2.75 mW/m<sup>2</sup> electromagnetic irradiation induced molecular responses in 40 days

**Gene expression profiling experiment following short duration electromagnetic irradiation in 40-day-old *Swarnaprabha* rice plants**

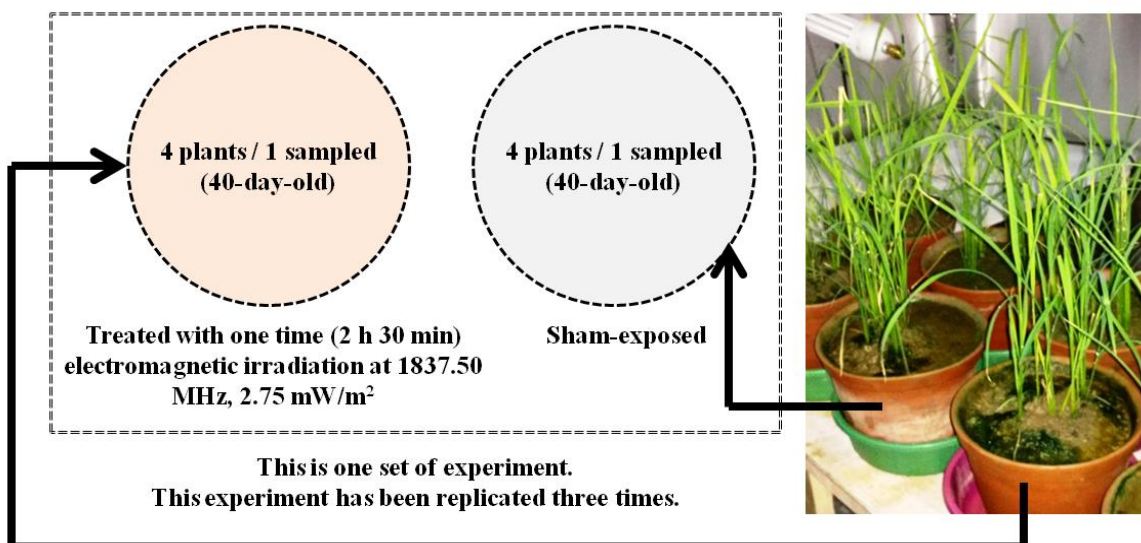


Fig. 8.4: Graphical scheme of gene expression profiling experiment in 40 days old *Swarnaprabha* rice plants following one-time electromagnetic irradiation

old rice plants. This investigation has been carried out at the main campus of Indian Institute of Science Education and Research Kolkata (22.9638° N, 88.5245° E) during the Monsoon with typical air temperature range 27 °C to 32 °C. At the initial stage, 30 *Swarnaprabha* seeds have been soaked in water for germination inside the electromagnetically quiet zone of the simple reverberation chamber – seeds have been kept in the dark and water was changed regularly for the first four days. After germination, eight healthy germinated seeds have been selected and directly seeded in two earthen pots (25.4 cm), each containing four germinated seeds. Next, those two earthen pots containing germinated seeds and saplings at a later stage have been grown together inside a Faraday cage made of metallic mesh. Thus, *Swarnaprabha* rice saplings have been allowed to grow under natural photoperiod with 800 μmol m<sup>-2</sup> s<sup>-1</sup> to 900 μmol m<sup>-2</sup> s<sup>-1</sup> photosynthetically active radiation for 12 h 30 min during daytime. It has allowed sufficient sunlight for photosynthesis and ensured isolation from unintended natural / technological electromagnetic frequencies present in surroundings. *Swarnaprabha* rice seedlings haven't been transplanted at the intermediate stage to avoid the possibility of uneven stress on rice seedlings during transplantation – seedlings in both the earthen pots have been allowed to grow for 40 days in an isolated electromagnetic quiet zone inside the Faraday cage. At the age of 40 days, typical



heights of all the rice plants have been observed to be in the range of 35 cm to 37 cm above soil level. All rice plants have been observed to be in active tillering stage with almost similar number of leaves in each plant.

#### **8.4.2 Electromagnetic Irradiation on *Swarnaprabha* Rice Plant**

The electromagnetic irradiation experiment on 40 days old *Swarnaprabha* rice plants is exactly similar as described earlier in case of 12 days old *Satabdi* rice seedlings – thus, the same is not repeated here. Targeted 40 days old *Swarnaprabha* rice plants have been exposed to 1837.50 MHz, 2.75 mW/m<sup>2</sup> electromagnetic radiation for 2 h 30 min – in contrast, the control rice plants for sham-exposure have been kept in electromagnetic quiet zone during the same time period. The schematic diagram to describe this experiment is illustrated in Fig. 8.4.

Right after the controlled electromagnetic irradiation (2 h 30 min), top-most first leaf of the targeted and sham-exposed *Swarnaprabha* rice plants have been collected, sliced into smallest possible pieces and stored in RNAlater solution at –20 °C till further use.

#### **8.4.3 Plant RNA Extraction and cDNA Synthesis (*Swarnaprabha*)**

For 40 days old *Swarnaprabha* plant samples, RNA extraction and cDNA synthesis techniques are exactly similar as in case of 12 days old *Satabdi* rice seedling samples.

#### **8.4.4 Quantitative Real-Time PCR (qRT-PCR)**

For *Swarnaprabha* plant samples, qRT-PCR protocol is also similar as described in case of *Satabdi* rice seedling samples – thus, the protocol is not repeated here again.

#### **8.4.5 Statistical Analysis**

For relative gene expressions analyses in electromagnetic radiation treated *Swarnaprabha* plant specimens, similar statistical data analyses have been performed as described earlier in case of *Satabdi* rice seedlings.

#### **8.4.6 Molecular Responses in *Swarnaprabha* Rice Plant**

In 40 days old *Swarnaprabha* rice plants, one-time controlled electromagnetic irradiation (2 h 30 min – 1837.50 MHz, 2.75 mW/m<sup>2</sup>) induced upregulation in relative transcript abundance of

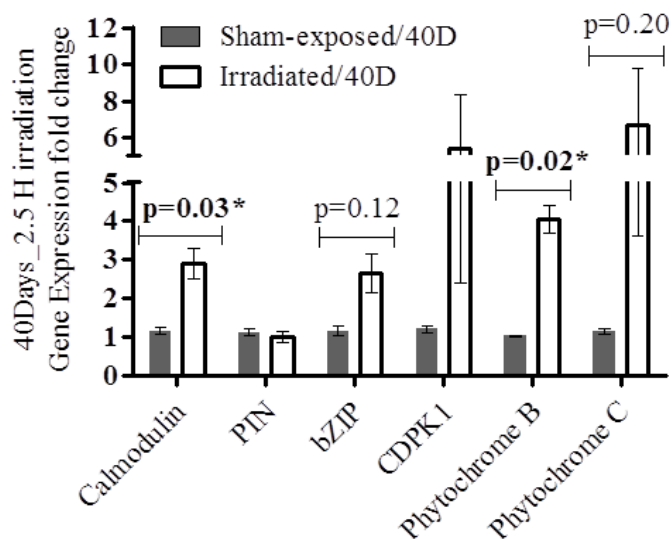


Fig. 8.5: Comparison of relative gene expression levels in 40 days old *Swarnaprabha* rice plants following one-time electromagnetic irradiation at 1837.50 MHz, 2.75 mW/m<sup>2</sup> for 2 h 30 min (data represent mean value  $\pm$  SEM from three independent experiments)

stress-responsive calmodulin (2.50 fold) and phytochrome B (3.98 fold) genes have been noted to be statistically significant at  $p$ -value = 0.03 and  $p$ -value = 0.02 respectively. In addition, relative expressions for bZIP1 (2.27 fold) and phytochrome C (5.87 fold) genes have also been observed to be upregulated following the electromagnetic irradiation – but, missed the statistical significance level of  $p$ -value = 0.05 by narrow margins. However, alterations in relative expressions for PIN and CDPK1 genes have been found to be statistically insignificant following the same electromagnetic irradiation. The normalized fold changes in relative expressions of the targeted stress-responsive genes are illustrated in Fig. 8.5 and respective  $p$ -values are indicated wherever applicable.

### 8.4.7 Discussions

One-time controlled electromagnetic irradiation at 1837.50 MHz, 2.75 mW/m<sup>2</sup> for 2 h 30 min has triggered significant transcriptional upregulation of the stress-sensitive transcripts in 40 days old *Swarnaprabha* rice plants. Upregulated expressions for some of these genes have also been recorded in 12 days old *Satabdi* rice seedlings under similar flash electromagnetic irradiation. Results indicate a direct relation between electromagnetic irradiation and induced strong

alterations in relative gene expressions – moreover, observed accumulation of the stress-sensing transcripts are in agreement with earlier reported plant responses following injurious treatments such as electromagnetic irradiation, leaf flaming or electrical stimulation [4-5, 7].

As discussed in the last chapter, calmodulin is a critical  $Ca^{2+}$  receptor in cell and also a key stress indicator in plants [5, 28]. At neutral pH, the cell membrane possesses negative surface potential – consequently,  $Ca^{2+}$  ions are attracted more over  $Na^{1+}$  or  $K^{1+}$ . In general,  $Ca^{2+}$  ions contribute in stabilizing plasma membrane, modulating membrane surface potential, activating several signaling pathways and so on [29-30]. However, incident time-alternating electromagnetic radiation can cause dislocation and subsequent replacement of few  $Ca^{2+}$  ions on cell membrane with the nearby  $Na^{1+}$  or  $K^{1+}$  ions – leading to membrane leakage and large influx of  $Ca^{2+}$  ions in cell cytoplasm. Electromagnetic irradiation induced imbalance of  $Ca^{2+}$ ,  $K^{1+}$  and  $Na^{1+}$  concentrations in the plant cell has substantial after effect [31-35]. Thus, one-time electromagnetic irradiation induced upregulation of calmodulin gene (in 40 days old *Swarnaprabha* rice plants) indicates early variations of  $Ca^{2+}$  concentration in cytoplasm and neighbourhood – and subsequently activates the essential defense mechanisms [4-5]. Moreover, the same electromagnetic irradiation has upregulated bZIP1, phytochrome B and phytochrome C gene expressions in 40 days old *Swarnaprabha* rice plants – as also reported earlier in case of 12 days old *Satabdi* rice seedlings. The consequences have previously been outlined in this chapter – thus, not repeated here.

Herein, transcript accumulation of stress-responsive genes in 40 days old *Swarnaprabha* rice plants is similar to the molecular responses in 12 days old *Satabdi* rice seedlings. Moreover, similar flash electromagnetic irradiation induced stress-responsive transcript accumulations have been reported in past [4-5, 7].

## 8.5 Conclusions

One-time hours-long electromagnetic irradiation (1837.50 MHz, 2.75 mW/m<sup>2</sup>) has evoked transcript accumulation of stress-responsive genes in both 12 days old *Satabdi* rice seedlings as well as 40 days old *Swarnaprabha* rice plants. All reported molecular responses, irrespective of rice variant and growth stage, have been noted at such an irradiation level (1837.50 MHz, 2.75 mW/m<sup>2</sup>) that is well below the standard electromagnetic regulatory guidelines [11-12]. Even

more, one-time electromagnetic irradiation induced stress-responsive transcript accumulation in rice plants is quite similar to the induced molecular responses under long-term periodic electromagnetic irradiation. Past reported one-time electromagnetic irradiation induced stress-responsive transcript accumulation in other plants endorses the outcome of this investigation [4-5, 7]. Long-term simultaneous electromagnetic irradiation at multiple frequencies can possibly induce more robust molecular responses in plants; however this needs to be validated at a large scale. Thus, transcript accumulations in plants and their dependence on applied electromagnetic radiation dose (i.e. frequency, power density and duration etc.) can be better understood. Taken together with the previous observations available in literature, the observed molecular responses not only confirm electromagnetic irradiation induced abiotic stress in rice plants but also demand for re-evaluating existing electromagnetic regulatory standards to protect the plant kingdom.

## References

- [1] S. O. Nelson, and S. Trabelsi, 'Dielectric Spectroscopy Measurements on Fruit, Meat, and Grain', *Transactions of the ASABE*, Vol. 51, No. 5, pp. 1829-1834, 2008.
- [2] S. O. Nelson, 'Dielectric Properties of Agricultural Products and Some Applications', *Research in Agricultural Engineering*, Vol. 54, No. 2, pp. 104-112, 2008.
- [3] A. Vian, C. Faure, S. Girard, E. Davies, F. Hallé, P. Bonnet, G. Ledoigt, and F. Paladian, 'Plants Respond to GSM-Like Radiations', *Plant Signaling & Behaviour*, Vol. 2, No. 6, pp. 522-524, 2007.
- [4] A. Vian, D. Roux, S. Girard, P. Bonnet, F. Paladian, E. Davies, and G. Ledoigt, 'Microwave Irradiation Affects Gene Expression in Plants', *Plant Signaling & Behavior*, Vol. 1, No. 2, pp. 67-69, 2006.
- [5] D. Roux, A. Vian, S. Girard, P. Bonnet, F. Paladian, E. Davies, and G. Ledoigt, 'Electromagnetic Fields (900 MHz) Evoke Consistent Molecular Responses in Tomato Plants', *Physiologia Plantarum*, Vol. 128, No. 2, pp. 283-288, 2006.
- [6] D. Roux, C. Faure, P. Bonnet, S. Girard, G. Ledoigt, E. Davies, M. Gendraud, F. Paladian, and A. Vian, 'A Possible Role for Extra-Cellular ATP in Plant Responses to High Frequency, Low Amplitude Electromagnetic Field', *Plant Signaling & Behaviour*, Vol. 3, No. 6, pp. 383-385, 2008.

- [7] D. Roux, A. Vian, S. Girard, P. Bonnet, F. Paladian, E. Davies, and G. Ledoigt, 'High Frequency (900MHz) Low Amplitude (5V m<sup>-1</sup>) Electromagnetic Field: A Genuine Environmental Stimulus that Affects Transcription, Translation, Calcium and Energy Charge in Tomato', *Planta*, Vol. 227, No. 4, pp. 883-891, 2008.
- [8] A. Vian, E. Davies, M. Gendraud, and P. Bonnet, 'Plant Responses to High Frequency Electromagnetic Fields', *BioMed Research International*, Article ID: 1830262, 2016.
- [9] International Electrotechnical Commission (IEC), '*IEC 61000-4-21 (2011) Electromagnetic Compatibility (EMC) – Part 4-21: Testing and Measurement Techniques – Reverberation Chamber Test Methods*', International Electrotechnical Commission, Geneva, 2011. [www.webstore.iec.ch/publication/4191](http://www.webstore.iec.ch/publication/4191) (subscription required) [Last accessed 01 December 2020]
- [10] E. Beaubois, S. Girard, S. Lallechere, E. Davies, F. Paladian, P. Bonnet, G. Ledoigt, and A. Vian, 'Intercellular Communication in Plants: Evidence for Two Rapidly Transmitted Systemic Signals Generated in Response to Electromagnetic Field Stimulation in Tomato', *Plant, Cell and Environment*, Vol. 30, No. 7, pp. 834-844, 2007.
- [11] R. F. Cleveland, Jr., D. M. Sylvar, and J. L. Ulcek, '*Evaluating Compliance with FCC Guidelines for Human Exposure to Radiofrequency Electromagnetic Fields*', FCC OET Bulletin, Vol. 65, Edition 97-01, Washington D.C., 1997.
- [12] International Commission on Non-Ionizing Radiation Protection (ICNIRP), 'Guidelines for Limiting Exposure to Electromagnetic Fields (100 kHz to 300 GHz)', *Health Physics*, Vol. 118, No. 5, pp. 483-524, 2020.
- [13] M. Czerwinski, L. Januszkiewicz, A. Vian, and A. Lazaro, 'The Influence of Bioactive Mobile Telephony Radiation at the Level of a Plant Community – Possible Mechanisms and Indicators of the Effects', *Ecological Indicators*, Vol. 108, Article No. 105683, pp. 1-11, 2020.
- [14] A. Grémiaux, S. Girard, V. Guérin, J. Lothier, F. Baluska, E. Davies, P. Bonnet, and A. Vian, 'Low-Amplitude, High-Frequency Electromagnetic Field Exposure Causes Delayed and Reduced Growth in *Rosa hybrida*', *Journal of Plant Physiology*, Vol. 190, pp.44-53, 2016.
- [15] M. N. Halgamuge, S. K. Yak, and J. L. Eberhardt, 'Reduced Growth of Soybean Seedlings After Exposure to Weak Microwave Radiation from GSM 900 Mobile Phone and Base Station', *Bioelectromagnetics*, Vol. 36, No. 2, pp. 87-95, 2015.

- [16] D. S. Pesnya, and A. V. Romanovsky, 'Comparison of Cytotoxic and Genotoxic Effects of Plutonium-239 Alpha Particles and Mobile Phone GSM 900 Radiation in the *Allium cepa* Test', *Mutation Research/Genetic Toxicology and Environmental Mutagenesis*, Vol. 750, No. 1-2, pp. 27-33, 2013.
- [17] V. P. Sharma, H. P. Singh, R. K. Kohli, and D. R. Batish, 'Mobile Phone Radiation Inhibits *Vigna radiata* (Mung Bean) Root Growth by Inducing Oxidative Stress', *Science of the Total Environment*, Vol. 407, No. 21, pp. 5543-5547, 2009.
- [18] H. P. Singh, V. P. Sharma, D. R. Batish, and R. K. Kohli, 'Cell Phone Electromagnetic Field Radiations Affect Rhizogenesis through Impairment of Biochemical Processes', *Environmental Monitoring and Assessment*, Vol. 184, No. 4, pp. 1813-1821, 2012.
- [19] A. L. Stefi, L. H. Margaritis, and N. S. Christodoulakis, 'The Effect of the Non-Ionizing Radiation on Exposed, Laboratory Cultivated Maize (*Zea mays L.*) Plants', *Flora*, Vol. 233, pp. 22-30, 2017.
- [20] C. Waldmann-Selsam, A. Balmori-de la Puente, H. Breunig, and A. Balmori, 'Radiofrequency Radiation Injures Trees around Mobile Phone Base Stations', *Science of the Total Environment*, Vol. 572, pp. 554-569, 2016.
- [21] CST Studio Suite, [www.3ds.com/products-services/simulia/products/cst-studio-suite](http://www.3ds.com/products-services/simulia/products/cst-studio-suite) [Last accessed 04 April 2022].
- [22] The National Center for Biotechnology Information (NCBI), [www.ncbi.nlm.nih.gov](http://www.ncbi.nlm.nih.gov) [Last accessed on 28 April 2022].
- [23] The Rice Annotation Project Database (RAP-DB), [rapdb.dna.affrc.go.jp](http://rapdb.dna.affrc.go.jp) [Last accessed on 28 April 2022].
- [24] J. H. Jung, M. Domijan, C. Klose, S. Biswas, D. Ezer, M. Gao, A. K. Khattak, M. S. Box, V. Charoensawan, S. Cortijo, and M. Kumar, 'Phytochromes Function as Thermosensors in Arabidopsis', *Science*, Vol. 354, No. 6314, pp. 886-889, 2016.
- [25] M. Takano, N. Inagaki, X. Xie, N. Yuzurihara, F. Hihara, T. Ishizuka, M. Yano, M. Nishimura, A. Miyao, H. Hirochika, and T. Shinomura, 'Distinct and Cooperative Functions of Phytochromes A, B, and C in the Control of Deetiolation and Flowering in Rice', *The Plant Cell*, Vol. 17, No. 12, pp. 3311-3325, 2005.

- [26] A. Para, Y. Li, A. Marshall-Colón, K. Varala, N. J. Francoeur, T. M. Moran, M. B. Edwards, C. Hackley, B. O. Bargmann, K. D. Birnbaum, and W. R. McCombie, 'Hit-And-Run Transcriptional Control by bZIP1 Mediates Rapid Nutrient Signaling in *Arabidopsis*', *Proceedings of the National Academy of Sciences*, Vol. 111, No. 28, pp. 10371-10376, 2014.
- [27] M. Obertello, G. Krouk, M. S. Katari, S. J. Runko, and G. M. Coruzzi, 'Modeling the Global Effect of the Basic-Leucine Zipper Transcription Factor 1 (bZIP1) on Nitrogen and Light Regulation in *Arabidopsis*', *BMC Systems Biology*, Vol. 4, No. 1, pp. 1-11, 2010.
- [28] T. Yang, and B. W. Poovaiah, 'Calcium/Calmodulin-Mediated Signal Network in Plants', *Trends in Plant Science*, Vol. 8, No. 10, pp. 505-512, 2003.
- [29] C. Larsson, I. M. Møller, and S. Widell, 'Introduction to the Plant Plasma Membrane – Its Molecular Composition and Organization', In *The Plant Plasma Membrane*, Springer, pp. 1-15, Berlin, Germany, 1990.
- [30] P. J. White, and M. R. Broadley, 'Calcium in Plants', *Annals of Botany*, Vol. 92, No. 4, pp. 487-511, 2003.
- [31] L. J. Challis, 'Mechanisms for Interaction between RF Fields and Biological Tissues', *Bioelectromagnetics*, Vol. 26, No. S7, pp. S98-S106, 2005.
- [32] S. Cucurachi, W. L. Tamis, M. G. Vijver, W. J. Peijnenburg, J. F. Bolte, and G. R. de Snoo, 'A Review of the Ecological Effects of Radiofrequency Electromagnetic Fields (RF-EMF)', *Environment International*, Vol. 51, pp. 116-140, 2013.
- [33] E. Davies, 'Electrical Signals in Plants: Facts and Hypotheses', In A. G. Volkov (eds): *Plant Electrophysiology*, Springer, pp 407-422, Berlin, Germany, 2006.
- [34] E. Davies, and B. Stankovic, 'Electrical Signals, the Cytoskeleton, and Gene Expression: A Hypothesis on the Coherence of the Cellular Responses to Environmental Insult', In F. Baluška, S. Mancuso, D. Volkmann (eds): *Communication in Plants*, Springer. pp 309-320, Berlin, Germany, 2006.
- [35] M. Levin, 'Bioelectromagnetics in Morphogenesis', *Bioelectromagnetics*, Vol. 24, No. 5, pp. 295-315, 2003.

# Chapter 9

## Conclusions and Future Scope

---

### 9.1 Introduction

The aim of this dissertation was to investigate Specific Absorption Rate (SAR) data and associated spatial distributions in different fruit, flower and plant models under diverse electromagnetic exposure scenarios – in addition, further plans were to investigate long duration as well as short duration, controlled and deterministic electromagnetic irradiation induced physiological and molecular responses in plants. Theoretical, simulation-based and practical investigations have meticulously been described in the previous chapters of this dissertation along with quantitative outcome analyses. Here, in this concluding chapter, the qualitative and quantitative accomplishments have been summarized along with a brief discussion on the potential extensions of the research work reported in this dissertation.

### 9.2 A Qualitative Summary of Research Achievements

At initial phase, this dissertation dealt with broadband complex dielectric properties ( $\epsilon_r$ ) characterization of several fruit and plant specimens – in general, all the measured results can contribute to the universal dielectric data base of fruits, crops and plants. The measured dielectric properties ( $\epsilon_r$ ) of mentioned fruit and plant specimens can be used in several microwave food processing applications in addition to SAR data evaluation under electromagnetic irradiation. Electromagnetic energy absorption rates estimation (SAR data and spatial distributions) in different fruit and plant models under diversified electromagnetic exposure scenarios is a unique research contribution in this dissertation. Reported SAR data and spatial distributions in fruit and plant models under practical exposure scenarios can facilitate the policy makers to reassess existing electromagnetic exposure guidelines for protecting fruits, crops and plants along with humans. Furthermore, a novel technique has been proposed in this dissertation to define effective dielectric properties ( $\epsilon_r$ ) of homogeneous phantom liquid that can represent random multilayer biological structure for accurate and realistic SAR measurement. In addition, a number of fruit and plant tissue layers equivalent homogeneous phantom liquid recipes have been prepared at



three different frequencies i.e. 947.50 MHz, 1842.50 MHz and 2450 MHz for SAR measurements in fruit and plant phantom models (in future). In this thesis, wireless channel propagation losses have been investigated due to electromagnetic absorption and scattering phenomena in plants – this experiment has been carried out at around 1800 MHz.

In the second phase of this dissertation, investigations on electromagnetic irradiation induced physiological and molecular responses have been reported. Based on the investigation's outcome, it has been reported that long duration cell phone irradiation causes reduced seed germination rate, enhanced plant growth and wrinkled leaves in *Capsicum annuum* saplings. Furthermore, irrespective of variant and plant growth stage, 1837.50 MHz, 2.75 mW/m<sup>2</sup> controlled and periodic electromagnetic irradiation induced physiological or molecular responses in rice (*Oryza sativa*) have been reported in this dissertation. The above mentioned periodic, controlled and deterministic electromagnetic irradiation has evoked reduction in rice seed germination rate and photosynthetic pigment concentration levels. In addition, significant upregulation in stress-responsive rice gene expressions has also been reported under the said periodic exposure (1837.50 MHz, 2.75 mW/m<sup>2</sup>) inside an electromagnetic reverberation chamber. In continuation, further investigations have been carried out. One-time (2 h 30 min) controlled electromagnetic irradiation (1837.50 MHz, 2.75 mW/m<sup>2</sup>) induced upregulation in stress-responsive rice gene expressions has also been reported in this thesis at different growth stages. Therefore, reported transcript accumulation of stress-sensitive rice genes under different exposure conditions indicates that plants perceive electromagnetic irradiation as an abiotic stress factor. This finding is also a distinct contribution in this dissertation.

### 9.3 Future Scope for this Dissertation

Some potential extensions of the work carried out in this dissertation can be outlined as follows,

- The dielectric properties ( $\epsilon_r$ ) measurement work can be extended further to prepare a comprehensive broadband dielectric data base of different plant, fruit and flower tissues considering temperature dependent variations.
- SAR evaluation work can be extended to investigate electromagnetic energy absorption rates in fruit, flower and plant models due to plane wave incidence with inclined linear polarization, circular polarization or elliptical polarization.

## Conclusions and Future Scope

- The concept of multilayer structure equivalent homogeneous phantom modeling can be pursued further to redefine existing phantom liquid dielectric properties ( $\epsilon_r$ ) for more realistic SAR measurements. Furthermore, applicable SAR measurement guidelines can be considered for probable revision.
- It should also be noted that a little amount of preservative can be added to fruit and plant tissue equivalent phantom liquid recipes for long-term storage.
- Customized fruit and plant phantom models can be fabricated for practical SAR measurements. Prepared homogeneous liquids can then be utilized to fill the phantom models for validating SAR data and distributions.
- The work in this dissertation can also be extended to investigate electromagnetic irradiation induced physiological and molecular effects on other plants, at different frequency bands, and at a larger scale – in this connection, field studies can be performed over elongated time duration.
- Appropriate research committees and policy makers can further pursue the investigation outcomes reported in this dissertation to protect fruits, crops and plants from potential hazardous effects of electromagnetic irradiation.

Research is a continuous journey with infinite number of possibilities to explore. Therefore, through this dissertation, a little incremental contribution has been added to the existing human knowledge base. It is expected that the content in this dissertation should encourage researchers to explore further in the future. The upcoming research direction in this field will be full of excitement with newer insights and therefore, will lead to balanced and sustainable development.

# Appendix I

---

## List of Journal Publications:

- [1] **Ardhendu Kundu**, Bhaskar Gupta, Amirul Islam Mallick, ‘Dependence of Specific Absorption Rate and its Distribution inside a Homogeneous Fruit Model on Frequency, Angle of Incidence and Wave Polarization’, *Frequenz*, Vol. 76, No. 1-2, 2022
- [2] **Ardhendu Kundu**, Bhaskar Gupta, Amirul Islam Mallick, ‘Estimation of Specific Absorption Rate Levels in a Typical Fruit Specimen and Observations on their Variations According to Different Electromagnetic Standards’, *Microwave Review (Mikrotalasna revija)*, Vol. 27, No. 2, December, 2021
- [3] **Ardhendu Kundu**, Sathish Vangaru, Sucharita Bhowmick, Somnath Bhattacharyya, Amirul Islam Mallick, Bhaskar Gupta, ‘One-time Electromagnetic Irradiation Modifies Stress-sensitive Gene Expressions in Rice Plant’, *Bioelectromagnetics*, Vol. 42, No. 8, December, 2021
- [4] **Ardhendu Kundu**, Sathish Vangaru, Somnath Bhattacharyya, Amirul Islam Mallick, Bhaskar Gupta, ‘Erratum: Electromagnetic Irradiation Evokes Physiological and Molecular Alterations in Rice’, *Bioelectromagnetics*, Vol. 42, No. 5, July, 2021
- [5] **Ardhendu Kundu**, Sathish Vangaru, Somnath Bhattacharyya, Amirul Islam Mallick, Bhaskar Gupta, ‘Electromagnetic Irradiation Evokes Physiological and Molecular Alterations in Rice’, *Bioelectromagnetics*, Vol. 42, No. 2, February, 2021
- [6] **Ardhendu Kundu**, Bhaskar Gupta, Amirul Islam Mallick, ‘Contrast in Specific Absorption Rate for a Typical Plant Model Due to Discrepancy Among Global and National Electromagnetic Standards’, *Progress In Electromagnetics Research M*, Vol. 99, January, 2021
- [7] **Ardhendu Kundu**, Bhaskar Gupta, Amirul Islam Mallick, ‘Specific Absorption Rate Evaluation in a Typical Multilayer Fruit: Coconut with Twig due to Electromagnetic Radiation as per Indian Standards’, *Microwave Review (Mikrotalasna revija)*, Vol. 23, No. 2, December, 2017
- [8] **Ardhendu Kundu**, Bhaskar Gupta, ‘Comparative SAR Analysis of Some Indian Fruits as per the Revised RF Exposure Guideline’, *IETE Journal of Research*, Vol. 60, No. 4, October, 2014

[9] **Ardhendu Kundu**, Kaushik Patra, Bhaskar Gupta, ‘Broadband Dielectric Properties Evaluation of Catharanthus Roseus Leaf, Flower and Stem Using Open Ended Coaxial Probe Technique’, *Journal of Physical Sciences*, Vol. 18, March, 2014

**List of Conference Publications:**

[1] **Ardhendu Kundu**, Amirul Islam Mallick, Bhaskar Gupta, ‘An Overview of Gene Expression Alterations in Plants Following Electromagnetic Irradiation’, *National Symposium on Engineering, Technology and Management – All Comprehensive Endeavors for Humanistic Growth*, Kolkata, December, 2021

[2] **Ardhendu Kundu**, Kaushik Patra, Bhaskar Gupta, Amirul Islam Mallick, ‘Role of Reverberation Chamber in Wireless Testing and Measurement with Emphasis on Investigating Biological Effects’, *IEEE Calcutta Conference (CALCON)*, Kolkata, February, 2020

[3] **Ardhendu Kundu**, Bhaskar Gupta, Amirul Islam Mallick, ‘Dependence of Electromagnetic Energy Distribution Inside a Typical Multilayer Fruit Model on Direction of Arrival and Polarization of Incident Field’, *Radio and Antenna Days of the Indian Ocean (RADIO)*, Reunion Island, September, 2019

[4] **Ardhendu Kundu**, Bhaskar Gupta, Amirul Islam Mallick, ‘Electromagnetic Radiation Absorption in Indian Flora and Related Consequences: A Critical Issue for Sustainable Growth’, *Radio and Antenna Days of the Indian Ocean (RADIO)*, Reunion Island, September, 2019

[5] **Ardhendu Kundu**, Bhaskar Gupta, ‘Review on Cell Tower Radiation Absorption in Indian Flora and Related Consequences: A Critical Issue for Sustainable Telecom Growth’, *National Conference on Sustainable Technology to Connect People with Nature*, Kolkata, June, 2017

[6] **Ardhendu Kundu**, Sharanbasappa B Belamgi, Kaushik Patra, Bhaskar Gupta, Amirul Islam Mallick, ‘A Practical Investigation on Radio Frequency Absorption and Shielding Effectiveness in Chinese *Tabernaemontana divaricata* Plants at GSM 1.8 GHz’, *24<sup>th</sup> West Bengal State Science and Technology Congress 2017*, Kolkata, February – March, 2017

[7] **Ardhendu Kundu**, Bhaskar Gupta, Amirul Islam Mallick, ‘Specific Absorption Rate Calculation in a Typical Bunch of Sapodilla Fruits (*Manilkara zapota*) as per Revised Indian RF Exposure Guidelines’, *URSI RCRS 2017*, Tirupati, March, 2017

- [8] **Ardhendu Kundu**, Bhaskar Gupta, Amirul Islam Mallick, ‘SAR Analysis in a Typical Bunch of Grapes Exposed to Radio Frequency Radiation in Indian Scenario’, 2016 *International Conference on Microelectronics, Computing and Communications (MicroCom)*, Durgapur, January, 2016
- [9] **Ardhendu Kundu**, Bhaskar Gupta, Amirul Islam Mallick, ‘Effects of Non-Ionizing Electromagnetic Radiation on Capsicum annum Seed Germination and Subsequent Sapling Growth – A Time Study’, 2016 *International Conference on Microelectronics, Computing and Communications (MicroCom)*, Durgapur, January, 2016
- [10] **Ardhendu Kundu**, Bhaskar Gupta, ‘Broadband Dielectric Properties Measurement of Some Vegetables and Fruits Using Open Ended Coaxial Probe Technique’, *International Conference on Control, Instrumentation, Energy and Communication (CIEC)*, Kolkata, November, 2014
- [11] **Ardhendu Kundu**, Bhaskar Gupta, ‘Specific Absorption Rate Evaluation of Apple as per FCC RF Exposure Guideline’, *Recent Development in Electrical, Electronics & Engineering Physics (RDE3P-2013)*, Howrah, October, 2013

# Appendix II

---

## List of Presentations in National/International Conferences/Workshops:

- [1] **Ardhendu Kundu**, Amirul Islam Mallick, Bhaskar Gupta, ‘An Overview of Gene Expression Alterations in Plants Following Electromagnetic Irradiation’, *National Symposium on Engineering, Technology and Management – All Comprehensive Endeavors for Humanistic Growth*, Kolkata, December, 2021
- [2] **Ardhendu Kundu**, Kaushik Patra, Bhaskar Gupta, Amirul Islam Mallick, ‘Role of Reverberation Chamber in Wireless Testing and Measurement with Emphasis on Investigating Biological Effects’, *IEEE Calcutta Conference (CALCON)*, Kolkata, February, 2020
- [3] **Ardhendu Kundu**, Bhaskar Gupta, Amirul Islam Mallick, ‘Dependence of Electromagnetic Energy Distribution Inside a Typical Multilayer Fruit Model on Direction of Arrival and Polarization of Incident Field’, *Radio and Antenna Days of the Indian Ocean (RADIO)*, Reunion Island, September, 2019
- [4] **Ardhendu Kundu**, Bhaskar Gupta, ‘Review on Cell Tower Radiation Absorption in Indian Flora and Related Consequences: A Critical Issue for Sustainable Telecom Growth’, *National Conference on Sustainable Technology to Connect People with Nature*, Kolkata, June, 2017
- [5] **Ardhendu Kundu**, Sharanbasappa B Belamgi, Kaushik Patra, Bhaskar Gupta, Amirul Islam Mallick, ‘A Practical Investigation on Radio Frequency Absorption and Shielding Effectiveness in Chinese *Tabernaemontana divaricata* Plants at GSM 1.8 GHz’, *24<sup>th</sup> West Bengal State Science and Technology Congress 2017*, Kolkata, February – March, 2017
- [6] **Ardhendu Kundu**, Bhaskar Gupta, Amirul Islam Mallick, ‘Specific Absorption Rate Calculation in a Typical Bunch of Sapodilla Fruits (*Manilkara zapota*) as per Revised Indian RF Exposure Guidelines’, *URSI RCRS 2017*, Tirupati, March, 2017
- [7] **Ardhendu Kundu**, Bhaskar Gupta, Amirul Islam Mallick, ‘SAR Analysis in a Typical Bunch of Grapes Exposed to Radio Frequency Radiation in Indian Scenario’, *2016 International Conference on Microelectronics, Computing and Communications (MicroCom)*, Durgapur, January, 2016

[8] **Ardhendu Kundu**, Bhaskar Gupta, Amirul Islam Mallick, ‘Effects of Non-Ionizing Electromagnetic Radiation on Capsicum annum Seed Germination and Subsequent Sapling Growth – A Time Study’, 2016 *International Conference on Microelectronics, Computing and Communications (MicroCom)*, Durgapur, January, 2016

[9] **Ardhendu Kundu**, Bhaskar Gupta, ‘Broadband Dielectric Properties Measurement of Some Vegetables and Fruits Using Open Ended Coaxial Probe Technique’, *International Conference on Control, Instrumentation, Energy and Communication (CIEC)*, Kolkata, November, 2014

[10] **Ardhendu Kundu**, Bhaskar Gupta, ‘Specific Absorption Rate Evaluation of Apple as per FCC RF Exposure Guideline’, *Recent Development in Electrical, Electronics & Engineering Physics (RDE3P-2013)*, Howrah, October, 2013

*Ardhendu Kundu*